Nano-MoO$_3$ as a efficient heterogeneous catalyst for one-pot synthesis of biscoumarin derivatives in water

Elham Zarenezhad*

Young Research and Elite Club, Darab Branch, Islamic Azad University, Darab, Iran.
Email address*: El_zarenezhad@yahoo.com*

Introduction: Biscoumarins derivatives comprise a diverse and interesting group of heterocyclic drugs which are extremely important for their biological activities. Some coumarin derivatives, in general, and biscoumarins, in particular, are known for their anti-HIV, antimicrobial, antifungal, antithrombotic, anticoagulant, anticancer and antioxidant,[1-4] urease inhibitory,[5] cytotoxicity and enzyme inhibitory activities [6]. Metal oxide nanoparticles are known as useful heterogeneous catalysts which traditionally can catalyze the organic reactions. MoO$_3$-nanoparticle has received considerable attention as an inexpensive, eco-friendly and highly reactive catalyst [7].

Methods / Experimentals: A aromatic aldehyde (1 mmol) and 4-hydroxycoumarin (2 mmol) were taken in 25 mL round bottom flask followed by addition of water (5 mL) and MoO$_3$ (10 mol) was stirred for the appropriate times (Table 4). The progress of the reaction was monitored by TLC, the reaction mixture was washed with H$_2$O (10 mL) and EtOAc (10 mL) to almost afford the pure product.

Results and Discussion: We herein report the synthesis of biscoumarins (**3**) by the reaction of aldehydes **(2)** and 4- hydroxycoumarin **(1)** in the presence of 10 mol% nano-MoO$_3$ in water (Scheme 1).
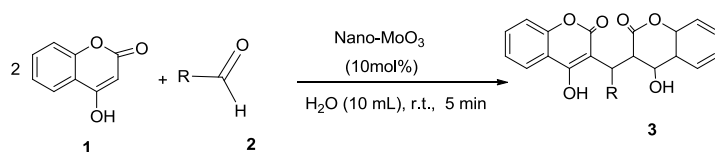
Scheme 1

As series of biscoumarins derivatives (**3a–h**) were synthesized and characterized. Two of which are new, the structure of all products was confirmed by appropriate spectroscopic and physical methods (Table 1).

Table 1. Synthesis of 1,3,4,5-tetrasubstituted 1,2,3,6-tetrahydropyrimidines derivatives (**3a–h**) using nano-MoO_3 in water

Entry	R	Product	Time (min)	Yield (%)
1	4-OH	3a	20	93
2	CH_3CH_2	3b	20	90
3	$4\text{-}CNC_6H_4$	3c	25	91
4	$3\text{-}C_6H_5OC_6H_4$	3d	22	90
5	$2\text{-}Cl,6\text{-}FC_6H_3$	3e	30	85
6	$3F,4\text{-}FC_6H_3$	3f	32	84
7	$2\text{-}OH,3\text{-}CH_3OC_6H_3$	3g	28	89
8	$3\text{-}ClC_6H_4$	3h	25	85

As can be seen in Table 1, this multi component approach can be used for both aromatic aldehyde with electron-withdrawing and electron-donating groups. Furthermore, a wide range of aromatic aldehyde were successfully used in this reaction with excellent results

Conclusion: In conclusion, we have developed MoO_3-nanoparticle -catalyzed simple, fast and efficient eco-friendly synthetic green protocol in water at room temperature and the present methodology was superior to the literature methods in terms of scalable green synthesis in water.

References

[1]. Borges F, Roleira F, Milhazes N, Santana L, Uriarte E. Current medicinal chemistry. **2005**; 12(8):887-916.

[2]. Su CX, Mouscadet JF, Chiang CC, Tsai HJ, Hsu LY. Chemical and pharmaceutical bulletin. **2006**;54 (5):682-6.

[3]. Nolan KA, Zhao H, Faulder PF, Frenkel AD, Timson JD, Siegel D, Ross D. T. J Med Chem. **2007**;5:6316.

[4]. Kancheva VD, Boranova PV, Nechev JT, Manolov **2010**, 30;92(9):1138-46.

[5]. Khan KM, Iqbal S, Lodhi MA, Maharvi GM, Choudhary MI, Perveen S., Bioorganic & medicinal chemistry. **2004** 15;12(8):1963-8.

[6]. Choudhary MI, Fatima N, Khan KM, Jalil S, Iqbal S. New biscoumarin derivatives-cytotoxicity and enzyme inhibitory activities. Bioorganic & medicinal chemistry. **2006** 1;14(23):8066-72.

[7]. Lin T. Nanofibers-production, properties and functional applications. InTech; **2011** Jan 1.

Catalytic Application of Pantothenic acid (vitamin B_5) Immobilized on the Starch Coated Magnetic Nanoparticles in the Condensation Reactions

Ameneh Eskandari, **Maasoumeh Jafarpour**[*], **Abdolreza Rezaeifard**[*]

Catalysis Research Laboratory, Department of Chemistry, Faculty of Science, University of Birjand, Iran
E-mail: mjafarpour@birjand.ac.ir; rrezaeifard@birjand.ac.ir

************************

Introduction:

Biocatalysis has now advanced to the point where we can seriously think about harnessing these biological catalysts for individual chemical reaction steps. The high selectivity and specificity is one reason for considering enzymes as catalysts for specific problems in synthetic chemistry [1].

In recent years, among the various approaches for immobilizing soluble catalysts, the covalent attachment has been the most frequently used strategy as the resulted heterogeneous catalysts have good stabilities during the course of catalytic reactions [2].

However, the small size of nanoparticles make their separation from the reaction solution and recycling difficult, which impedes their use in industrial processes. In order to circumvent such recycling problems, magnetic nanoparticles, whose flocculation and dispersion can be controlled reversibly by applying a magnetic field, were extensively employed as a recyclable support matrix in past decade [3].

Method:

γ-Fe_2O_3 MNPs were synthesized by a reported chemical co-precipitation technique of ferric and ferrous ions in alkali solution with minor modifications followed by coating with starch to modify its surface [4]. Pantothenic acid was attached to starch coated magnetic nanoparticles under ultrasonic irradiation producing a magnetically separable nanobiocatalyst (B_5@SMNP) (Fig. 1).
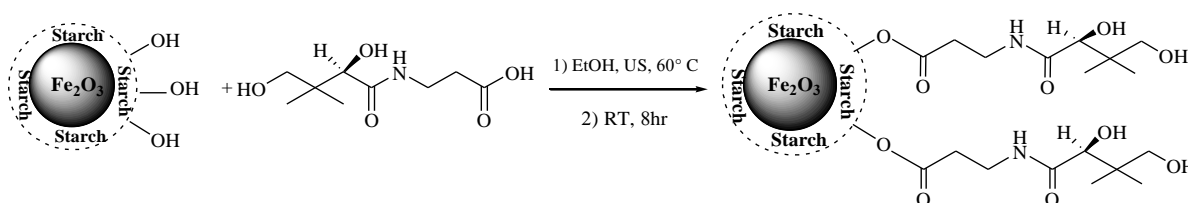
Scheme 1. Preparation of [B_5@SMNP]

Results and Discussion:

At the first step of this work, the γ-Fe_2O_3 (MNP) was prepared with a diameter of approximately 10 nm using a co-precipitation method [4]. It was coated with a dense starch layer (SMNP) followed by loading with pantothenic acid under ultrasonic irradiation. The nanobiocatalyst was characterized by different techniques such as FT-IR, VSM, TEM, XRD. Transmission electron microscopy (TEM) image revealed a uniform rod shape with the length of 10-14 nm and with a diameter 154-159 nm.

The as-prepared [B_5@SMNP] nanoparticles possess excellent catalytic properties for the aerobic synthesis of benzimidazoles in ethanol as a safe solvent. Spectral results and leaching experiments revealed that the structural integrity of the solid catalyst being well preserved after many reusing.

Conclusion:

In conclusion, [B_5@SMNP] nanoparticles was prepared by immobilizing of pantothenic acid on the starch coated γ-Fe_2O_3 nanoparticles. The title nanocatalyst was used successfully as a biocatalyst for practical production of benzimidazol derivatives in ethanol providing a novel environmentally benign catalytic condensation method. The employment of ethanol as an environmentally benign solvent in this high yielding method along with reusability of the biocatalyst provide ready scalability and make it appropriate for practical applications.

Rerferences:

[1] Nestl, B. M.; Hammer, S. C.; Nebel, B. A.; Hauer, B. *Biocatalysis*, **2014**, *53*, 3070-3095.
[2] Jafarpour, M.; Rezaeifard, A.; Ghahramaninezhad, M.; Feizpour, F. *Green Chemistry*, **2014**, 1-25.
[3] Jafarpour, M.; Rezaeifard,A.; Yasinzadeh,V.; Kargar, H. *RSC Advances*, **2015**, 1-21.
[4] (a) Massart, R.; Dubois, E.; Cabuil, V.; Hasmonay, E.; Magn, J. *Magn. Mater*, **1995**,*149*, 1–5. (b) Tang, B. Z.; Geng, Y.; Lam, J. W. Y.; Li, B.; Jing, X.; Wang, X.; Wang, F.; Pakhomov, A. B.; Zhang, X. X. *Chem. Mater*. **1999**, *11*, 1581–1589.

Electrochemical Determination of Tryptophan by using of Modified Multi-walled Carbon Nanotube/Ionic Liquid Electrode

Elham Rezaee[a], Fatemeh Honarasa[a,*]

[a] Department of Chemistry, Shiraz Branch, Islamic Azad University, Shiraz, Iran

*[*]*fhonarasa@gmail.com

Introduction: Tryptophan is one of the most important amino acids and found in natural proteins. This amino acid is widely used in the food industry as an antioxidant and in the pharmaceutical industry as a biomarker. Inaddition, it plays an important role in several biological processes [1].Various methods such as flow injection chemiluminescence[2], high pressure liquid chromatography[3], colorimetry[4], chromatography-spectrophotometry[5] and electroanalytical methods[6] have been reported for determination of tryptophan. However, electrochemical detection has been found more attractive technique for the determination of electroactive compounds because of its sensitivity, fast operation, reproducibility, accuracy, low-cost and analysis in trace samples.

Experimental: A conventional three electrode system consisting of Ag/AgCl reference electrode, platinum disk counter electrode and modified multi-walled carbon ionic liquid working electrode were used. In this work, multi-walled carbon ionic liquid electrode was prepared by hand-mixing of the synthesized 1-octylpyridinium hexafluoro phosphate and multi-walled carbon nanotube. A new surface was obtained by smoothing the electrode onto a weighing paper. For constructing modified electrode, the electrode was cycled in a solution containing $K_4Fe(CN)_6$ and KNO_3.

Result and Discussion: The cyclic voltammetric behavior of tryptophan at bare and modified multi-walled carbon nanotube/ ionic liquid (MWIL) electrodes was depicted in Figure 1. Clearly, a large increase in current can be observed at modified MWIL. Also, modified electrode shows facile electro-oxidation of tryptophan at peak potential of ~0.6 V.
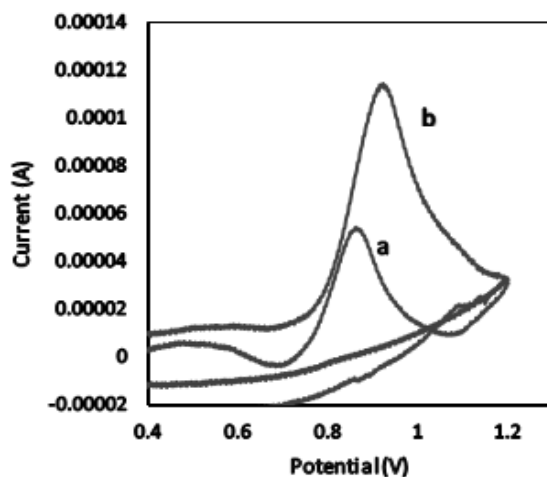
Figure 1. Cyclic voltammograms of (a) bare and (b) modified MWIL electrode toward 1 mM tryptophan in acetate buffer pH=4.

Also, effect of pH on oxidation peak of tryptophan was explored and results show equality of proton and electron in the process. In addition, since αn was obtained as 0.72 by using of Tafel plot, a two-electron transfer process is confirmed for the rate-determining step of the oxidation of tryptophan.

Finally, calibration curve for tryptophan was obtained. Calibration curve has linear range of 1×10^{-6} to 1×10^{-3} M and the detection limit is 1×10^{-6} M. The reproducibility of the electrode response, based on 5 measurements, was 2.4% for the slope of the calibration curve.

Conclusion: The electrochemical behavior of tryptophan on the surface of modified MWIL electrode was studied by cyclic voltammetry method. The modified electrode showed a low detection limit, wide linear concentration range and good reproducibility, for the detection of tryptophan.

References:

J.M.Silván, J.vande Lagemaat, A.Olano, M.D.delCastillo, *J.Pharm.Biomed.Anal.*, **2006**, 41, 1543–1551.

[2].J.Zhou,S.Chen,F.Sun,P.Luo,Q.Du,S.Zhao, *J.Chromatogr.B*, **2015**, 1006, 65.

[3]Q.Zhen, B.Xu,L.Ma,G.Tian,X.Tang,M.Ding, *Clin.Biochem.* **2011**, 44, 226.

[4]Y.Huang,S.Xiong,G.Liu,R.Zhao, *Chem.Commun.* **2011**, 47, 8319.

[5]J.Vignau, M.C.Jacquemont, A.Lefort, M.Imbenotte, M.Lhermitte, *Biomed.Chromatogr.*, **2004**, 18, 872.

[6]O.A.Farghaly, R.S.A.Hameed, A.A.H.Abu-Nawwas, *Int.J.Electrochem.Sci.,* **2014**, 9, 3287.

Interaction of Zinc (II) Schiff Base Coordination Polymer with BSA

Zahra Asadi[*], Maryam Golchin

Department of Chemistry, College of Sciences, Shiraz University, Shiraz 71454, Iran

E-mail address: zasadi@shirazu.ac.ir

＊＊＊＊＊＊＊＊＊＊＊＊＊＊＊＊＊＊＊＊

Introduction

It is proven that multinuclearity increases the efficiency and selectivity of the anticancer drugs due to the potential cooperative between the metal centers [1]. Recently, coordination polymers (CPs) and metal organic frameworks (MOFs) with muli-metal centers have attracted intense attention in cancer therapy and multi-carrier of drugs. Many drugs are bound to albumin and transported in the blood. Thus formation of complexes between drugs and protein are important from the point of view of transportation and mechanism of drug – protein interaction [2].

Methods / Experimentals

Synthesis of complex: A mixture of 2,6-diformyl-4-methylphenol and glycine were refluxed for 3h then zinc (II) chloride was added to the solution and the system refluxed again for 4h. The binding properties of complex with BSA were investigated using electronic absorption spectroscopy and fluorescence measurements. The docked conformation of the complex with BSA was generated by the molecular docking program (MVD).

Results and discussion

The synthesized compounds were identified FT-IR, ^{1}HNMR, electronic spectra and elemental analyses.

The effect of complex on BSA fluorescence intensity is shown in Figure 1. It is obvious that serum albumin reveal strong fluorescence emission peaks around 340 nm.

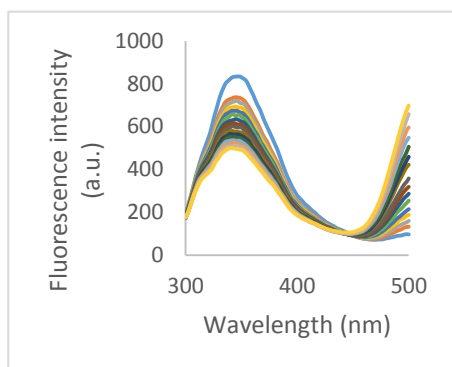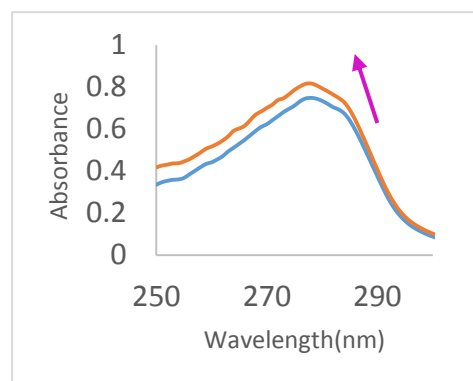Figure 1. Effect of complex on the fluorescence spectra of BSA (λ_{EX}=280)

Figure 2. UV–Vis absorption spectra of BSA in the absence and presence of the complex

The absorption spectra of BSA in the absence and presence of complex is shown in Figure 2 which displayed that by addition the compound absorption intensity of BSA enhanced with a slight blue shift. This result suggested a static interaction between the complex and BSA due to the formation of a complex-BSA ground state system.Thermodynamic parameters determined from the linear van't Hoff plot. The ΔH and ΔS values suggest that the binding between BSA and complex was exothermic and entropy-driven process.

Quenching of the fluorescence of BSA with both $\Delta\lambda = 15$ and 60nm indicated that the complex could bind to tyrosine and tryptophan residues simultaneously. The maximum emission wavelength of tyrosine residues had a blue shift but no obvious wavelength shift of tryptophan residues was observed, which suggested that the polarity around tyrosine residues decreased and the hydrophobicity increased, yet the polarity around tryptophan residues had no remarkable change during the binding process.

Conclusion

Coordination polymer was synthesized and characterized by elemental analysis, FT-IR, ^{1}H NMR and UV-Vis spectroscopy. The binding interaction of this complex with BSA was investigated by spectroscopic methods. Competitive experiments also showed that the complexes were bounded to site II of serum albumins.

References

[1] A. Arbuse, M. Font, M. A. Martínez, X. Fontrodona, M. J. Prieto, V. Moreno, X. Sala and A. Llobet. *Inorganic chemistry*, 2009, **48**, 11098-11107.

[2] H. Farrokhpour, H. Hadadzadeh, F. Darabi, F. Abyar, H. A. Rudbari and T. Ahmadi-Bagheri. *RSC Advances*, 2014, **4**, 35390-35404.

Green Tea extract as an efficient green reagent for recovery of silver Nano particles by Interacting waste photography solution

Hamid Reza Safaei*, sorayya afrasiabi

^{a} Department of Applied Chemistry, Shiraz Branch, Islamic Azad University, PO Box 71993-5, Shiraz, Iran

E-mail: hrsafaei@yahoo.com

****

Introduction: More than 18% of the world's silver needs are provided by recycling from photographic fixer solution [1]. Nano metallic particles show unique feature [2]. In recent years, Silver nano particles are gaining in popularity for their strong antimicrobial activity [3] and its relatively low toxicity towards humans [4]. Plant extracts are often environmentally and economically friendly materials. The reason plant extracts work so well in the synthesis of nanoparticles is because they act as reducing agents as well as capping agents [5]. Although there are several synthetic routes to make silver nanoparticles, However, None of them have noted to recovery as a goal. They have used standard solution of silver nitrate as a source of silver ions, while there are substantial difference between the chemical composition of photography waste solution and standard solution of $AgNO_3$ [6]. We herein report an efficient bio-recovery of silver nanoparticles from photography waste solution by Green tea (Camellia sinensis) extracts have been examined as reducing and stabilizing agents in Ag NPs production because,This plant is rich of natural antioxidants cause stability of nano particle by capping of silver particles.

In this study to the best of our knowledge for the first time silver nano particles was obtained from waste photography solution. The condition of the reaction were optimized and characterization of obtained Ag NPs were assessed by instrumental methods such as UV-Visible and IR spectroscopy, dynamic light scattering (DLS), X-ray diffraction analysis and Scanning Electron Microscope (SEM) images.

Methods:

10 g of dried prepared green tea was extracted for 20 min with 100mL ethanol 50% and filtered by using Whatman filter paper.5ml of green tea extract was add into 50 ml of fixer solution

(8 gL^{-1}) in 70 °C within 15 min time period with vigorous stirring.
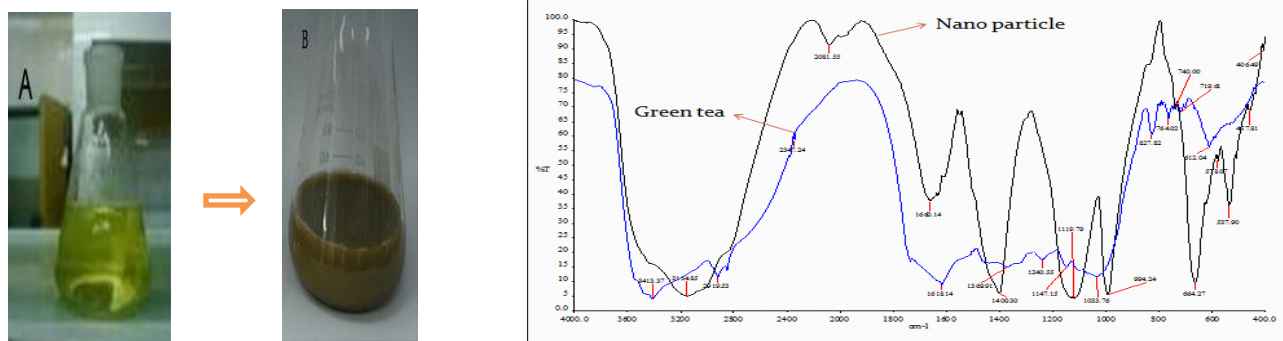
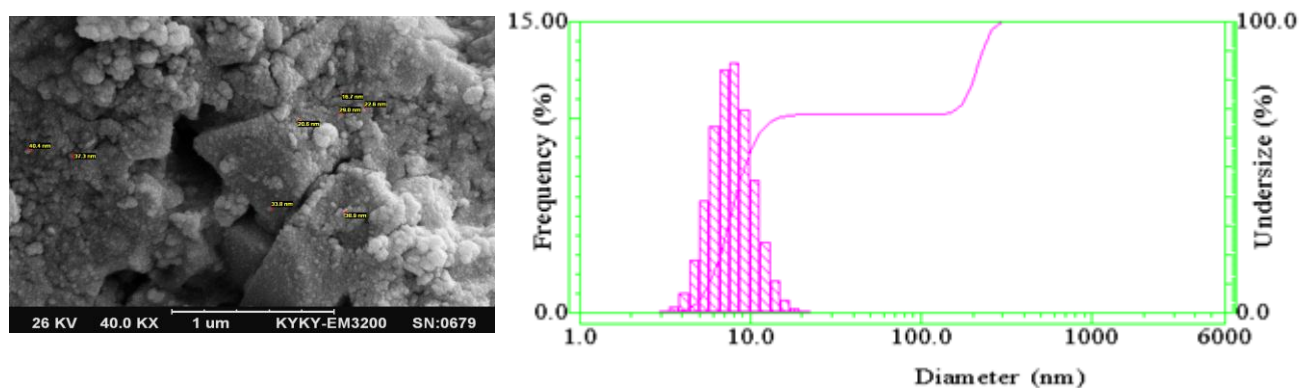**Fig 1.** Nano particle of Ag$^+$(B) and FT-IR Spectra

Fig 2. SEM image of silver nanoparticles and Particle Size Analyzer

Results and Discussion:

It was found that green tea extracts can reduce silver cations into metallic silver nanoparticles whitin a simple and efficient reaction.In this method average diameter of Ag nanoparticles was obtained 9.3 nm. Obtained silver nanoparticles was characterized by UV-Visible, PSA, FT-IR, SEM analysis.

Conclusion:

This is novel environmental friendly method that use of external stabilizing to the best our knowledge this is report.

References
[1] O. Okorosaye, K and Jack, I.R. *Amer. J. sci. and ind. Res*. 2012, 390.
[2] Kholoud M. M. et al. Arab. J. Chem. 2009. 3, 135.
[3] Edwards-Jones V. *Lett Appl Microbiol*. 2009. 49(2):147.
[4] Lansdown ABG. Crit Rev Toxico. 2007, 37(3):237.
[5] D. Hebbalalu, J. Lalley, et al., *Sustainable Chem. Eng*. 2012. 703.

Nucleophilic reaction of aliphatic amines on hydroquinolines in different situation for investigation of their pharmaceutical properties

Mohammad Hakimi, Jalil Lari, Elahe sadat Mousavi*, Reza tavakkoli
Payame Noor University of Mashad
E-mail: elahesadatmousavi65@gmail.com

In recent years, more attention has focused on synthesis of 1-Cyclopropyl-7-dimethylamino-6-fluoro-4- oxo-1, 4-dihydro-quinoline-3-carboxylic acid because of their application in pharmaceutical industry, such as Antibacterial, antifungal, antimicrobial and etc. 1-Cyclopropyl-7-dimethylamino-6-fluoro-4-oxo- 1,4-dihydro-quinoline-3-carboxylic acid also can be used as a ligand in synthesis of metal complexes which have specific pharmaceutical properties. In this research we synthesized the 1-Cyclopropyl-7- dimethylamino-6-fluoro-4-oxo-1, 4-dihydro-quinoline-3-carboxylic acid by nucleophilic reactions with amines such as piperazine, N-methyl piperazine, N-ethyl piperazine, diethanolamine and diethylamine. These synthetic works were carried in different protic solvents, ethanol and water, and the results were compared with solvent free condition and investigated their pharmaceutical properties. At the end, synthesized ligands were proved by using CNMR, HNMR, FT-IR, melting point and elemental analysis method.

Introduction:

Ciprofloxacin is a drug belongs to an antibacterial group of pharmaceutical compounds and is a broad antibiotic which includes the all gram positive and negative bacteria. This material has poor adsorption and solubility in an alkali environment. An investigation in Cambridge Structural Databases showed that 82 structures contain Ciprofloxacin which only 17 of these structures belong to multi- component forms of CIP.

Experimental:

In this project for synthesis of our product, we mixed carboxylic acid (0.5g) and diethanol amine (0.5mL) in two solvents a) butanol (1.6mL) b) water (1.2mL) and c) solvent-free condition. Time duration for each condition has been shown below.

Solvent	buthanol	water	Solvent-free
Time (h)	48	60	20

Results and discussion:

In this project we found a new path for synthesis our product which has advantages such as reducing costs and time, increasing yield in an environmentally friendly condition.
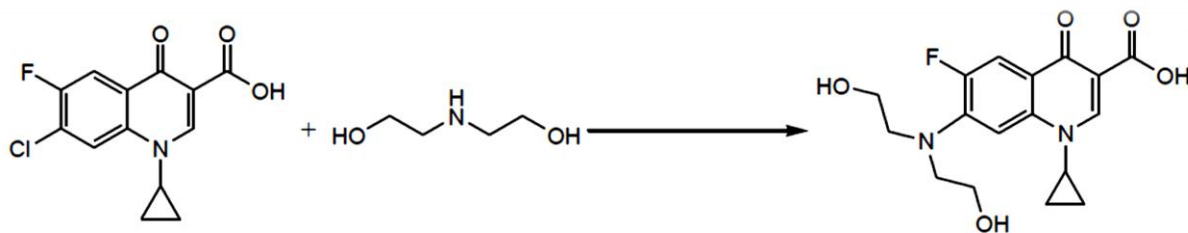
Conclusion:

In summary, we found out the buthanol as the solvent has no significant effect on the yield of reaction and solvent-free condition is more desirable.

References:

[1] Kaminsky, D; Meltzer, R I.*J.Med. Chem* 11, 160, 1968.

[2] Laucr, W M; Kaslow, C E.*Org. Synthesis Coll.* Vol. III, 580, 1955.

[3] Goswami, M; Mangoli, S; Jawali, N. *Int J Antimicrob Agents* 2014;43(4):387-388.

[4] Cheng, G; Hao, H; Dai, M; Liu, Z; Yuan, Z; Eur, *J. Med. Chem* 2013;66:555-562.

[5] Liang-Cai, Yu; Zi-Long Tang; Pin-Gui, Yi, Sheng-Li Liu, Xia Li, *J. Coord Chem* 2008;61(18):2961-67.

[6] Florence, AJ; Kennedy, AR; Shankland, N; Wright, E; Al-Rubayi, A. *Acta Crystallogr Sect C* 2000;56:1372-3.

[7] Turel, I; Bukovec, P; Quiro´s, M. *Int J Pharm* 1997;152:59-65.

[8] Prasanna, MD; Guru Row, TN. *J Mol Struct* 2001;559:255-61.

[9] Wallis, SC; Gahan, LR; Charles, BG; Hambley, TW. *Aust J Chem* 1994;47:799-806.

[10] Turel, I; Gruber, K; Leban, I; Bukovec, N. *J Inorg Biochem* 1996;61:197-212.

[11] El-Subbagh, H I; Abu-Zaid, S M; Mahran, M A; Badria, F A; Al-Obaid, A M. *J. Med. Chem*, 43, 2915, 2000.

[12] Jerom, B R; Spencer, K H; *Eur. Pat. Appl*. EP 277794, 1988.

[13] Kaminsky, D; Meltzer, R I. *J. Med. Chem*. 11, 160, 1968.

[14] Musiol, R; Jampilek, J; Buchta, V; Silva, L; Niedbala, H; Podeszwa, B; Palka A,Majerz-Maniecka, K; Oleksyn, B; Polanski, J; Bioorg. *Med. Chem*. 14, 3592, 2006.

Using Modified Acceptor Phase for Extraction and Preconcentration of Triazine Herbicides from Cucumber Peel by Three Phase Hollow Fiber Liquid Phase Microextraction

Mohammad Mahdi Khataei[a], Yadollah Yamini[a]*, Ali Esrafili[b]

a Department of Chemistry, Tarbiat Modares University, Tehran, Iran

b Department of Environmental Health Engineering, School of Public Health, Iran University of Medical Sciences, Tehran, Iran

***E-mail:** yyamini@modares.ac.ir

****

Introduction:

Hollow fiber liquid-phase microextraction (HF-LPME) offers an efficient alternative to classical techniques for sample preparation and preconcentration [1]. Within the framework of green chemistry, non-toxic, biodegradable, recyclable and low price solvents occupy a strategic place. In this study, two types of quaternary ammounnium salts that are cheap and safe and even one of them was used as animal's food [2] were used for modifying acceptor solvent. This modified solvent was located in the lumen of hollow fiber as acceptor phase in three phase hollow fiber liquid phase microextraction (HF-LPME) for extraction and preconcentration of triazine herbicides from cucumber peel.

Methods/Experimental:

Skin of cucumbers were peeled and dried in freeze dryer for 24 hr. Cucumber peel was grind homogenously and desire amount of standards were added to 250 mg of it with excess amount of methanol for reaching standards to whole of them. After being dried, whole of it was placed in 15 mL centrifuge tube and 3 mL methanol was added to it. Back extraction was performed 4 minutes under ultrasonic probe. Two mL of extraction solvent was poured into donor phase and diluted to 20 mL and 4 g salt was dissolved in it. Organic solvent (*n*-dodecane) was immobilized in the pores of the hollow fiber and acceptor phase (methanol containing quaternary ammonium) was filled within the lumen of hollow fiber.

Results and discussion:

Based on our previous experience *n*-dodecane containing 7.5% TOPO was used as supported liquid membrane. Effects of other parameters such as type of acceptor phase solvent, type and amount of modifier, amount of salt, stirring rate, fiber length and extraction time on the extraction efficiency of the analytes were investigated. In additional, for extraction of triazine herbicides from skin of cucumbers three factors were investigated and optimized. These parameters include: type of extraction solvent and effect of its amount in the donor phase on extraction efficiency of the analytes by HF-LPME method and extraction time of ultrasonic probe were optimized. Under the optimized conditions, preconcentration factors in the range of 301-404 were obtained. The performance of the proposed method was studied in terms of linear

ranges (LRs from 1 to 10 mg kg^{-1}), linearity (R^2 ≥0.999), precision (RSD % ≤5.5) and limits of detection (LODs in the range of 0.2-0.3 mg Kg^{-1}). In addition to preconcentration, HF-LLLME also served as a technique for sample clean-up.

Conclusion:

Triazine herbicides from skin of cucumber was extracted successfully by ultrasonic probe and its clean-up and preconcentration was performed by three phase hollow fiber liquid phase microextraction under optimized condition. Quaternary ammonium salts modified acceptor phase that produced additional interaction with analytes. Results show that this method has good linear range that is capable for determination of triazine herbicides in cucumber peel.

References:

[1] M. Ghambarian, Y. Yamini, A. Esrafili. *Microchim. Acta*, **2012**, 177, 271-294.

[2] Q. Zhang, K.D.O. Vigier, S. Royer, F. Jérôme. *Chem. Soc. Rev.*, **2012**, 41, 7108-7146.

Contradictory Dual effects: water uptake and proton conductivity inducement based on direct or indirect insertion of -SO$_3$H onto imidazole ring

Koorosh Firouz Tadavani[a], **Amir Abdolmaleki** [a,b,*] , **Mohammad Reza Molavian** [a], **Mohammad Zhiani** [a]

[a]*Department of Chemistry, Isfahan University of Technology, Isfahan 84156-83111, I. R. Iran.*

[b]*Department of Chemistry, College of Sciences, Shiraz University, Shiraz 71467-13565, I. R. Iran.*

E-mail address: abdolmaleki@cc.iut.ac.ir, abdolmaleki@shirazu.ac.ir (A. Abdolmaleki)

Introduction

Nowadays, environmental and energy issues such as global warming, fossil fuel resource depletion, etc., have caused the development of alternative energy resources. Fuel cells (FCs) as a clean and safe energy resource is a good candidate to replace fossil fuels. Proton exchange membrane (PEM) is the key component of FCs, that duo to the inefficient Nafion commercial membrane at high temperatures (low conductivity, membrane decomposition, etc.) increase regarding new membranes, particularly heat resistant polymers. Among which PBIs are good candidates for proton exchange membrane as they exist in two tautomeric forms. In fact, a proton transfer pathway can be recognized when a proton moves from imidazolium cation to other imidazole groups [1, 2].

Methods / Experimentals

poly(benzimidazole-imide) (PBII) was obtained from the synthesized diamine and corresponding aromatic dianhydride by a two-step mechanism. In the first stage, poly(amic acid) (PAA) was synthesized by the condensation polymerization and in the second stage, the film was converted to polyimide by exposure to different temperature range. Then, sulfonated side chains were added to PBII by sultone (Indirect insertion of sulfonate group onto imidazolic nitrogen) and ClSO$_3$H (direct insertion of sulfonate group onto imidazolic nitrogen).

Result and discussion

All the monomers and polymers were characterized by FT-IR spectra, ^{1}H-NMR and elemental analysis. The thermal stability of poly(benzimidazole-imide)s (PBIIs) was studied by TGA in the nitrogen atmosphere. X-Ray diffraction analyses of PBIIs show different crystallinity. Proton conductivity and water uptake of the membranes was measured in different

conditions that indirect insertion of sulfonate group onto imidazolic nitrogen of PBII increases water uptake to 160 %. Also the maximum proton conductivity (0.067 S.cm^{-1}) is observed at 80 ˚C and RH 60 % for this membrane (PBII2); however, at temperatures higher than 80 ˚C, proton conductivity of the PBII2 becomes similar to the Nafion (the more temperature, the less proton conductivity). However, when sulfonate group is directly placed on the imidazolic nitrogen by ClSO$_3$H (PBII3), water uptake is reduced to approximately zero percent and shows very poor conductivity at ambient temperature. By increasing temperature, proton conductivity is amplified which at 160 ˚C and RH 30 %, the proton conductivity of the membrane reach to 0.026 S.cm^{-1}. Single cell performance was measured under 120°C and anhydrous conditions for PBII3 and obtained results compared with those for PBII2.

Conclusion

1. Sulfonation by 1,4-butan sultone causes high water uptake and good proton conductivity at low temperatures. Nevertheless, high temperature and reducing proton carrier decrease proton conductivity.

2. Sulfonation thought the chlorosulfonic acid due to direct insertion of –SO$_3$H on the imidazole ring, form an ionic like structure that presence of strong electrostatic interactions prevents to water diffusion. Therefore, at low temperatures, proton conductivity is very poor, but with increasing temperature, proton conductivity incease through the hopping mechanism.

References

[1] W.-Q. Deng; V. Molinero; W.A. Goddard. J. Amer. Chem. Soc, 2004, 126, 15644-15645.

[2] S. Bureekaew; S. Horike; M. Higuchi; M. Mizuno; T. Kawamura; D. Tanaka; N. Yanai, S. Kitagawa. Nature Mater, 2009, 8, 831-836.

Modified natural biomembrane for mucoadhesive drug delivery

Hamidreza Gharibi[a], **Amir Abdolmaleki** [a,b,*]

[a]*Department of Chemistry, Isfahan University of Technology, Isfahan 84156-83111, I. R. Iran.*

[b]*Department of Chemistry, College of Sciences, Shiraz University, Shiraz 71467-135065, I. R. Iran.*

E-mail address: abdolmaleki@cc.iut.ac.ir, abdolmaleki@shirazu.ac.ir (A. Abdolmaleki)

Introduction: Many authors have investigated polymers with various molecular characteristics essential for mucoadhesion. The presences of polar chemical functional groups increase their interaction with the mucin glycoproteins and favors' adhesion. At present, the most widely conducted group of mucoadhesives are anionic, cationic and thiolated polymers [1].

Additionally the use of synthetic polymers may have cytotoxic effects and economically unfavorable. Clearly, the development of natural biomembrane such as Eggshell membranes (ESM) that can be used as mucoadhesives is of significant importance and no attempts have been reported to modification of natural biomembrane as mucoadhesive drug delivery systems. Herein, citric acid (CA) functionalized biomembrane using ESM as a model (ESM-CA) has been synthesized for the first time.

Methods/Experimantals: The ESM–CA was made by thermo-chemical modification. The ESM contains amines, hydroxyls, amides, carboxylic and other hydrophilic surface functional groups which anchoring the CA molecules to the membrane fiber surface by hydrogen bond linkage where modification can occur. As the temperature was increased, the adjacent carboxylic acid groups on CA dehydrated to yield a cyclic anhydride, and consequently citric anhydrides could react with free amine and hydroxyl groups in the ESM to form amide and ester linkages and the chains were gradually cross-linked by CA.

Results and discussion: FTIR spectroscopy and CHN analysis demonstrating the successful reaction of ESM with CA. Also, successful modification of the ESM also was observed by the change in thermogravimetric analysis.
SEM micrographs of neat ESM and ESM-CA give further insight into ESM morphology and its modification. The ESM-CA displayed dense and orderly shapes.

Tensile strength values for ESM-CA indicate superior ESM-CA mechanical strength.

Have proved that the ESM-CA can induce enhanced mucoadhesion, owing to the presence of large amounts of functional groups ($-OH$, $-CO_2H$, $-NH_2$, $-CHO$, $-SO_4H$, $-SH$, $-S-S-$) [2].

The indomethacin release decreases for ESM-CA treated at pH 2 compared to pH 7 and pH 10. Definitely, carboxylic acid groups on the ESM-CA matrix transformed into negatively-charged carboxylate groups as the samples were immersed in pH 7 medium with loss of a proton [3,4]. The formed carboxylate groups repelled each other within the matrix and the cross-linked network began to expand, conducive to a fast rate of drug permeation. As the pH value reached higher than 10, the charge-screening effect was caused, and also the ester and amide groups were hydrolyzed seriously, which weakened the water absorption and because of the deterioration of 3D structure and salt bridges within the ESM drug release enhanced abruptly.

Kinetics of release from the ESM-CA showed different release mechanism in different environments.

Conclusion: In this study, we developed a mucoadhesive network made from ESM-CA. ESM-CA network is denser than neat ESM, thus allowing for a slower degradation and drug release. Although the mechanical properties of ESM-CA networks are comparable to those of ESM. We envision that these networks could be successfully used as mucoadhesive drug delivery system for other applications, including for example gastrointestinal tract targeting for the treatment of diseases such as ulcerative colitis.

Reference

[1] J. D. Smart. *The basics and underlying mechanisms of mucoadhesion*, Advanced Drug Delivery Reviews, 2005, 57, 1556– 1568.

[2] T.N. Nakano and L. Ozimek. *Chemical composition of chicken eggshell and shell membranes.* Poultry Science, **2003**, 82(3), 510-514.

[3] A. Verma and J. K. Pandit, Trop. *Rifabutin-loaded floating gellan gum beads: effect of calcium and polymer concentration on incorporation efficiency and drug release.* J. Pharm. Res., 2011, 10, 61–67.

[4] X. Huang and C. S. Brazel. *On the importance and mechanisms of burst release in matrix-controlled drug delivery systems.* J. Controlled Release, 2001, 73, 121–136.

Synthesis of new derivatives 1,2,3- Triazoles using copper catalyst

Ahmad Kakavand Ghalenoei[*], Mohammad Bakherad, Ali Keivanloo

School of Chemistry, Shahrood University of Technology, Shahrood, I. R. IRAN

Corresponding Author E-mail: Kakavand.ahmad@yahoo.com

1. Introduction

1,2,3-Triazole finds use in research as a building block for more complex chemical compounds, including pharmaceutical drugs such as antibacterial, antifungal, antiviral, anticancer, antimicrobial, antidepressant, anticonvulsant, central nervous system modulators, and anti-inflammatory [1]. Several methods have been reported for the synthesis of 1,2,3-triazoles. The conventional method of synthesizing 1,2,3-triazoles is by addition of organoazides to alkynes [2]. The well-appointed procedure applied thus far for the synthesis of the [1,2,3]-triazole system based on the thermal 1,3-dipolar Huisgen cycloaddition of organic azides with alkynes [3].

Recently, some methods to outreach the above drawbacks have been reported through the one pot, three-component reaction in the presence of catalysts such as Cu_2O [4], $CuSO_4$ [5] and Cu/SiO_2 [6].

2. Experimental

2.1. *Preparation of propargyl amine*

A mixture of calcium carbide (1.2 mmol), aldehyde (1.0 mmol), amine (1.5 mmol), and CuI (0.1 mmol) were added to a 5 mL round-bottom flask containing CH_3CN (2 mL).After the mixture was stirred for 8 hours at 70 °C, propargyl amines were obtained as determined by ^{1}H NMR spectroscopy.

2.2. *Preparation of 1,2,3- triazoles in the presence of copper catalyst*

In a typical procedure, a mixture of propargyl amine, aryl azids, $Cu(AOC)_2$ and NaAs was stirred for 4 hours at 70 °C (TLC). The mixture was then extracted with ethyl acetate (3×10 mL). The combined organic phases are washed with brine (2×5 mL), dried overe Na_2SO_4, and concentrated under vacuum to give the crude product. The residue was subjected to flash column chromatography with hexane/EtOAc (6/1) as eluent to obtain the desired product.

3. Results and discussion

We decided to attempt reactions with copper (II) in different solvents such as ethanol, DMSO, water and acetonitrile using $Cu(OAc)_2$ (10 mol%) and NaAs (20 mol%) at 80 °C. The reaction was incomplete when attempted in ethanol even after 8 h with 60% yield of desired product. Reactions using DMSO, water and methanol as solvent required longer reaction times and gave inferior yields compared to acetonitrile. The reaction of propargyl amines and aryl azids in acetonitrile was then attempted at lower temperature and also with lower catalyst loading. The reactions at lower temperature (60 °C) and with lower catalyst loading (5 mol%) resulted in increase in reaction time and decrease in product yield. Moreover, No product was obtained in absence of catalyst. Thus, the optimized reaction conditions for this reaction are the $Cu(OAC)_2$ (10 mol%) in CH_3CN using NaAs (20 mol%) as base at 80 °C.
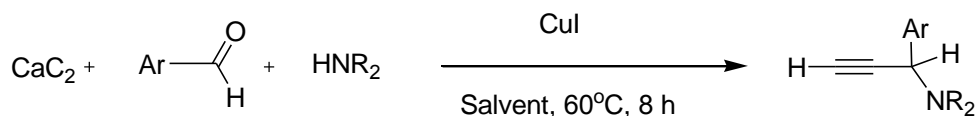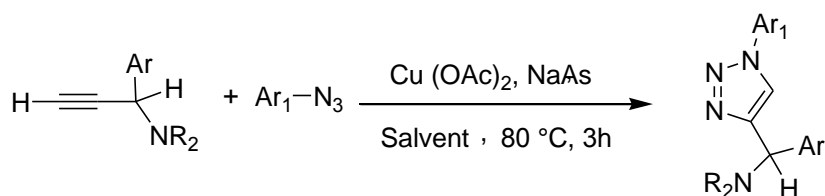
Ar: C_6H_4 , 4-Br-C_6H_4 , 4-Me-C_6H_4

Ar$_1$: 4-Me-C_6H_4 , 4-NO_2-C_6H_4, 4-Cl-C_6H_4

NR_2:
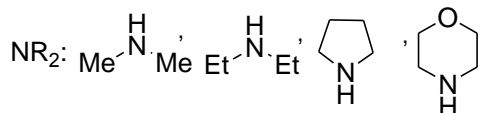
4.Conclusion

we have reported a practical and general method for the synthesis of 1,2,3- triazoles through a cross-coupling/click reaction sequence. This approach uses simple and readily available starting materials and shows good functional compatibility. The procedure can be successfully performed without isolation and purification of any compounds during the process. These features make this protocol potentially attractive for the synthesis of 1,4-disubstitued 1,2,3-triazoles through the 1,3-dipolar cycloaddition of propargyl amines and aryl azids in the presence of hemogeneous catalyst supports.

References:

[1] (a) Abdo, N. Y. M.; Kamel, M. M. *Chem. Pharm. Bull*. **2015**, *63*, 369. (b) Tang, R.; Jin, L.; Mou, C.; Yin, J.; Bai, S.; Hu, D.; Wu, J.; Yang, S.; Song, B. *Chem. Cen. J*. **2013**, *7*, 30.

[2] M. Meldal, C.W. Tornøe, *Chem. Rev*. **2008**, *108*, 2952.

[3] Karlsson, S.; Hogberg, H. E. *Org. Prep. Proced. Int.* **2001**, *33*, 103–172

[4] F. Alonso, Y. Moglie, G. Radivoy, M. Yus, *Synlett* **2012**, 2179.

[5] N. Mukherjee, S. Ahammed, S. Bhadra, B. C. Ranu, *Green Chem.* **2013**, *15*, 389.

[6] P. Veerakumar, M. Velayudham, K.L. Lub, S. Rajagopal, *Catal. Sci. Technol*. **2011**, *1*, 1512.

DFT Study of The Complexation of Nicotinic Acid with Poly(Amidoamine)-G1 Dendrimers

Farideh Badalkhani-Khamseh[a],*, Nasser L. Hadipour[a]

[a] *Tarbiat Modares University, Tehran, Iran*

Introduction

In the pharmaceutical area, the key factors upon which the medical success of any drug is based are efficiency, toxicity, solubility, and bioavailability. Based on recent studies, about 40% of newly developed active pharmaceutical ingredients are not exploitable by the pharmaceutical industry because of low water solubility and, thus, bioavailability [1]. Therefore, the development of molecular-level drug carriers, which enhance water solubility of the drug while maintaining essential pharmacophoric features, has been of particular interest. Given the aforementioned challenges and opportunities, DFT computations have been applied to inspect the specifics of the encapsulation behavior of niacin to NH_2-terminated PAMAM-G1 dendrimers.

Methods

All geometry optimizations and energy calculations were performed based on M06-2X/6-31G(d) level of theory as implemented in GAMESS software package. We used the following definition as the enthalpy change under encapsulation of NA into PAMAM-G1 at $T = 298$ K and $P = 1$ atm

$$\Delta H = \left[(H + ZPE)_{complex}\right] - \left[(H + ZPE)_{G1}\right] - \left[(H + ZPE)_{NA}\right] \qquad (1)$$

Implicit solvent effects were addressed through polarizable continuum model (PCM) considering the dielectric constant of water. NMR and NBO analyses were performed at the M06-2X/6-311+G(d) // 6-311++G(d,p) levels of theory, respectively.

Results and discussion

The predicted energetic data for the most stable configuration deliver preliminary information about relatively strong interactions between G1 and NA. According to table 2,

1

HOMO-LUMO energy gap indicates that the electronic properties of G1 dendrimer are sensitive to NA molecule.

The calculated geometrical parameters, NMR, and NBO calculations for NA molecule, G1 dendrimer and G1@NA complex in gas and solvent phase propose

1) An intermolecular hydrogen bond formation between carbonyl oxygen of surface group of G1 dendrimer and hydroxyl group of drug molecule.
2) A relatively weak hydrogen bonding is formed between oxygen of carbonyl group of NA and amide group of G1 dendrimer.
3) An intermolecular hydrogen bonding between amine groups at the peripheral monomers and the nitrogen of NA molecule.

Table 1. Calculated energetic data (kcal mol^{-1}), minimum and maximum modes of vibrational frequencies (cm^{-1}) for G1@NA complex.

G1@NA	ΔH	ΔG	$E_{binding}$	v_{min}	v_{max}
Gas	-33.18	-13.99	-32.32	2.93	3677.75
Solvent	-25.62	-6.08	-24.95	4.90	3664.92

Table 2. Calculated HOMO and LUMO energies E_g for G1 dendrimer and G1@NA (eV)

Configuration		E_{HOMO}	E_{LUMO}	E_g	ΔE_g (%)
G1	Gas	-7.43	1.52	8.95	___
G1@NA		-7.42	-0.82	6.60	26.26
G1	Solvent	-7.54	1.82	9.36	___
G1@NA		-7.56	-0.77	6.79	27.46

Conclusion

We investigated the encapsulation of niacin into PAMAM G1 dendrimers using DFT method. The geometrical parameters of optimized structures, NMR, and NBO calculations showed that the intermolecular hydrogen bonding formed between NA and functional groups of dendrimer are responsible for the encapsulation process.

References

(1) Svenson, S.; Chauhan, A. S. *Nanomedicine.* **2008**, 3, 679-702.

Biosorption of nickel Ion by Biomass of Silybum marianum

F. Nazeri[a], A. A. Amiri[a,*]

[a] Department of applied Chemistry, Shiraz Branch, Islamic Azad University, Shiraz, Iran

[*]amiri1355@gmail.com

Introduction: Heavy metals have been a major preoccupation for many years because of their toxicity towards aquatic life, human beings and the environment[1]. A number of technologies such as adsorption, precipitation, solvent extraction, ion exchange have been developed for the removal of metal ions[2]. Adsorption is now recognized as an effective and economic method for heavy metal wastewater treatment. The adsorption process offers flexibility in design and operation and in many cases will produce high-quality treated effluent[3]. Biosorption of heavy metals from solutions is a new process that has been confirmed a promising process in the removal of heavy metal [3].

Experimental: In this project, Silybum marianum biomass (mass index) has been used for the removal of nickel as heavy metal. The effect of pH, amount of the absorbent, ion concentration and the time of exposure are the parameters that have been evaluated.

Result and Discussion: In this project the most appropriate pH level reported for Nickel was 3. The best time of exposure that has been achieved in this biomass is 60 minutes and it has been observed that after increasing the amount of absorbent to its optimum amount, 2 grams, the amount of adsorption remained unchanged. As ion concentration, the percentage of ion removal has reduced while the amount of ion in the solution increased. Furthermore, Langmuir adsorption model was determined as the best adsorption isotherm for the element. When increasing pH above 6 while adjusting it, metal ions deposit (precipitate). Hydrolysis and precipitation of metal ions by changing its concentration and the shape of absorbable metallic species that are available for absorption, influence the process of absorption.

Consistency in the absorption efficiency in higher grams than the optimal amount can be explained as a result of minor accumulation absorbent, leading to the reduction (decrease) of effective surface area to absorb the metal ions. Because the absorbent level is fixed and does not change, so by the increase of concentration of absorption

sites ions in the biomass, it has less ability to absorb and therefore the elimination percentage is reduced.

Conclusion: According to the results, Silybum marianum biomass can be used as an appropriate biomass with a quick and high level of adsorption of Nickel ions in aqueous solutions. Nickel adsorption in the Silybum marianum biomass is a chemical adsorption. The best isotherm for Nickle was Langmuir. Two factor, pH of samples and the amount of biosorbents have the greatest effect on the efficiency of extraction.

References:

[1] Chiron, N., Guilet, R., & Deydier, E. (2003). Adsorption of Cu (II) and Pb (II) onto a grafted silica: isotherms and kinetic models. Water Research, 37(13), 3079-3086.

[2] Eloussaief, M., Benzina, M., 2010. Efficiency of natural and acid-activated clays in the removal of Pb(II) from aqueous solutions. J. Hazard. Mater. 178, 753e757.

[3] Fu, F., & Wang, Q. (2011). Removal of heavy metal ions from wastewaters: a review. Journal of environmental management, 92(3), 407-418.

Introduction of 2-aminoethanesulfonic acid as a Mild and Efficient Green Bio-organic Catalyst for the Knoevenagel Reaction in Green Media

Farhad Shirini,[a,b]* Nader Daneshvar[b]

[a]Department of Chemistry, College of Sciences, University of Guilan, 41335, Rasht,Iran. Tel: +981313233262
*[b] Department of Chemistry, College of Sciences, University of Guilan, university campus 2*
E-mail: shirini@guilan.ac.ir

Intorduction: The Knoevenagel reaction, treatment of an aldehyde with a compound containing an active methylene group which was reported by Emil Knoevenagel in 1894, is one of the most important and noticeable reactions for C=C bond formation [1]. This reaction is suitable for the preparation of alkenes with electron-withdrawing groups and its products can be used as intermediates for many other types of reactions [2].

2-Aminoethane sulfonic acid (Taurine) is an amino acid that is found in high concentration in the tissues of animals [3]. It is being used for many years as ingredient of energy drinks, nutrient, supplement and has many biological properties such as osmoregulation, immunomodulation and bile salt formation [4].

Methods / Experimentals: In a 25 mL round-bottomed flask a mixture of aldehyde (1.0 mmol) malononitrile (1.1 mmol) and taurine (0.025 g, 20 mol%) in water (2 mL) was heated at reflux temperature for the appropriated time. After the compilation, 10 mL of water was added and stirred for 3 minutes. Then the product was precipitated and separated by filtration. The separated product was washed several times with water. After drying, the pure product was obtained (scheme 1).
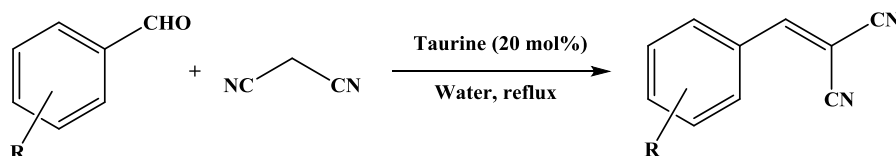
Scheme1. Knoevenagel reaction catalyzed by taurine

Results and Discussion: After the optimization of the conditions and amount of the catalyst, a series of aromatic aldehydes containing either-electron-donating or electron-withdrawing substituents successfully reacted in 6-19 minute and produced the products in 86-98% yield under the selected conditions. The nature and electronic properties of the substituents had no obvious effect on the rate and yield of the reaction. Meanwhile the catalyst showed excellent reusability for this reaction.

Conclusion: In this work, we have introduced an amino acid (taurine) as a green organo catalyst for the efficient synthesis arylidene malononitrile compounds with good to excellent yields during short reaction times in green media and also the reusability of the catalyst was excellent.

References:

[1] L. F. Tietze, U. Beifuss. *Comprehensive Organic Synthesis,* Oxford, uk, **1991**, ch 1, pp 341-394.

[2] F. Freeman. *Chem. Rev.,* **1969**, *69*, 591-624.

[3] R. J. Huxtable. *Physiol. Rev.*, **1992**, *72*, 101-163.

[4] (a) G. P. Salz, D. A. Davis. *Aquaculture*, **2015**, *437*, 215-229; (b) J. M. Menzie, C. Pan, H. Prentice, J. Y. Wu. *amino acids*, **2014**, *46*, 31-46.

Synthesis of 1,8-dioxo-octahydroxanthenes in presence of titanium dioxide-coated carbon nano tube

Bita Baghernejad[a]*, Fatemeh nohi [a]

Department of Chemistry, School of Sciences, Payame Noor University (PNU), Iran

Email: bitabaghernejad@yahoo.com

Introduction: Xanthene derivatives are very important heterocyclic compounds and have been widely used as dyes fluorescent materials for visualization of bio-molecules and laser technologies due to their useful spectroscopic properties [1]. They have also been reported for their agricultural bactericide activity [2], photodynamic therapy [3], antiflammatory effect and antiviral activity [4].

In our continued interest in the development of highly expedient methods for the synthesis of heterocyclic compounds and in continuation of our investigation on the use of water as solvent for chemical preparation, we report here a facile and improved protocol for preparation of xanthene derivatives, from benzaldehydes, dimedon and titanium dioxide-coated carbon nano tube as a catalyst in ethanol at ambient conditions (Scheme 1).
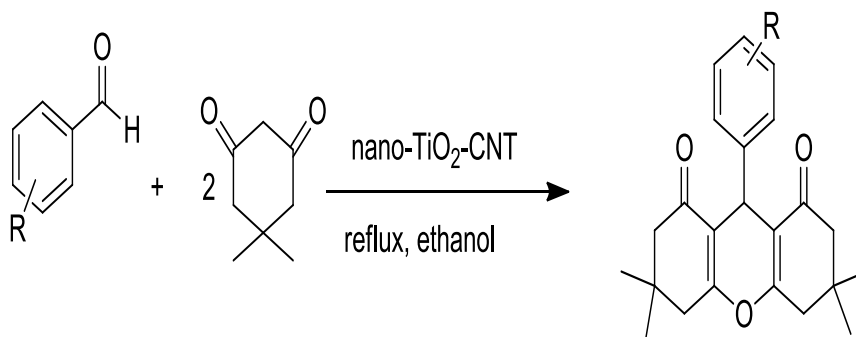
Scheme 1

Experimentals: A mixture of an aromatic aldehyde (1 mmol), dimedone (2 mmol) and titanium dioxide-coated carbon nano tube (5 mol%) in Ethanol (5 mL) was refluxed. The progress of the reaction was monitored by TLC. After completion of the reaction, the mixture was cooled and filtered off. The pure product was obtained by recrystallization from ethanol.

Result and discussion: In order to show the general applicability of the method, the reaction of structurally diverse aldehydes with dimedone under similar conditions was investigated. By this method, the reactions were carried out easily and very cleanly in the presence of titanium dioxide-coated carbon nano tube to produce xanthene derivatives in good to excellent yields and no undesirable by-products are observed. This protocol offers advantages in terms of its simple procedure and work-up and excellent yields. The experimental procedure is very simple, convenient, and has the ability to tolerate a variety of other functional groups such as methyl, methoxy, nitro, hydroxyl, halide under the reaction conditions. It was indicated that both electron rich and electron deficient aldehydes worked well, mostly leading to high yields of products.

Conclusion: Some advantages of this procedure are: 1) the experimental simplicity and the easy work-up procedure, 2) the compatibility with various functional groups, 3) use of the green, easy to handle and reusable catalyst, and 4) high yields of the products. The procedure is very simple and can be used as an alternative to the existing procedures.

References

[1] A. Banerjee; A.K. Mukherjee. *Stain Technol*. **1981,** 56, 83-85.

[2] J.P. Poupelin ; G. Saint-Ruf ; O. Foussard-Blanpin ; G. Narcisse ; G. Uchida-Ernouf; R. Lacroix. *Eur. J. Med. Chem*. **1978**, 13, 67-71.

[3] G. Saint-Ruf; A. De; H.T. Hieu. *Bull. Chim. Ther*. **1972**, 7, 83–86.

[4] C.G. Knight;T. Stephens. *Biochem. J*. **1989**, 258, 683–689.

Synthesis and characterization of anionic polyurethane dispersion nano hybrid with nano Sio2

*Tayebe Shirkavand[1], Behzad Shirkavand Hadavand[2]

1Department of Organic Chemistry, Payam-e-NoorUniversity,Tehran,Iran,P.O.Box:19395-4697, t.sh2011@yahoo.com
 2 Department of Organic Chemistry, Institute for Color Science and Technology, Tehran, Iran, P.O.Box:16765-654, shirkavand@icrc.ac.ir
Email address:t.sh2011@yahoo.com
****

Introduction: Polyurethane dispersions are high solids dispersions of polyurethane polymers in water. They provide the performance of polyurethane and the convenience of waterborne latex. Polyurethane polymers have traditionally exhibited high toughness and versatility in coating, adhesive, sealant and elastomer applications [1-3].
Waterborne dispersion technology allows ease of formulation, application and cleanup as well as environmental advantages such as the elimination of monomers, odor and production of volatile organic compounds (VOC). Since the polyurethane reactive chemistry is performed at Dow, the user does not have to work with reactive materials; in addition, this product has no residual (i.e., free) isocyanate. Polyurethane dispersions allow the many advantages of polyurethane polymers to be brought to many applications, without these conventional handling concerns. However, formulating skill is required to obtain optimum properties from polyurethane dispersions. This formulating guide is designed to help a formulator get started using polyurethane dispersions, and successfully deliver high-performance products that are environmentally and user friendly [4, 5]

Methods/Exprimentals: In this study, the of anionic waterborne polyurethane hybrid nano-SiO_2 was synthesized by isophoren diisocyanate (IPDI), 1, 6- hexandiol (HD), triethoxysilyl propylamine (APTMS), dibutyltin dilaurate (organometallic catalysts), triethylamine in acetone solvent in foure steps. In the first step the anionic polyurethane with NCO end group was synthesized at 45 °C for two hours. In the second step triethoxysilyl propylamine was added and the reaction was continiued at the same condition for two hours. In the thirth step triethylamine was added for neutralizing. In the last step the solvent was evaporated and the synthesized resin was dispersed in water. Prepared resin was characterized by FT-IR spectroscopy; calorimetry (DSC and TGA) and the size if particles were identified by particle size analyzer. The morphology of the polymer and hybrid nanoparticles was studied by scanning electron microscopy.
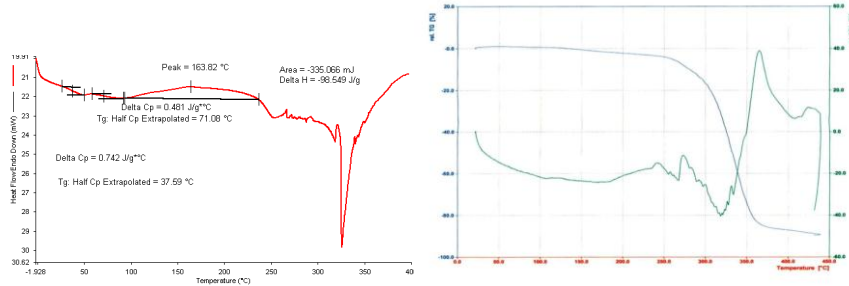
Results and disucssion:
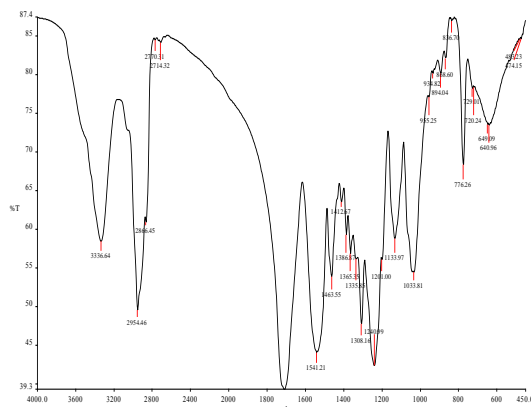
FTIR spectra of anionic waterborne polyurethane hybrid nano-SiO_2.
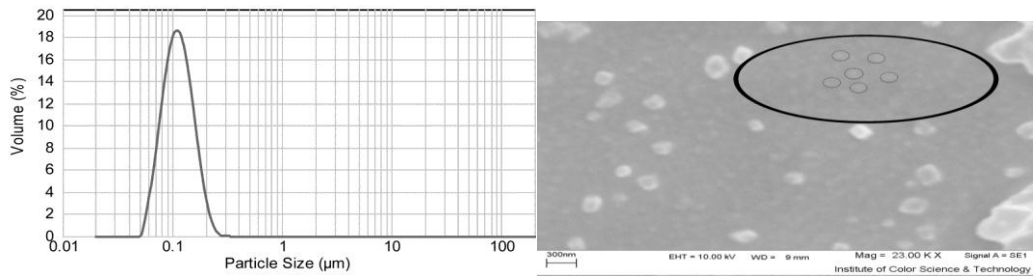
Particle size diagram (a) and SEM (b) image of anionic waterborne polyurethane hybrid nano-SiO$_2$.

DSC (a) and TGA (b) thermograms of anionic waterborne polyurethane hybrid nano-SiO2.

Conclusion: Infrared spectroscopicresults corroborant the thynthesis of nano structured hybrid.The confirming particle size test in equality of size and scanning electronic microscope was representative of spheral structure and adaptable scattering in producedcoverage.Also the result of thermometry test shows thermal constancy of nano hybrid for consumption.

References

[1] M.M. Rahman, W.K. Lee, Properties of isocyanate-reactive waterborne polyurethane adhesives: Effect of cure reaction with various polyol and chain extender content, J Appl Polym Sci, 114 (2009) 3767-3773.

[2] M.M. Rahman, H.D. Kim, W.K. Lee, Properties of waterborne polyurethane adhesives: effect of chain extender and polyol content, J Adhes Sci Technol, 23 (2009) 177-193.

[3] M.S. Yen, P.Y. Tsai, P.D. Hong, The solution properties and membrane properties of polydimethylsiloxane waterborne polyurethane blended with the waterborne polyurethanes of various kinds of soft segments, Colloids Surf. A: Physicochem. Eng. Aspects, 279 (2006) 1-9.

[4] H. Du, Y. Zhao, Q. Li, J. Wang, M. Kang, X. Wang, H. Xiang, Synthesis and characterization of waterborne polyurethane adhesive from MDI and HDI, J Appl Polym Sci, 110 (2008) 1396-1402.

[5] S.A. Madbouly, Y. Xia, M.R. Kessler, Rheological behavior of environmentally friendly castor oil-based waterborne polyurethane dispersions, Macromolecules, (2013) 4606-4616.

Removal of Cadmium ions from synthetic wastewater by micellar-enhanced ultrafiltration using SDS

Atieh Hasani[a], Masod Nasiri Zarandi[b*]

mnasiri@semnan.ac.ir

****

Introduction: Micellar-enhanced ultrafiltration (MEUF) is a new technology developed for treating the wastewater containing metal ions [1]. In MEUF, surfactants are added to wastewater at levels equal to or higher than their critical micelle concentrations (CMCs) and surfactant monomers will aggregate to form micelles, then the micelles are able bind ions on the surface of the opposite charged micelle via electrostatic interactions [2] which aims to promote the removal of metal ions or organic matters. In this study, MEUF is proposed to be a viable technique to remove cadmium ions from synthetic wastewater.

Methods / Experimentals: Fig. 1 illustrates the experimental setup. MODDE 7.0.0 software was used for the design of experiments and data analysis. The experimental design was a full Response Surface design complemented to a central composite design (CCD). The factors and the levels studied are summarized in Table 1.
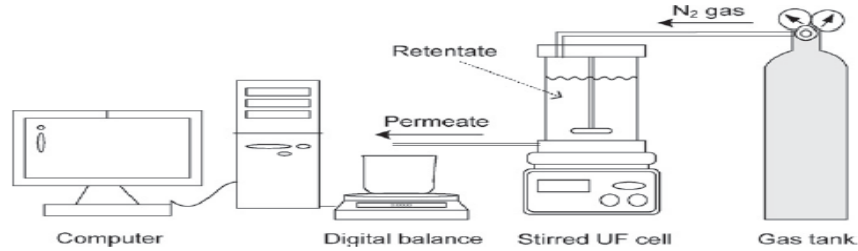

Fig.1. Schematic diagram of the experimental setup of dead-end UF process.

All the experiments were conducted at temperature 25 ± 2 °C and difference pressure at 3bar which was controlled by nitrogen gas. The stirring speed was 400rpm. The ultrafiltration membrane used was a polyether sulfone flat membrane. The average rejection of Cd(II) was obtained as follows:

$$\text{Observed retention(\%)} = \left(1 - \left(\frac{C_p}{C_f}\right)\right) \times 100 \qquad \text{(Eq.1)}$$

Table 1
coded and actual levels of the factors studied at RSM part of the study.

Factors	Level		
	Start points (-1)	Center (0)	Start points (+1)
Cd(II) concentration (ppm)	100	200	300
SDS concentration (mM)	16.724	25.086	33.448

Results and Discussion: The empirical model is a quadratic model which is fitted to the experimental data (Eq. 2).

$$(\text{observed retention percent})^3 = 6.172 \times 10^5 - 75630.55X_1 - 79658.30 \times 10^5 X_2 + 11.1890 \times 10^6 \ X_1^2$$

$$(\text{Eq2.})$$

Where X_1 is Cd(II) concentration in feed and X_2 is SDS feed concentration. The model is significant. The response variation percentage explained by the model (R^2) is 0.747 and R^2_{adj} is 0.6204 which are required for a good model. In addition, Fig. 2 shows the actual vs. predicted values of the response. These results are satisfactory and demonstrate a good model validity.
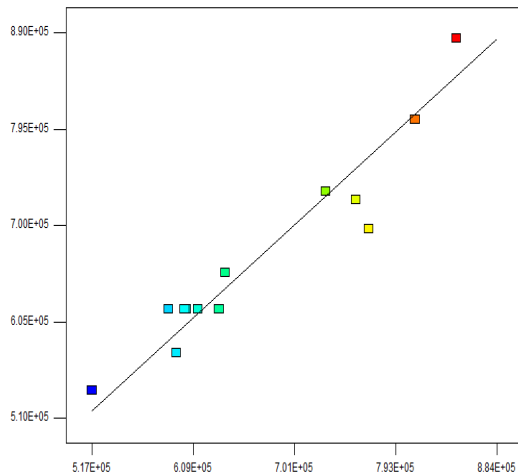

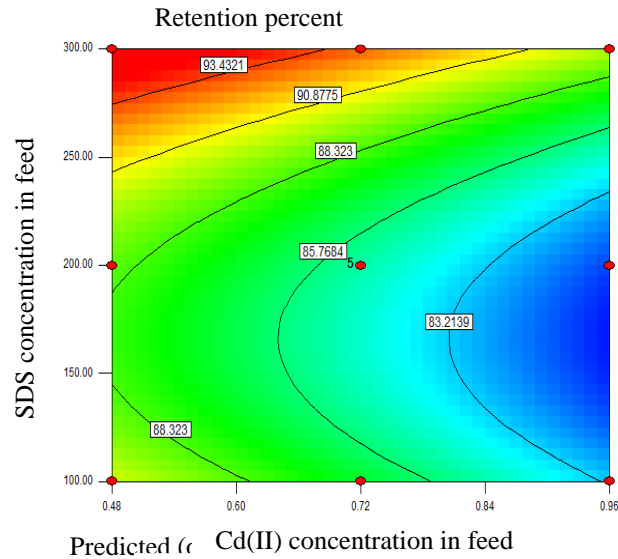Fig. 2. Actual vs. predicted values of the response.

Fig. 3. Contour form of response surface.

As it can be observed in Fig. 3 at low concentration of SDS the removal of Cd(II) is better than when the concentration of SDS is high. This can be due to the concentration polarisation. The concentration polarisation phenomenon is caused by the build-up of surfactant and other molecules on the membrane surface. The SDS feed concentration affected negatively on the heavy metal rejections.

Conclusions: Micellar-enhanced ultrafiltration of Cd(II) from a synthetic wastewater has been studied at 25 °C and 3 bar with the anionic surfactant SDS. Removal of 300 ppm of Cd(II) higher than 90% could be achieved at 16.724 millimolar of SDS. It was shown that the SDS concentration played a crucial role in metal rejection.

References

[1] Huang J, Liu L, Zeng G, Li X, Peng L, Li F, Jiang Y, Zhao Y, Huang X. Influence of feed concentration and transmembrane pressure on membrane fouling and effect of hydraulic flushing on the performance of ultrafiltration. Desalination, 2014, 335(1):1-8.

[2] Fang YY, Zeng GM, Huang JH, Liu JX, Xu XM, Xu K, Qu YH. Micellar-enhanced ultrafiltration of cadmium ions with anionic–nonionic surfactants. Journal of membrane science, 2008, 320(1):514-519.

Biosorption of cadmium ion by Biomass of Ginger

Zahra rashidi[a], A. A. Amiri[a,*]

[a] *Department of applied Chemistry, Shiraz Branch, Islamic Azad University, Shiraz, Iran*

[*]amiri1355@gmail.com

Introduction: Today Environmental pollution is one of the important issues that different communities face. Human being in his daily and industrial activities inter large amounts of industrial pollutants into the environment[1]. Various heavy metals are of the environmental pollutants and due to toxicity and accumulation features are in attention for the health aspects.Today the use of bio sorbents for the treatment of materials is highly regarded due to economic and environmental sustainability. The aim of this study is to evaluate the rate of heavy metal chromium absorption by the biomass ginger[2].

Experimental: In this study, which is conducted in laboratory scale, first, the ginger powder was prepared in several stages. Then cadmium removal efficiency was determined by varying factors under different conditions including pH, contact time, initial concentration of ion and adsorbent dosage. The Langmuir and Freundlich isotherms were evaluated.

Result and Discussion: In this project the most appropriate pH reported for cadmium was 4. The best time of exposure that has been achieved in this biomass is 60 minutes and it has been observed that after increasing the amount of absorbent to its optimum amount, 2 grams, the amount of absorption remained unchanged. As ion concentration, the percentange of ion removal has reduced while the amount of ion in the solution increased. When increasing pH above 4 while adjusting it, metal ions deposit (precipitate). the maximum amount of biomass removed, initial concentration of 20 ppm. Hydrolysis and precipitation of metal ions by changing its concentration and the shape of absorbable metallic species that are available for absorption, influence the process of adsorption. Consistency in the adsorption efficiency in higher grams than the optimal amount can be explained as a result of minor accumulation absorbent, leading to the reduction (decrease) of effective surface area to absorb the metal ions. Because the absorbent level is fixed and does not change, so by the increase of concentration of adsorption sites ions in the biomass, it has less ability to absorb and therefore the elimination percentage is reduced.

Conclusion: According to the results, ginger biomass can be used as an appropriate absorbent with a quick and high level of adsorption of cadmium ions in aqueous solutions.

cadmium adsorption in the ginger biomass is a chemical adsorption. The best cadmium adsorption isotherm was determined for Freundlich model.

Sample solution pH and the amount of bio sorbents are two factors which have the greatest effect on the efficiency of extraction.

References:

[1]Chong, A. M. Y.; Wong, Y. S.; Tam, N. F. Y., 2000. Performance of different microlgal species in removing nickel and zinc from industril wastewater , Chemosphere, Vol. 41, pp. 251-257.

[2] Chojnacka, K. 2011, Biosorption and bioaccumulation-the prospects for practical applications. Environment intemational. 36(3): 299-307

Efficient Synthesis of New Pyrrolo[2,3-b]quinoxalines through Palladium-Catalyzed coupling Reaction/ Heteroannulation Process

Tayebeh Besharati-seidani[a], <u>Ali Keivanloo</u>[a]*, Babak Kaboudin[b]

[a] *School of Chemistry, Shahrood University of Technology, shahrood, 36199-95161, Iran Fax: +98-233-2395441 E-mail: keivanloo@shahroodut.ac.ir , t.besharati@yahoo.com*

[b] *Department of Chemistry, Institute for Advanced Studies in Basic Sciences, Gava Zang, Zanjan 45137-66731, Iran, Fax: +98-241-4214949, E-mail: kaboudin@iasbs.ac.ir*

Introduction:

The Pd-catalyzed Heck reaction is one of the most powerful methods for the arylation and vinylation of alkenes [1]. Chalcones are an important class of biologically active compounds, which have been reported to exhibit a wide range of pharmacological properties, including anticancer, anti-inflammatory, antioxidant, antimicrobial, and antiallergic activity. Compounds belonging to this structural class are also recognized as important intermediates for the synthesis of heterocyclic systems and functional materials [2].

Methods / Experimentals:

For the synthesis of 1,2,3-trisubstituted pyrrolo[2,3-b]quinoxalines we used, 3-chloroquinoxalin-2-amines and chalcones as the starting materials. Reaction of 2,3-dichloroquinoxaline with primary alkyl amines in ethanol produced 3-chlorolquinoxalin-2-amines in good-to-high yields. Chalcones were prepared from aldehydes and ketones via Claisen-Schmidt condensation.

Results and Discussion:

In this work we developed a reaction pathway for the synthesis of new pyrrolo[2,3-b]quinoxalines via palladium catalysed coupling Heck reaction followed by heterocyclization process. Reaction of 3-chloroquinoxalin-2-amines and chalcones in presence of 5 mol% $PdCl_2$, 10 mol% PPh_3, 3 eq K_2CO_3 in DMF (3 mL) at 80 °C under inert atmosphere led to desired product with good yields. All new synthesized compounds were characterized by spectroscopic data and screened for their invitro-antibacterial activities against Gram-positive and Gram-negative bacteria using a well-diffusion method.
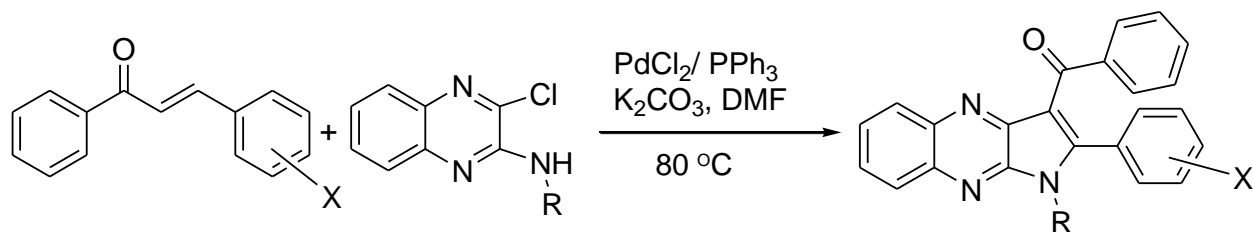
Conclusion:

In summary, we have developed a palladium-catalyzed Heck reaction/annulation process for the construction of a variety of novel 1,2,3-trisubstituted pyrrolo[2,3-b]quinoxalines from 3-

chloroquinoxalin-2-amines and chalcones. Further investigations into the mechanism and regioselectivity are undergoing in our laboratory.

References

[1] R. F. Heck. *Accounts of Chemical Research*, **1979**, 12, 146-151.

[2] T. Guo, Q. Jiang, L. Yu, Z. k. Yu. *Chinese Journal of Catalysis*, **2015**, 36, 78–85.

Synthesis of new nano water-soluble [M(٥-CH٢PPh٢-٣,٤-salpyr)](ClO₄)٢ (M= Ni, Zn) complexes characterization, DNA binding, cleavage activity, and molecular docking studies

Zahra Asadi,*[a] Mozaffar Asadi,[a] Zeinab Mandegani,[a]

[a]Department of Chemistry, College of Sciences, Shiraz University, Shiraz ٧١٤٥٤, Iran.

E-mail: zeinab mandegani@gmail.com;

Introduction:

The interactions between small molecular ligands and deoxyribonucleic acid (DNA) are of great importance biological and medicinal processes.[١] Complexes of nickel(II)[٢] and zinc(II)[٣] have variety of biological activity and show cytotoxicity against human cancer cell lines.[٤]. Water solubility of complexes have been increased by functionalizing the ligand by charged or polar groups.[٥] The application of nanoparticles (NPs) for biomedical usages is usual in the literature and continues to be a rapidly growing research field, with great emphasis on imaging and drug delivery e.g., to smart drugs and assisting in achieving maintainable development, e.g., reducing of energy and pollution.[٦, ٧]

Methods / Experimentals:

General procedure for synthesis of nano [N,N′-bis{٥-[(triphenyl phosphonium chloride)-methyl] salicylidine}-٣,٤-diaminopyridine] M(II) perchlorate. [M(٥-CH٢PPh٢-٣,٤-salpyr)](ClO₄)٢ (١-٥):
Nano complex was synthesized by slow addition of a solution of (٣-formyl-٤-hydroxybenzyl)triphenylphosphonium chloride (٠.٦ g, ١.٢٥ mmol) in ٥٠ mL water during ٧ h into a hot solution of M(acetate)٢.٢H٢O (٠.١٤ g, ٠.٦٢ mmol) dissolved in water and then a solution of ٣,٤-diaminopyridine (٠.٠٧ g, ٠.٦٢ mmol) in ٢٠ mL ethanol was added in this mixture for ٣٠ min.

Result and discussion:

The complexes [M(٥-CH٢PPh٢-٣,٤-salpyr)](ClO₄)٢ (M=Zn (١,٢) Ni (٣,٤) that the complexes ١ and ٣ were synthesized with nano size) and [Ni(٥-CH٢PPh٢-٢,٣-salpyr)](ClO₄)٢ (٥) were isolated using the procedure reported (Scheme ١).

All the complexes were characterized by elemental analysis, FT-IR, ١H NMR, ١٣C NMR,٣١P NMR, UV−vis. Spectroscopy and the morphology of the nano complexes were determined using FE-SEM and TEM. ١H NMR spectral data of the zinc and nickel complexes are given in experimental part.
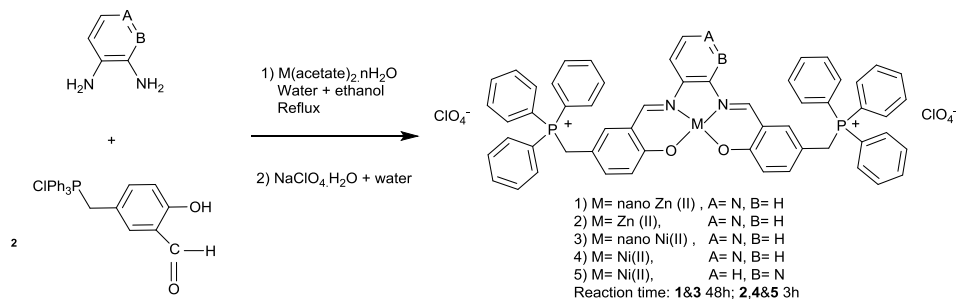
Scheme ١ Synthetic route for complexes ١-٥.

Absorption spectral studies

Electronic absorption spectroscopy is one of the most common methods to explore the interaction of complexes of ١-٥ with DNA. The change in absorbance and shift in wavelength upon addition of DNA solution in a fixed concentration of metal complexes gives important information on the type of interaction.[٨] From the results obtained, it has been found that complexes strongly bound with DNA relative to ligand and Ni(II) complexes are better relative to Zn(II) complexes. Furthermore the size of particles influences the interaction. The order of binding affinity is ٣ > ٤ > ٥ > ١ > ٢ > **L**.

Viscosity measurements

Viscosity measurement is often considered as an effective mode to determine the binding mode between small molecules and DNA. Intercalating agents are expected to lengthen the double helix to accommodate the ligands in between the bases, leading to an increase in the viscosity of DNA.[٩] The increased degree of viscosity, which may depend on its affinity to DNA, follows the order of ٣ > ٤ > ٥, which parallels the hypochromism and DNA binding affinities.

Electrochemical studies

Cyclic voltammetry has demonstrated to be a very sensitive analytical method to determine changes in redox behavior of metallic species in the presence of biologically important molecules.[١٠, ١١] Cyclic voltammetry of complexes (١-٤) in H₂O/DMSO showed oxidation waves in the sweep range from -١ V to +١.٥ V.

Conclusions

The ligand (**L**) and new complexes have been synthesized and well characterized. The DNA binding properties of **L** and complexes ١–٥ were examined by UV-Vis absorption spectra, emission spectra, viscosity, voltammetric techniques, and gel electrophoresis. The DNA binding properties of the free ligand and Zn(II) and Ni(II) complexes were investigated by absorption and fluorescence measurements. While **L** and complexes ١, ٢ interact with DNA, presumably by groove binding mechanism, complexes ٣–٥ intercalated with DNA through intercalation which was also confirmed by viscosity measurements and voltammetric techniques of DNA solutions in the presence of the complexes.

References
[١] A. Rajendran, C. J. Magesh, P. T. Perumal *Biochim. Biophys. Acta.* ٢٠٠٨, ١٧٨٠, ٢٨٢-٢٨٨.
[٢] F. Meyer, H. Kozlowski in ٦.٣ - *Nickel, Vol.* (Ed. J. A. M. J. Meyer), Pergamon, Oxford, ٢٠٠٣, pp.٢٤٧-٥٥٤.
[٣] W. Maret *BioMetals.* ٢٠١١, ٢٤, ٤١١-٤١٨.
[٤] B. S. Mendiguchia, D. Pucci, T. F. Mastropietro, M. Ghedini, A. Crispini *J. Chem. Soc. Dalton Trans.* ٢٠١٣, ٤٢, ٦٧٦٨-٦٧٧٤.
[٥] K. I. Ansari, J. D. Grant, G. A. Woldemariam, S. Kasiri, S. S. Mandal *Org. Biomol. Chem.* ٢٠٠٩, ٧, ٩٢٦-٩٣٢.
[٦] H. L. Karlsson *Anal. Bioanal. Chem.* ٢٠١٠, ٣٩٨, ٦٥١-٦٦٦.
[٧] K. K. Jain *BMC med.* ٢٠١٠, ٨, ٨٣.
[٨] Z.-C. Liu, B.-D. Wang, B. Li, Q. Wang, Z.-Y. Yang, T.-R. Li, Y. Li *Eur. J. Med. Chem.* ٢٠١٠, ٤٥, ٥٣٥٣-٥٣٦١.
[٩] J. M. Kelly, A. B. Tossi, D. J. McConnell, C. OhUigin *Nucleic Acid Res.* ١٩٨٥, ١٣, ٦٠١٧-٦٠٣٤.
[١٠] S. Srinivasan, J. Annaraj, P. Athappan *J. Inorg. Biochem.* ٢٠٠٥, ٩٩, ٨٧٦-٨٨٢.
[١١] A. M. Leone, J. D. Tibodeau, S. H. Bull, S. W. Feldberg, H. H. Thorp, R. W. Murray *J. Am. Chem. Soc.* ٢٠٠٣, ١٢٥, ٦٧٨٤-٦٧٩٠.

New Generation of Antidote Agent: EDTA-modified Mesoporous Silica in Iron Detoxification

Fatemeh Farjadian [*a], **Sahar Ghasemi** [a], **Reza Heidari** [a], **Soliman Mohammadi-Samani** [a, b]

a Pharmaceutical Sciences Research Center, Shiraz University of Medical Sciences, P.O. Box 71345-1583, Shiraz, Iran

b Department of Pharmaceutics, School of Pharmacy, Shiraz University of Medical Sciences, P.O. Box 71345-1583-Shiraz, Iran

Email: farjadian_f@sums.ac.ir

Introduction

Porous and highly dispersed materials have attracted significant attention from both academic and commercially[1]. Among different types of these materials, ordered mesoporous Silica (MS) are much more interesting for scientists[2]. In addition to good chemical and thermal stability, these materials are potential candidates for key biological applications.

Recently, we reported novel application of nanosphere MCM-41 as potent adsorber of drugs [3] . The efficiency of synthesized structures was evaluated in adsorption of phenobarbital and acetaminophen. Here, we introduced EDTA-modified MCM-41 and the efficiency of this structure was evaluated in adsorption of ferrous sulphate.

Methods/Experimental:

MCM-41 functionalized with amine (MSN-NH$_2$) was prepared according to reported procedure[4]. Conjugation of EDTA to modified MSN-NH$_2$ samples was performed with a similar procedure [5]. To determine the iron adsorption capacity (q) according to the adsorbed iron (mmol) per gram of MSN (g), the following model was used:

$$q = (C_0 - C_e)V/m$$

Results and Discussion:

Well-suspended MSNs of MCM-41 type, containing EDTA were prepared and characterized. FT-IR spectrum of MCM-41 containing amine and MCM-41 containing EDTA were recorded. The asymmetric stretching vibrations (Si–O–Si) appear at about 1090 cm^{-1} and a characteristic band of N-C=O related to amide functional groups at 1480 and 1520 cm^{-1} and C=O of carboxylic acid at 1630 cm^{-1} [6]. The powder X-ray diffraction (XRD) patterns for synthesized samples showed the expected crystallinity of MCM-41 nanoparticles. The surface area and porosity of our synthesized materials, was investigated using N$_2$ adsorption isotherms. A BET surface area of 800 m^2/g, pore diameter was obtained.To obtain the size, SEM and TEM were performed. SEM pictures showed well-dispersed and fine ordered nano-sized spherical particles with smooth surfaces. The TEM images showed that mesoporous silica nanoparticles are well-ordered and dispersed in solution, the average sizes was around 60 nm. Finally, *In vitro* adsorption evaluation was executed in simulating gastric (pH 1.2) and intestinal aqueous media (pH 7.2). The adsorption isotherms were plotted by defining the amount of iron adsorption per MSNs (mmol g^{-1}) against the concentration of iron (mmol L^{-1}) in equilibrium (Figure 1).
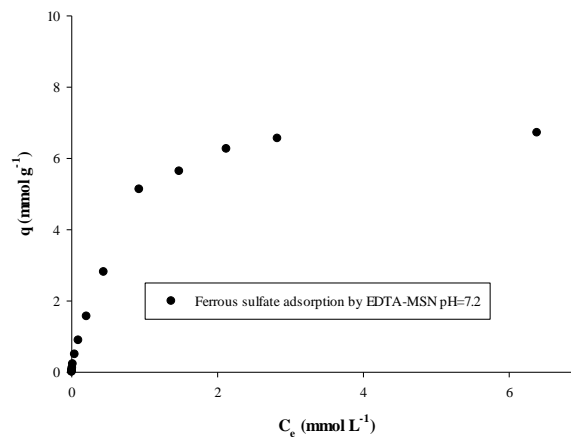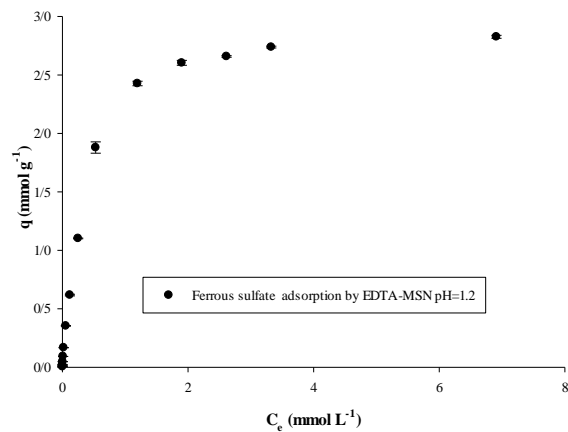
Conclusion

EDTA-modified MS material were synthesized and characterized. The synthesis conditions were controlled and nano-spheres with sizes less than 50 nm were synthesized. The highest porosity was observed for MSN-NH$_2$ hence functionalization with EDTA resulted in decreasing surface area. The efficiency of MSNs to adsorb drug was tested for ferrous sulphate in physiological pH conditions. The structures of the sorbent and adsorbent were shown to play a significant role in adsorption.

References

[1] Mesoporous materials: properties, preparation and application, Nova Science Publishers **2009**.
[2] F. Hoffmann, M. Cornelius, J. Morell, M. Fröba, Angewandte Chemie International Edition, **2006**, 45, 3216-3251.
[3] F. Farjadian, P. Ahmadpour, S.M. Samani, M. Hosseini, Microporous and Mesoporous Materials, **2015**, 213, 30-39.
[4] F. Lu, S.H. Wu, Y. Hung, C.Y. Mou, Size Effect on Cell Uptake in Well- Suspended, Uniform Mesoporous Silica Nanoparticles, Small, **2009**, 5, 1408-1413.
[5] W.-J. Liu, F.-X. Zeng, H. Jiang, X.-S. Zhang, Chemical Engineering Journal, **2011**, 170, 21-28.
[6] F. Farjadian, B. Tamami, ChemPlusChem, 2014,79, 1767-1773.

Research Progress on Phase Equilibrium and Thermo-physical Properties Measurements: Applications to Oil and Gas Industry in Iran

Amir Hossein Jalili[*], Ali Taghi-Zoghi, Mohammad Shokouhi

Gas Refining Technology Group, Gas Research Division, Research Institute of Petroleum Industry (RIPI), West Blvd. Azadi Sports Complex, P.O. Box 14665-137, Tehran, Iran.

Email address: jaliliah@ripi.ir

****

Industrial development in a country without basic experimental and computational facilities for measuring and generating physico-chemical properties of substances is impossible. In this respect, measurement and modeling phase equilibrium and thermo-physical properties of binary and multi-component mixtures are of special practical importance for development of industrial processes such as oil and gas as well as petrochemical and pharmaceutical industries. In every process accompanied with phase change such as crystallization, vaporization/distillation and extraction, which are used in purification of raw starting materials, intermediates and final products, phase equilibrium data, play an essential role.

In this presentation, the status of the vapor-liquid equilibria and thermo-physical properties measurements, during more than ten years of research and development in the Research Institute of Petroleum Industry (RIPI) in Iran [1-20], with accentuate on the fundamental principles and ideas used to design and build up the new apparatuses and measurement systems, will be discussed extensively. Especial emphasize will be put to the experimental setups developed in the Thermodynamics Research Center (TRC) in RIPI, which have been forming an important part of infrastructures for developing a newly rising technology, i.e. the ParsiSol technology, in the natural gas processing industry. The Future plans to design and extend new apparatus to overcome the existing shortcomings will be discussed as well. The presentation will highlight the practical applications of one of the most traditional yet one of the most imperative disciplines of physical chemistry, i.e. the chemical thermodynamics, in the industry.

References

[1] A. H. Jalili; A. Pourbashiri; C. Ghotbi. *14th International Conference on Properties and Phase Equilibria for Product and Process Design (PPEPPD **2016**)*, Porto, Portugal, May 22-26, 2016.

[2] M. Nematpour; A. H. Jalili; C. Ghotbi; D. Rashtchian. *J. Nat. Gas Sci. Eng.* **2016**, *30*, 583 − 591.

[3] A. H. Jalili; M. Shokouhi; F. Samani; M. Hosseini-Jenab. *J. Chem. Thermodyn.* **2015**, *85*, 13 − 25.

[4] M. Shokouhi; A. H. Jalili; F. Samani; M. Hosseini-Jenab. *Fluid Phase Equilibr.*, **2015**, *404*, 96 − 108.

[5] M. Shokouhi; H. Farahani, M. Hosseini-Jenab; A. H. Jalili. *J. Chem. Eng. Data.* **2015**, *60*, 499 − 508.

[6] A. Najafloo; A. T. Zoghi; F. Feyzi. *J. Chem. Thermodyn.* **2015**, *82*, 143 − 155.

[7] A. H. Jalili; M. Shokouhi; G. Maurer; M. Hosseini-Jenab. *J. Chem. Thermodyn.* **2013**, *67*, 55 − 62.

[8] M. Shokouhi; A. H. Jalili; A. H. Mohammadian; M. Hosseini-Jenab; S. Sadraei Nouri. *Thermochim. Acta.* **2013**, *560*, 63 − 70.

[9] M. Shokouhi; A. H. Jalili; M. Hosseini-Jenab; M. Vahidi. *J. Mol. Liq.* **2013**, *186*, 142 − 146.

[10] A. T. Zoghi; F. Feyzi; M. R. Dehghani. *Ind. Eng. Chem. Res.* **2012**, *51*, 9875 − 9885.

[11] A. T. Zoghi; F. Feyzi; S. Zarrinpashneh. *Int. J. Greenhouse Gas Control* **2012**, *7*, 12-19.

[12] A. H. Jalili; M. Safavi; C. Ghotbi; A. Mehdizadeh; M. Hosseini-Jenab; V. Taghikhani. *J. Phys. Chem. B*, **2012**, *116*, 2758 − 2774.

[13] H. Mazloumi; A. Haghtalab; A. H. Jalili; M. Shokouhi. *J. Chem. Eng. Data* **2012**, *57*, 2625 − 2631.

[14] S. Ahmad Kelayeh; A. H. Jalili; C. Ghotbi; M. Hosseini-Jenab; V. Taghikhani. *J. Chem. Eng. Data* **2011**, *56*, 4317 − 4324.

[15] A. H. Jalili; A. Mehdizadeh; M. Shokouhi; H. Sakhaeinia; V. Taghikhani. *J. Chem. Thermodyn.* **2010**, *42*, 787 − 791.

[16] A. H. Jalili; A. N. Ahmadi; A. Mehdizadeh; M. Shokouhi; M. Hosseini-Jenab; F. Fateminasab. *J. Chem. Thermodyn.* **2010**, *42*, 1298 − 1303.

[17] H. Sakhaeinia; A. H. Jalili; V. Taghikhani; A. A. Safekordi. *J. Chem. Eng. Data* **2010**, *55*, 5839 − 5845.

[18] M. Rahmati-Rostami; C. Ghotbi; M. Hosseini-Jenab; A. N. Ahmadi; A. H. Jalili. *J. Chem. Thermodyn.* **2009**, *41*, 1052 − 1055.

[19] A. H. Jalili; M. Rahmati-Rostami; C. Ghotbi; M. Hosseini-Jenab; A. N. Ahmadi. *J. Chem. Eng. Data* **2009**, *54*, 1844 − 1849.

[20] A. H. Jalili; M. Sina. *J. Chem. Eng. Data*, **2008**, *53*, 398 − 402.

Synthesis of fluorescent multi-functional C- tethered bispyrazolones

Adeleh Moshtaghi Zonouz[*], **Masumeh Beiranvand**

Chemistry Department, Faculty of Science, Azarbaijan Shahid Madani Univercity, Tabriz, Iran

(E-mail: adelehmz@yahoo.com)

Introduction:

Fluorescent compounds have attracted much attention recently due to their potential applications. As they are fluorescent in the solid state, they could be good candidates for photoluminescent or electroluminescent materials. Also because of their fluorescent in solution, they could be used as fluorescent sensor for application in biology and environmental science [1]. Pyrazoles are pluripotent ligands in coordination chemistry, as building blocks in heterocycle synthesis, as optical brighteners and UV stabilizers, as photoinduced electron transfer systems [2].
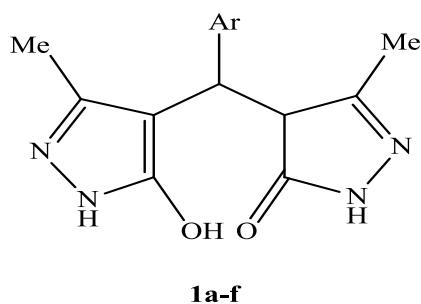
Methods / Experimentals:

General procedure. A mixture of 3-methyl-1H-pyrazol-5(4H)-one (obtained from condensation of hydrazine hydrate and ethyl acetoacetate at room temperature under solvent-free condition) (2 mmol) and benzaldehyde (1 mmol) in choline Chloride-Urea based DES (1 ml) was stirred at 100 $^{\circ}$C till the completion of reaction as indicated by TLC. After which it was cooled and the precipitated solid was filtered, washed with cold ethanol and recrystallized from ethanol to afford the pure 4,4'-(phenylmethylene)bis(pyrazolone) **1a** as white powder in 58% yield.

Results and Discussion:

The reaction was carried out in two stages. In the first step, 3-methyl-1H-pyrazol-5(4H)-one was prepared from condensation of ethyl acetoacetate and hydrazine hydrate at room temperature under solvent-free condition. At the second step, Knovenagel condensation of obtained pyrazolone derivative with aromatic aldehydes followed by Michael addition resulted 4,4'-(arylmethylene)bis(pyrazolone) derivatives **1a-f** (Table 1).

The obtained products were characterized by spectroscopic methods such as IR, ^{1}H and ^{13}C NMR. In addition, the structure of compound **1a** was determined by X-ray crystallographic study. Finally, the absorption and emission properties of the products have been studied with UV/Vis and fluorescence spectroscopy. The flouresence spectrum for compound **1b** was shown in figure **1**. In this spectrum, a broad emission centered at 441 nm was observed in the emission spectrum with an excitation wavelength at 264 nm.

Table **1**. Synthesis of 4,4'-(arylmethylene)bis(pyrazolones) in Chloride-Urea DES medium.

1a-f

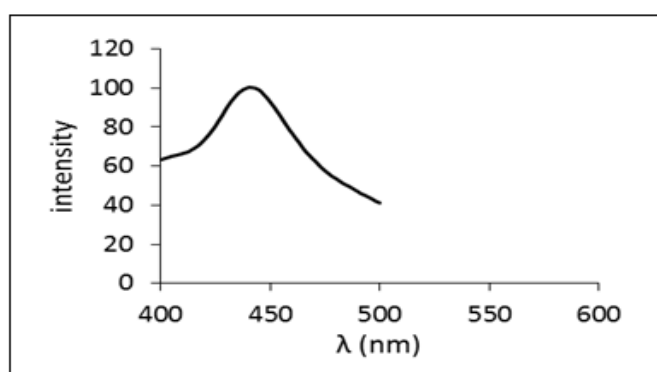| Entry	Ar	Product	Mp ($^\circ$C)	Yield (%)
١	C_6H_5	**1a**	٢٢٩–٢٣٠	٥٨
٢	2-MeC$_6$H$_4$	**1b**	٢٧٧–٢٧٩	٦٤
٣	3-O$_2$NC$_6$H$_4$	**1c**	٢٥٩–٢٦١	١٧
٤	2-ClC$_6$H$_4$	**1d**	١٧٩–١٨١	٢٥
٥	3-MeOC$_6$H$_4$	**1e**	٢٦٩	٤٤
٦	2-BrC$_6$H$_4$	**1f**	٢٨٣–٢٨٥	٧٠

Figure 1. Photolominesence spectrum of compound **1b**.

Conclusion:

We have developed a simple and efficient protocol for synthesis of some new fluorescent multi-functionalized C-tethered bispyrazols derivatives in DES as green solvent. Features of this strategy include the mild condition, good yields, short reaction time and avoiding the use of environmentally hazardous solvents and catalysts.

References

[1] J. Lu; L. Zhang; L. Liu; G. Liu; D. Jia; D. Wu; G. Xu. *Spectrochimica Acta Part A: Molecular and Biomolecular Spectroscopy*, **2008**, *71(3)*, 1036-1041.

[2] B. Willy; T. J. J. Müller. *Organic letters*, **2011**, *13(8)*, 2082-2085.

Comparison of Long-Heating Kinetic Process of Frying Oil In Presence and In Absence of Potato Slices Using ATR-FTIR and Chemometrics Tools

Marjan Mahboubifar[a, b]**, Bahram Hemmateenejad**[c, *]

[a]Medicinal and Natural Products Chemistry Research Center, Shiraz University of Medical Sciences, Shiraz, Iran
[b]Student Research Committee, Shiraz University of Medical Sciences, Shiraz, Iran
[c]Chemistry Department, Shiraz University, Shiraz, Iran

 Email address: hemmatb@shirazu.ac.ir; hemmatb@sums.ac.ir

 Introduction: Oxidation of oil induced by heating is an important degradation reaction and an undesirable chemical change with significant effect on the oil's nutritional quality and also may cause side effects on human health [1-3].
 Investigation of oil's oxidation processes is an approach for evaluation of its quality but most of the official methods are time-consuming, laborious and are environmentally hazardous. Due to the vast using of frying oil in the restaurant, especially for long-time frying of foodstuffs, we decided to survey on the long-heating kinetic process of frying oil in absence and in presence of potato to find the difference between them at this situation. For this purpose, we combined ATR-FTIR and chemometrics to survey the heating degradation of frying oil. Multivariate curve resolution-alternative least square (MCR-ALS) was utilized to resolve spectral and concentration pattern of the main produced/degraded species during the long-time heating (36-hours heating) treatment of frying oil in absence and in presence of potato slices.

 Methods / Experimentals: Frying oil was heated for 36 hours in absence and in presence of potato slices. Sampling was done every 3 hours. IR spectra of the oil samples were collected in absorption mode. The spectra were collected in the range 4000–550 cm^{-1}. For estimating the number of components in the data matrix the singular value decomposition (SVD) and evolving factor analysis (EFA) methods were used. Then MCR-ALS optimization program was applied for evaluation of the difference between the long-heating (36-hours heating) kinetic process of frying oil in the absence and in the presence of potato.

 Results and Discussion: The concentration and spectra of three main formed/degraded compounds during long heating process for frying oil in the absence and in the presence of potato were detected utilizing MCR-ALS method.
The main differences between the three detected compounds at the spectral profile resolved by MCR-ALS, can be observed around 1650-970, 3008 and 3450 cm^{-1}, due to changes in their composition. It is clear that the differences are mainly located at the frequencies of the characteristic bands correspond to trans (-CH=CH-), aliphatic (-CH2-), the (C=O) group, cis (-CH=CH-) and OH intermolecular bendings [2, 4, 5].
Description of results of the extracted concentration profile during the time and the resolved pure spectra of each compound showed that these three compounds were related to the deduction of

triacylglycerol of unsaturated acid, appearance of hydroperoxides form of triacylglycerols and secondary oxidation products during the 36-hours oxidation.

The changing pattern in the concentration profile of triacylglycerol of unsaturated acid for the oil which was heated alone was almost in opposite direction of the changing of secondary products of oxidation. However the changing pattern of this component in the oil which was heated in presence of potato was almost in opposite direction of the changing of the hydroperoxides form of unsaturated acid. These observations express the close relationship between the increasing and depression of these two compounds in these two different conditions.

Conclusion: Three main compounds during long heating process were detected utilizing MCR-ALS method. These compounds were related to triacylglycerol, hydroperoxides form of triacylglycerols and secondary oxidation products. The result shows that heating the oil in presence of potato lead to more formation of free radicals and hydroperoxides. But the formations of the secondary oxidation products are more in the oil which was heated in absence of potato.

 References

[1] Gonçalves, R. P., Março, P. H., Valderrama, P., *Food Chemistry,* **2014**, 163, 83–86.

[2] Le Dréau, Y., Dupuy, N., Artaud, J., Ollivier, D., Kister, J., *Talanta,* **2009**, 77, 1748–1756.

[3] Ng, C.-Y., Leong, X.-F., Masbah, N., Adam, S. K., Kamisah, Y., Jaarin, K., *Vascular Pharmacology*, **2014**, 61, 1–9.

[4] Moros, J., Roth, M., Garrigues, S., Guardia, M. de la., Food Chemistry, **2009**, 114, 1529–1536.

[5] Pinto, R.C., Locquet , N., Eveleigh, L., Rutledge, D. N., Food chemistry, **2010**, 120, 1170-1177.

A New Efficient Method for Synthesis of Dihydroquinqzoline Derivatives in Presence of TBAOH

Somayeh Ghorbanzadeh [a], Hamid Reza Safaei [a]*, Reza Khalifeh[b], Vahid Rahmanian[c]

[a]Department of Applied Chemistry, Faculty of Science, Shiraz Branch, Islamic Azad University, P.O. Box 71993-5, Shiraz, Iran

[b]Department of Chemistry, Faculty of Science, Shiraz University of Technology, Shiraz, Iran

[a]Department of Industrial Polymer Eng., Faculty of Engineering, Shiraz Branch, Islamic Azad University, Shiraz, Iran

*Corresponding Author(email: safaei@iaushiraz.ac.ir)

****

Introduction:

Quinazolinone derivatives have drawn much attention because of their broad range of pharmacological activities, [1] such as anticancer, anti-inflammatory, and anticonvulsant activities. Therefore, considerable efforts have been made to explore new, simple, and direct approaches toward the construction of 4(3H)-quinazolinone skeletons, for example, via amidation of 2-aminobenzonitrile followed by oxidative ring closure and Pd-catalyzed heterocyclization of nitroarenes. Recently, a number of classical methods for the synthesis of 2,3-dihydroquinazolin-4(1H)-ones have been reported in the literature, involving the condensation of 2-aminobenzamidewith aldehydes or ketones in the presence of various catalyst such as $CuCl_2$ and $TiCl_4$ –Zn. However, most of the reported methods suffer from tedious procedures and often from low yields. Therefore, the development of simpler, environmentally benign, high-yielding, and clean syntheses of 2,3-dihydroquinazolin-4(1H)-ones is in demand. So, in connection with our previous work [2,3] for the synthesis of quinazoline derivatives we report here an efficient and new synthetic route for this type of heterocyclic compounds.

Methods/Experimental:

Try to find new source and precursor for synthesis of organic compounds is desirable for chemistry researchers and chemical industries all the time because of making diversity in raw materials and methods. As I mentioned before there are two most popular methods for the synthesis of 2- sustituted quinazolines. The first one is based on the condensation of 2-aminobenzamide with aromatic aldehydes and ketones that is promoted in the presence of various catalytic systems and the other one is one-pot condensation of isatoic anhydride and amines with aldehydes. Moreover, reductive condensation of 2-nitrobenzamide and aldehydes, or ketones was also reported in the presence of reducing metallic catalyst.
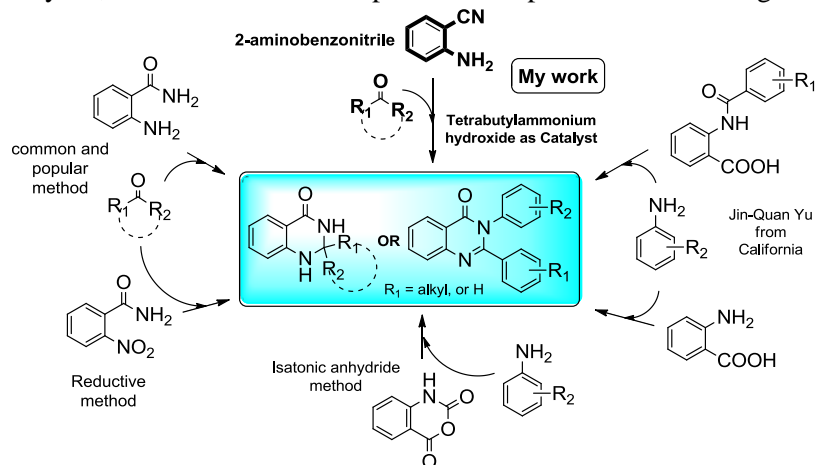
Recently, Professor Yu from Scripps Research Institute in California have introduced new precursor for quinazoline synthesis in J of American Chemical Society. In my project we did the reaction with *o*-cyano aniline as a new and unprecedented precursor for synthesis of derivatives of quinozalinon. In this novel reaction to a stirred solution of 2-aminobenzonitrile and tetrabutylammonium hydroxide was added ethanol at room temperature. The reaction mixture is vigorously stirred at 80°C for appropriate time. then aldehyde/ketone was added and The resulting solution was stirred under 65-75 °C. After the completion of the reaction, the precipitated product was filtered and recrystallized in order to obtain pure product.

Results and Discussion:

aim of this project focused on introduce and applied new precursor in order to expand diversity of synthetic method of quinozaline derivatives, but it has been succeeded to synthesis of widespread new and unreported structures of quinozalinones. I believe that the results of this project will open the door for scientist in chemistry and pharmaceutical fields.

References

[1] Z. B Xie, Sh.G Zhang, G.F Jiang, D.Zh Sun, Zh.G Le. "The green synthesis of 2, 3-dihydroquinazolin-4(1H)-ones via direct cyclocondensation reaction under catalyst-free conditions", Green Chemistry Letters and Reviews. 2015, 8, 95-98.
[2] H. R Safaei, M Shekouhy, S Khademi, V Rahmanian, M Safaei. "Diversity-oriented synthesis of quinazoline derivatives using zirconium tetrakis(dodecylsulfate) [Zr(DS)4] as a reusable Lewis acid-surfactant-combined catalyst in tap water", J. Ind. Eng. Chem. 2013, 20, 3019-3024.
[3] H. R Safaei, M Shekouhy, V Shafiee, M Davoodi. "Glycerol based ionic liquid with a boron core: A new highly efficient and reusable promoting medium for the synthesis of quinazolinones", J. Mol. Liq. 2013,180, 139-144.

The synthesis of new 5-[2-aryl-2-oxo-ethyl]-1,3-dimethyl-pyrimidine-2,4,6-trione derivatives

**Parinaz Madadi***, **Jabbar Khalafy, Mahnaz Ezzati**

Department of Chemistry, Faculty of Science, Urmia University, Urmia 5756151818, Iran

Email address: parinaz.madadi@gmail.com

Introduction:

The Knoevenagel condensation is an organic reaction used to convert an aldehyde or ketone and an activated methylene to a substituted olefin using an amine base as a catalyst [1].
In 2008 Gozalishvili and Co-workers reported the knoevenagel condensation reaction of 1,3-dimethyl barbituric acid, arylglyoxals in presence of acetic acid at room temperature affording 5-(2-arylethylidene-2-oxo)-1,3-dimethyl-pyrimidin-2,4,6-trione derivatives [2] as shown in Scheme 1.
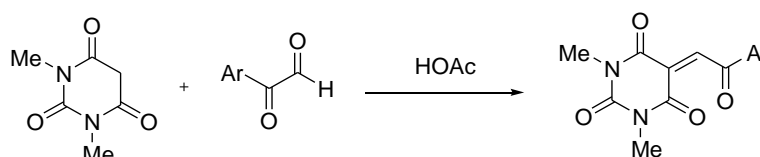
Scheme 1

In continuation of our research on reactions of arylglyoxals with methylene active compounds, Here, we have report the synthesis of 5-[2-aryl-2-oxo-ethyl]-1,3-dimethyl-pyrimidine-2,4,6-trione by reaction of arylglyoxals with *1,3*-dimethylbarbituric acid in presence of L-Cysteine.
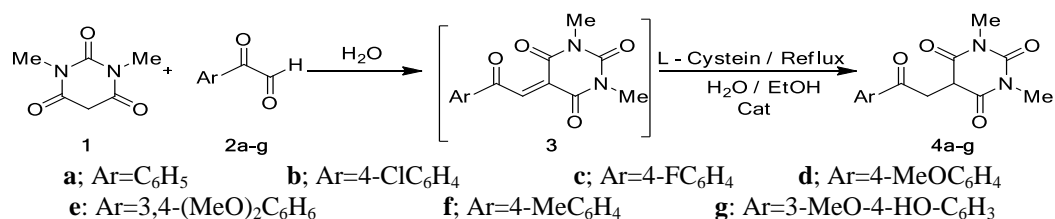
Methods / Experimentals:

To a mixture of arylglyoxal (**1a-g**, 1 mmol), 1,3-dimethylbarbituric acid (**2**, 1mmol) in water (4 mL), L-Cysteine (2 mmol) and Tungstophosphoric acid (10 mg) were added. The reaction mixture was refluxed in H_2O/EtOH (1:1) for 2-3 h and was left to cool to room temperature, the precipitate was fiterred, washed with water and dried to give the products (**4a-g**) as crystalline solids in 69-81% yield.

Results and Discussion:

The reaction of corresponding arylglyoxals [3] with *N,N*-dimethylbarbituric acid in H_2O at room temperature gave the corresponding intermediate, which was treated with L-Cysteine under H_2O/EtOH reflux conditions gave the desired products as a crystalline solids in high

yield. There was no sign of any heterocyclic products formation as expected (Scheme 2).

a; Ar=C$_6$H$_5$ **b**; Ar=4-ClC$_6$H$_4$ **c**; Ar=4-FC$_6$H$_4$ **d**; Ar=4-MeOC$_6$H$_4$
e: Ar=3,4-(MeO)$_2$C$_6$H$_6$ **f**; Ar=4-MeC$_6$H$_4$ **g**: Ar=3-MeO-4-HO-C$_6$H$_3$

Scheme 2

The structure of all product were confirmed by their FT-IR, ^{1}H-NMR, ^{13}C-NMR and X-ray crystallography. The spectral data are give below for **4a**, **4d** as an example.

1,3-Dimethyl-5-(2-oxo-2-phenyl-ethyl)-pyrimidine-2,4,6-trione: (4a): Colorless crystals, 71%, mp 190 ^{o}C. ^{1}H-NMR (300 MHz, CDCl$_3$) δ (ppm): 7.96 (d, J = 8.1 Hz, 2H, Ar), 7.69 (d, J = 6.6 Hz, 1H, Ar), 7.49 (t, J = 8.1 Hz, 2H, Ar), 4.05 (d, J = 3.3 Hz, 2H, CH$_2$), 3.61 (t, J = 3.3 Hz, 1H, CH), 3.37 (s, 6H, 2 × NMe). ^{13}C-NMR (75 MHz, CDCl$_3$) δ (ppm) : 167.92, 135.27, 135.00, 129.88, 129.79, 129.31, 127.61, 127.26, 45.35, 43.71, 37.81, 27.92, 27.74, 25.98. FT-IR V$_{max}$: 3428, 2892, 1667, 1463, 1390, 1306, 1218, 1114, 1031, 764, 691.

5-[2-(4-Methoxy-phenyl)-2-oxo-ethyl]-1,3-dimethyl-pyrimidine-2,4,6-trione   **(4d):** Colorless crystals, 69%, mp 197 ^{o}C. H-NMR (300 MHz, CDCl$_3$) δ (ppm) : 7.93 (d, J = 9 Hz, 2H, Ar), 6.95 (d, J = 9 Hz, 2H, Ar), 4.01 (d, J = 3.9 Hz, 2H, CH$_2$), 3.89 (s, 3H, CH$_3$), 3.56 (t, J = 3.3 Hz, 1H, CH), 3.37 (s, 6H, 2 × NMe). ^{13}C-NMR (75 MHz, CDCl$_3$) δ (ppm) : 195.24, 168.11, 164.1 , 151.75, 130.66, 128.3, 113.88, 55.50, 44.52, 37.58, 29.66, 28.74. FT-IR V$_{max}$: 3391, 3320, 2942, 2891, 1664, 1604, 1375, 1250, 1167, 1111, 1027, 827, 749, 563.

Conclusion:

We have reported a convenient and simple synthesis of 5-[2-aryl-2-oxo-ethyl]-1,3-dimethyl-pyrimidine-2,4,6-trione via the reactions of arylglyoxals with *N,N*-dimethylbarbituric acid in presence of Tungstophosphoric acid as a catalyst in H$_2$O/EtOH and L-Cysteine under reflux conditions. The advantageous features of this procedure are mild reaction conditions, high yields, operational simplicity, ready availability of starting materials.

References
[1] Knoevenagel, E. Ber. *Dtsch. Chem. Ges.* **1898**, *31*, 2596–2619.
[2] Lali L. Gozalishvili, Tetyana V. Beryozkina, Irina V. Omelchenko, Roman I. Zubatyuk, Oleg V. Shishkin, Nadezhda N. Kolos, Tetrahedron, **2008**, 64, 8759–8765.
[3] Riley, H. A.; Gray, A. R. *Organic Syntheses* Collect. In Wiley & Sons: New York, **1943**, *II*, 509.

Sensitive self-powered and low-cost DNA biosensor based on microbial fuel cell to diagnose genetic defects

Maryam Asghary[a], Jahan Bakhsh Raoof[*a], Mostafa Rahimnejad[b], Reza Ojani[a]

[a]*Electroanalytical Chemistry Research Laboratory, Department of Analytical Chemistry, Faculty of Chemistry, University of Mazandaran, Babolsar, Iran*

[b] *Biofuel and Renewable Energy Research Center, Department of Chemical Engineering, Babol Noshirvani University of Technology, Babol, Iran*

E-mail address: j.raoof@umz.ac.ir

Introduction

DNA biosensors, as detectors of nucleic acid sequences, have attracted an enormous attention over the last three decades with a vast area of applications such as gene analysis, clinical diagnostics, or even forensic applications [1]. Microbial fuel cells (MFCs) as bio-electrochemical systems represent a new promising source and power technology for the sustainable production of green energy [2,3]. As a continuous, portability, long life, and safe power source, the MFC technology has been widely used as energy source in electronic devices, implantable medical devices, biosensors for measuring biochemical oxygen demand, and water toxicity [4].

Methods and experimental

The laboratory-scale MFC system was set up by connecting two 750 mL Plexiglas chambers as anodic and cathodic compartments with an operating volume of 600 mL. The cathode consisted of a graphite electrode (0.22 cm^2) coated with synthesized AuNPs. An unmodified graphite plate (12 cm^2) was used as the anode. The anodic chamber was filled with the domestic sludge collected from the anaerobic process tank of the waste water treatment center of Ghaemshahr in the north of Iran. The voltage was continuously measured by a digital multimeter.

Results and discussion

Sensitive detection of DNA hybridization in the two-chambered MFC system

The detection of DNA hybridization was carried out by applying the MFC as a new power technology. To demonstrate the ssDNA probe immobilization and hybridization with complementary target DNA on the surface of an AuNP/graphite cathode in a pH 7.00 phosphate buffer, the variation of power density curves vs. current density was obtained in the cathodic chamber. As can be observed in Fig. 1, the maximum power density of 241.55 mW/m^2 was achieved by 1.0 µM ssDNA probe modified AuNP/graphite electrode at a current density of 851.69 mA/m^2. While, after the hybridization of ssDNA probe on the

surface of AuNP/graphite electrode with ١.٠ μM complementary target DNA, the maximum power density decreased and reached to ١٩٠.٣٦ mW/m^٢ at a current density of ٧٣٠.٧٦ mA/m^٢, under the steady state condition. Thus, the obtained power density of the MFC system with complementary DNA hybrid was less than that of with ssDNA. This revealed that the ssDNA probe immobilization and hybridization were effectively detected by the MFC system on the surface of AuNP/graphite cathode in the MFC system. Also, the low values of relative standard deviation (RSD) for three replicate measurements (n=٣) proved that the proposed biosensor could be potentially used as a sensitive and precise device for diagnosis applications with acceptable reproducibility.
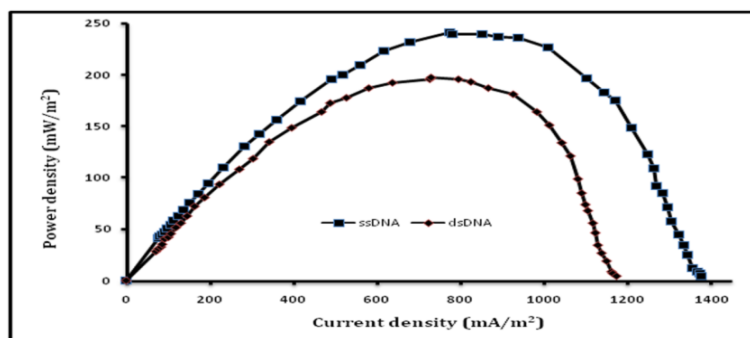

Fig. ١. Variation of power density as a function of current density of ١.٠ μM ssDNA probe modified AuNP/graphite electrode and after hybridization with ١.٠ μM complementary target DNA in the presence of a pH ٧.٠٠ phosphate buffer as an electrolyte under the steady state condition.

Conclusion

A truly low cost, easy-to-use, rapid, and portable self-powered DNA biosensor was constructed using a MFC system as a core portion and power supply to identify the genetic defects. The current changes before and after hybridization of the ssDNA probe with target sequence were sensitively detected by a digital multimeter. The constructed DNA biosensor exhibits a successful performance in detection and determination of the complimentary target DNA in spiked human serum sample.

References

[١] P. Du, H. Li, Z. Mei, S. Liu, *Bioelectrochemhstry*, ٢٠٠٩, ٧٥, ٣٧-٤٣.

[٢] M. Ghasemi, W.R.W. Daud, M. Rahimnejad, M. Rezayi, A. Fatemi, Y. Jafari, M. Somalu, A. Manzour, *International Journal of hydrogen energy*, ٢٠١٣, ٣٨, ٩٥٣٣-٤٠.

[٣] Y. Qiao, C.M. Li, S.-J. Bao, Q.-L. Bao, *Journal of Power Sources*, ٢٠٠٧, ١٧٠, ٧٩-٨٤.

[٤] C. Dai, S. Choi, *Open Journal of applied Biosensor*, ٢٠١٣, ٢, ٨٣-٩٣.

QUANTUM MECHANICAL LOCAL REACTIVITY INDICES OF INTERACTION OF IBUPROFEN AND FULLERENE C$_{60}$

P.Salimpour*, S.Yeganegi

[1]*Department of Physical Chemistry, Faculty of Chemistry, University of Mazandaran, Babolsar, Iran*

Introduction

Ibuprofen(IBU) is a non-steroidal anti-inflammatory drug (NSAID). This drug reduces hormones that cause inflammation and pain in the body. Therefore used to reduce fever and treat pain caused by many conditions. Fullerenes are Nanomolecular carbon cages that can serve as platforms for the delivery of drugs and imaging agents. According to the experimental studies, it has been found that fullerenes have good properties as adsorbent and transporter drugs. The objective of present is the study of interaction between fullerene and the IBU drug based on understanding the local reactivity through electrophilic and nucleophilic Parr functions.

Methods

The electrophilicity index as defined by Parr et al.[1] is given by the expression:

$$\omega = \frac{\mu^2}{2\eta} \tag{1}$$

Tetracyanoethylene (TCE) is used as a reference in the nucleophilicity scale

$$N = E_{HOMO(Nu)}(eV) - E_{HOMO(TCE)}(eV) \tag{2}$$

The local electrophilic, p_k^+, and nucleophilic, p_k^-, Parr functions are obtained from the analysis of the Mulliken atomic spin density (ASD) at the rdical cation and at the radical anion. These local functions allow for the characterization of the most electrophilic and nucleophilic centres in a molecule.

$$p^-(k) = \rho_s(k) \quad \text{for electrophilic attacks} \tag{3}$$

$$p^+(k) = \rho_s(k) \quad \text{for nucleophilic attacks} \tag{4}$$

DFT calculations were carried out using the B3LYP exchange–correlation functional, together with the standard 6-31+G** basis set[2,3]

Results and discussion

Analysis of the local electrophilicity (ω_{max}) and nucleophilicity (N_{max}) indices for IBU and Fullerene, allows for an explanation of the regio- and chemoselectivity in additions of IBU to Fullerene.
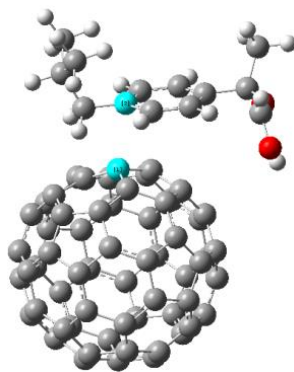
Fig.1. Optimized geometries of IBU adsorbed on the Fullerene.

Table.1. Quantum molecular descriptors for IBU, Fullerene, and Fullerene with IBU drug molecules in gas phase (eV)

Descriptors	Ibuprofen	Fullerene	Fullerene-Ibuprofen
HOMO energy	-6.6449	-6.4	-5.8
LUMO energy	-0.751	-3.6734	-3.22
LUMO – HOMO gap	5.8939	2.7266	2.58
Electron affinity (A)	0.751	3.6734	3.22
Ionization potential (I)	6.6449	6.4	5.8
Global hardness (η)	2.9469	1.3633	1.29
Chem. Potential (μ)	-3.6973	-5.0367	-4.51
Electrophilicity (ω)	2.3201	9.304	7.883

Table 1, shown that binding energy of IBU drug to Fullerene is -21.5 Kcal/mol and equilibrium nearst distance between atoms is 2.65 Å.

Conclusions

In this work we present ASD for the radical anion and at the radical cation of the reagents provides the characterisation of the most electrophilic and nucleophilic centres of the molecules, and thus makes it possible to establish the regio- and chemoselectivity in this reaction. Our results showed that thermodynamically is favorable and energetically the fullerene-IBU system is stable.

References

[1]   R. G. Parr, L. v. Szentpaly, and S. Liu, "Electrophilicity index," *Journal of the American Chemical Society,* vol. 121, pp. 1922-1924, 1999.
[2]   D. A. Yalalov, S. B. Tsogoeva, and S. Schmatz, "Chiral Thiourea-Based Bifunctional Organocatalysts in the Asymmetric Nitro-Michael Addition: A Joint Experimental-Theoretical Study," *Advanced Synthesis & Catalysis,* vol. 348, pp. 826-832, 2006.
[3]   W. J. Hehre, *Ab initio molecular orbital theory*: Wiley-Interscience, 1986.

Quasi-classical trajectory study on the reaction of O(^3P) + H$_2$S($^1A_1$)

Mousavipour S. H.^{a,*}, Masoumpour M. S.^{a}

^{a}*Department of Chemistry, College of Science, Shiraz University, Shiraz, Iran*

Email address: mousavipour@shirazu.ac.ir

****

Introduction: Oxidation of H$_2$S has an important role on the chemistry of atmosphere and combustion of sulfur-containing fossil fuels [1]. The most important oxidation reactions of sulfur containing pollutants in remote atmosphere are with ozone, hydroxyl radical, hydrogen peroxide, and atomic or molecular oxygen [2]. In the present study we report the results of a theoretical study on the dynamics of the title reaction. The effect of the initial relative translational energy on the kinetics and dynamics of the O(^3P) + H$_2$S($^1A_1$) reaction is investigated.

Methods: A primary potential energy surface for the title reaction at the MPWB1K level of theory is constructed. GROW program from Collins is used to study the dynamics of the title reaction. The method calculates the energy, gradient, and second derivative of the potential at important sampled locations on the PES. To grow the potential energy surface for a reaction, an iterative procedure automatically places new data points in regions of configuration space that are important dynamically.

Results and Discussion: The PES of the stationary points at the MPWB1K level of theory are shown in Figure 1. Dynamics of the main reactions are investigated.

$$H_2S + O(^3P) \rightarrow OH + SH \qquad\qquad\qquad R1$$
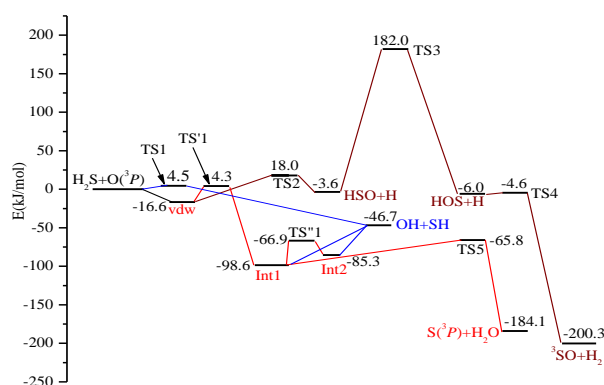
$$\rightarrow HSO + H \qquad\qquad\qquad R2$$

Figure 1. Potential energy surface for the title reaction at the MPWB1K level.

The interpolated PES was grown with classical trajectories which were carried out at fixed initial internal energy in H_2S and relative translational energy for the reactants from 13.1 kJ mol^{-1} to 78.8 kJ mol^{-1}. The reactive reaction cross sections for each of the reactions R1 and R2 as a function of relative translational energy is shown in Figure 2.
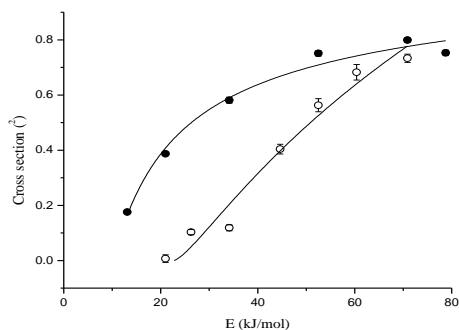

Figure 2. Reactive cross sections for reactions R1 ($\bullet$) and R2 (o) as a function of the initial collision energy.

The reaction cross sections $\sigma(E)$ can be related to the reaction rate constants based on simple collision theory at temperature T.

$$k(T) = g_e(T)\sqrt{\frac{8}{\pi\mu(KT)^3}}\int_0^\infty E\sigma(E)\exp(-\frac{E}{KT})\,dE$$

where $g_e(T)$ is the electronic degeneracy, μ is the reduced mass and K is Boltzmann's constant. As shown in Fig. 2, fitted cross sections for reactions R1 and R2 are expressed as

$$\sigma_{R1}(E) = (0.63 \pm 0.23)\frac{(E - (10.03 \pm 1.24))^{(1.08\pm0.09)}}{E} \quad , \sigma_{R2}(E) = (0.21 \pm 0.08)\frac{(E - (22.66 \pm 1.71))^{(1.44\pm0.11)}}{E}$$

The integrated rate constant for reactions R1 and R2 is evaluated as

$$k_1(T) = \frac{5.82\times10^{-13}T^{0.59}e^{-1207.00/T}}{e^{-326/T}+3e^{-228/T}+5} \quad , k_2(T) = \frac{4.21\times10^{-14}T^{0.94}e^{-2726.08/T}}{e^{-326/T}+3e^{-228/T}+5}$$

Conclusion: The cross sections and probabilities for different products are evaluated. The reaction cross section for reaction R1 does not change significantly at higher collision energy but the reaction R2 showing a monotonic increase with the increase in collision energy. The energy partitioning among the main products are investigated. The calculated rate constants are in reasonable agreement with the reported experimental results.

References

1.   M. A. Collins, *Theor. Chem. Acc.* **2002**, *108*, 313.
2.   E. Miliordos; S. S. Xantheas. *J. Am. Chem. Soc.*, **2014**, *136*, 2808.

Binding of Distamycin to DNA and G-Quadruplex by Molecular Dynamics Simulation

Mina Maddah[a]*, **seifollah Jalili**[a,b]

[a]*Department of Chemistry, K. N. Toosi University of Technology, P. O. Box 15875-4416, Tehran, Iran.*
[b]*Computational Physical Sciences Research Laboratory, School of Nano-Science, Institute for Research in Fundamental Sciences (IPM), P.O. Box 19395-5531 Tehran, Iran.*
madahmina@gmail.com

Introduction: DNA can be folded apart from B-DNA double helix, in another biological structure which is named G-quadruplexes. G-quadruplexes inherently have greater selectivity than duplex DNA [1,2]. The telomeric DNA could fold into DNA quadruplex structures and been as a potential target for novel small molecules based anticancer therapy [2,3]. Since telomerase is activated in more than 90% of all cancers [4], G-quadruplex in telomeres have been established as promising anticancer targets. By adding of small molecules or ligands, these quadruplex structures become more stable. The hole between G-tetrads is well suited to coordinating cationic drugs. Moreover small molecules such as many antibiotics and cationic ligands bind in the minor groove of DNA. In this study the binding of distamycin as an anticancer drug with B-DNA and G-quadruplexes is compared.

Methods: The starting structures were based on X-ray crystal structure of distamycin/5'd(CGCAAATTTGCG)3'(PDB:2DND) [5] and NMR solution structure of the 4:1 distamycin/[d(TGGGGT)]$_4$ complex (PDB:2JT7) [6]. Both structures were solvated in periodic octahedron box of TIP3P water molecule, with a distance of 10 Å from the edge of the solute in each direction. Simulations were performed using AMBER10 package [7]. Two stages of energy minimization and tree stage of equilibration were performed, and finally, 20 ns NPT simulations were done. The parameters for the distamycin were generated with ANTECHAMBER [8] with the general AMBER force-field [9], and the ff9SB force-field [10] was used for nucleotides.

Results and Discussion: The RMSD of the DNA backbone was calculated against the initial structure for G-DNA and B-DNA, and results were shown in Fig. 1. Throughout the simulation, the G-quadruplex backbone is well-maintained in compared with double-helical DNA, because distamycin causes more changes in DNA than G-quadruplex. There are 8 donor hydrogen and 4 acceptor oxygen atoms in distamycin drug. The amide nitrogen atoms of distamycin were positioned between A4–T8 base pairs in B-DNA T1-G5 in G-quadruplex. All the amidium hydrogens form hydrogen bonds to N3 atoms of adenine and O2 atoms of thymine in the minor

groove while N2, N3, N7 and, N9 atoms of bases and O3' and O5'atoms of sugar have donor role in G-quadruplex. The occurrence of hydrogen bonds between distamycin-bases along the simulation time is evaluated as the extent of stability of hydrogen bonds. It is shown the hydrogen bonds are well preserved between all of the base pairs in G-quadruplex more than B-DNA. The binding free energy and their energetic components are summarized in Table 1. Regarding the negative value of ΔG_{bind}, it can be concluded that binding of distamycin in both complexes in water is favorable. ΔG_{bind} for binding of distamycin to G-quadruplex is more negative than B-DNA. This fact shown, the binding of distamycin to quadruplex are more favorable than B-DNA.

Table 1 Binding free energies for two complexes.

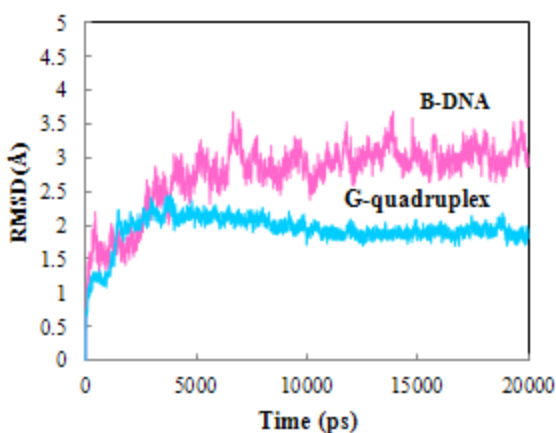| Energy (kcal/mol)	B-DNA		G-DNA	
	Mean	std	Mean	std
ΔE_{ele}	-48.21	30.6	-55.96	5.76
ΔE_{vdw}	-137.04	5.51	-75.86	2.97
ΔE_{init}	0.00	0.0	0.00	0.0
ΔG_{PBSUR}	-11.12	0.18	-5.23	0.08
ΔG_{PBCAL}	111.47	33.1	39.50	2.52
ΔG_{PBSA}	-84.90	15.4	-97.55	12.5
$T\Delta S$	-55.61	11.8	-33.97	6.26
ΔG_{bind}	-29.29	-	-63.58	-

Figure 3 Root mean square (rms) deviation profiles, during the MD simulation of G-DNA and B-DNA.

Conclusion: Distamycin bind between strands of DNA and quadruplex by forming Hydrogen bond, van der Waals and electrostatic interaction. There are four positions in G-quadruplex structure for distamycin so the number of H-bonds and extent of interaction helps to more stability of this structure than B-DNA.

Reference
[1] Oganesian L; TM Bryan; Bioessays, **2007**, 29,155-165.
[2] Neidle S; *Current opinion in structural biology,* **2009**, 19, 239-250.
[3] Cuesta J; Read MA; Neidle S; *Mini reviews in medicinal chemistry*, **2003**, 3, 11-21.
[4] Shay J; Bacchetti S; *European journal of cancer*, **1997**, 33, 787-791.
[5] Coll M; et al; *Proceedings of the National Academy of Sciences*, **1987**, 84, 8385-8389.
[6] Martino L; et al; *Journal of the American Chemical Society*, **2007**,129, 16048-16056.
[7] Pearlman DA; et al; *Computer Physics Communications*, **1995**, 91, 1-41.
[8] Wang J; et al; *Journal of molecular graphics and modelling*, **2006**, 25, 247-260.
[9] Wang J; et al; *Journal of computational chemistry*, **2004**, 25, 1157-1174.
[10] Cheatham III TE; Cieplak P; Kollman PA, *Journal of Biomolecular Structure and Dynamics*, **1999**,16, 845-862.

Study of the inclusion complex and antioxidating activity of amlodipine besylate with β-cyclodextrin and γ-cyclodextrin

Alizadeh N[*] **and** __malakzadeh Sh__

* Department of Chemistry, Faculty of Science, University of guilan, Rasht, Iran

Email address: n-alizadeh@guilan.ac.ir

****

Introduction: The aim of the study was to synthesize and Characterization the inclusion complexes of amlodipine besylate with β-cyclodextrin (β-CD) and γ-cyclodextrin (γ-CD) which have antioxidating activity property. Kinetic studies of 2,2-diphenyl-1-picrylhydrazyl (DPPH˙) with with Wogonin and cyclodextrins (CDs) complexes were done[1].

Methods / Experimentals: β-cyclodextrin (β-Cyd) and γ-cyclodextrin (γ-CD) inclusion complexs containing amlodipine besylate as a guest was prepared by soluble method in doubly distilled water. The product was characterized by Fourier Transform Infrared (FTIR) spectrometer, ultraviolet-visible spectroscopy (UV-vis). The antioxidant activity was measured, wherein the bleaching rate of a stable free radical, DPPH˙ is monitored at a characteristic wavelength in the presence of the sample.

Results and Discussion: The interaction of β-Cyd and and γ-Cyd with amlodipine besylate was also analyzed by means of spectrometry by UV-Vis spectrophotometer to determine the formation constant and Scavenging study of the DPPH˙ radical. The formation constant was calculated by using a modified Benesi-Hildebrand equation at 25°C. Besides that, the stoichiometry ratio was also determined to be 1:1 for the inclusion complexs of β-Cyd and γ-Cyd with amlodipine besylate and the experimental resulted confirmed the forming of amlodipine besylate complexes with CDs by Fourier Transform infrared spectra.

Conclusion: This proves the formation of the inclusion complex where the benzyl part of amlodipine besylate has been encapsulated by the hydrophobic cavity of β-Cyd and γ-Cyd. The results obtained indicated that the amlodipine besylate/ β-CD and the amlodipine besylate/γ-CD complexs was the most reactive than theirs free form into antioxidant activity.

References

[1] Jinxia Li[1] , Huizhi Zhang[2], Yanyan Yan[3], Shumao Sun[4] , J Incl Phenom Macrocycl Chem, 2016, 84, 115–120.

A novel Isocyanide base three-component reaction for synthesis of new derivatives of 1,5-dihydro imidazole

Mahboobeh Zebarjad[a], Hamidreza Safaei[a],*

**Department of Applied chemistry,Faculty of science,Shiraz Branch,Islamic Azad University,P.O.Box 71993-5,Shiraz,Iran**

*Corresponding Author(email:safaei@iaushiraz.ac.ir)

****

Abstract:

Three-component one pot reaction involving urea, aldehydes, and isocyanide in CH_3CN/H_2O was prinvestigated. The structures of products were determined by spectroscopic data.

Introduction:

Within the realms of organic synthesis, cycloaddition reactions hold a distinction for ever-increasing importance. This distinction is driven by the nature of cycloaddition process, in which multiple bond formation and cyclization take place synchronously, making it a unique tool to convert simple precursors into complex cyclic products in a rapid and efficient manner. There has been a stupendous growth of cycloaddition reactions over the past half century which has been utilized in almost every area of chemistry from materials chemistry to drug discovery. Amongst a variety of cycloaddition sequences, isocyanide-based cycloaddition reactions have been widely reconnoitered owing to the ability of isocyanides to act as electrophiles as well as nucleophiles.
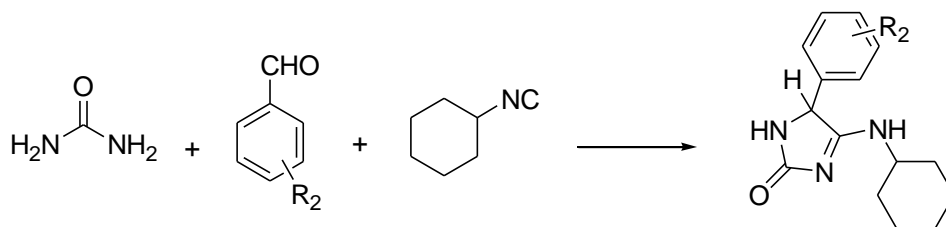
This feature providing them excellent opportunities towards construction of heterocyclic entities and bioactive natural products Heterocyclic compounds play an important role in the drug discovery process Among numerous heterocycles, the imidazole core is one of the most prominent
groups because it is a constituent of many important natural products and medicinal agents. So, due to our interest to Isocyanide base multicomponent reaction [1,2] herein report a facile, environmentally benign isocyanides based one-pot three-component strategy for the synthesis of novel 1,5-dihydroimidazole derivatives in H_2O/CH_3CN as reaction medium.

Methods/Experimentals: General procedure:

A solution of urea,3-Nitrobenzaldehyde, cyclohexyl isocyanide were disolved in acetonitrile /water. Then after catalytic amount of NH$_4$Cl (20%mol) was added and the mixture was stirred at 70°C for 5h.the progress of the reaction was monitored by TLC (ethyl acetate-hexane 3:1).After completion of the reaction, the solvents was evaporated under low pressure the reaction mixture was then washed with ice-water and acetone.The solid product was recrystallized from MeOH to give pure product.

Results and Discussion:

In conclusion, we report a convenient, simple, efficient, and environmentally friendly approach for the three-component condensation reaction of urea ,aldehydes,and cyclohexyl isocyanide resulting in the formation of derivations of imidazole. To the best of our knowledge, this is the first report on synthesis of five members nitrogen heterocyclic compounds based on isocyanide cyclo addition reaction.

Reference:

1. Hamid Reza Safaei, Najva Shioukhi, Mohsen Shekouhy "Isocyanide-based one-pot three-component synthesis of novel spiroiminolactone derivatives in water" *Monatsh Chem*., **2013**, 144: 1855–1863. DOI 10.1007/s00706-013-1060-1.

2. Hamid Reza Safaei, Farbod Dehbozorgi "Isocyanide-based three component reaction for synthesis of highly cyano substituted furan derivatives" *RSC Adv*., **2016**, 6, 26783-26790. DOI: 10.1039/c5ra22293a. Publisher is Royal Society of Chemistry

Magnetic nanoparticle assisted gemini-based supramolecular solvent extraction of heavy metals prior to their determination by ICP-AES

Neda Feizi Gilandeh, Yadollah Yamini [*]

Department of Chemistry, Tarbiat Modares University, P.O. Box 14115-175, Tehran, Iran

*yyamini@modares.ac.ir

Introduction: Microextraction based on SUPRASs requires a centrifugation step for phase separation, and this is time consuming. Another problem of centrifugation is its low efficiency in separation of aggregates from aqueous solution. Due to solve the problem, we describe a method for the microextraction of heavy metals from waste water samples. It is based on the use of the gemini-based supramolecular solvent and magnetic nanoparticles (NPs) which are applied to magnetically separate the supramolecular aggregates contains complex of heavy metals. Following desorption of the coating from the magnetic NPs with methanol, the solution was submitted to ICP-AES.

Experimental: SUPRAS was formed by adding 20 mg of 14-2-14 in 5.0 mL of propanol to 35.0 mL of water samples contains 10 % w/v of NaCl and 0.1 mM of PAN at pH 4.0. After extraction, 20 mg of MNPs were added to the solution and vortexed for 2 min. After collection of the MNPs with a magnet, the supernatant was decantated and the adsorbent was eluted with 100 μL of methanol. Finally, the eluent was injected into the ICP-AES for analysis of extracted metal ions.

Results and Discussion: Effects of different parameters on the extraction efficiency of metal ions by the proposed method were investigated. The following optimized parameters were obtained: an amount of 20 mg of gemini surfactant; 5.0 mL of propanol; a sample solution pH of 4.0; an extraction time of 10 min; a stirring rate of 3500 rpm; 20 mg of adsorbant; an ionic strength of the solution of 10 % w/v. Under optimal conditions, the preconcentration factors of 183 to 256 were obtained.

The analytical ranges extend from 0.3 to 250 μg L^{-1}, and the limits of detection (LODs) are between 0.3 and 0.5 μg L^{-1}. The precision of the method, expressed as relative standard deviation for extraction and determination of the 100 μg mL^{-1} analytes in the samples solution is in the

range from 6.5 to 12 %. Finally, to test the applicability of the established method, it was successfully applied to the determination of heavy metals in aqueous samples.

Conclusions: A new technique of gemini-based supramolecular solvent-assisted by nanomagnetic particles has been developed. The technique was applied for extraction and determination of heavy metals from water samples. The main advantages of the new supramolecular solvent assisted by magnetic nano particles methods is elimination of centrifugation step for collection of extraction solvent, which makes the procedure faster and robust.

Reference

[1] A. Spietelun, A. Kloskowski, W. Chrzanowski, J. Namieśnik, Chem. Rev., **2013**, 113, 1667-1685.

Studying Mechanism of Performance of Specialized Compact Integrated Narcotic Drugs Detecting Device (CINDI) in Identifying and Discovering Drugs

Sh. Arjmand ,A. Sharifnia

Department of Chemistry, University of Applied Sciences Pars Special Economic Energy Zone,*Assalouyeh,Bushehr Iran*

Email: shahriar_arjmand@yahoo.com

Abstract

Need to use devices with high technology for identifying and discovering narcotic drug resulted in supplying new generation of specialized portable devices to the market. Of these devices, it should be referred to Compact Integrated Narcotic Drugs Detecting Device (CINDI) [١]. Compact Integrated Narcotic Drug Detecting Device is a portable and light device with a source of californium – ٢٥٢ which is ascended from inside front chamber of Compact Integrated Narcotic Drug Detecting Device (CIND) and its performance for various samples is as follows: The device penetrates into materials with very dense structure with the least energy change but it is backscattered through materials rich in hydrogen like narcotic drugs. Backscatter mechanism is operated in such a way that will lead to the detection of hidden materials [٢-٣].

Mechanism of performance of the device is discussed at the present study and method of identifying and discovering narcotic drugs by this detector device and also advantages and disadvantages of the device is analyzed. The results of studies indicate that CINDI uses a very sensitive detecting approach which allows safe use of weak radioactive sources without reducing detection power. CINDI is able to detect materials rich in hydrogen with more efficiency and directly behind panels made of steel, wood, fiberglass, or even materials with lead coating [٤]. This issue causes this method to be useful for inspecting marine equipment, hulls of ships, cars, construction walls and sealed small-size containers. Meanwhile, lightness and portability of the device and application of the device in specific condition can be considered as its salient advantages.

Keyword: CINDI، Narcotic Drugs ، analyze, detect

Introduction
Detection of drug traces is of considerable importance for forensic applications. Traditional drug analysis requires a rather large sample and is time-consuming. The ideal analytical tool for forensic applications should be fast and of very low detection limits.

CINDI incorporates a highly sensitive detection scheme which permits the use of weak radioactive sources for safety without compromising detectability. CINDI is able to detect hydrogen-dense materials most effectively directly behind panels made of steel, wood, fiberglass, or even lead-lined materials. This makes it useful for inspecting marine vessels, ship bulkheads, automobiles, structure walls, or small sealed containers. The present CINDI version selectively detects hydrogen rich substances only. The new technique will detect both neutrons and gamma rays simultaneously. The backscatter mechanism of gamma rays and neutrons are sufficiently different that they complement each other and lead to a higher likelihood of identifying the concealed material.

References
[١] T. O Tumer, R. M. Pierce, K. C. Dotson, Joseph R. Jadamec and Chin-Wu Su, Portable narcotics detector with identification capability, ١٩٩٤
[٢] C.Vallvey LF, A . LJ, L J, Frames MD, Palma AJ. Oxygen-sensing film coated photo detectors for portable instrumentation. Anal Chim Acta, ٢٠٠٧; ٥٨٢(١): ١٦٦-٧٣.
[٣] Minata K. Reflective thermal lens detection device. Lab Chip, ٢٠٠٦; ٦(١): ١٢٧-٣٠
[٤] N. S, Lynd's P, Powel J. A new thermal desorption solid phase system for hand-held ion mobility micro extraction spectrometry. Analytical Chemical Act ٢٠٠٦; ٥٥٩(٢):١٤٠-١٦٩

Investigating the Effect of Pore-widening Process on Pore Diameter and Transparency of Al$_2$O$_3$-Nanoholes Array Fabricated by a Two-Step Anodization

S. Barzegar[a], G. Absalan*[a], M. Moradi[b], and S. Behaein[b]
[a] Department of Chemistry, College of Sciences, Shiraz University, Shiraz, Iran.
[b] Department of Physics, College of Sciences, Shiraz University, Shiraz, Iran.
* gubsulun@yahoo.com

Introduction: Many studies have been done to optimize the pore parameters of anodized aluminum oxide (AAO). It has been reported previously that the pore diameter and thickness of AAO can be controlled by changing different parameters of anodization. The diameters of the pores also can be adjusted by wet chemical etching which is called pore widening process. This process decreases the thickness of barrier layer at the bottom of AAO pore array. The barrier layer thinning is essential in order to increase the electrical contact between AAO and electrode especially in facilitating the process in electrodeposition of nanomaterials in AAO template [1].

Methods / Experimentals: The nanohole arrays fabricated using high-purity Al discs (thickness: 1.0 mm) by two step anodization method in a mixture of oxalic acid (0.30 M) and phosphoric acid (0.30 M) as the electrolytes were utilized in the process of pore widening. The arrays were etched in CuCl$_2$ in HCl solution for 30 minutes to dissolve Al substrate and obtain free oxide films. Then the oxide films were kept in 0.5 M H$_3$PO$_4$ (30^{0C} [2]) for 10 minutes 32 times.

Results and Discussion: In the pore widening process anion incorporated layers of the pore walls were dissolved in H$_3$PO$_4$ 0.5 M without any changes in the interpore distance and pore density. Besides, the size uniformity is increased and the hexagonal pattern is more obvious [1]. It is considered in figure 1a and b that the holes became wider from 133 to about 440nm and apparently, the walls became narrower. The long time etching results in filter structures (figure 1c) which means that the barrier layers of holes were dissolved.
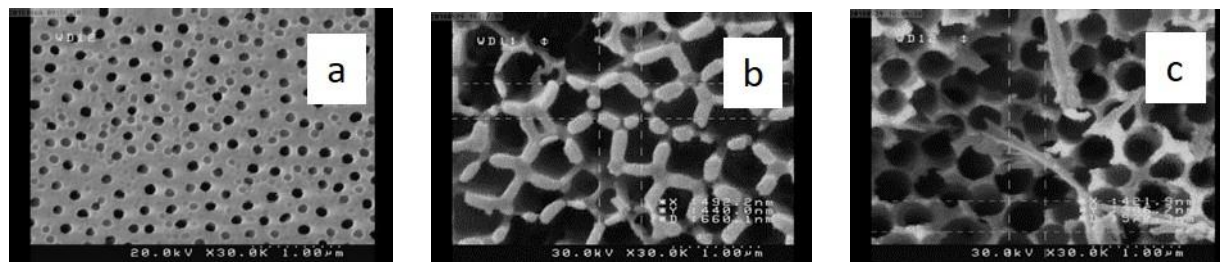

Figure 1 SEM image of the AAO. top profile without pore widening, a, top profile after pore widening for 320 min in 0.5 M H$_3$PO$_4$, b, back profile of the etched structure in which the dead end dissolved, c.

Pore widening process for a long period of time make the opportunity to achieve different pore size arrays. After each pore widening step, the optical transparency of the oxide film was checked by a spectrophotometer. 100 min etching achieved a film with higher transparency in the range of 500 to 900 nm (figure 2). Pore widening for more than 100 min result in reduction of peak resonance intensity in transmittance [3]. Low transmittance level is probably due to light scattering losses [2].

These results should be taken into account for designing Anodized Aluminum oxide (AAO) based optical metamaterials especially for plasmonic systems [2].
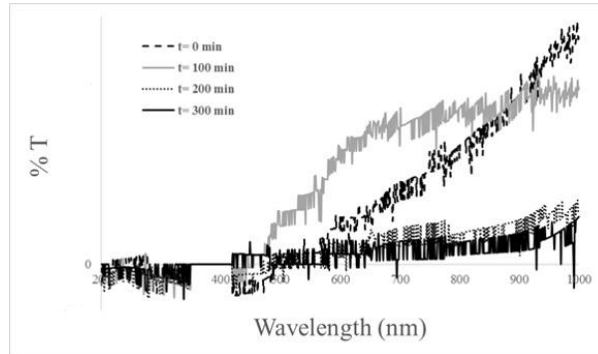

Figure 2 Effect of pore-widening process in 0.50 M H_3PO_4 for t=0, 100, 200, 300 min on transparency of AAO.

Conclusion:
The pore diameter can be tuned by widening process. The final structures with desired pore dimensions can be used as templates for fabrication of nano rods, nanotubes and nanowires with different size distributions. Long time etching achieve filter structures that can be used for size selective filtration and flow through nanohole arrays. The process of pore widening increase the transparency of the oxide films in limited conditions.

References

[1] J. Zhang; J. E. Kielbasa; D. L. Carroll. *Materials Chemistry and Physics*, **2010**, *122*, 295–300

[2] A. Hierro-Rodriguez; P. Rocha-Rodrigues; F. Valdés-Bango; J. M. Alameda; P. A. S. Jorge; J. L. Santos; J. P. Araujo; J. M. Teixeira; A. Guerreiro. *Journal of Physics D: Applied Physics*, **2015**, *48*, 455105-455111

[3] A. Kassu1; C. Farley; A. Sharma. *Proc. of SPIE*, **2014**, *9106*, 91060M-1

Synthesis of new arylidene Meldrum's acid derivatives

Elham Moosazadeh, Enayatollah Sheikhhosseini*, Dadkhoda Ghazanfari

Department of Chemistry, Kerman Branch, Islamic Azad University, Kerman, Iran,

Email address: sheikhhosseiny@gmail.com.

****

Introduction: Alkylidene and Arylidene Meldrum's acids are very reactive acceptors in conjugate additions, and are known to be significantly more electrophilic than other α, β-unsaturated carbonyl electrophiles. Arylidene Meldrum᾽s acid derivatives are used in cycloaddition reactions, 1,4-conjugated addition reactions, preparation of mono alkyl Meldrum᾽s acid derivatives, preparation of deuterated carboxcylic acid derivatives and so forth [1, 2]. Knovenenagle condensation of Meldrum᾽s acid and aromatic aldehydes under variety condition furnishing corresponding Arylidene derivatives (5-Arylidene-2,2-dimethyl-1,3-dioxane-4,6-dione), which are versatile substrates for variety of reactions. This condensation is generally catalysed by bases, such as pyridine [3, 4], pyrrolidinium acetate [5] and piperidine/glacial acetic acid in benzene with water removal [6, 7]. Uncatalysed reaction was reported in the literature using DMF, DMSO and water as solvent [8, 9].

Methods / Experimentals:

General procedure for the synthesis of ethylene glycol-based dialdehyde derivatives: A mixture of polyethylene glycol ditosylate (10 mmol), salicylaldehyde (25 mmol), and K_2CO_3 (50 mmol) in acetonitrile (50 mL) was heated at reflux for 24 h. After completion of the reaction monitored by TLC. The reaction mixture was filtered off; then, the solvent of filtrate was evaporated and purified by recrystallization from water/acetone.

General procedure for the synthesis of benzylidene Meldrum᾽s acid derivatives containing ethylene glycol spacers: A mixture of ethylene glycol based dialdehyde derivatives (5 mmol) and Meldrum᾽s acid (10 mmol) in ethanol (10 mL) was heated at reflux for 2-3 h. Upon cooling, solid materials were precipitated from the solution. These precipitates were filtered off, washed with hot water, and recrystalized from EtOH to afford pure products.

Results and Discussion: Oligo ethylene glycol ditosylate was obtained from the reaction of oligo ethylene glycol with para-tolyl solfunyl chloride stirring in dichloromethane. Optimization study for determining the reaction conditions for Knoevenagel condensation

reaction was initiated with Meldrum's acid. Dialdehyde obtained from the reaction of salicylaldehyde with ethylene glycol ditosylate in the presence of K_2CO_3 was reacted with the Meldrum's acid in ethanol at reflux (Scheme 1). It was satisfying to observe that the reaction was complete in 2-3 h and was typically characterized by the separation and spectroscopic characterization of a solid product in the reaction mixture.

Afterward, a variety of dialdehydes to check the viability of this protocol in obtaining a library of arylidene Meldrum's acid derivatives were used.

n = 0, 1, 2
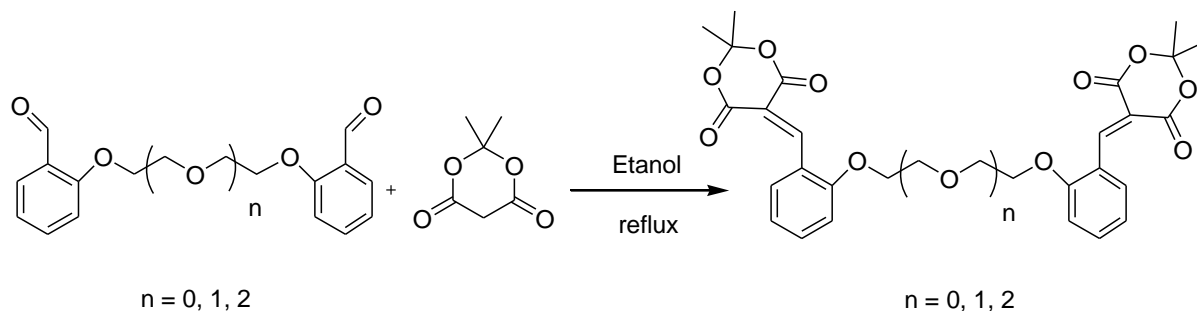
Scheme 1:. Synthesis of new arylidene Meldrum's derivatives

Conclusion: Reaction of ethylene glycol-based aromatic aldehyde derivatives with Meldrum's acid in ethanol produced novel benzylidene Meldrum's acid derivatives which contain good yields of ethylene glycol spacers. Structures of the products were deduced from their IR, ^{1}H-NMR, and ^{13}C-NMR spectroscopy.

References

[1] Zemtsov, A.; Levin, V. V.; Dilman, A. D.; Struchkova, M. I.; Belyakov, P. A.; Tartakovsky, V. A. *Tetrahedron Lett*., **2009**, *50*, 2998–3000.

[2] Fillion, E.; Carret, S.; Mercier, L. G.; Tre´panier, V. EA. *Org. Lett*., **2008**, *10*, 437- 440.

[3] Davidson, D.; Bernhard, S. A. *J. Am. Chem. Soc.,* **1948**, *70*, 3426–3428.

[4] Corey, E. J. *J. Am. Chem. Soc*., **1952**, *74*, 5897–5905.

[5] Aaron, M.; Dumas, Adam Seed, Alexander K. Zorzitto, and Fillion, *etrahedron Lett*., **2007**, 48, 7072–7074.

[6] Kraus, G. A.; Krolski, M. E. *J. Org. Chem.,* **1986**, *51*, 3347–3350.

[7] Scuster, P.; Polansky, O. E.; Wessely, F. *Monatsch. Chem*., **1964**, *95*, 53–58.

[8] Hedge, J. A.; Kruse, C. W.; Snyder, H. R. *J. Org. Chem*., **1961**, *26*, 3166–3170.

[9] Bigi, F.; Silvia Carloni, S.; Ferrari, L.; Maggi, R.; Alessandro, M.; Sartori, G. *Tetrahedron Lett*., **2001**, *42*, 5203–5205.

Theoretical study of a proposed molecular wire using quantum theory of atoms-in-molecules (QTAIM)

Safari, Reza[*]; Vahid dastjerdy, Mani

Department of Chemistry, University of Qom, Iran.

Email: safari_physicalchemistry@yahoo.com

****

Introduction: A wide variety of molecules have been suggested for uses as molecular devices (such as molecular wires, molecular diodes, molecular switches and so on). Among in a variety of molecules that can act as molecular device, the conjugated organic molecules and their derivatives are favorable molecules, due to their characteristic structures in electron transport [1-3]. Investigations on the electronic structures of any molecule as molecular device and its physical or chemical properties in conjugation systems are very important to understanding the electron transport in the nanowire. The current study investigated a proposed molecular device, using the quantum theory of atoms-in-molecules (QTAIM)[2]. Based On the QTAIM, the atomic electronic energy, $E_{elec}(\Omega)$, is given by $E_{elec}(\Omega) = K_{elec}(\Omega) + V_{elec}(\Omega)$, where $K_{elec}(\Omega)$ and $V_{elec}(\Omega)$ are total atomic kinetic and potential energies of the atomic basin(Ω), respectively. In this work, the external electric field effect on a proposed molecular system (M) were studied and thus analyzed. Then, using the results of QTAIM, suitable atomic basins to connect were identified the metal electrodes (Au4) to the proposed system and consequently to identified design of molecular device (E-M-E), Fig.1. In addition, using the Landauer formula ($G = \frac{2e^2\tau}{h}$, where τ is the electron transmission through the molecule, i.e., $\tau = \exp(-\beta L)$, here L is he molecular length and β is the tunneling decay parameter), electrical conductivity of molecular device (E-M-E), was investigated, Fig. 2.

Computational Methods: In this study investigated the electric field effects on structural, electronic and vibrational characteristics of a proposed molecular system (M) and then electrode − molecule − electrode (E-M-E) device, using density functional theory (DFT) at the UB3LYP/6-31G* level of theory, and LANL2DZ pseudopotential for gold atoms. To this end, the quantum theory of atoms-in-molecules (QTAIM) was used. Under a specific filed intensity, the voltage difference (V) applied on the two ends of the molecular wire, depends on the distance (L) of the two ends of molecule. Therefore, each applied field strength value (E) corresponds to a particular bias voltage V, applied over the length L of the molecular wire, as V = E.L. The values of electrical field intensities applied on the molecular wire are -10^{-2} to 10^{-2} a.u (in the X axis).

Results and Discussion: The results showed that the HLG (energy gap between frontier orbitals HOMO and LUMO) and consequently the electrical conductivity, electronic energy of atomic basin and electrical dipole moment were dependent on applied electric field properties (intensity and direction) in a nonlinear manner, Fig.3. In addition, the current–voltage characteristic curve is estimated for the proposed molecular device and results showed that the proposed molecular device, could be used in real nanoelectronic circuits as a molecular wire, considering the acceptable electrical conductivity of the device. Moreover, analysis of the results obtained from QTAIM showed that the pattern of electron density topology (and it's Laplace, corresponding electronic kinetic energy) in molecular systems is

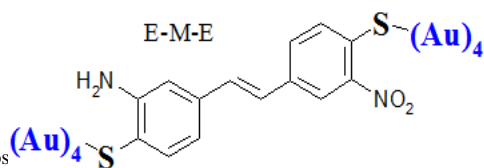related to the applied field properties, Tab. 1, and the electronic properties of atomic basins system, Fig. 4.
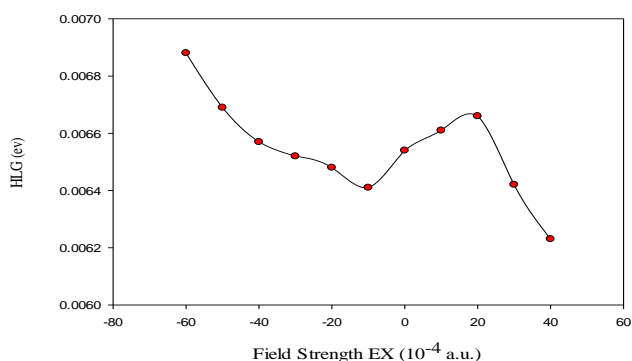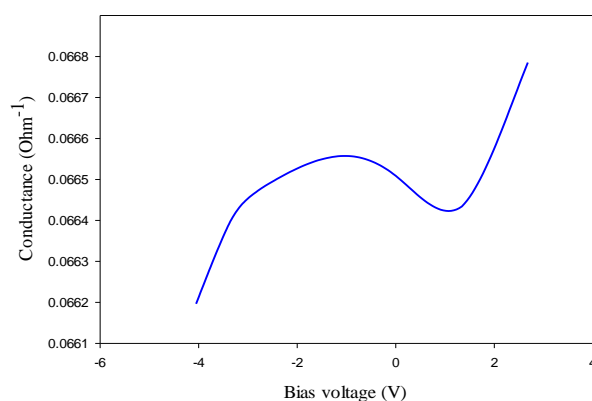

Fig.1: A propos

Fig. 2: The G-V (conductance – voltage) characteristic curve at various electric field intensities, calculated at DFT-UB3LYP/6-31G* level of theory and landuer Formula, for the proposed molecular wire ,Fig. 1.

Fig. 3: Electric field effects on the HLG of the proposed molecular wire, Fig.1.

S (left) Field Intensity	$\rho(r)$	$\nabla^2\rho(r)$	q (Ω)	E_{elec}
-100	1.57663	-6.78200	2.33633	-3.98726
-60	1.56955	-6.77472	3.04466	-3.98700
0	1.56059	-5.86773	3.94083	-3.98684
60	1.55284	-8.57446	4.71536	-3.98671
100	1.54487	-7.80885	5.51232	-3.98664

Table 1: Electric field effects on the electron density, $\rho(r)$, Laplacian of the electron density, $\nabla^2\rho(r)$, electrical charge, q (Ω), and electronic energy ,E_{elec}, of the left sulfur atomic basin (all in a.u.).
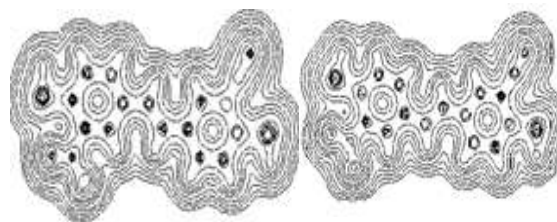

Fig. 4: Contour maps of the electron density of the proposed molecular system (M) in E =10^{-3} a.u.(left) and in E =10^{-2} a.u.(right) electric field intensities .

Conclusion: Investigations on the geometric, vibrational and electronic structures of any molecule as molecular device are very important to understanding the electron transport in the molecular electronic device (wire). Therefore, the study of electronic and vibrational response to any atomic basins in applied electric field can be an approach for theoretical design of optimal field-effect molecular devices (with high performance). In this regard and based on the method used in this article and using QTAIM, it is expected that we conduct a fundamental (atomic scale) study of molecular electronic device.

References:

[1] R. F. W. Bader, *Atoms in Molecules*: *A Quantum Theory*, Oxford University Press: Oxford, U.K, 1990.
[2] A. Salomon, D. Cahen, S. Lindsay, J. Tomfohr, V. B. Engelkes, C. D. Frisbie, *Adv. Mater*, **15**, 1881 (2003).
[3] H. Sabzyan, R. Safari, *Europhys. Lett*. **77**, 39335 (2012).

Simultaneous differential pulse voltammetry measurement of epinephrine, acetaminophen and tryptophan on a modified glass carbon electrode (GCE) by polymer(7,11b-Dihydroindeno[2,1-c]chromene-3,4,6a,9,10(6H)-pentol)(Haematoxylin)

**AzamGholinia**[*] **, DR.Taee , DR.Hasanpoor**

Omid5458@ymail.com

❊❊❊❊

Introduction: The modified electrodes is one of the exciting developments in the field of electro analytical chemistry. The different strategies have been employed for the modificationof the electrode surface. The motivations the modifications of the electrode surface are: (a) improved electro catalysis, (b) freedom from surface fouling and (c) prevention of undesirable reactions competing kinetically with the desired electrode process. Epinephrine (EP) is an important catecholamine neurotransmitter in the mammalian central nervous system. Therefore, the determination of EP has attracted much attention of researchers.Acetaminophen (AC),tryptophan (Trp) are oxidized at nearly the same potential with poor sensitivity at unmodified electrodes. The overlap of their voltammetry responses makes their simultaneous determination highly difficult.

Methods / Experimentals: In this study, simultaneous determination of AC, EP, andTR were carried out by differential pulse voltammetry in modified GCE. A modified electrode was fabricated by electro polymerization of polymer on a bare glassy carbon surface. The effect of different variable

such as pH, scan rate, Curves adjustment monomer concentration in electro polymerization was studied and optimized.Individual and simultaneous determination of EP,AC,and,TR were carried out by differential pulse voltammetry.

A higher catalytic activity was obtained for electro catalytic Oxidation of epinephrine (EN),Acetaminophen (AC) andtryptophan (Trp) in pH 5 phosphate buffer solution (PBS) at polymer modified glassy carbon electrode due to an enhanced peak current and well-defined peak separations compared with bare glassy carbon electrode (GCE).
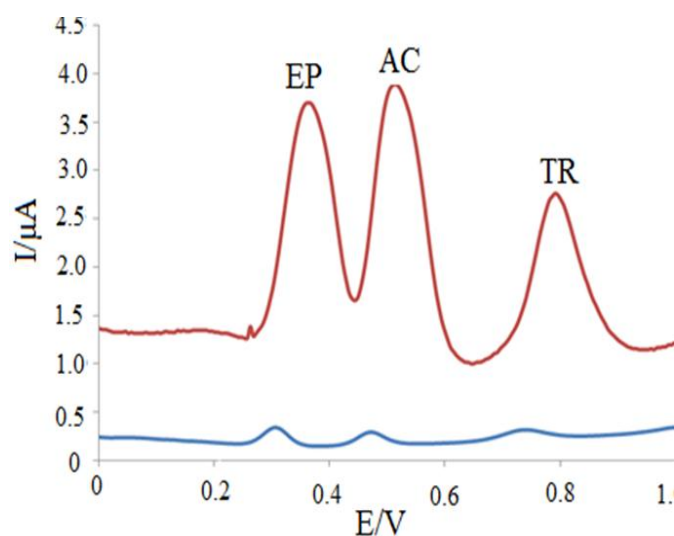
For the ternary mixture containing EP,AC and TR, the three compounds can well separate from each other at the scan rate of ٠.٠-١.٥ mVs−١ with a potential difference of ٣.٤٢E-٦ , ٥.٤٢E-٦,٧.٧٢E-٦ mV between EP,AC,TR respectively, which was large enough to determine EP,AC,and,TR individually and simultaneously.

Conclusion: The oxidation peak potentials of the threecompounds were observed to shift positively with an increasein the scan rate. The oxidation processes of EP, AC and TR in the ternary mixture at the (Haematoxylin)modified electrode were the same as that of the individual compound.
.

References

[١] Cag˘rıCeylanKocak, ZekeryaDursunJournal of Electro analyticalChemistry(٢٠١٣) ٦٩, ٩٤–١٠٣

[٢] Wang Ren, Hong QunLuo, Nian Bing LiBiosensors and Bioelectronics (٢٠٠٦) ٢١, ١٠٨٦–١٠٩٢

[٣] Mohammad Mazloum-Ardakania,∗, HadiBeitollahi a, Mohammad KazemAminib, FakhradinMirkhalafc, Bibi-FatemehMirjalili a, Biosensors and Bioelectronics (٢٠١١),٢٦, ٢١٠٢–٢١٠٦

Synthesis of different shape of gold nanoparticles and investigation of particles shape on photothermal therapy of cancer cells.

Asrin Pakravan, Roya Salehi, Mehrdad Mahkam*

Department of Chemistry, Faculty of Basic Sciences, Azarbaijan Shahid Madani University, Tabriz, Iran
Mmahkam@yahoo.com

Introduction

To date, surgical resection has been employed as the widespread therapeutic method for the most cancers. There are, however, several drawbacks such as a required large incision accompanied by pains and a second operation for bilateral diseases[1]. Photothermal therapy (PTT), one of the major modalities for the treatment of cancer, has experienced a tremendous revolution from traditional laser therapy to nanotechnology driven photothermolysis[2]. Well-designed photothermal nanostructures have attracted many scientists pursuing a better means to assess the efficacy of cancer treatment. Recently, gold-based nanostructures have enabled photothermal ablation of cancer cells with near-infrared (NIR) light without damaging normal human tissues [1]. One particularly promising area of research focuses on the unique optical properties of metal nanostructures known as localized surface plasmon resonance (LSPR). When a metal nanostructure is illuminated with light, the photons are strongly absorbed or scattered at specific resonant wavelengths.
The absorbed light can be transformed into heat, a process known as the photothermal effect, allowing for an increase in temperature to be triggered and managed from a distance. When tissues are heated above the hyperthermia temperature (42°C), irreversible cellular damage occurs. The heat generated from the photothermal effect can be used to destroy cancer cells directly or trigger drug release.
 To maximize the amount of heat generated, it is important both to match the resonant wavelength of the nanostructure with the light source and to ensure that the maximum amount of radiation reaches the treatment site[3]. By changing the structure and shape, the LSPR frequency of gold nanoparticles can be tuned to near infrared (NIR) region, where light penetration in tissue is optimal. Current gold analogs under study include spherical Au NPs, gold nanoshells, gold nanorods, gold nanocages and gold nanostars[4].

Experimentals

Gold nanoparticles are made in different sizes, shapes, and structures by the chemical method in presence of reduction agent and effective surfactant to prevent aggregation of fine nanoparticles and functional shaping agent to form the different AuNPs in one step. The morphology, size, monodispersional state and shape of synthesized gold nanoparticles were determined using typa of analysis.Note that all the glassware before of uses should be washed with Aqua Regia (HCl and HNO_3 at the ratio of 3:1 by volume) and rinsed with ultrapure water repeatedly before use.

Results and Discussion

To measure the photothermal conversion performance of different shape AuNPs, the solution of the gold nanoparticles quartz cell and exposed to the 808 nm laser source at a distance of 2 cm. The original temperature was maintained at ~25° C. The synthesized AuNRs were characterized by the TEM image and UV-vis absorption spectrum analysis. Gold nanospheres

have one visible absorption band around 520 nm. The surface plasmon absorption of gold nanorods have two bands: a strong long-wavelength band due to the longitudinal oscillation of electrons around 800nm and a weak short-wavelength band around 520 nm due to the transverse electronic oscillation and for gold nanostars has a broader absorption peak at about 700 nm are showen in figure1A. The transmission electron microscopy (TEM) image of the nanorods with an aspect ratio of 3.9 is shown in Figure 1B.
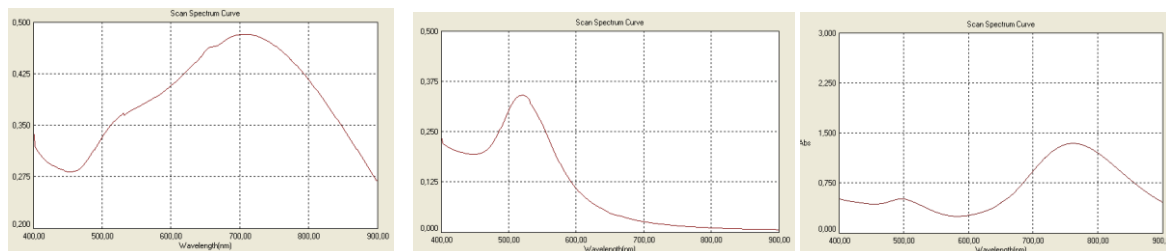

Figure1, A) UV_vis spectra taken from aqueous suspensions of Au nanostars, Au nanoparticles and
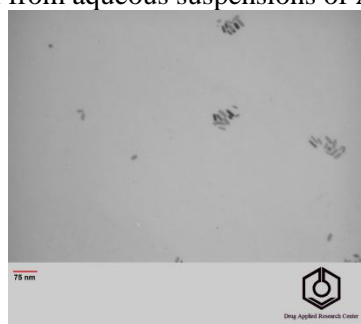

Figure1 B) TEM of Au nanorods

The surface plasmon absorption spectra of gold nanospheres shift to the NIR region as the diameter of the nanoparticle increases. Gold nanorods can be is red-shifted when the aspect ratio increases, but the absorption peaks are also weak compared to stars as seen in figures 1.

Conclusion

Our comparison studies for applications in photothermal cancer treatment potential use of different Au nanoparticles, indicated that all Au nanostructures could absorb and convert NIR light into heat. We compared the photothermal conversion efficiencies of different types of Au nanostructures by measuring the temperature rise for their aqueous suspensions upon laser irradiation. The photothermal conversion efficiency per Au atom was highest for nanostars, followed by nanorods, and then nanoparticles.

References
[1] Jihye Choi1; Jaemoon Yang2; Eunji Jang. *Anti-Cancer Agents in Medicinal Chemistry,* **2011***, 11,* 1-12.

[2] Xiaohua Huang; Bin Kang Wei Qian Megan A. Mackey; Po C. Chen Adegboyega K. Oyelere. *Journal of Biomedical Optics*, **2010**, *15(5),* 1-7.

[3] Claire M Cobley; Leslie Au; Jingyi Chen. *Expert Opin. Drug Deliv*, **2010**, *7(5)*, 577-587.

[4] Xiaohua Huang a; Mostafa A; El-Sayed. *Alexandria Journal of Medicine*, **2011**, *47*, 1–9.

Synthesis of mesoporous molybdenum sulfide and the study of its photocatalytic applications for removal of organic dyes

Mohammad Hadi Mokari-Manshadi[a], Mohamad Mahani[a,*], Zahra Hassani,[b] Dariush Afzali,[c] Esmat Esmaeilzadeh,[d]

[a] *Department of Chemistry and Nanochemistry, Faculty of Sciences and Modern Technologies, Graduate University of Advanced Technology, Kerman, Iran.*

[b] *Department of New Materials, Institute of Science, High Technology and Environmental Sciences, Graduate University of Advanced Technology, Kerman, Iran.*

[c] *Environment Department, Institute of Science, High Technology and Environmental Sciences, Graduate University of Advanced Technology, Kerman, Iran*

[d] *Research & Development Centre, Water & Environment Researches, Sarcheshmeh Copper Complex, Rafsanjan, Iran.*

Corresponding Author E-mail: mohmahani@gmail.com

****

Introduction: Due to with weak van der Waals gap and thus excellent properties in the field of heterogeneous catalysis and lubrication, molybdenum sulfide have attracted many researchers in recent years [1]. In addition to the narrow band gap of about 1.8 eV that results in strong absorption in the solar spectrum region, MoS_2 is nontoxic, environmental friendly and abundant semiconductor. On the other hand mesoprous materials, due to their high surface area, larger pore volume and diameter attracting much attentions [2]. Molybdenum disulfide nanostructures were synthesized by different methods such as gas phase reactions, laser and sonochemical routes. These methods are expensive and need special devices. Thus simple and low cost procedures such as hydrothermal methods are highly regarded. Removal of harmful organics by mesoporous materials has drawn much attention recently. Organic dyes are aromatic chemical colors that widely used in the textile industry. As a result of aromaticity properties, these colors are often toxic, carcinogenic, mutagenic and resistant to biodegradation. MoS_2 shows unique properties in the photodegradation of organic compounds such as methyl orange and phenol [3].

Methods: In a typical synthesis, 3 mmol of Na_2MoO_4 (0.73g) and 9 mmol of Na_2S were added into 30 mL of deionized water. Then 12 mol/L HCl was dropped into the solution while stirring to adjust the pH value to less than 1. The solution was transferred into a Teflon-lined stainless steel autoclave and heated at 180°C for 24 h. After cooled to room temperature, the resulting mixture of MoS_2 were centrifuged at 10000 rpm for 10 minutes, washed with distilled water, dried at 60 °C for 12 h and then was annealed in a conventional tube furnace at 750 °C for 2 h with the argon gas flow to prevent oxidation.

In order to study the removal of methylene blue (MB), the batch experiments were carried out with 10 ml of 5 mg/L dye solutions prepared using deionized water. The MB solution with the 2 mg of nanostructures was stirred by a magnetic stirrer with speed 200 rpm in room temperature. During the experiments, 1ml of solutions were withdrawn at regular intervals. The absorbance (A) of MB solution was measured every 15 min by a Uv-Vis spectrophotometer.

Results and Discussion: In this study mesoporous molybdenum sulfide were synthesized successfully by hydrothermal method. The morphology and structural properties of the annealed nanostructures were studied by SEM analysis. It can be seen that the SEM image of the MoS_2 sample reveals a mesoporous morphology. These nanostructures were used as adsorbent and heterogeneous nanocatalyst for remove of methylene blue as an environmental pollutant organic dye. Optimum condition for removal process was neutral pH and room temperature. The removal efficiency of methylene blue on the MoS_2 mesoporous nanostructures was evaluated using the absorbance of MB solution at a wavelength of 665 nm from the formula: $E= (A_0-A)/A_0\times100$, where A_0 is the initial absorbance. The removal yields of methylene blue by annealed MoS_2 mesoporous nanostructure was 98% in 30 minutes which is high enough in comparison to bulk MoS_2 with 54% yields and other metal sulfide photocatalysts such as NiS_2, FeS_2 and CoS_2.

Conclusion: In summary, mesoporous MoS_2 nanostructures were prepared by a facile and effective hydrothermal approach. Synthesized MoS_2 mesoporous show excellent performance as a photocatalyst for removal of methylene blue under visible light in comparison to its bulk counterpart due to high surface area. MoS_2 may be more active than other photocatalyst because of its effective absorption in the solar spectrum region due to a narrow band gap.

References

[1]   Shi X-R, Jiao H, Hermann K, Wang J, CO hydrogenation reaction on sulfided molybdenum catalysts, Journal of Molecular Catalysis A: Chemical, 2009, 312, 7-17.
[2]   Yonemoto BT, Hutchings GS, Jiao F, A General Synthetic Approach for Ordered Mesoporous Metal Sulfides, Journal of the American Chemical Society, 2014, 136, 8895-8898.
[3]   He Z, Que W, Dang Y, He Y, Hou Z, Characterization and adsorption characteristics of mesoporous molybdenum sulfide microspheres, Materials Letters, 2014, 120, 58-61.

Intercalation of Vanadate Ions in Ni-Fe-Layered Double Hydroxide Nanoparticles

Kamellia Nejati [a]*, Soheila davari [a], Alireza Akbari [a], Parvaneh dalir kheyrollahi [a], Zolfagar rezvani [b], Karim Asadpoor Zeynali [c]

a Department of chemistry, Payam-e- Noor University, P.O.Box,19395-3697 Tehran, Iran

b Department of chemistry, Azarbaijan university of Tarbiat Moallem, 5375171379,Tabriz,Iran

c Department of Analytical Chemistry, Faculty of chemistry, Tabriz University, Tabriz, Iran

e- mail: nejati_k@yahoo.com

****

Introduction

The cationic and anionic clays having surface charge and layered structure are used to intercalate organic and inorganic anions to alter the properties[1]. Layered double hydroxides (LDHs) are considered to be the new generation materials in areas such as nanomedicine, adsorbents, catalysis, etc [2]. LDHs have the general formula $[(M^{II})_{1-x}(M^{III})_x(OH)_2]^{x+}(A^{n-})_{x/n} \cdot mH_2O$, where M^{II} and M^{III} are divalent and trivalent metal cations, respectively, and A^{n-} is an anion. Due to their ion exchange capability many novel compounds can be synthesized. Therefore, by changing metal ions, composition, and interlayer anions, a series of materials can be generated with different structures and properties. As an illustration, complex ions such as $[Fe(CN)_6]^{3-}$ and $[Mo(CN)_8]^{4-}$,vanadate and etc, become electroactive when intercalated in LDHs films, which has been used to enhance the efficiency of electrodes[3]. We report here the synthesis and characterization of vanadate intercalated Ni^{II}/Fe^{III} layered double hydroxide nanoparticles.

Methods/Experimental

In a typical synthesis, 0.45mmol of $Ni(NO_3)_2.6H2O$, 0.05 mmol $Fe(NO_3)_3.9H2O$ and 0.1gr vanadate were first dissolved in 10mL of distilled water. Then 0.12gr of urea was added to the above solution and stirred for 30min. The resulting solution was transferred into 20mL Teflon-lined autoclave and hydrothermally treated at 160 °C for 10h.The final products were collected by centrifugation, repetitively washed and vacuum dried.

Results and Discussion

In the FT-IR spectra of vanadate intercalated Ni^{II}/Fe^{III} layered double hydroxide nanoparticles, the broad band in the range of 3200 – 3700 cm^{-1} is related to the O–H stretching of the metal hydroxide layers and interlayer water molecules. The band at1625 cm^{-1} is due to bending vibrations of water molecules. Another bands (<800cm^{-1})are attributed to the M-O-H and O-M-O bending vibrations[3]. The absorption close to 1415cm^{-1} is due to

the interlayer vanadate species in LDH. The XRD patterns of the vanadate intercalated- LDH (Fig 2) showed the characteristic reflections related to (003), (006), (009) and (110) plans respectively. In comparison with Ni–Fe–NO$_3$-LDH precursor, the increase in basal spacing and shift of the basal reflection (003) to a lower 2θ angle indicated that vanadate ions were intercalated into LDH by replacing NO$_3^-$ ions.
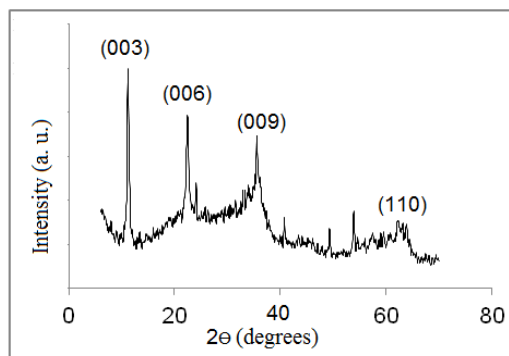

Fig. 2. The XRD patterns of the vanadate intercalated Ni/Fe- LDHϴ

Transmission electron microscope was used to examine the size of the crystals and morphology of the LDH. The TEM image of vanadate intercalated Ni/Fe- LDH showed that the nanoparticles has a plate-like shape.

Conclusion

Vanadate intercalated Ni/Fe- LDH   nanoparticles with an Ni/Fe ratio of 9 has been successfully synthesised by a coprecipitation technique. The XRD, FT-IR and TEM analysis show that the original interlayer nitrate anions of hydrotalcite can be replaced by vanadate anions. The larger interlayer spacing for vanadate -intercalated LDHs determined by XRD analyses. The TEM image of vanadate intercalated Ni/Fe- LDH showed LDH had a plate-like shape.

References

 [1] S.Kwak; W. M.Kriven; M. A.Wallig; J.Choy, *Biomaterials ,***2004**, *25*, 5995-5999.

 [2] A. I.Khan; L.Lei; A. J.Norquist; D. Hare, *Chem Commun. (Cambridge)* **2001**, 2342-2348

[3] H. S.Panda; R.Srivastava; D. J. Bahadur, *Nanosci. Nanotechnol.* **2008**, *8*, 4218-4230.

Microwave-assisted synthesis and Biological Evaluation of 2-Hydrazolyl-4-Thiazolidinones

Department of Organic Chemistry, University of Guilan, PO Box 41335-1914, Rasht, Iran

Samaneh Mohammad Gholipour, Nosratollah Mahmodi*

Email: mahmoodi@guilan.ac.ir

Introduction:

4-Thiazolidinones are an important group of heterocycles found in numerous natural products and pharmaceuticals. Thiozolidinones possess various biological activities such as antitumor, anti-HIV, antibacterial, and antidegenerative.

Multi-step or cascade reactions can be defined as the combination of two or more reactions in a specific order rather that occur in one pot. They are very attractive due to their ease of setup in comparison to the traditional single-step processes, the reaction and product isolation are carried out independently and repeatedly to synthesize the target compounds. The former process allows a minimization of waste and compared to stepwise reactions, the amount of solvent, reagents, adsorbents, and energy is extensively decreased.

Methods / Experimentals:

To a stirred solution of benzaldehyde (300 mg, 2.0 mmol) in toluene (1 mL) and DMF (1 mL) were added thiosemicarbazide (220 mg, 2.4 mmol), Ksf@Ni (30 mg, 0.2 mmol,), and maleic anhydride (987 mg, 10.0 mmol).The reaction mixture was heated in a stirred microwave vial for (3-10) min at 120 (200 W), poured into water (30 mL), and extracted with ethyl acetate (3 x30 mL). The combined organic layers were dried (Na2SO4), filtered, andconcentrated. The residue was finally recrystallized from methanol to give as a white solid.
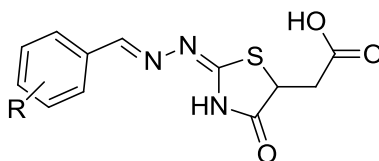
Results and Discussion:

 we explored the microwave mediated tandem reactions of aldehydes, thiosemicarbazide, and maleic anhydrides to produce 2-hydrazolyl-4-thiazolidinones, with reasonable yields. The advantages in the use of this methodology are shorter reaction times, higher yields, and a minimization of synthetic operations, solvent use, and waste generation. When we investigated the scope of the tandem synthesis for hydrazolyl-4-thiazolidinones 5, we were able to demonstrate that the process is general for electron withdarwing, electrondonating aldehydes. In continuation to our previous studies in synthesis of novel heterocyclic compounds [1-2] here, we decided to synthesize thiazolidinones via three component one-pot reaction of aldehydes, thiosemicarbazide and maleic anhydride in the presence of heterogeneous catalyst KSF@Ni under microwave irradiation. The use of microwave ovens to perform organic synthesis has

received a great deal of attention over the last 10 years. Several publications have shown that microwave irradiation can circumvent the need for prolonged heating, and it is generally accepted that this source of energy minimizes side reactions and acceleratesthe rate of chemical reactions. Herein, we wish to report an efficienttandem procedure for the synthesis of 2-hydrazolyl-4-thiazolidinones under microwave conditions.Different solvents and various reaction equivalents were explored until we obtained good isolated yields of thiazolidinones Microwave heating for the synthesis of thiazolidinone resulted in a significantly better yield compared tothermal conditions Microwave irradiation also allowed for a faster conversion .

Conclusion:

In summary, in this investigation we explored the microwavemediated tandem reactions of aldehydes, thiosemicarbazide,and maleic anhydrides to produce 2-hydrazolyl-4-thiazolidinones,with yields ranging from 70% to 97%. The advantages in the use of this methodology are shorter reaction times, higher yields, and a minimization of synthetic operations, solvent use, and waste generation.

References:

[1] B. Sharifzadeh, N. O. Mahmoodi, M. Mamaghani, K. Tabatabaeian, A. SalimiChirani, I.Nikokar,

Bioorg. Med. Chem. Lett.23(2012) 548.

[2] N. O. Mahmoodi, S. Ramzanpour, F.GhanbariPirbasti, Arch. Der pharm. 348 (2015) 275.

Synthesis of new derivatives 1,2,3- Triazoles catalyzed by MCM-41-supported aminothiophenol-Cu (I)

Ahmad Kakavand Ghalenoei, Mohammad Bakherad*, Ali Keivanloo

School of Chemistry, Shahrood University of Technology, Shahrood, I. R. IRAN

Corresponding author E-mail: m.bakherad@yahoo.com

1. Introduction

1,2,3-triazoles have received significant attention as one of the most important heterocycles displaying interesting biological activities, such as anti-HIV4 and GSK-3 inhibiting activity [1], and have been widely applied in many research fields [2].

The classical method for their synthesis involved thermal 1,3-dipolar cycloaddition of organic azides with alkynes [3]. Nevertheless, this approach researcher have reported methods for the synthesis of 1,2,3-triazoles suffer from drawbacks such as high temperature, lack of selectivity, drippy work-up procedures owing to the application of homogeneous catalyst and low yields [4]. Thus to overcome these drawbacks an improved procedure involving Cu(I)-catalyzed azide alkyne 1,3-dipolar cycloaddition was reported, which provided high regioselectivity, room temperature reaction and enlarged scope [5].

2. Experimental

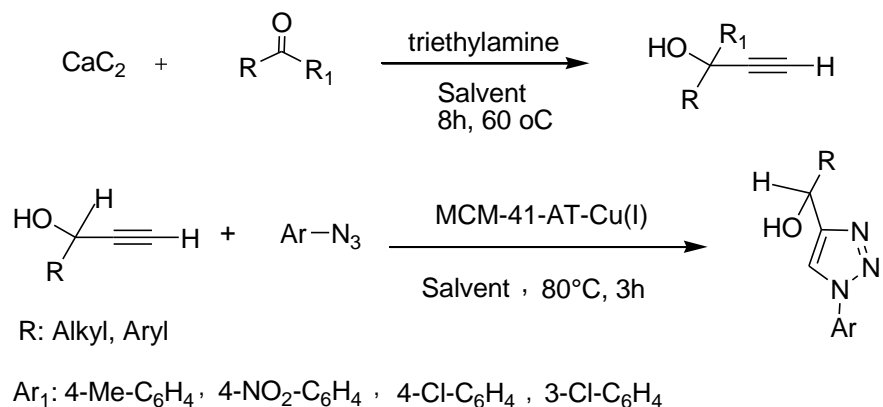### 2.1. *Preparation of propargyl alcohol*

Aldehydes or ketones (1 mmol), calciumcarbide (2.5 mmol) and triethylamine (0.2 mmol) were added to the solvent DMSO/H2O 50:1. After the mixture was stirred for 8 hours at 70 °C, propargyl alcohols were obtained in good to high yields.

2.2. *Preparation of 1,2,3- Triazoles in the presence of MCM-41-aminothiophenol-Cu(I)*

In a typical experimental procedure, a mixture of propargyl alcohol and aryl azids over a surface of MCM-41-aminothiophenol-Cu(I) was stirred for 3 hours at 80 °C (TLC). The mixture was then extracted with ether (3×10 mL). The combined organic phases are washed with brine (2×5 mL), dried over anhydrous MgSO4 and concentrated in vacuo. The residue was subjected to flash column chromatography with hexane/EtOAc (9/1) as eluent to afford the pure product.

3. Results and discussion

At the beginning of, we encouraged by the successful synthesis of 1,4-disubstitued 1,2,3-triazoles through the 1,3-dipolar cycloaddition of propargyl alcohol and aryl azids in the presence of MCM-41-aminothiophenol-Cu(I) as semi heterogeneous catalyst supports. We have created 1,3-dipolar cycloaddition of propargyl amines and aryl azids to regioselectively construct 1,4-disubstitued 1,2,3-triazoles. We report the synthesis of MCM-41-supported aminothiophenol-Cu (I) complex (MCM-41-AT-Cu(I) as an efficient catalyst for the synthesis of 1,4-disubstitued 1,2,3-triazoles. The (MCM-41-AT-Cu(I) catalyst was prepared by stirring MCM-41-$(CH_2)_3$-Cl and aminothiophenol in n-hexane for 24 h, then MCM-41-aminothiophenol was treated copper iodide was added and the resulting mixture was refluxed for 15 h. The resulting yellow solid impregnated with the metal complex was filtered and washed with ethanol to obtain MCM-41-AT-Cu(I).

CaC$_2$ + R−CO−R$_1$ →(triethylamine, Salvent, 8h, 60 oC)→ HO−C(R)(R$_1$)−C≡C−H

HO−C(R)(H)−C≡C−H + Ar−N$_3$ →(MCM-41-AT-Cu(I), Salvent, 80°C, 3h)→ triazole product

R: Alkyl, Aryl

Ar$_1$: 4-Me-C$_6$H$_4$, 4-NO$_2$-C$_6$H$_4$, 4-Cl-C$_6$H$_4$, 3-Cl-C$_6$H$_4$

4.Conclusion

In conclusion, we described a novel and an efficient method for the synthesis of 1,4-disubstitued 1,2,3-triazoles in good to high yields *via* copper (I)-catalyzed reaction of propargyl alcohol and aryl azids under mild conditions. In addition, this methodology offered the competitiveness of recyclability of the catalyst, and the catalyst could be readily recovered by a simple filtration and reused for 5 cycles, and thus making the procedure environmentally more friendly

References:

[1] P.H. Olesen, A. R. Sørensen, B. Ursø, P.Kurtzhals, A.N. Bowler, U. Ehrbar and B. F. Hansen, J. Med. Chem., **2003**, *46*, 3333–3341.

[2] (a) N. J. Agard, J. A. Prescher and C. R. Bertozzi, J. Am. Chem. Soc., **2004**, *126*, 15046–15047; (b) H. C. Kolb and K. B. Sharpless, Drug Discovery Today, **2003**, *8*, 1128–1136.

[3] L. D. Pachón, J. H. van Maarseveen and G. Rothenberg, Adv. Synth. Catal., **2005**, *347*, 811; (e) G. Molteni, C. L. Bianchi, G. Marinoni, N. Santo and A. Ponti, New J. Chem., **2006**, *30*, 1137.

[4] K.V. Gothelf and K.A. Jorgensen, Chem. Rev. **1998**, *98*, 863.

[5] (a) V. V. Rostovtsev, L. G. Green, V. V. Fokin and K. B. Sharpless, Angew. Chem.. Int. Ed., **2002**, *41*, 2596; (b) C. W. Tornoe, C. Christensen and M. Meldal, J. Org. Chem., **2002**, *67*, 3057.

Catalyst-free dehalogenation of 5-bromopyrimidine derivatives using DMF/trialkylamine as the hydrogen source

Mahsa Mousavi, **Mehdi Bakavoli**[*]**, Ali Shiri, Hossein Eshghi**

Department of Chemistry, Faculty of Science, Ferdowsi University of Mashhad, 91775-1436 Mashhad, Iran

**Email address:** mbakavoli@um.ac.ir

Introduction:
A wide range of synthetically valuable transformations in organic chemistry involve reduction process through which functionalization can be easily performed over the course of the reaction. While several reduction methodologies utilizing transition metals as catalysts, non-catalytic methods are of more interest as they offer safe and inexpensive synthetic protocols. Reports on dehalogenation of halo-uracils involve photochemical reductions through irradiation in aqueous alcoholic solvents [1-4], thermolysis in acetamide [5], sonication in the presence of Indium metal[6], and reduction under physiological conditions [7-8].

Experimental:
A mixture of 5-bromo-2,4-diamino-6-substituted pyrimidine and trialkylamin in DMF was heated with stirring over the range of 80 – 120 °C. After the completion of the reaction, the solvent was evaporated under reduced pressure and the product was purified by column chromatography.

Result and discussion:
The reaction of halogenated pyrimidines with the mixture of DMF/R_3N gives rise to the dehalogenated product. The reaction can be completed within hours and the obtained product can be easily purified by column chromatography. The optimum temperature for this reaction is set on 80 to 120°C. Other trialkylamine also was tested to efficiently work in this reaction as well. (Scheme 1)
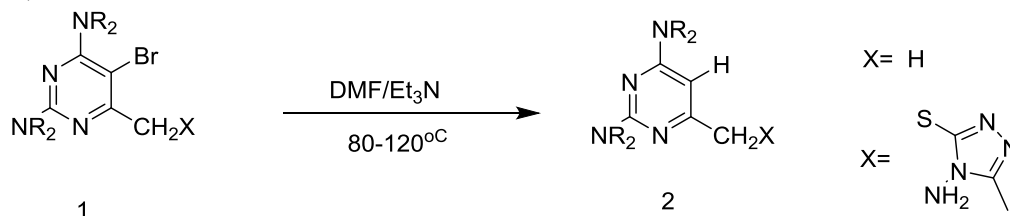
X \ NR₂	NR₂						yield
X= H	O⟶N	⟶N	Me⟶N	Ph—N⟶N	Me⟶N⟶Me	⟶N	Up to 85%
X= (triazole)	O⟶N	⟶N	Me⟶N	Ph—N⟶N	Me⟶N⟶Me	⟶N	Up to 80%

Scheme1

To propose a mechanism we referred to the frequently reported publications wherein amines are well-known as efficient electron-donors in Electron Transfer catalytic reactions [9,10]. Owing to the molecular orbital theory calculations which considers pyrimidine as a moderate electron acceptor [11], it is estimated that temperature could have initiated the Electron Transfer process (Thermal Electron Transfer); leading to a single electron transfer from Et_3N-DMF complex to the 5-bromopyrimidine. At least 10 several derivatives of 5-halogenopyrimidines and uracil were successfully reduced under the same reaction conditions. In all cases emerging a singlet signal between 5-6 ppm in ^{1}H NMR and a signal at 91 ppm in ^{13}C NMR besides other spectral characterizations, strongly confirms the replacement of bromide with a hydrogen atom in the product.

Conclusion:
We have developed a novel metal catalyst-free procedure for reduction of 5-bromo pyrimidines using Et_3N/DMF as a potential reducing system. To the best of our knowledge this is the first report of dehalogenation reaction using DMF, in the absence of metals. The system can tolerate amine and sulfide functionalities. Our results may provide a new route to the reduction of more other organic compounds.

References:
[1]   B. Matasovic, M. Bonifacic. *Radiation Phys. Chem.***, 2011**, 80, 750–754.
[2]   B. J. Swanson, J. C. Kutzer, T. H. Koch. *J. Am. Chem. Soc*, **1981**, 103, 1274-1276.
[3]   T. M. Dietz, T. H. Koch. *Photochem. Photobio.*, **1989**, 49, 121-129.
[4]   L. Venkatarangan, D.H Yang, G. A. Epling, A. K. Basu. *Tetrahedron Lett.*, **1999**, 40, 1441-1444.
[5]   M. Sako, M. Suzuki, M. Tanabe, Y. Maki. *J. Chem. Soc., Perkin Trans. 1*, **1981**, 3114-3117.
[6]   K. Tanaka, T. Kamei, A. Okamoto. *Tetrahedron Lett.*, (**2007**), 48, 3167–3169.
[7]   S. Mondal, D. Manna, G. Mugesh. *Angew.Chem. Int. Ed*, **2015**, 54, 9298 –9302.
[8]   H. W. Barrett, R. A. West. *J. Am. Chem. Soc*, **1956**, 78, 1612–1615.
[9]   S. Nad, H. Pal, *J. Chem. Phys*, **2002**.116, 1658-1670.
[10]   J. Hu, J. Wang, T. Nguyen, N. Zheng, *Beilstein J. Org. Chem*, **2013**, 9,1977–2001.
[11]   B. Pullman, A. Pullman, *Biochemistry*, **1958**, 44, 1197-1202.

Synthesis of Co Doped ZnO Nanorods and Their Solar Photocatalytic Properties for Dye Degradation

F. Ebrahimzadeh,[*١] **A. Abasi,**[١] **R. Rooydell,**[٢] **C.P Liu**[٢]

[١]Department of Chemistry, Marvdasht Branch, Islamic Azad University, Marvdasht, Iran.

[٢] National Cheng Kung University, Department of Materials Science and Engineering, Tainan, Taiwan

Email: polychemfar@miau.ac.ir,

Introduction

Nanostructures ZnO have many potential application in photocatalysis, solar cell, antibacterial action and so on. [١] Recently, modified ZnO was prepared by doping with transition metal such as Ag [٢], Mn [٣], Co[٤] and Pd,[٥].The results of these transition metals doped ZnO show that the optical, magnetic and electrical properties changed with the change in concentration of transition metal. The doping of Co in ZnO is expected to modify absorption, and other physical or chemical properties of ZnO.

Experimental

٠.٢٥M of $Zn_xCo_{1-x}AA$ was dissolved in distilled (DI) water/ethanol (H_2O/EtOH) solution of ٢٠ ml under magnetic stirring for ٢٠ minutes. [٦] The mixture solution was then sealed up in a ٢٠ ml bottle that was subsequently heated up slowly to ٨٥°C and kept for١h, prior to the immersion of a substrate [Si substrate (١ cm^2] coated with a ZnO film obtained by sputtering) into the solution to grow Co-doped ZnO NRs using $Zn_xCo_{1-x}AA$ precursors with various x via hydrothermal method.

Result and discussion

In this work, we present a simple hydrothermal route to the synthesis of Co doped ZnO nanorods with controllable doping concentration at a low temperature (٨٥°C) by using a bi-metallic metal-organic complex comprising of both Zn and Co in a single metal-organic precursor as continue of our research [٧]. The resultant nanorods were characterized by X-ray diffraction (XRD), energy dispersive X-ray analysis (EDX), and X-ray photoelectron spectroscopy (XPS), and scanning electron microscopy (SEM).

The morphology of the as-synthesized ZnO NRs and also the comparison between X-ray diffraction of Co-doped ZnO nanorods with ZnO nanorod was shown in figure ١ . The derived products are all shaped in ١D short rods. The density and diameters of the NRs exhibit dependence on the presence of Co and the Co concentration in the precursor.
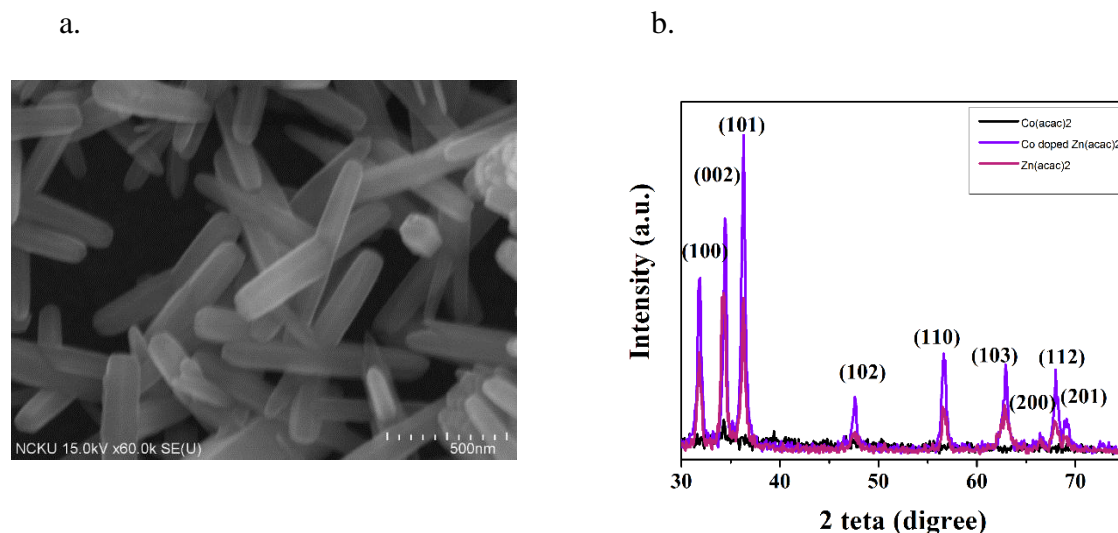
a.   b.

Figure ١.(a) SEM of Co-doped ZnO Nanorods (b) comparison between X-ray diffraction of Co-doped ZnO and their precursors.

The potential of Co doped ZnO nanorods towards solar degradation of dye solution was tested by adding different mass of catalyst (٥, ١٠, ٢٠, ٥٠ and ١٠٠ mg) in ٢٠ ppm ٢٥ ml methyl orange solution at pH = ٦ under atmospheric pressure and at room temperature. This result indicates that the Co-doped ZnO nanorod shows high activity in degradation of organic dyes.

١ Xu, F. and Sun, L.T. *Energy & Environmental Science*, ٢٠١١, ٤, ٨١٨-٨٤١

٢ Fageria, P., Gangopadhyay, S. and Pande, S. *RSC Advances*, ٢٠١٤, ٤, ٢٤٩٦٢-٢٤٩٧٢.

٣ Wu, D.W., Huang, Z.B., Yin, G.G., Ya, Y.D., Lia, X.M., Han, D., Huang, X. and Gu, J.W.. *CrystEngComm*, ٢٠١٢, ٢٠١٢, ١٢, ١٩٢-١٩٨.

٤ Kuriakose, S., Satpatib, B. and Mohapatra, S. *Physical Chemistry Chemical Physics*, ٢٠١٤, ١٦, ١٢٧٤١-١٢٧٤٩.

٥ Li, L., Wang, W., Liu, H., Liu, X., Song, Q. and Ren, S. *The Journal of Physical Chemistry C*, ٢٠٠٩, ١١٣, ٨٤٦٠-٨٤٦٤.

٦ R. Rooydell, R-C Wang, S. Brahma, F. Ebrahimzadeh , C.P Liu, *Dalton Transactions*, ٢٠١٥, DOI: ١٠.١٠٣٩/c٥dt٠٠٨٠٨e

٧ R. Rooydell, S. Brahma, R.C Wang, F. Ebrahimzadeh, C.P. Liu, *Journal of Alloys and Compounds* ٢٠١٦, doi: ١٠.١٠١٦/j.jallcom.٢٠١٦.٠٨.٣٢٤

Synthesize of $CaCu_3Ti_4O_{12}$ nanosturucture by electrospinning

M. Mohammadi[a], P. Alizadeh[a,*], F.J. Clemens[b]
a. School of Engineering, Tarbiat Modares University, Tehran, Iran.
b. Swiss Federal Laboratories for Materials Science & Technology (Empa), Duebendorf8600, Switzerland.
* E-mail address: p-alizadeh@modares.ac.ir

Introduction

Electrospinning is a remarkably simple method for generating one-dimensional polymeric fibers with diameter in the nanometer and micrometer ranges [1]. When combined with conventional sol–gel preparation, it provides a versatile technique for producing ceramic nanofibers with either a solid, porous, or hollow structure [2].

$CaCu_3Ti_4O_{12}$ (CCTO) has attracted much attention for its giant dielectric permittivity over a wide temperature range from 100 K to 500 K [3]. Ceramic materials with a high dielectric constant, such as oxides with perovskite and related structures, are widely used in capacitors, memory devices, power systems and the automotive industry [4,5].

This article presents effect of SiO_2 on sintering and morphology of $CaCu_3Ti_4O_{12}$ nanofibers.

Experimental

To synthesize 95wt% $CaCu_3Ti_4O_{12}$-5wt%SiO_2 in system (CaO-Cu_2O-TiO_2-SiO_2), according to table 1, appropriate quantities of raw materials were mixed for 1h to form ceramic solutions and Polymeric solution. The electrospinning solutions were obtained after mixing 50 vol% the polymeric solution and 50 vol% the ceramic solution for 1h stirring at room temperature. The electrospinning solutions were subsequently electrospun using Nabond electrospinning equipment. Feeding rate, accelerating voltage and working distance were 0.6 ml/h, 20kV and 16 cm, respectively. To obtain CCTO nanofibers, the resulting mat of fibers were calcined and sintered at 800 °C for 4h.

Table.1. Compositions of electrospinning solution.

Precursor	ceramic solution						Polymeric solution	
	$Ti(C_4H_9O)_4$	$Cu(NO_3)_2.3H_2O$	$Ca(NO_3)_2.4H_2O$	Acetic acid	$Si(C_2H_5O)_4$	Methanol	PVP	Ethanol
Solution	3.52gr	1.87gr	0.62gr	0.60	0.29gr	15ml	8gr	15ml

Results and Discussion

The thermal analysis of as-electrospun CCTO from room temperature to1000°C is shown in Fig 1. The DSC curve showed three reactions at 74.94, 205.36 and 418.36°C, respectively.

XRD patterns of as-electrospun fibers and the fibers which were sintered at different temperatures for 4h are shown in Fig.2. No diffraction peaks are observed for as-electrospun fibers. As the sintering temperature gradually increased to 800 °C, the characteristic peaks of $CaCu_3Ti_4O_{12}$ appeared in XRD patterns of fibers. According to the patterns, crystallization of SiO_2 happened at 1000 °C. It can be inferred that CCTO nanofibers consist of amorphous SiO_2 and $CaCu_3Ti_4O_{12}$ phase at temperatures lower than 1000 °C.

Figure 3(a) and 3(b) show the SEM images of as-electrospun nanofibers and calcinated electrospun of nanofibres, respectively. Nano crystals of CCTO with diameters ranging <50 nm can be observed on the surfaces of the fibers which heat treated at 800 °C (inset of Fig.3(b)).
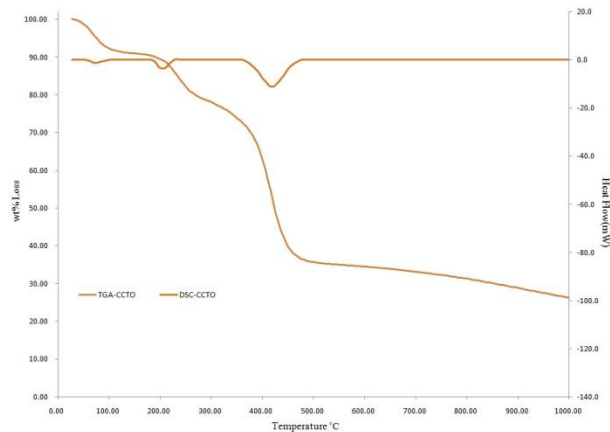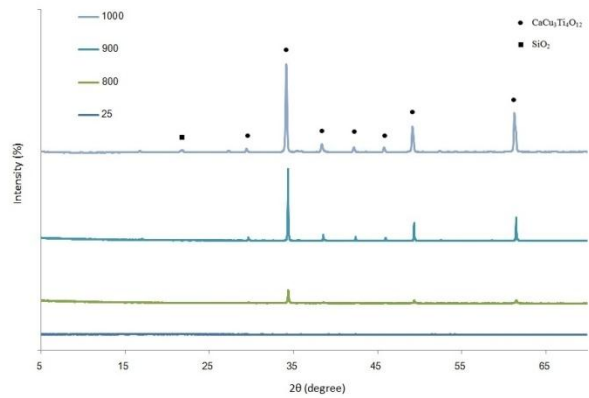
Fig.١. DSC-TG of as-electrospun CCTO.

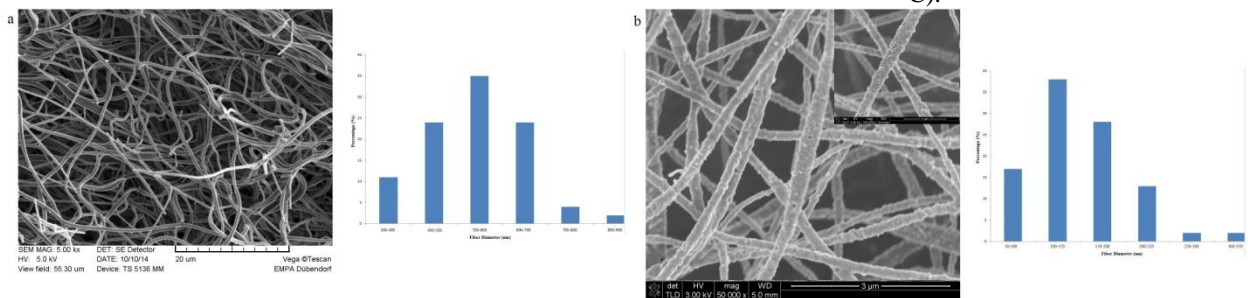Fig.٢. XRD patterns of various CCTO nanofibres samples at different temperatures (٢٥,٨٠٠,٩٠٠ and ١٠٠٠ °C).

Fig.٣. SEM images of the electrospun ٩٥CCTO nanofibres (a) before and (b) after heat treatment at ٨٠٠°C.

Conclusions

CCTO nanofibres can be easily synthesized by the electrospinning method followed by sintering at ٨٠٠°C for ٤h. The size of sintered CCTO nanofibers was in the range of ٥٠–٢٥٠ nm. The results of SEM demonstrated that polycrystalline nanostructure $CaCu_3Ti_4O_{12}$ nanofibers that could be obtained using $CaO-Cu_2O-TiO_2-SiO_2$.

Reference

[١] Y. Ishii, H. Sakai, H. Murata, "A new electrospinning method to control the number and a diameter of uniaxially aligned polymer fibres", *Journal of Materials Letters*, ٦٢(٢٠٠٨)٣٣٧٠–٧٢.

[٢] D. Li, J.T. McCann, Y. Xia, M. Marquez, "Electrospinning: A Simple and Versatile Technique for Producing Ceramic Nanofibers and Nanotubes", *Journal of American Ceramic Society*, ٨٩(٢٠٠٦)١٨٦١–٦٩.

[٣] C.C. Homes, T. Vogt, S.M. Shapiro, S. Wakimoto, A.P. Ramirez, "Optical response of high dielectric constant perovskite related oxide", *Journal of Science*, ٢٩٣(٢٠٠١)٦٧٣-٧٦.

[٤] T. Shimada, K. Touji, Y. Katsuyama, H. Takeda, T. Shiosaki, "Lead free PTCR ceramics and its electrical properties", *Journal of European Ceramic Society*, ٢٧(٢٠٠٧)٣٨٧٧-٨٢.

[٥] Y. Kobayashi, A. Kurosawa, D. Nagao, M. Konno, "Fabrication of barium titanate nanoparticles-polymethylmethacrylate composite films and their dielectric properties", *Journal of Polymer Engineering and Science*, ٤٩(٢٠٠٩)١٠٦٩-٧٥.

Synthesis of novel 1,2,3-triazole tethered *β*-carboline derivatives with cytotoxic and antibacterial activities

Peyman Salehi[a],*, Kosar Babanezhad[a], Morteza Bararjanian[a], Mohammad-Ali Esmaeili[a], Atousa Aliahmadi[a]
[a] Medicinal Plants and Drugs Research Institute, Shahid Beheshti University, Tehran, Iran
p-salehi@sbu.ac.ir

Introduction: *β*-Carbolines, containing tricyclic pyrido[3,4-0]indole ring structure, are a large group of indole alkaloids. *β*-Carbolines have a great importance because of their various pharmacological activities such as sedative, anxiolytic, anticonvulsant, hypnotic, anticancer, antiparasitic, antiviral, antithrombotic and antimicrobial [1]. 1,2,3-Triazole ring is an important class of *N*-heterocycles with a wide range of pharmacological activities, such as antibacterial, anthelmintic, antifungal [2], antimalarial, trypanocidal and anticancer [3]. In this paper the synthesis of new *β*-carboline derivatives possessing the 1,2,3-triazole ring at C-1 substituent from *L*-tryptophan by Pictet-Spengler reaction followed by a Huisgen 1,3-dipolar addition is reported.

Methods / Experimentals: The products were synthesized in four steps starting from *L*-tryptophan (Scheme 1). All of the products were fully characterized by NMR spectroscopy and HRMS. Antibacterial activity of each synthetic material was evaluated by broth micro-dilution susceptibility method to determine the minimum concentration of each antibacterial agent required for inhibition of visible growth of bacteria (MIC). The following bacteria strains were included in the study: *Escherichia coli* ATCC 25922, *Staphylococcus aureus* ATCC 25923, *Enterococcus faecalis* ATCC 29212, Vancomycin resistant strain of *Enterococcus faecium* (MIC value: 64 µg/ml) and *Bacillus cereus* PTCC 1015. Cytotoxicity of the products was determined using the MTT assay [4].

Results and Discussion: The overall strategy for the synthesis of novel *β*-carboline derivatives containing the 1,2,3-triazole ring is shown in Scheme 1. 1,2,3,4-Tetrahydro-*β*-carboline compounds **4a-c** were synthesized by Pictet-Spengler reaction of *L*-tryptophan methyl ester (**2**) with *O*-propargylated benzaldehydes (**3a-c**). 1,2,3,4-tetrahydro-*β*-carboline derivatives **4a-c** converted to the corresponding *β*-carbolines with sulfur in refluxing xylene. Then the terminal alkyne moiety of *β*-carboline derivatives were reacted with alkyl and aryl azides by using CuSO$_4$.5H$_2$O and sodium ascorbate as catalyst.

In vitro cytotoxicity and antibacterial activity of synthetic compounds were investigated. The cytotoxic activity of novel *β*-carboline derivatives **4a–c**, **5a–c** and **7a–i** were evaluated *in vitro* against two cancer cell lines, namely Hela and HepG2, by the standard MTT assay. Paclitaxel was used as the positive control. Compound **7f** demonstrated the highest cytotoxicity against both cancer cell lines, Hela and HepG2, with IC$_{50}$ values equal to 46 µM and 32 µM, respectively. These results showed that R group of 1,2,3-triazole ring has a detrimental effect on the cytotoxic activity of *β*-carbolines and their activity could be tuned by linking appropriate groups.

Antibacterial activities of the synthesized *β*-carboline derivatives were assessed against *Staphylococcus aureus*, vancomycin resistant strain of *Enterococcus faecium*, *Enterococcus faecalis*, and *Bacillus cereus* as Gram-positive bacteria and one Gram negative bacterium,

Escherichia coli. Chloramphenicol and cefixime were used as the standard antibiotics. Compounds **7d** and **7i** and **5c** showed excellent inhibition activity for *Enterococcus faecium* with MIC of 8 μg/mL.
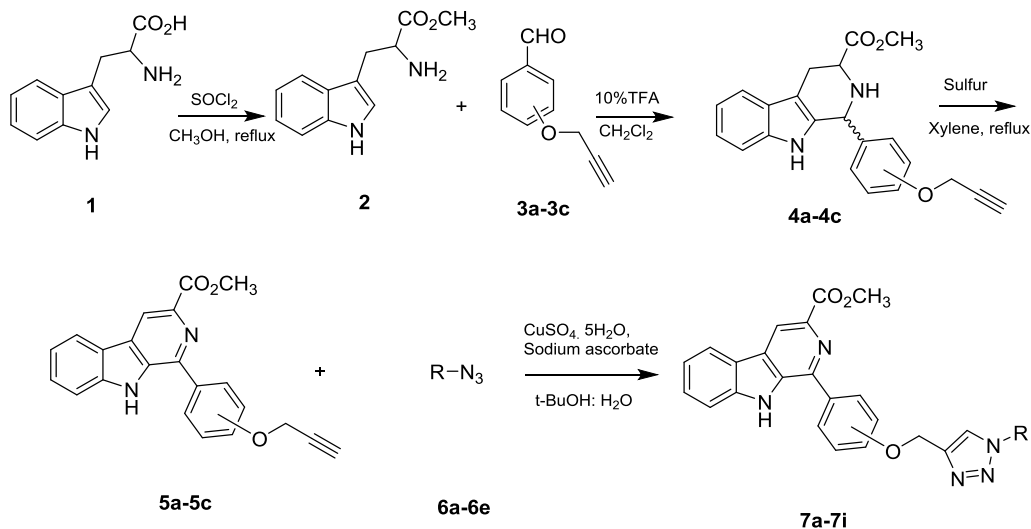
Scheme 1. The synthesis of novel *β*-carboline derivatives

Conclusion: In this paper several novel 1,2,3-triazole tethered *β*-carboline derivatives were synthesized. The cytotoxic and antibacterial activity of the compounds was evaluated. A number of the products showed promising cytotoxicity in the range of 32 to 100 μM. Also compounds **7d**, **7i** and **5c** showed the excellent inhibition against *E. faecium* with MIC equal to 8 μg/mL.

References:

[1] Cao R; Peng W; Wang Z; Xu A. Current Medicinal Chemistry, **2007**, 14, 479.

[2] Carvalho I, Andrade P, Campo VL, Guedes PMM, Sesti-Costa R, Silva JS, Schenkman S, Dedola S, Hill L, Rejzek M, Nepogodiev SA, Field RA. Bioorganic Medicinal Chemistry, **2010**, 18, 2412.

[3] Naresh Kumar R; Jitender Dev G; Ravikumar N; Krishna Swaroop D; Debanjan B; Bharath G; Narsaiah B; Nishant Jain S; Gangagni Rao A. Bioorganic and Medicinal Chemistry Letters, **2016**, 26, 2927.

[4] Jorgensen J H; Turnidge J D; Antibacterial susceptibility tests: dilution and disk diffusion methods. In: Murray P R; Baron E J; Jorgensen J H; Pfaller M A; Yolken F C; Yolken R H; Manual of Clinical Microbiology, 9th ed. Washington DC: American Society for Microbiology. **2007**, 1152.

Immobilization of platinum nanoparticles on para- aminobenzene modified electrode and investigation of its electrocatalytic activity for methanol oxidation

Fatemeh Abazari, Esmaeil Shams
E-mail address: e_shams@chem.ui.ac.ir

Introduction

Due to direct conversion of chemical energy to electrical energy, fuel cells have attracted great deal of attention in recent years. Amongst different types, direct methanol fuel cells (DMFCs) as candidates for portable power sources, have devoted a significant amount of research in the field. The expensive catalytic materials, such as platinum, and relatively low electrocatalytic efficiency for electrochemical reactions of the fuel are drawbacks to be circumvented for commercial applications. To improve the catalytic activity of methanol electrooxidation, an enormous effort has been devoted towards the development of catalysts [١]. In this research, platinum nanoparticles were deposited on the surface of para-aminobenzene modified glassy carbon electrode (GCE). The electrocatalytic activity of the modified electrode for methanol oxidation reaction was investigated.

Methods / Experimental

Modification of glassy carbon electrode surface

The surface modification of glassy carbon electrode with nitrobenzene was carried out in acetonitrile (ACN) solution containing ١.٠×١٠^{-٣} M nitrobenzenediazonium tetrafluoroborate and ٠.١ M tetrabuthylammonium tetrafluoroborate (TBATFB) by repetitive cyclic scanning from ٠.٤ to -٠.٠٣ V (vs. Ag/AgCl reference electrode) at the scan rate of ١٠٠ mV$s^{-١}$. The electrodes were then removed and rinsed with large volumes of ACN, followed by ultrasonication for ٥ min. The procedure for reduction of nitrobenzene was to perform six cyclic scanning between ٠.٧ and -١.٥V at the scan rate of ٢٠٠ mV$s^{-١}$ in a ٠.١ M KCl solution in water: ethanol (٩:١, v/v). The resulting aminobenzene modified electrode was thoroughly rinsed with water and transferred into a ٠.١ mM $H_٢PtCl_٦$ + ٠.٥ M $H_٢SO_٤$ solution, the potential was cycled at -٠.٢٢ to ١.٠١V (٥٠ cycles) for immobilization of platinum nanoparticles onto GCE. The resultant modified electrode was used as a working electrode for methanol oxidation in ٠.٥ M sulfuric acid solution.

Results and Discussion

Nitrobenzene was covalently attached to the surface of GCE and then electrochemically reduced to aminobenzene according to our previously reported work [٢]. The modification was completed by attachment of platinum nanoparticles via electrochemical reduction of $PtCl_٦^{-٢}$ on the surface of aminobenzene-modified-GCE.

Fig. ١ showed the CVs of GC electrodes containing Pt–GCE and Pt-aminobenzene modified GCE (Pt-NH₂-GCE) in ٠.٥ M H₂SO₄ solution containing ١.٠ M CH₃OH. Typical feature of methanol oxidation is observed. Two oxidation peaks, which are related to the oxidation of methanol and intermediates, appear at ٠.٦٢ and ٠.٤٤ V vs Ag/AgCl, respectively. It can be observed that the catalytic activity of Pt-NH₂-GCE is higher than that of Pt-GCE by about ١.٥ times. In addition, it is known that the ratio of the forward oxidation current peak (I_f) to the reverse current peak (I_b), I_f/I_b, shows the amount of methanol oxidized to carbon dioxide relative to carbon monoxide [٣]. The

If/Ib ratio of Pt-NH$_\Upsilon$-GCE is substantially higher than that of the Pt-GCE, showing better catalyst tolerance of Pt-NH$_\Upsilon$-GCE. Moreover, the prepared Pt-NH$_\Upsilon$-GCE showed better stability during the long-term circle experiment.
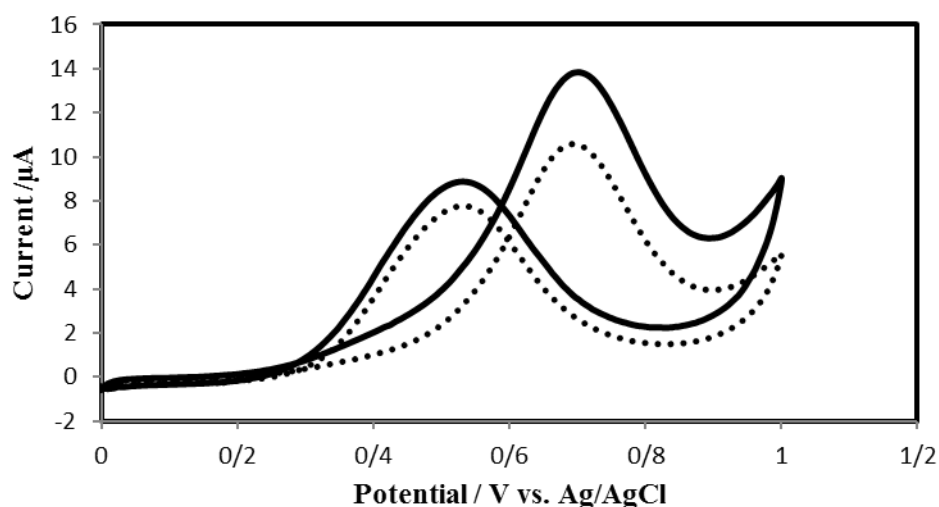

Fig. ١. CVs of Pt-NH$_\Upsilon$-GCE (solid line) and Pt − GCE (dot line) recorded in ٠.٥ M H$_\Upsilon$SO$_٤$ in the presence of ١.٠ M methanol.

Conclusion
In this research platinum nanoparticles were electrodeposited on the surface of aminobenzene modified GCE. The electrochemical oxidation of methanol on the surface of this modified electrode was investigated. The Pt-NH$_\Upsilon$-GCE showed a higher electrocatalytic activity towards methanol oxidation reaction than did a Pt–GCE.

References
[١] M.M. Bruno, F.A. Viva, M.A. Petruccelli, H.R. Corti J. Power Sources, ٢٠١٥, ٢٧٨, ٤٥٨‑٤٦٣.

[٢] Z. Nazemi, E. Shams, M.K Amini Electrochim. Acta, ٢٠١٠, ٥٥, ٧٢٤٦‑٧٢٥٣.

[٣] S. Li, X. Yu, G. Zhang, Y. Ma, J. Yao, P. de Oliveira, Carbon, ٢٠١١, ٤٩, ١٩٠٦‑١٩١١.

An efficient synthesis of dihydropyrano[c]chromene derivatives using by a polymeric catalyst

Leila nazemi –nasyrmahale, Farhad Shirini*

Department of chemistry, Faculty of Science, University of Guilan, Rasht, Iran

Corresponding author E-mail: shirini@guilan.ac.ir

Introduction:

Multi-component reactions (MCRs) play an important role in modern synthetic organic chemistry since they generally occur in a single pot and exhibit a high atom–economy and selectivity. They also deliver fewer byproducts compared to the classical step wise synthetic routes. 3,4-Dihydropyrano[c]chromenes and their derivatives are of considerable interest as they possess a wide range of biological properties such as antimicrobial [1], antibacterial [2], spasmolytic, diuretic, anti-coagulant, anti-cancer, and anti-anaphylactic activity [3,4].

Experimentals:

A mixture of aldehyde (1 mmol), 4-hydroxycoumarin (1 mmol), malononitrile (1.1 mmol) and catalyst (20mg) in H_2O/EtOH was stirred at 70^oC. The reaction progress was monitored by TLC [nhexane-EtOAc (10:2)]. After completion of the reaction (TLC), the mixture was diluted with water and the catalyst was decanted and recrystallization of the solid residue from hot ethanol to be obtained the pure products in high yields.

Results and Discussion:

To study the effect of catalyst loading on the synthesis of dihydropyrano[c]chromene derivatives the condensation reaction of malononitrile, 4-chlorobenzaldehyde, and 4-hydroxycoumarin was chosen as a model reaction (scheme 1).A series of different 3,4-dihydropyrano- [c]chromene derivatives were prepared successfully from different aldehydes bearing electron-with- drawing and electron donating groups, 4-hydroxycoumarin and malononitrile under the selected conditions.
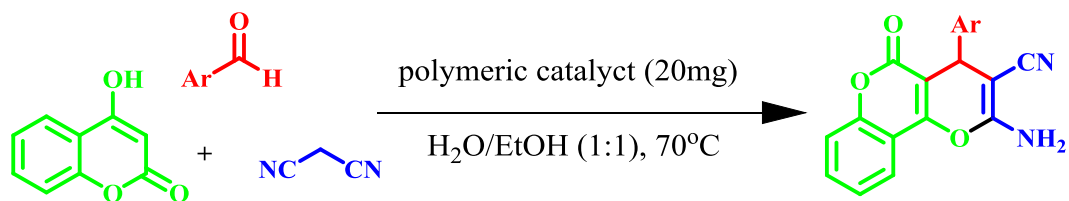
Scheme 1. Synthesis of dihydropyrano [c]chromene derivatives in the presence of polymeric catalyst.

Conclusion:

In conclusion, we developed an efficient, and simple procedure for synthesis of various dihydropyrano[c]chromene derivatives in the presence of polymeric catalyst at $H_2O/EtOH$ conditions. The easy work-up procedure, short reaction times and high yields of the products are significant advantages of this method.

References

[1]. A. Kumar; Maurya, R. A.; Sharma, S. A.; Ahmad, P.; Singh, A. B.; Bhatia, G;. Srivastava, A. K. *Bioorg. Med. Chem. Lett*. **2009**, 19, 6447-6451.

[2]. Raj, T.; Bhatia, R. K.; Kapur, A.; Sharma, M.; Saxena, A. K.; Ishar, M. P. S. *Eur. J. Med. Chem*. **2010**, 45, 790-797.

[3]. Abdelrazek, F. M.; Metz, P.; Farrag, E. K. Arch. *Pharm*. **2004**, 337, 482-485.

[4]. Symeonidis, T.; Fylaktakidou, K. C.; Hadjipavlou-Litina, D. J.; Litinas, K. E. *Eur. J. Med. Chem*. **2009**, 44, 5012-5017.

Adsorption Capability for Congo red on Nanocrystalline MAl_2O_4 (M =Fe, Co, Ni) spinel

Zahra Sadeghi*, Sepide Sarlak, Hossein Salavati

Chemistry, Department, Payame Noor University,19395-4697 Tehran,I.R. of IRAN
za.sadeghi@gmail.com

Introduction: Spinel compounds have a general formula AB_2O_4, in which the A-site is tetrahedrally coordinated and generally occupied by divalent cations (Co, Mn, Ni, and Zn) and the B-site is octahedrally coordinated and occupied by trivalent cations (Al, Cr, and Fe). In solid-state science, oxides with spinel structures are some of the most studied compounds due to their wide range of applications. The structure of spinel oxide is responsible for a variety of interesting properties. Determination of cation distribution is of considerable relevance because the theoretical interpretation of the chemical and physical properties of these compounds depends on this distribution [1].

The removal of dyes from aqueous environment has been widely studied and numerous methods such as coagulation [2], oxidation [3], photocatalysis [4], adsorption [5], nanofiltration [6], micellar enhanced ultrafiltration [7] etc, have been developed. Adsorption technology is currently being applied extensively to the removal of dyes from aqueous solutions. Several adsorbents have been investigated by previous researchers such as activated carbon [8], natural materials [5,9] and synthetic resins [10].

In this contribution, we compare the adsorption capacity of different MAl_2O_4 (M = Fe, Co, Ni) ferrite nanocrystals synthesized by hydrothermal method for Congo red. Itis the first time to give a comprehensive comparison and analysis of the adsorption capacity of ferrite nanocrystals with spinel structure for Congo red. Research indicates that the cations distribution of MAl_2O_4 ferrites is the most important factor to decide their adsorption capacity. Electrostatic absorption was conceived as the main adsorption mechanism.

By the calculation of Langmuir isotherm model, the maximum adsorption capacity of $CoAl_2O_4$ for Congo red is 244.5 mg g^{-1}.

Methods / Experimentals:

2.1. Synthesis of the material

The starting materials were $M(NO_3)_2$-$6H_2O$ (Merck, 99.9%), zeolite Y ($Na_{59}Al_{59}Si_{133}O_{384}$-$234H_2O$, structure type FAU) (Merck, 95.0%), aqueous NH_3 (Reidel, 33.0%) and were used as supplied. The spinel particles crystallize during the calcination of transition metal exchanged zeolites. Calcination destroys the zeolites, and the spinels grow in the resulting amorphous silicate matrix.

2.2. Adsorption studies

A stock solution of 100 mg/L of Congo red was prepared. The necessary dilutions were carried out in 25 mL of distilled water in order to prepare 1, 3, 5, 7, 9 and 11 mg/L solutions. The quantity of the powder added was 0.1 g in each flask and the all the flasks were shaken for an optimized time of 160 min at room temperature and the absorption spectrum of the filtrate solutions were studied at the λmax of the dye which is 497 nm which is measured by using Perkin Elmer UV/VIS Lambda 25 spectrophotometer [23].

Results and Discussion:

The FESEM image (Fig. 1a) shows that the product zeolite Y consists of irregular polyhedral, their edge lengths are in the range of 50–400 nm. Uniform nanoparticles with particle sizes around 25 nm are observed from Fig. 1b. In Fig. 1c, we can observe large numbers of octahedral with some small nanoparticles adsorbed on their surfaces. The lateral sizes of octahedral are ranging from 80 to 100 nm and the nanoparticles with about 10–20 nm in diameters.
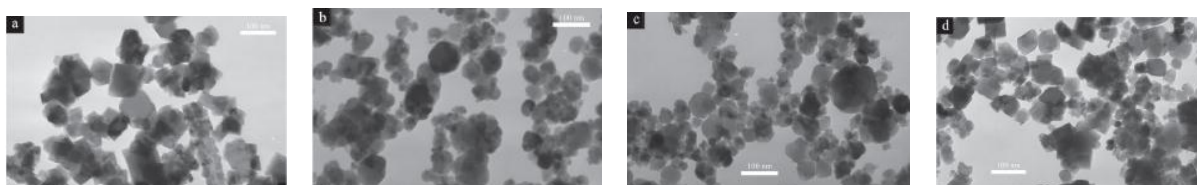
Fig. 1. FESEM analyses of a: zeolite Y b: $NiAl_2O_4$ c: $FeAl_2O_4$ d: $CoAl_2O_4$

Thermodynamic parameter related to the adsorption process i.e., free energy change (ΔG, kJ mol^{-1}) for adsorption was calculated using the following equation:

$\Delta G = -RTlnK_c$ $\quad$ (1)

Where R is the universal gas constant (8.314 J mol−1 K−1), T is the temperature (K) and K_c is equilibrium constant the Kc value is calculated from Eq. (2):

$Kc = C_{AE}/C_{SE}$ $\quad$ (2)

Where Kc is the adsorption equilibrium constant C_{AE} is the amount of dye (mg) adsorbed on the adsorbent per litre of the solution at equilibrium. C_{SE} is the equilibrium concentration (mg L^{-1}) of the dye in the solution.

The use of an adsorbent in the wastewater treatment depends not only on the adsorptive capacity, but also on how well the adsorbent can be regenerated and used again for repeated use of an adsorbent, adsorbed dye should be easily desorbed under suitable conditions. Desorption process was conducted by mixing 5 mg of CR-loaded modified MFe2O4 with 30 mL of acetone solutions or alcohol and shaking for 30 min. The desorption efficiency calculated as:

Desorption ratio (%) = amount of desorbed Congo red / amount of adsorbed Congo red × 100

Conclusion:

The prepared adsorbent can be easily separated from the aqueous solution. The effects of various operating conditions, like initial dye concentration, pH and temperature, were investigated. It was observed that the adsorption of Congo red is favored at low pH (130.6 mg g^{-1} at pH = 3.2). The maximum monolayer adsorption capacity of magnetic $CoAl_2O_4$ was found to be 111.1 mg g^{-1}. This value was higher than those reported by other researchers with the exception of A. filiculoides, natural clay, and calcined alunite. Adsorption data were described using the pseudo-first-order kinetic model, the pseudo-second-order model, and the intraparticle diffusion model. The adsorption kinetics was well described by pseudo-second-order model. The data were analyzed by the Langmuir and Freundlich models of adsorption. The equilibrium data fitted well with the Langmuir model. The thermodynamic study indicated that the adsorption of Congo red onto $CoAl_2O_4$ was spontaneous and an exothermic process.

References
1. S. Lv, X. Chen, Y. Ye, S. Yin, J. Cheng, M. Xia, *Hazard. Mater*. **2009**, *171*, 634–639.
2. M.L. Marechal, Y.M. Slokar, T. *Dyes Pigments* **1997,** *33*, 181–298.
3. W.X. Chen, W.Y. Lu, Y.Y. Yao, M.H. Xu, *Environ. Sci. Technol.* **2007,** *41*, 6240–6245.
4. J. Fernandez, J. Kiwi, C. Lizama, J. Freer, J. Baeza, H.D. Mansilla, *J. Photochem. Photobiol. A* **2002**, 151, 213–219.
5. M. Arami, N.Y. Limaee, N.M. Mahmoodi, N.S. Tabrizi, *J. Colloid Interface Sci.* **2005,** *288*, 371–376.
6. S. Chakraborty, M.K. Purkait, S. Dasgupta, S. De, J.K. Basu, *Sep. Purif. Technol.* **2003,** *31*, 141–151.
7. M.K. Purkait, S. DasGupta, S. De, *Sep. Purif. Technol.* **2004,** *37*, 81–92.
8. M.K. Purkait, A. Maiti, S. DasGupta, S. De, *J. Hazard. Mater.* **2007,** *145*, 287–295.
9. R. Jain, S. Sikarwar, *J. Hazard. Mater.* **2008,** *152*, 942–948.
10. Y. Yu, Y.Y. Zhuang, Z.H. Wang, M.Q. Qiu, *Ind. Eng. Chem. Res.* **2003**, *42*, 6898–6903.

Novel bis-pyrimidine derivatives: Synthesis and characterization
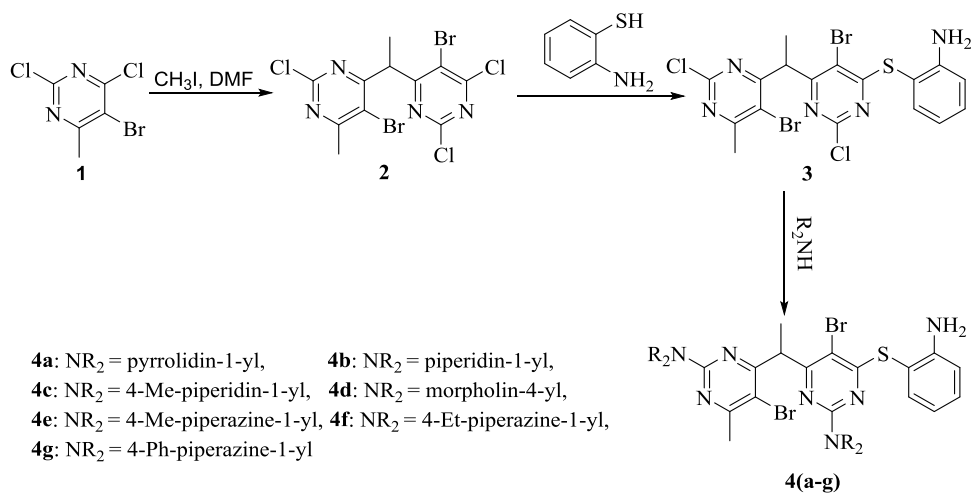
Toktam Afrough, Mehdi Bakavoli[*], Hossein Eshghi

Department of Chemistry, Faculty of Science, Ferdowsi University of Mashhad, Mashhad, Iran.

Email address: *mbakavoli@um.ac.ir, mbakavoli@yahoo.com*

Introduction: Pyrimidine nucleus has played crucial role in the history of heterocyclic chemistry and has been used extensively as important pharmacophor and synthon in the field of organic chemistry and drug design. Bis-heterocyclic compounds are considered as bis-drugs, due to their double therapeutic behavior compared to their mono-heterocyclic analogues. For example, bis-pyrimidines show various biological properties such as anti-bacterial [1], anti-inflammatory [2] and anti-amobeic [3]. Here, we wish to report the synthesis of new series of bis-pyrimidine derivatives.

Methods / Experimentals: Initially, bis-pyrimidine (**2**) was prepared from reaction of compound (**1**) [4] with methyl iodide in DMF. Consecutive reaction of compound (**2**) with 2-aminothiophenol and secondary amines gave compound (**3**) and the desired bis-pyrimidine derivatives (**4a-g**), respectively.

Results and Discussion: The general route for the synthesis of 2-((5-bromo-6-(1-(5-bromo-6-methyl-2 (substituted)pyrimidin-4-yl)ethyl)-2-(substituted)pyrimidin-4-yl)thio)aniline (**4a-g**) is depicted in scheme 1.

4a: NR$_2$ = pyrrolidin-1-yl,   **4b**: NR$_2$ = piperidin-1-yl,
4c: NR$_2$ = 4-Me-piperidin-1-yl,   **4d**: NR$_2$ = morpholin-4-yl,
4e: NR$_2$ = 4-Me-piperazine-1-yl, **4f**: NR$_2$ = 4-Et-piperazine-1-yl,
4g: NR$_2$ = 4-Ph-piperazine-1-yl

Scheme 1

Attempted heterocyclization of these compounds (**3**) and (**4a-g**) in the presence of NaNH$_2$ and CH$_3$CN as have been reported for the synthesis of pyrimido[4,5-*b*][1,4]benzothiazine derivatives [5] was not successful. This reaction did not even proceed when different base/solvent systems was employed and each time the starting material was recovered. The poor electrophilicity of C-5 of these compounds can be accounted on the fact that the methine's hydrogen is more acidic than NH$_2$ hydrogens. For tentative confirmation of this idea, we exchanged acidic hydrogen of compound **3** in isopropanol-*d8* and obtained deuterated product **3′**. In the ^{1}H NMR spectrum of compound **3′** quartet peak at δ 4.91 ppm belonging to hydrogen of methine adjoined to methyl group disappeared. Antimicrobial activities of the new products were evaluated against a variety of Gram-positive and -negative bacteria.

Conclusion:

In summary, new bis-pyrimidine derivatives (**4a-g**) were prepared in a three-step procedure based on 5-bromo-2,4-dichloro-6-methylpyrimidine (**1**) as starting material. In spite of our expectation based on our previous studies, the heterocyclization of compounds (**3**) and (**4a-g**) was not performed. It is proved that the poor electrophilicity of C-5 of these compounds can be responsible for synthesis of new bis-pyrimidine derivatives (**4a-g**) despite pyrimido[4,5-*b*][1,4]benzothiazine derivatives.

Refrences

[1]   N. O. Mahmoodi; S. Shoja; B. Sharifzadeh; M. Rassa. *Med. Chem. Res*, **2014**, *23*, 1207-1213.

[2]   Sh. M. Sondhi; Sh. Jain; M. Dinodia; R. Shukl; R. Raghubir. *Bioorg. Med. Chem*, **2007**, *15*, 3334–3344.

[3]   H. Parveen; F. Hayat; S. Mukhtar; A. Salahuddin; A. Khan; F. Islam; A. Azam. *Eur. J. Med. Chem*, **2011**, *46*, 4669-4675.

[4]   M. Bakavoli; M. Nikpour; M. Rahimizadeh. *J. Heterocycl. Chem*, **2006**, *43*, 1327-1329.

[5] M. Bakavoli; M. Nikpour; M. Rahimizadeh; M. R. Saberi; H. Sadeghian. *Bioorg. Med. Chem*, **2007**, *15*, 2120–2126.

A New Method for Synthesis of Ni-Co Layered Double Hydroxides and Structural Characterization of Nanoparticles

Kamelia Nejati[a]*, Soheila davari[a], Alireza Akbari[a], Parvaneh dalir kheyrollahi[a], Zolfagar rezvani[b], Karim Asadpour Zeynali[c]

a Department of chemistry, Payam-e- Noor University, P.O.Box19395-3697 Tehran, Iran

b Department of chemistry, Azarbaijan university of Tarbiat Moallem, 5375171379,Tabriz,Iran

c Department of Analytical Chemistry, Faculty of chemistry, Tabriz University, Tabriz, Iran

email: nejati_k@yahoo.com

****

Introduction

Layered double hydroxides (LDHs) belong to a general class called anionic clay minerals. They can be of both synthetic and natural origin. The most commonly known naturally occurring LDH clay is hydrotalcite. The general chemical formula of LDH clays is written as: $[M^{II}_{1-x}M^{III}_{x}(OH)_2]^{x+} (A^{n-})_{x/n}.yH_2O$ where M^{II} is a divalent metal ion, such as Mg^{2+},Ca^{2+},Zn^{2+} ,etc, M^{III} is a trivalent metal ion, such as $Al^{3+},Cr^{3+},Fe^{3+},Co^{3+}$,etc and A^{n-} is an anion , such as Cl^-,CO_3^{2-}, NO_3^-,etc. The anions occupy the interlayer region of these layered crystalline materials. Although a wide range of values of x is claimed to provide LDH structure, the pure phase of LDH clays is usually obtained for a limited range as 0.2>x >0.33 [1]. The structure of LDHs can best be explained by drawing analogy with the structural features of the metal hydroxide layers in mineral brucite or simply the $Mg(OH)_2$ crystal structure. Brucite consists of a hexagonal close packing of hydroxyl ions with alternate octahedral sites occupied by Mg^{2+} ions. The metal hydroxide sheets in brucite crystal are neutral in charge and stack one upon another by Van der Waal's interaction. In LDH, some of the divalent cations of these brucite-like sheets are isomorphoulogy substituted by a trivalent cation and the mixed metal hydroxide layers, thus formed acquire a net positive charge. This excess charge on the metal hydroxide layers is neutralized by the anions accumulated in the interlayer region. The interlayer region in LDHs also contains some water molecules for the stabilization of the crystal structure[1-4].The purpose of this work is to study the effect of hydrothermal and thermal treatment conditions on structural and textural properties of synthetic Ni-Co-NO_3^- LDH .

Methods/Experimental

A mixed solution of $Ni(NO_3)_2.6H_2O$ and $Co(NO_3)_2.6H_2O$ with Ni^{2+}/ Co^{2+} ratio of 2 by dissolving in distilled water and methanol, was added dropwise under N_2 to a vigorously stirred solution of 0.5M NaOH until the PH adjusted to 10 . The resulting suspension was aged at 180 °C for 24h. The mixture was centrifuged at a speed of 1300 rpm for 20min and

the solid washed thoroughly with deionised water and dried at 70 °C in the oven for 24 h . This reaction repeated in temperature 80 °C for thermal conditions.

Results and Discussion

The FT-IR spectra of LDH materials provide many important. As shown in Fig 1 The broad band in the range 3200 – 3700 cm^{-1} originates from the O–H stretching of the metal hydroxide layer and interlayer water molecules. The band at1643 cm^{-1} is due to the bending vibrations of water molecules. Another two bands ($<800cm^{-1}$)are attributed to the M-O-H and O-M-O bending vibrations[5]. The narrower absorption close to $1382cm^{-1}$ is due to mode ν_3 of the interlayer nitrate anions in Ni/Co-NO$_3$LDH. The XRD patterns of the precursor Ni-Co-LDH showed the characteristic diffractions peaks from (003), (006), (009) and (110) plans. The XRD pattern of the Ni-Co- LDH are shown in Fig.2 .
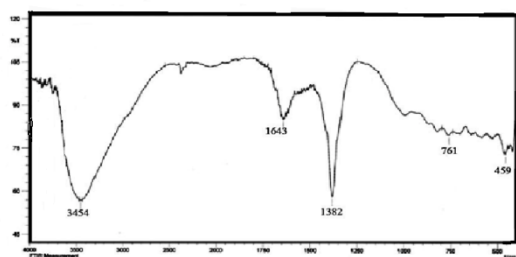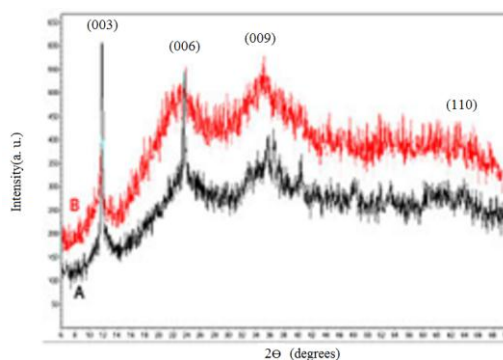

Fig.1. FT–IR spectra of the Ni-Co- LDH

Fig.2. XRD pattern of the Ni-Co- LDH
(A=180 °C, B=80 °C in PH~10)

Conclusion

In the present study a hydrotalcite-like material Ni-Co- LDH with a molar ratio of 2 have been obtained. The effect of hydrothermal and thermal conditions on structural and textural properties was studied in the temperature range 80°C, 100°C for 24 h. The characterization of the Ni-Co- LDH were carried out extensively using various analytical techniques, like XRD and FTIR. Layered double hydroxides can be considered a group of promising materials in the development of new applications.

References

 [1] F. Cavani; F. Trifiro; A. Vaccari. Catalysis Today, 1991, 11,273 – 301.

[2] V. RIVES (Editor). Nova Science Publishers, Inc, 2001, New York.

[3] S. M. Lomakin ; G. E. Zaikov. VSP Publishers, Netherlands, 2003.

[4] M . K . Titulaer ; J . B. H . Jansen ; J . W. Geus. Clays Miner,1994,33, 242 - 249.

[5] A.Vaccari.,Catal.Today, 1991,11 ,173-189

Cu(II) Schiff base complexes encapsulated in nanocavities of zeolite-Y: catalytic activity toward reduction of aldehydes

Saeed Rayati[a], *, Saeedeh Shokouhi[a]

[a] Department of Chemistry, K.N. Toosi University of Technology, P.O. Box 16315-1618, Tehran 15418, Iran

Email address: rayati@kntu.ac.ir.

****

Introduction: Zeolites and mesoporous silica nanoparticles are silicate or aluminosilicate nanomaterials with well-defined pore networks. Zeolites are widely used in industry for applications such as catalysis, separations and gas adsorption [1].

One of the most convenient methods for preparation of the reusable catalysts is encapsulation of catalyst in the cavities of zeolites. Also, the product selectivity and the lifetime of the catalyst can also be improved by encapsulation. Accordingly many research groups investigated the catalytic properties of the complexes entrapped within the supercages of Y-zeolite. [2-5]

The present study describes the synthesis and characterization of the copper(II) Schiff base complexes encapsulated in the nanocavity of zeolite-Y. Also, the catalytic activities of the prepared materials for the reduction of aldehyde with $NaBH_4$ has been investigated.

Experimental: To an ethanolic solution of 1,2-diaminopropane (H_2L_1) or ethylendiamine (H_2L_2), 2,4-dihydroxyacetophenone was added. The solution was stirred and heated to reflux for 1 h. Then obtained precipitate was filtered off and washed with warm ethanol.

The procedures for the preparation of metal complexes are as follows: 1 mmol H_2L_1 or H_2L_2 were dissolved in ethanol. Ethanolic solutions of 1 mmol copper(II) acetate were added to above solution and the reaction mixture was refluxed for 2 h. The colored solution was concentrated to yield colored powders. The products were washed with warm ethanol.

Incorporation of Cu(II) in Na-Y (metal exchanged Y-zeolite) Cu–Y was prepared by ion-exchange method: 5 g Na-Y zeolite was suspended in 100 mL distilled water containing copper (II) acetate (12 mmol). The mixture was then stirrer for 24 h. The solid was filtered and washed with deionized water and dried at room temperature to give the light-blue powder of Cu-Y.

Immobilization of the free base ligands in Cu-Y: An amount of 1.0 g Cu(II)-Y and 2.5 g of ligand H_2L were mixed in 100 mL of methanol and the reaction mixture was refluxed for 15 h in an oil bath with stirring. The resulting material was separated by filtration and then extracted with methanol using Soxhlet extractor to remove unreacted ligand from the cavities of the zeolite as well as those located on the surface of the zeolite along with neat complexes, if any. The unreacted copper(II) ions present in the zeolite was removed by stirring with aqueous 0.01 M NaCl solution. The resulting solid was filtered and washed with distilled water until free from chloride ions. Finally, it was dried at 120 °C in an air oven for several hours.

General reduction procedure: To a mixture of aldehyde (0.1 mmol) and catalyst (0.003 mmol) in methanol (1 mL), 1.8 mg $NaBH_4$ (0.05 mmol) was added. The reaction mixture was stirred

magnetically at room temperature for 2 min and the progress of the reaction was monitored by GC.

Result and Discussion: The prepared heterogeneous catalysts have been characterized by FTIR, NMR and atomic absorption spectroscopy, X-ray diffraction patterns, scanning electron microscopy and BET.

SEM spectroscopy illustrate the cubic structure of zeolite by alone and after encapsulation [Fig1]. Also according to EDX spectroscopy investigated the percentage of metal in complex CuL_1-Y and compare with Na-Y.

The percentages of metal content of various catalysts estimated by atomic absorption spectroscopy, approximately Metal content of the CuL_1-Y is 2.86% and CuL_2-Y is 2.56%.

The catalytic activities of the encapsulated complexes were studied in the reduction of aldehydes with NaBH4. Reduction of 4-methyl benzaldehyde in the presence of CuL_1-Y led to 89.9% reduction of the aldehydes to the corresponding alcohol. Also The catalytic activity of the recovered catalysts was compared with the fresh ones.

Conclusion: It can be concluded that CuL_x (x= 1 and 2) complexes can be encapsulated in Na–Y zeolite supercages without structural modification or loss of crystallinity of the zeolite framework. The physico-chemical studies confirmed the encapsulation of metal complexes in the supercages of zeolite Y. Catalytic activity of the prepared catalysts in the reduction of aldehydes with $NaBH_4$, was investigated.

Fig1. SEM spectroscopy of complexes.

Reference:

[1] Sean E. Lehman; Sarah C. Larsen. *Environ. Sci.: Nano, 2014, 1,* 200–213.

[2]S.M. Bonesi, E.Carbonell, H. Garcia, M.Fagnoni, A.Albini. *Appl.Catal. B: Env*, **2008**, *79* , 368-375.

[3] M.R. Maurya, A.K. Chandrakar, S. Chand, *J. Mol.Catal. A: Chem*, **2007**, *274*, 192-201.

[4]M.R. Maurya, M. Bisht, N.Chaudhary, F. Avecilla, U. Kumar, H.-F. Hsu. *Polyhedron*, **2013**, *54*, 180-188.

[5] S.Rayati, S.Shokoohi, E.Bohloulbandi. *J Iran Chem SOC*, **2016**, *13*, 1983-1991.

Immobilized NNN Pd-complex on magnetic nanoparticles: Efficient and reusable catalyst for Heck coupling reaction

Fahimeh Dehghani Firuzabadi, Zahra Asadi*

Department of Chemistry, College of Sciences, Shiraz University, Shiraz 71454, Iran

Email address: zasadi@shirazu.ac.ir

****

Introduction:

Immobilization of Pd species on different supports including silica, porous materials, magnetic nanoparticles and etc. were used to prepare heterogeneous Pd catalyst systems. Compared with other supports, magnetic nanoparticles (MNPs) show obvious superiority and have recently received considerable attentions as excellent supports [1]. This class of supports enables facile separation of the catalyst from the reaction medium by employing an external magnetic field [2].This kind of separation hampers wasting of the catalyst and saves time when compared with filtration method [3].

Here we report the synthesis of a highly efficient Pd complex supported on magnetic nanoparticles for application in Heck reaction.

Experimental:

For the synthesis of catalyst, first $Fe_3O_4@SiO_2$ nanoparticles were obtained and functionalized with (3-chloropropyl)-trimethoxysilane (3-CPTMS) in order to functionalized MNPs surface with alkyl halide group for substitution reaction. For the synthesis of the NNN Schiff base ligand diethylenetriamine and isovaniline were used. The substitution reaction on C-Cl bond of 3-CPTMS with amine groups of NNN ligand yields the production of CPS-MNPs-NNN substrate. Finally, palladium was immobilized on the CPS-MNPs-NNN substrate surface, leading to the formation of CPS-MNPs-NNN-Pd catalyst.

Results and Discussion:

FT-IR, XRD and EDX techniques were used to prove the successful functionalization of the MNPs. According to the TEM image, the size of catalyst particles is estimated to be in the range of 8-15 nm and SEM image shows that the nanoparticles are formed in nearly spherical shape. The values of the saturation magnetization are 22 emu g^{-1} for CPS-MNPs-NNN ligand and 28 emug^{-1} for CPS-MNPs-NNN-Pd catalyst. The decrease in the saturation magnetization is due to the presence of Pd immobilized on the surface of the CPS-MNPs-NNN ligand.

The catalytic applicability of the CPS-MNPs-NNN-Pd catalyst was investigated in the Heck coupling reaction. To explore the optimal reaction conditions, a series of circumstances were evaluated including time duration, solvent, base, and temperature.

The optimal reaction conditions and the model reaction are shown in Scheme 1. In order to explore the scope of the reaction, several differently substituted aryliodides with acrylonitrile were examined (Scheme 2). In our catalytic system, due to the magnetic nature of the CPS-MNPs-NNN-Pd catalyst, it could be recovered from the reaction mixture by magnetic separation and recycled at least 5 times without a significant loss in its catalytic activity.

Conclusion:

To sum up, CPS-MNPs-NNN-Pd complex acts as an efficient, economic and green catalyst that shows an extraordinary robustness, moisture stability and catalytic activity in Heck coupling reaction in the presence of only 0.5 mol% of supported Pd catalyst and generated the corresponding products in good to excellent yields. This catalyst is prominent due to the efficient recoverability for at least 5 times in consecutive runs with negligible loss of its reactivity.
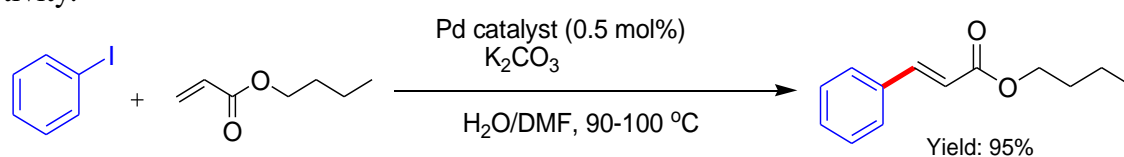
Scheme 1. The optimal reaction conditions and the model reaction.
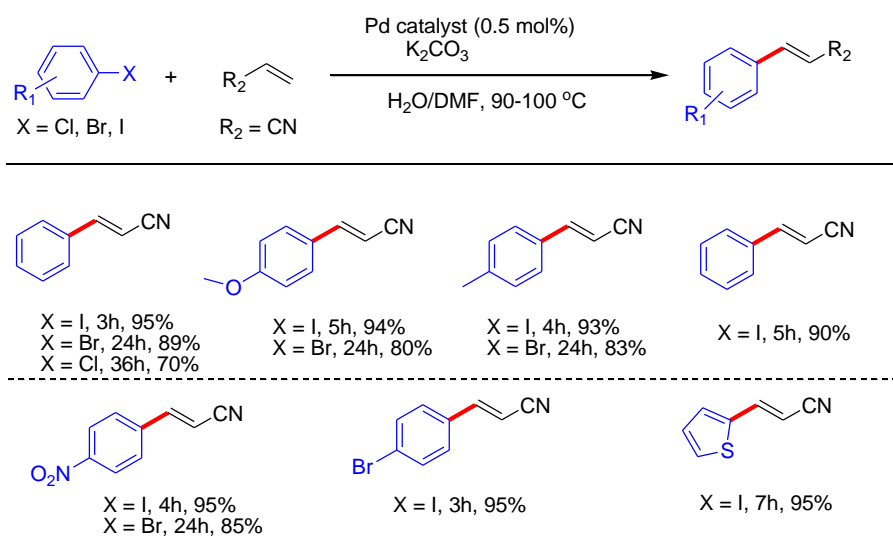
Scheme 2. Heck reaction of different aryl halides with acrylonitrile under the optimized conditions. Reaction conditions: aryl halide (1 mmol), alkene (1.2 mmol), K_2CO_3 (2.0 mmol) in H_2O/DMF [2/1 (v/v), 2.5 mL]. Yields are isolated.

References

[1] M. B. Gawande; P. S. Brancoa; R. S. Varma. *Chem. Soc. Rev.*, **2013**, 42, 3371-3393.

[2] V. Polshettiwar; R. Luque; A. Fihri; H. Zhu; M. Bouhrara; J.-M. Basset. *Chem. Rev.*, **2011**, 111, 3036-3075.

[3] A. Kumar; R. Parella; S. Arulananda Babu. *Synlett*, **2014**, 25, 835-842.

Riboflavin mediated photo-oxidation of crystallin proteins in the presence of ascorbic acid and glutathione as two natural antioxidants of eye lens.

Afrooz Anbaraki, Reza Yousefi[*]

Protein Chemistry Laboratory (PCL), Department of Biology, College of Sciences, Shiraz University, Shiraz, Iran

[*]**Email address: ryousefi@shirazu.ac.ir**

Introduction: Exposure to sunlight has long been recognized as a source of aging of lens crystallins and an important risk factor for the cataract development [1]. The solar radiation wavelengths greater than 280 nm reach the eye lens but shorter wavelengths being effectively filtered by the ozone layer. Riboflavin (RF) is a normal component of eye lens which acts as a photosensitizer molecule. Upon absorption of the solar radiation, RF is converted to its triplet state and subsequently initiates the formation of different types of reactive oxygen species resulting in important structural damages of biomolecules [2].

Methods: Lens proteins were exposed to the sunlight with different concentrations of RF. The RF-mediated photo-damaging of these proteins were studied in the presence of lens antioxidant components such as ascorbic acid and glutathione. The photo-induced crosslinking and formation of high molecular weight protein species were analyzed by electrophoresis and dynamic light scattering analyses. Also, Uv-visible and fluorescence spectroscopic techniques were applied to evaluate the structural damages and aggregation of the photo-damaged lens proteins.

Results and Discussion: The results of both Uv-visible absorption studies and fluorescence emission assessments suggested important structural damages in the lens proteins upon exposure to the solar radiation. Also, as a result of exposure to the sun light new chromophores were appeared in the structure of lens crystallins. The results of both electrophoresis and dynamic light scattering analyses suggested increased oligomeric size distribution of the photo-damaged lens crystallins. In addition, we indicated that photo-damaging of these proteins was reduced to the significant level in the presence of ascorbic acid and glutathione.

Conclusion: The results of our study suggest that the powerful antioxidant defense mechanism of eye lens may prevent/attenuate the molecular photo-damaging effects of solar radiations during the life span.

References

[1] A. Midelfart. Acta Ophthalmologica Scandinavica, **2005**, 83, 642-645.

[2] G. Viteri; A. M. Edwards; D. L. Fuente; E. Silva. Photochemistry and Photobiology, **2003**, 77, 535-540.

Theoretical studies of the Bergman cyclization reactions of enediynes

Parvin Ghasemi[a,*] and Avat (Arman) Taherpour[a,b*]

[a,b]*Department of Organic Chemistry, Faculty of Chemistry, Razi University, Kermanshah, Iran*
[b]*Medical Biology Research Center, Kermanshah University of Medical Sciences, Kermanshah, Iran*
[*]Corresponding authors Email: **avatarman.taherpour@gmail.com** and **ghasemi_pr66@yahoo.com**
****

Introduction: The enediynes are organic molecules that readily undergo a Bergman cyclization thermal rearrangement. In 1972, Bergman published a detailed study of the thermal behavior of simple acylic (Z)-enediynes [1]. When enediyne was heated in solution, the products observed were benzene or its derivatives, depending on the solvent used. Bergman had suggested the intermediacy of the highly unstable *p*-benzyne biradical to explain the results. One of the most important motivations for the investigation of *p*-benzyne and the Bergman reaction was the discovery of the enediyne cytostatics, namely, calicheamicins, esperamicins and dynemicins that they are able to cleave the DNA double strand sequence specifically in vivo [2]. A variety of rearrangements followed Bergman cyclization in (Z)-enediynes equipped with n-membered ring (n=0,3,5). In the first step of this process, H-atom abstraction efficiently intercepted the *p*-benzyne product of the Bergman cyclization through a transition state with six-membered ring and transformed the *p*-benzyne into a new more stable radical (Figure 2). H-abstraction occurred through external H-atom donor.

Methods: The computational chemistry package *Spartan '10* [3] was used to determine the structures of the (Z)-enediynes equipped with n-membered ring (n=0,3,5), as well as the products of their rearrangements. Geometries of all species and molecules were optimized at the MP2-6-31G* level of theory. The procedure employed to obtain transition states was a bit more involved than for other species. For each of the transition states, the molecule's geometry was optimized with the length of the bond formed or broken during the rearrangement fixed at several different values, by MP2-6-31G*. The energies of biradical species and transition states from singlet state calculations will be presented.

Results and Discussion: The (Z)-enediyne series was selected as the one on which the effect of basis set on the description of reactivity would be tested. The product resulted from the process initiated by the Bergman cyclization of enediyne was given in Figure 1. all optimized structures and their corresponding energies were successfully obtained. The results of this investigation are given in table 1. This table contains the singlet electronic state of energy at the optimized geometry and the transition states. All of the calculated species were obtained by the MP2/6-31G* level of theory. Moller-Plesset calculation method on these systems modeling led to a number of geometrical parameters which correlated well with their tendencies to undergo the Bergman cycloaromatization reaction. Depending on the size of n-membered ring and their conformational forms, kinetic data of the Bergman reaction led to the different thermodynamic values.
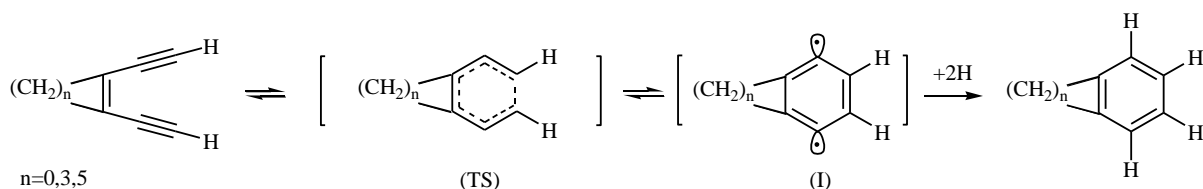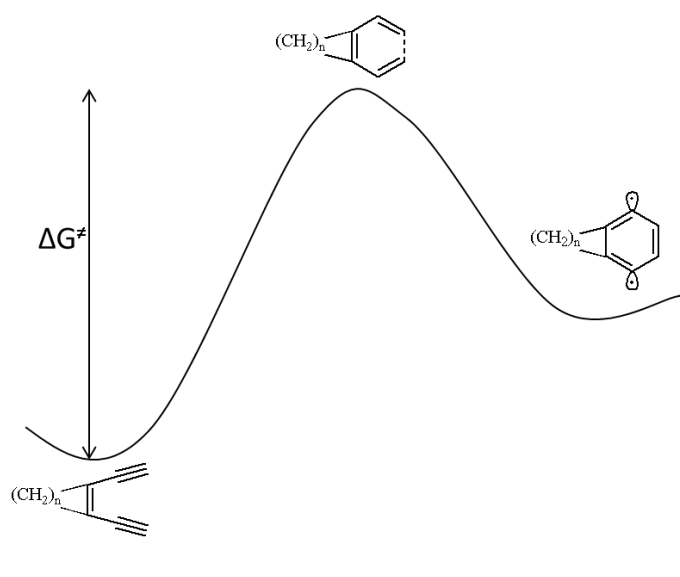

Figure 1. The Bergman cyclization

Figure 2. The energy profiles of the Bergman cyclization

Table 1: Calculated Energies Of the (z)-enediyne series using the MP2-6-31G* basis set

State	$\Delta G^{\neq}$, kcal mol^{-1}	K
n=0	-35.41	9.34×10^{25}
n=3	-13.16	4.48×10^{9}
n=5	-10.18	2.92×10^{7}

Conclusion: The theoretical studies have shown that the kinetic of the Bergman cyclization would be faster by increasing the ring size of the fused ring to the (Z)-enediyne structure. The result of the studies was interpreted by the free activation energy of the cyclization reaction.

References

[1] Jones, R.R.; Bergman, R.G. *J. Am. Chem. Soc*. **1972**, *94*, 660.
[2] Ogozelski, W.K.; Tullius, T. D. *Chem. Rev*. **1998**, *98*, 1089.
[3] Spatran '10-Quantum Mechanics Program: (PC/x86)-1.1.0v4.2011, Wavefunction Inc USA.

# Synthesis and Study of Coordination of ligands containing Imidazolidine to Manganese (II) Ion

Ahmad Ali Dehghani-Firouzabadi[*], Zahra Samadifar

Department of Chemistry, Yazd University, Yazd, aadehghani@yazd.ac.ir

Introduction: Imidazolidin and compounds of similar structure constitute a widespread structural motif in natural products and pharmaceutical [1,2]. Imidazolidin derivatives have shown a range of biological activities such as antimalarialactivity, antiproliferative activity for melanoma and so forth [3-6]. Specific imidazoline receptors have been proposed to be responsible for various pharmacological effects of imidazolin-containing drugs [7]. Due to the utility of imidazolidins, a number of methods have been developed for their construction. The most commonly employed method for the synthesis of these compounds involves the generation of 1,2-diamines [8].

Methods: A solution of ethylenediamine in ethanol was added dropwise to an ethanolic solution of pyridine-2-carbaldehyde and stirred for 12 h at room temperature. Solid sodium borohydride was then added slowly and the reaction mixture heated at the reflux for 2 h. Then excess water was added and the product was extracted with chloroform. The resulting product was dissolved in ethanol and aldehyde (various) was added. The mixture was heated for 6 h and then was evaporated to small volume and the crystalline precipitate filtered off. A solution of these compounds in hot ethanol was added to a solution of $MnCl_2 \cdot 4H_2O$ in the same solvent and stirred for 4 h. The solvent was evaporated in air to small volume and the product was filtered off, washed with cold diethyl ether.

Results and Discussion: The synthetic procedure adopted for the imidazolidin derivatives and their chemical structures are illustrated in Scheme. These compounds were prepared via [1+1] condensation of various aldehyde with N,N′-bis((pyridin-2-yl)methyl)ethane-1,2-diamine in the solvent of acetonitrile and characterized by the appropriate spectroscopic methods (FT-IR, UV–Vis, 1H and 13C NMR, EI-Mass). Then in this research, Manganese (II) complex of these compounds were synthesized and characterized by FT-IR, UV–Vis spectroscopy, molar conductivity, EI-Mass spectrometry and X-ray crystallography. The spectroscopic data for the imidazolidin derivatives and the complexes confirm the formation of them.
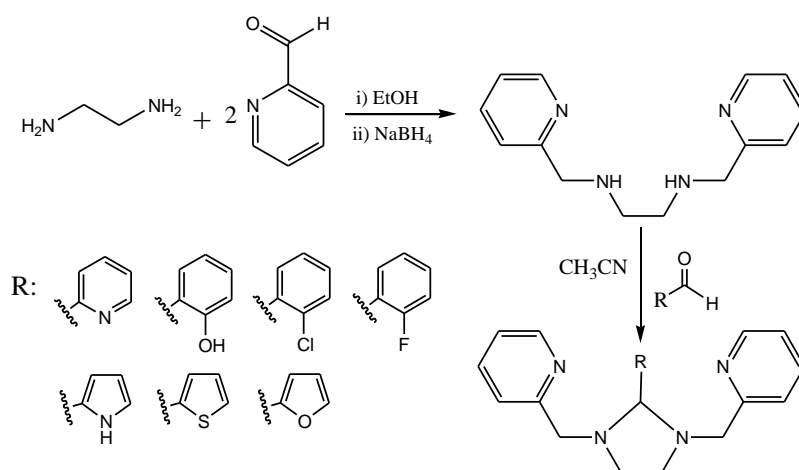
Conclusion: In summary, we have successfully synthesized the N,N´-bis((pyridin-٢-yl)methyl)ethane-١,٢-diamine from a tetradentate Schiff base ligand and then the imidazolidin derivatives have been obtained. These compounds were characterized by FT-IR, UV–Vis, ¹H and ¹³C NMR spectroscopy and EI-Mass spectrometry and the synthesized complexes characterized by FT-IR, UV–Vis spectroscopy, molar conductivity, EI-Mass spectrometry and X-ray crystallography. In this study, we has shown that the imidazolidin ring in manganese (II) complex is unstable and ring in complex can be opened.

Keyword: manganese (II) complex; unstable ring; imidazolidin; Mass spectrometry.

References:

[١] G. Schneider, U. Fechner, Nat. Rev. *Drug Discovery* ٢٠٠٥, ٤, ٦٤٩–٦٦٣.

[٢] S. B. Mhaske, N. P. Argade, *Tetrahedron* ٢٠٠٦, ٦٢, ٩٧٨٧–٩٨٢٦.

[٣] N. Vale, M. S. Collins, J. Gut, R. Ferraz, P. J. Rosenthal, M. T. Cushion, R. Moreira, P. Gomes, *Bioorg. Med. Chem. Lett.* ٢٠٠٨, ١٨, ٤٨٥–٤٨٨.

[٤] P. Gomes, M. J. Araujo, M. Rodrigues, N. Vale, Z. Azevedo, J. Iley, P. Chambel, J. Morais, R. Moreira, *Tetrahedron* ٢٠٠٤, ٦٠, ٥٥٥١–٥٥٦٢.

[٥] M. J. Araffljo, J. Bom, R. Capela, C. Casimiro, P. Chambel, P. Gomes, J. Iley, F. Lopes, J. Morais, R. Moreira, E. de Oliveira, V. do Rosario, N. Vale, J. *Med. Chem.* ٢٠٠٥, ٤٨, ٨٨٨–٨٩٢.

[٦] J. Chen, Z. Wang, Y. Lu, J. T. Dalton, D. D. Miller, W. Li, Bioorg. *Med. Chem. Lett.* ٢٠٠٨, ١٨, ٣١٨٣–٣١٨٧

[٧] G. A. Head, D. N. Mayorov, *Cardiovasc. Hematol. Agents Med. Chem.* ٢٠٠٦, ١٧–٣٢.

[٨] G. Sartori, R. Maggi, in: *Science of Synthesis* (Houben-WeylMethods of Molecular Transformations. S. V. Ley, J. G. Knight, editors). Thieme: Stuttgart; ٢٠٠٥, ١٨, ٦٦٥-٧٥٨.

Other Statistical Mechanics (Non-extensive Thermodynamics) to Describe The Thermodynamic Properties of LJ Nanoclusters

Mozhgan sabzehzari[*a], **Ezzat Keshavarzi**[b]

aDepartment of Chemistry, Jondi Shapor University of Technology, Dezful, Iran
bDepartment of Chemistry, Isfahan University of Technology, Isfahan, Iran

[*]**Email address**: msabzehzari@jsu.ac.ir

Abstract

In this article we have shown that the nonextensive vibration partition function of harmonic oscillator in Tsallis statistical mechanics may be used for prediction of the behavior of the L.J-nanoclusters, for example for sub-extensivity of the configuration energy.

1. Inroduction

Recently, the Tsallis nonextensive statistics have been attracted more attention in different fields because of its ability in prediction of some phenomena for which Boltzmann Gibbs statistics fails. There are systems which are nonextensive because of their microscopic (interactions) correlations, not dynamic (statistic) correlations. The examples of nanoextensive systems are nanoclusters which are in the concern of nanotechnology field. In fact the origin of the nonextensivity in internal energy of nanoclusters is related to the microscopic interactions rather than its statistics correlations, While in Tsallis framework, nonextensivity originates from statistic in definition of the entropy, by entropic index, q[1].

2. Dynamics Correlation and Nonextensivity

It has been known that for two independent subsystems,*A* and *B*,with probabilities, $P_i^A, and \ \ P_j^B$, respectively, the probabilities corresponding to $A \bigcup B$ satisfy $P_{ij}^{A \cup B} = P_i^A P_j^B$. By substituting the probability function defined in Tsallis statistical mechanics [2] will lead to

$$\varepsilon_{ij}^{A \cup B} = \varepsilon_i^A + \varepsilon_j^B + \beta^* (q^* - 1) \varepsilon_i^A \varepsilon_j^B$$

(1)

In spite of independent probabilities, the combined energy of these two systems is not the sum of their individual energies. There is always a statistic (dynamic) correlation between them. To do so we consider a system with N independent and identical harmonic oscillators in Tsallis statistical framework. The internal energy for a system which it has been composed from two independent and identical harmonic oscillators may be obtained by using Eq.(1), and the definition of the internal energy in the Tsallis statistics[1], $U_A = \frac{\sum_i^w \varepsilon_i p_i^q}{\sum_i^w p_i^q}$,as

$$U_{A \cup A} = 2U_A + \beta^*(q^* - 1)U_A^2$$
(2)

Therefore the internal energy of N independent and identical harmonic oscillators, U_N will be written as the following analytical equation interestingly:

$$U_N = \frac{[(\alpha U + 1)^N - 1]}{\alpha}$$
(3)

3. The Nonextensivity of Internal Energy of Nanoclusters

To show the nonextensivity in energy of nanoclusters, the data of molecular dynamic simulation for configuration energies of stable structures of L.J-nanoclusters have been used. Figure1 shows the behavior of the configuration energy of L.J-nanoclusters per atom, U/n, versus the number of atoms exists in a nanocluster, n. In fact the decreasing behavior of the configuration energy per atom with respect to N is a representation of the subextensivity of configuration energy for theses nanoclusters. We have also plotted the behavior of the internal energy of the clusters composed from $N=3n-5(6)$ harmonic oscillator at $kT/ hv=1$ versus the number of harmonic oscillator in Tsallis statistics mechanics with q equals to 0.993. As it is clear the agreement between internal energies predicted by Tsallis statistical mechanics and MD simulations is so good.
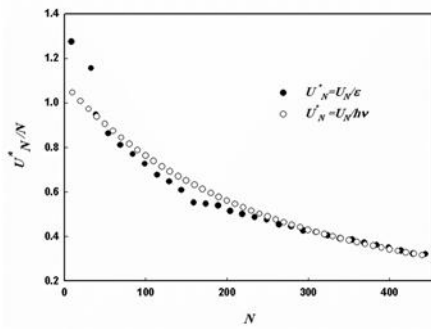

Figure.1 Internal energy which predicted by Tsallis statistical mechanics(°),MD simulations(•).

5. Conclusion
It seems that instead of considering the microscopic correlations in usual statistical mechanics, it is possible to investigate the independent particles or quasi particles in nonextensive statistics with definition of q parameter. Although we investigated only the L.J nanoclusters but we believe such a comparison may be done for other nanoclusters. The values of q for other nanoclusters are strongly depend on the kind of intermolecular interactions.

References
[1] C.Tsallis. *J. Stat. Phys.,* 1988,52,479-487.

[2] S. Mart´ınez; F. Nicols; F. Pennini; A. Plastino. *Physica A*,2000, *286 (3-4),* 489-502 .

Structural Features of Several Cu-Based Layered Double Hydroxides

S. Hosein Mousavipour*, <u>Fatemeh Keshavarz</u>

Department of Chemistry, College of Science, Shiraz University, Shiraz, Iran
Email: mousavipour@shirazu.ac.ir

Introduction: Layered double hydroxides (LDHs) are ionic compounds that are composed of positively charged layers and an interlayer region with compensating anions and solvation molecules. Their generic formula for metals M and non-framework anion A^{n-} is $[M^{2+}_{1-x}M^{3+}_x(OH)_2][A^{n-}]_{x/n}\cdot zH_2O$ [1]. LDHs can be used as precursors for preparing CO_2 adsorbents and as catalysts, ion exchange hosts, drug delivery hosts, etc. [2]. Here, $Cu_{7.4}M_{1.6}Al_4$ LDHs (M=Cu, Zn, Cd or Ni) are synthesized, characterized by several spectroscopic techniques and some structural features of each LDH is unraveled by DFT calculations and NBO analysis.

Methods: Temperature controlled urea hydrolysis was employed to obtain mono-dispersed LDH particles through homogeneous co-precipitation that was inspired from reference [3]. Some structural properties of the LDHs were revealed by FT-IR, XRD, and SEM. More structural insight was gained from quantum mechanical calculations by Gaussian 09W [4] on models of the type $[Cu^{II}M^{II}Al^{III}(OH)_4(H_2O)_9]^{3+}$ using B3LYP method, with 6-31+G(d) basis set for O, H and Al atoms and LANL2DZ pseudo potentials for the transition metals.

Results and Discussion: The FT-IR results depict the well-known LDH features with the carbonate, metal-hydroxyl and water components while SEM results declare that application of urea method has eliminated unwanted rigid sand rose morphology which is common in conventional co-precipitation synthesis methods. The lattice parameters are outlined in Table 1. Agreement of the theoretical and experimental results approves application of the LDH model and method/basis set combination. According to the DFT calculations, Cu, Zn, Ni and Cd containing LDHs with triplet, doublet, quadruplet, and doublet spin multiplicities exhibit the highest structural stability with no spin contamination, respectively. For CuCuAl, CuZnAl, CuCdAl and CuNiAl LDHs, the HOMO-LUMO energy gap respectively equals 0.26290, 0.26097, 0.24777, 0.25695 hartree. While the weakest reactivity is expected from CuCuAl-LDH, the CuCdAl-LDH possesses the highest chemical reactivity. Molecular orbitals of the LDHs are shown in Figure 1.

Conclusion: Here, spectroscopic and electronic structure details of some Cu-based LDHs are provided. The DFT results show that substitution of a third metal in the CuAl-LDH framework alters LDH reactivity through changing the HOMO, LUMO and their corresponding gap energies.

Table 1. Lattice parameters of the LDHs based on the XRD results. a, c and D_c represent the mean cation–cation distance within the layer, layer thickness and crystallite size, respectively.

LDH	a/ Å	c/ Å	Dc/ Å
Cu_9Al_4-LDH	3.77587	22.68114	6.61920
$Cu_{7.4}Zn_{1.6}Al_4$-LDH	3.76621	22.60997	8.48699
$Cu_{7.4}Cd_{1.6}Al_4$-LDH	3.75932	22.55592	11.9375
$Cu_{7.4}Ni_{1.6}Al_4$-LDH	3.78074	22.70400	5.97889
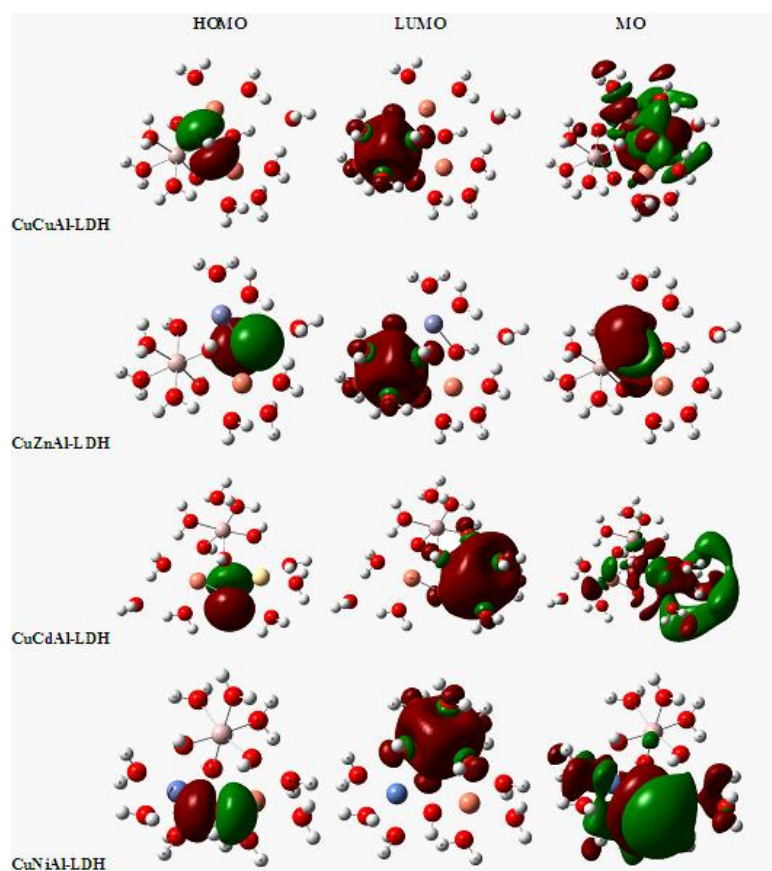
Figure 1. HOMO, LUMO and molecular orbitals (MOs) of the $[Cu^{II}M^{II}Al^{III}(OH)_4(H_2O)_9]^{3+}$ LDHs. Cu, Al, Zn, Cd, Ni, O and H atoms are in orange, pink, bluish purple, yellow, blue, red and white colors, respectively.

References

[1] S. Miyata. *Clays and Clay Minerals*, **1975**, 23, 369-375.
[2] J. Plank; D. Zhimin; H. Keller; et al. *Cement and concrete research*, **2010**, 40(1), 45-57.
[3] C. Li; Y. Chen; S. Zhang; et al. *Chemistry of Materials*, **2013**, 25(19), 3888-3896.
[4] M. J. Frisch; G. W. Trucks; H. B. Schlegel; et al. Gaussian 09w, version 7.0, Gaussian. Inc, Wallingford, **2009**.

Preparation of novel deoxycholic-calixarene chiral stationary phase and evaluation of its chiral discrimination property in the HPLC resolution of racemic compounds

S. Yaghobnejad, K. Tabar Heydar*, S. H. Ahmadi, R. Zadmard

Chemistry and Chemical Engineering Research Center of Iran

*E-mail: Ktabarh@ccerci.ac.ir

Introduction

Calix[n]arenes are the cyclic oligomers or metacyclophanes that composed of phenol units linked by methylene bridges at positions ortho to the hydroxyl groups[1]. Calix[n]arenes are often referred to as the third generation of supramolecular receptors after crown ethers and cyclodextrins[2]. The interest in use of calix[n]arene derivatives as stationary phase is rapidly increasing because these derivatives can form inclusion complexes and hydrophobic, π–π interactions with solutes. For these reasons some functionalized calix[n]arenes have been synthesized and their applications have been reported in a variety of chromatography fields[3]. In this paper, we describe the synthesis and separation performance of deoxycholic-calixarene-bonded silica gel as a new HPLC stationary phase for chiral separation (Figure 1).
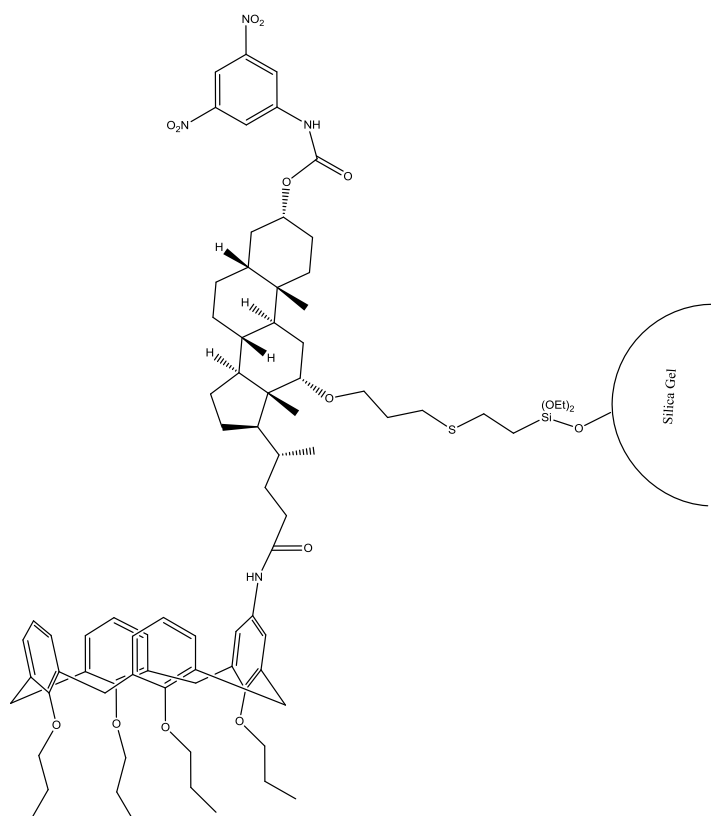

Figure 1.

Methods / Experimentals

The chiral selector was synthesized by use of calix[4]arene, deoxycholic acid and 3,5-dinitrophenyl isocyanate in 9 steps. The phase was prepared by covalently bonding deoxycholic-calixarene to thiopropyl-modified silica by thiol-ene click chemistry reaction then end-capping with 1-hexene. The synthetic stationary phase is characterized by means of elemental analysis. The chiral stationary phase (CSP) was slurry packed into stainless steel column (250mm × 4.6mm i.d.) and tested under normal phase.

Results and Discussion

The results show that the CSP has excellent selectivity for the separation of selected racemic amino acid derivatives and enantiomers of chiral compounds due to the cooperative functioning of calix[4]arenes, deoxycholic acid and 3,5-dinitrobenzoyl group. Figure 2. illustrates the separation of the N-3,5-dinitrobenzoyl derivatives of four amino acids.
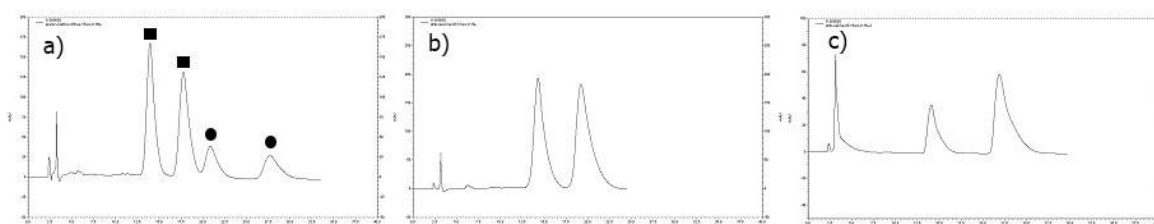

Figure 2. Separation of the enantiomers of the racemic N-3,5-dinitrobenzoyl derivatives of a) alanine (■), methionine (●) b) Leucine c) Valine using 5% isopropyl alcohol in hexane, flow rate 1 ml/min, detection UV at 254 nm

Conclusion

This CSP containing both π-acidic (with π-electron-donor phenyl groups) and π-basic (with π-electron-accepting phenyl group) groups on the deoxycholic acid molecule, therefore, this CSP is very effective for the chiral resolution of racemic compounds containing both π-electron-donating and π -electron-accepting groups.

References

[1] A. Ikeda and S. Shinkai, *Chemical reviews* **1997**, *97*, 1713-1734.
[2] A. Sirit and M. Yilmaz, *Turk. J. Chem* **2009**, *33*, 159-200.
[3] a) G. Arena, A. Casnati, A. Contino, L. Mirone, D. Sciotto and R. Ungaro, *Chemical Communications* **1996**, 2277-2278; b) K. Baechmann, A. Bazzanella, I. Haag, K.-Y. Han, R. Arnecke, V. Boehmer and W. Vogt, *Analytical Chemistry* **1995**, *67*, 1722-1726; c) S. Gebauer, S. Friebe, G. Scherer, G. Gübitz and G.-J. Krauss, *Journal of chromatographic science* **1998**, *36*, 388-394; d) J. Glennon, E. Horne, K. Hall, D. Cocker, A. Kuhn, S. Harris and M. McKervey, *Journal of Chromatography A* **1996**, *731*, 47-55; e) J. D. Glennon, K. O′ Connor, S. Srijaranai, K. Manley, S. J. Harris and M. A. McKervey, *Analytical letters* **1993**, *26*, 153-162; f) Y. Lee, Y. Ryu, J. Ryu, B. Kim and J. Park, *Chromatographia* **1997**, *46*, 507-510; g) M. Sánchez Peña, Y. Zhang and I. M. Warner, *Analytical chemistry* **1997**, *69*, 3239-3242; h) S. Sun, M. J. Sepaniak, J.-S. Wang and C. D. Gutsche, *Analytical chemistry* **1997**, *69*, 344-348; i) X.-Z. Xiao, Y.-Q. Feng, S.-L. Da and Y. Zhang, *Chromatographia* **1999**, *49*, 643-648.

Molybdenum Nanoparticles Encapsulated Into Zr-MOF Metal-Organic Framework: Highly efficient and reusable catalyst for alkene epoxidation

Niloufar Afzali[a], **Shahram Tangestaninejad[b]***, **Iraj Mohammadpoor-Baltork[c]***, **Majid Moghadam[d]**,

Valiollah Mirkhani[e], **Reihaneh Kardanpour[f]**, **Zahra Zamani Noori[g]**

[a] *PhD student of Inorganic Chemistry*

[b] *Professor of Inorganic Chemistry*

[c] *Professor of Organic Chemistry*

[d] *Professor of Inorganic Chemistry*

[e] *Professor of Inorganic Chemistry*

[f] *PhD in inorganic chemistry*

[g] *PhD student of Inorganic Chemistry*

Department of Chemistry, University of Isfahan, Isfahan 81746-73441, I. R. Iran

E-Mail Address: Stanges@sci.ui.ac.ir (S. Tangestaninejad) *and* Imbaltork@sci.ui.ac.ir (I. Mohammadpoor-Baltork).

Introduction

Metal−organic frameworks (MOFs) are a class of crystalline and porous materials formed by coordination bonds between metal-containing nodes and organic linkers [1]. Because of prominent properties of MOFs such as their flexible pore size, shape and structure, high surface area and tuneability, they have found applications in different field. Especially, they can be applied in catalysis field as both catalyst and support [2]. So far, only a handful of MOF materials have been reported to be used as catalysts for organic catalysis and even fewer of them as host matrices to support metal nanoparticles (NPs) as catalysts for heterogeneous catalysis [3-5]. The mesoporous cages can be used to confine the metal nanoparticles and to restrict their growth, which are pertinent features for their applications in heterogeneous catalysis. Furthermore, the mesoporous cages and large microporous windows may allow the large reactant molecules to reach the active site in the pores and the large product molecules to leave from the active sites easily [6].

As the ideal MOF support platform, we selected the Zr-based MOF known to have exceptional thermal and mechanical stability [7,8]

In this manner, a heterogeneous catalyst containing highly dispersed Mo nanoparticles using Zr-MOF as host compound for epoxidation of different alkenes is reported. The high dispersion of the Mo nanoparticles on Zr-MOF and the big pore size of MOF guarantee sufficient contact between substrate and catalytic active center, thus accelerating the rate of reaction and providing improved catalytic efficiency. Finally, the prepared catalysts were characterized. The Mo-containing MOFs were reused several times without any appreciable loss of their efficiency.

Methods / Experimental

Initially, the parent framework was synthesized by two different methods. The first one was solvothermal method as a typical procedure and the second one was large-scale method. To

synthesis of Mo@Zr-MOF catalysts the activated framework was reacted with $MoO_2(acac)_2$ in the reflux conditions followed by chemical reduction with$NaBH_4$. The prepared catalysts was used in epoxidation of cyclooctene as reaction model.

Results and Discussion

The known metal-organic framework (MOF) was synthesized by both solvothermal and ultrasonic methods and used as support for molybdenum nanoparticles. To prove the successful synthesis of molybdenum nanoparticles encapsulated into framework, different methods such as FT-IR, UV-vis, X-ray diffraction (XRD), inductively coupled plasma atomic emission spectroscopy (ICP-AES)), transmission electron microscopy (TEM) was used. The catalytic activity of this heterogeneous catalyst was investigated in epoxidation of alkenes with *tert*-butyl hydroperoxide (TBHP) in CCl_4.

Conclusion

One of the important key point for application of MOF is their stability. The Zr MOF that selected as support for immobilization of Mo nanoparticles known as a most stable MO [7,8]. It is also stable to water and many organic solvents. Molybdenum nanoparticle based on Zr MOF catalysts have been prepared for the epoxidation of olefins with *tert*-butyl hydroperoxide (TBHP) (Scheme 1). The recyclability of the catalysts was investigated. Easy work up, convenient and steady reuse and high activity and selectivity are prominent properties of these new catalysts.

Mo@Zr-MOF-S or Mo@Zr-MOF-L

CCl_4, TBHP, reflux
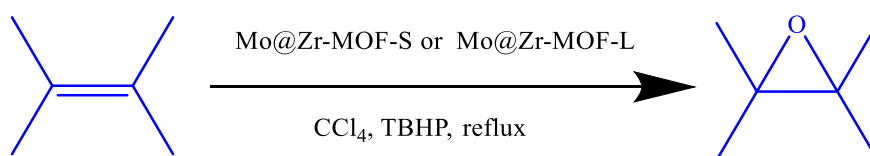
(Scheme 1)

References

[1] Kitagawa, S.; Kitaura, R.; Noro, S. i. *Angew. Chem. Int. Ed.* **2004**, *43*, 2334-2375.
[2] Aijaz, A.; Xu, Q. *J. Phys. Chem. Lett* **2014**, *5*, 1400-1411.
[3] Cho, S.-H.; Ma, B.; Nguyen, S. T.; Hupp, J. T.; Albrecht-Schmitt, T. E. *Chem. Commun.* **2006**, 2563-2565.
[4] Lee, J.; Farha, O. K.; Roberts, J.; Scheidt, K. A.; Nguyen, S. T.; Hupp, J. T. *Chem. Soc. Rev.* **2009**, *38*, 1450-1459.
[5] Aijaz, A.; Karkamkar, A.; Choi, Y. J.; Tsumori, N.; Rönnebro, E.; Autrey, T.; Shioyama, H.; Xu, Q. *J. Am. Chem. Soc.* **2012**, *134*, 13926-13929.
[6] Pan, Y.; Yuan, B.; Li, Y.; He, D. *Chem. Commun.* **2010**, *46*, 2280-2282.
[7] Cavka, J. H.; Jakobsen, S.; Olsbye, U.; Guillou, N.; Lamberti, C.; Bordiga, S.; Lillerud, K. P. *J. Am. Chem. Soc.* **2008**, *130*, 13850-13851
[8] Valenzano, L.; Civalleri, B.; Chavan, S.; Bordiga, S.; Nilsen, M. H.; Jakobsen, S.; Lillerud, K. P.; Lamberti, C. *Chem. Mater.* **2011**, *23*, 1700-1718.

Synthesis, Characterization and Computational Studies of Symmetrical Binuclear Complex containing bridging biphosphine ligand from Cyclometalated Bis-Chelate Organoplatinum (II) Complex

Seyed Reza Barzegar Kiadehi[a], Mohsen Golbon Haghighi[a*]

[a] Department of Chemistry, Shahid Beheshti University, Evin, Tehran, 19839-69411, Iran,
mohsen_golbon@yahoo.com , m_golbon@sbu.ac.ir

****

Introduction: The study of the cyclometalation reactions have considerable interest from its role in many applications, such as the fuctionalization of C-H bonds, anti-cancer drug, luminescence, etc [1]. The ligand substitution reaction involving transition metal complexes, is usually considered as a key step in many catalytic reactions [2]. However, such reactions have rarely been considered on cycloplatinted complexes [3]. In particular, cyclometalated organoplatinum (II) complexes have been developed for their application in OLEDs as phosphorescent emitters and other unique emitter devices [4-5]. Complexes of this class, exhibit triplet excited states of mixed ligand-centred/metal-to-ligand charge-transfer character (^{3}LC/MLCT), which are usually capable of producing efficient luminescence due to the spin-orbit coupling effects induced by the metal [6].

Methods: The reaction of [Pt(ppy)(dppm)]X, **2**, (ppy = 2-Phenylpyridine; dppm = bis(diphenylphosphino)methane, X = CF_3CO_2 or Cl) with 1 equiv [Pt(ppy)(X)(L)] , **1**, (L = SMe_2 or DMSO) in benzene gave symmetrical binuclear complexes of the type [$Pt_2X_2(ppy)_2(\mu$-dppm)] , **3** . All complexes were fully characterized by using ^{1}H-NMR and ^{31}P{^{1}H}-NMR spectroscopy. Single crystals of **1a** were grown from a concentrated CH_2Cl_2 solution by slow diffusion of n-Hexane. Density functional calculations were performed with the program suite Gaussian03 using the B3LYP level of theory. The LANL2DZ basis set was chosen to describe Pt. The 6-31G(d) basis set was used for other atoms .
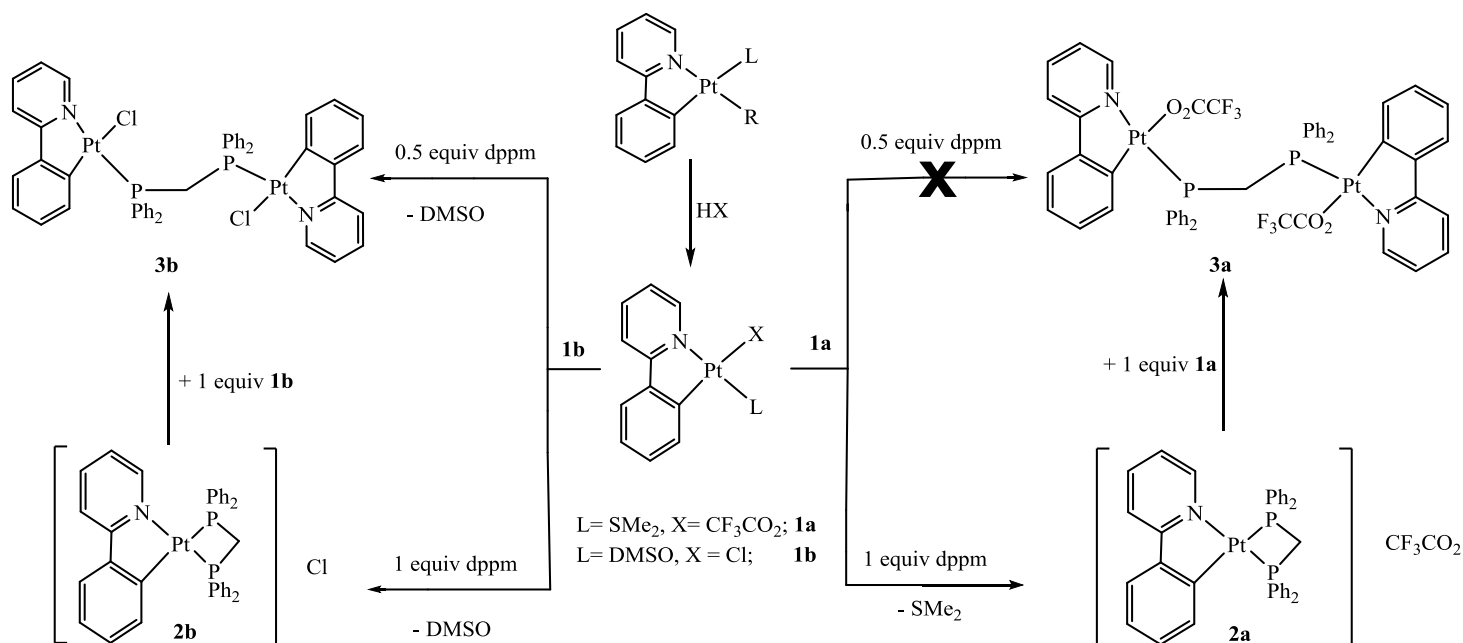
Scheme 1. Synthesis route for preparation of cyclometalated organoplatinum (II) complexes containing chelate and bridge dppm ligand **2**-**3**.

Results: Structures of the complexes in solution were deduced from the ^{1}H, and ^{31}P NMR spectra . Typically, ^{31}P NMR spectrum of the complex **2a**, having a chelating dppm ligand, contains two doublet resonances with ^{2}J$_{PP}$ coupling being 37 Hz for the P trans to C [δ = -25 ppm , ^{1}J$_{PtP}$ = 1400 Hz] and P trans to N with a much bigger ^{1}J$_{PtP}$ value [δ = -33 ppm, ^{1}J$_{PtP}$ = 3400 Hz], confirming that the biphosphine ligand dppm is chelated. In the ^{1}H NMR spectrum of complex **2a**, there are one notable signals that are coupled to the platinum center, at δ = 4.87 ppm (coupling to Pt center with ^{3}J$_{PtH}$ ≈ 48 Hz, ^{2}J$_{PH}$ = 11 Hz which is attributed to the CH$_2$ group of the dppm ligand, confirming that apart from ppy, the dppm ligand is also chelated. The ^{31}P NMR spectrum of the complex **3a** having a bridging dppm ligand, contains one singlet resonances with ^{1}J$_{PtP}$ coupling being 4400 Hz with δ ≈ 7 ppm , confirming that the dppm ligand is bridged. In the ^{1}H NMR spectrum of complex **3a** there are one notable signals that are coupled to the platinum center, at δ = 4.17 ppm (^{3}J$_{PtH}$ ≈ 42 Hz, ^{2}J$_{PH}$ = 13 Hz which is attributed to the CH$_2$ group of the dppm ligand, confirming that the dppm ligand is bridged.
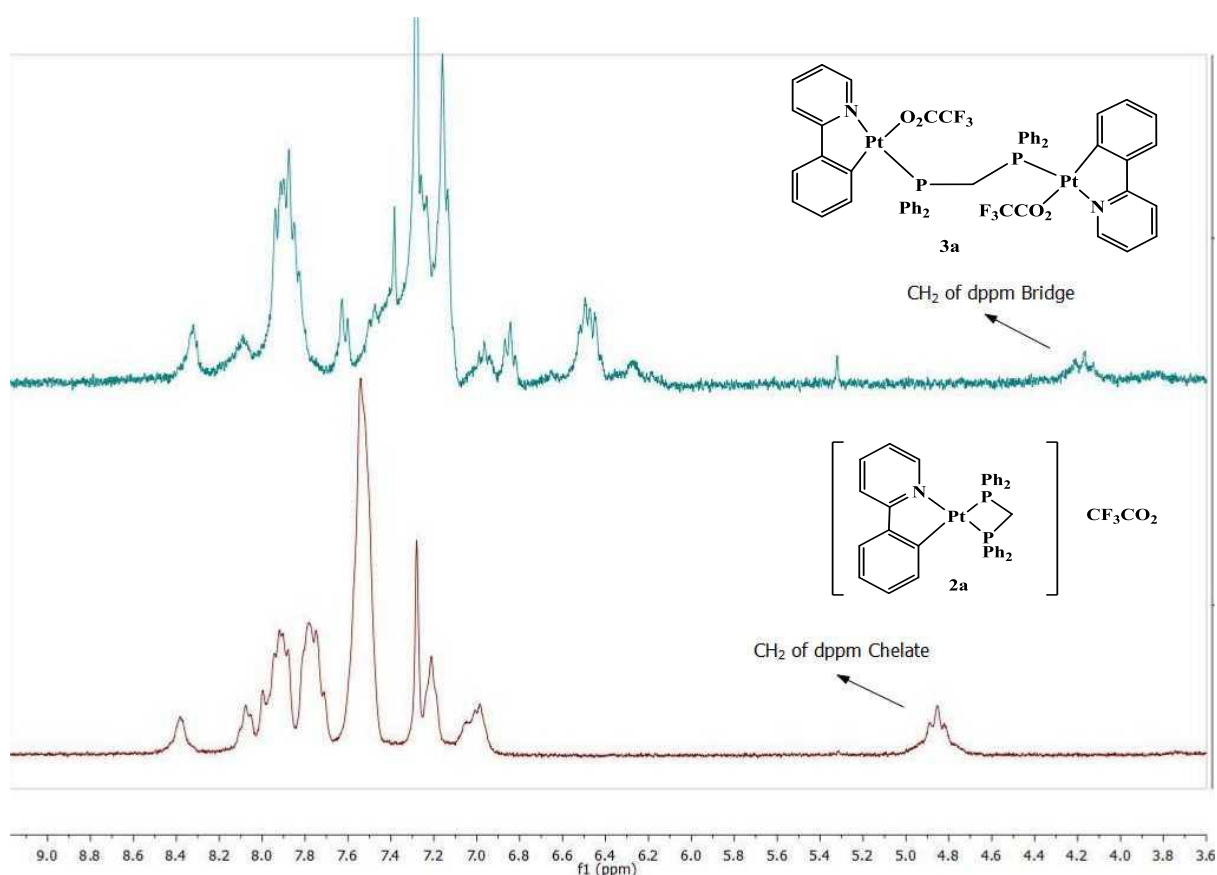
Conclusion: A series of cationic monomers and their corresponding neutral dimers, with general formula respectively [Pt(ppy)(dppm)]X, **2**, and [Pt$_2$X$_2$(ppy)$_2$(μ-dppm)] , **3**, (X = CF$_3$CO$_2$ or Cl) were synthesized and characterized in this work. Also by computational studies, the energies for mentioned transformations in above scheme were calculated.

References
[1] J. Dupont, C. S. Consorti and J. Spencer, *Chem. Rev.*, **2005**, 105, 2527.
[2] M. L. Tobe and J. Burgess, *Inorganic Reaction Mechanism*, Logman, Essex, UK, **1999**.
[3] S. M. Nabavizadeh, M. Golbon Haghighi, A. R. Esmaeilbeig, F. Raoof, Z. Mandegani, S. Jamali, M. Rashidi and R. J. Puddephatt, *Organometallics*, **2010**, 29, 4893.
[4] L. Xiao, Z. Chen, B. Qu, J. Luo, S. Kong, Q. Gong and J. Kido, *Adv. Mater.*, **2011**, 23, 926- 952.

[5] J. Kalinowski, V. Fattori, M. Cocchi and J. A. G. Williams, *Coord. Chem. Rev.*, **2011**, 255, 2401-2425.

[6] H. Yersin, A. F. Rausch, R. Czerwieniec, T. Hofbeck, T. Fischer, *Coord. Chem. Rev*. **2011**, 255, 2622 2652

Fluidity Equation for the Temperature Dependence of Viscosity of 1-Alkyl-3-methylimidazolium Bis(trifluoromethylsulfonyl)imide Ionic Liquids: Effect of Side Chain Length

Morteza Zare[a,*], Mohammad Hadi Ghatee[b,*], Rayhaneh Sami[b]

[a] *Department of Chemistry, Shahid Chamran University of Ahvaz, Ahvaz, Iran*
[b] *Department of Chemistry, Shiraz University, Shiraz 71946, Iran*
Email address: m.zare@scu.ac.ir; ghatee@susc.ac.ir

Introduction

Ionic liquids (ILs) are a class of low melting point compounds that result from combination of organic cations and organic or inorganic anions [1]. Due to their unique properties, such as low vapor pressure and good thermal stability, ILs are extensively investigated for many applications. They are vastly utilized as solvents for reactions media and as lubricants. To develop new solvents or lubricants, it is appropriate to conduct an analysis of behavior of viscosity as a function of temperature. In this work, fluidity equation is used to describe the viscosity of 1-alkyl-3-methylimidazolium bis(trifluoromethylsulfonyl)imide series ([$C_n$mim][Tf_2N], where n=2–10, 12, 14) as a function of temperature.

Method

Viscosity of the ILs shows non-Arrhenius temperature dependence. We have proposed a three-parameter equation for temperature dependent of viscosity, which successfully applies for a variety of ILs [2]:

$$\left(\frac{1}{\eta}\right)^{\varphi} = a + bT \qquad (1)$$

where a and b are specific adjustable parameters and φ is a characteristic exponent. This equation also can be successfully applied as a two-parameter equation where a universal value for the exponent (φ=0.3) is applied accurately. The Eq. (1) is used to correlate viscosity of [$C_n$mim][Tf_2N], where n=2–10, 12, and 14 with temperature.

Results and Discussion

The values of the viscosity of [$C_n$mim][Tf_2N] are fitted using the Eq. (1) in two-parameter form with φ=0.3 as a universal exponent. The range of temperature, number of data points, fitting parameters (a and b), correlation coefficient squared (R^2), and percent absolute average deviation (%AAD) are displayed in Table 1. The values of R^2 and %AAD indicate the Eq. (1) can describe the temperature dependent viscosity quite accurately.

If φ is allowed to adjust for each IL, we have a three-parameter relation. The fitting parameters (a, b, and φ), R^2, and %AAD of ILs are displayed in Table 2. The values of R^2 and %AAD indicate that three-parameter equation provides a better description than the two-parameter one, as expected.

Table 1. Temperature range (ΔT), number of viscosity data points, fitting parameters of Eq. (1) with φ=0.3, R^2, and %AAD of studied ILs. Viscosity data are taken from Ref [3].

ILs	ΔT/K	# of data points	- a	$b.10^2$	R^2	%AAD[a]
[C_2mim][Tf_2N]	278-358	17	0.68321	0.346	0.9981	2.67
[C_3mim][Tf_2N]	278-373	18	0.76094	0.362	0.9973	3.56
[C_4mim][Tf_2N]	278-393	19	0.74527	0.354	0.9954	5.10
[C_5mim][Tf_2N]	278-373	18	0.79941	0.368	0.9964	3.82
[C_6mim][Tf_2N]	278-393	19	0.79658	0.361	0.9974	4.18
[C_7mim][Tf_2N]	278-363	18	0.83633	0.371	0.9996	1.61
[C_8mim][Tf_2N]	278-363	18	0.83339	0.366	0.9984	2.54
[C_9mim][Tf_2N]	278-358	17	0.84972	0.368	0.9998	1.03
[C_{10}mim][Tf_2N]	278-393	19	0.81496	0.354	0.9984	3.51
[C_{12}mim][Tf_2N]	283-363	17	0.84527	0.358	0.9999	0.15
[C_{14}mim][Tf_2N]	313-363	11	0.84462	0.351	0.9999	0.43

[a] $\%\text{AAD} = \frac{1}{m}\sum_m \left|\eta_{\text{expt.}} - \eta_{\text{calc.}}/\eta_{\text{expt.}}\right| \times 100$

Table 2. Fitting parameters of Eq. (1) (a, b and φ), R^2, and %AAD of ILs. The temperature range, and number of viscosity data points are the same as Table 1.

ILs	$-a$	$b \cdot 10^2$	φ	R^2	%AAD
[C$_2$mim][Tf$_2$N]	0.78574	0.336	0.4409	0.9999	0.30
[C$_3$mim][Tf$_2$N]	0.84215	0.348	0.4292	0.9998	0.84
[C$_4$mim][Tf$_2$N]	0.84394	0.343	0.4418	0.9996	1.61
[C$_5$mim][Tf$_2$N]	0.85578	0.347	0.4265	0.9990	2.10
[C$_6$mim][Tf$_2$N]	0.86029	0.351	0.3956	0.9997	1.51
[C$_7$mim][Tf$_2$N]	0.85922	0.365	0.3379	0.9998	1.16
[C$_8$mim][Tf$_2$N]	0.85246	0.351	0.3641	0.9983	1.87
[C$_9$mim][Tf$_2$N]	0.85797	0.362	0.3241	0.9999	0.70
[C$_{10}$mim][Tf$_2$N]	0.84089	0.342	0.3630	0.9995	2.23
[C$_{12}$mim][Tf$_2$N]	0.84839	0.356	0.3090	0.9999	0.64
[C$_{14}$mim][Tf$_2$N]	0.86579	0.345	0.3363	0.9999	0.11

There is no clear trend in the parameters of the Eq. (1) with alkyl chain length. However, from Fig. (1), two distinct regimes characteristics of short ($n<6$) and long alkyl chain length ($n>6$) can be identified for the value of φ parameter. The similar patterns have been observed for surface tension and melting point of ILs. An initial decrease in the surface tension values from $n=1$ to $n=6$ and then achieving to a constant value for $n>6$ have been observed for [C$_n$mim][Tf$_2$N] [4]. Moreover, for short alkyl chains the melting point decreases with increasing alkyl chain length but increases for long alkyl chains [5]. It seems that cation-anion interaction, mostly Coulombic, is dominated in ILs with short alkyl chain length, while dispersion interactions between long alkyl chains on neighboring cations overcome to Coulombic ones for [C$_n$mim][Tf$_2$N] with $n>6$.
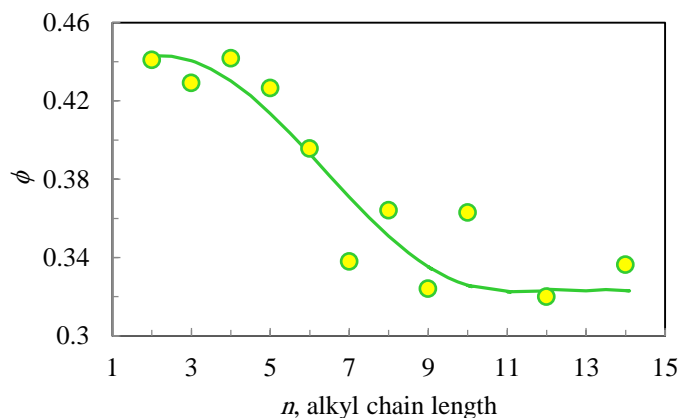

Figure 1. General trend in φ values dependence on the increasing alkyl chain in the cation. The line is the trend line.

Conclusion

The fluidity equation was utilized to describe the viscosity of [C$_n$mim][Tf$_2$N] with temperature. We can adequately assume constant value for the exponent ($\varphi=0.3$), which reduces the equation to a two-parameter one. The exponent φ can be related to predominant intramolecular and intermolecular interactions in ILs. More studies on the various types of ILs with different cations and anions are required to achieve a correlation between the exponent of proposed equation and viscous behavior of the fluid at molecular level. This work is under proceed in our group.

References

[1] K.N. Marsh; J.A. Boxall; R. Lichtenthaler. *Fluid Phase Equilib*., **2004**, *219*, 93–98.
[2] M.H. Ghatee; M. Zare; A.R. Zolghadr; F. Moosavi. *Fluid Phase Equilib.*, **2010**, *291*, 188–194.
[3] M. Tariq; P.J. Carvalho; J.A.P. Coutinho; I.M. Marrucho; J.N.C. Lopes, L.P.N. Rebelo. *Fluid Phase Equilib.*, **2010**, *301*, 22–32.
[4] A.M. Fernandes; M.A.A. Rocha; M.G. Freire; I.M. Marrucho; J.A.P. Coutinho; L.M.N.B.F. Santos. *J. Phys. Chem. B*, **2011**, *115*, 4033–4041.
[5] U.L. Bernard; E.I. Izgorodina; D.R. MacFarlane. *J. Phys. Chem. C*, **2010**, *114*, 20472–20478.

Synthesis of Novel Heterocyclic compound from reaction of some nitrogen nucleophile with perhalo compound

Reza Ranjbar-Karimi[a], **Tayebeh Davodian**[b]*.

a *Department of Chemistry, Faculty of Science, Vali-e-Asr University, Rafsanjan 77176, Islamic Republic of Iran.*
b *Department of Chemistry, Faculty of Science, Vali-e-Asr University, Rafsanjan 77176, Islamic Republic of Iran.*
(E-mail: T.Davodian83@yahoo.com).

Introduction: Perhalogenated aromatic and heteroaromatic compounds are important starting materials for the synthesis of other heterocyclic and macrocyclic compounds [1–3]. Many researchers are interested in the reactions of various N, O, S, C, and P nucleophiles with perhalogenated compounds [4–8]. The natures of nucleophile, reaction condition, and solvent have a basic role in the regiochemistry of the reactions. Pentachloropyridine reacted with bulky nucleophiles at 2-position of pyridine ring and with small nucleophiles at 4-position of pyridine ring [9].

Experimentals: In the bottom flask 4- iodotetrachlouropyridine 1(1mmol, 0.271gr) with potassium tiocyanate (1.5mmol, 0.95gr) was stirred and refluxed in dry THF for 48h and column chromatography on silica gel gave 2,3,5,6-tetrachloro-4-thiocyanatopyridine (2). In following, the mixture of benzyl amine (1mmol, 0.107gr) with potassium carbonate (2mmol, 0.27gr) was added to 2 (1mmol, 0.276gr) and stirred and refluxed for 5h. After completion of the reaction, the reaction mixture was cooled and the solvent was evaporated and extracted with chloroform, and evaporated to yield the crude product, which was then purified by column chromatography on silica gel to gave product(3).

Results and Discussion: In this work we would like to report the site reactivity of tiocyanate with 4-iodo tetrachloropyridine 1 in dry THF. In proceed, reaction of appropriate nitrogen nucleophile derived from benzyl amines derivatives with 2,3,5,6-tetrachloro-4-thiocyanatopyridine in the presence of potassium carbonate in dry CH_3CN as solvent was investigated. Our study indicated that the initial nucleophilic of thiocyanate attack at 4-position of pyridine ring and followed by cyclization of 2 by reaction with amines at the geometrically assessable 3 position of pyridine ring. The structure of compounds were confirmed with ^{1}H-NMR,^{13}C-NMR and IR spectroscopy (Scheme 1).
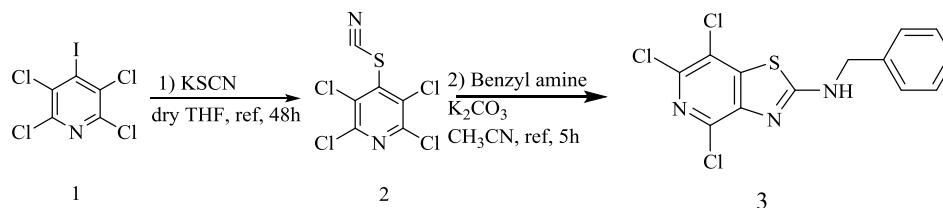
Scheme1- The possible reaction of 2 with benzyl amine

Conclusion: In conclusion, we demonstrated that the synthesis of N-benzyl-4,6,7-trichlorothiazolo[4,5-c]pyridin-2-amine from the reaction of benzyl amine compounds with 2,3,5,6-tetrachloro-4-thiocyanatopyridine.

References

[1]R. D. Chambers; A. Khalil, C. B. Murray; G. Sandford; A. S.Batsanov and J. A. K. Howard, *J. Fluorine Chem*, **2005**, 126,1002–1008.

[2] R. Ranjbar-Karimi; G. Sandford; D. S. Yufit and J. A. K.Howard, *J. Fluorine Chem*, **2008**, 129, 307–313.

[3] G. Sandford; R. Slater; D. S. Yufit; J. A. K. Howard andA. Vong, *J. Org. Chem*, **2005**, 70, 7208–7216.

[4] R. E. Banks; J. E. Burgess;W.M.ChengandR.N.Haszeldine,*J. Chem. Soc*., **1965**, 575–581.

[5] R. E. Banks; R. N. Haszeldine; D. R. Karsa; F. E. RickettandI. M. Young, *J. Chem. Soc. C*, **1969**, 1660–1662.

[6] R. E. Banks; R. N. Haszeldine; E. Philips and I. M. Young,*J. Chem. Soc. C*, **1967**, 2091–2095.

[7] R.D. Chambers, B. IddonandW. K. R. Musgrave, Tetrahedron,**1968**, 24, 877–885.

[8] B. V. Nguyen and D. J. Burton, *J. Fluorine Chem*, **2012**, 135,144–154.

[9] R. Ranjbar-Karimi, G. Sanford, D. S. Yufit, J. A. K. Howard, *J. Fluorine Chem*, **2008**,129, 307.

Application of chemometrics methods for simultaneous spectrophotometric determination of some industrial dyes using graphene oxide nano particles

Mahboobeh Razi Asrami [a]**, Jahan B. Ghasemi** [b]*

[a] Faculty of Chemistry, K. N. Toosi University of Technology, Tehran, Iran
[b] Faculty of Chemistry, University of Tehran, Tehran, Iran
* **E-mail address**: jahan.ghasemi@ut.ac.ir (J.B. Ghasemi).

Introduction: The removal of pollutants from wastewaters has become an important issue because of the environmental concerns [1]. Despite the toxic nature and high stability, dyes are widely used. Therefore, treatment of industrial effluents containing dyes, is important and necessary to be monitored before entering into water resources due to the widespread use of the dyes in the cosmetics, fungicides, parasiticides and aquaculture antiseptics, dyeing of cotton, wool, nylon, acrylic, leather, distilleries, manufacturing and so on [2]. Presence of these dyes in water resources, even in trace amounts is undesirable [3]. These dyes may reportedly exhibit humans gastrointestinal irritation including nausea, vomiting and diarrhea or respiratory irritation such as coughing and shortness of breath or even carcinogenesis, mutagenesis and other many environmental problems [4]. The aim of this project is the synthesis of graphene oxide nanoparticles and its application to extract Crystal Violet and Malachite Green from the water samples and their simultaneous determination by UV-Vis spectroscopy device and data analysis using central composite design (CCD) and partial least squares (PLS).

Experimental: Graphene oxide was synthesized by Hummers method. At first, 1 gr of graphite powder, 0.5 gr of sodium nitrate and 23 ml of concentrated sulfuric acid were stirred in a 1000 mL beaker. The beaker was put to the ice bath to reduce the mixture temperature below 20 °C. Then 3 gr of potassium permanganate was slowly added to the solution over a period of 20 min. The ice bath was removed and the temperature was kept constant at 35 ° C for half an hour. Then, 46 ml of water was slowly added to the mixture. The temperature rose to 98 ° C and was maintained at this extent for 15 minutes. The mixture was diluted with 140 ml of distilled water and 2.5 ml of hydrogen peroxide (30%) was added. The supernatant was removed by centrifugation (8000 rpm for 10 min). The sediment solid was washed, and then was placed in the oven at 60 ° C for 4 hours.

To find the optimum conditions for adsorption of dyes on the absorbent surface (GO) were used from Central composite design (CCD). In this work, based on studies and preliminary experiments, the effect of three factors including pH, extraction time and amount of adsorbent, on the extraction efficiency has been effectively detected.

Results and discussion: As can be seen in Fig. 1 there is considerable overlap between the absorption spectrum of CV and MG. Conventional methods are not suitable for quantitative determination of this complex system, to deal with this problem PLS method can be used. PLS technique that uses mathematical calculations compared to many separation methods that require complex sample preparation and separation can be used as a simplicity and low-cost technique for Simultaneous determination of CV and MG.

GO has a very large particular surface area with various functional groups. These hydrophilic functional groups of GO lead to that, it is well dispersed in an aqueous phase and by contact via

significant $\pi-\pi$ interaction and electrostatic interaction with CV and MG cause to remove them efficiently during mixture.
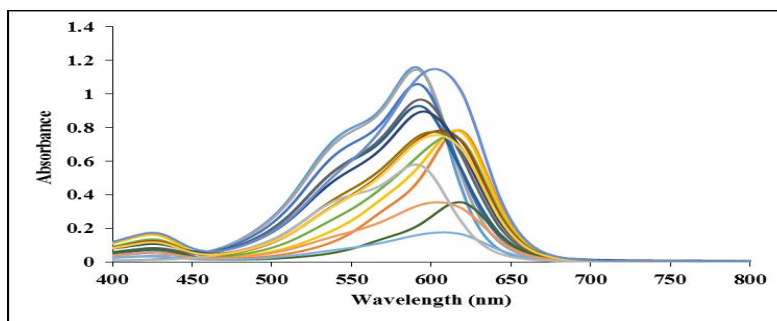

Fig. 1. Absorption spectra of CV and MG in the different concentration.

The interference due to several cations and anions on the simultaneous determination of CV and MG by the proposed method was studied in detail and the results are given in Table 1. When a change of more than $\pm 5\%$ in the absorbance of the analytes by an ion be created ‹then the ion is considered as interference [4].

Table 1   Tolerance limit of foreign ions.

Foreign ions	Tolerance ratio
K^+, Cu^{2+}, NH^{4+}, Co^{2+}, Ni^{2+}, Mg^{2+}, Pb^{2+}, Cd^{2+}, Ca^{2+}, Zn^{2+}, Hg^{2+}, Fe^{2+}, Al^{3+}, F^-, Cl^-, I^-, NO_3^-, CO_3^{2-}, SO_4^{2-}, PO_4^{3-}	1000
NO_2^-, SO_3^{2-}	500
CH_3COO^-, $B_4O_7^{2-}$, Na^+	250

Conclusion: In this paper, a method for Simultaneous determination of CV and MG in water samples were presented. The method that is the unique combination of DSPE preconcentration and multivariate calibration, can be applied in each laboratory with simple equipment. This method has many advantages such as simplicity, low cost, lack of need for professional technician. The sorbent was successfully used to Simultaneous determination of CV and MG from water samples.

References

[1] G. Crini, H. N. Peindy, F. Gimbert, C. Robert, Separation and Purification Technology 53 (2007), pp. 97-110.
[2] S. Srivastava, R. Sinha , Aquatic toxicology 66 (2004), pp. 319-29.
[3] V. K. Gupta, Journal of environmental management 90 (2009), pp. 2313-42.
[4] L. An, J. Deng, L. Zhou, H. Li, F. Chen, H. Wang, Y. Liu, Journal of hazardous materials 175 (2010), pp. 883-8.

Platinum Nanoparticles Supported on Thiol Containing Dendrimer: An Efficient Catalyst for Synthesis of Benzimidazoles and Benzothiazoles from Benzyl alcohols

Zahra Zamani−Noori[a], Amir Landarani Isfahani[b], Majid Moghadam[c]∗, Valiollah Mirkhani[d], Shahram Tangestaninejad[e], Iraj Mohammadpoor−Baltork[f], Niloufar Afzali[g]

[a] *PhD student of Inorganic chemistry*

[b] *PhD of organic chemistry*

[c] *Professor of Inorganic chemistry*

[d] *Professor of Inorganic chemistry*

[e] *Professor of Inorganic chemistry*

[f] *Professor of organic chemistry*

[g] *PhD student of Inorganic chemistry*

Department of Chemistry, Catalysis Division, University of Isfahan, Isfahan 81746-73441, Ira

*e-mail[*]:* **moghadamm@sci.ui.ac.ir**

Introduction
In recent years, platinum have been used as a catalyst for the synthesis of benzimidazoles and benzothiazoles [1]. Benzimidazoles and benzothiazoles are aromatic heterocycles which are chemically and biologically very significance [2]. Dendrimers are highly branched, spherical and three-dimensional materials and their unique structures are suitable for application in a wide range of catalytic systems because of their architectural excellent design [3 , 4].

Experimental
To a mixture of nano-silica supported dendrimer was added K_2PtCl_4 .The mixture was stirred at room temperature. The solution was subsequently reduced with an equal volume of fresh $NaBH_4$.

Result and Discussion
In this research, a reusable platinum base catalyst is reported for synthesis of Benzimidazoles and benzothiazoles. In this manner, Pt nanoparticles were immobilized on nanosilica-coated a novel and unique dendrimer containing thiol groups. The nanocatalyst, $Pt_{np}@nSTDP$, was characterized by FE-SEM, TEM, ICP, XPS and DR-UV-Vis techniques. The catalytic performance of $Pt_{np}@nSTDP$ was investigated for synthesis of benzimidazoles and benzothiazoles derivatives by the reaction of between benzyl alcoholes and 2-aminothiophenole or 1,2-phenylenediamine (Scheme 1).
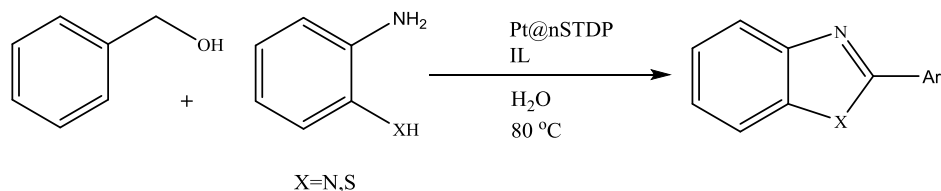
(Scheme 1)

Conclusion

These reactions were performed in H_2O as green media in the presence an IL. Desired products were obtained in high yields in short reaction time under mild conditions. Furthermore, the catalyst was stable under the reaction conditions and easily recovered and reused several times.

References

[1] Chaudhari, C.; Siddiki, S. H.; Shimizu, K.-i. *Tetrahedron Lett.,* **2015**, *56*, 4885-4888.
[2] Nasr-Esfahani, M.; Mohammadpoor-Baltork, I.; Khosropour, A. R.; Moghadam, M.; Mirkhani, V.; Tangestaninejad, S. *J. Mol. Catal. A: Chem.,* **2013**, *379*, 243-254.
[3] Anderson, R. M.; Yancey, D. F.; Loussaert, J. A.; Crooks, R. M. *Langmuir,* **2014**, *30*, 15009-15015.
[4] Isfahani, A. L.; Mohammadpoor-Baltork, I.; Mirkhani, V.; Khosropour, A. R.; Moghadam, M.; Tangestaninejad, S.; Kia, R. *Adv. Synth. Catal.,* **2013**, *355*, 957-972.

Master Equation Modeling of HCOH$_2$ Complex Unimolecular Decomposition

S. Hosein Mousavipour[a],*, Elham mazarei[a]

[a]*Department of Chemistry, College of Science, Shiraz University, Shiraz, Iran*

Email address: mousavi@susc.ac.ir

Introduction: Collision energy transfer plays a key role in unimolecular reactions [1,2]. Theoretical calculations provide a useful tool for estimating the rate constant of a system over wide ranges of temperature and pressure. Master equations (ME) describe the time evolution of the population distributions as molecules undergo reactive or non-reactive collisions. HCOH$_2$* is an intermediate formed during the reaction of CH (X^{2}II) with H$_2$O (^{1}A). Dynamics and kinetics of this intermediate is investigated through ME, in this work.

Methods: Time-dependent population of species calculated by MESMER [4] (Master Equation Solver for Multi Energy well Reactions) can be written as Eq. (1):

$$\frac{dn_i(E)}{dt} = Z_i \int_{E_{0i}}^{\infty} P_i(E, E') n_i(E') dE' - Z_i n_i(E) - \sum_{j \neq i}^{M} k_{ji}(E) n_i(E) + \sum_{j \neq i}^{M} k_{ij}(E) n_j(E) - k_{d_i}(E) n_i(E) +$$

$$K_{eqi} k_{d_i}(E) F_i(E) n_R n_m - \sum_{p=1}^{N_p} k_{p_i}(E) n_i(E) \qquad i = I, \ldots, M \qquad (1)$$

The canonical rate constant can then be computed according to Eq. (2):

$$k(T) = \frac{1}{Q(\beta)} \int_{E_i} k(E_i) \rho(E_i) e^{-\beta E_i} dE_i \qquad (2)$$

Given a potential energy surface (PES) with an arbitrary number of intermediates, the coupled deferential equations describing both reactive and non-reactive processes are solved allowing the role of the pre-reaction complex to be considered.

Results and Discussion: The *ab initio* data including geometrical information, symmetry numbers, PES of the system, vibrational frequencies and classical rotor moments of inertia and zero-point energies (ZPEs) at theMPWB1K/6-31++g(2df,2p) level of theory were used to calculate temperature and pressure dependence of the fractional populations of different species involved in this reaction. The most probable initiation step for the CH (X^{2}II) reaction with H$_2$O(^{1}A) is a barrier less association reaction to form a chemically activated intermediate

$HCOH_2{}^*$. The fractional populations and rate constant for each individual path for the title reaction have been calculated by solving one-dimensional chemical master equation. The PES for the title reaction is shown in Figure 1. The fractional populations of the species in this system are shown in Figure.2 at translational temperature of 1000 K and 1 atm pressure. The total rate constant of the main species are reported as:

$$k_{total} = 3.43 \times 10^{11} T^{-0.67} e^{\frac{1.35 kJmol^{-1}}{RT}}$$

$$k_{CH_2O+H} = 5.0 \times 10^{12} T^{-1.59} e^{\frac{3.65 kJmol^{-1}}{RT}}$$
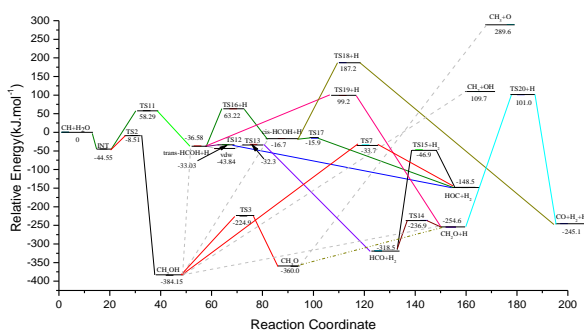
Fig. 1 The PES and relative energies of stationary points at the MPWB1K/6-31++g(2df,2p) level of theory.
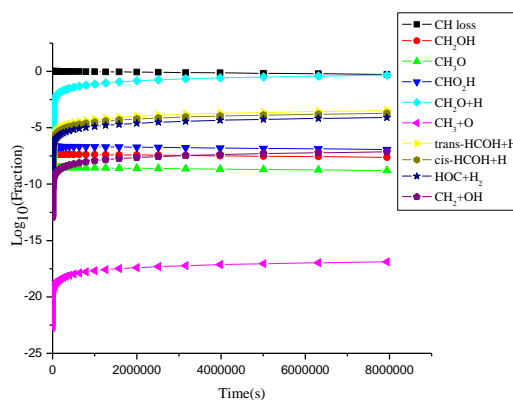
Fig. 2 Time evolutions of fractional concentrations of different species during the stages of the reaction at 1000 K and 1 atm.

Conclusion: Fractional profile for the species were studied by chemical ME simulation. Total rate constant of the reaction and rate constant for the main product (CH_2O) are in good agreement with the reported results in literature.

References

[1] Christiansen, J. A.; Kramers, H. A. Z. Phys. Chem. **1923**, *104*,451–471.
[2] Barker, J. B.; Weston, Jr. R. E. *Phys. Chem. A*.**2010**, *114*, 10619–10633.
[3] Glowacki, D.R.; Liang, C.H.; Morley, C.; Pilling M.J.; Robertson, S.H. *J. Phys. Chem. A*.**2012**, *116*, 9545−9560.
[4] Robertson, S. H.; Glowacki, D. R.; Liang, C.-H.; Morley, C.; Shannon, R.; Blitz, M.; Seakins, P. W.; Pilling, M. J., MESMER (Master Equation Solver for Multi-Energy Well Reactions), **2008-2013**; an object oriented C++ program implementing master equation methods for gas phase reactions with arbitrary multiple wells. http://sourceforge.net/projects/mesmer.

Lens electrolyte imbalance and chemical modification of crystallin proteins are two important causative players in senile and diabetic cataract development.

Reza Yousefi[*].

Protein Chemistry Laboratory (PCL), Department of Biology, Shiraz University, Shiraz, Iran

Email: ryousefi@shirazu.ac.ir

Introduction: The altered level of certain metal ions in eye lenses may play an important role in pathomechanism of both age-related (senile) and diabetic cataract disorders. In addition, various chemical modifications (i.e. deamidation, oxidation, acetylation, glycation, and proteolysis) of eye lens proteins (α-, β-, and γ-crystallins) have been indicated to participate in the pathogeneses of cataract which is known as a primary cause of blindness worldwide [1, 2].

Experimentals: We have used various spectroscopic techniques, gel electrophoresis and microscopic visualization assessments to investigate the particular impact of calcium and copper ions, as well as the effect of various chemical modifications on structure, stability, function and aggregation/fibrillation of lens crystallins.

Results and Discussion: Our recent investigations suggested that highly reactive endogenous chemical agents such as peroxynitrite, methylglyoxal, dehydroascorbic acid and homocysteine thiolactone can play important roles in structural and functional damages of lens proteins and they likely have significant contribution to the pathogenesis of diabetic and senile cataract development. We are also searching for those chemical compounds which are capable to prevent or attenuate the structural and functional insults of lens proteins. Our recent findings suggested lens antioxidant defense components as important barriers against various structural and functional damages of lens crystallins occurring by either highly reactive endogenous chemicals or by increased level of the metal ions such as copper.

Conclusion: The results of our earlier studies are to shed light on the molecular mechanisms underlying cataract development occurring by some endogenous chemical metabolites and also by unbalanced levels of some metal ions.

References

[1] M. Zhang; M. Shoeb; P. Liu; T. Xiao; D. Hogan; I. G. Wong; G. A. Campbell; N. H. Ansari. **2011**, Journal of Toxicology and Environmental Health, 74, 380-391.

[2] P. G. Hains; R. J. Truscott. Journal of Proteome Research, **2007,** 6, 3935-3943.

Novel and Highly Selective Cyanide Sensor Based on Green Synthesised of AuNPs in Honey

Mohammad Jafar Samimipour, Mohammad Mahdi Bordbar, Javad Tashkhourian*

Department of Chemistry, Shiraz University, Shiraz, 71454, Iran

E-mail: Tashkhourian@susc.ac.ir

Introduction: Environmental pollution with toxic materials is the detrimental issues facing our world in recent years [1]. Cyanide is extremely toxic substance due to its tendency to bind with iron in cytochrome oxidase causing hypoxia that inhibit the mitochondrial electron-transport chain [2]. In recent years, noble metal nanoparticles have been attracting extensive research interest, due to their unique optical, electrical and catalytic properties [3]. In this study honey was used as a reduction and stabilization of green synthesis of gold nanoparticles. The nanoparticles in aqueous solutions was used to measure cyanide in various aquatic environments.

Methods/Experimentals: For synthesis of AuNPs, 50 mg of $HAuCl_4$ was dissolved in 120 mL deionized water, 20 g of honey was diluted to 70 mL. 10 mL of this aqueous solution of honey was added to 30 mL of $HAuCl_4$ and stirred well. The complete reduction of $AuCl_4$ is evidenced by light purple color of the solution. Working solution was prepared by adding 0.5 mL stock AuNPs solution into 2.5 mL universal buffer solution. Similarly, a 10 µL aliquot of different concentration of cyanide was added this solution and the UV–Vis absorption spectrum was recorded at room temperature.

Result and Discussion: In this work we designed a chemosensor for determination of cyanid anions. Some important parameters such as the effect of pH, kind of buffer, volume of nanoparticle and time were optimized. Under optimized experimental conditions, relationship between difference of absorbance and cyanide concentration was linear in the ranges of 5×10^{-8} to 5×10^{-6} and 5×10^{-6} to 10^{-4} $molL^{-1}$ cyanide was obtained. Repeatability of method investigated by five different sensor and RSD = 1.36 were obtained for these sensors. AuNPs in the absence (a) or the presence (b) of cyanide is shown in figure 1. The absorbance of these particles at 539 nm is shown in figure 2.
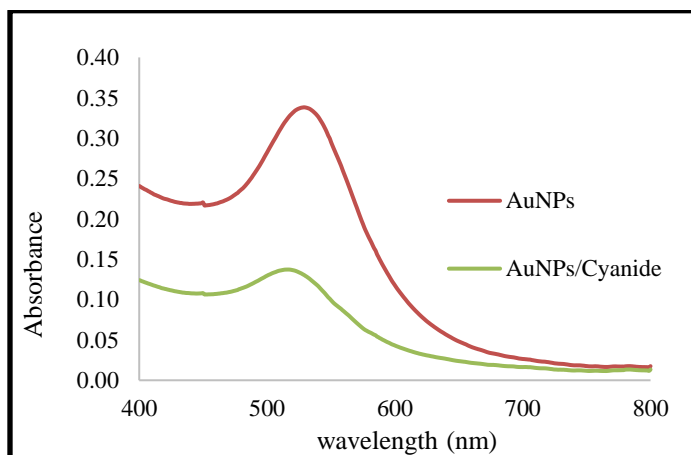

Figure1

Figure2

Conclusion: In summary, we have developed a novel chemosensor based on green synthesis of AuNPs for wide concentration range detection and determination of cyanide anion in environmental samples by UV/Vis spectrophotometry. At higher concentration in the hundreds of micromolar level, the colorimetric method can be used directly as a suitable tool for industrial sewage monitoring with the naked-eye. Compared to traditional methods, this system is relatively simple, without requiring complex organic synthesis and uses only commercially available materials, but has an excellent selectivity towards cyanide over other common anions and metal ions.

References

[1] O. A. Adegoke; T. E. Adesuji; O. E. Thomas. *Spectrochimica Acta Part A: Molecular and Biomolecular Spectroscopy,* **2014**,*128*, 147–152.

[2] H. M. Al-Saidi; S. A. Al-Harbi; E. H. Aljuhani; M. S. El-Shahawi. *Talanta*, **2016**, 159, 137–142

[3] S. Chen; J. M. Sommers. *J. Phys. Chem. B***, 2001**, *105*, 8816-8820.

Synthesis and Characterization of Superparamagnetic Nanoparticles of γ-Fe₂O₃@SiO₂@L-Leucine as a Green Catalyst for Preparation of Thiazoloquinolines

## Zahra Arabpoor [a], Hamid Reza Shaterian [a, *]

[a] *Department of Chemistry, Faculty of Sciences, University of Sistan and Baluchestan, PO Box 98135-674, Zahedan, Iran*

[*] *Corresponding author E-mail:* hrshaterian@chem.usb.ac.ir

Introduction

Magnetic nanoparticles (MNPs) have been well employed to immobilize organocatalysts and biocatalysts through the formation of covalent bonds [1]. Thiazolyl compounds and annulated thiazoles are applied in human therapeutics, veterinary remedy and leading structure for drugs[2].

In this research, we represented synthesis of MNPs-L-Leucine as an efficient heterogeneous catalyst, and its application in the preparation of thiazoloquinolines was investigated under thermal solvent-free conditions (Scheme 1).
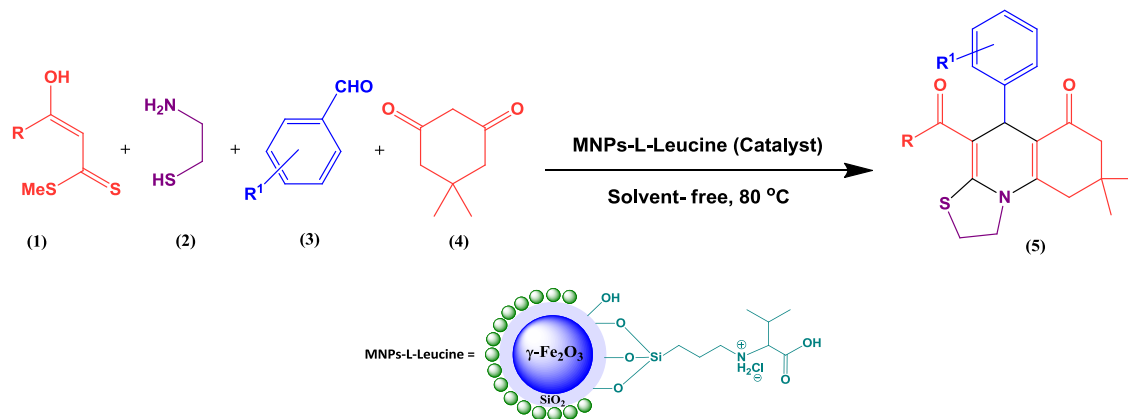
Scheme 1: γ-Fe₂O₃@SiO₂@L-Leucine catalyzed the preparation of thiazoloquinolines

Experimental

Synthesis of γ-Fe₂O₃@SiO₂@L-Leucine: The Fe_3O_4 nanoparticles were synthesized by a chemical co-precipitation technique[3, 4].The prepared nanoparticles were heated at 300 °C for 3 h to convert to γ-Fe₂O₃ nanoparticles. Chloro-functionalized γ-Fe₂O₃@SiO₂ was prepared according to the literature [5] and then converted to MNPs-L-Leucine.

Synthesis of thiazoloquinolines: A mixture of α-enolicdithioesters (0.5 mmol), cysteamine (0.5 mmol), aldehyde (0.5 mmol), cyclohexane-1,3-dione(0.5 mmol) and MNPs-L-Leucine (0.025 g) were stirred at 80 °C under solvent-free conditions.

Results and Discussion

The XRD pattern of MNPs-L-Leucine had six characteristic peaks which have a good accordance with the cubic structure of γ-Fe_2O_3 (Fig.1). XRD showed that SiO_2 and L-Leucine had amorphous phases. SEM image of MNPs-L-Leucine shows spherical morphology and average size 17.5 nm using histogram curve (Fig.2).The EDS spectrum implicates the presence of atoms Fe, O, Si, C, N and Cl in the catalyst (Fig.3).
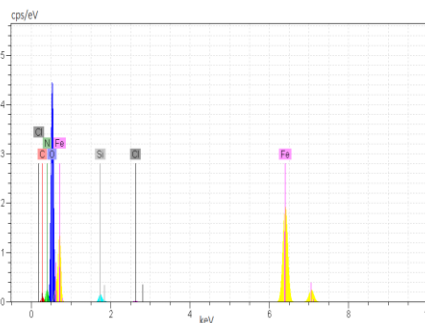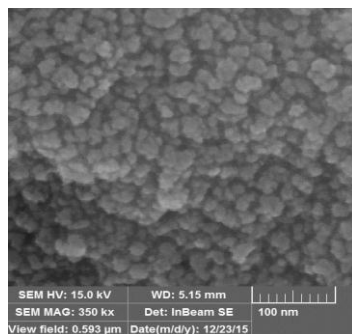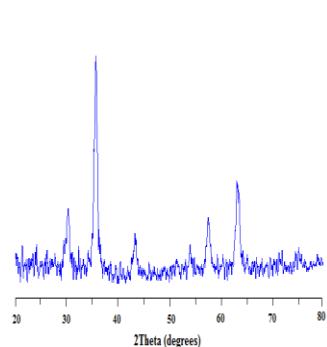

Fig.1: XRD of MNPs-L-Leucine

Fig.2 : SEM image of MNPs-L-Leucine

Fig.3: EDS spectrum of MNPs-L-Leucine

To evaluate the best optimum activity of the catalyst, MNPs-L-Leucine was applied in the one-pot four-component reaction of 3-hydroxy-3-phenyl-prop-2-enedithioate, cysteamine, 4-nitrobenzaldehyde and dimedone as a selected model. The best efficiency was obtained at 80 ^{o}C, with 0.025 g of the catalyst under solvent-free conditions. According to optimal considered conditions, various structurally derivatives of the desired products were synthesized. The products are synthesized in suitable times and good yields.

Conclusion

In summary, we represented synthesis and characterization of MNPs-L-Leucine as an efficient nanocatalyst. Its application in the preparation of thiazoloquinolines was investigated under thermal solvent-free conditions. MNPs-L-Leucine catalyzes the reaction with good yields, in short times, and under mild conditions. The catalyst was separated for the reaction mixture by an external magnet. The catalyst is reused at least for five runs without significant loss of its activity.

References

[1]   Y.Huan and W. Zhang; *Green Processing and Synthesis*, **2013**, *2*, 603-609.
[2]   M.Chakrabarty; A. Mukherji; S. Karmakar; R. Mukherjee; K. Nagai; A. Geronikaki and P. Eleni; *Arkivoc*, **2010**, *xi*, 265-290.
[3]   K. M. Ho and P. Li; *Langmuir*, **2008**, *24*, 1801-1807.
[4]   K.Azizi and A. Heydari; *RSC Advances*, **2014**, *4*, 8812-8816.
[5]   Z.Arabpoor and H. R. Shaterian; *RSC Advances,***2016**, *6*, 44459-44468.

Application of quantitative structure-retention relationship in the retention behavior of some nitroimidazole derivatives in high performance liquid chromatography

S. Mollazadeh Sadeghion[a], A. A. Amiri[a*]

[a] Department of Applied Chemistry, Shiraz Branch, Islamic Azad University, Shiraz, Iran

*amiri1355@gmail.com

Introduction: High performance liquid chromatography (HPLC) is a well-matured technique currently employed in the vast majority of analytical laboratories for research, routine analysis and quality control. The number of HPLC trials carried out daily in the world, specially using reversed-phase chromatography is enormous. On the other hand, the composition of mobile phase in liquid chromatography has a primary role both in isocratic and gradient elution, since it determined the possibilities offered for optimization of solvent strength and selectivity. Hence, optimization of the mobile phase composition and prediction of retention behavior are important aspects of method development in HPLC [1]. The use of suitable binary solvent mixtures provides the most common solution to achievement of sufficient resolution and selectivity. However, ternary or even higher order solvent mixtures are expected to be a more advanced and flexible solution [2]. Although, separations are still being optimized in a non-systematic manner, often by empirical optimization strategies, but in ternary solvent mixtures, as the number of possible combinations of solvents is very large, the trial-and-error approach is time-consuming and also very expensive. Recently, modeling of retention behavior is extremely attractive, as only limited input data is required in order to rapidly obtain accurate optimum separation conditions [3,4].

Methods / Experimentals:

10 mg of each substance were dissolved in 10 mL of acetonitrile to obtain a stock solution with a concentration of 1000 mg L^{-1}. Working standards were prepared by diluting these stock solutions with acetonitrile to yield concentration of 100 mg L^{-1} for all substances. 20 µL of these working standards injected to HPLC with a 20 µL loop at ambient temperature. All experiments carried out at flow rate 1 mL min^{-1} of mobile phase in isocratic mode. The wavelength 280 nm was selected for monitoring of studied compounds.

Results and Discussion: The molecular structures of the two compounds used in this study are reperesented in Figure 1. We used these molecules to identifying retention behavior affecting mobile phase parameters. Since the most of these compound have NH group as substituent, standard silica-based reversed-phase columns could not be suitable for our purpose because the analytes interacted very strongly with the stationary phase support and result in broaden peaks. In this study a µBondapak C_{18} endcapped stationary phase with a very low metal content was used. The peaks asymmetry for all compounds were determined using the expression: $A_s = W_{2/2} / W_{1/2}$, where $W_{1/2}$ is peak first half width and $W_{2/2}$ is peak second half width. Using this stationary phase, almost all peaks were symmetrical (A_s= 0.91-1.37). Typical chromatograms of compound NI1 and NI15 recorded for mobile phases of acetonitril-methanol-water 20-40-40% are shown in Figure 1. Obviously, with increase the volume fraction of water in solvent, retention times of compound increase. Preliminary studies showed that logarithmic transformation of capacity factor (log k) resulted in more straightforward models, which is in agreement

with LSFER concept. Thus, in all derived models, log k was used as dependent variable. LSFER equations obtained for each solute using volume fraction of each pure solvent, products of volume fractions of solvent and solvatochromic parameters of pure solvents as independent (or predictor) variables. For each substance, the significant independent variables were selected by applying a stepwise procedure to build up the model. The quality of each model was estimated by its coefficient of multiple determination (R^2), standard error of regression (SE) and variance ratio (F-value). For all solutes, the model equations contain the volume fraction of water (f_w) and product of volume fraction of water and volume fraction of methanol ($f_w f_m$) of ternary mixed solvent, which suggests that amount of water and methanol are the main factors controlling the interaction of these derivatives with acetonitrile-methanol-water mixed solvents.
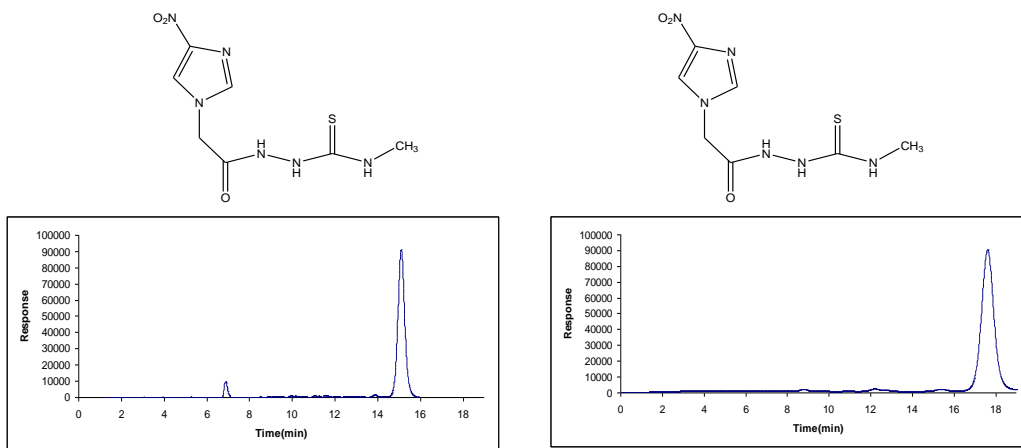

Figure 1. Chromatograms of NI1 and NI2

Conclusion: Multi linear regression was used to find those properties of acetonitrile-methanol-water mixtures which affect the retention time of 18 synthesized Nitroimidazoles .Influence of the composition of mobile phase on the retention time was investigated and among the solvent properties, volume fraction of water (f_w) and product of volume fraction of water and volume fraction of methanol ($f_w f_m$) were identified as controlling factors the retention times of these derivatives and a reduced equation Log k = $b_0 + b_1 f_w + b_2 F_{AC} \pi^*_{AC} + b_3 f_w f_m$ was obtained. Coefficient of f_w is positive which indicates that longer retention times are obtained in solvent systems of higher f_w values. By using this equation, one is able to obtain qualitative information about solute-solvent interaction and also to predict the quantitative estimate of retention times of new or non-tested compounds.

Refrences

[1] R. Beges, V. Sanz-Nebot, J. Barbosa, *J. Chromatogr. A*, **2000**, *869*, 27
[2] A. Pappa-Louisi, P. Nikitas, A. Papageorgiou, *J. Chromatogr. A*, **2007**, *1166*,126.
[3] M. L. Hajnos, M. Waksmundzka-Hajnos, K. Glowniak, *Acta chromatogr.* **2002**, *12*, 211.
[4] B. Hemmateenejad, K. Javidnia, M. Elyasi, *Anal. Chim. Acta*, **2007**, *592*, 72.

[Pyridine–SO$_3$H]NO$_3$ as a tasked specific ionic liquid for the synthesis of TEX

Saeid Moradi, Mohammad Ali Zolfigol[*], Mahmood Zarei

Depatment of Organic Chemistry, Faculty of Chemistry, Bu-Ali Sina University, Hamedan 6517838683, Tel: +988138282807, Fax: +988138380709 Iran. E-Mail: zolfi@basu.ac.ir&mzolfigol@yahoo.com.

Introduction: Nitro compounds are one of the most important starting materials for the synthesis of energetic compounds, dyes, pharmaceuticals, and polymers so that finding novel nitrating agents has great demand in organic methodology [1]. In this regard, developing green nitrating systems is also attractive [2]. Cyclic molecules with multi N–NO$_2$ functionalities, such as hexahydro-1,3,5-trinitro-1,3,5-triazine (RDX), octahydro- 1,3,5,7-tetranitro-1,3,5,7-tetrazocine (HMX) as well as 2,4,6,8,10,12-hexanitro-2,4,6,8,10,12 hexaazaisowurtzitane (HNIW),are important class of highly explosive compounds (Figure 1) [3,4].Thus, much effort has been put into the development and synthesis of this class of compounds. One of them, 4,10-dinitro-2,6,8,12-tetraoxa-4,10-diazaisowurtzitane or 4,10-dinitro-2,6,8,12-tetraoxa-4,10-diazatetracyclo[5.5.0.05,903,11]dodecane(TEX), [5,6] is an attractive nitro amine explosive, due to its energetic activity, high density, high detonation velocity, and great explosion potential. The presence of NO$_2$ functional groups and skeletal strain are the major reasons for these properties [7]. In this paper we obtained (TEX) by 1-sulfopyridinium chloride [Pyridine–SO$_3$H]NO$_3$.
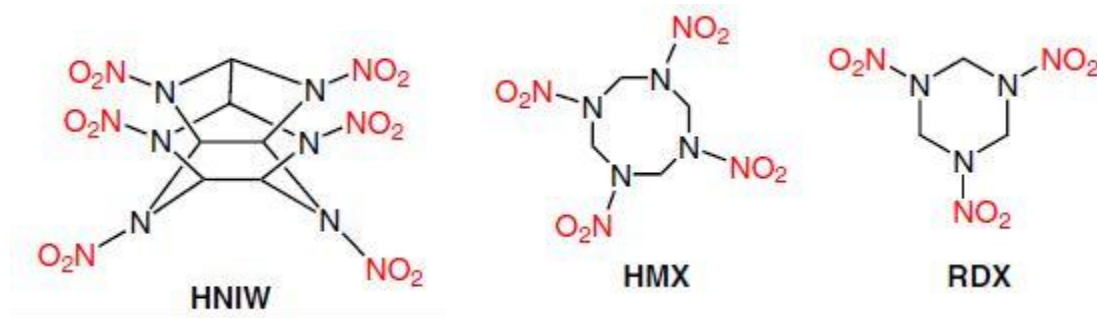

Fig. 1.Molecular structure of HNIW, HMX and RDX

Methods / Experimentals: [Pyridine–SO$_3$H]NO$_3$ was prepared according to our previously reported procedure. During the synthesis of TEX the temperature of the reaction should be slowly increased and, on workup, shock, heat, friction, and impact on the product must be avoided. To a round-bottomed flask (10 mL) was added [Pyridine–SO$_3$H]NO$_3$ (0.222 g, 1.5 mmol). 1,4-diformyl-2,3,5,6-tetrahydroxypiperazine (DFTHP) (1 mmol) and oxalaldehyde (1 mmol) were then added, and the mixture was stirred at room temperature. After the reaction was completed (monitored with TLC), dichloromethane (5 mL) was added to the reaction mixture, and the mixture was stirred for 2 min and separated. The organic solvent was evaporated, and the product was easily purified by short column chromatography. Note: For the nitration of aniline, after the reaction was completed, the reaction mixture was basified to pH 8 by the slow addition of 10% NaOH solution. The organic layer was separated, and the aqueous layer was extracted with dichloromethane. The combined organic solution was washed with brine, dried over MgSO$_4$, filtered, and concentrated to give a crude product, which was purified with short column chromatography. (Scheme1)
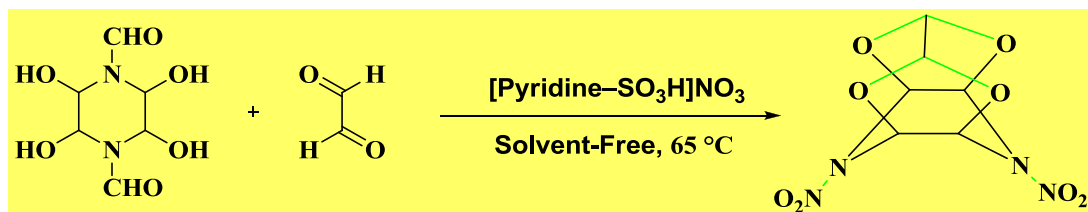
Scheme 1. Synthesis of TEX

Results and Discussion: In continuation of our knowledge based development of nitration of aromatic rings, synthesis of energetic materials and preparation of TEX [6], herein, we wish to develop the ability of [Pyridine–SO$_3$H]NO$_3$ as an efficient nitrating agent for the synthesis of TEX. [Pyridine–SO$_3$H]NO$_3$ is a suitable alternative for nitrating mixture of concentrated HNO$_3$ and H$_2$SO$_4$, because it has both nitrate and sulfonic acid moieties in its structure. It is obvious that synthesis of TEX via [Pyridine–SO$_3$H]NO$_3$ is better than another method such as NaHSO$_4$·H$_2$O/NaNO$_3$, NaHSO$_4$·H$_2$O/HNO$_3$, silica sulfuric acid (SSA)/NaNO$_3$, SSA/HNO$_3$, nanometa silica mono sulfuric acid sodium salt (NMSMSA)/ HNO$_3$, nano meta silica disulfuric acid (NMSDSA)/HNO$_3$, C$_2$H$_2$O$_4$.2H$_2$O/NaNO$_3$, Fe(HSO$_4$)$_3$/HNO$_3$, Al(HSO$_4$)$_3$/HNO$_3$, CuNO$_3$·3H$_2$O, Fe(NO$_3$)$_3$·9H$_2$O, Fe(NO$_3$)$_3$·9H$_2$O/FeCl$_3$, Ce(HSO$_4$)$_3$·7H$_2$O/HNO$_3$, NH$_4$NO$_3$/NaNO$_3$.

Conclusion: In conclusion, we have developed a nitrating system for the synthesis of TEX by using [Pyridine–SO$_3$H]NO$_3$ under mild conditions. TEX was prepared in good yield, high purity, and short reaction time with a simple workup procedure.

References:
[1] G. Yan; M. Yang, Org. Biomol.Chem.**2013**, 11, 2554.
[2] G. K. S. Prakash; L. Gurung; K. E. Glinton; K. Belligund; T. Mathew; G. A. Olah, Green Chem. **2015**, 17, 3446.
[3] (a) Y. Bayat; M. A. Zolfigol; A. Khazaei; M. Mokhlesi; M. Daraei; M. A. Heydari Nezhad Tehrani; G. Chehardoli, Propellants, Explos., Pyrotech., **2013**, 38, 745. (b) Y. Bayat; S. S. Hajimirsadeghi; S. M. Pourmortazavi, Org. Process Res. Dev. **2011**, 15, 816. (c) Y. Bayat; Y. M.Zarandi; M. A.Zarei; R.Soleyman; V. Zeynali, J. Mol. Liq. **2014**, 193, 83. (d) Y. Bayat; J. Mokhtari, Def. Sci. J. **2011**, 61, 171.
[4] S. S. Sysolyatin; A. A. Lobanova; Y. T. Chernikova; G. V. Sakovich, Russ. Chem. Rev. **2005**, 74, 757.
[5] V. T. Ramakrishnan; M. Vedachalam; J. H. Boyer, Heterocycles **1990**, 31, 479.
[6] (a) M. A. Zolfigol; A. Khazaei; A. R. Moosavi-Zare; A. Zare; H.G. Kruger; Z. Asgari; V. Khakyzadeh; M. Kazem-Rostami, J. Org. Chem, **2012**, 77, 3640. (b) A. R. MoosaviZare; M. A. Zolfigol; M. Zarei; E. Noroozizadeh; M. H. Beyzavi, RSC Adv., **2016**, 6, 89572–89577. (c)H. Ghaderia; M. A. Zolfigol; Y. Bayat; M. Zareia; E. Noroozizadeha, Synlett, **2016,** 27, A–E
[7] K. Karaghiosoff,; T. M. Klapotke; A. Michailovski; G. Holl, Acta Crystallogr., Sect. C: Cryst. Struct.Commun.**2002**, 58, o580.

A novel approach to synthesis of new imidazo[2',1':2,3]thiazolo[5,4-d]pyrimidines as a class of heterocyclic compounds

Maria Asgari, Mehdi Bakavoli *

Department of Chemistry, School of Sciences, Ferdowsi University of Mashhad, 91775-1436 Mashhad

Email address: mbakavoli@yahoo.com

Introduction: The thiazolo [5,4-d] pyrimidines have a wide range of biological activities such as immunosuppressive agents ['], anti-agiogenic agents [2] and potential anti-Parkinson's disease agents [3]. The synthetic routes to thiazolo[5,4-d]pyrimidines mainly start from either pyrimidine or thiazole precursors. In this way, treatment of 5-amino- or 5-nitro-pyrimidines with reagents such as acid anhydrides, phosgene, carbon disulphide or isothiocyanates affords thiazolo[5,4-d]pyrimidines [4-7]. On the other hand, the imidazole moiety is present in a wide range of naturally occurring molecules as well as in a number of important synthetic compounds such as fungicides, herbicides, plant growth regulators, and therapeutic agents [8].

Methods / Experimentals. Initially, the mixture of compound (**1**) and glycine in the presence of K_2CO_3 was refluxed in CH_3OH/H_2O. Then, the resulting compound (**2**) underwent cyclization in refluxing $POCl_3$ to give compound (**3**). Finally, new derivatives of heterocyclic system limidazo[2',1':2,3]thiazolo[5,4-d]pyrimidin 4(a-g) was obtained through S_NAr reaction of several secondary amines with compound (**3**).

Results and Discussion: Our approach is based on the 2,5-dichloro-7-methylthiazolo[5,4-d]pyrimidine as starting material [10]. Reaction of compound (**1**) with glycine as the representative of amino acids in the presence of K_2CO_3 proceeded smoothly in a selective manner to give the substituted derivative (**2**). The latter compound on exposure to $POCl_3$ at reflux temperature underwent cyclisation to give 2-chloro-4-methylimidazo[2',1':2,3]thiazolo[5,4-d]pyrimidin-6(7H)-one (**3**). The proof for the cyclisation process came from spectroscopic data. For example, the ^1H NMR spectrum of compound (**3**) showed a singlet at 2.07 ppm corresponding to the methyl group and another singlet at 5.26 ppm for the methylene moiety. The mass spectrum of compound (**3**) showed the molecular ion peak at m/z 240 (M^+) corresponding to the molecular formula $C_8H_5ClN_4OS$. Compound (**3**) has the potential to react with nucleophiles such as secondary amines to give new substituted products (scheme 1).

Entry	a	b	c	d	e	f	g
R₂N-							
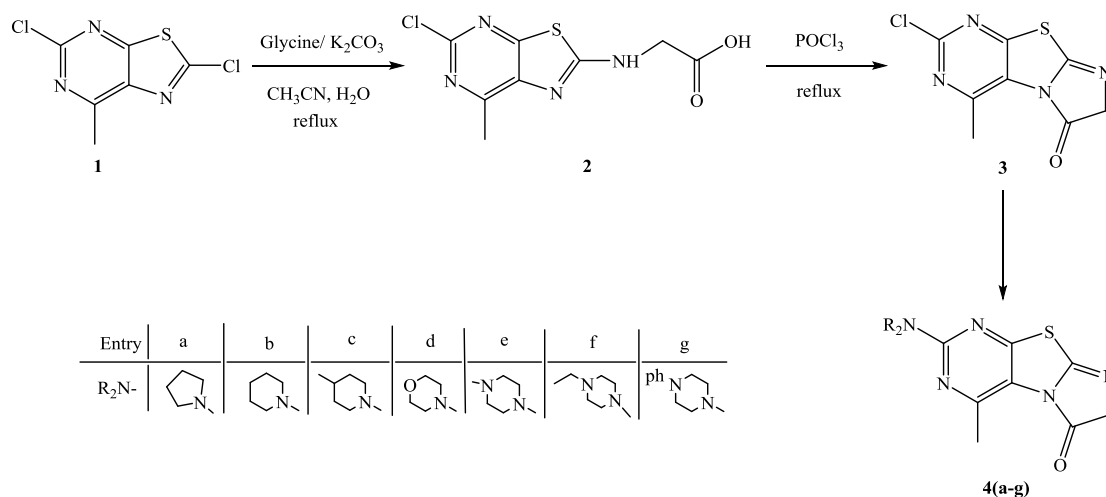
Scheme 1

Conclusion: In conclusion, we have presented an efficient synthetic pathway for the synthesis of new derivatives of imidazo[2´,1´:2,3] thiazolo[5,4-*d*]pyrimidin 4(a-g) *via* the heterocyclization of 2,5-dichloro-7-methylthiazolo[5,4-*d*]pyrimidine **(1)** with glycine. The foregoing tricyclic heterocyclic derivatives can be useful templates in drug discovery.

References:

[1] M.-Y. Jang; Y. Lin; S. De Jonghe; L.-J. Gao; B. Vanderhoydonck; M. Froeyen; J. Rozenski; J. Herman; T. Louat; K. Van Belle; M. Waer ; P. Herdewijn. *J. Med. Chem.*, **2011**, 54, 655-668.

[2] R.W.A. Luke; P. Ballard; D. Buttar; L. Campbell, J. Curwen; S.C. Emery; A.M. Griffen; L. Hassall; B.R. Hayter; C.D. Jones; W. McCoull; M. Mellor; M.L. Swain ; J.A. Tucker. *Bioorg. Med. Chem. Lett*., **2009**, 19, 6670–6674.

[3] F. Varano; D. Catarzi; L. Squarcialupi; M. Betti; F. Vincenzi; A. Ravani; K. Varani; D.D. Ben; A. Thomas; R. Volpini; V. Colotta. *Eur. J. Med. Chem.,* **2015**, 96, 105–121.

[4] S.J. Childress ; R.L. McKee. *J. Am. Chem. Soc*., **1951**, 73, 3862–3864.

[5] E. Suzuki; S. Sugiura; T. Naito; S. Inoue. *Chem. Pharm. Bull*., **1968**, 16, 750–755.

[6] D.J. Brown; W.C. Dunlap; G.W. Grigg; J. Kelly. *Aust. J. Chem*., **1977**, 30, 1775 – 1783.

[7] J. Liu; R.J. Patch; C. Schubert; M.R. Player. *J. Org. Chem*., **2005**, 70, 10194–10197.

[8] Y. S.Lo; J. C.Nolan; T. H.Maren; W. J., Jr.Welstead; D. F.Gripshover; D. A. Shamblee. *J. Med. Chem.* **1992**, 35, 4790–4794.

[9] H. Moradi; H. Eshghi; M. Bakavoli. *J. Chem. Res*., **2016**, 40, 276–279.

Efficient synthesis of^{2}H labeled compounds related to Chemical Weapons Convention

**Sajjad Mousavi Faraz[a], Hamid Saeidian[b,∗], Mehran Babri[a,∗]**

[a]Defense Chemical Research Lab (DCRL), P.O. Box 31585-1461, Karaj, Iran

[b]Department of Science, Payame Noor University (PNU), P.O. Box 19395-4697, Tehran, Iran. E-mail: Sadjadmousavie@gmail.com

****

Introduction: Chemical warfare agents (CWAs), were used on a large scale during World War I. Neurotoxic or nerve agents, e.g. sarin, soman, VX, and tabun, were used for the first time during the Iran–Iraq war[1] and subsequently in some terrorist attacks in Japan and Syria. Among chemical weapons, nerve agents constitute the greatest concern due to their high toxic effects on human[2]. The Organization for the Prohibition of Chemical Weapons (OPCW) maintains a networkof designated laboratories in order to provide off-site analytical services [3]. Gas chromatograph (GC) coupled with mass spectrometer (MS) is widely used for the analysis of CWAs, because most CWAs are volatile and nonpolar compounds[4].The OPCW Central Analytical Database (OCAD) is the major source for CWC-related reference mass spectra. This database is being developed in OPCW under supervision of a special validationgroup [5].^{2}H labeled nerve agents and their related-CWC compounds were prepared from dialkyl methyl(d$_3$)phosphonate. These labeled compounds are useful as internal standards in mass spectrometry for monitoring chemical warfare agents and their metabolites[6]. On the other hand, the knowledge on fragmentation mechanismsin MS spectra becomes important from the verification spoint of view for on/off site analysis. Proposed fragment structures were confirmed through analyzing fragment ions of deuterated analogs.

Representativemethods/experimentals: To a solution of methyl(d$_3$)phosphonic dichloride (0.2 mmol) and triethylamine (0.4 mmol) in CH$_2$Cl$_2$(1 mL), appropriate alcohol(0.2mmol) in CH$_2$Cl$_2$(300 µL) was added drop wise, while stirring. The reaction mixture was stirred at ambient temperature for 10 min. The ammonium fluoride (0.2 mmol) was added to the solution. The mixture was stirred for an hourat ambient temperature. The resulting solution was analyzed using GC/MS as required.

Results and Discussion: A key intermediate in the synthesis of ^{2}H labeled nerve agents and their related-CWC compounds was dialkylmethyl(d$_3$)phosphonate **1**. These compounds were prepared from commercial available trimethylphosphite and triethylphosphite and methyliodide(d$_3$) through Arbuzov reaction (Scheme1).
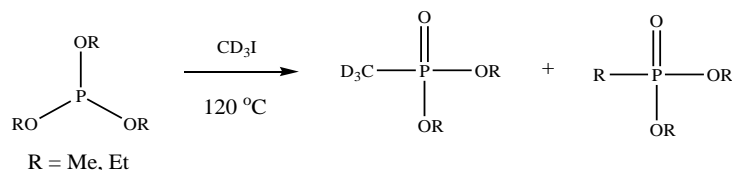
Scheme 1. The Arbuzov reaction for synthesis of dialkyl methyl(d$_3$)phosphonate.

Trimethylphosphite in this reaction was not work well and dimethyl methylphosphonate was produced as a major product. Use of Triethylphosphite (3eq.) and CD_3I (1 eq.) gave the desired product in high yield.

As shownin Scheme 2, isotopomer of nerve agents and their related-CWC chemicals were synthesized from diethyl methyl(d$_3$)phosphonate with good yields. The structure of the desired compounds **2-10** were confirmed by ^{13}CNMR, ^{31}PNMR and GC-MS (EI and CI) spectrometry.
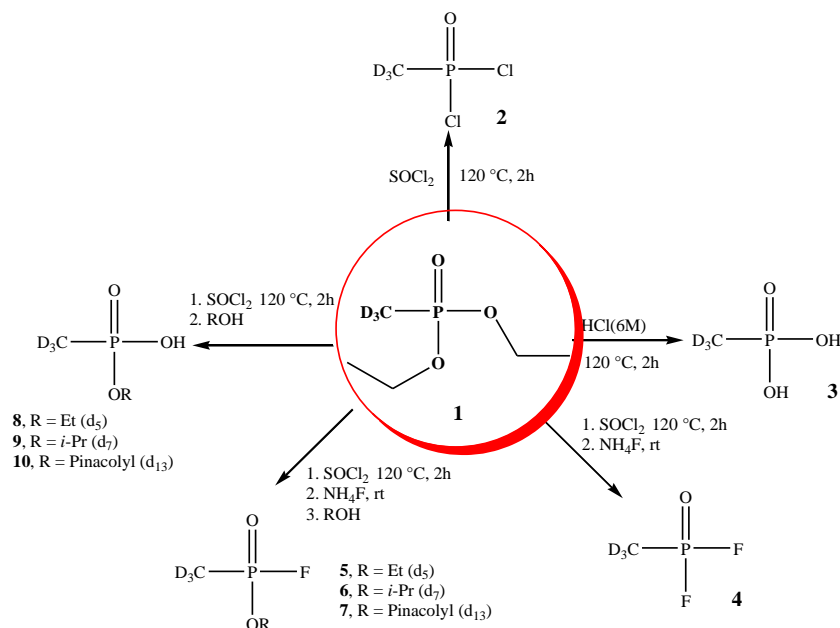
Scheme 2.Thesynthesized related-CWC chemicals from diethyl methyl(d$_3$)phosphonate.

Conclusion: Through a series of reactions, diethyl methyl (d$_3$) phosphonate was converted to some isotopomer of nerve agents and their related-CWC compounds with high yields. Theresults show that the synthesis of ^{2}H labeled compounds need special reaction conditions.

References

1. UN Report S/117911 (**1986**) United Nations, New York.
2. R.T. Delfino; T.S. Ribeiro; J.D. Figueroa-Villar.*J. Braz. Chem. Soc*. **2009**, *20*, 407-412.
3. J. Hendrikse, Comprehensive review of the Official OPCW Proficiency Test, in:M. Mesilaakso (Ed.), Chemical Weapons Convention Analysis, Sample Collection, Preparation and Analytical Methods, John Wiley & Sons Ltd, Chichester,UK, **2005**, p. 89.
4. H. Saeidian; M. Babri; D. Ashrafi; M. Sarabadani; M.T. Naseri.*Anal. Bioanal. Chem.***2014**, *406*, 5221-5230.
5. OPCW Technical Secretariat, Report of the forty-second meeting of the validation group for the updating of the OPCW central analytical database, 2 and 3September **2015**.
6. R. Wu;N. L. Siegfried;G. Schmidt; R. F. Williams; L. A. Silksa. *J. Label Compd. Radiopharm***2012**, *55,* 211–222.

Solid state linkage isomerization in thiocyanato-bipyridineplatinum (II) complexes: A DSC and DFT analysis on the kinetic and thermodynamic of the metastable isomers

Fahime Nasouti, Abbas Eslami

Department of Inorganic Chemistry, Faculty of Chemistry, University of Mazandaran,

P.O.Box 47416-95447, Babolsar, Iran

Email address: nasouti.fahime@gmail.com

Introduction

The coordination mode of ambidentate ligands toward transition metal ions may be predicted based on ligand-binding selectivity to various factors [1,2]. The thiocyanate ion is regarded as a good candidate to produce linkage isomerism with transition metal complexes. For thiocyanate platinum(II) complexes, presence of a π-acceptor ligand trans to the thiocyanate lead to preferred N-bonded isomer and in the absence of that, the S-bonded thiocyanate was proposed to be favored [3]. $[Pt(bipy)(NCS)_2]$ complex can be dominated as a N-bonded isomer at ambient temperatures, the S-bonded isomer as a kinetic product can be achieved at lower temperatures [4,5]. The kinetic and thermodynamic parameters of this interconversion are still unknown. we have used DSC method to report these parameters for first time. DFT calculations were employed to elucidate the relative stabilities of isomers and suggested transition states.

Experimental

The $[PtCl_2(bipy)]$ complex was prepared according to a previous report in the literature [6]. To a DMSO solution of $[PtCl_2(bpy)]$, an aqueous solution containing $AgNO_3$ was added. A gray precipitate of AgCl was removed by filtration. To the resulting yellow filtrate, an aqueous solution of excess KSCN was added at ca. 5°C, resulting in the immediate formation of the yellow precipitate. The yellow precipitate was filtered and repeatedly washed with water. This process of washing is very important to avoid the conversion of the yellow crystals to the red ones.

Results and discussions

DSC curves of solid samples of $[Pt(bipy)(SCN)_2]$ at several heating rates exhibit a fine exothermic peak in the range 120–190 °C, which can be ascribed to $(-SCN)_2$ to $(-NCS)_2$ linkage isomerization upon heating (Fig. 1). The isomerization DSC curves were resolved into two distinct peaks (by using PeakFit® software) that correspond to stepwise isomerization reactions. The stepwise enthalpy changes of the isomerization, ΔH^1_{SCN} (first stage) and ΔH^2_{SCN} (second stage) which are (–2.999) and (–2.817) kJ mol^{-1} can be determined upon mathematical resolution of the DSC peaks. The thermokinetic parameters (table 1) were calculated by Kissinger method [6], an isoconversional (model-free) method and using Eyring equation [7]. According to the negative value of activation entropy and activation volume of isomerization, we could assign an association mechanism or bond

making in the transition states. The electronic structures of the reactant, intermediate and also product were optimized in the gas phase using DFT/B3LYP and 6-31G(d,p)/LANL2DZ basis sets. The platinum atom is surrounded by two nitrogen atom of bipy ligand and two SCN groups, which form a square planner structure. The transition states for the stepwise isomerization were described as pentacoordinate structures in the gas phase. The activation energies (E_a) of linkage isomerization were calculated by energy differences between the transition state and the reactant for each stage of conversion. The activation energies for the first (E_{a1}) and second stage (E_{a2}) were obtained as 114.4 and 119.5 kJ mol^{-1}, respectively.
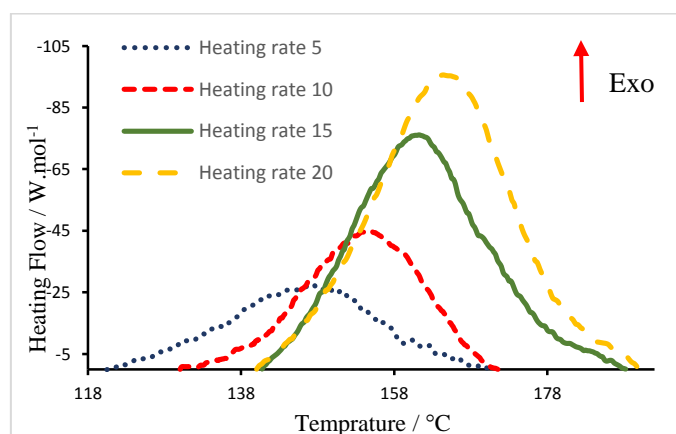

Fig.1. DSC curves of linkage isomerization of solid samples of [Pt(bipy)(SCN)$_2$] at heating rates of 5, 10, 15 and 20 ⊙C min^{-1}

Table. 1. Activation parameters for the stepwise thermal isomerization of [Pt(bipy)(SCN)2]

$E_{a1}^{\#}$	$E_{a2}^{\#}$	$\Delta H_1^{\#}$	$\Delta H_2^{\#}$	$\Delta S_1^{\#}$	$\Delta S_2^{\#}$	$\Delta G_1^{\#}$	$\Delta G_2^{\#}$	$\Delta V_1^{\neq}$	$\Delta V_2^{\neq}$
kJ.mol^{-1}	kJ.mol^{-1}	kJ.mol^{-1}	kJ.mol^{-1}	J.mol^{-1}.K^{-1}	J.mol^{-1}.K^{-1}	kJ.mol^{-1}	kJ.mol^{-1}	Å	Å
101.788	106.261	77.965	78.094	-92.871	-92.663	117.468	118.252	-0.9686	-0.9309

Conclusion

For the first time DSC analysis was employed to studying the isomerization of thiocyanate platinum complexes. The resolution of the DSC peaks allowed us to investigate the thermodynamics and thermokinetics of linkage isomerization in the solid state which were still unknown. DFT calculations of these linkage isomers show that (-NCS)$_2$ isomer is thermodynamically more stable than (-SCN)$_2$ isomer.

References:

[1]   H.E. Toma, R.C. Rocha, Croat. Chem. Acta. 2001, 74, 499-528.
[2]   E.V. Boldyreva, Russ. J. Coord. Chem. 2001, 27, 297–323.
[3]   A. Turco, C. Pecile, Nature, 1961, 191, 66-67.
[4]   I. Bertini, A. Sabatini, Inorg. Chem. 1966, 5, 1025-1028.
[5]   Sh. Kishi, M. Kato, Inorg. Chem. 2003, 42, 8728-8734.
[6]   A.K. Burnhamb, S. Vyazovkin, J.M. Criadoc, L.A. Perez Maquedac, C. Popescud, N. Sbirrazzuolie, Thermochim. Acta, 2011, 520, 1-19.
[7]   G. Lente, I. Fabian, A.J. Poe, New J. Chem. 2005, 29, 759-760.

Synthesis and characterization of novel nanostructure zinc(II) Schiff base coordination compounds and its possible application for preparation of nanostructure zinc oxide

S. Khani[a], M. Montazerozohori[a,*]

[a] Department of Chemistry, Yasouj University, Yasouj 75918-74831, Iran

Email address: mmzohori@yu.ac.ir; S.khani62@yahoo.com

****

Introduction: Schiff base ligands are one of the most important classes of donor compounds forming metal coordination materials [1, 2]. Schiff base compounds containing an imine group, are usually formed by the condensation reaction between a primary amine and an active carbonyl. In recent decades, various uses of the metal coordination compounds have been discovered [3, 4]. Metal Schiff bases complexes have been the focus of extensive studies because of their applications in various chemical and biological areas such as organic synthesis, catalyst, models for active sites of metalloenzymes and drug design [5, 6], optoelectronic devices, sensors, antimicrobial, antivirus, antibacterial and antifungal agents. The potential of the schiff bases and their complexes for binding or DNA cleavage has conducted the biochemists to study the activities of these compounds in the biochemistry point of view. Zinc complexes with schiff base ligands have been studied in different fields of medicinal chemistry including treatment of Alzheimer disease, enzyme inhibitors, DNA interaction or as antitumor, antibacterial, antidiabetic, antioxidant, anticancer, antifungal agents. In most cases, it was found that Zn complexes were generally more active than their free ligand. In continuation of our studies on the synthesis of metal schiff base complexes, the aim of the present research is the synthesis and spectral characterization of some novel nano-structure zinc complexes of a new schiff base ligand.

Methods / Experimentals:

Materials

All solvents and chemicals used in the synthesis and analysis were purchased from Aldrich and Merck, and used without any further purification. Zinc azide and thiocynate were freshly synthesized based on our previous report.

Synthesis of schiff base ligand and its zinc complexes

The ligand was prepared by drop-wise addition of 1 mmol (0.1032 g) of diethylenetriamine in ethanol (5 cm^3) to 2mmol (0.3504 g) of 4-(dimethylamino)cinnamaldehyde dissolved in ethanol (5 cm^3) under severe stirring according to our previous report. Synthesis of ligand takes 4-h time at room temperature, and the reaction is completed by the appearing of a yellow solution in reaction pot that confirmed the formation of ligand. For the synthesis of the zinc complexes, the ligand solution (10 cm^3) was drop-wise added to the stoichiometric amount of zinc halide, thiocyanate, or azide salts (1 mmol) in ethanol (5 cm^3) under strong stirring for 15 min. Afterward, the reaction mixture was stirred for 4-5 h at room temperature.

Results and discussion

Physical properties of the ligand and its complexes are given in Table 1. Ligand is naturally liquid but all complexes are as solid powders; and all compounds are stable at room temperature. The molar conductivity for all compounds has been measured in 10^{-3} M solutions in DMF. The low molar conductance values in the range of 14.40-23.1 Ω^{-1} cm^2 mol^{-1} confirm that these compounds are non-electrolyte. SEM image was also used to present the morphology of the complexes. SEM image showed that the particles are agglomerated and are observed as nanostructure and as non-uniform needle like.

Thermo-gravimetric analysis (TG/DTG) of ligand(Fig. 1) and all complexes has been performed in the temperature range of room temperature to 1000 ˚C under N$_2$ atmosphere with a heating rate of 10˚per minute for investigation of their thermal stability and existence of water molecules inside or outside the coordination sphere of metal ion.

Table 1 Physical data of the Schiff base ligand and its zinc complexes

Compounds	Color	Melting point (˚C) (Dec.)	Yield (%)	$\Lambda^{\circ}_M/cm^2 \, \Omega^{-1} \, mol^{-1}$
Ligand	Orange liquid	-	78	21.7
ZnLCl$_2$	Orang	182	82	14.4
ZnLBr$_2$	Yellow	198	76	20.4
ZnLI$_2$	Dark orange	228	87	23.1
ZnL(SCN)$_2$	Yellow	214	74	21.6
ZnL(N$_3$)$_2$	Yellow	207	68	20.8
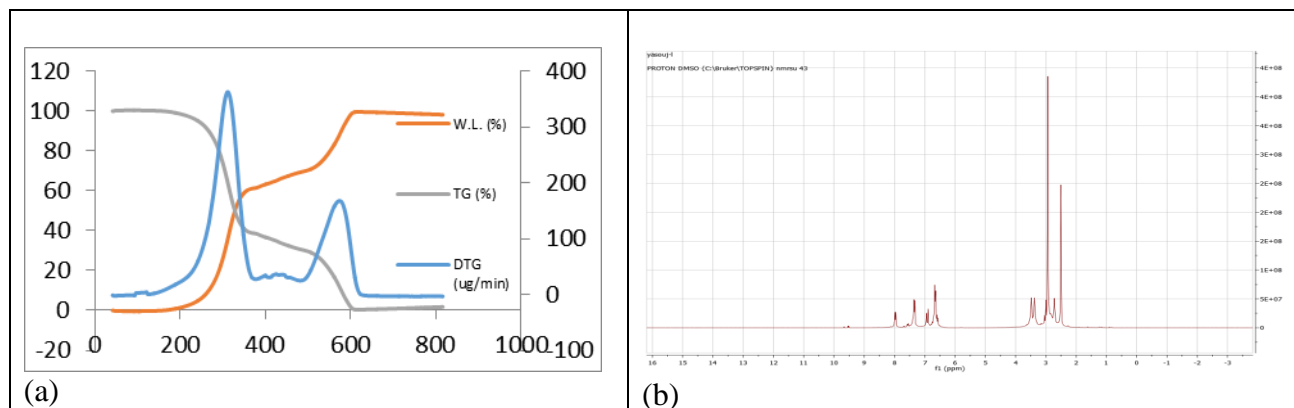
Fig. 1 The TG/DTG graphs for ligand (a) ^{1}H NMR of ligand (b)

IR spectral analysis was used to identify the nature of the functional groups attached to the metal atom. An IR spectral comparison between the free ligand and its zinc complexes shows some changes in position of peaks. The spectrum of the free Schiff base ligand showed the peak of azomethine group (–CH=N) at 1631 cm^{-1}, which is shifted to lower wavenumbers in the zinc complexes, that this shift confirms the involvement of ligand azomethine nitrogen in linkage to zinc ion. The electronic absorption spectrum of the ligand shows one important absorption band. The absorption band observed at 336 nm in ligand spectrum were attributed to $\pi-\pi^*$ electronic transition. The spectra of the zinc complexes showed a band too, a band at 381–385 nm assignable to $\pi-\pi^*$ transition that have been redshifted to longer wavelengths due to the promotion of electron back donation from the highest occupied molecular orbital of the zinc ion to the lowest unoccupied molecular orbital of ligand. ^{1}H and ^{13}C NMR of ligand (Fig. 1) and its complexes were recorded in the DMSO-d6 solution. The resulting data from ^{1}H and ^{13}C NMR confirm the proposed structure for schiff base ligand and its complexes.

Conclusion

In this research, some new nano-structure zinc(II) coordination compounds of an schiff base ligand were synthesized and then characterized by spectral (FTIR, UV–visible, ^{1}H and ^{13}C NMR) and physical techniques such as melting points, molar conductivity, Scanning electron microscopy (SEM) and X-ray powder diffraction (XRD). thermal analysis of ligand and its complexes revealed that they are decomposed via 2–3 thermal steps in the range of room temperature to 1000 ˚C.

References

[1] M. Montazerozohori; H. Mohammadi; A. Masoudiasl; M.Nasr-Esfahani; R. Naghiha; A. Assoud. J. Iran. Chem. Soc., **2016**, DOI 10.1007/s13738-016-0978-8
[2] M. Montazerozohori; F. Parsi; A. Masoudiasl; R. Naghiha; M. Montazer Zohour. Synth. React. Inorg. Met.-Org. Chem. Nano Met. Chem., **2016**, DOI 10.1080/15533174.2016.1218511
[3] S. Nur Alam; R.Shahidur; R. Arifur; S. Abdus; Abu Yousuf; I. Farhadul; A. Azharul. Bangladesh Pharm J., **2012**, 15, 83–7.
[4] K. Gupta; A. Sutar; C. Lin. J Coord Chem Rev., **2009**, 253, 1926–46.
[5] S. Akin; T. Taniguchi; W. Dong; S. Masubuchi; T. Nabeshima. J. Org. Chem., **2005**, 70, 1704.

Theoretical studies of Polycaprolactone (PCL) as nano-carrier for anticancer drug delivery

Afshan Mohajeri[*], Soode Amigh

Department of Chemistry, College of Sciences, Shiraz University, Shiraz, Iran

Email: amohajeri@shirazu.ac.ir

Introduction

Drug delivery is the method or process of administering a pharmaceutical compound to achieve a therapeutic effectin humans or animals [1].

Polymeric nanoparticles (PNPs) are types of nano-carriers for drug delivery systems (DDS). Drugs can be immobilized on PNPs surface after a polymerization reaction or can be encapsulatedon PNP structure during a polymerization step [2].Drugs may be released by desorption, diffusion, or nanoparticle erosion in target tissue. The examples of drug-polymeric nano-carrier conjugates used as drug delivery systems [3]. In this work we have studied drug delivery systems for transporting anticancer drugs such as mitomycin C. In our model, the adsorption of mitomycin C on to Polycaprolactone (PCL) as a PNP by hydrogen bonding is investigated.

Methods

We have applied density functional theory (DFT) at M06-2X level using TZV basis set. The adsorption energies were calculated as $E_{ads} = E_{\text{complx}} - (E_{\text{drug}} + E_{\text{PCL}})$ where E_{complex}, E_{drug} and E_{PCL} represent the total electronic energies of drug/PCL complexes, free drug and PCL respectively. The adsorption energy were then corrected for BSSE using counterpoise method $E_{ads}^{corr} = E_{ads} + BSSE$.

Results and Discussion

Figs. 1 show the graphical representations of mitomycin C and Polycaprolactone (PCL).
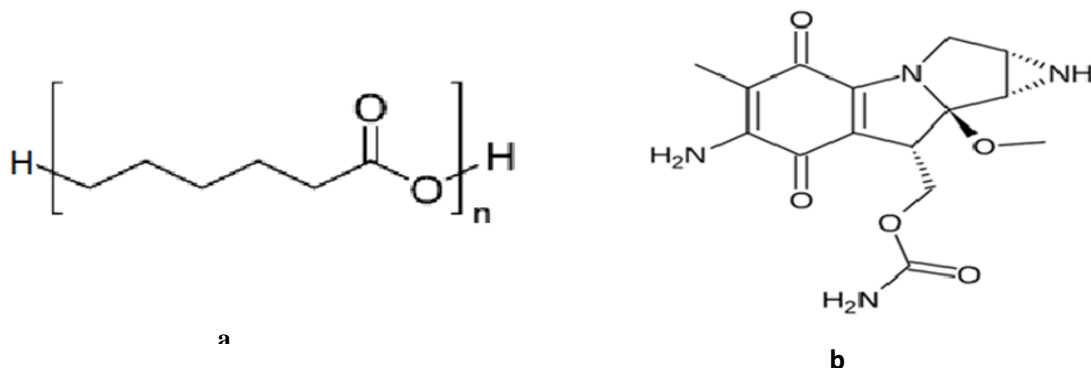

Fig1. a) polycaprolactone (PCL) and b) mitomycin C

Adsorption of mitomycin on PCL can occur from eight different adsorption sites. The adsorption energies were calculated and found position that the most stable configuration was found (Fig. ٢).
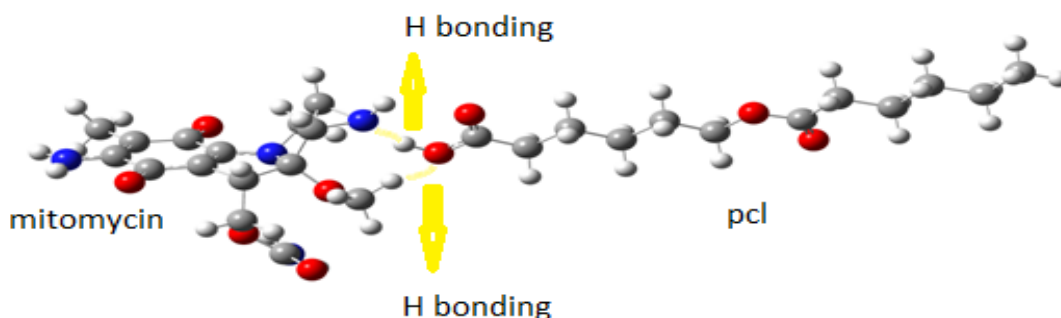

Fig٢. Lowest energy structure for adsorption of mitomycin on PCL.

In order to evaluate the reactivity of different sites in drug and carrier, Fukui functionswere calculated for all local reactive sites [٤]. The results of Fukuifunctions are in agreement with the adsorption energies, indicating that maximum Fukui correlates with the largest adsorption energies. For the best adsorption positionunder scrutiny, the nature of interactions between drug and PCL was analyzed using AIM theory with the help of AIM٢٠٠٠ software. Furthermore, NBO calculations have been employed to describe the state of charge transfer upon drug adsorption [٥].

Conclusion

We have performed DFT calculations on the PCL as nano-carrier in order to find the best adsorption position for drug delivery of mitomycin C. In all of the adsorptions, the interaction between mitomycin and PCL is through hydrogenbonding. We found that in the lowest energy structure two strong hydrogen bonds exits between mitomycin and PCL.

References

[١] Tiwari G, Tiwari R, Sriwastawa B, Bhati L, Pandey S, Pandey P, BannerjeeSK.*Int.J. Pharma.Investig.,*٢٠١٢, ٢, ٢-١١.

[٢] Mora-Huertas CE, Fessi H, Elaissari A. *Int.J. Pharm.,* ٢٠١٠, ٣٨٥, ١١٣-١٤٢.

[٣] Wilczewska AZ, Niemirowicz K, Markiewicz KH, Car H. *Pharmacol. Rep.,*٢٠١٢, ٦٤, ١٠٢٠-١٠٣٧.

[٤]Yang W, Mortier WJ.*J. Am. Chem. Soc.,*١٩٨٦, ١٠٨, ٥٧٠٨-٥٧١١.

[٥] A.E. Reed, L.A. Curtiss, F.A. Weinhold.*Chem.Rev.,*١٩٨٨, ٨٨, ٨٩٩-٩٢٦.

Theoretical Study of Mg-porphyrin-C_{70} Fullerene: a Novel Sensor of Oxygen in the Presence of Carbon Oxides

Sattar Arshadi[a]

[a]*Department of chemistry, Payame Noor University, 19395-4697, I.R. of Iran*

Chemistry_arshadi@pnu.ac.ir

Introduction: According to importance of O_2 gas, the designing and developing of efficient sensors for detecting the trace concentrations of this gas seems to be essential [1]. The very high surface to volume ratio and the hollow structure of nanomaterials such as fullerenes make them ideal materials for adsorption, detection and storage of gas molecules. On the other hand, doping with heterocyclic macrocycle compounds such as porphyrins and their metal complexes can improve the nanomaterial properties [2].

Computational methods: The studied compounds were $C_{70}F$ molecule with D_{5h} point group, the Porphyrin-C_{70} Fullerene ($PIC_{70}F$), Mg- $PIC_{70}F$, O_2 and CO. The geometries of the considered compounds were optimized at the B3LYP/6-31G (d) as implemented in Gaussian 98 suite of program [3]. In order to make defect similar to porphyrin in fullerene, the fullerene C_{70} molecule was selected with D_{5h} point group. Finally, the adsorption configurations of O_2 and CO gas molecules on Mg-$PIC_{70}F$ were studied. To that end, the adsorption energies were corrected using BSSE correction through the counterpoise method with "ghost" atoms [37] according to the following equation:

$$E_{ads}^{BSSE} = E_{Mg-PIC70F/gas} - \left[E_{Mg-PIC70F/gas\,ghost} + E_{gas/\,Mg-PIC70F\,ghost} \right] \qquad (1)$$

Where the E_{ads}^{BSSE} is the BSSE corrected adsorption energy. The "ghost" gas and M-$PIC_{70}F$ corresponds to additional basis wave functions centered at the position of the O_2, CO and CO_2 or the Mg-$PIC_{70}F$, without any atomic potential.

Results and discussion: The geometrical structures, binding energies, electronic properties, ΔN, FOT, DOS, distribution of the HOMO and LUMO, NBO basis analysis (such as charges and donor–acceptor interactions) and TD-DFT absorption spectra are scrutinized to

predict the adsorption properties and mechanism of *metal-PIC$_{70}$F-gas* systems. Relative stabilities of studied compounds have been verified through binding energy.

Due to strong chemisorption of Mg^{2+} ions on 18-membered porphyrin like cavity of PIC$_{70}$F, the band gap, work function and total dipole moments have been reduced. In this process electrons will flow from conjugate carbons of PIC$_{70}$F to metal ion and consequently, the cavity size will be increased. These occurrences make the Co-N ionic which is in agreement with *NBO* analyses results.
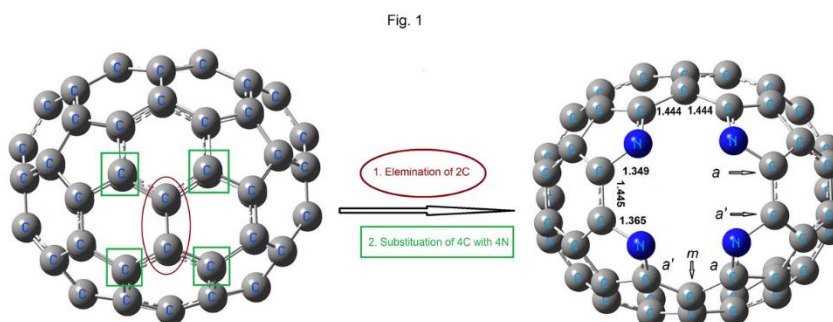

Fig 1. The formation schematic of porphyrin induced C$_{70}$ fullerene (PIC$_{70}$F) (right) from fullerene C$_{70}$ (left)

Conclusion: During the O$_2$ and CO adsorption, for all configurations, the cavity size will be decreased and conjugated carbon atoms of fullerene transfer charge to adsorbed gas *via* nitrogen$_{porphyrin}$ –metal bridge and increase the negative charge on its surface. Consequently the total dipole moment especially for higher E_{ads}^{BSSE} will be increased.

The obtained results revealed that only with adsorption of O$_2$ gas molecule on Mg-PIC$_{70}$F, the amount of E$_g$ has been considerably decreased. Based on calculated E_{ads}^{BSSE} and E$_g$, it is expected that the Mg-PIC$_{70}$F could be a promising candidate in gas sensor devices for selective detection of O$_2$ even in the presence of CO.

References

[1] Mowery MD, Hutchins RS, Molina P, Alajarín M, VidalL A, Bachas LG. Anal Chem. 1999;71:201-204.

[2] Hassani F, Tavakol H. Sens Actuators, B: Chemical. 2014;196:624-630.

[3] Frisch, M J. et al. Gaussian 98A.11.3, Gaussian Inc., Pittsburg: USA,2002.

Preparation and Characterization of Eggshell Membrane Electrospun Nanofibers

Leila Mohammadzadeh , Mehrdad Mahkam[a]*, Roya Salehi[b]

[a]*Department of Chemistry, Faculty of Basic Sciences, Azarbaijan Shahid Madani University, Tabriz, Iran*
[b]*Drug Applied Research Center and Faculty of advanced Medical Science, Tabriz University of Medical Sciences, Tabriz, Iran*
Mmahkam@yahoo.com

Introduction:

Electrospinning of various natural protein-based materials, such as keratin, collagen has been widely investigated in recent years [1]. Protein-based electrospun nanofibers have a high surface area to volume ratio, unique physical properties, and biocompatibility, which make them suitable to mimic the scaffolds of human skin tissue in biomedical applications, such as wound dressings and cosmetic sheets. Eggshell membrane (ESM), which contains collagen types I, V, and X, is a common waste material in daily life. ESM exhibits the cell-producing action of amino acids, adherence to textured surfaces due to a network structure, appropriate moisture retention, and air permeability, which are suitable characteristics for medical applications [2].

Experimentals:

SEP was prepared by dissolving raw ESM powder in aqueous 3-mercaptopropionic acid and acetic acid followed by neutralizing to pH 5.

Electrospinning of S-ESM blend fibers: Spinning solutions were prepared by dissolving PVAو silk fibroin and SEP in solvent with concentrations of 10% (w/w) blending ratio (SEP/PVA/ silk fibroin = 15:15:70). This mixture was vigorously stirred at room temperature for 12h. An electrospinning apparatus was designed and built, composing of a syringe and stainless needle, a ground electrode, a copper plate covered by aluminum foil as a collector, and an adjustable high voltage supply. The prepared solution was filled into the 5mL syringe, and anode is attached to the external surface of the metal needle. When the high voltage was applied across the syringe and the grounded collector, the solution would be ejected from the tip of the needle to produce nanofibers and deposit on the grounded collector as fibrous membranes. The as-spun mats were dried under vacuum for 24h to remove residual solvent and then used for further studies.

Results and Discussion:

We first studied the dissolution process using 3-mercaptopropionic acid as a reductive reagent to cleave the disulfide bonds existing in ESM. The results are: Both temperature and concentrations of 3-mercaptopropionic acid and acetic acid can all affect the time taken for dissolution and sometimes the yield. The concentration of 3-mercaptopropionicacid is crucial. When it was too dilute, for example, raw ESM could not be dissolved at 80ºC even after 48h. With increasing concentration of 3-mercaptopropionic acid, the dissolution becomes faster, and the yield increases initially then levels off at about 55%.
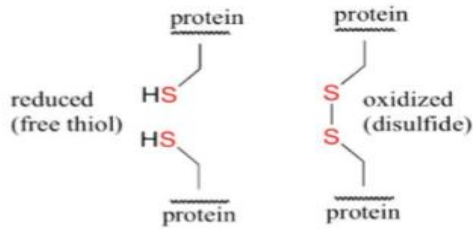
Figure1: cleave the disulfide bonds in ESM

In this study, ESM was chosen as the protein- based material for electrospinning. The low molecular weight of ESM reveals its low viscosity and no stable drop could be formed on the tip of needle for the formation of fibers. The addition of PVA increased the solution viscosity, formed a more stable liquid jet, and greatly improved the electrospinnability of SEP, PVA were selected as supporting polymer for incorporation with ESM, because It has been shown to have good processability for blending with many natural materials favored for electrospinning. ESM nanofibers were successfully electrospun with silk fibroin and PVA. Uniform fibers were produced for a ESM/silk fibroin/PVA blend ratio of 15:15: 70 and a 10 wt % total solute concentration .
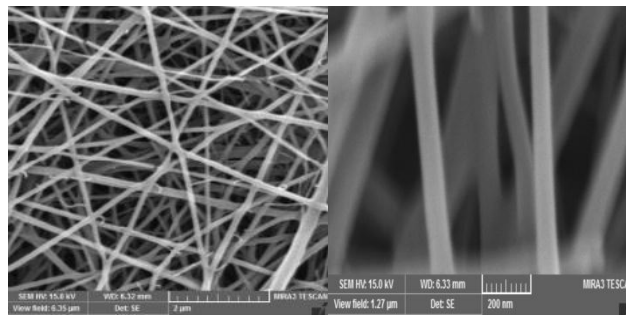

Figure 2: SEM photographs of electrospun ESM/silk fibroin/PVA fibers

Conclusion:

 Electrospinning. Spinning solutions were prepared by dissolving PVAو silk fibroin and SEP in solvent with concentrations of 10% (w/v) blending ratio (SEP/ silk fibroin /PVA = 15:15:70) and ESM nanofibers were successfully electrospun with silk fibroin and PVA. .Nanofibers obtained in this study could be potentially applied as wound dressings or as cosmetic sheets in the biomedical field.

References

[1]. Aluigi, A.; Varesano, A.; Montarsolo, A.; Vineis, C.; Ferrero, F.; Mazzuchetti, G.; Tonin, C. J Appl Polym Sci **2007**, 104, 863.

[2]. Mo, X. M.; Chen, Z. G.; Weber, H. J. Front Mater Sci China **2007**, 1, 20.

A novel and convenient procedure for the synthesis
Of 3-(benzylthio)-9b-hydroxy-1*H*-imidazo[5,1-*a*]isoindole-1,5(9b*H*)-dione Derivatives

Mohammad Reza Mohammadizadeh[a] , **Azar Jamaleddini**[a*], **S. Hekmat Mousavi**[a]
[a]Department of Chemistry, Faculty of sciences, Persian Gulf University, Bushehr 75169, Iran
Email address: azar_jamaleddini@yahoo.com

Introduction: Heterocyclic compounds have embraced significant space in synthetic chemistry. Heterocyclic molecules having imidazole have wide-range applications in developing new drugs [1], organometallic catalysis [2], coordination chemistry [3], and asymmetric catalysis [4].
Isoindole is a hetero ring system which attract considerable attention due to their diverse pharmacological profile such as, antimicrobial, insecticidal and anticancer activity [5]. Among the imidazole fused isoindoles, imidazo[5,1-*a*]isoindole derivatives are common compounds. There are several procedures about the preparation of these compounds, but the majority of the reported methods suffer from one or more drawbacks such as use of complex, expensive catalyst and low chemoselectivity [6].

Experimental: In this method, imidazo[5,1-a]isoindole derivatives **2** were prepared by oxidative cleavage of several indenoimidazol derivatives **1**. Initially a mixture of periodic acid and indenoimidazol **1** in ethanol was stirred for several minutes at room temperature. The oxidation reaction of all diols **1** were rapidly completed and crude products **2** were precipitated. Pure products 2 were simply obtained by filtration of reaction mixture and washing the filtrate with water. Using this procedure, imidazo[5,1-*a*]isoindole derivatives **2** were obtained in excellent yields.

Results and Discussion: As part of our continuing interest on the development of new synthetic methods for heterocyclic compounds, and in continuation of our previous work on the oxidation of cyclic diols1 [7], here, we wish to report a new, one-pot procedure for the synthesis of imidazo[5,1-*a*]isoindole derivatives **2** by the room temperature oxidation of a series of vicinal cyclic diols **1** with periodic acid in ethanol (Scheme 1)**.**
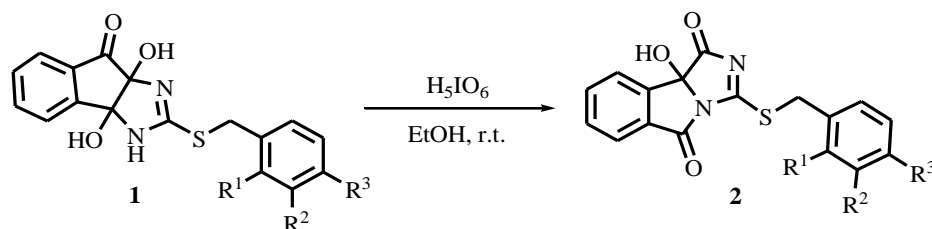
Scheme 1. Efficient synthesis of 9b-hydroxyimidazo[5,1-*a*]isoindoles 2 *via* oxidation of 3a,8a-dihydroxyindenoimidazoles 1

Using this one-pot procedure, imidazo[5,1-a]isoindole derivatives **2** were obtained in excellent yields and their structures were characterized based on their IR, ^{1}H and ^{13}C-NMR and mass spectroscopy data. For example, the ^{1}H NMR spectrum of **2a** exhibited an AB-quartet pattern at

4.60 ppm readily recognized as arising from two diastereotopic CH_2 protons along with a broad singlet at $\delta = 8.15$ for the OH proton. Nine aromatic H-atoms are located as multiplets in the range of $\delta = 7.20–8.05$. The ^{1}H-decoupled ^{13}C NMR spectrum of **2a** showed 15 distinct resonances in agreement with the proposed structure. The signals at $\delta= 36.1, 166.1, 180.9$ and 185.1 correlated with the benzylic CH_2 of imidazole moiety and carbonyl groups, respectively. The quaternary carbon attached to hydroxyl group (C-OH) resonated at 90.6 ppm. The structure of product **2a** was further confirmed by mass spectrometry, which showed a molecular ion peak at 324. The procedure was successfully worked for a variety of dihydroxyindenoimidazole derivatives **1**. The results for synthesis of various 9b-hydroxyimidazo[5,1-*a*]isoindole derivatives **2a-h** are collected in table 1.

Table 1

Entery	R^1	R^2	R^3	Product	Yield%
1	H	H	H	2a	98
2	Me	H	H	2b	95
3	H	Me	H	2c	97
4	H	H	Me	2d	97
5	H	OMe	H	2e	94
6	H	H	OMe	2f	92
7	H	H	CN	2g	90
8	Cl	H	Cl	2h	90

Conclusion: In summary we have studied the oxidation of dihydroxyindeno[1,2-*d*]imidazolones using periodic acid in ethanol at room temperature. Using this oxidation system we could to introduce a new, fast, highly efficient, and environmentally friendly procedure for the synthesis of 9b-hydroxy-1*H*-imidazo[5,1-*a*]isoindole-1,5(9b*H*)-dione derivatives. Furthermore, we could clear some mechanistic feature of the reaction.

References:

[1]. (a) Boiani, M.; Gonzalez, M. *Mini-Rev. Med. Chem.* **2005**, *5*, 409-424. (b) Lipshutz, B. H. *Chem. Rev.* **1986**, *86*, 795-819.
[2]. Herrmann, W. A. *Angew. Chem., Int. Ed.* **2002**, *41*, 1290-1309.
[3]. Nieto, I.; Cervantes-Lee, F.; Smith, J. M. *Chem. Commun.* **2005**, *30*, 3811-3813.
[4]. Cesar, V.; Bellemin-Laponnaz, S.; Gade, L. H. *Chem. Soc. Rev.* **2004**, *33*, 619-636.
[5]. (a) Speck, K.; Magauer, T. *Beilstein J. Org. Chem.* **2013,** *9*, 2048-2078. (b) Neves, R. A. W. Jr.; Palm-Forster, M. A. T.; de Oliveira, R. N. *Synth.Commun.* **2013**, *43*, 1571-1576.
[6]. Xu, X.; Zhao, L.; Li, Y.; Soul, J.-F.; Doucet, H. *Adv. Synth. Catal.* **2015**, *357*, 2869-2882.
[7]. Mohammadizadeh, M.R.; Bahramzadeh, M.; Taghavi, S. *Tetrahedron Lett.* **2010**, *51* , 5807-5809.

Cobalt binuclear complex with tridentate N, N, O Donor Hydrazone Ligand Derived from 2-Pyridine Carboxaldehyde: Synthesise, Study and Crystal Structure Characterization

Mir A. Naziri*[1], E. Sahin[2] and B. Shaabani[3],

1,2:*Depatment of Inorganic Chemistry, Faculty of Chemistry, University of Ataturk, Erzrum, Turkey,*
1,3:*Deprtment of Inorganic Chemistry, Faculty of Chemistry, University of Tabriz, Tabriz, Iran,*
E-mail:a.naziri@tabrizu.ac.ir

****

Introduction: The hydrazon Schiff bases have become a frequently used ligands to get a chelating compounds in coordination chemistry [1-3], in catalysis, antioxidative activity, medicine as antibiotics, anti-inflammatory agents and industry for anticorrosion properties [4-5]. The hydrazon Schiff base complexes also have used as drugs and they possess a wide variety of antimicrobial activity against bacteria, fungi and they inhibit the growth of certain types of tumors [6]. In this work the reaction of Cobalt (II) chloride with 2- pyridine carboxaldehyde derived hydrazon ligand (HL) formed a new binuclear complex, (**[Co(C$_{13}$H$_{11}$N$_3$O$_2$)Cl]$_2$Cl)** . The complex crystallizes in the monoclinic system, space group P21/c and a= 9.7764(10), b=22.829(2), c=7.2116(8) Å parameters, z=4.

Keywords: Crystallography, Hydrazine, Schiff base, Cobalt (II) complex.

Methods / Experimentals: The crystalline tridentate ligand HL (Figure 1) was prepared by condensation of 4-Hydroxybenzhydrazide with 2-pyridine carboxaldehyde respectively in the absolut ethanol. The Brown colored crystals of Co (II) complex, (CoLCl)$_2$Cl of HL was synthesized by reaction of CoCl$_2$ with ligand (HL). X-ray data were recorded by Rigaku R-ZXIS RAPID-S diffractometer and XSCANS METHOD. IR spectra were recorded on a FT-IR Bruker Tensor 27 spectrometer in the wave number region of 400-4000 cm^{-1} using KBr pellets. Solution electronic absorption spectra in the UV-Vis region were recorded by SPECORD UV- Analytik Jena, and all electrochemical experiments are performed with a Metrohm 757 VA processor.
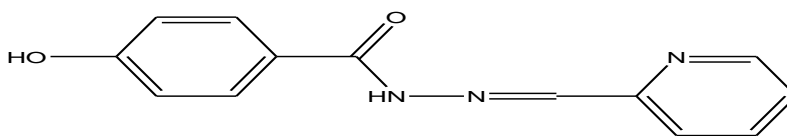

Figure.1. Structure of HL ligand

Results and Discussion: The structures of complex and ligand were illuminated by single crystal X-ray analysis method. X-ray data shows that Cobalt complex has a triclinic system and reacted with ligand in 2:2 ratio with one chloride anion (Figure 2). The IR spectra of the ligand and its complex display characteristic bands of immine (C=N) groups. The complex exhibits a sharp and strong band at 1603 cm^{-1}, attributable to the C=N. The absorption of the C=N stretching vibration in the ligand occurs as a medium band at 1644 cm^{-1}. Also, the presence of a new absorption band at 3131 cm^{-1} in the complex can be attributed to the terminal OH group of coordinated ligand. The UV−Vis data for the Schiff-base ligand in ethanol shows two absorption bands at 330 and 390 nm corresponding to a π-π* transition of the chromophore and an n-π* transition of the aromatic ring, respectively. The electronic spectrum of the complex in ethanol

solution is not similar to that of the free ligand. The cobalt complex of this ligand shows four peaks in UV-Vis region. The week peak absorption band at 229 nm corresponding to a π-π^* transition of the pyridine rings, a strong absorption band at 211 nm corresponding to π-π^* transition of (R–C=N–NH–CO–R') and a band around 290 nm probably corresponding to the n-π^* transition of the non-bonding electrons of nitrogen to the p orbital of the imine group, and a bond around 377 nm and a weak shoulder at 442 nm can be designed as d-d transitions of d^7 configuration of Co^{2+} in octahedral geometry ($^4T_{1g}(F) \rightarrow {}^4T_{2g}$ and $^4T_{1g}(F) \rightarrow {}^4T_{1g}(P)$ (Figure 2)).
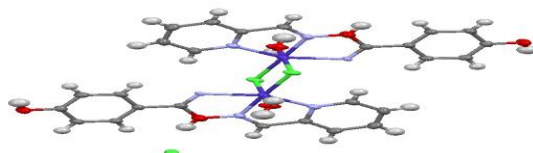

Figure.2. Binuclear complex of cobalt

The electrochemical responses of the ligands and its complex with cobalt cation were studied by recording the cyclic voltammograms in the potential range +1.0 V to -1.0 V. One pair anodic and cathodic peaks observed for complex of cobalt. These peaks could be related for oxidation and reduction of cobalt in the complex as the equation:

$A)\quad Co^{2+}_{Complex} \rightarrow Co^{3+}_{Complex} + e \quad$ and $\quad B)\quad Co^{3+}_{Complex} + e \rightarrow Co^{2+}_{Complex}$

Conclusion: With considering X-ray strutures and its data about complex of cobalt, and spectroscopic data, FT-IR, CV and UV-Vis of ligand and its complex, we could conclude that ligand acted as a tridentate and coordinated to cobalt via N imine, N pyridine and O benzohydrazide atoms. From the UV-Vis data and different absorptions ligand and its complex we sure that the complex is succesfully synthesised. Also IR spectra showed different peaks for –C=N- group in ligand. The results of CV of ligand and its complex showed that cobalt complex is electroactive but the ligand is nonelectroactive.

References

[1].   M. Tumer, D. Ekinci, F. Tumer, A. Bulut, Synthesis, Characterization and properties of some divalent metal (II) complexes, Acta Part A, 2007; 67; 916-929
[2].   S. Tabassum, M. Zaki, F. Arjmand, I. Ahmad, Synthesis of hetrobiometallic complexes: Journal of photochemistry and photobiology B: Biology 2012; 114: 108-118
[3].   D. Lahiri, R. Majumdar, Anrerobic DNA cleavage in red light by dicopper(II) complexes on disulphide bond activation, J. Chem. Sci 2010; 122(3) 321-333.
[4].   Costamagna J, Vargas J, Latorre R, Alvarado A, Mena G, coordination compounds of copper, nikel and iron with Schiff bases derived from hydroxynaphthaldehydes and salicylaldehydes, Coord. Chem. Res 1992; 119: 67-88
[5].   R. Rajavel et al.The template synthesis, spectral and antibacterial investigation of new N₂O₂ donor Schiff base Cu(II), Ni(II), Co(II), Mn(II) and VO(IV) complexes, Journal of Chemical and Pharmaceutical Research, 2013, 5(1):57-63
[6].   M. M. Deshpande et al.: Synthesis and Structural Characterization of…. , J. Curr. Chem. Pharm. Sc.: 4(4), 2014, 152-156

Synthesis of Some Novel Diastereoselective Benzothiazoleβ-lactam Conjugates

Maryam Alborz[a], Aliasghar Jarrahpour[a*], Hashem Sharghi[a], MahdiAberi[a]

[a] Department of Chemistry, College of Sciences, Shiraz University, Shiraz 71454, Iran

Email address: jarrah@susc.ac.ir;aliasghar6683@yahoo.com

Introduction: Since the introduction of penicillin in the 1940s, antibiotics have become a milestone of modern medicine. Penicillins, cephalosporins and monobactams all belong to the family of β-lactam antibiotics [1]. The azetidin-2-one (β-lactam) derivatives have been reported to possess a wide range of biological activities like antimalarial, cholesterol absorption inhibitors, antifungal, and anticancer agents [2-4].Similarly, benzothiazole derivatives are present in natural products and in synthetic pharmaceuticals. They have biological and therapeutic activities such as anticancer, orexin-1 receptor antagonist, and HIV reverse transcriptase inhibitor [5]. Today, despite an enormous number of synthetic strategies to prepare the β-lactam ring, the Staudinger approach using ketenes and imines is regarded as themost effective and versatile procedure for the synthesis of 2-azetidinone rings [1].

Experimental: General procedure for the synthesis of benzothiazole β-lactam conjugates 5a-q

A mixture of (benzo[*d*]thiazol-2-yl)phenol **1a-b** (1.00 mmol), bromoacetic acid **2** (1.50 mmol), and K_2CO_3 (5.00 mmol) in DMF (5 mL) was stirred at 70 °C for overnight. Then the mixture of reaction was cooled to room temperature, neutralized with HCl (1N) and the crude solid acetic acid derivatives **3a-b** were washed with hot ethanol. Finally a mixture of Schiff bases **4a-m** (1.45 mmol), triethylamine (7.27 mmol), substituted acetic acids **3a-b** (2.18 mmol) and tosyl chloride (2.18 mmol) in dry CH_2Cl_2 (15 mL) was stirred at room temperature for several hours. Then it was washed with HCl 1N (20 mL), saturated $NaHCO_3$ (20 mL) and brine (20 mL). The organic layer was dried (Na_2SO_4), filtered and the solvent was evaporated to give the crude products **5a-q**. Crude conjugates **5a-q** were purified by recrystallization from dichloromethane (Scheme 1).

Results and Discussion: The synthesis of β-lactam conjugates **5a-q** was achieved according to the outlined procedure in Scheme 1. Schiff bases **4a-m** were treated with acids **1a-b** in the presence of triethylamine and tosyl chloride to afford the expected benzothiazole β-lactam conjugates **5a-q** in good to excellent isolated yields varying from 82 to 98 %. The observed coupling constants of these protons confirmed the *cis* stereochemistry for these β-lactams. The *cis* and *trans* stereochemistries of 2-azetidinones were deduced from the coupling constants of H-3 and H-4 ($J_{3,4}>4.0$ Hz for the *cis* and $J_{3,4}<3.0$ Hz for the *trans* stereoisomer) [6]. The structure of the products was fully characterized by IR, ^{1}H and ^{13}C NMR spectra. The ^{1}H NMR spectrum of **5a** exhibited two doublets at $\delta = 5.52$ and 5.70 ppm ($^3J_{HH}= 4.75$ Hz) for vicinal methane of β-lactam protons along with a multiplet at $\delta = 6.80−8.20$ ppm for phenyl ring protons. The ^{1}H-decoupled ^{13}C NMR spectrum of **5a** showed 20 distinct resonances in agreement with the suggested structure. Characteristic ^{13}C NMR signals were shown due to carbonyl groups at $\delta = 161.2$ ppm, signals at $\delta = 80.9$ and 81.6 ppm for C-3, and C-4 (β-lactam ring), and at $\delta = 55.5$ ppm for methoxy group. Also the IR spectrum of compound **5a** indicated a characteristic absorption band of a β-lactam carbonyl moiety at 1743 cm^{-1}.
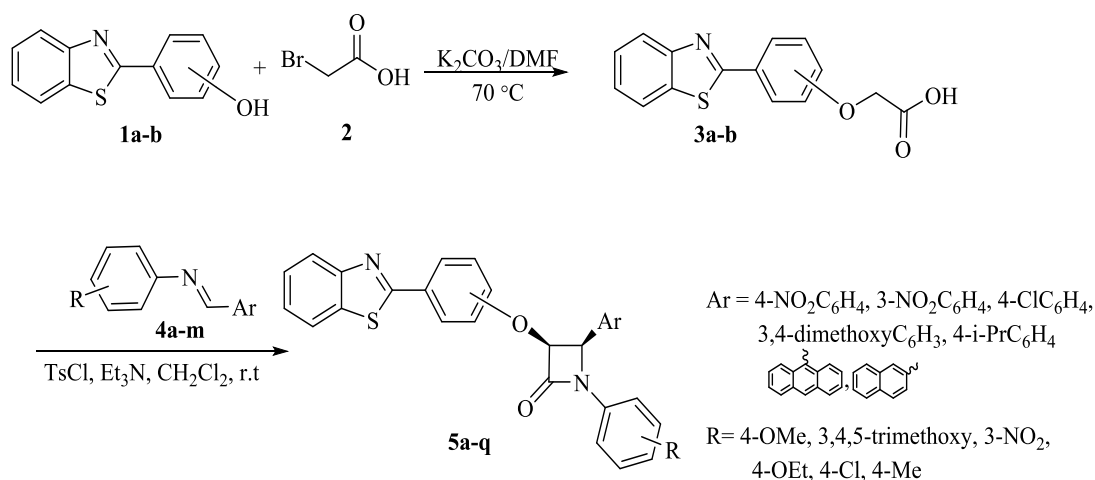
Scheme 1: Synthesis of new (benzo[*d*]thiazol-2-yl) azetidin-2-one **5a-q**

Conclusion: In summary, 17 new benzothiazole β-lactam conjugates were synthesized from a novel ketene derived from 2-(4-(benzo[d]thiazol-2-yl)phenoxy)acetic acid. All of the synthesized β-lactam hybrids were *cis* stereoisomers. Also these new β-lactam derivatives were easily prepared and further studies are now under current investigation to evaluate their biological activities, such as anticancer, antifungal, antimalarial, and antibacterial.

References:

[1]. Rajamäki, S. H. M.; De Luca, L.; Capitta, F.; Porcheddu, A. A. *RSC Adv*., **2016**, *6*, 38553- 38557.

[2]. Ebrahimi, E.; Jarrahpour, A.; Heidari, N.; Sinou, V.; Latour, C.; Brunel, J. M.; Zolghadr, A. R.; Turos, E. *Med. Chem. Res*. **2016**, *25*, 247-262.

[3]. Jarrahpour, A.; Shirvani. P.; Sinou, V.; Latour, C.; Brunel, J. M. *Med. Chem. Res*. **2016**, *25*, 149-162.

[4]. Jarrahpour, A.; Nazari, M. *Iran. J. Sci. Technol. Trans A. Sci*. **2015**, *39*, 259-265.

[5]. Sharghi, H.; Aberi, M.; Doroodmand, M. M. *J. Iran. Chem. Soc*.**2012**, *9*, 189-204.

[6]. Jarrahpour, A.; Aye, M.; Sinou, V.; Latour, C.; Brunel, J. M. *J. Iran. Chem. Soc*. **2015**, *12*, 2083-2092.

Synthesis of 4H-chromenes catalyzed by thioreandioxide-functionalized γ-Fe$_2$O$_3$ magnetic nano particles

Davood Azarifar *[1] , Jahangir Ashnood [2] , Masoumeh Ghaemi [3]

1. Professor, Bu Ali Sina University in Hamedan, azarifar@basu.ac.ir

2. Graduate Student, Bu Ali Sina University in Hamedan, j.ashnood@che.basu.ac.ir

3. PhD student, Bu Ali Sina University in Hamedan, m.gh_251@yahoo.com

*Corresponding author: azarifar@basu.ac.ir

Introduction: 4*H*-chromenes are common and important in compounds which are found in a variety of natural products [1-3] , and perform important biological activities [4]. Among the chromene derivatives, 2-amino-4*H*-chromenes with a nitrile functionality are known as favourite compounds for medicinal chemists because of their potential biomedical applications as novel anticancer agents [5-7]. Also these compounds are industrially important as cosmetics, pigments and potentially biodegradable agrochemicals [8]. In this study **,** thioreandioxide-functionalized γ-Fe$_2$O$_3$ magnetic nano particles have been used as efficient catalyst to effect the one-pot three-component condensation reactions between aromatic aldehydes , malononitrile and 1,3 dimethylebarbituric acid .

Methods / Experimentals: To a mixture of aldehyde, malononitrile and 1,3 dimethylebarbituric acid , was added γ-Fe$_2$O$_3$@HAP-TUD MNPs catalyst and the mixture was heated at 100 °C with sterring for an appropriate time . The progress of the reaction was monitored by TLC. After completion of the reaction, the resulting reaction mixture was diluted with hot ethanol and the catalyst was magnetically separated by using an external magnet. The solid product was isolated by filtration followed by recrystallization from hot ethanol to obtain the pure product.

Results and Discussion: Herein ,we describe the synthesis of thioreandioxide - functionalized γ-Fe$_2$O$_3$ MNPs grafted with thioureadioxide and their characterization by x-ray diffraction (XRD), thermo gravimetric analysis (TGA) , Fourier transform infrared spectroscopy (FT-IR) , energy dispersive x-ray spectroscopy (EDX) ,scanning electron microscopy (SEM) and vibrating sample magnetometer (VSM) techniques . This newly nanocatalytic system has been explored as an efficient and recycle nanocatalyct to effect the one-pot three component condensation

reactions of various aromatic aldehydes , malononitrle and 5,5-dimethylcyclohexan-1,3-diones under solvent-free conditions with excellent yields .

Conclusion: In summary , the titled products 4H-chromens were conveniently synthesized in high yields and low reaction times using thioreandioxide-functionalized γ-Fe_2O_3 MNPs as an efficient and non-toxic catalyst .

References:

[1]. S. Hatakeyama ; N .Ochi ; H . Numata ; S . Takano . *J Chem* Soc , *Chem Commun*, **1988**, 42, 1202 -1204 .

[2]. R. Gonzalez ; N. Martin ; C . Seoane ; J . L . Marco ; A . Albert ; H . Cano . *Tetrahedron Lett*, **1992**, 33, 3809-3812 .

[3] . C. Yao ; B . Jiang ; T. Li ; Qin . B ; Feng . X ; Zhang ; H , Wang ; C. S. Tu . *Bioorg Med Chem* Lett, **2011**, 21, 599-608 .

[4]. L . Alvey ; S . Prado ; B . Saint-Joanis ; S . Michel ; M . Koch ; S. T . Cole ; F . Tillequin ; Y .L . Janin . *Eur J Med Chem*, **2009**, 44, 2497-2505

[5]. J . Skommer ; D . Wlodkowic ; M. Maettoe ; M . Eray ; J. Pelkonen . Leuk *Res*, **2006**, 30, 322

[6]. J. M . Doshi ; D . Tian ; C . Xing . *J Med Chem* , **2006**, 49, 7731-7739 .

[7]. M. N . Erichsen ; T. H .V . Huynh ; B . Abrahamsen ; J. F . Bastlund ; Bundgaard . C ; O . Monrad ; A . Bekker-Jensen ; C . W . Nielsen ; K . Frydenvang ; A. A . Jensen ; L . Bunch . *J Med Chem*, **2010**, 53,7180- 7191 .

[8] S . Khaksar ; A. Rouhollahpour ; S . Mohammadzadeh Talesh , J. Fluorine Chem. **2012**, 141, 11 -15 .

Synthesis of pyrano[2,3-*c*]pyrazole catalyzed by thioureandioxide functionalized γ-Fe$_2$O$_3$ magnetic nano particles.

Davood Azarifar *[1] ,Mehrdad Tadayoni Motakallem [2] , Masoumeh Ghaemi [3]

1. Professor, Bu Ali Sina University in Hamedan, azarifar@basu.ac.ir

2. Graduate Student, Bu Ali Sina University in Hamedan, Mehrdad.tad@gmail.com

3. PhD student, Bu Ali Sina University in Hamedan, m.gh_251@yahoo.com

 *Corresponding author: azarifar@basu.ac.ir

Introduction: Multi component reactions (MCR) approach emerged as the most suitable protocol for the synthesis of functionalized organic compounds due to the fact that the synthesis can be performed without the isolation of the intermediates and discharge any functional groups in short reaction time [1]. Pyrazoles and their derivatives constitute an important class of natural and non-natural hetrocycle products, many of which show useful biological activities as pharmaceuticals and agrochemicals[.2-8]Among such compounds, pyrazole fused heterocyclic derivatives are interesting due to their pharmacological properties and clinical applications.[9,10]They have been widely used as antimicrobial, insecticidal, and anti-inflammatory compounds[11] .

Methods / Experimentals: To a mixture of aldehyde, malononitrile and 3-methyl-1-phenyl-2-pyrazoline-5-on, added γ-Fe$_2$O$_3$@HAP-TUD MNPs as catalyst and the mixture was heated at 100 °C with sterring for an appropriate time . The progress of the reaction was monitored by TLC. After completion of the reaction , the resulting reaction mixture was diluted with hot ethanol (5 mL) and the catalyst was magnetically separated by using an external magnet.

Results and Discussion: Herein, we describe the synthesis of thioreandioxide - functionalized γ-Fe$_2$O$_3$ MNPs grafted with thioureadioxide and their characterization by x-ray diffraction (XRD), thermo gravimetric analysis (TGA) , Fourier transform infrared spectroscopy (FT-IR) , energy dispersive x-ray spectroscopy (EDX) ,scanning electron microscopy (SEM) and vibrating sample magnetometer (VSM) techniques . This newly nanocatalytic system has been explored as an efficient and recycle nanocatalyct to effect the one-pot three component condensation reactions of various aromatic aldehydes , malononitrle and 3-methyl-1-phenyl-2-pyrazoline-5-on under solvent-free conditions with excellent yields .
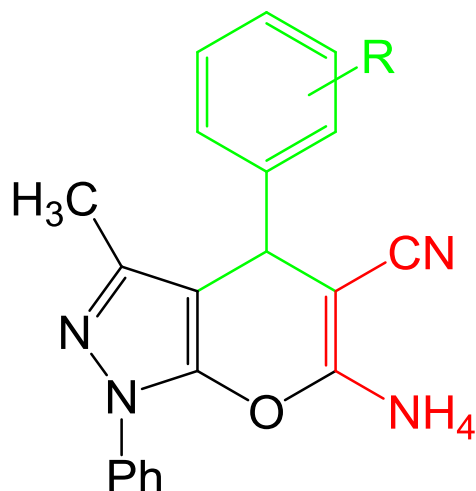
Conclusion: In summary, the titled products pyrano[2,3-*c*] pyrazole were conveniently synthesized in high yields and low reaction times using thioreandioxide-functionalized γ-Fe_2O_3 MNPs as an efficient and non-toxic catalyst .

References:

[1]   Boulard. L ; BouzBouz. S ; Cossy. J , *Tetrahedron Lett.* **2004**, *45*, 6603.

[2]   Lv. P-C ; Li. H-Q ; Sun. J ; Zhou. Y ; Zhu. H-L . *Bioorg. Med. Chem.* **2010**, *18*, 4606.

[3]   Bonesi. M ; Loizzo. M. R ; Statti. G. A ; Michel. S ; Tillequin. F ; Menichini. F , *Bioorg. Med. Chem. Lett.* **2010**, *20*, 1990.

[4]   Bondock. S ; Fadaly. W ; Metwally. M. A , *Eur. J. Med. Chem.* **2010**, *45*, 3692.

[5]   Barsoum. F. F ; Girgis. A. S , *Eur. J. Med. Chem.* **2009**, *44*, 2172.

[6]   El-Sabbagh. O. I ; Baraka. M. M ; Ibrahim. S. M ; Pannecouque. C ; Andrei. G ; Snoeck, R ; Balzarini. J ; Rashad. A. A , *Eur. J. Med. Chem.* **2009**, *44*, 3746.

[7]   Abdel-Aziz. M ; Abuo-Rahma. G. E-D. A ; Hassan. A. A , *Eur. J. Med. Chem.* **2009**, *44*, 3480.

[8]   Rosiere. C.E ; Grossman. M.I , *Science* **1951**, 113, 651.

[9]   Tanitame. A ; Oyamada. Y ; Ofuji. K ; Fujimoto. M ; Iwai. N ; Hiyama. Y ; Suzuki. K ; Ito. H ; Terauchi. H ; Kawasaki. M. *J. Med. Chem.* **2004**, *47*, 3693.

[10] Cali. P ; Nærum. L ; Mukhija. S ; Hjelmencrantz. A. *Bioorg. Med. Chem. Lett.* **2004**, *14*,5997.

[11] Zonouz. A. M ; Eskandari. I ; Khavasi. H. R. *Tetrahedron Lett.* **2012**, *53*, 5519.

Preparation of polyvinylchloride containing graphene (reduced by extracted Lavandula Angustifolia) and study of its electrical properties

Sedighe Jangavar and   **Nooredin Goudarzian***

Department of Applied Chemistry, Shiraz Branch, Islamic Azad University, Shiraz, Iran
Corresponding author*: Sedighe Jangavar   email: Sjangavar@yahoo.com

1. Introduction

Several methods have been reported for reduction of graphene oxide [GO]. But the toxic nature of these chemical reducing agents (hydrazine, hydroquinone, sodium borohydride), are harmful for the environment. Consequently, new approaches need to be explored for the effective conversion of GO into graphene [RGO] under mild conditions and by utilizing environmentally friendly reducing agents. Extracted Lavandula Angustifolia[ELA] has been used extensively for the reduction of aliphatic and aromatic ketones, cyclic ketones, b-keto esters, and azidoketones[1]. Therefore, microorganisms in Extracted ELA are expected to remove oxygen functionalities from the surface of GO and restore electronic conjugation in RGO. This work reports the simple reduction of GO sheets by using ELA in aqueous solution at room temperature. Most significantly, in comparison with other strong reducing agents used in GO reduction, extracted Lavandula Angustifolia is readily available and has low environmental impact [2].

2. Experimental

2.1. Synthesis of GO: GO was synthesized from natural graphite by a modified Hummers method [1].

2.2. Reduction of GO by ELA: In a typical experiment GO dispersed in ELA at room temperature. The mixtures were magnetically stirred at room temperature for various time and then refluxed and finally sonicated in ultrasonic bath. The purified RGO was finally found to be stable for a long time.

2.3. Formation of nano composite layers on polyvinylchloride [PVC]: RGO suspended in acetone gradually added to the samples of PVC were put in THF and acetone and sonicated. This process was performed to reveal the best time for adequate swelling in order to control the depth of RGO diffusion into PVC. Since the weight percent composition of RGO in top layer of PVC is important and must be controlled.

2.4. Testing: FT-IR analysis was performed to make sure graphene oxide is reduced to graphene. We studied the dispersion and distribution of nano particles and the depth of diffusion of layer by SEM and optical imaging. XRD test was performed to check the distance between layers. For characterizing electrical behavior of samples electrical impedance and 4-point probe electrical conductivity were performed.

3. Results and discussion

X-ray diffraction (XRD) patterns of graphene oxide, GO, RGO and PVC-RGO are shown in Fig.1 a-c. Pristine graphite exhibits a basal reflection (002) peak at $2\emptyset = 26.6$ (d spacing = 0.335 nm). Upon oxidation of pristine graphite, the 002 reflection peak shifts to the lower angle ($2\emptyset = 11.2$, d spacing = 0.79 nm). The increase in d spacing is due to the intercalation of water molecules and the formation of oxygen-containing functional groups between the

layers of the graphite. The XRD of RGO show the appearance of a broad band centered at 2Ø ~ 23.96 corresponding to the stacking of graphene layers. The disappearance of 002 reflection peak of graphene oxide and appearance of a broad band at 2Ø ~ 23.96 in the RGO indicate the formation of few-layer graphene.
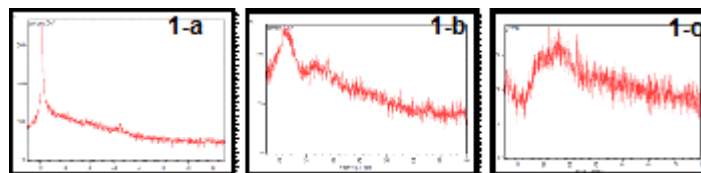
FT-IR analysis: Fourier transform infrared (FT-IR) spectra of pure GO, RGO and PVC-RGO samples showed that the intensities of the FT-IR peaks corresponding to the oxygen functionalities such as the C=O stretching vibration peak at 1728 cm^{-1} and O–H deformation peak at 1395 cm^{-1} decreases to a significant extent after reduction of GO by ELA. The intensities of the C–O(epoxy) stretching vibration peak of GO at 1223 cm^{-1}, and the C–O (alkoxy) stretching vibration peak at 1051 cm^{-1} significantly changed in the RGO. This is attributable to the partial reduction of GO to graphene. The intensity of the peak at 1628 cm^{-1} increases significantly in the R-GO.

3.6. Thermo gravimetric analysis: The TGA curve of GO shows a small mass loss (3 wt.%) at ca. 100°C, attributable to the loss of adsorbed water from the surface of graphene. Pure GO exhibits two degradation steps; the first commencing at 165 $^{\circ}$C, due to the loss of hydroxyl, epoxy functional groups and remaining water molecules. The second step degradation (450–600 $^{\circ}$C) involves the pyrolysis of the remaining oxygen-containing groups as well as the burning of ring carbon. This suggests that most of the labile oxygen functionalities have been removed from the RGO.

3.6. Electrical characterization of PVC/GO composites: The empedance of and PVC-GO and PVC-RGO nanocomposite films. The dispersion of nano filler in the polymer matrix can be directly correlated with significant improvement in several properties of polymer nanocomposites, including electrical properties, together with ease of processing. A significant change in the electrical properties such as dielectric constant and dielectric loss of PVC/GO nanocomposites was observed at various frequencies. Thus, nanocomposite which can offer improved dielectric properties at low frequency with high flexibility and easy processing can be used in fabrication of electronic devices.

4. Conclusion: An environmentally friendly reduction system by using ELA as a biocatalyst for the reduction of graphene oxide is described. The reduction was carried out in aqueous medium at room temperature. FTIR and XPS analysis provide evidence for the elimination of oxygen functionality from the surface of GO. Thermal stability data of GO and RGO from TGA are also in line with the other experimental data. The main advantages of this technique over the traditional chemical reduction are the cost-effectiveness, environmentally friendly approach and simple product isolation process. Electrical impedance and conductivity test showed that all nanocomposites containing 2% nano particle has the highest conductivity compared to other compositions.

References: [1] Sun Z, Yan Z, Yao J, Beitler E, Zhu Y, Tour JM., *Nature*, 2010; 468,549. [2] Park S, Ruoff RS. *Nat Nanotechnol*., **2009**; 4, 217

Label-Free Colorimetric Detection of Methiocarb insecticid Based on Aggregation of Gold Nanoparticles

Aliakbar Mohammadi[1], Forough Ghasemi[1], M. Reza Hormozi-Nezhad[1, 2*]

[1]Department of Chemistry, Sharif University of Technology, Tehran, 11155-9516, Iran

[2]Institute for Nanoscience and Nanotechnology, Sharif University of Technology, Tehran, Iran

hormozi@sharif.edu

****

Introduction: Methiocarb [3,5-dimethyl-4-(methylthio) phenol methyl-carbamate] also known as mercaptodimethur or mesurol, is an N-methylcarbamate registered as a molliscicide with neurotoxic action[1]. Methiocarb is particularly effective as insecticide and bird repellent when applied to rice seed. Because carbamate pesticides are acetylcholinesterase inhibitors, they are considered to be carcinogens and mutagens[2]. Thus, to prevent their harmful effects on animals, humans, and the environment, it is of crucial importance to develop simple and sensitive methods for detection of methiocarb.

Colloidal gold nanoparticles (AuNPs) have recently gained much interest for colorimetric assays due to their extremely large extinction coefficients. Colorimetric sensing strategies using AuNPs are usually based on the change of optical properties because of their aggregations and morphology changes[3]. In this study, we report a highly selective colorimetric probe for methiocarb detection based on aggregation of AuNPs.

Methods: *Synthesis of citrate coated AuNPs;* Briefly, 50 mL of HAuCl$_4$ solution (1.0 mmol L^{-1}) was boiled and then 5 mL of sodium citrate (38.8 mmol L^{-1}) was added. The solution was refluxed for 30 min and then allowed to cool and stored at 4°C.

Procedure for determination of methicarb; A solution contained citrate coated AuNP with a final concentration 0.27 nmol L^{-1}, NaCl with final concentration 22.5 mmol L^{-1} was prepared. Then, different concentrations of methiocarb was added as the total volume was constant for all experiments with pH 4. All spectra were recorded 15 min after the addition of the last drop of analyte.

Results and Discussion: It is well recognized that the displacement of the citrate group shell, which have lower affinity to surface of AuNPs, with thiol containing compounds induces the aggregation process. As citrate AuNPs were stable only in neutral and basic pH, so pH 4 was

selected as an optimal pH. To determine the best concentration of NaCl (as electrolyte), different concentrations of NaCl were added to AuNPs, and UV–vis spectra were recorded over time. The concentrations of 22.5 mmol L^{-1} was selected as ptimized salt for citrate. Further experiments under the optimum conditions showed good linear relationship between absorption ratio (A_{650}/A_{520}) and methiocarb concentration (see Figure 1). To investigate the applicability of the proposed technique in real samples, paddy water and tab water were tested. The results summarized in Table 1 show the feasibility and usability of this method for determination of methiocarb in real samples.
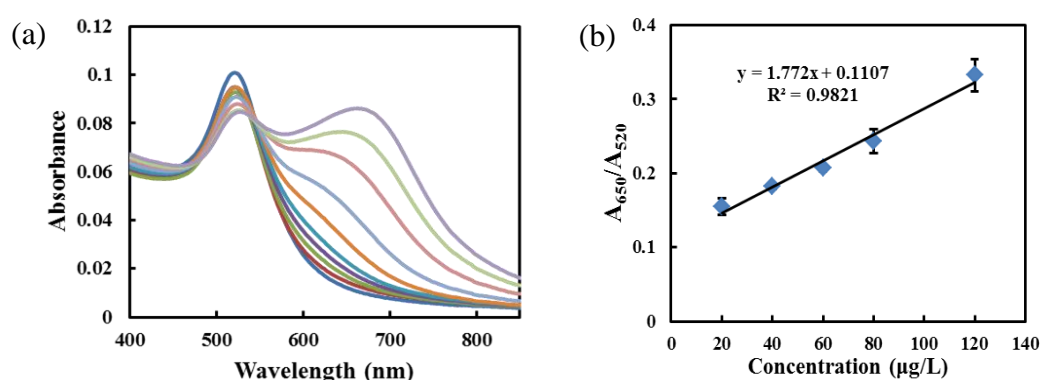
Figure 1. (a) UV– vis spectra of AuNPs in the presence of different concentrations of methiocarb, and (b) Calibration curve of A_{650}/A_{520} versus metiocarb concentration under optimum conditions.

Table 1. Determination of methiocarb in different water samples

Samples	Spiked (µg L^{-1})	Recovery	RSD%
Paddy water	180	108.40	2.20
Tap water	180	105.20	0.84

Conclusion: In summary, the potential and feasibility of AuNPs for the colorimetric determination of methiocarb have been demonstrated. The developed methodology, based on aggregation of AuNPs,could achieve a quantification limitat low levels, and good linearity, accompanied by acceptable accuracy and reproducibility, permitting determination of methicarb in paddy and tab water.

References

[1] A. Placido, P. Paiga, D.H. Lopes, M. Correia, C. Delerue-Matos, Journal of agricultural and food chemistry, 61, 325-331.

[2] J. Zhang, H.K. Lee, Journal of Chromatography A, 2006, 1117, 31-37.

[3] F. Ghasemi, M.R. Hormozi-Nezhad, M. Mahmoudi, Analytica Chimica Acta, 2015, 882.

A TD-DFT study of the lowest excitation energies of Schiff base ligand

Moslem Sedaghat, Zahra Asadi*

Department of Chemistry, College of Sciences, Shiraz University, Shiraz 71454, I.R. Iran

Email address: zasadi@shirazu.ac.ir

****

Introduction: The density functional formalism of Hohenberg and Kohn and Sham has become a powerful tool in computational chemistry to determine a variety of ground state properties of molecules. Since density functional theory (DFT) has been recognized as an inexpensive and reasonably accurate method that rectify many problems of the Hartree–Fock (HF) approximation, there has been a great interest to extent the DFT approach to excited electronic states. Today, the most successful and widely used method to calculate excitation energies and electronic spectra is the time-dependent generalization of DFT theory (TD-DFT). Time-dependent density functional theory (TD-DFT) extends the basic ideas of ground-state density-functional theory (DFT) to the treatment of excitations or more general time-dependent phenomena [1].

Methods: In this work we present TD-DFT calculations of the excited electronic states of a Schiff base Ligand. The ground-state structures of the ligand was optimized by the DFT (B3LYP/6/311+G*) level of theory [2]. Using the optimized ground-state structure, the absorption properties of the compound in methanol (CH_3OH) media were calculated by time-dependent density functional theory (TD-DFT). The lowest 14 singlet-singlet transitions were computed and it was observed that the results of the TD calculations are qualitatively matched with the experimental spectra. All the calculations were performed using the GAUSSIAN03 program package.

Results and Discussion: The molecular structure of Schiff base ligand have been fully optimized in their singlet spin state. In Fig. 1, the optimized structures of the ligand, a comparison between the experimental and theoretical spectra and molecular orbital diagram are shown. The absorption spectrum of this ligand is calculated by TD-DFT in Methanol solution at room temperature. For the analysis of molecular orbital in order to recognize the type of transition we used the Canonical Molecular Orbitals (CMO) techniques. The partial frontier

molecular orbital compositions and energy levels are listed in Table 1. The vertical excitation energy and oscillator strength along with the main excitation configuration are listed in Table 2.
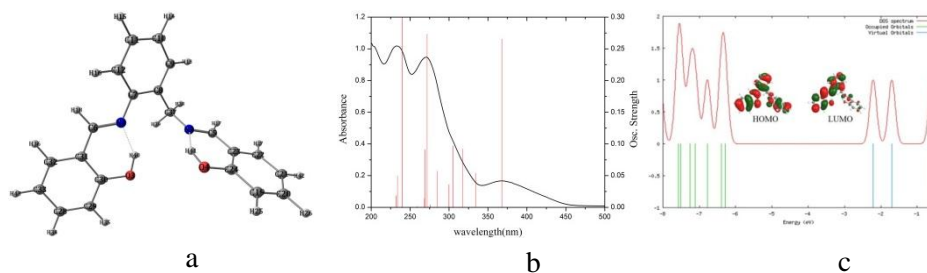

Figure 1. a) Optimized structures of Schiff base ligand, b) Overlaid experimental absorbance (spectra) and calculated TD-DFT (bars), c) molecular orbital diagram

Table 1. Frontier molecular orbital composition (%)

Orbital	Energy (eV)	Contribution (%)
L+3	-0.309	31.2%($\pi^*_{C29-C30}$)+ 27.1 %($\pi^*_{C31-C32}$)+ 11.7%($\pi_{C28-C33}$)+ 6.5%($\pi^*_{C10-C11}$)+ 5.9%(π^*_{C7-C12})
L+1	-1.691	44.6%(π^*_{N2-C5})+ 16%($\pi^*_{C22-C23}$)+ 10.7%($\pi^*_{C20-C21}$)+ 10%($\pi_{C19-C24}$)+
L	-2.208	41.4%(π^*_{N1-C6})+ 10%($\pi^*_{C31-C32}$)+ 7.5%($\pi_{C29-C30}$)+ 7.2%(π^*_{C7-C12})+ 7%($\pi_{C28-C33}$)
H	-6.283	14.5%($\pi_{C28-C33}$)+ 11.5%(Lp_{O3})+11%($\pi_{C29-C30}$)+8%(π_{N1-C6})+7.5%(π_{C7-C12})+ 7%($\pi_{C10-C11}$)
H-2	-6.770	18.2%($\pi_{C29-C30}$)+ 11.7%($\pi_{C10-C11}$)+ 9.6%(Lp_{O3})+ 9.4%(π_{C7-C12})+ 6.5%($\pi_{C31-C32}$)+ 5.2%(Lp_{N1})
H-3	-7.108	30.4%($\pi_{C22-C23}$)+ 12.1%(π_{N2-C5})+ 11.4%($\pi_{C19-C24}$)+ 7%(π_{C8-C9})
H-4	-7.252	27.8%(π_{C8-C9})+ 7.3%(π_{C7-C12})+ 6.5%($\pi_{C10-C11}$)+ 6.3%(Lp_{N2})
H-5	-7.507	17.6%($\pi_{C31-C32}$)+ 7.3%(π_{C7-C12})+ 6.7%($\pi_{C28-C33}$)+ 5.7%(π_{C8-C9})+ 20.1%(Lp_{N1})
H-6	-7.572	6.9%(π_{C8-C9})+ 6.5%(σ_{C5-H17})+ 5.3%(σ_{O4-H41})+ 46%(Lp_{N2})+ 7.2%(Lp_{O4})
H-7	-8.080	20.8%(Lp_{N1})+ 13.6%($\pi_{C10-C11}$)+ 7.5%($\pi_{C31-C32}$)+ 6.5%($\pi_{C28-C33}$)+ 6.4%(π_{C7-C12})+ 5.2%(Lp_{O3})

Table 2. Computed excitation energies, electronic transition configurations, and oscillator strengths (f)

Excitation	Composition (%)	λtheo (nm)	(f)	Assignment
1	H→L (93%)	368.385	0.2655	$\pi{\to}\pi^*$, n$\to \pi^*$
2	H-5->LUMO (22%), H-4->LUMO (25%) H-3->LUMO (31%), H-2->LUMO (10%)	271.870	0.2735	$\pi{\to}\pi^*$, n$\to \pi^*$
3	H-5->LUMO (48%), H-4->LUMO (10%) H-3->LUMO (25%)	269.394	0.091	$\pi{\to}\pi^*$, n$\to \pi^*$
4	H-6->LUMO (14%), H-6->L+1 (13%) H-2->L+1 (64%)	268.362	0.0143	$\pi{\to}\pi^*$, n$\to \pi^*$
5	H-6->L+1 (10%), H-3->L+1 (72%)	239.664	0.3492	$\pi{\to}\pi^*$, n$\to \pi^*$
6	H-6->L+1 (31%), H-4->L+1 (52%)	233.731	0.0498	$\pi{\to}\pi^*$, n$\to \pi^*$
7	H-7->LUMO (58%), HOMO->L+3 (16%)	232.216	0.0184	$\pi{\to}\pi^*$, n$\to \pi^*$

Conclusion: The TD-DFT study was applied to calculation the (π-π^*, n-π^*) excitation energies in Schiff base compounds with emphasis on the accuracy of the method. Also, the TD-DFT calculations described the spectral features due to the good qualitative agreement of line shape and relative strength with experimental results.

References:

[1] M. Parac; S. Grimme. *Chemical physics*, **2003**, *292*, 11-21.
[2] D.F. Back; C.R. Kopp; G.M. de Oliveira; P.C. Piquini. *Polyhedron,* **2012**, *36*, 21-29.

A facile, one-pot procedure for the synthesis of spiro[benzo[g]indole-2,1'-isobenzofuran]-3,3',4,5(1*H*)-tetraone derivatives

S. Hekmat Mousavi[a]*, Mohammad Reza Mohammadizadeh[a], Azar Jamaldini[a]

[a]Department of Chemistry, Faculty of Sciences, Persian Gulf University, Bushehr 75169, Iran

Email: hekmat.1368@yahoo.com

Introduction: Oxygen- and nitrogen-containing heterocycles are important in the area of pharmaceuticals and agrochemicals. Substituted phthalides (isobenzofuran-1(3*H*)-ones) represent an important class of natural products that possess significant biological properties [1]. In particular, 3-substituted phthalides are vital heterocyclic motifs in many bioactive compounds such as isocoumarins, anthraquinones, anthracyclines, and several alkaloids [2]. Their notable characteristics include antibacterial, anticonvulsant, anti-HIV, antiasthmatic, antitumor, antiplatelet activities, anesthesia prolongation, and PGF2a inhibitory properties [3]. Furthermore, the chemistry of isobenzofurans is of great importance, because they are 10p electron systems with a quinoid nature, which makes them attractive as unique building units for oligomeric and polymeric p-conjugated compounds [4].

Experimental: Amine **1** was added to a solution of sodium 3,4-dioxo-3,4-dihydronaphthalene-1-sulfonate **2** in water. The reaction mixture was stirred at room temperature for 20 min. After completion of the reaction, the mixture was filtered and the filtrate washed with water a dried under vacuum.

Then to a mixture of ninhydrin in acetic acid, 4-(amino)naphthalene-1,2-dione derivatives 3 was added and the reaction mixture was stirred under the reflux for 1 h. the reaction mixture was cooled to room temperature, H_5IO_6 was added and stirring was continued for 1 h. The mixture was filtered, and the products were purified by recrystallization from EtOH.

Results and Discussion: In continuation of our programs to develop more efficient processes for the synthesis of oxygen- and nitrogen-containing heterocycles, herein, we describe a novel and practical one-pot procedure for the preparation of some new spiro[benzo[g]indole-2,1'-isobenzofuran]-3,3',4,5(1*H*)-tetraones. As shown in Scheme 1, diols **4**, were efficiently synthesized from the reaction of ninhydrin **1** and 4-(amino)naphthalene-1,2-dione **3** [5]. Oxidative cleavage of these diols using periodic acid resulted in the formation of spiro[benzo[g]indole-2,1'-isobenzofuran]-3,3',4,5(1*H*)-tetraone derivatives **5**. The procedure worked efficiently under the one-pot conditions and either the reaction times were reduced or the yields of products **5** were comparable with respect to the overall yields of the two-step procedure.
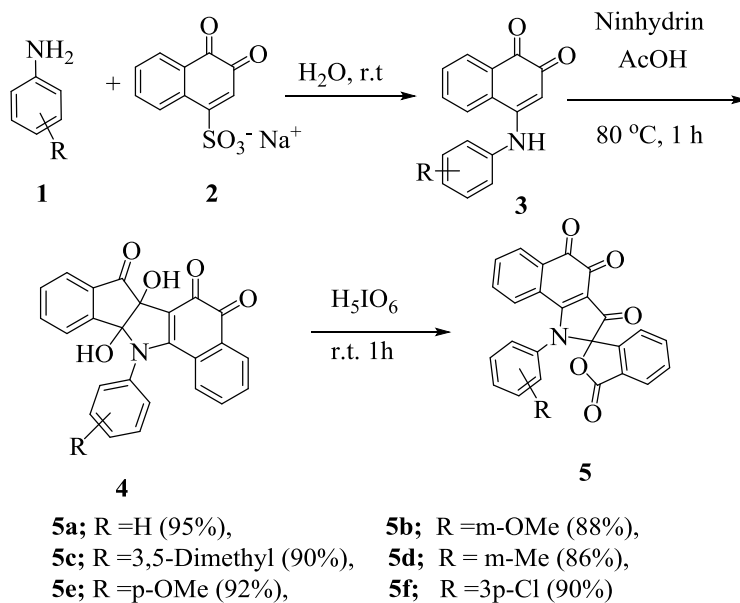
Scheme 1: Synthesis of 3'H-spiro[benzo[g]indole-2,1'-isobenzofuran]-3,3',4,5(1H)-tetraone derivatives **5a-f**

The structures of the products **5** were established by spectroscopy data. The ^{1}H NMR spectrum of **5c** exhibited two sharp singlets at δ 2.08 and 2.28 due to the methyl protons, along with multiplets at δ 6.76–8.21 for the aromatic protons. ^{13}C NMR spectrum of **5c** showed 25 distinct resonances, in agreement with the proposed structure. The signal at δ 95.8 is consistent with the presence of the spiro carbon.

Conclusion: In summary, we have reported a new, efficient procedure involving the addition reaction of ninhydrin and 4-(amino)naphthalene-1,2-dione derivatives, which leads to 11*b*,12-dihydrobenzo[*g*]indeno[1,2-*b*]indole-5,6,7(6b*H*)-trione derivatives and their subsequent conversion to 3'*H*-spiro[benzo[*g*]indole-2,1'-isobenzofuran]-3,3',4,5(1*H*)-tetraone derivatives in the presence of periodic acid sodium salt. The combination of generality, high yields, short reaction times, and mild conditions makes this method a novel and efficient useful procedure synthesis of the titled compound.

References

[1] S. M. Landge; M. Berryman; B. Tçrçk. Tetrahedron Lett, 2008, 49, 4505.
[2] J. E. Baldwin; K.W. Bair. Tetrahedron Lett, 1978, 19, 2559.
[3] J. Safari, H; Naeimi; A. A. Khakpour; R. S. Jondani; S. D. Khalili. Chem, 2007, 270, 236.
[4] A. O. Patil; A. J. Heeger; F. udl; Chem. Rev, 1988, 88, 183.
[5] P. Rashidi-Ranjbar; A. Mohajeri; M. Ghiaci. Iran J. Chem. Chem. Eng, 2001, 20, 102.

An Efficient Synthesis of Pyrido[2,3-*d*]pyrimidine Derivatives in Water Catalyzed by TiO$_2$-SiO$_2$ Nanocomposite

Minoo Shariati[a], Shahrzad Abdolmohammadi[b,*]

[a] *Department of Chemical Engineering, Tafresh University, Tafresh 39518 79611, Iran*

[b] *Department of Chemistry, Faculty of Science, East Tehran Branch, Islamic Azad University, P.O. Box 18735-138, Tehran, Iran*

*Email address: s.abdolmohamadi@iauet.ac.ir and s.abdolmohamadi@yahoo.com

****

Introduction: Pyridopyrimidines have been identified as an important class of nitrogen containing heterocycles, which display wide range of biological properties such as antibacterial [1], antiallergic [2], antifolate [3] activities. Currently, nanostructured metal oxides based their high physical and chemical abilities promote numerous organic transformations [4-5]. Among them TiO$_2$-SiO$_2$ nanocomposite with improved the catalytic efficiency has been found as a new efficient catalyst. We wish to report herein a very simple route to synthesize some of pyrido[2,3-*d*]pyrimidines **4** *via* a condensation reaction of aromatic aldehydes **1**, methylcyanoacetate **2**, and 4(6)-aminouracil **3** in aqueous media by using TiO$_2$-SiO$_2$ nanocomposite with a molar ratio of 1:1 as an efficient catalyst (**Scheme 1**).
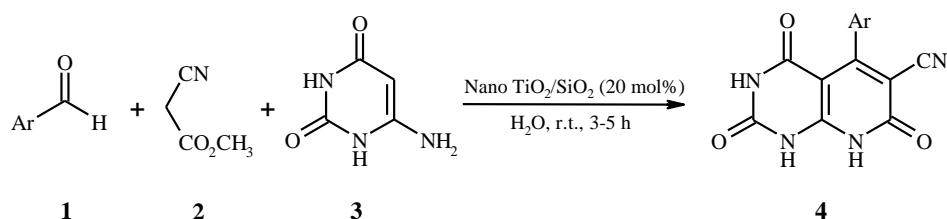
Scheme. 1. Synthesis of 2,4,7-trioxo-5-aryl-1,2,3,4,7,8-hexahydropyrido[2,3-*d*]pyrimidine-6-carbonitriles.

Methods / Experimentals: A mixture of aromatic aldehydes **1** (1 mmol), methylcyanoacetate (**2**, 1 mmol), 4(6)-aminouracil (**3**, 1 mmol), and TiO$_2$-SiO$_2$ nanocomposite (28 mg, 20 mol %) in H$_2$O (2 mL) was stirred at room temperature for appropriate time. After completion of the reaction (TLC), DMF (2 mL) was added to the reaction mixture, and catalyst was removed by filtration. The filtrate was cooled to 0 °C over night and the pure product was obtained by crystallization from this mixture.

Results and Discussion: In the preliminary experiments, we prepared TiO$_2$-SiO$_2$ nanocomposite catalyst according to a known non thermal sol-gel process [6]. The crystalline structure and purity of the synthesized nanocomposite was confirmed from XRD analysis (**Fig 1**). The TEM image of as-prepared TiO$_2$-SiO$_2$ nanocomposite is also presented in **Fig. 2** showing grainy structure of nanoparticles with sizes of 5-9 nm. The chemical composition of as-prepared nanocomposite was determined by X-ray fluorescence (XRF) technique and the results show that the molar ratio was 1:1.
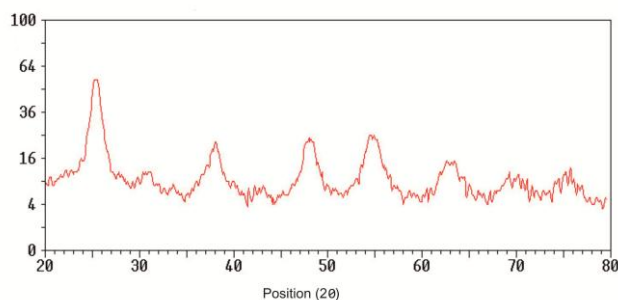
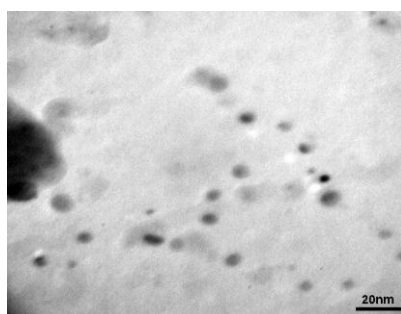**Fig. 1.** XRD pattern of the synthesized TiO$_2$-SiO$_2$ nanocomposite.

Fig. 2. TEM image of the synthesized TiO$_2$-SiO$_2$ nanocomposite.

We then studied on the reaction conditions optimization using a model reaction of 4-bromobenzaldehyde, methylcyanoacetate, and 4(6)-aminouracil under various reaction conditions. The best results were obtained with 20 mol% of TiO$_2$-SiO$_2$ nanocomposite (with respect to TiO$_2$) in H$_2$O at room temperature.

Conclusion: In summary, we have developed a novel and highly efficient procedure for the synthesis of pyrido[2,3-*d*]pyrimidines *via* the three-component reaction of aromatic aldehydes, methylcyanoacetate, and 4(6)-aminouracil efficiently, that was catalyzed by TiO$_2$-SiO$_2$ nanocomposite in aqueous media. The simplicity of operation, improved product yields, shorter reaction time, using non-toxic and readily available catalyst, and eco-friendly procedure make this approach more attractive compared to previous method.

References

[1] Nargund, L.V.G.; Reddy, Y.S.R.; Jose, R. *Indian Drugs*, **1991**; *9*, 45-46.
[2] Furukawa, K.; Hasegawa, T.; Can. *Pat*. 2151971; *Chem. Abstr*., **1996**; *124*, 289568c.
[3] Rosowsky, A.; Mota, C.E.; Queener, S.F.; *J. Heterocycl. Chem*., **1995**; *32*, 335-.
[4] Reddy, V.P.; Kumar, A.V.; Swapna, K.; Rao, K.R. *Org. Lett*., **2009**; *11*, 951-953.
[5] Mittapelly, N.; Reguri, B.R.; Mukkanti, K. *Der Pharma Chem*., **2011**; *3*, 180-189.
[6] Nilchi, A.; Janitabar-Darzi, S.; Rasouli-Garmarodi, S. *Mater. Sci. Appl.*, **2011**; *2*, 476-480.

Microencapsulated Phase Change Material with PMMA shell: Synthesis and Characterization

Somayeh Lashgari[a,b], **Mehdi Ghafele Bashi**[a], **Hassan Arabi**[b*], **Ali Reza Mahdavian**[a]

a National Petrochemical Company, Petrochemical Research & Technology Company - P.O. 1435884711, Tehran, Iran.

b Iran Polymer & Petrochemical Institute, P.O. Box 14965-115, Tehran, Iran

Email address: H.arabi@ippi.ac.ir

Introduction:

Energy conservation has become an important issue nowadays due to the limitation of conventional fossil energy and the increase of greenhouse emission level. For this reason much attention has been focused on exploitation of new substances and study on phase change materials (PCMs) and their microcapsules for thermal energy storage as an area of extensive research works[1,2]. PCMs divided to three main categories namely organic, inorganic and eutectics [3]. Paraffin and n- alkanes as organic PCMs are in large interest due to their high latent heat storage capacity, chemical and thermal stability, low vapor pressure, cheapness, and availability. In this research, n-hexadecane microcapsules with poly methyl methacrylate (PMMA) shell has been synthesized and the effect of core content and crosslinker has been investigated.

Methods / Experimental:

The polymerization was carried out in a double-jacketed glass reactor equipped with stirrer, nitrogen inlet and outlet and circulating cooling system. At first hydrophilic phase was added to the reactor, then the hydrophobic phase including monomers and PCM was transferred to the reactor. The polymerization temperature was 70 °C and the reaction continued for 5 hrs.

Results and Discussion:

The morphology of the microcapsules has been illustrated in Fig. 1. All microcapsules have spherical shape with average diameter of 220 μm. The comparison of PCM microcapsules with neat one shows that the surface of microcapsules is wrinkled while neat particles owe a smooth surface, free of wrinkle. This phenomenon could be attributed to the interfacial tension between HD and PMMA which impose internal stress on polymer chains and due to rigidity of PMMA chains it is not possible to relax and make a smooth surface. Moreover the breakage area of samples in Fig. 1 displays multi-nucleus morphology.

Thermal behavior of samples has been characterized by differential scanning calorimetry (DSC) and has been illustrated in Fig. 2. As expected the melting enthalpy of microcapsules has been increased by increment of HD content. The experimental and theoretical core content (C_E, C_t) has been calculated by the following equations respectively and the results have been summarized in Table 1.

$$C_E = {\Delta H_m}/{\Delta H_{HD}} \times 100\% \qquad\qquad C_t = \left(\frac{W_{HD}}{W_{HD} + W_m}\right) \times 100$$

ΔH_m is the melting enthalpy of microcapsules and ΔH_{HD} is melting enthalpy of hexadecane and is equal to 218 J/g. The results show that the experimental core content is close to theoretical one, which illustrates the good encapsulation of HD. Moreover to evaluate the cycling performance of the microcapsule, all samples were thermally heated and cooled for 200 times and after that their melting enthalpy has been measured through DSC ($\Delta H'$). The

decrement of melting enthalpy for M1 was sensible in contrast to others. This shows the presence of cross linker is vital for minimizing the leakage of PCM through shell.

Table 1: formulation recipes and thermal properties of samples.

	MMA %	EGDM %	HD %	ΔH_m	$\Delta H'_m$	C_E	C_t
M1	60	0	40	84	71.9	38.7	40
M2	65	5	30	62	61.5	28.8	30
M3	55	5	40	86.2	86	39.5	40
M4	45	5	50	106.3	105	48.7	50
MN	95	5	0	-	-	-	-
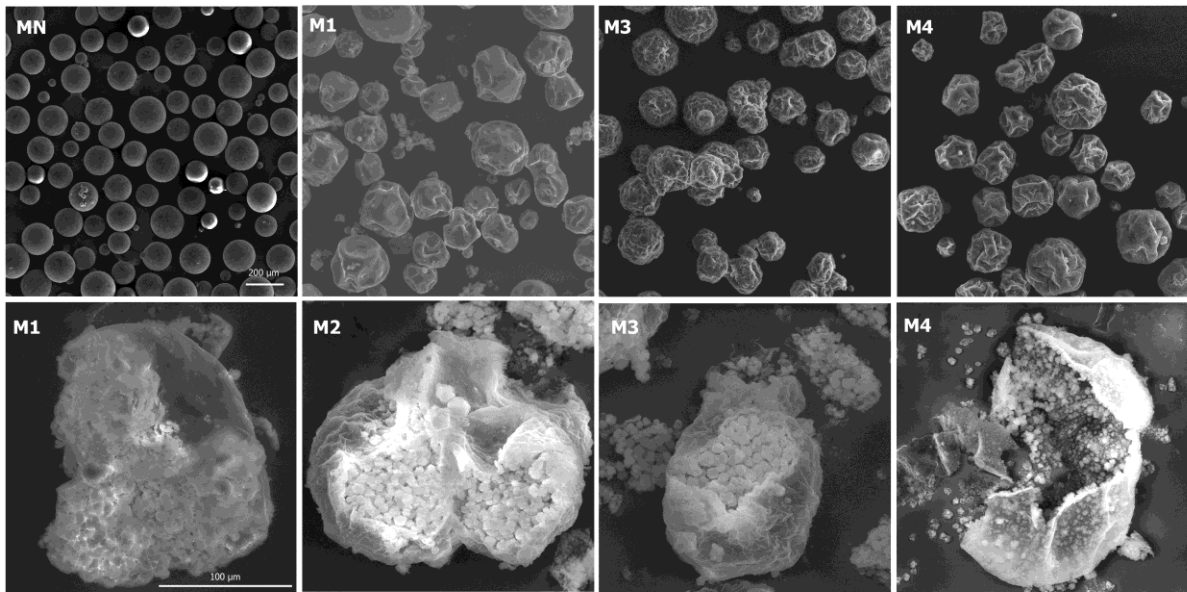
Fig. 1: SEM micrographs of microcapsules.
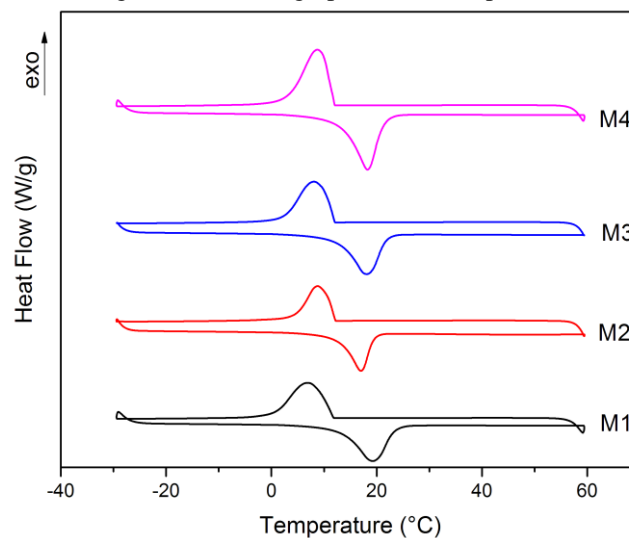
Conclusion:

HD/PMMA microcapsules were synthesized successfully. They had spherical morphology and showed good thermal properties.

References:

[1] Konuklu Y, Paksoy HO, Appl Energy, **2015**, 150, 335.
[2] Yu S, Wang X, Wu D, Appl Energy , **2014**, 114, 632.
[3] Sharma A, Tyagi V V, Renew Sustain Energy Rev, **2009,** 13, 318.

Simultaneous determination of acetylsalicylic acid (ASA) and ascorbic acid (AA) in their binary mixtures by novel spectrophotometric methods

Raziyeh Rahdari*, Ghadamali Bagherian, Mansour Arab Chamjangal

College of Chemistry, Shahrood University of Technology, Shahrood, P.O. Box 36155-316, Iran.

E-mail: ra.rahdari@gmail.com

Introduction

Three simple, accurate, and precise spectrophotometric methods, manipulating ratio spectra, were developed for simultaneous determination of aspirin (acetylsalicylic acid, ASA) and ascorbic acid (AA). These methods include extended ratio subtraction method (EXRSM) [1], simultaneous ratio subtraction method (SRSM) [2], and simultaneous ratio subtraction coupled with constant multiplication method (SRS-CM) [3]. A combination of AA and ASA, which are perhaps the two mostly consumed drugs in the world, is widely employed in pharmaceutical formulations for pain and fever relief including fevers associated with cold and flu [4]. These procedures do not require a preliminary separation step, and do not require a special program.
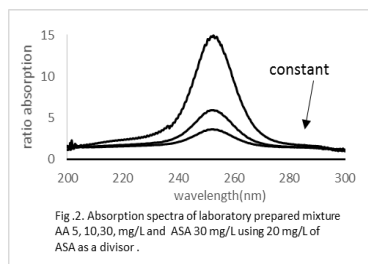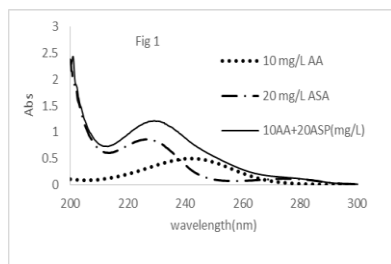
Method/Experimental

The absorption spectra for the two compounds ASA and AA and their mixture can be seen in Fig. 1. The factors such as pH affecting the sensitivity of these three methods were first optimized. For three methods, the absorption spectra for the standard solutions containing 10-50 mg/L of ASA, 5-40 mg/L of AA, and their mixtures were then recorded in the range of 200-300 nm.

Results and discussion

For SRSM, AA was determined by dividing the spectrum for the mixtures by the absorption spectra for 20 mg/L of ASA, as a divisor (ASA'). The division gave a new curve that represented $\frac{AA}{ASA'} + constant$. By measuring this constant, which is parallel to the wavelength axis in the region where ASA is extended ($\sim$280-295 nm), then a new curve was obtained after subtraction of the constant. This can be summarized as $\frac{AA+ASA}{ASA'} = \frac{AA}{ASA'} + \frac{ASA}{ASA'} = \frac{AA}{ASA'} + constant$ (1), is shown in Fig. 2. $\frac{AA}{ASA'} + constant - constant = \frac{AA}{ASA'}$ (2) is shown in Fig. 3. The concentration of AA was calculated using the regression equation representing correlation between the amplitudes of ratio spectra $\frac{AA}{ASA'}$ and the corresponding concentration of AA. The concentration of ASA was calculated via a measured constant value using the regression equation representing correlation between the amplitudes of ratio spectra $\frac{ASA}{ASA'}$ and the corresponding concentration of ASA.

For SRS-CM, the concentration of AA was determined as previously detailed in SRSM, while the concentration of ASA was determined using the constant multiplication method by multiplying the previously measured constant value $\frac{ASA}{ASA}$ in SRSM by the divisor ASA' using $\frac{ASA}{ASA'} \times ASA' = ASA$ (3) to get a zero-order spectrum (D0) for ASA, and then using the

regression equation representing correlation between the absorbance values for D0 of ASA at its λ_{max}= 275 nm against the corresponding concentrations.

Fig 1
10 mg/L AA
20 mg/L ASA
10AA+20ASP(mg/L)

Fig .2. Absorption spectra of laboratory prepared mixture AA 5, 10,30, mg/L and ASA 30 mg/L using 20 mg/L of ASA as a divisor .

Fig. 3. Division spectra of laboratory prepared mixture of AA 5,10,30 mg/L and ASA 30 mg/L using 20 mg/L ASA as a divisor aftersubtraction of the constant
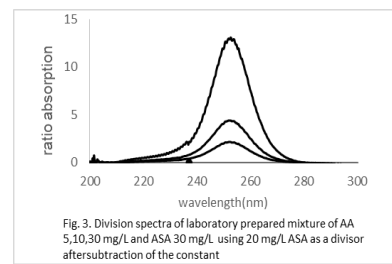
For EXRSM, the mixture of the two components was analyzed using well-established SRSM, where D0 of AA could be obtained by multiplying $\frac{AA}{ASA'}$ by divisor ASA$^{'}$ ($\frac{AA}{ASA'} \times ASA' = AA$ (4)). D0 of ASA was obtained by dividing D0 of AA in equation (4) by the absorption spectra for 10 mg/L of AA, as a divisor (AA'), to get the constant $\frac{AA}{AA'}$ for each concentration in the mixtures. Then the same ratio subtraction procedure was followed by dividing each mixture using 10 mg/L of AA, as a divisor, and then subtracting the corresponding constant $\frac{AA}{AA'}$ and multiplying by ASA'. Then the concentrations of AA or ASA in the mixture were calculated using the corresponding regression equations obtained by plotting the absorbance D0 values for each drug at its maximum absorbance against its corresponding concentration.[3]

Conclusion

In this work, three smart and simple recently developed spectrophotometric methods were validated by analyzing synthetic mixtures containing the cited drugs. The accuracy, precision, and detection limit of the proposed methods were determined. These methods were successfully applied for the simultaneous determination of the cited drugs in synthetic mixtures and tap water samples. These methods are also sensitive and selective, and could be used for routine analysis of ASA and AA in their available dosage form without prior separation.

References

[1] H.M. Lotfy; M.A.Hagazy, Spectrochimica Acta Part A: Molecular and Biomolecular Spectroscopy, **2012**, *96*, 259-270.
[2] H. M.Lotfy; M. A. Hegazy, Spectrochimica Acta Part A: Molecular and Biomolecular Spectroscopy, **2013**, *113*, 107-114**.**
[3] H.M.Lotfy; M.A.Hegazy; M.R.Rezk; Y.R.Omran, Spectrochimica Acta Part A: Molecular and Biomolecular Spectroscopy, **2014,** *126*, 197-207.
 [4] M.R.Khan; Z .Alothman; M.Naushad; A.A. Ghfar; S.M, Journal of Liquid Chromatography

Improved desalination performance of reverse osmosis membranes modified with boehmite nanoparticles

Mahdie Safarpour[1,*], Vahid Vatanpour[2], Hamed Zarrabi[2] and Ehsan Yekavalangi[2]

[1]*Research Laboratory of Advanced Water and Wastewater Treatment Processes, Department of Applied Chemistry, Faculty of Chemistry, University of Tabriz, Tabriz, Iran*
(E-mail: safarpour_88@yahoo.com)
[2]*Faculty of Chemistry, Kharazmi University, Tehran, Iran*
****

Introduction

Reverse osmosis (RO) process is economical for the production of potable water from brackish water or seawater. Although many RO plants have been established by now, research effort to increase the membrane flux, rejection and antifouling properties is still needed. Lots of strategies have been proposed to develop antifouling RO membranes in recent years, including the selection of new monomers, improvement of fabrication process, surface modification of RO membrane by physical and chemical methods as well as the hybrid organic/inorganic RO membrane [1]. Boehmite is an aluminum oxide hydroxide (γ-AlOOH) particle, containing hydroxyl groups attached to its surface. In the current study, RO membranes were modified with boehmite nanoparticles [2].

Experimental

RO membranes were prepared by interfacial polymerization method. Specific amount of boehmite were first dispersed in deionized water under ultrasonic treatment, and then 2.0 wt% m-phenylenediamine (MPD) was added to it. Polyamide RO membranes were formed by immersing the polysulfone support membrane in this solution for 5 min. The MPD saturated support was then immersed into the organic solution of trimesoyl chloride (TMC) for 60 s. The resulting composite membranes were cured at 70 ºC for 10 min.

Results and Discussion

The surface hydrophilicity of membranes is usually expressed in terms of water contact angle to evaluate the tendency of water to wet the membrane surface. Hydrophilicity is one of the most important properties of membranes which it influence the flux and antifouling ability of the membranes [3]. As presented in Table 1, the contact angle decreased by addition of the boehmite nanofiller. The reduced contact angle implies the enhancement in hydrophilicity, which comes from natural high hydrophilicity of the nanoboehmite due to the presence of hydroxyl groups on the nanoparticles surface [2].

Table 1. Water contact angle of the RO membranes modified with boehmite.

[Boehmite] (wt.%)	0	0.002	0.005		0.01	0.02
Contact angle (º)	67.8	49.8	61.3		57.3	51.1

Figure 1 and 2 shows the water flux and salt rejection versus boehmite content in the prepared RO membranes. As can be seen in Figure 1, the addition of boehmite increased the water flux of the membranes. The higher water flux of the modified membranes compared to the bare membrane is attributed to the more hydrophilic surface of these membranes as confirmed by contact angle results. As shown in Figure 2, the salt rejection values were increased in all of the modified membranes compared to bare membrane. The maximum salt rejection was observed for RO membrane containing 0.002 wt.% boehmite (97.41%).
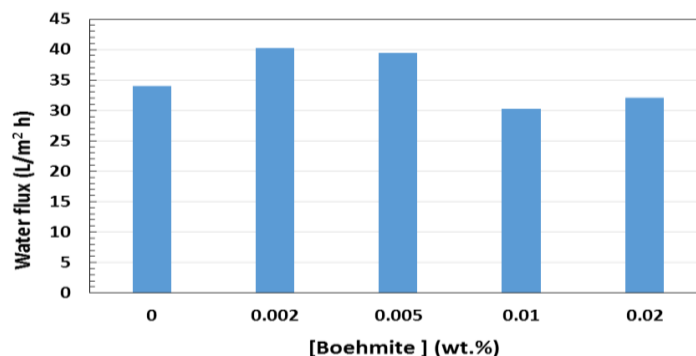
Figure 1. Effect of boehmite loading on the water flux of RO membranes.
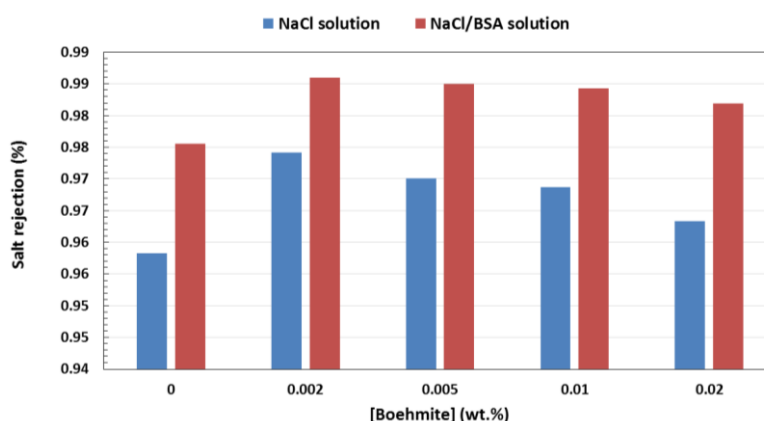
Figure 2. Effect of boehmite loading on the salt rejection performance of RO membranes.

Conclusion

Thin film composite reverse osmosis (TFC-RO) membranes incorporating boehmite nanoparticles were prepared by interfacial polymerization of MPD and TMC. It was shown that the addition of hydrophilic boehmite additive improved the surface hydrophilicity, permeability and salt rejection performance of the RO membranes.

References

[1] Zhao, H., Qiu, S., Wu, L., Zhang, L., Chen, H. and Gao, C., Journal of Membrane Science, 2014, 450, 249-256.
[2] Vatanpour, V., Madaeni, S. S., Rajabi, L., Zinadini, S. and Derakhshan, A. A., Journal of Membrane Science, 2012, 401–402, 132-143.
[3] Safarpour, M., Khataee, A.R. and Vatanpour, V., Journal of Membrane Science, 2015, 489, 43-54.

Synthesis, characterization and antimicrobial studies of some new zinc, cadmium and mercury nitrates complexes: new precursors for nanostructure metal oxide

Sajjad Mojahedi Jahromi [a], Morteza Montazerozohori [a*], Samaneh mojahedi-jahromi [b]
[a]Department of Chemistry, Yasouj University, Yasouj 75918-74831, Iran
[b]MSc, Drug and Food Department, Jahrom University of Medical Sciences, Jahrom, Iran
Email address: mmzohory@yahoo.com

Introduction: Metal coordination compounds have been a subject of particular interest due to broad spectrum of application in science and technology such as catalysis, medicine, polymer industries, optical industries and microbiological fields [1-3]. Using different type of ligands and metal ions in synthetic process of metal coordination complexes provides an opportunity to design various compounds for different scientific target. Among of various complexes, those with Schiff base ligands are important [4]. They have easy synthetic processes and coordinate with a broad spectrum of metal ions. In addition Schiff base complexes have many applications as catalyst and/or as industrial and pharmaceutical materials [5-7]. All these features causes that metal complexes of Schiff base have an outstanding role in many scientific field. Synthesis of coordination compound in nano-meter size is a new trend in inorganic chemistry and attracted more attention due to their unique properties that is related to the large numbers of surface molecules in comparison of the bulk forms. A literature survey indicate that synthesis of different inorganic Zn, Cd and Hg compounds have been reported [8, 9] but the reports for nano structure coordination compound with tridentate Schiff base complexes and using them as precursors for nanostructure metal oxide are rarely found. Metal oxides play an important role in many areas of chemistry, physics and materials science [10, 11]. In technological applications, oxides are used in the fabrication of microelectronic circuits, sensors, piezoelectric devices, fuel cells, coatings for the passivation of surfaces against corrosion, and as catalysts. Herein, the synthesis and characterization of some new Zn, Cd and Hg complexes of a tridentate Schiff base ligand entitled as (E)-N1-((E)-3-phenylallylidene)-N2-(2-((E)-((E)-3-phenylallylidene) amino) ethyl) ethane-1, 2-diamine are presented. The nano-structure and metal oxide of the complexes were also prepared under ultrasonic irradiation and calcination method respectively. Furthermore, thermal behaviors (TG/DTG/DTA) of all complexes are investigated.

Experimental: The ligand was synthesized via a condensation reaction between trans-3-phenyl-2 propenal, and diethylenetriamine in 2:1 M ratio in ethanol solvent under ultrasonic wave at room temperature. For the synthesis of Zn, Cd and Hg complexes, the ligand solution (1 mmol in 15 mL of ethanol) was drop wise added to the stoichiometric amount of Zinc, Cadmium and Mercury nitrate salts in ethanol (10 mL) during 10 min under ultrasonic wave. Then, the reaction mixture was maintain under ultrasonic wave more for 15 min at room temperature. Finally, the obtained precipitate of complexes was filtered and washed with ethanol several times. The resultant compounds were placed at 70–100 ^{O}C under vacuum and then kept in a desiccator over silica gel. The metal oxide was prepared from the complexes by calcination method at 500 ^{O}C.

Results and discussion: The ligand and all complexes were characterized by physico-chemical and spectroscopic methods such as FT-IR, UV–visible, ^{1}H, ^{13}C NMR spectra, melting points, and conductometric measure-ments. Furthermore the scanning electron microscopy (SEM), X-ray powder diffraction (XRD) and transmission electron microscopy (TEM) were used to investigate the particle sizes and morphologies of the complexes. Also the ligand and all complexes exhibited acceptable antibacterial and antifungal activity against bacterial and fungal strains comparable with standard drugs such as amoxicillin, penicillin and cephalexin.

Table 1
Vibrational (cm^{-1}) and electronic (nm) spectral data of tridentate Schiff base (L) and its Mercury (II) complexes.

Compoud	νCH_{arom}	$\nu N\text{-}H_{amine}$	νCH alkene	νCH aliph.	νCH imine	$\nu C{=}N$	$\nu C{=}C$	$\nu M{-}N$	$\lambda_{max}(nm)(\varepsilon, cm^{-1} M^{-1})$
Ligand	3056	3245	3025	2925	2834	1635	1492-1450	506	228(33951)-281(30840)
ZnL(NO$_3$)$_2$	3060	3253	3025	2937	2896	1634	1488-1446	512	233(99837)-283(82309)
CdL(NO$_3$)$_2$	3055	3223	3023	2917	2860	1633	1488-1448	507	225(16369)-289(22928)
HgL(NO$_3$)$_2$	3054	3245	3025	2919	2857	1629	1488-1448	507	258(51202)-288(51202)

(ε) Refers to absorption coefficient.
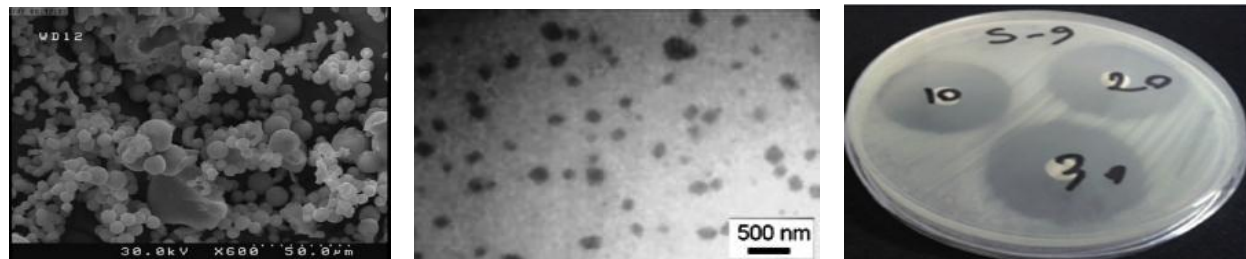
Fig1.From left to right SEM, TEM and Antimicrobial image of Zn, Cd and Hg complexes respectively.

Conclusion: In this study, we prepared some novel Zinc, Cadmium and Mercury complexes with a new tridentate Schiff base ligand. All the analytical data confirmed that the ligand and all complexes were synthesis successfully. The antibacterial and antifungal activities of free ligand and its complexes were screened in vitro against various bacteria. Evaluation of antibacterial and antifungal activities of the complexes with respect to free ligand was performed. Accordingly, HgL(NO$_3$)$_2$ were found as the most effective agents among other complexes against B. subtilis and S. aureus while CdL(NO$_3$)$_2$ showed good inhibitory effects against P. aeruginosa and E. coli respectively. Also among the complexes, ZnL(NO$_3$)$_2$ were found as more impressive in fighting with C. albicans and A. niger with respect to others .Moreover, interaction of these complexes with DNA indicated that all complexes can degrade DNA structure so that they may inhibit the growth of microorganisms via binding to DNA of them in addition to degradation of cell membrane. Furthermore thermal analyses of all complexes revealed that they are decomposed via 2–4 thermal steps from room temperature to 1000 ^{O}C. Finally, some thermo-kinetic parameters such as activation energy (ΔE^*), enthalpy (ΔH^*), entropy (ΔS^*) and Gibbs

References

[1] A. Scozzafava, C.T. Supuran, J. Med. Chem. 43 (2000) 3677.

[2] A. Scozzafava, L. Menabuoni, F. Mincione, G. Mincione, C.T. Supuran, Bioorg. Med. Chem. Lett. 11 (4) (2001) 575.

[3] M. Montazerozohori, S. Mojahedi Jahromi, A. Naghiha. J. Ind. Eng. Chem. 22 (2015) 248.

[4] A.K.M. Nur Alam Siddiki, Md. Shahidur Rahman, Md. Arifur Rahman, Md. Abdus Salam, Md. Abu Yousuf, Md. Farhadul Islam, et al., Bangladesh Pharm. J. 15 (1) (2012) 83-87.

[5] M. Shebl, S.M.E. Khalil, S.A. Ahmed, H.A.A. Medien, J. Mol. Struct. 980 (2010)39–50.

[6] S.K. Bharti, G. Nath, R. Tilak, S.K. Singh, Eur. J. Med. Chem. 45 (2010) 651−660.

[7] G. Kumar, V. Singh, K. Singh, I. Ahmad, D.S. Yadav, J. Pharm. 2 (2012) 45.

[8] M. H. Habibi, E. Askari, M. Habibi, M. Zendehdel, Spectrochim. Acta A 104 (2013) 197.

[9] M. Montazerozohori, S. Mojahedi Jahromi, A. Masoudiasl, P. McArdle, Spectrochim. Acta A. 138 (2015) 517–528.

[10] J. A. Rodríguez, M. Fernández-García, (Eds.) Whiley: New Jersey, 2007.

[11] M. Fernández-García, A. Martínez-Arias, J. C. Hanson, J. A. Rodríguez, Chem. Rev. 104 (2004) 4063.

One-pot synthesis of 5-substituted 1H-tetrazoles using Schiff base complex of Ni(II) supported on superparamagnetic Fe$_3$O$_4$@SiO$_2$ magnetic nanospheres as a recyclable catalyst

Ali Reza Sardarian∗, Iman Dindarloo Inaloo, Mohsen Esmaeilpour

Chemistry Department, College of Sciences, Shiraz University, Shiraz 71454 (Iran),
E-mail: asardarian55@yahoo.co.uk (A.R. Sardarian)

1. Introduction

Tetrazoles are an increasingly popular functionality with a wide range of applications such as in pharmaceuticals as lipophilic spacers and metabolically stable surrogates for carboxylic acids in medicinal chemistry, ligands in coordination chemistry, special explosives in materials science, in photography and information recording systems and valuable precursors to a variety of nitrogen-containing heterocycles in organic synthesis [1]. They have been found to be potential TNF alpha inhibitors, P2X7-antagonists and inhibitors of anandamide cellular uptake [2]. Furthermore, tetrazoles are screened for various biological activities such as anticonvulsant, antiulcer, anti-inflammatory, antifungal, antiviral, antibacterial, antiulcer and antitubercular activities [3]. Many methods for the synthesis of 5-substituted tetrazoles have been proposed based on [3+2] cycloaddition of azide ion to corresponding organic nitriles. The reactions were carried out using numerous catalysts such as BF$_3$-OEt$_2$ [4], γ-Fe$_2$O$_3$ [5], nano-CuFe$_2$O$_4$ [6] and Zn/Al hydrotalcite [7]. However, most of the reported methodologies suffer from various disadvantages, therefore, the choice of catalyst is one of the most crucial steps for achieving good results. In the present research, we wish to describe an efficient, facile and convenient procedure for the synthesis of 5-substituted 1H-tetrazoles from nitriles in the presence of Fe$_3$O$_4$@SiO$_2$/Schiff base of Ni(II) magnetic catalyst (Scheme1).
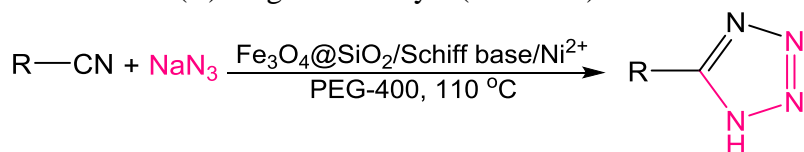
Scheme.1 One-pot synthesis of 5-substituted 1H-tetrazoles using the Fe$_3$O$_4$@SiO$_2$/Schiff base/ Ni(II) catalyst.

2. Experimental

2.1. *Preparation of* Schiff base complex of Ni(II) functionalized Fe$_3$O$_4$@SiO$_2$ nanoparticles

Fe$_3$O$_4$@SiO$_2$/Schiff base of Ni(II) nanoparticles were prepared in our previous work [8].

2.2. *General procedure for synthesis of 5-substituted 1H-tetrazole derivatives in presence of Fe$_3$O$_4$@SiO$_2$/Schiff base of Ni(II) catalyst*

Fe$_3$O$_4$@SiO$_2$/Schiff base of Ni(II) (0.02 g) was added to a mixture of nitrile (1 mmol), sodium azide (1.2 mmol) and DMF (3 ml) and PEG-400 stirred at 110 °C. After completion of the reaction, the reaction mixture was cooled down, and catalyst was isolated by simple filtration and HCl (1 N, 10 mL) was added to the filtrated solution. The products extracted with ethyl acetate (3×10 mL). The organic solvent was dried over anhydrous sodium sulfate, and concentrated to give the crude solid product.

3. Results and discussion

The catalytic activity of $Fe_3O_4@SiO_2$/Schiff base of Ni(II) was studied in order to optimize the protocol for formation of 5-substituted $1H$-tetrazoles using benzonitrile and NaN_3 as model reaction. Our optimization data are: 1 mmol of benzonitrile, 1.2 mmol of sodium azide, 0.9mol% of 0.02 catalyst and 5ml of peg-400 at 110 °C. After optimizing the reaction conditions, we next examined the generality of the reaction using sodium azide and various benzonitriles. As can be seen, the yields were good to excellent without the formation of any side products and the reaction times are very low.

Table 1. $Fe_3O_4@SiO_2$/Schiff base/Ni(II)-catalysed synthesis of 5-substituted $1H$-tetrazoles.

Entry	R	Time (h)	Yield (%)[b]	M.p. (lit.) (°C)
1	C_6H_5	4	93	216-218(215-217)[1]
2	$4\text{-}CN\text{-}C_6H_4$	6	95	255-257 (255)[1]
3	$4\text{-}NO_2\text{-}C_6H_4$	8	92	214-216 (217-218)[1]
4	$4\text{-}MeO\text{-}C_6H_4$	12	91	229-230 (230-231)[1]
5	$4\text{-}Me\text{-}C_6H_4$	12	89	247-248 (249-250)[1]
6	2-Pyridyl	10	93	209-210 (211-212)[1]
7	1-Naphthalene	13	84	260-261 (261-262)[1]
8	9-Phenanthrenyl	14	82	217-218 (216)[1]
9	$C_6H_5CH_2$	16	80	119-121 (121-122)[1]

In order to confirm the reusability and stability of this magnetic catalyst it was recovered by applying a magnetic field and the catalyst reused for subsequent reactions at least 6 times without any activation process.

4. Conclusions

In summary, we have reported that $Fe_3O_4@SiO_2$/Schiff base of Ni(II) nanoparticles can be an efficient and reusable catalyst for one-pot syntheses of 5-substituted $1H$-tetrazoles from nitriles in good to excellent yields. This method has notable advantages such as thermal stability, heterogeneous nature, easy preparation and easy separation of catalyst, short reaction time, clean and simple procedure, excellent yields, easy product separation and purification and lower loading of catalyst compared with other methods.

Acknowledgements

References

[1] Mohsen Esmaeilpour, Jaber Javidi ,Saeed Zahmatkesh, *Appl. Organometal. Chem*. **2016**, *30*, 897-904.
[2] Ortar, Giorgio, Aniello Schiano Moriello, Maria Grazia Cascio, Luciano De Petrocellis, Alessia Ligresti, Enrico Morera, Marianna Nalli, Vincenzo Di Marzo. *Bioorg. Med. Chem. Lett*. **2008**, *18*, 2820-2824.
[3] Malik, Sachin, Suroor A. Khan. *Med. Chem. Res*. **2014**, *23*, 207-223.
[4] Kumar, Anil, Ramamurthi Narayanan, Harold Shechter. *J. Org. Chem*. **1996**, *61*, 4462-4465.
[5] Qi, Gang, Yong Dai. *Chin. Chem. Lett*. **2010**, *21*, 1029-1032.
[6] Sreedhar, B., A. Suresh Kumar, Divya Yada. *Tetrahedron Lett*. **2011**, *52*, 3565-3569.
[7] Kantam, M. Lakshmi, KB Shiva Kumar, and K. Phani Raja. *J. Mol. Catal. A*. **2006**, *247*, 186-188.
[8] Mohsen Esmaeilpour, Ali Reza Sardariana, Jaber Javidi, *Applied Catalysis A: General*. **2012**, *445*, 359-367.

Biosynthesis and application of magnetically recyclable nanocatalys of Fe3O4@SiO2–Ag in the reduction of organic dyes in water

Neda Seyedi, Mohaddeseh Shahabi Nejad, Pourya Mohammadi, Hassan Sheibani, Kazem Saidi

nseyedi2013@gmail.com

Department of Chemistry, Shahid Bahonar University of Kerman, Kerman 76169, Iran

nseyedi2013@gmail.com

Introduction: Among of these noble metals, silver nanoparticles (Ag NPs) have been known as an inexpensive metal and were applied in a variety of catalytic reactions, such as selective epoxidations, oxidations, and reduction [1-4]. Several methods have been reported to synthesize of $Fe_3O_4@SiO_2$-Ag NPs but there is still a critical need to develop facile and practical methods to get small and highly dispersed Ag NPs with a thin size distribution on the $Fe_3O_4@SiO_2$ support. Although there are several available methods for the syntheses of silver nanoparticles but these one some contain such as use of toxic chemicals, high temperature, pressure and production of hazardous by-products [5,6]. The plant extracts for the synthesis of silver nanoparticles have been proposed as a valuable alternative to chemical methods to avoid from cited disadvantages. Therefore, in order to investigate the catalytic activity of $Fe_3O_4@SiO_2$-Ag we have chosen the reduction of chemical compounds such as organic dyes.

Experimental: The characterization of this catalyst has been done with transmission electron microscopy (TEM), X-ray powder diffraction (XRD), vibration sample magnetometer (VSM).

Freshly collected plant leaves were shad dried and powdered. Then, the dry powdered samples were extracted with ethanol as a solvent. The prepared extracts were kept in sterile bottles and put in refrigerator at $3\text{-}5^{°}C$ until further use. we synthesized Fe_3O_4 NPs from iron salts and coated it to form a core–shell ($Fe_3O_4@SiO_2$) structure A simple in situ wet chemistry method was employed for the the synthesis of $Fe_3O_4@SiO_2$–Ag nanoparticles. Firstly, $Fe_3O_4@SiO_2$ was dispersed in a solution of $AgNO_3$. Then, the prepared leaf extract was added to the reaction mixture. The mixture was cooled down to an ambient temperature, the precipitates were collected using an external magnet and washed distilled water. Finally, in order to investigate the catalytic activity of $Fe_3O_4@SiO_2$-Ag we have chosen the reduction of chemical compounds such as organic dyes.

Result and discussion: The morphology and size distribution of $Fe_3O_4@SiO_2$-Ag NPs were analyzed using TEM (Fig. 1).

Fe_3O_4 NPs exhibit dominantly near spherical morphology which a thin layer of silica coted each of these Fe_3O_4 NPs. The phase and purity of $Fe_3O_4@SiO_2$-Ag NPs was examined by XRD. Fig. 2 shows XRD powder pattern of the $Fe_3O_4@SiO_2$-Ag NPs. In the case of $Fe_3O_4@SiO_2$–Ag (Fig. 3c), besides the characteristic diffraction of Ag NPs, the obvious diffraction peaks at 2θ= $37.9^{°}$, $44.1^{°}$, $64.3^{°}$ and $77.2^{°}$, which can be attributed to the reflections of the (1 1 1), (2 0 0), (2 2 0), and (3 1 1) crystalline planes of cubic Ag, respectively [7].

The magnetic properties of the synthesized nanocatalyst ($Fe_3O_4@SiO_2$-Ag) were characterized using vibrating sample magnetometry (VSM). Figure 3 shows a typical magnetization curve. It should be noted that the core–shell structured $Fe_3O_4@SiO_2$–Ag NPs still shows strong magnetization, suggesting its suitability for magnetic separation and recovery.

Figure1   Figure2   Figure3
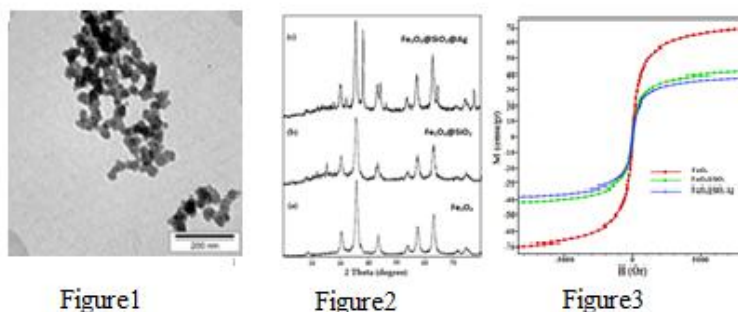
In order to investigate the catalytic activity of $Fe_3O_4@SiO_2$-Ag NPs, the reduction of organic dyes was chosen as a model reaction in the presence of $NaBH_4$. The reaction can be monitored easily by measuring the change in UV–Vis absorbance at 400 nm and 300 nm. The result showed that this catalyst possessed high performance in reduction of organic dyes

Conclusions: In summary, a simple and green process for the synthesis of $Fe_3O_4@SiO_2$-Ag NP by using leaf extract of plant has been demonstrated. The synthesized Ag NPs display both catalytic and magnetic properties which can be easily recycled by an external magnet after the catalytic reduction of organic dyes by using $NaBH_4$ as a reducing agent at room temperature in aqueous media. This catalyst retains its high activity for the degradation even after 10 cycles. This approach would hold great promise an ideal platform for the fabrication of highly efficient magnetically catalysts for various heterogeneous catalytic reduction applications.

References

[1] J. Chen; X. Tang; J. Liu; E. Zhan; J. Li; X. Huang; W. Shen, *Chem. Mater*. **2007**, *19*, 4292-4297.

[2] J.W. Medlin; J.R. Monnier; M.A. Barteau, *J. Catal.* **2001**, *20*, 471-477.

[3] K. Shimizu; K. Sawabe; A. Satsuma; *Sci. Technol*. **2011**, *1*, 331-336.

[4] T. Ung; L.M. Liz-Marzán; P. Mulvaney; *J. Phys. Chem. B*, **1999**, *103*, 6770-6779.

[5] P. Logeswari; S. Silambarasan; J. Abraham; *Sci Iran*. **2013**, *20*, 1049-1054.

[6] S. Ahmed, Saifullah; M. Ahmad; BL. Swami; S. Ikram; et al. , *J Rad Res App Sc*. **2015**, *7*, 1131-1139.

[7] T. Bárbara; M. António; R. Cristina; S. Carmo; M. Olívia; N. Nuno R; N. José M F; S. Jorge Alexandre; N. Maria Leono; *Journal of the Science of Food and Agriculture*, **2013**, *93*, 2707–14.

[8] A. L. Morel; S. I. Nikitenko; K. Gionnet; A. Wattiaux; J. Lai-Kee-Him; C. Labrugere; B. Chevalier; G. Deleris; C. Petibois; A. Brisson; *ACS Nano*, **2008**, *2*, 847-852.

Synthesis, characterization and DNA interaction of vanadyl Schiff base complex

Raziyeh Kalantari, Zahra Asadi[*]

Department of Chemistry, College of Sciences, Shiraz University, Shiraz ٧١٤٥٤, I.R. Iran

Email address: zasadi@shirazu.ac.ir

****

Introduction:

Organic ligands containing Schiff bases, considered privileged structures, have attracted considerable attention due to their facile synthesis and variable coordination behavior toward metal ions, as well as their wide applications in various fields [١].

Schiff base ligands are capable to coordinate to metals and have a variety of applications such as biological. The interest in coordination chemistry of vanadium has increased in the last decades because of its catalytic and medicinal importance.

Deoxyribonucleic acid, DNA, is a molecule of great biological significance since it is one of the targets for the drugs. Studies of the interaction between metal complexes and DNA have been pursued in recent years [٢].

Methods / Experimental:

Synthesis of vanadyl Schiff base complex: glycylglycine (٨mmol) was dissolved in water and then sodium acetate trihydrate (١٦mmol) and ٥-(triethylammoniummethyl)salicylaldehyde chloride (٨mmol) were added. The solution became yellow due to the formation of the Schiff base. After that a solution of $VOSO_4.5H_2O$ (٨mmol) in water was added. Green precipitate was formed and washed with diethyl ether.

The binding propensity of the synthesized complex with biomolecules was investigated using electronic absorption spectroscopy, fluorescence measurements, viscosity measurement and cyclic voltammetry.

Results and Discussion:

The complex was characterized by FT-IR, elemental analysis and electronic spectra. Figure ١ shows the Ft-IR spectra of vanadyl Schiff base complex. The peaks at ١٦٢٧ (due to C=N) and ٩٧٩ (due to V=O) proved the successful synthesis of the Schiff base compound.
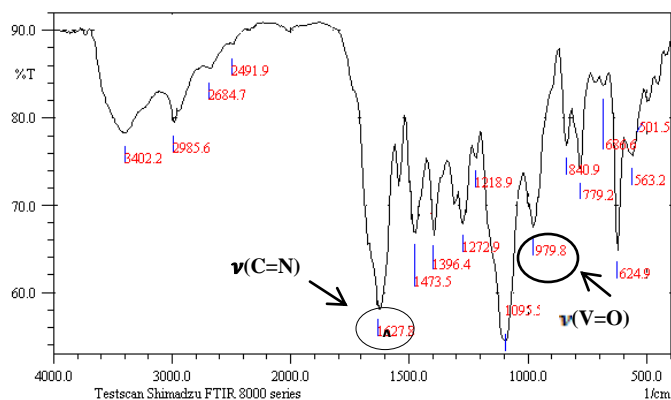
Figure ١. FT-IR spectra of vanadyl Schiff base complex.

Figure ٢ shows the absorption spectra of the complex in the absence and presence of varying amounts of HS-DNA. The interaction of complex with DNA caused a decrease in absorbance (hypochromism) in the π-π* transition.In general, hypochromism is associated with the binding of the complex to the helix by an intercalative mode involving strong stacking interaction of the aromatic chromophore of the complex between the DNA base pairs.
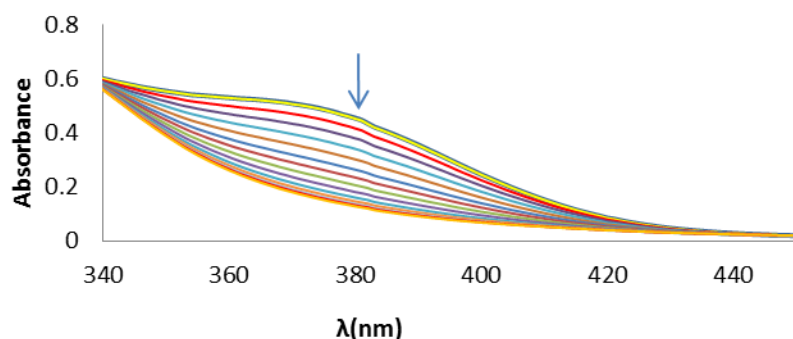

Figure ٢: Titration of the complex solution with varying amounts of DNA.

Conclusion:

In this study a new vanadium (IV) complex was synthesized and characterized. UV-Vis spectroscopy, fluorescence and viscosity studies were revealed that this complex can bind to DNA by an intercalation binding mode.

References:

[١] Cao, Y; Yi, C; Liu, H; Li, H; Li, Q; Yuan, Z; Wei, G. *Transit Met Chem*, ٢٠١٦, ٤١, ٥٣١-٥٣٨.

[٢] Alaghaz, A. M. A; El-Sayed, B. A; El-Henawy, A. A; Ammar, R. A. A. *J. Mol. Struct*, ٢٠١٣, ١٠٣٥, ٨٣-٩٣.

Highly Efficient Synthesis of *N*-Alkyl Theophylline derivatives from Alcohols using P₂O₅/KI

Somayeh Behrouz*, <u>Samira Ahmadi</u>

Department of Chemistry, Shiraz University of Technology, Shiraz 71555-313, Iran

E mail: behrouz@sutech.ac.ir

****

Introduction: Methylxanthines including theophylline, caffeine and theobromine are one of the significant ingredients found in major dietary sources like coffee, tea, cola beverages, energy drinks and chocolates [1,2]. Among methylxanthines, theophylline has attracted considerable interest due to its greater binding efficacy with DNA compared to theobromine and caffeine [3]. The *N*-alkyl theophylline derivatives exhibit diverse chemotherapeutic activities including bronchodilator activity, analeptic, diuretic, cardiotic, CNS stimulant and so on (Figure 1) [4]. In this research, we would like to report a straightforward and highly efficient approach for direct synthesis of *N*-alkyl theophyllines from alcohols using P₂O₅/KI in the presence of DBU in refluxing acetonitrile.

Acefylline
(cardiotic, diuretic, antipasmodic bronchodilator)

Diprophylline
(expectorant, bronchodilator)

Fenethylline
(CNS stimulant)

Etamiphylline
(cardiotonic, diuretic)

Proxyphylline
(cardiotonic, bronchodilator)

Theofibrate
(antihyperlipoproteinemic)

Theodrenaline
(circulary analeptic, diuretic, cardiotonic)

Xantinol
(vasodilator)
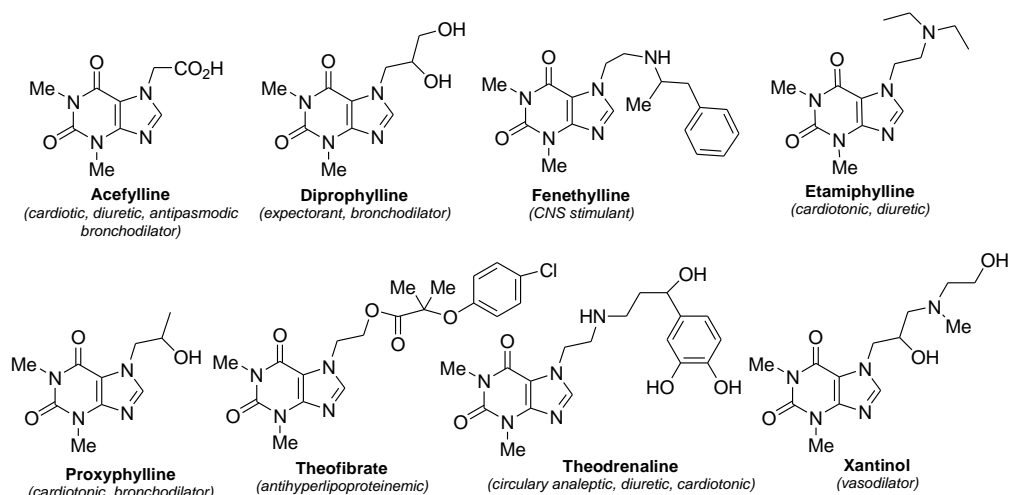
Figure 1

Experimental: To a double-necked round-bottom flask (50 mL) equipped with a condenser was added a mixture of theophylline, P₂O₅, KI, and DBU in refluxing acetonitrile. After completion of the reaction (TLC monitoring), the solvent was evaporated under vacuum and the remaining foam was diluted in CHCl₃ (100 mL) and subsequently washed with H₂O (2 × 100 mL). The organic layer was dried on Na₂SO₄ and evaporated. The crude product was purified by short column chromatography on silica gel eluting with a mixture of *n*-hexane/EtOAc.

Results and Discussion: To identify the optimized reaction conditions, the *N*-alkylation of theophylline with benzyl alcohol in the presence of P_2O_5/KI was selected as the sample reaction. Since the solvent has undeniable role in reaction progress; therefore, our preliminary effort was focused on selecting an appropriate solvent. The best result was obtained using acetonitrile as the solvent. We further explored the effect of several organic and inorganic bases on the progress of sample reaction. Among the examined bases, DBU was proved to be the most suitable base.

We then investigated the scope and general applicability of the present protocol for direct *N*-alkylation of theophylline with various structurally diverse alcohols. In general, good to excellent yields were obtained, when both primary and secondary alcohols were applied. However, the use of tertiary alcohol such as *t*-butyl alcohol did not afford the desire product. The versatility of the method was confirmed with respect to allylic, benzylic, aliphatic, alicyclic and other alcohols containing *N*-heterocycles.

We also examined the selectivity of this method. To this end, a competitive reaction in a binary mixture of 1-butanol and 2-butanol was investigated under the optimized conditions. High selectivity for *N*-alkylation of theophylline was observed for primary alcohol compared to its secondary analogue.

Conclusion: We have developed a simple and convenient method for direct *N*-alkylation of theophylline with primary and secondary alcohols using P_2O_5/KI. The ease of operation, use of safe and cheep reagent for activation of alcohol, good to excellent yields of the product, and the applicability of the method in large scale synthesis make this process as an attractive protocol for synthesis of structurally diverse *N*-alkyl theophyllines as potential chemotherapeutic agents.

References

[1] Roberts, M. F.; Wink, M. In *Alkaloids: Biochemistry, Ecology, and Medicinal Applications*, Plenum Press, New York 1998.

[2] Scheindlin, S.; *Mol. Interv.,* **2007**, *7*, 236-242.

[3] Nafisi, S.; Manouchehri, F.; Tajmir-Riahi, H.-A.; Varavipour, M. *J. Mol. Struct.,* **2008**, *875*, 392-399.

[4] Kleeman, A.; Engel, J.; Kutscher, B.; Reichert, D. In *Pharmaceutical Substances*, 3rd edn., Thieme, Stuttgart, 1999.

Highly Efficient and Ligand-Free Protocol for *N*-Arylation of Imidazole with Aryl Halides Using Novel Nano Silica-Based Copper Catalyst

Somayeh Behrouz*, <u>Mehrnaz Amirabadi</u>

Department of Chemistry, Shiraz University of Technology, Shiraz 71555-313, Iran

E mail: behrouz@sutech.ac.ir

<div align="center">*********************</div>

Introduction: *N*-Arylimidazoles are useful substrates due to their biological effects and medicinal applications [1]. The most common route to access *N*-arylimidazoles is the copper-catalyzed Ullmann coupling reaction [2]. However, such reactions have traditionally suffered from harsh reaction conditions and the need for stoichiometric amounts of copper catalyst that make scale up unfeasible and ecologically unfriendly. Hence, the development of efficient heterogeneous catalytic systems under milder conditions has been actively pursued. Herein, we wish to report highly efficient Ullmann-type synthesis of *N*-arylimidazoles using a novel nano silica-based copper catalyst in the presence of DBU in refluxing acetonitrile (Scheme 1).

X = Br, I
R = H, Me, OMe, Cl, ...
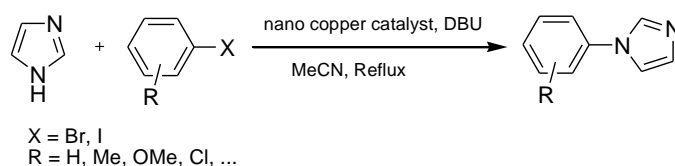
Scheme 1

Experimental: To a double-necked round-bottom flask (50 mL) equipped with a condenser was added a mixture of imidazole, DBU, and catalyst in refluxing acetonitrile. After completion of the reaction (TLC monitoring), the solvent was evaporated under vacuum and the remaining foam was diluted in CHCl$_3$ (100 mL) and subsequently washed with H$_2$O (2 × 100 mL). The organic layer was dried on Na$_2$SO$_4$ and evaporated. The crude product was purified by short column chromatography on silica gel eluting with a mixture of *n*-hexane/EtOAc.

Results and Discussion: In order to optimize the reaction conditions, the *N*-arylation of imidazole with iodobenzene in the presence of a nano silica-based copper catalyst was selected as the sample reaction. To this end, our preliminary effort was focused on selecting an appropriate solvent for progress of the reaction. Among the examined solvents used in these experiments, acetonitrile affords the best results and thus it was applied for all subsequent reactions. The reaction base was another important factor

that affects the progress of the reaction. Thus, the effect of several organic and inorganic bases on the progress of sample reaction was evaluated. Among the examined bases, DBU provides the higher yield of product in short reaction times.

We then screened the scope and general applicability of this protocol for *N*-arylation of imidazole with different aryl halides. Aryl bromides and aryl iodides efficiently converted to the corresponding *N*-arylimidazoles. In addition, aryl halides having both electron-rich and electron-deficient groups perform the *N*-arylation of imidazole to afford the corresponding products in good yields. The recyclability and the reusability of catalyst were also investigated under the optimized reaction conditions. The results confirm the reusability of catalyst without any significant loss of its activity after 8 consecutive runs.

Conclusion: We have described a simple and highly efficient method for Ullmann-type *N*-arylation of imidazole with structurally diverse aryl halides using a novel nano silica-based copper catalyst. The thermal and chemical stability, reusability as well as the ease of recovery of catalyst allows it to be a highly efficient and suitable heterogeneous catalyst for different organic transformations. This method is attractive for the synthesis of different *N*-aryl heterocyclic derivatives as important potential biological active compounds.

References

[1] Zhong, C. L.; He, J. T.; Xue, C. Y.; Li, Y. J. *Bioorg. Med. Chem.*, **2004**, *12*, 4009-4015.

[2] Hassan, J.; Sevignon, M.; Gozzi, C.; Schulz, E.; Lemaire, M. *Chem. Rev.*, **2002**, *102*, 1359-1470.

An efficient synthesis of pyrano[2,3-*d*]pyrimidinones using by a organo catalyst

Mandana momenpour, Farhad Shirini*

Department of chemistry, Faculty of Science, University of Guilan, Rasht, Iran

Email address*: shirini@guilan.ac.ir

Introduction: Pyrano[2,3-*d*]pyrimidine derivatives are annulated uracils that have received great attention due to their wide range of biological activity such as antitumor, antihypertensive, cardiotonic, bronchiodilators and antiallergic activities. The conventional synthetic method for the preparation of this type of compounds is based on the condensation of barbituric acid with aldehydes and malononitrile. For this purpose, a variety of catalysts have been used to facilitate this reaction that have some disadvantage such as toxicity, expensive and high require time for preparation of catalyst. In this work we used a organo catalyst for the efficient synthesis of pyrano[2,3-*d*]pyrimidinone Derivatives.[1-5]

Experimental: A mixture of aldehyde (1 mmol), barbituric acid (1 mmol), malononitrile (1.1 mmol) and organo catalyst (10 mg, 6.5 mol%) in EtOH:H$_2$O (1:1) (5 mL) was heated at 70 °C. The progress of the reaction was monitored by TLC (EtOAc: Hexane [1:5]). After completion of the reaction, water was added to the mixture of the reaction then the product was filtrated. Pure product was obtained after recrystallization from ethanol.

Result and discussion: We have used of basic organo catalyst as a highly powerful catalyst for the simple and efficient synthesis of pyrano[2,3-*d*]pyrimidinones. We explored the protocol with a variety of aromatic, aliphatic and heterocyclic aldehydes under the optimal conditions that results shown that the desired products were obtained in good to excellent yields. The work-up of the reaction is accomplished by simple filtration, followed by recrystallization (Scheme 1).
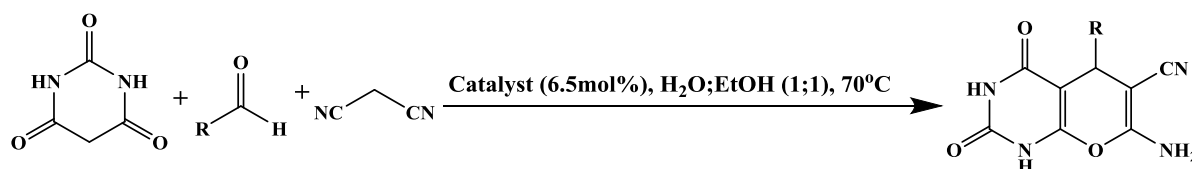
Scheme 1. Synthesis of pyrano[2,3-*d*]pyrimidinone derivatives in the presence of organo catalyst

Conclusion: We have developed an efficient and ecologically safe method for the synthesis of pyrano[2,3-d]pyrimidine derivatives using a green procedure. Our method is simple as no special apparatus, reagents or chemicals, and work up are required, and the formed compound is filtered and purified just by simple crystallization.

References

[1] J. Davoll; J. Clarke; E. F. Eislager. *J. Med. Chem.*, **1972**, 15, 837–839.
[2] G. L. Anderson; J. L. Shim; A. D. Broom. *J. Org. Chem*, **1976**, 41, 1095–1099.

[3] E. M. Griva; S. Lee; C. W. Siyal; D. S. Duch; C. A. Nichol. *J. Med. Chem.*, **1980,** 23, 327–329.

[4] D. Heber; C. Heers; U. Ravens. *Pharmazie*, **1993**, 48, 537–541.

[5] M. M. Ghorab; A. Y. Hassan. *Phosphorus, Sulfur, Silicon Related Elem.*, **1998**, 141, 251–256.

Iron and manganese (III) porphyrin covalently bound to poly(acryloyl chloride) as biomimetic heterogeneous catalysts for alkene epoxidation by NaIO$_4$: advantage of iron (III) porphyrin and significance of nitrogen donor axial ligands

Gholamreza Karimipour[a], Saeed Kowkabi[a,*]

[a] Department of Chemistry, Yasouj University, Yasouj 75918-74831, Iran

Email address: kowkabi.saeed@yahoo.com

Introduction:

Metalloporphyrins may structurally and functionally resemble the cytochrome P-450 monooxygenase enzymes [1, 2] that have been used as model compounds for oxidation reactions [3, 4]. Metalloporphyrin catalysts are generally destroyed by the oxidants or by their metal-oxo intermediates, leading to obtain low yields, low selectivities and turnover frequencies. The strategy prevents the degradation and inactivation of heme groups as active site of the enzymes. Similarly, the use of synthetic metalloporphyrins substituted with active groups and their immobilization on an appropriate support has resulted in efficient, reusable and selective catalysts for catalytic oxidation reactions. Furthermore, the use of supported metalloporphyrins as the active heterogeneous catalyst provides an easy way to handle and eliminate the difficulty in recovery and recycle of these expensive catalysts from the reaction media. Poly(acrylic acid) (PAA) is a hydrophilic; water soluble polymer used in many applications including surface medication, biotech and pharmaceuticals [5, 6]. In this work, the carboxyl end group of PAA was converted to acyl group by using thionyl chloride to obtain poly (acryloyl chloride) (PAC). The prepared PAC was used for supporting of iron and manganese tetrakis(4-benzylamine)porphyrins to attain Fe(T$_{Bamin}$P)OAc@PAC and Mn(T$_{Bamin}$P)OAc@PAC as heterogeneous catalysts for epoxidation of alkenes by sodium periodate (NaIO$_4$).

Methods / Experimentals:

Tetrakis(4-benzylamine)porphyrin ligand, (T$_{Bamin}$)P, was successfully synthesized previously by our group through the reduction of tetrakis(4-cyanophenyl)porphyrin (T$_{CN}$)P with lithium aluminum hydride in anhydrous diethyl ether [7]. Fe(T$_{Bamin}$P)OAc and Mn(T$_{Bamin}$P)OAc are obtained by metallation of the (T$_{Bamin}$)P with iron(II) acetate or manganese(II) acetate in DMF according to the method described by Buchler et al. [8]. Poly(acryloyl chloride) (PAC) was prepared following literature procedure by the reaction of commercial PAA (average Mv ca. 450,000) with thionyl chloride [9]. Fe(T$_{Bamin}$P)OAc@PAC catalyst was prepared by the interaction of Fe(T$_{Bamin}$P)OAc and PAC in the presence of triethylamine. In a 500 mL round bottom flask, 3.0 g of PAC was suspended in 150 mL of tetrahydrofuran/toluene (1:1; v/v) and the suspension was stirred vigorously for 30 min. Another 150 mL tetrahydrofuran/toluene (1:1 v/v) containing 0.6 g (0.72 mmol) Fe(T$_{Bamin}$P)OAc and 2.91 g (28.81 mmol) triethylamine was prepared and added dropwise to the polymer suspension. The mixture was then refluxed for 12 h

and cooled down to room temperature. The resulting brown solid was filtered off, washed thoroughly with MeOH and CH_2Cl_2 and dried under vacuum at 90 °C. A similar procedure was followed for preparing $Mn(T_{Bamin}P)OAc@PAC$ as a slime green solid using $Mn(T_{Bamin}P)OAc$ and PAC in the presence of triethylamine. In epoxidation reactions, to an acetonitrile solution (2 mL) containing alkene (0.3 mmol), axial ligand (i.e., imidazole; 0.025 mmol; 0.0017 g) and $Fe(T_{Bamin}P)OAc@PAC$ (0.1 g), an aqueous solution (1.0 mL) of $NaIO_4$ (0.325 mmol; 0.069 g) was added. The reaction was stirred at room temperature for required time and monitored by gas chromatography.

Results and Discussion:

The overall reaction pathway for preparing supported metalloporphyrin catalysts is shown in Scheme 1. The carboxylic acid groups in PAA were converted to acyl chloride to obtain PAC and then the Fe and Mn porphyrin catalysts were reacted with PAC to obtain the heterogeneous catalysts. The FT-IR spectroscopy gives valuable information about covalent anchoring of $Fe(T_{Bamin}P)OAc@PAC$ on the functionalized polyacrylic acid that is obtained by comparison of the IR spectra of PAA, PAC and Fe $(T_{Bamin}P)OAc@PAC$ (Fig. 1). The EDX analysis of the catalyst showed presence of Fe as shown in Fig. 2 that confirmed the loading of $Fe(T_{Bamin}P)OAc$ on the polymer support. From the EDX data (not shown) we have found that the amount of the Fe-porphyrin loaded on PAC was ca. 504 mmol per gram of the catalyst. This result is coincident with that obtained by AAS, and consequently all the oxidations under study (vide infra) were achieved by ca. 0.1 g of $Fe(T_{Bamin}P)OAc@PAC$ which contains 0.005 mmol of the catalyst. The particle size and structural morphology of the $Fe(T_{Bamin}P)OAc@PAC$ were also investigated by TEM technique(Fig. 3). Also scanning electron micrograph (SEM), was recorded for PAC, $Fe(T_{Bamin}P)OAc@PAC$ and $Mn(T_{Bamin}P)OAc@PAC$ to examine the morphological changes occurring on the surface of the polymer. A clear change in the morphology of the polymer, after supporting of the porphyrin complexes, was observed by SEM (Fig. 4). The Mn content of $Mn(T_{Bamin}P)OAc@PAC$ was determined by AAS, which showed a value of 846 μmol per gram of the catalyst. Therefore, the oxidation reactions catalyzed by $Mn(T_{Bamin}P)OAc@PAC$ were performed with 0.006 g of the catalyst which is equivalent to ca. 0.005 mmol of $Mn(T_{Bamin}P)OAc$.

Epoxidation reactions:

It should be noted that the epoxidation does not proceed in the absence of catalyst or in the presence of PAA and or PAC. So, the catalytic experiment was carried out with styrene and $NaIO_4$ in the presence of both the heterogeneous and homogeneous Fe and Mn porphyrin catalysts. The heterogeneous Fe and Mn catalysts are more effective than that of the homogeneous catalysts. This may be related to high specific surface area of the catalyst which resulted from supporting of the catalyst to the PAC chain. The optimal conditions were applied for epoxidation of some other alkenes. The results are summarized in Table 1. As it can be seen, epoxidation of styrene with $Fe(T_{Bamin}P)OAc$ as heterogeneous catalyst leaded to 28.4 % conversion with 60.2 % selectivity for styrene epoxide (Table 1, run 1). Moreover, the turnover frequency is very low (4.1 h^{-1}) in this case. However, $Fe(T_{Bamin}P)OAc@PAC$-Im/$NaIO_4$ system shows better catalytic activity toward alkenes, so that styrene was epoxidized in 56 % with ca.

96.9 % selectivity and 22.4 h^{-1} TOF (Table 1, run 2). No benzaldehyde or other products were found, probably due to the formation of a high valent Fe-oxo porphyrin intermediate which could epoxidize styrene directly through the interaction of the intermediate and the alkene substrate [10]. It is reasonable to assume that the epoxidation was achieved directly with the high valent Fe-oxo porphyrin without any allylic oxidation which results benzaldehyde and other by products. Although, the C=C ond in α-methylstyrene (Table 1, run 3) is more electronrich than styrene, the epoxide yield of α-methylstyrene is lower than that of styrene. This may be related to the stericindrance existing in the former. Cyclohexene (Table 1, run 4) and cyclooctene (Table 1, run 5) were epoxidized moderately with 100 % selectivity and high TOFs. Although, the epoxide yield obtained for trans-stilbene (Table 1, run 6) is lower than that of cis-stilbene (Table 1, run 7) which may attribute to steric effect of the former, the TOF value of cis-stilbene was higher than that of trans-isomer. In 1-octene (Table 1, run 8), the C=C bound is an electron poor double bond and thus give low yield and low TOF.

Conclusion:

In conclusion, poly(acryloyl chloride) (PAC) is a convenient support for Fe(T$_{Bamin}$P)OAc and Mn(T$_{Bamin}$P)OAc, because the active -NH$_2$ functional groups in the porphyrin could easily react with the acyl groups in PAC and produce polymer-anchored metalloporphyrin complexes as stable heterogeneous catalysts. We have found that (1) Fe(T$_{Bamin}$P)OAc@PAC is the best among other homogenous and heterogeneous Fe and Mn porphyrin catalysts for alkene epoxidation with NaIO$_4$; (2) acetonitrile/water (2:1, v/v) has been found to be the best solvent for reaction performed in the presence of the Fe(T$_{Bamin}$P)OAc@PAC, (3) nitrogen donor axial ligands (i.e., imidazole) can greatly enhance the catalytic activity of the metalloporphyrin, (4) only a 0.005 mmol of the Fe(T$_{Bamin}$P)OAc@PAC catalyst was taken to achieve the epoxidation reactions and the optimal molar ratio of the catalyst, imidazole, alkene and NaIO$_4$ was 1.5:60:65, respectively, which applied for alkene epoxidation at room temperature, (5) the epoxidations were achieved in moderate yields with high selectivity for epoxide, and (6) the catalyst is reusable and can be applied at least for four times without any significant loss of its activity.

References
[1] B. Meunier, S.P. de Visser, S. Shaik. *Chem. Rev,* **2004**, 104, 3947.
[2] S. Zakavi, F. Heidarizadi, S. Rayati. *Inorg. Chem. Commun*, **2011**, 14, 1010.
[3] F. Lingling, C. Yuan, L. Zhigang. *J. Mol. Catal. A-Chem*, **2015**, 408, 91.
[4] B.A. Arndtsen, R.G. Bergman, T.A. Mobley, T.H. Peterson. *Acc. Chem. Res*, **1995**, 28, 154.
[5] G. Saunders, B. Mac Creath, *Biodegradable polymers analysis of biodegradable polymers by GPC-SEC application compendium,* **2010** (Agilent Technologies Inc, Santa Clara).
[6] C.F. Jones, D.W. Grainger, *In vitro assessments of nanomaterial toxicity. Adv Drug Deliv Rev*, **2009** 61, 438.
[7] G. Karimipour, M. Ghaedi, M. Behfar, Z. Andikaey, S. Kowkabi, A.H. Orojloo. *I.E.E.E. Sens, J.* **2012**, 12, 2638.
[8] J. W. Buchler, G. Eikelmann, J. Puppe, K. Rohback, H. Schneehage, D. Weck. *Liebigs Ann. Chem*, **1971**, 745, 135.
[9]. M.Y. Abdelaal, M.S.I. Makki, T.R.A. Sobahi. *Am. J. Polym. Sci*, **1971**, 2, 73.
[10] S. Tangestaninejad, M. Moghadam, V. Mirkhani, I. Mohammad-poor-Baltork, N. Hoseini. *J. Iran. Chem. Soc*, **2010**, 7, 663.
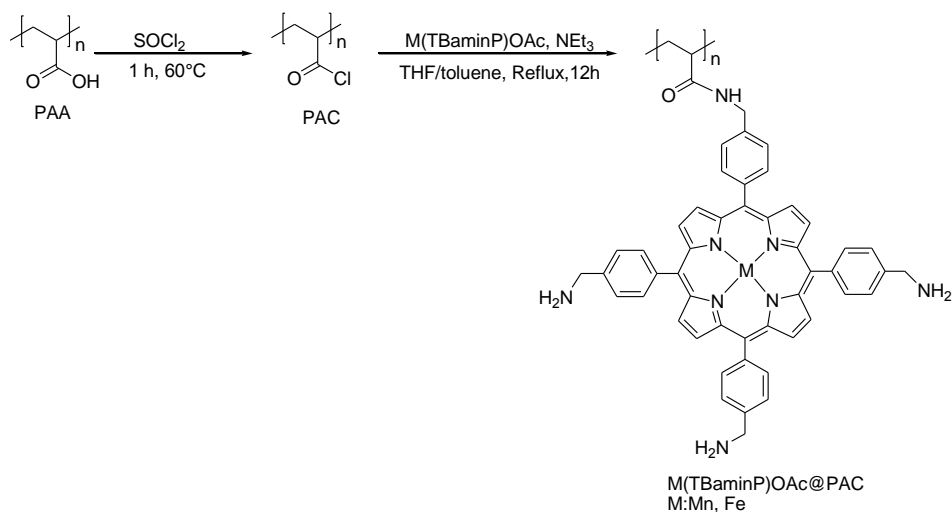
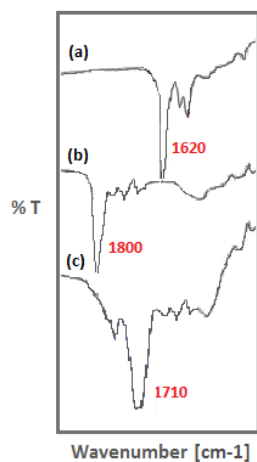**Scheme 1** Overall reaction pathway for preparation of Mn and Fe(T$_{Bamin}$P)OAc@PAC

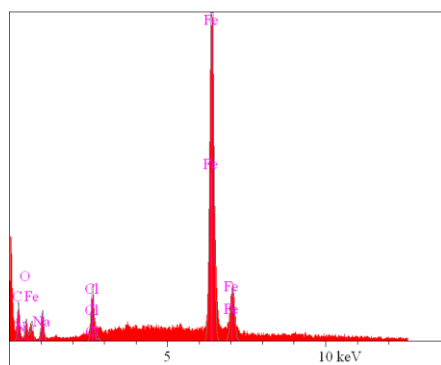**Fig. 1** The FT-IR spectra(C=O Stretching region) of Fe(T$_{Bamin}$P)OAc@PAC (a), PAC (b) and PAA(c).
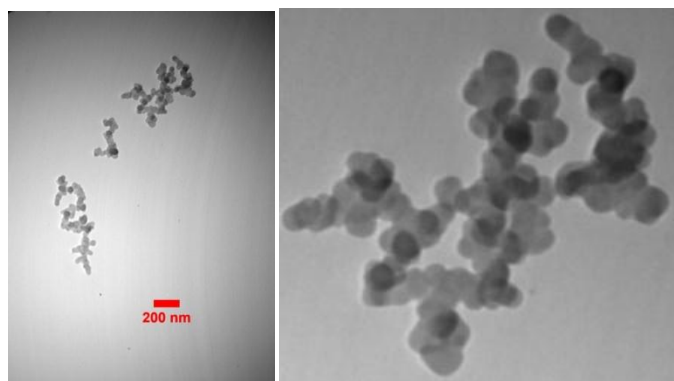

Fig. 2 The EDAX pattern of Fe(T$_{Bamin}$P)OAc@PAC
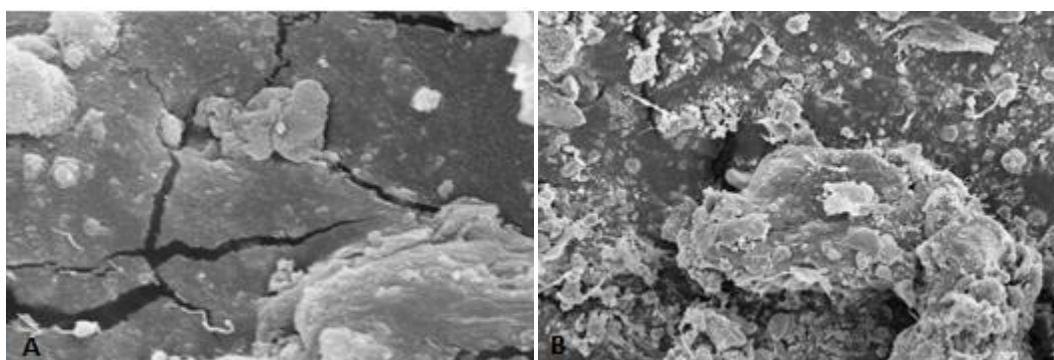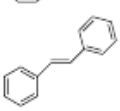
Fig. 3 TEM image of Fe(T$_{Bamin}$P)OAc@PAC

Fig. 4 Scanning electron Micrograph(SEM) of: (A) Poly(acryloyl chloride); (B) FeT(4-CH$_2$NH$_2$)PP@PAC

Table 1 Epoxidation of alkenes with NaIO$_4$ catalyzed by Fe(T$_{Bamin}$P)OAc@PAC and imidazole

Run	Alkene	Conv. (%)	Epox. (%)	Epoxide selectivity (%)	Time (h)	TOF (h^{-1})[a]
1		28.4	17.1	60.2	2.5	4.1
2		57.8	56.0	96.9	1.5	22.4
3		49.4	49.4	100	1.5	19.7
4		72.5	72.5	100	2	21.7
5		79.2	79.2	100	2.5	19.0
6		47.7	46.0	96.4	1	27.6
7		56.0	54.7	97.0	1	32.4
8		23.8	21.0	88.2	2.5	5.0

Green synthesis of high conductivity thiolated graphene oxide /reduced Graphene oxide/polyaniline nanocomposite film

Sajad Amirzadeh and Nooredin Goudarzian*
Department of Applied Chemistry, Shiraz Branch, Islamic Azad University, Shiraz, Iran
Corresponding author*: Sajad.amirzadeh2620@gmail.com

1. Introduction

This paper proposes a fast, facile, low cost, large-scale, and environmentally friendly preparation method for preparation of thiolated graphene oxide (TGO)/reduced graphene oxide(RGO)/polyaniline(PA) nanocomposite film by in situ ultra-sonication at room temperature with the assistance of the extract of Teucrium Polium (TP), which is a natural antioxidant essential for many metabolic , as a nontoxic reducing agent. In addition, the formation of dimension-controlled of TGO and RGO on PA by ultra-sonication assistance and its growth mechanism is proposed. On the other hand, the fabrication of TGO/RGO/PA thin film via solvent treatment was carried out and electrical properties of the nanocomposite film was investigated.

2. Experimental

2.1 Preparation of polyaniline: Freshly distilled aniline was added into HCl in a beaker. Ammonium persulfate (NH4)2S2O8 solution, was added from a burette into the monomer solution. Then the polymer was filtered, washed to remove impurities and remainder monomers. Then the product was dried. The synthesized polymer powder (PA/HCl) was treated with a solution of ammonia at room temperature in order to change the polymer into emeraldine base (EB)state.

2.2 Synthesis of TGO/RGO/PA nanocomposites: Graphene oxides and TGO/RGO nanocomposite were prepared. Subsequently, extract of Teucrium Polium was added slowly to the reaction mixture. The suspension was then washed and dried to obtain the as-prepared TGO/RGO nanoparticles. TGO/RGO nanoparticles were dispersed in tetrahydrofuran (THF). Dispersions were then sonicated and then the appropriate amounts of PA placed in the TGO/RGO nanoparticles dispersion and sonicated again under the same conditions then washed and dried to obtain the TGO/RGO/PA nanocomposite film. Conductivity and transmittance have been measured for five different nanocomposite polymer strips and an average value was calculated for each case.

3. Results and Discussion

3.1 Green reduction of GO by Teucrium Polium: It was demonstrated that the studied plant Teucrium Polium extracts have the potential to be used as reducing agents for the reduction of graphene oxide in an environmentally benign synthetic protocol. The optimized reaction conditions for the reduction of grapheme oxide was determined to be a reaction time, temperature and Teucrium Polium extracts concentration. Various characterization techniques such as gravimetric analysis, UV-Vis spectroscopy and FT-IR, and TGA confirmed that graphene oxide was reduced with Teucrium Polium extracts. This environmental-friendly reduced graphene oxide can potentially be used in various areas such as biomedical applications.

3.2 Conductivity and morphology: Electrical DC-conductivity of TGO/RGO/PA nanocomposite films (doped with HCl) was measured using conventional 4-point probe

technique. In order to measure conductivity, the polymer samples were cut into optimum strips for conductivity. Conductivity measurements were carried out after doping the polymer nanocomposite films with HCl solution at room temperature after drying at ambient conditions. Conductivity of TGO/RGO/PA nanocomposite after doping with HCl, was much higher than pure PA. With increasing the percentage of /GO/RGO nano particles, conductivity of polymer nanocomposite increase gradually. TGO/RGO/PA nanocomposite were changed into insulator when treated with a dilute ammonia solution. Characterization of TGO/RGO/PA nanocomposite was also carried out using scanning electron microscopy (SEM). SEM images have shown the well dispersion of nanoparticles in polymer bed (Fig.1-a and 1-b).
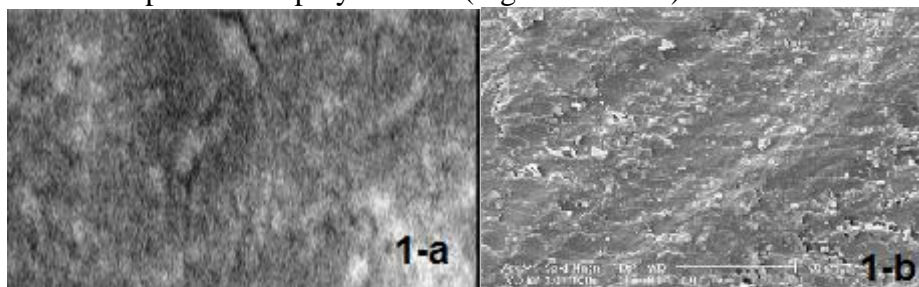
4. Conclusions

Based on the results, a new prospective green facile synthesis route in controlling the morphology of the nano particles in reduced graphene oxide composites with ultra-sonication and annealing assistance was obtained. Therefore, it is expected that this green synthesis approach of TGO/RGO/PA nanocomposite hybrids will lead to the further development of a broad new class of graphene oxide composite films with enhanced properties for many technological applications.

References:

[1]. Kudin KN, Ozbas B, Schniepp HC, Prud'homme RK, Aksay IA, Car R. Raman spectra of graphite oxide and functionalized graphene sheets. *Nano Lett*. **2007**;*8*:36–41.

 [2] S. Gawande, S.R. Thakare, One-pot sonochemical synthesis of CdS-reduced graphene oxide composite and its application for photocatalytic degradation of methylene blue, *Indian Journal of Chemistry Section A: Inorganic Bio-Inorganic Physical Theoretical & Analytical Chemistry*, **2013**, *52 (5)*, 614–618.

Kinetic investigation of antibiotic amoxicillin degradation over ZnO nano-catalyst using Monte Carlo simulation

Hamed Moradmand Jalali*

Department of physical chemistry, Faculty of science, University of Guilan, Rasht, Iran

*email: Haamedmoradmandjalali@gmail.com

Introduction

Antibiotics are dangerous pollutants in water owing to their adverse effects on aquatic life and human health. Amoxicillin (AMX) is antibiotics that extensively prescribed in order to treat numerous diseases [1]. This antibiotic has antimicrobial properties due to existence of a beta-lactam ring in its chemical structure (Fig.1). Non-biological technologies have been developed to remove antibiotics from aquatic. Elmolla *et al*. have reported photo-decomposition of AMX in aqueous systems using ZnO nanoparticles as photocatalyst [2]. In the present work, the kinetic parameter and mechanism of the AMX degradation by ZnO nanoparticle has been studied using kinetic Monte Carlo (KMC) simulation.
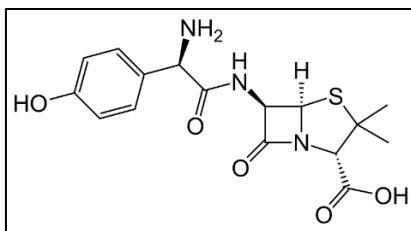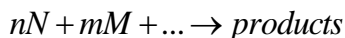

Fig.1. Chemical structure of antibiotic amoxicillin

Kinetic Monte Carlo Methods

In KMC simulation the reaction mechanism is considered as a collection of several reactions [3]:

$$nN + mM + ... \rightarrow products$$

The input data are steps and their rate constants, k_i. The rate of ith step, R_i, is taken to be proportional to probability, P_i, of its occurring in a particular time interval.

$$P_i \propto R_i = k_i[N]^n[M]^m$$

The algorithm is based on probability density function:
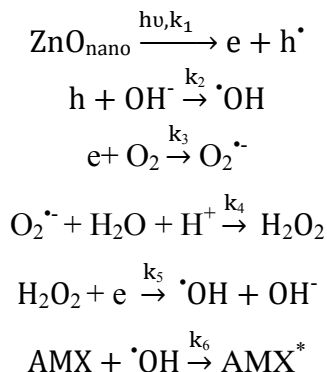
$$P(\tau,i)=k_iC_i\exp\{-\Sigma k_iC_i\tau\}$$

The time step Δt is the mean time for a system obeying Poisson statistics:

$$\Delta t = \frac{-\ln \rho}{\sum R_i}$$

where ρ is a random number between 0 and 1.

Results and discussion

In the mechanism which has a good fitting with experimental kinetic data, electron/hole pair is formed by irradiation of ZnO nanoparticles photocatalyst. In the subsequent steps hydroxyl radical is formed by photocatalytic processes of electron and hole (reactions 2-5). This radical is strong oxidant which can participate in the oxidation of AMX antibiotics over ZnO surface. These steps can be described below:

$$ZnO_{nano} \xrightarrow{h\upsilon, k_1} e + h^\bullet$$

$$h + OH^- \xrightarrow{k_2} {}^\bullet OH$$

$$e + O_2 \xrightarrow{k_3} O_2^{\bullet -}$$

$$O_2^{\bullet -} + H_2O + H^+ \xrightarrow{k_4} H_2O_2$$

$$H_2O_2 + e \xrightarrow{k_5} {}^\bullet OH + OH^-$$

$$AMX + {}^\bullet OH \xrightarrow{k_6} AMX^*$$

The values of the rate constants of each step in the aforementioned mechanism were obtained as adjustable parameters. The AMX concentrations versus time curves were achieved using KMC simulation. Well agreement is observed between calculated and experimental [2] data (Fig. 2.)
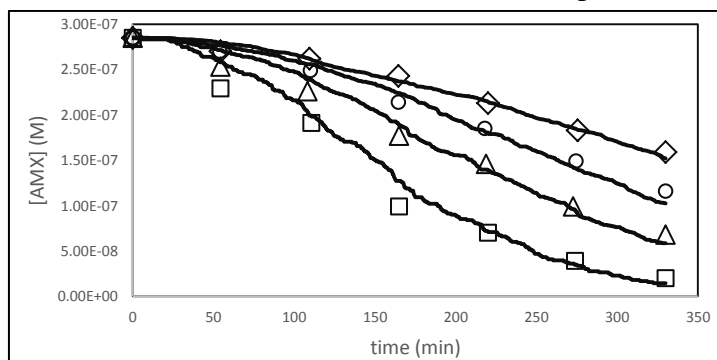

Fig.2. Kinetic data for AMX degradation by different concentrations of ZnO nanoparticle: (◊) 0.2, (○) 0.35, (△) 0.5, (□) 1.0 g/L. Experimental data (open markers) and simulated data (solid lines).

Conclusion

KMC simulation was used as an effective method to investigation the kinetics of photo-catalytic activity of ZnO nano-catalyst applied in AMX destruction. The rate constant of each steps were obtained. The KMC simulation results exhibit qualitative agreement with the experimental kinetic curves for different concentration of ZnO nano-catalyst. Therefore the obtained mechanisms can be suitable for the kinetic study of photo-catalytic removal of antibiotics by ZnO nanoparticles.

References

1 S. Su, W. Guo, C. Yi, Y. Leng, Z. Ma, *Ultrason. Sonochem.* **2012**, *19*, 469–474
2 E.S. Elmoll, M. Chaudhuri, *J. Hazard. Mater.* **2010**, *173*, 445–449
3 D.T. Gillespie, *J. Comp. Phys*. **1976**, *2*, 403-434.

CuCr$_2$O$_4$ nanoparticles as a new and efficient catalyst for the sonogashira coupling of triarylamines and arylacetylene by microwave irradiation

Javad Safaei-Ghomi*, Zeinab Akbarzadeh

Department of Organic Chemistry, Faculty of Chemistry, University of Kashan, Kashan, 51167, I. R. Iran

*email: safaei@kashanu.ac.ir

Introduction

Ethynyl linked aromatic amines are often applied as a significant part in electrophotography [1] and light-emitting devices [2]. Also these compounds are used in synthesis of natural products [3], polymers [4] and inmolecular wires [5]. Synthesis of ethynyl linked aromatic amines has been carried out by Sonogashira coupling [6] which is a palladium-copper catalyzed reaction of halides substituted triarylamines and aryl acetylenes. In this research we combined the advantages of microwave irradiation and nanotechnology to find the more convenient and efficient reaction of triarylamine substituted iodide and aryl acetylenes to produce ethynyl linked triarylamines.

Experimental

Copper chromite nanoparticle has been prepared by coprecipitation method in 86% yield. For the synthesis of ethynyl-linked-triarylamines, a mixture of iodo-substituted-triarylamine-arylacetylene, CuCr$_2$O$_4$ nanoparticles and Pd(PPh$_3$)$_2$Cl$_2$ in Et$_3$N was being stirred at 50 °C. At the end of reaction, the mixture was separated on a silica gel column chromatography to afford products in 47-55 % yields. In the similar process, the mixture was irradiated by microwave irradiation (600 W) at 25 °C and ethynyl-linked-triarylamines was produced in 77–86% yield.

Results and discussion

The SEM image of the produced nano CuCr$_2$O$_4$ illustrates particles with diameters in the range of nanometers (Figure 1).
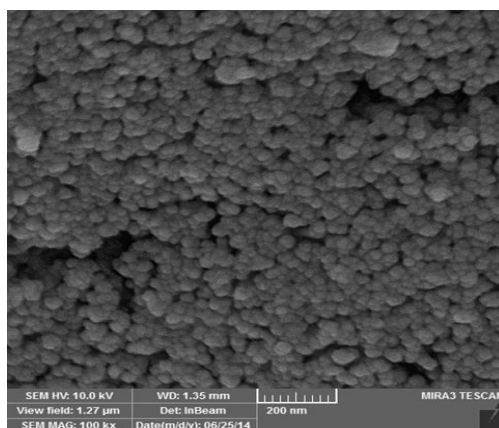

Figure-1: SEM image of the CuCr$_2$O$_4$ nanoparticles

Ethynyl linked triarylamines were synthesized from the Sonogashira coupling of iodo-substituted triarylamine with arylacetylene in the presence of $CuCr_2O_4$ nanoparticles and $Pd(PPh_3)_2Cl_2$ as a catalytic system and trietylamine (Et_3N) as the base under conventional and microwave conditions (scheme 1). In order to find the best catalyst, a variety of catalysts were examined (Table 1). Obviously, 2% mol of $Pd(PPh_3)_2Cl_2$/ nano $CuCr_2O_4$ is the most effective catalytic system for this reaction (Table 1, entry 5).
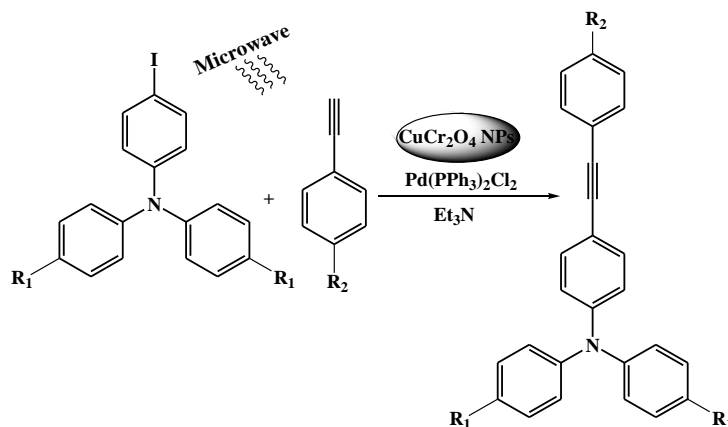
Scheme-1: Synthesis of ethynyl linked triarylamine

Table 1. Synthesis of ethynyl linked triarylamines by various catalyst under microwave irradiation

Entry	Catalytic system (mol%)	Time (min)	Yield[a] (%)
1	$CuCr_2O_4$/$Pd(PPh_3)_2Cl_2$ (12%)	20	55
2	CuI/$Pd(PPh_3)_2Cl_2$ (12%)	25	40
3	CuCl/$Pd(PPh_3)_2Cl_2$ (12%)	25	42
4	Nano $CuCr_2O_4$/$Pd(PPh_3)_2Cl_2$ (1%)	15	73
5	**Nano $CuCr_2O_4$/$Pd(PPh_3)_2Cl_2$ (2%)**	**15**	**79**
6	Nano $CuCr_2O_4$/$Pd(PPh_3)_2Cl_2$ (3%)	15	79

[a] Isolated yields

Conclusion

As the result, this work indicates a simple and efficient approach for the synthesis of ethynyl linked triarylamine using $CuCr_2O_4$ nanoparticles and $Pd(PPh_3)_2Cl_2$ as a highly efficient catalytic system under microwave condition. This microwave method represents several advantages such as green procedure, mild reaction conditions, short reaction times and high yields.

References

1. M. J. Plater, T. Jackson, *Tetrahedron*, **2003**, *59*, 4673-4677.
2. Z.J. Zhao, X.J. Xu, X.P. Chen, X.M. Wang, P. Lu, G. Yu, *Tetrahedron*, **2008**, *64*, 2658-2662.
3. M. Toyota, C. Komori, M. Ihara. *J. Org. Chem.* **2000**, *65*, 7110-7117.
4. W. Shi, L. Wang, M. Umar, T. Awut, H. Mi, C. Tana, I. Nurulla, *Polym. Int.* **2009**, *58*, 800-814.
5. W. P. Hu, H. Nakashima, K. Furukawa, Y. Kashimura, K. Ajito, Y. Q. Liu, *J. Am. Chem. Soc.* **2005**, *127*, 2804-2809.

6. K. Sonogashira, *Comprehensive Organic Synthesis*, Trost, B. M., Fleming, I., Eds.; Pergamon Press: New York, 1991; Vol. 3, pp 521-549.

Low frequency vibrational modes of alkaline earth metals acetylacetonates

Hamideh Fakheri,[a] Mahboobeh Gholamhoseinpour,[b] Sayyed Faramarz Tayyari,[a]
Mohammad Momen Heravi,[a] Ali Morsali[a]

[a] Chemistry Department, Mashhad Branch, Islamic Azad University, Mashhad
[b] Chemistry Department, Mashhad Branch, Islamic Azad University, Mashhad

1. Introduction

The infrared spectra of many acetylacetonates complexes have been assigned by a number of investigators [1,3], but the attention so far has mostly been confined to the middle infrared region (700-1600 cm^{-1}), and little is known about the low-frequency part of the spectra. These studies indicate that several vibrations in the low-frequency region involve metal-oxygen, M-O, stretching character to a varying degree through the vibrational coupling. The M-O stretching bands are metal sensitive; they are shifted to higher or lower frequencies by changing the metal in a series of compounds having the same structure.

The aim of the present work is the investigation of the low frequency IR absorption and Raman scattering spectra of Be, Mg, Ca, Sr, and Ba acetylacetonates by means of density functional theory (DFT) approach. The effect of changing the metal on the frequency of metal-oxygen vibrational bands and the nature of metal-oxygen bond are discussed in this work.

2. Experimental

Alkaline earth metals acetylacetonates were prepared and purified according to the method described in the literature [4].

The IR spectra were recorded on a Bomem B-154 Fourier transform spectrophotometer in the region 900-600 cm^{-1} by averaging 20 scans with a resolution of 2 cm^{-1}. The spectra were measured as KBr pellets.

The Far-IR spectra in the region 600–50 cm^{-1} were obtained using a Thermo Nicolet NEXUS 870 FT-IR spectrometer equipped with a DTGS/polyethylene detector and a solid substrate beam splitter. The spectrum of the polyethylene pellet was collected with a resolution of 2 cm^{-1} by averaging the results of 64 scans.

The FT-Raman spectra were recorded employing a Bomem MB-154 Fourier transform Raman spectrometer.

3. Method of analysis

In this study, the molecular equilibrium geometry, harmonic force field, and vibrational transitions of alkaline earth acetylacetonates were computed with the GAUSSIAN 09 software system [5] by using density functional theory. The B3LYP level, using 6-311++G**basis set, have been used for Be, Mg, Ca acetylacetonates and LanL2DZ for all complexes.

LanL2DZ basis set (adding d and f orbitals as extrabasis) was also used for calculating the vibrational frequencies and IR and Raman intensities of all compounds.

Orbital population and Wiberg bond orders [6] were calculated with NBO 3.0 program implemented in Gaussian 09.

For better elucidation of nature and strength of the M-O bonding interactions of the titled complexes, a topological analysis, using Bader's theory of Atoms in Molecules. The bond energies of metal-oxygen, E(r), are calculated by the $E(r) = -\frac{1}{2} V(r)$ relation [7], which V(r) is the potential energy of critical point calculated by AIM program.

4. Results and discussion

The vibrational normal modes were recognized by GaussView software.

Excellent correlations between observed and calculated metal-oxygen vibrational modes with the M-O bond orders and M-O energies and also between M-O energies and stability of complexes were obtained. These correlations indicate that in the alkaline earth acetylacetonates the stability constants are directly dependent to the M-O strength. No linear correlation was observed between M-O vibrational frequencies and reverse of squre root of metal atom, which indicates that the change in the vibrational wavenumbers is not solely caused by metal mass.

Considering similar works on other metals and ligands may be needed to find a way for calculating the stability constants of unknown complexes.

References

[1] J. P. Dismukes, L. H. Jones, J. C. Bailar, Jr., J. Phys. Chem. 65 (1961) 792.
[2] K. E. Lawson, Spectrochim. Acta 17 (1961) 248.
[3] R. D. Gillard, H. G. Silver, J. L. Wood, Spectrochim. Acta 20 (1964) 63.
[4] W.C. Fernelius and B.E. Bryant, Inorg. Synth. 5 (1957) 105.
[5] Gaussian 09, Revision A.02, M. J. Frisch, et al. Gaussian, Inc., Wallingford CT, 2009.
[6]   K.W. Wiberg, Tetrahedron 24 (1968) 1083.
[7]   E. Espinosa, E. Molins, C. Lecomte, Chem. Phys. Lett. 285 (1998) 170

Fabrication of the titanium dioxide nanotubes using anodization method and considering the deposition of the silver nanosheets with different thickness on them using AC pulse electrodeposition

Saeid Behaein , Marzie Asoodeh , Razieh Khaki

North Tehran Azad Unuversity

Shiraz University

Introduction:

Electrochemical anodization is a cheap method to produce the titanium base nanotubes. In the nanotubes structures the thickness, height and diameters are important parameters [1]. In the electrochemical anodization the surface of the metal oxidizes under applying the potential or electric field produced by two electrodes floated in an electrolyte [2]. In the electrochemical deposition the ionic solution is used. In this method a metallic layer is deposited on the surface by an electric current [3].

Methods:

In this study the pure titanium (99.9%) foil with 0.2 millimeters thickness has been used. The sample is washed in the acetone, ethanol and water using the ultrasonic bath, each one for 5 minutes. To produce nanotubes the anodization process is started under the voltage of 60 Volt at room temperature. In this experiment titanium is considered as the anode and graphite as the cathode. The solution is including 0.3% Wt Ammonium fluoride (NH4F) and 2% by volume water in ethylene glycol. Then to coat the silver nanosheets on the walls and surface of the TiO$_2$ nanotubes the prepared sample of the previous step is used as the cathode and a platinum plate as the anode and the silver nitrate and boric acid solution are used as the electrolyte. The deposition of metallic layer on a matter is done by considering the material which is depositing as the cathode and it's plunging in a solution including the salt of considered metal.

Discussion and results:

In this research, the titanium dioxide nanotubes are produced using the electrochemical anodization. In this experiment the distance between the two electrodes is considered very low (4 millimeters) and this condition leads to the short nanotubes. In this study very high ordered nanotubes with maximum height 2.8 micrometers and the average internal diameter: 35 nanometers which anodized under the voltage 60 volt are produced. For silver deposition the electrochemical deposition is used and the distance of the cathode and anode is changing and this condition leads to silver nanosheets production with different thicknesses on the surface of the

nanotubes. The SEM image of the nanotubes produced by the electrochemical method is indicated in Fig.1. After the nanotubes production, in the silver deposition step, by applying the alternative pulses and finding the suitable oxidation voltage, oxidation time, reduction voltage, reduction time, the silver nanotubes start to deposit on the walls and surface of the titanium dioxide nanotubes. The XRD results also confirm this deposition (Fig.2).
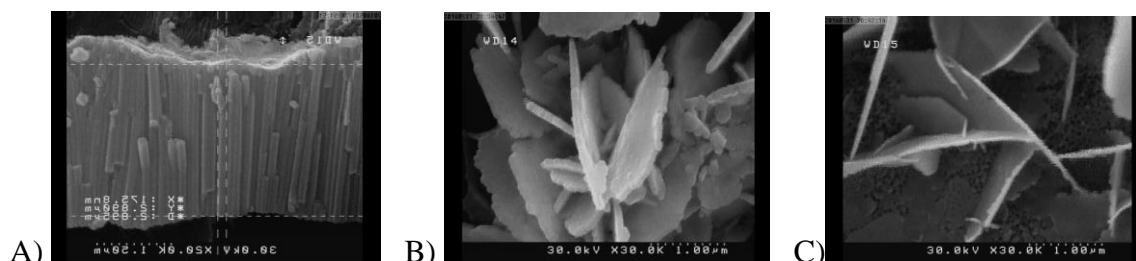

Fig.1. A) The SEM image of the produced nanotubes at anodization voltage of 60 Volt and at room temperature, B & C) The SEM image of the produced silver nanosheets on the nanotubes with thickness: 100(related to 2cm distance of cathode and anode) and 50 nanometers (related to 2cm distance of cathode and anode), respectively.
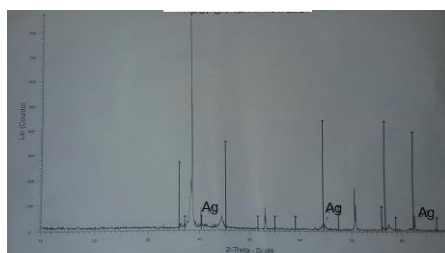

Fig.2. Diagrams of density of current versus time.

Conclusion:

The SEM image of the coated silver shows that the distance between the cathode and anode completely depend on both anodizing and electrochemical deposition processes, in the anodization process here very short nanotubes are produced due to the 4 millimeter distance of the cathode and anode and in the electrochemical deposition process the silver nanosheets with thicknesses 50 to 100 nanometers are produced.

References:

[1]. P. Roy; S. Berger; P. Schmuki. " TiO2 nanotubes: synthesis and applications", *Journal of Angew Chem Int Ed Engl*, Mar **2211**,*50*, 2904-39.

[2]. Y. T. Sul; C. B. Johansson; Y. Jeong; T. Albrektsson. "The electrochemical oxide growth behaviour on titanium in acid and alkaline electrolytes", *Med Eng Phys*. **Jun 2001,** 323-44.

[3]. S. Shingubara. "Influence of substrate microstructure on longitudinal correlation length of porous system of anodic alumina: Small-angle scattering study" *Nanopart*. Res.sep **2013**.

Density functional theory (DFT) studies of some water soluble metal Schiff base complexes and their docking studies with DNA

Narges Samimi, Zahra Asadi[*]

Department of Chemistry, College of Sciences, Shiraz University, Shiraz 71454, I.R. Iran

Email address: zasadi@shirazu.ac.ir

****

Introduction

Schiff bases are condensation products of primary amines with carbonyl compounds. They were first reported by Schiff in 1864[1]. Density functional theory (DFT) has been remarkably successful in providing means for an accurate evaluation of ground state properties. On these regard, interest is shifting toward an accurate and physically sound extension of DFT to the study of excited electronic states [2]. Molecular docking techniques are an attractive scaffold to understand the drug–DNA interactions in rational drug design, as well as in the mechanistic study by placing a small molecule into the binding site of the target specific region of the DNA mainly in a non-covalent fashion [3].

Methods/ Experimentals:

The GAUSSIAN 03 program package was employed to carry out DFT calculations at the Becke's three-parameter functional and Lee–Yang–Parr functional (B3LYP) level of calculation and the 6-311G++ (d, p) basis set was used for ground state geometry optimization calculations of the complex. The structure with the lowest energy was selected for the docking study. The molecular docking program Molegro Virtual Docker (MVD) was employed to generate a docked conformation of the complex with DNA.

Results and Discussion:

DFT or ab initio studies: Ground state optimization calculations (in the gas phase) of the complex was achieved using DFT at B3LYP/6-311G (d, p)/ LANL2DZ (Ni) basis set. The highest occupied molecular orbital (HOMO) and lowest unoccupied molecular orbital (LUMO) of the complex (Figure 1) and geometrical parameters including bond lengths, bond angles and other parameters were obtained from these calculations.

Docking Study: Validation of docking was used to ensure orientation and position of ligand binding that was obtained from docking studies by MVD program with ten replication of each running (Figure 2).

Conclusion:
DFT calculations at the B3LYP/6-31G (d, p) / LANL2DZ (Ni) basis set level of theory were performed in order to analyse structural properties and UV-Vis absorption of complex. The energies for the various possible conformers of the title compound were calculated and the minimum energy structure was chosen for the computational study as well as for docking. The minimum-energy docked model suggests that complex interacts with the minor groove of DNA.
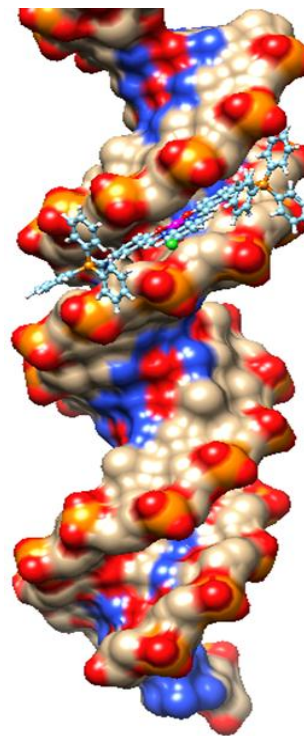
LUMO
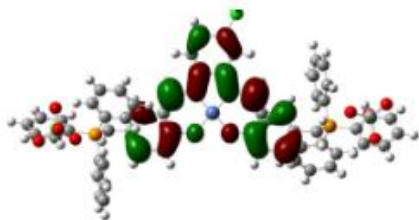
HOMO

Figure 1

Figure 2

References:

[1] Sharma, A; Shah, M. K . *Chem Sci Trans*, **2013**, *2(3)*, 871-876.

[2] Jung, H. S; Park, M; Han, D. Y; Kim, E; Lee, C; Ham, S; Kim, J. S. *Organic letters ,* **2009**,*11(15)*, 3378-3381.

[3] Bindu, P. J; Mahadevan, K. M; Naik, T. R; Harish, B. G. *MedChemComm* , **2014**, *5(11),* 1708-1717.

Experimental design by response surface methodology (RSM) for indirect determination of dichromate by a zeolite modified electrode

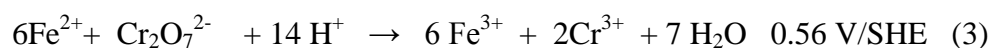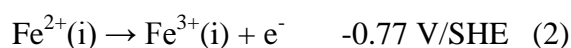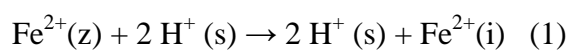Motahare Nosuhi[a,b], Alireza Nezamzadeh-Ejhieh[*,a,b,c]

Corresponding Author E-mail address: arnezamzadeh@iaush.ac.ir

Introduction: Due to the toxicity and harmful effects, chromium is one of the most important contaminants in the surface waters, groundwater resources, soil, and sewage [1]. Oxidation state and solubility of Cr compounds determines their toxicity. Cr(III) is a trace nutrient for the proper functioning of living organisms. Cr(VI) have a greater mobility than Cr(III), and penetrate rapidly into any environmental object surface and ground waters and soils, producing hazardous effects on human health and living nature [2, 3]. Generally, Cr(VI) compound is considered to be 100-1000 times more toxic than Cr(III) [5,6]. Furthermore, Cr(VI) is soluble in the full pH range increasing its transport speed and potential hazards [7].

Methods/Experimentals: Natural clinoptilolite was crushed with an agate mortar and sieving in analytical sieves for the separation of micronized clinoptilolite particles (MClin) with mesh -400. MClin powder was used for preparation of nano-particles of zeolite using a planetary ball mill under controlled milling conditions such as rotational speed, ball to powder ratio as well as, grinding time, so the crystallinity retained during the size reduction process. To prepare Fe^{2+}-exchanged form of NClin and MClin, nanoparticles and micro particles were added individually to Fe^{2+} solution and shaken for 8h (3 times) and centrifuged.

Results and Discussion: Effect of Fe^{2+}-NClin on the Behavior of Electrode.

Cyclic voltammograms behavior of the CPE, NClino/CPE and Fe^{2+}-NClin/CPE was studied in the supporting electrolyte solution (pH 3). As shown in Figure 1a and b no voltammetric responses were observed for these electrodes in the applied potential range. On the other hand no electroactive species are present in solution or in the carbon paste electrode to carry out redox reactions at the electrode-solution interface. Voltammogram 'd' is related to CPE in the supporting electrolyte containing 1 mM $Cr_2O_7^{2-}$ (pH 3) that shows cathodic and anodic currents in potentials 0.65 V and 0.35 V, respectively. Voltammograms 'e' and 'c' are related to Fe^{2+}-NClin/CPE in absence and presence of 1 mM $Cr_2O_7^{2-}$, respectively. As can be seen in presence of $Cr_2O_7^{2-}$ ions in primary voltammograms (1 to 4) only cathodic peak can be observed with severe decrease in current (Ep = 0.7 V). These responses are justifiable according to the flowing reactions:

$$Fe^{2+}(z) + 2 H^+ (s) \rightarrow 2 H^+ (s) + Fe^{2+}(i) \quad (1)$$

$$Fe^{2+}(i) \rightarrow Fe^{3+}(i) + e^- \qquad -0.77 \text{ V/SHE} \quad (2)$$

$$6Fe^{2+} + Cr_2O_7^{2-} + 14 H^+ \rightarrow 6 Fe^{3+} + 2Cr^{3+} + 7 H_2O \quad 0.56 \text{ V/SHE} \quad (3)$$

In absent of $Cr_2O_7^{2-}$, in surface of modified electrode reactions 1 and 2 occur. By entering $Cr_2O_7^{2-}$ ions in solution, reaction 3 competes with reaction 2 in taking $Fe^{2+}(i)$ ions. Therefore decrease in the current of the oxidation-reduction reaction of iron can be seen. Hence, this decrease in peak current was considered for indirect voltammetric determination of dichromate by the proposed electrode.
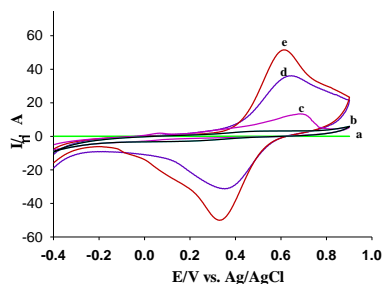

Figure 1. Cyclic voltammograms of the a) CPE, b) NClin/CPE and e) Fe^{2+}-NClin/CPE in HCl (pH 3) and d) CPE, c) Fe^{2+}-NClin/CPE in HCl (pH 3) + 1 mM $Cr_2O_7^{2-}$, $\upsilon = 100$ mV s^{-1}

Conclusion: In conclusion, we have developed a new electrode for indirect detection of Cr(VI). This sensor has proven to be highly sensitive, specific, and selective. The use of low-cost, carbon paste-based electrodes further improves the applicability of this sensor for real world analysis of environmental and hazardous material samples. Under optimum conditions, the current response of Fe^{2+}-NClin on the carbon paste modified electrode was inversely proportional to $Cr_2O_7^{2-}$ in the concentration range from 4 mM to 2000 μM with a detection limit (3S/N) of 1100 μM. The method showed high selectivity, good reproducibility and was successfully applied to the determination of Cr(VI) in natural water samples and industrial waste water

References

[1] Lee E. Korshoj, Anita J. Zaitouna, Anal. Chem. **2015**,87, 2560–2564

[2] Wei Jin Hao Du ShiliZheng Yi Zhang,ElectrochimicaActa, **2016**,191, 1044–1055

[3] CM. Thompson, JC. Wolf, RH. Elbekai, Mutat Res Genet Toxicol Environ Mutagen, **2015**, 789-790, 61-66.

[4] S. I. Ohira, K. Nakamura, C. P. Shelor, P. K. Dasgupta, K, Toda, Anal. Chem. **2015**, 87(22) 11575–11580

[5] D. Rai, B.M. Sass, D.A. Moore, Inorg. Chem. **1987**,26, 345.

[6] C.D. Pereira, J. G .Techy,E.M. Ganzarolli, S.P. Quinaia,**2012**, 14, 1559.

[7] L.L. Wei, R. German, J- .M. Lee ,Appl. Catal. B: Environ.**2015**, 176-177, 325.

Fabrication of flaky 3-dimensional Aluminum oxide nanopores using the hard anodize

Mohammad Panahian; Mahmood Moradi; Saeid Behaein

Shiraz University

Introduction

Recently fabrication of different kind of nanostructures has attracted lots of attention. Some methods with high accuracy are usually expensive. Among many methods the electrochemical method is cheap with high enough accuracy. One of the methods is anodization process, in particular, using the anodization method to produce Alumina nanopores. For the first time the anodization was done using chromic acid. Alumina nanostructures with suitable porosity and large band gap are one of the suitable materials to produce the photonic crystals and this material has high refractive index compare to the air. After obtaining the photonic band gap in the anodic alumina oxide, many researches have been fabricated this kind of template in order to improve the photonic crystal characteristic by producing the very regular arrays of nanopores to achieve the required forbidden band including low transmission and adjustable condition[1]. Beside the various available methods, different kind of anodization potential, in particular pulse and alternative potential, to produce modulated and three dimensional pores to investigate many different kinds of optical properties of these nanostructures is used.

Methods:

In our experiment we wash the sample of the pure aluminium (99.999%) in the acetone and ethanol by the ultrasonic bath and DI water. Then before anodizing, to electropolish the sample we put the sample under the voltage 20 volt and current 60mA in the perchloric acid+ethanol (with the ratio 1 to 4) solution in 5 minutes. To anodize the sample we use the solution of oxalic acid and sulfuric acid with concentration 0.4 molar and 0.08 molar, respectively. One of the electrodes is the aluminum plate and the other one is the sample. In the first step we apply the anodization voltage of 40 Volt for 10 minutes (soft anodizing) and then we apply the voltage of 47.5 Volt for 5000 seconds. After we make the sample ready to investigate the optical property we stick the sample on a glass and then we put in the CuCl +HCl solution to completely remove the aluinium of the sample. In the next step the obtained membrane is set in the UV-Vis spectrophotometer to get the required optical properties.

Results:

After anodizing with switching the agitator, which is inside the reactor, on and off we produced flaky nanostructures. In this experiment we produced the modulated three-dimensional nanopores with the help of soft and hard two step anodizing in the voltages 40 and 47.5 volts, respectively and switching the agitator on and off. Fig.1 is the SEM image of the sample in which the flaky structure is completely obvious. After producing the nanopores to pore widening we put the sample in the phosphric acid with concentration 0.5 molar in the 140 minutes at the 30 degrees Celsius. To study the value of light transmission in different wavelenghts we put the pore widened sample in the spectrophotometer again and the spectrophotometer curves revel that after pore widening for 140 minutes, a gap is observed in the wavelenghts between 280 and 400 nanometers. Fig.2 shows the transmission spectrum.
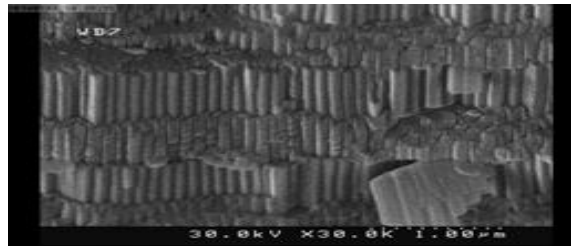

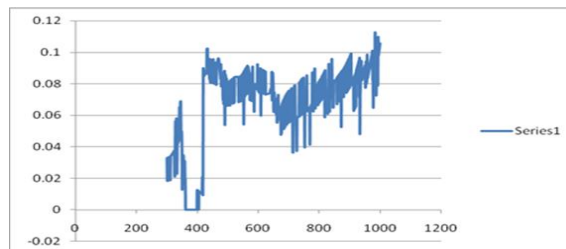Fig.1. is the SEM image of the sample. The flaky structure is completely obvious.

Fig. 2. The transmission spectrum of the anodized sample in the voltage of 47.5 Volt after putting in the phosphoric acid for 30 minutes.

Conclusion:

In this study with the 2step anodizing and switching the agitator on and off, we produced the modulated 3-dimensional nanopores and its transmission spectrum shows that the maximum attraction occurs in the wavelenghts between 280 and 400 nanometers, i.e the transmission of light vanishes in a bandwidth, and this can prepare the start of photonic crystals production.

References:

[1]. F. Cerdeira, I. Torriani, P.Motisuke, V. Lemos, F. Deker, Optical and Structural Properties of Polycrystalline CdSe Deposited on Titanium Substrates", Appl. Phys., Vol.46, 107, (1988).

Synthesis of Cyclometalated Platinum (II) Complexes Containing 2-Vinylpyridine with Pendant Vinyl Group: Oxidative-Addition to Platinum(II) vs Addition to Alkene

Sirous Jamali,* **Zohreh Hendi**
aChemistry Department, Sharif University of Technology, P.O. Box 11155-3516, Tehran, Iran
Email address: Sirousper@gmail.com

Introduction

The design and development of new transition metal complexes containing two reactive centers (metals and ligands) in which they act together in a cooperative manner to assist chemical processes, have recently attracted a great deal of attention because of their potential applications in many fields, such as catalysis in biological systems, organic synthesis and small molecule activations [1]. Two reactive centers can participate in the bond rupturing or bond formation steps and the coordination mode of the ligand modified and experience a change during the reaction. The C–X (X=heteroatom) bonds are often formed in chemical processes, such as substitution or addition to C=C double bonds. For example, there are two possible routes for addition of the molecular halogen to the cyclometalated platinum (II) complexes containing 2-vinylpyridine with a pendant vinyl group. The first route is oxidative-addition of the X_2 to the metal center and the second pathway is direct attack of the electrophilic reagent (X_2) at the ligand center. With these precedent as well as our interest in study of the oxidative-addition reaction to platinum(II) complexes [2] led us to incorporate an appropriate pendant unsaturated functional group in a platinum(II) complex and use them as precursor in reaction with Br_2.

Experimentals

As summarized in scheme 1, the reaction of the cyclometalated platinum(II) complexes [Pt(*p*-tolyl)(ppy)(SMe₂)], **1a, 1b** (that in **1a**: R=Me, cyclometalated ligand = bhq and in **1b**: R= p-tolyl, cyclometalted ligand = ppy) with 1 equiv 2-vinylpyridine in acetone at room temperature gave the platinum(II) complexes **2a** and **2b**, in good yield by replacement of the SMe_2 ligand with the N ligating atom of 2-vinylpyridine. The product complexes **2a** and **2b** are stable in dichloromethane and chloroform and characterized using NMR spectroscopy, elemental microanalysis and X-ray crystallography. The reaction of **2a** with Br_2 in has been investigated.
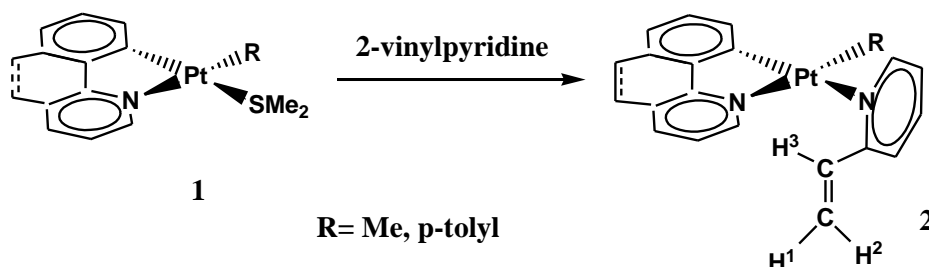
Scheme 1

Results and Discussion

The cyclometalated complex **2a** and **2b** is stable in dry chlorinating solvents but undergoes complex reactions in wet acetone. The NMR spectroscopy and X-ray crystallogrsaphy results (Figure 1) illustrate that the cyclometalated platinum(II) complexes **2a** and **2b** are successfully synthesized. The reaction of **2** with 1 equiv Br_2 gave the binuclear platinum(IV) complex $[Pt_2Br_2Me_2(bhq)_2(\mu\text{-}Br)_2]$, **3** and organic products. Complex **3** characterized using X-ray crystallography in the solid state.

| 3 | 2b |
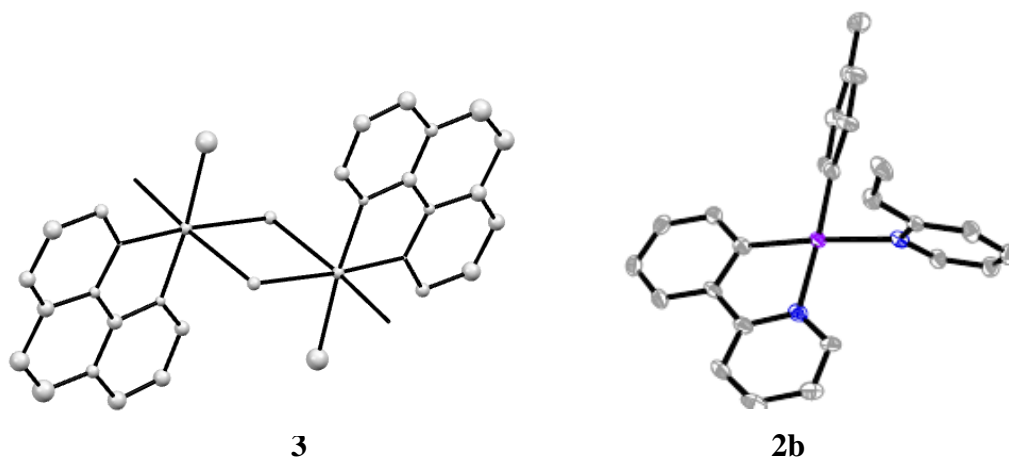
Figure 1. crystal structure of **2b** and **3**

Conclusion

In summary, the new complexes **2a** and **2b** were prepared and characterized. The reaction of **2a** with Br_2 shows that the 2-vinylpyridine ligand is completely removed complex as organic products and complex **3** is formed.

References

[1] Y. Zhang; J. Anand Garg; C. Michelin. *Inorg. Chem.* **2011**, *50*, 1220-1228.
[2] S. Jamali; M. Nabavizadeh; M. Rashidi. *Inorg. Chem.* **2005**, *44*, 8594-8601.

Preparation of graphene oxide supported hydroquinone and study of its stability and delivery

Sahar Abbasian and **Nooredin Goudarzian***
Department of Applied Chemistry, Shiraz Branch, Islamic Azad University, Shiraz, Iran
Corresponding author: **saharabbasian7090@gmail.com**

1. Introduction

Advances in Nanoscience and nanotechnology, enabling the synthesis of new nanomaterials, have led to the development of a number of new drug delivery systems. The recent discovery of graphene oxide (GO) has been accompanied by increasing research attention to explore this new material for drug delivery applications. GO, a single layer of sp2 hybridized carbon atoms arranged in a honeycomb two-dimensional crystal lattice, has evoked enormous interest throughout the scientific community since its first appearance in 2004. Due to its unique structure and geometry, GO possesses remarkable physical and chemical properties, including a high Young's modulus, high fracture strength, and excellent electrical and thermal conductivity, fast mobility of charge carriers, large specific surface area and biocompatibility. These properties enable graphene to be considered as an ideal material for a broad range of applications, ranging from quantum physics, Nano electronics, energy research, catalysis and engineering of Nano composites and biomaterials .Therefore, it is not surprising that GO has generated great interest in Nano medicine and biomedical applications, where suitably modified GO can serve as an excellent drug delivery platform .In this research we report the applications of GO supported hydroquinone as a nanocarriers for hydroquinone loading, based on surface modifications and functionalization of GO, followed by discussion related to its toxicity [1,2].

2. Experimental

2**.1. Synthesis of GO:** The most common method adapted for large-scale production of graphene and GO is based on top-down approaches using mechanical, physical and chemical exfoliation of graphite pioneered by Hummers et al. using strong acids and oxidants [1, 2]. These methods require extensive oxidation of aromatic structure in order to weaken Van der Waals interaction between GO sheets followed by their exfoliation and dispersion in solution. Resulting GO multilayered or single sheets have high density OH and COOH groups. The optimization of the exfoliation process using more gentle approaches based on surfactants, electrochemistry and other methods are progressing to address this challenging problem toward a green, low waste, scalable and low cost production of GO .

2.2. Surface modification and functionalization of GO: GO is soluble in water, it aggregates in physiological buffers in the presence of salts due to the charge screening effect. It is well known that the surface chemistry of nanomaterials is key to building drug carriers with good biocompatibility and controlled behavior in biological systems. Therefore, the modification of GO to build   desired hydroquinone carrier is of great significance. Two main methods for the surface modifications using covalent or noncovalent methods have been investigated. The covalent method is usually achieved via a few techniques such as atom doping or reaction of hydroquinone with oxygen groups of graphene oxide structure. In contrast, non-covalent

methods employ Van der Waals forces and electrostatic binding without affecting graphene oxide's natural structure and hydroquinone molecules.

3. Results and discussion

3.1. Covalent modifications: The surface modification of GO by covalent chemical bonding is possible due to the presence of defects and reactive oxygen groups in the GO lattice function as a site for reaction with hydroquinone molecules . The covalent modifications can be archived by several different methods, including nucleophilic substitution, electrophilic addition, condensation and addition. The main reactive sites for the reaction by nucleophilic substitution are the epoxy groups of GO. This is a simple reaction which occurs at room temperature and in aqueous medium, and hence is a promising method for large-scale modification of GO using a broad range of molecules including all types of aliphatic and aromatic compound's, amino acids, polymers, ionic liquid and specially hydroquinone molecules .

3.2. Non-covalent modifications: Non-covalent modifications including Van der Waals forces, electrostatic interaction, hydrogen bonding, coordination bonds and p–p stacking interaction have been extensively used in the modifications of GO with hydroquinone molecules. Non-covalent functionalization can be achieved by polymer wrapping, adsorption of surfactants or small molecules and interactions with biomolecules.
3.3. Chemical control drug release: When the hydroquinone's molecules are attached onto the drug carriers such as GO via pH-sensitive linkers, it is possible control the release of the hydroquinone by manipulating the pH value of environments. Another strategy to control the hydroquinone release is to use the hydrolysis technique. These chemical methods allow for the accurate control of hydroquinone release.

4. Conclusion
As a result of the remarkable structural and chemical properties of GO supported hydroquinone, and its application for drug delivery system has been report. In this study clearly indicate that significant and exciting progress has been made in this field, and that these emerging biomaterials demonstrate great potential for biomedical applications. GO supported hydroquinone obviously display many advantages compared with other drug delivering systems, with the ability to provide high drug loading capacity. Both covalent and non-covalent surface modifications have been successfully used to impart specific activity to GO supported hydroquinone, as well as to improve the colloidal stability. Therefore, more toxicity studies using in vivo animal models are required in future to prove the biocompatibility of GO supported hydroquinone.

References:
[1]. Jingquan Liu, Liang Cui, Dusan Losic, Graphene and graphene oxide as new nanocarriers for drug delivery Applications, *Acta Biomaterialia,* 2013, 9, 9243–9257
[2]. Mendes RG, Bachmatiuk A, Büchner B, Cuniberti G, Rümmeli MH. Carbon nanostructures as multi-functional drug delivery platforms, J *Mater Chem B,* 2013, 1,401–28.

Carrier-Mediated Hollow Fiber-Liquid Phase Microextraction for Preconcentration Followed by Spectrophotometric Determination of Amoxicillin

Batool Zare Khafri, Morteza Akhond*, Ghodratollah Absalan

Professor Massoumi Laboratory, Department of Chemistry, Shiraz University, Shiraz 71454 , Iran

*E-mail: akhond@susc.ac.ir

Introduction

Amoxicillin (Amox) is a β-lactam antibiotic that is widely used to treat infectious human and animal diseases. Considering environmental pollution problem, development of sensitive and simple methods for separation and determination of Amox is highly demanded. In this regard various analytical methods have been reported such as HPLC [1] and capillary electrophoresis [2]. However, the main disadvantages of these methods are corresponding complicated procedures and expensive instrumentation. Hollow fiber-liquid phase microextraction (HF-LPME) technique has advantages including lower capital and operating costs, lower energy consumption, less solvent usage and good selectivity. This work proposes UV-Vis spectrophotometric detection system which is simple, fast and inexpensive.

Methods / Experimentals

A piece of hollow fiber was inserted in the organic phase for 10 s in order to impregnate its pores with this solvent. Aliquot of 26 μL of the receiving solvent was injected into the channel of the hollow fiber. Then it was introduced into the aqueous analyte sample. After a prescribed period of time, the receiving phase was withdrawn by the microsyringe and was diluted with the receiving phase and then was poured into a UV cell in order to take the absorption spectrum of the analyte.

Results and Discussion

Amoxicillin (Amox) is a practically challenging drug because it is a hydrophilic compound with high solubility in aqueous media. Depending on solution pH, it can exist at various chemical forms due to having different acidic and basic functional groups. Therefore, the direct passive transport of Amox from aqueous sample to receiving phase (RP) using organic impregnated solvents is difficult. At pH 8–11, Amox is mainly present at its anionic form. Therefore, by utilizing a cationic carrier in membrane solvent, it is possible to actively transport $Amox^-$ from the aqueous sample into the RP. To do this, Aliquat-336, $R_3NCH_3^+Cl^-$

was chosen as cationic carrier and was dissolved in the membrane solvent. In the aqueous sample–membrane interface, Amox$^-$ forms a neutral ion-pair with Aliquat-336 as $(R_3NCH_3)^+Amox^-$, while releasing the Cl$^-$ anion. Due to concentration gradient, the ion-pair diffuses across the membrane. At the RP-membrane interface, Amox$^-$ is released from the organic phase while Cl$^-$ is diffused back to the carrier. In this process, the driving force for transport of Amox is the gradient of pH and concentration of Cl$^-$ between the aqueous sample and RP.

Conclusion

Carrier-mediated three-phase HF-LPME combined with UV-Vis spectrophotometry was applied for the extraction and determination of Amox in aqueous and biological samples. The method exhibited a low LOD with a high preconcentration factor. The developed method was simple, inexpensive, fast, and was successfully applied in the separation, preconcentration and determination of Amox in different real samples.

References

[5] E. Benito-Pena, J. L. Urraca, M. C. Moreno-Bondi, J. Pharm Biomed Anal, 2009, 49, 289-294.

[6] M. Hernandez, F. Borrull, M. Calull, J Chromatogr. B, 1999, 731, 309-315

Theoretical Study of Anti-HIV Medication Azidothymidine (AZT) Interactions with Non-functionalized and Functionalized Nanotubes

Yaqhoub Hatami [a]*, Mohammad Momen Heravi[b], Ali Morseli[b], Mohammad Reza Bozorgmehr[b]

[a]Department of Chemistry , Jiroft Branch, Islamic Azad University

[b]Department of Chemistry, Mashhad Branch, Islamic Azad University

y.hatami٥٠@gmail.com

Introduction: *The ability of carbon nanotubes in penetration in biological cells introduced them as a drug carrier to transport low molecular weight drugs.But the low rate of spread as a result of strong Van der Waals intermolecular interactions between the nanotubes and the formation of toxic accumulation of carbon nanotubes are the fundamental problem ahead of their use [١]. Now, functionalized carbon nanotubes (F-CNT) are known as new compounds in nano carriers equations to deliver drug molecules to the aimed cell[٢]. Covalent functionalization of carbon nanotubes and addition of medication molecules to them (anticancer, antiviral and antibacterial), is a new and emerging field of research [٣].Zidovudine is a medicine widely used in the fight against HIV or AIDS. It'sCombine it with nanotubes is a promising way to overcome the increasing the cellular uptake and internalized by functionalized carbon nanotubes, respectively.Thus, the understanding of nanotube interactions with Zidovudine can be a good guide to better understanding of drug interactions with nanotubes and evaluate changes to improve effectiveness or reduce its toxicity.*

Methods/Computational details: *DFT was used in the current study to evaluate the interactions and all calculations were performed using Gaussian ٠٩ software. Calculations were performed using the B٣LYP level of theory and basis set ٦-٣١G(d, p) molecule drugs (Zidovudine), single walled carbon nanotubes (CNT) and functionalized nanotubes (f-CNT) for all configurations. All configurations have been tested. All configurations in the gas-solvent phase (water) were applied with the Polarizeable ContinuumModulation (PCM) method. This section examines the interaction of single-walled carbon nanotubes (٥ , ٥) with the medication Zidovudine. This section applies ZIDO goes for the medication Zidovudine, CNT goes for pure carbon nanotubes and f-CNT goes for functionalized carbon nanotubes with COOH [٤].*

Results and discussion: *For the calculation of the interaction of Zidovudine with functionalized carbon nanotubes (٥ , ٥) the optimal structure of each is separately required. Zidovudine, carbon nanotubes (٥ , ٥) and functionalized nanotubes in the gas phase and solvent phase are individually optimized. Five configurations were considered to investigate the interaction of nanotubes with Zidovudine. optimized configuration structure includ CNT-ZIDO ١, CNT-ZIDO ٢, CNT-ZIDO٣, f-CNT-ZIDO ١ and f-CNT-ZIDO ٢ in gas and solvent (water) phase, in each of these configurations Zidovudine interacts from Deoxythymidine ring with π-π interaction; RCH٢OH groups oxygen and van der Waals interactions from the N٣ group with natural carbon nanotubes (CNT), and also has covalent binding from Alcohol Group and Deoxythymidine ring. According results seems that f-CNT-ZIDO ١ configuration in the solvent phase has more stability than that of f-CNT-ZIDO ٢, so that the f-CNT-ZIDO ٢ configuration lacks anoptimal structure.The increased reactivity for configuration is as follows:*

$$CNT - ZIDO \, \backslash > CNT - ZIDO \, \backslash > CNT - ZIDO \, \backslash > f - CNT - ZIDO \, \backslash > f - CNT - ZIDO \, \backslash$$

It seems that the Zidovudine place on carbon nanotubes increases reactivity. E_gap data show that f-CNT-ZIDO ١, unlike other complexes; is more stable, with more electron affinity and less ionization energy than other configurations when exposed to solvent phase.structure despite good strong bond. This can be a main reason for that transfer from Alcohol Group is never possible.

Conclusion*: We can conclude that configurationsthat usenon-functionalized carbon nanotubesshow direct effect of the solvent and the interaction between the nanotubes and Zidovudine is under the effect of solvent.On the other hand the interaction between functionalized nanotubes andZidovudine in a covalent bond of Zidovudine and functional groups on the nanotubesshows that the best type of Zidovudine and nanotubes bond is covalent. It should be noted as a conclusion that the presence of ٢ ketones in the Pyrimidine – ٢ structures inf − CNT − ZIDO١ covalent structure leads to increased electron affinity of nitrogen in NH group in the ring with more acidic property than other hydrogen contents. Generally, it can be predicted that the binding of medicationoccurs through NH group of Pyrimidine ring- ٢, ٤ Dionne .It should be noted that in HOMO and LUMO orbitals the green color indicates a negative charge and the red indicates a positive charge.*

References

[١]Allen T.M; Cullis P.R. Drug delivery systems, entering the mainstream, Science, ٢٠٠٤, ٣٠٣, ١٨١٨ـ ١٨٢٢.

[٢]Assovskii I; Kozlov, G. Synthesis of single-walled carbon nanotubes by the laser ablation of graphite under normal conditions, Doklady Physical Chemistry, Springer, ٢٠٠٣, ١٣ـ ١٧.

[٣]Bianco A, Prato M. Can carbon nanotubes be considered useful tools for biological applications? Advanced Materials, ٢٠٠٣, ١٥, ١٧٦٥ـ ١٧٦٨.

[٤]Feazell R.P, Nakayama-Ratchford N,Dai H,Lippard S.J. Soluble single-walled carbon nanotubes as longboat delivery systems for platinum (IV) anticancer drug design, American Chemical Society, ٢٠٠٧, ١٢٩, ٨٤٣٨ـ٨٤٣٩

In situ production of silver nanoparticles for high sensitive detection of ascorbic acid via inner filter effect

B. Rezaei*, <u>M. Shahshahanipour</u>, Ali A. Ensafi

m.shahshahanipour@ch.iut.ac.ir

Introduction

Conventional sensing assays are used for the fluorescent chemosensor can lead to a complicated and time-consuming technique as well as the limits in practical applications. But recognize the analyte based on the formation or presence absorber species, like silver nanoparticles (SNPs) which resulted in alterations in the absorption and fluorescence intensities [2,3]. Dispersion of SNPs in solution caused a substantial UV-visible extinction compared to when the silver used in the bulk form. It can be explained that resonates between the incident photon frequency and the excitation band of conduction electrons leads to mention extinction band. This phenomenon is identified as the surface plasmon resonance (SPR) [4]. Because of their exclusive electronic and optical specifications, semiconductor nanocrystals or quantum dots (QDs) show great potential, especially in used as probes and luminescent labels in biological detection [5]. Ascorbic acid plays a crucial role in various essential biological functions [10] and has been used for prevention and treatments of common cold, mental illness, infertility, coronary heart diseases, and cancer and in some clinical exhibitions of HIV infections [2].

Methods / Experimental:

To obtain the fluorescence spectra, a solution mixture (containing CdTe QDs, $AgNO_3$ and AA solutions in universal buffer (pH 9.5), was transferred into a 1.0-cm quartz cell and the fluorescence emission spectra were recorded. For the determination of AA at a constant wavelength (575 nm) a freshly prepared mixture containing 100 μL of 0.32 μmol L^{-1} CdTe QDs and 20 μL of 1.0×10^{-7} mol L^{-1} $AgNO_3$ solution in universal buffer (pH 9.5), plus an appropriate volume of a sample solution were added in a vial and they were stirred for 30 min. Then, the mixture was transferred into a 1.0-cm quartz cell and the fluorescence emission was recorded at 575 nm (excitation wavelength 524 nm). The response function (F0 - F) values of the sensor were obtained as an analytical signal with different concentrations of AA, where F0 and F referred to the fluorescence intensity at 575 nm in the absence and presence of AA respectively.

Results and discussion

The size, shape, and distribution of the CdTe QDs and SNPs were characterized by TEM and DLS images, Ag^+, had fluorescence quenching effect on the fluorescence signal of QDs. AA acts as a reducing agent for Ag ions [25]. SNPs have broad UV-Vis absorption spectra and a good spectral overlap with the excitation and emission band of the QDs (fluorophore). Therefore, it seems that there could be suitable absorber and fluorophore pair for the high efficiency IFE-based fluorescent chemosensor [28, 29]. The effect of pH, amount of CdTe QDs, Effect of Silver Nitrate Concentration and effect of incubation time were studied. Also the effect of Foreign Substance and application of this sensor in real samples were investigated.

Conclusions

In the present study, the SNPs, which were prepared chemically in-situ due to the one-step reduction of silver salt ($AgNO_3$) by AA case to the efficient quenching of CdTe QDs. The proposed method can be used as a very delicate, cost-effective and rapid approach for determining AA in real samples. The other merits of this nanosensor are low detection limit (0.02 ng mL^{-1}), wide linear range (0.2 to 88.0 ng mL^{-1}) and ease of production.

References

[2] M. Zheng, Z. Xie, D. Qu, On−Off−On Fluorescent Carbon Dot Nanosensor for Recognition of Chromium(VI) and Ascorbic Acid Based on the Inner Filter Effect, 2013, 5, 13242–13247.

[3] Y. Sun, Y. Xia, Gold, and silver nanoparticles: a class of chromophores with colors tunable in the range from 400 to 750 nm, 2003, 128, 686-691.

[4] A.D. McFarland, R.P. Van Duyne, Single silver nanoparticles as real-time optical sensors with zeptomole sensitivity, 2003, 3, 1057-1062.

[5] X. Liu, H. Jiang, J. Lei, Anodic Electrochemiluminescence of CdTe Quantum Dots and Its Energy Transfer for Detection of Catechol Derivatives, 2007, 79, 8055-8060.

[10] C.S. Tsao, Marcel Dekker, New York, An overview of ascorbic acid chemistry and biochemistry In Vitamin C in Health and Disease 1997, 25.

Removal of lead by using polyaniline/maghemit magnetic nanocomposite

Leyli Irannejad[1], Fatemeh Sabermahani[1]

[1]*Department of Chemistry, PayameNoor University, PO BOX19395-4697, kerman, IRAN*

Email:leylii1368@gmail.com

Introduction

Water pollution by toxic heavy metal occur globally. Strict environmental regulations on the discharge of heavy metal ions and rising demand for clean water with extremely low level of heavy metal ions make it greatly important to develop different efficient technologies for heavy metal ions removal. Chemical precipitation, ion exchange, membrane filtration, electrochemical methods, and adsorption are some of the conventional methods that have been used for removal of heavy metals. [1-6]. Adsorption technology is commonly used for heavy metal ions removal from water samples and aqueous solutions. We examined the use of polyaniline/maghemite (PAni/ Fe_2O_3) magnetic nanocomposite (MNCs) for removal of lead from aqueous media.

Experimental

Chemical co-precipitation was used to prepare the maghemite nanoparticles. Subsequently, we synthesized the PAN/MNCs through emulsion polymerization of aniline. Firstly, a certain amount of nanoparticles were dispersed in HCl (0.1 M) under mechanical stirrer and sonication simultaneously. Aniline (1 mL) was added to the container and sonicated for 15 min to obtain a homogenous dispersion. Afterwards, the solution of APS (1 M) was added drop-wise under constant stirring. The precipitates were filtered and washed several times with distilled water. The dark green products dried at room temperature for about 48 h.

Results and Discussion

Batch adsorption experiments were carried out by shaking 0.04 g of the sorbent with the solutions 30 µg mL^{-1} of Pb. After adjusting pH, the solutions were shacked for 150 min. Then the mixtures were filtered out and the Pb was determined by FAAS.

The effect of pH, adsorbent dosage (m), contact time, concentration and temperature on adsorption of lead were examined. The best pH was 6 for removal of lead. Langmuir and Freundlich isotherms have been used to describe adsorption phenomena on the adsorbent and sorption data have been analyzed according to the linear form of the Langmuir isotherm. Effect of temperature was examined at 303, 308, 313 and 318 K. Adsorption ability of the sorbent increased with increasing temperature, illustrating that adsorption is an endothermic process. The standard enthalpy (H^0) and standard entropy (S^0) can be obtained from the slope and intercept of van t Hoff equation of G^0 versus T. The values S^0 and H^0 were 405.79 J mol^{-1} K^{-1} and =+120.916 kJ mol^{-1}, respectively.

Conclusions

PAN/MNCs showed significant potential for removal of Pb from aqueous solutions. Kinetics data were best described by pseudo-second order model. The thermodynamic studies indicated that the adsorption was spontaneous and endothermic

References:
[1] Y. Kong, J. Wei, Z. Wang, T. Sun, C. Yao, Z. Chen, *J. Appl. Polym. Sci.* **2011**, 122, 2054–2059.
[2] M. Ghorbani, H. Eisazadeh, *Synthetic Met.* **2012,** 162, 1429–1433.
[3] G. Zhao, X. Wu, X. Tan, X. Wang, *Open Colloid Sci. J.* **2011**, 4, 19–31.
[4] F.-M. Pellera, A. Giannis, D. Kalderis, R. Stegmann, ,E. Gidarakos, *J. Environ. Manage.* **2012,** 96, 35–42.
[5] K.Z. Setshedi, M. Bhaumik, S. Songwane, M.S. Onyango, A. Maity, Chem. Eng. J. **2013**, 222 , 186–197.
[6] F. Fu, Q. Wang, *J. Environ. Manage.* **2011**, 92, 407–418.

Preparation and Study of Swelling Behavior of Polyacrylamide-based Hydrogels for Enhancement Oil Recovery (EOR)

Ali Rahmatpour[*], **Mehrdad Shojaei**

a_rahmatpour@sbu.ac.ir
Polymer Chemistry Group, College of Chem. Shahid Beheshti University, Tehran, Iran

Introduction:

Hydrogel products constitute a group of polymeric materials, the hydrophilic structure of which renders them capable of holding large amounts of water in their three-dimensional networks [1]. Hydrogel is a polymeric material that exhibits the ability to swell and retain a significant, but will not dissolve in water. The ability of hydrogels to absorb water arises from hydrophilic functional groups attached to the polymeric backbone, while their resistance to dissolution arises from cross-links between network chains [2]. Polymer gels for water control are obtained by cross-linking a polymer in solution. The chemical gelling solution (gelant) is prepared by adding the polymer to water. With temperature and time, a cross-linking reaction (gelation) takes place between the two components to form a three-dimensional cross-linked polymer network. This structure (including the encapsulated water) is referred to as gel. In continuing research on the preparation of polymer-based hydrogels for water production control, HPAM hydrogels were prepared by crosslinking of the aqueous solutions of the HPAM with chromium triacetate can. The gelation process and the effect of HPAM and salt concentration on the swelling behavior of synthesized hydrogels were studied. In addition, due to applications of polyacrylamide gels in EOR treatments, the swelling behavior of the prepared hydrogels in synthetic oil reservoir water was also investigated.

Methods/Experimentals: The polymer used is partially hydrolyzed polyacrylamide (HPAM). HPAM, with an average molecular weight of 3×10^6 Dalton was prepared by the suspension method. Chromium triacetate, as an ionic cross-linker, was purchased from Carlo Erba (Italy).The cross-linker is a chromium (III) complex ion system. First, screening tests were conducted to determine the gelation range. Here, the gelation range is defined as the polymer and cross-linker concentration range in which a gel can be formed. Second, several factors, such as temperature, concentration, and pH value, were studied to determine their effects on the gelation time.

Preparation of Hydrogel: HPAM solutions were prepared by gradual addition of its powder to tap water while stirring, to obtain clear viscous solutions. Cross-linking of the prepared HPAM solutions was performed by adding chromium triacetate/water solutions and then stirring the

aqueous reaction mixtures (gelant solutions) at ۷۵°C using an overhead electronic stirrer PZR ۲۱۰۲ (Heidolph, Germany) for ۶۰–۷۰ min. The products were immersed in an excess of tap water for ۷ days to remove the residual, uncross-linked polymers and impurities.

Results and Discussion:

Gelation range

Gelation range of HPAM and cross-linker system was studied. The results obtained show that there are two concentration boundaries between the gel system and the colloidal sol. Approximately, only when the polyacrylamide concentration is above ۲۰۰۰ ppm and the cross-linker concentration is over ۲۰ ppm will a gel system be formed.

Gelation time

The influence of temperature on gelation time was studied. The results obtained show that gelation time is very sensitive to temperature. The elevated temperature greatly shortens gelation time. The gelation time required at a practical reservoir temperature can be interpolated from this curve. The effects of polymer concentration and cross-linker concentration on the gelation time were studied. It is found that with the increase in polymer concentration, the gelation time is reduced. The major reason is that the cross-link reaction is accelerated at a higher polymer concentration. Similarly, the higher the cross-linker concentration is, the shorter the gelation time is. The pH value also affects the gelation time to some extent. The results indicates that the gelation time decreases as pH value increases.

Swelling Behavior The effect of HPAM content on the swelling behavior of the hydrogels in tap water and different electrolytes solutions was studied. The swelling capacity of the polyacrylamide hydrogels was investigated in NaCl and $CaCl_2$ electrolyte solutions.

Conclusion: In this paper, the detailed experimental data for a novel gel system consisting of polymer and cross-linker are presented and discussed. The gelation process and effects of pH, polymer content and ionic strength on the swelling behavior of these hydrogels were investigated.

References:

[۱] Wang W., Liu Y., Gu Y., Colloid Polym. Sci., ۲۰۰۳, ۲۸۱, ۱۰٤٦-۱۰۵۷.

[۲] Lake LW., *Enhanced oil recovery*. Prentice -Hall, New Jersey, ۱۹۸۹

[۳] Aalaie J., Rahmatpour A., *J. Macromol. Sci. Part B: Physics* ۲۰۱۳, ۵۲, ۶۰٤- ۶۱۳.

[٤] Aalaie J., Rahmatpour A., Vasheghani-Farahani E., *Poly. Adv. Tech.* ۲۰۰۹, ۲۰, ۱۱۰۲.

[۵] Aalaie J., Rahmatpour A., *J. Macromol. Sci. Part B: Physics* ۲۰۰۸, ٤۷, ۹۸.

Highly Stereoselective Synthesis of tolmetin-Substituted β‑Lactams by [2π+2π] cycloaddition reaction of imine and the novel ketene

Behjat Bananezhad *[a] , **Mohammad Reza Islami** [b] , **Nafiseh Kamali nezhad**[c], **Mahnoosh Rashidi**[d]

Department of Chemistry, Shahid Bahonar University of Kerman, Kerman 76169, Iran

b_bananezhad@sci.uk.ac.ir

Introduction: The 2-azetidinone (β-lactam) are an Interesting and extensively investigated heterocyclic ring system [1.2]. These compounds have many biological and medical properties. These compounds have anti-bacterial and anti-microbial properties, etc [3-4]. Recently, researchers have discovered new and important properties of beta lactams, which increases the incentives for the synthesis of these compounds [5-6]. Several chemical methods have been reported for the synthesis of beta-lactam. One of the most important methods for the synthesis of azetidin-2-ones involves the use of ketenes [7-8]. In this present work we have synthesized new β-lactam compounds in a highly stereoselective manner by in situ production of a novel ketene.

Experimental: The best result was obtained when the reaction was carried out in two steps. In the first step, acid (tolmetin) was refluxed with Mukaiyama's reagent [9] in the presence of Et_3N in CH_2Cl_2. In the next step, imine and base (Et_3N) were injected and refluxed for ten hours. The reaction of acid and Mukaiyama's reagent with triethylamine in dichloromethane in the presence of imines led to the formation of the corresponding azetidinones. The reaction was found to be highly stereoselective, and the trans-isomers were formed as the only products (Table1).

Results and Discussion: The structures of products fully characterized by IR, ^{1}H NMR, and ^{13}C NMR spectroscopy. The IR spectra of these compounds showed absorption bands due to the carbonyl group at 1737-1762 cm^{-1}. ^{1}H NMR spectra of products indicated that the trans-β-lactams were formed as the only products. In 1H NMR spectrum of compounds exhibited two doublets at $\delta = 4.34$ and 4.93 ppm ($^3J_{HH}= 2.8$ Hz) for vicinal methine protons. Characteristic ^{13}C NMR signals were shown due to two carbonyl groups at $\delta = 186.19$ and 163.32 ppm.
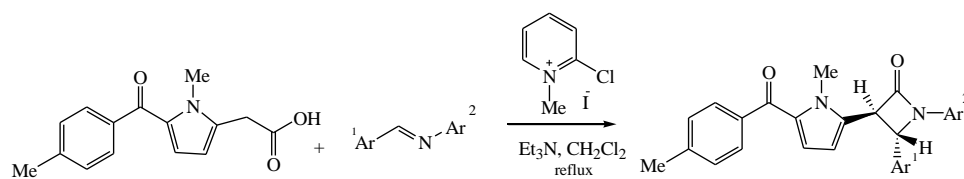
Scheme 1 Synthesis of the β-lactam compound from 2-[1-methyl-5-(4-methylbenzoyl) -1H-pyrrol-2-yl] acetic acid (Tolmetin)

Table 1 Synthesis of 3-[1-Methyl-5-(4-methyl-benzoyl)-1H-pyrrol-2-yl]-1, 4-diphenyl-azetidin-2-one

Product	Ar^1	Ar^2	Yield (%)
1	Ph	Ph	75
2	Ph	$4\text{-MeOC}_6\text{H}_4$	88
3	Ph	$4\text{-MeC}_6\text{H}_4$	70
4	$4\text{-ClC}_6\text{H}_4$	Ph	60
5	$4\text{-MeC}_6\text{H}_4$	Ph	65
6	Naphthyl	Ph	55
7	Naphthyl	$4\text{-ClC}_6\text{H}_4$	75

In summary, the present work describes the synthesis of a series of novel β-lactams comprising the tolmetin via reaction tolmetin, aromatic imines and Mukaiyama's reagent the presence of triethylamine. The reaction proceeds through in situ generation of a novel ketene and a pursuant electrocyclic reaction of a zwitterionic intermediate. The reactions were highly stereoselective and trans-β-lactams were obtained as the only observed products.

[1] Fisher, J. F.; Meroueh, S. O.; Mobashery, *S. Chem. Rev*. 2005, 105, 395-424.

[2] Elander, R. P. *Appl. Microbiol. Biotechnol.* 2003, 61, 385-392.

[3] Sheehan, J. C.; Henery-Logan, K. R. *J. Am. Chem. Soc.* 1957, 79, 1262−1263.

[4] Staudinger, H. *Ber. Dtsch. Chem. Ges.* 1905, 38, 1735-1739.

[5] Banik, B. K.; Becker, F. F.; Banik, I. *Bioorg. Med. Chem.* 2004, 12, 2523-2528.

[6] Banik, B. K.; Banik, I.; Becker, F. F. *Eur. J. Med. Chem.* 2010, 45, 846-848.

[7] Staudinger, H. *Justus Liebigs Ann. Chem.* 1907, 356, 51−123.

[8] Islami, M. R.; Allen, A. D.; Vukovic, S.; Tidwell, T. T. *Org. Lett*.2011, 13, 494−497.

[9] Mukaiyama, T. *Pure Appl. Chem.* 1979, 51, 1337-1346

Highly Stereoselective Synthesis of Novel Azetidinones from 2-(2,4-dichlorophenoxy)ethenone as novel ketene

Mahnoosh Rashidi[a*], Mohammad reza Eslami, Ahmad moemeni, Nafiseh kamali nezhad, Behjat bananezhad

Department of Chemistry, Shahid Bahonar University of Kerman, Kerman 76169, Iran

mahnooshrashidi@yahoo.com

Introduction:β-Lactams (azetidinones) are an important class of antibiotics[1,2]. and in recent years their clinical use has expandedsignificantly because of the medicinal properties of penicillin and the cephalosporins[3]. The history of the first synthetic β-lactamdates back to 1907, when H. Staudinger reported that he added zinc powder to 2-chloro-2,2 diphenylacetyl chloride in thepresence of an imine and 2-azetidinone was formed as the finalproduct [4]. One of the most important methods for the synthesis of 2-azetidinones is the use of ketenes. Theyhave long been known for their unique reactivity in [2 + 2] cycloaddition reactions[5,6]. To the best of our knowledge, 2,4-Dichlorophenoxy acetic acid has not beenemployed as a substituent for the synthesis of β-lactam (2-azetidinone).In this present work, we have synthesized new2,4-dichlorophenoxyaceticacid including a β-lactam ring.

Experimental: Highly stereoselective synthesis of 2,4-Dichlorophenoxyacetic acid derivatives containing functionalized 2-azetidinone moiety was achieved starting from by areaction of 2,4-Dichlorophenoxyacetic acid, aromatic amines, andMukaiyama's reagent in the presence of base shift in dichloromethane at was refluxed. The approach to these valuable heterocyclic scaffolds involves aformal [2π + 2π] cycloaddition between Schiff bases and the novel ketene which was generated in situ. The *cis*-β-lactam wasformed either as a single isomer or as the major isomer.

Result and Disciscussion: In contrast to the obtained products from the reaction of 2-(2,4-dichlorophenoxy)ethenoneketene with imines in which *cis*-azetidinones were formed as only products.
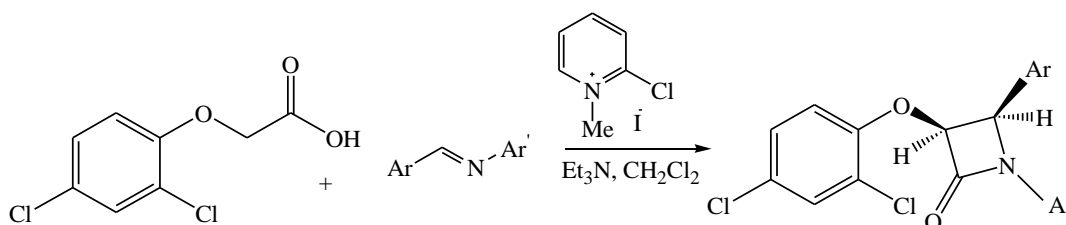
We synthesis 15 novel β-lactams on the basis of spectroscopicanalysis. The structure of the products was fully characterized by IRand ^{1}H and ^{13}C NMR spectra along with elemental analysisdata. ^{1}H NMR spectroscopy is generally used for distinguishing between cis and trans-isomers of β-lactam using H−H couplingconstants. The J value is smaller (2−2.5 Hz) in a trans-isomerthan in a cis isomer (5−6 Hz)[7].^{1}H NMR spectra of products exhibiting the cis-β-lactams were formed as the only product.The ^{1}H NMR spectrum exhibited two doublets at δ =5.54 and 5. 45 ppm ($^3J_{HH}$= 5Hz) for vicinal methine protonsalong with a multiplet at δ = 7.45−7.03 ppm for phenyl ringprotons. The ^{1}H-decoupled ^{13}C NMR showed21 distinct resonances in agreement

with the suggestedstructure. Characteristic ^{13}C NMR signals were shown due to one carbonyl groups at δ = 162.33and signals at δ = 61.44 and 81.6 ppm for CH groups, respectively. To identify the 2-(2,4-dichlorophenoxy)ethenoneKeteneas an intermediate in thesynthesis of β-lactam ring, we have under taken further reaction of the mentioned ketene with aminoxyl radicals.

Conclution:we have synthesized novel β-lactams bythe reaction of 2,4-Dichlorophenoxyacetic acid with aromaticimines and Mukaiyama's reagent in the presence oftriethylamine. The reaction proceeds through in situ generationof a novel keteneand a

subsequent electrocyclic reaction of a zwitterionic intermediate.It is worthy of note that, in contrast tothe products obtained from the reaction of 2-(2,4-dichlorophenoxy)ethenoneketenewith imines, in the present work *cis*-β-lactams were isolatedas the main products.

References:

[1]. Elander, R. P. *Appl. Microbiol. Biotechnol.* **2003**, *61*, 385-389

[2]. Fisher, J. F.; Meroueh, S. O.; Mobashery, S. *Chem. Rev.***2005**, *105*, 395-402

[3]. O'Boyle, N. M.; Carr, M.; Greene, L. M.; Bergin, O.;Nathwani, S. M.; McCabe, T.; Lloyd, D. G.; Zisterer, D. M.;Meegan, M. J. *J. Med. Chem.* **2010**, *53*, 8569-8574

[4]. Woodward, R. B.; Heusler, K.; Gosteli, J.; Naegeli, P.; Oppolzer,W.; Ramage, R.; Ranganathan, S.; Vorbruggen, H. *J. Am. Chem. Soc.***1966**, 88, 852−853

[5]. Brady, W. T.; Saidi, K. J. Org. Chem. **1980**, 45, 727−729.

[6]. Merino, I.; Hegedus, L. S. *Organometallics* **1995**, *14*, 2522.

[7]. Brady, W. T.; Saidi, K. *J. Org. Chem.* **1980**, 45, 727−729.

Why Dibromocarbazole Derivative (P7C3) Is an Effective Neuroprotective Drug but Not Dichlorocarbazole or Parent Carbazol?

Amin Reza Zolghadr*, <u>Maryam Heydari Dokoohaki</u>

Department of Chemistry, Shiraz University, Shiraz 71946-84795, Iran

Email address: <u>arzolghadr@shirazu.ac.ir</u>

****

Introduction: The new approach on treating Alzheimer's disease suggests drugs that promote hippocampal neurogenesis [1]. A novel carbazolium based neuroprotective small molecule was discovered using a target-agnostic in vivo screen in living mice [2]. This aminopropyl carbazole (P7C3), is non-toxic at doses several fold higher than the efficacious dose. The bromines on the carbazole group of P7C3 appear particularly important as the derivatives with dichloro (P7C3-Cl) and parent carbazole (P7C3-H) abrogate activity at the concentrations tested [2].

As a pharmaceutical application of liquid–liquid interfaces, study of octane–water interface in the presence of drugs is a significant achievement. To provide the proof of concept, in this work we studied the conformation of P7C3 molecule and its derivatives at octane/water interface, with the aim to find a reason for the better activity of P7C3 in comparison to dichloro derivative and parent carbazole by molecular dynamics simulation.

Methods: All simulations were run in DL_POLY program by using three-dimensional periodic boundary conditions. Parameters employed to model the intramolecular and intermolecular interactions of octane and drug molecules were obtained from the General Amber Force Field. The initial configurations were set up by making water/octane interfaces for conducting the hydrophilic/hydrophobic simulation. After achieving the state of equilibrium, the simulation ensemble was completed by adding 24 drug molecules to both sides of n-octane slab surface. MD simulations were extended for additional 20 ns to ensure that the results are equilibrated.

Results and Discussion: At the start of the simulations, the drug molecules were distributed in the water phase. As simulation proceeded, the P7C3 and P7C3-Cl molecules very quickly migrated toward the octane phase and reached the interface within 1 ns. During this process the drug molecules are aggregated and stable self-assemblies are formed. Once the aggregated molecules equilibrated at octane side of the interface within 6 ns, they remains there until the end of the simulation (see Figure 1). In the case of P7C3-H stable aggregates are formed in the water

phase in the self-assembly process. The density profiles of octane/drug/water systems indicate that the P7C3 molecules are mainly accumulated at the interface of octane/water system and protrude in a higher extent toward octane phase (see Figure 2). The area below density curve of drug candidate molecules at the interface indicate that P7C3 accumulated 1.22 times more than the P7C3-Cl molecules. The calculated values of diffusion coefficient for P7C3 and P7C3-Cl are 5.23×10^{-10} m^2.s^{-1} and 0.934×10^{-10} m^2.s^{-1}, respectively. Therefore, the self-diffusion of the P7C3-Cl molecules is much slower than those of P7C3 due to the interfacial confinement effect. The electrostatic potential map of P7C3 clearly shows the presence of numerous electrophilic and nucleophilic sites in this compound (see Figure 3). This map and more considerations reveal that the polarizability of P7C3 molecules (especially around Br groups) is higher than P7C3-Cl and
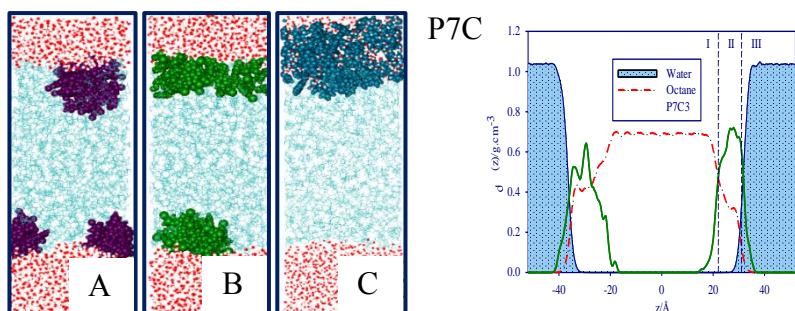

Figure 1. Sample snapshots of (A) octane/P7C3/water, (B) octane/P7C3-

Figure 2. Total density profile of octane/P7C3/water

Figure 3. Electrostatic potential map of P7C3.

Conclusion: Molecular dynamics simulations were performed to examine the partitioning behavior of P7C3 and its analogous at octane/water interface. The simulation shows the rapid formation of P7C3 and P7C3-Cl assemblies at the octane/water/interface and the migration and equilibration of self-assembled molecules to the octane side of the interface while they were initially in the water phase. The diffusion of P7C3 molecules are much higher than P7C3-Cl. In contrast, P7C3-H molecules form self-assemblies in the water phase.

References:

[1] Faghih, Z.; Fereidoonnezhad, M.; Tabaei, S. M. H.; Rezaei, Z.; Zolghadr, A. R. *Chemical Physics*, **2015**, *459*, 31-39.

[2] MacMillan, K. S.; Naidoo, J.; Liang, J.; Melito, L.; Williams, N. S.; Morlock, L.; Huntington, P. J.; Estill, S. J.; Longgood, J.; Becker, G. L; McKnight, S. L. *Journal of the American Chemical Society*, **2011**, *133*, 1428-1437.

Synthesis of graphene oxide and graphene supported acetyl salicylic acid as nano drug

Seideh Masoumeh Mousavi and Nooredin Goudarzian*

Department of Applied Chemistry, Shiraz Branch, Islamic Azad University, Shiraz, Iran

Corresponding author*: Ngoudarzian@iaushiraz.ac.ir

1. Introduction

Graphene, a very recent rising star, with an atomically thin, 2D honeycomb lattice that consists of sp2-hybridized carbons, exhibits remarkable electronic, thermal, optical, and mechanical properties. Particularly, graphene oxide (GO), Reduced graphene oxide (RGO) water soluble derivative, has been found important potential applications in drug delivery due to their large specific surface area and abundant functional groups .The controlled loading and targeted delivery drug by GO and RGO based drug carriers remain unexplored. Herein, we designed and prepared acetyl salicylic acid (ASA) conjugated GO and RGO as drug delivery system. In our strategy, sulfonic acid groups were introduced to GO, which rendered it stable under physiological conditions, and ASA molecules were conjugated with the RGO for targeting specific cells with acid receptors. Furthermore, controlled loading and targeted delivery ASA using the GO as a carrier were investigated.

2. Experimental

2.1 Synthesis of graphene oxide: Synthesis of graphene oxide

GO was prepared using nature graphite powders as the raw materials by a modified Hummers method [1].

Conjugation of acetyl salicylic acid with reduced graphene oxide (RGO-COOH)**:** ASA molecules were conjugated to the RGO according to the literature [1]. Briefly, appropriate amounts of ASA and NaOH were added to RGO suspension. After sonicated, the resulting product (RGO-COOH) was neutralized with dilute HCl and. Then, the RGO-COOH suspension was dialyzed against DD water to remove any ions. Finally, the pure product separated by ultra-centrifuge and vacuum dried.

Results

Synthesis and characterization of GO and FA-GO

GO was prepared using nature graphite powders as the raw materials through a modified Hummers method. The morphology of as prepared GO was characterized by AFM and SEM. The results indicated that the GO existed in the sheet like shapes. The thickness, measured from the height profile of the AFM image. The as prepared GO was also determined by FTIR and UV-vis spectroscopy. The FTIR spectrum of GO showed that there are ester, hydroxyl, and epoxide groups in the GO sheets. The procedure for preparation of RGO was same as GO layer except that after preparing of GO in mixture we added appropriate amounts of leaf extracts of Allium Ampeloprasum(AA) and let to be stirred under reflux and then , the pure product separated by ultra-centrifuge and vacuum dried.

Loading Efficiency Measurements: The loading efficiency of RGO-COOH was calculated by using RGO-COOH, UV calibration curve. The correlation between the UV absorbance and the concentration of RGO-COOH was normalized by linear regression, which showed a well correlated linear relationship ($R^2=0.9948$). The standard curve had a good linear relation.

Conclusion

We have demonstrated that a novel drug delivery system based on ASA -conjugated RGO could be developed with good solubility and low cytotoxicity. The RGO-COOH has been

effectively loaded into the system via hydrophobic interactions and π-π stacking. Further development of RGO-based drug delivery system, the size of RGO should be controlled, and the surface of RGO should be modify to prevent fluorescence quenching of ASA with RGO and improve the photodynamic effect.

References:

[1]. Xu Y, Liu Z, Zhang X, Wang Y, Tian J, Huang Y, et al. A graphene hybrid material covalently functionalized with porphyrin: synthesis and optical limiting property. *Adv. Mater.* 2009; 21:1275-9.

Cyclopalladated Complex of Auramine-O: Catalytic Activity of Functionalized Titania-Supported Pd Catalyst in the Copper-Free Sonogashira Cross-Coupling Reactions

Sedigheh Abedanzadeh, Kazem Karami,*

*Department of Chemistry, Isfahan University of Technology, Isfahan, 84156, I.R. Iran*

karami@cc.iut.ac.ir

****

Introduction: The Sonogashira cross-coupling reaction is one of the most important methods for the synthesis of natural products, pharmaceutical compounds and polymeric materials which is generally catalyzed by homogeneous palladium complexes in the presence of toxic phosphine ligands, using copper salts as co-catalysts and amine as a solvent or base, under inert condition [1-4]. There have been many efforts to introduce highly active and easily reusable supported palladium catalysts to address the limited practical application of homogeneous type through the convenient Cu-, amine and phosphine- free methods under environmentally friendly conditions.

Methods / Experimentals: All the reactants and solvents were used as commercially available chemicals without any purification. bis[4-(dimethylamino)phenyl]methaniminium chloride (Auramine-O) was added to the solution of $Pd(OAc)_2$ in toluene and the resulting mixture was refluxed to give chloro-bridge dimeric cyclopalladated complex. The functionalized titania-supported Pd catalyst was prepared by stirring a mixture of surface bound ligand and synthesized complex in dry acetone.

Results and Discussion: Nitrogen-containing palladacycles have attracted much attention as exciting catalyst precursors for cross coupling reactions due to their accessibility, thermal stability, slow decomposition and high catalytic activity [5]. A general approach has been designed to synthesize a new dinuclear CN-palladacycle deriving from bis[4-(dimethylamino)phenyl]methaniminium chloride (Auramine-O) which was fully characterized by IR, multinuclear NMR spectroscopies and elemental analysis technique. In order to convert a homogeneous catalyst into a heterogeneous one, CN-palladacyclic complex was stabilized onto the large surface area of inorganic TiO_2 support by an organic spacer to create organic-inorganic hybrid catalyst. The heterogeneous Pd catalyst system has been fully characterized by FT-IR, XRD, FE-SEM, EDX, TEM and XPS techniques. To study the performance of the resulting low Pd-loaded catalyst for the Sonogashira cross-coupling reaction of

aryl halides with phenylacethylene, optimization of the reaction conditions with various solvents and catalyst dosages were applied in the different range of time reactions and temperatures. The generality of the current system has been investigated with several electronically diverse aryl aryl iodide, bromide and chlorides under the optimized conditions.
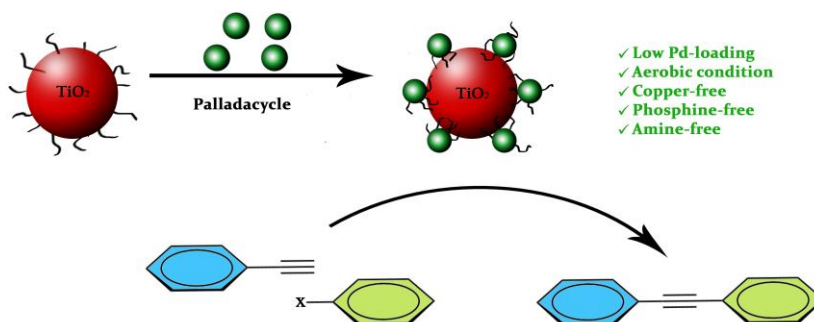
Conclusion: The present work describes the preparation of the heterogeneous TiO_2-supported palladium catalyst originated from the new bezophenone imine-derived CN-palladacyclic precursor which is fully characterized by FT-IR, XRD, SEM, EDX, TEM and XPS techniques. This hybrid catalyst demonstrated high catalytic activities in the copper-, amine and phosphine-free Sonogashira coupling reactions of phenylacetylene with aryl halides in the presence of very low catalyst Pd-loading. This class of heterogeneous Pd catalyst allows the reaction of phenylacethylene and aryl iodides to promote with remarkable yields under environmentally green condition.

References

[1] C. N´ajera; R. Chinchilla, *Chem. Rev.*, **2007**, *107*, 874-922.

[2] H. Doucet; J. -C. Hierso, *Angew. Chem. Int. Ed.*, **2007**, *46*, 834-871.

[3] L. Yin; J. Liebscher, *Chem. Rev.*, **2007**, *107*, 133-173.

[4] K. C. Nicolaou; P. G. Bulger; D. Sarlah, *Angew.Chem. Int. Ed.*, **2005**, *44*, 4442-4489.

[5] D. A. Alonso; C. Na´ jera, *Chem. Soc. Rev.*, **2010**, *39*, 2891-2902.

A highly efficient and recyclable Fe_3O_4 magnetic nanoparticles immobilized copper catalyst for the O-arylation reaction

Razieh Zahedi, Zahra Asadi*

Department of Chemistry, College of Sciences, Shiraz University, Shiraz 71454, I.R. Iran

Email address**:** zasadi@shirazu.ac.ir

****

Introduction: Heterogeneous catalysts are especially interesting in academic and industrial research, mainly because of their simple separation from a mixture of products and due to their reusability [1]. However, the heterogeneous catalysts broadly need tedious preparation and separation processes, and there is a necessity to obtain new materials with special properties such as magnetism in order to overcome these weaknesses. Magnetic nanoparticles are an important class of nanostructures materials of current interest, mostly due to their advanced technological and medical applications. Among the various magnetic nanoparticles, Fe_3O_4 nanoparticles are arguably the most extensively studied and have recently emerged as promising supports for the immobilization of core–shell metal nanoparticles [2].

Methods / Experimentals: Fe_3O_4 magnetic nanoparticles were prepared using co-precipitation method. In order to avoid from aggregation of MNPs they were coated with a silica layer using tetra ethyl ortho silicate (TEOS). The $Fe_3O_4@SiO_2$ was further functionalized with 3-aminopropyltriethoxysilane (3-APTES) and then reacted with 2-Hydroxybenzophenone. The resulting NPs were metallated with copper (II) acetate to produce the final catalyst (Cu-HB@ASMNPs).

Procedure for O-arylation reaction: A mixture of phenol (1mmol), iodobenzene (1mmol), base (1mmol), and catalyst (10 mol%) was added to 2.5ml of Solvent. The reaction mixture was heated for the required time. The progress of the reaction was monitored by TLC.

Results and discussion: Cu-HB@ASMNPs catalyst was synthesized and characterized by different techniques such as FT-IR, CHN and ICP. The coupling of iodobenzene with 4-tert-Butyl phenol was initially studied as a model reaction and the effects of the type of solvent, base, temperature, as well as catalyst loadings were investigated. Therefore, the optimal reaction conditions and the model reaction are shown in Scheme 1. O-arylation reactions were done using different phenols and aryliodides and the product were obtained in good yields. The catalyst was

recovered from the reaction mixture by magnetic separation after each experiment, washed with n-hexane and ethanol to remove the base. The recovered catalyst was used for several times in consecutive runs without a significant loss in its catalytic activity.
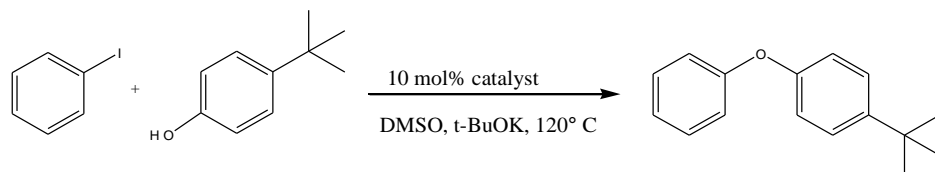
Scheme 1: The optimal reaction conditions and the model reaction for the Ullmann coupling of O-arylation.

Conclusion: In summary, a highly stable magnetically recoverable catalyst formed by very small copper nanoparticles well distributed and stabilized in the magnetizable support surfaces. The catalytic activity of the catalyst was investigated in O-arylation reaction. After each reaction, the catalyst could be easily separated magnetically from the reaction products minimizing the generation of organic residues and avoiding the use of additional solvents and environmentally non-friendly procedures.

References:

[1] V. Polshettiwar; R. S. Varma. *Green Chem.* **2012**, *12*, 743-754.

[2] H. Wang; A. Yu; A. Cao; J. Chang; Y. Wu. *Appl. Organometal. Chem.*, **2013**, *27*, 611–614.

# Water-Mediated Amide Formation in *o*-Aminophenol Copper Complex versus Zinc Analogue

Zahra Alaji [a], **Elham Safaei** [b]*,

[a] *Institute for Advanced Studies in Basic Sciences (IASBS), 45137-66731, Zanjan, Iran*
[b] *Department of Chemistry, College of Sciences, Shiraz University, Shiraz, 71454, Iran*

E-mail*:* e.safaei@shirazu.ac.ir

****

Introduction. The electronic properties of transition metal complexes and their multi-electron redox chemistry may affect by the redox-active ligands [1]. In metalloenzymes, radical participation with the surrounding ligands is an effective strategy to overcome one-electron chemistry to promote a net two-electron transformation [2,3]. Oxidation of organic functions assisted by metal coordination is an interesting reaction in chemistry[4]. This work is concerned to develop redox active systems promoting the reaction of eq 1 where the functional transformation of imine to amide occurs.

$$\underset{H}{\overset{}{>}}C=N\overset{M}{\underset{}{<}} \longrightarrow \underset{O}{\overset{}{>}}C-N\overset{M}{\underset{}{<}} \qquad \text{eq 1}$$
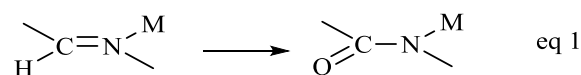
Experimental methods. The ligand HL^{IPIP} was synthesized through the sequential condensation of 2-aminobenzylamine with 3, 5-DTBQ and then pyridine-2-carbaldehyde, HL^{IPIP}. Next, HL^{IPIP} was treated immediately with Cu(OAc)$_2$·2H$_2$O to afford the copper complex. For Synthesis of Zn complex, the ligand HL^{IPIP} was treated immediately with Zn(OAc)$_2$·4H$_2$O. The synthesized complexes were characterized by X-Ray crystallography and ESI-MS spectroscopy.

Results and discussions.
The dark red-brown crystals of the copper complex for X-ray analysis were obtained from n-hexane/dichloromethane (1:1) mixture (Figure 1). IR analysis of Cu^{II}L^{APIP} revealed a sharp band at 1642 cm^{-1}, attributed to the $\nu_{C=O}$ stretch of an amide substituent. ESI-MS analysis confirmed the presence of the Cu^{II}L^{APIP} complex at m/z 491.2. A prominent parameter in ligand structure is the oxidation of imine bond to amide. The C=O bond length of 1.232 Å is consistent with the value reported for amide group [1] .
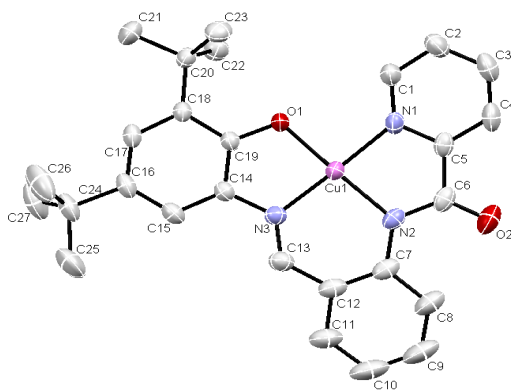

Fig.1 Molecular structure of Cu^{II}L^{APIP} ·Hydrogen atoms have been omitted for clarity.

In order to determine the susceptibility of this imine bond to the nucleophile substitution, we tried to obtain the structure of this complex exposing another nucleophile such as methanol. A remarkable parameter in the ligand framework of the single crystals obtained from methanol/dichloromethane mixture (1:1) is the coordination of methoxy group to C6 (Figure 2). It clearly shows that methanol can substitute to imine bond at the absence of water, not further oxidized to amide moiety.
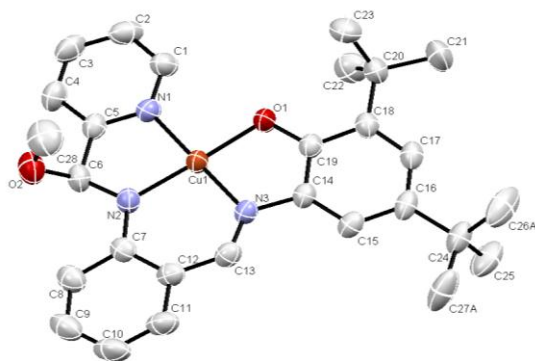

Fig. 2 Molecular structure of $Cu^{II}L^{MeOPIP}$ Hydrogen atoms have been omitted for clarity.

Firstly, zinc complex of this ligand was synthesized under the same condition as copper complex, and the dark brown single crystals were obtained from methanol (Figure 4). The most interesting part is that the imine bond remained intact even in the presence of the water molecule in the coordination environment.
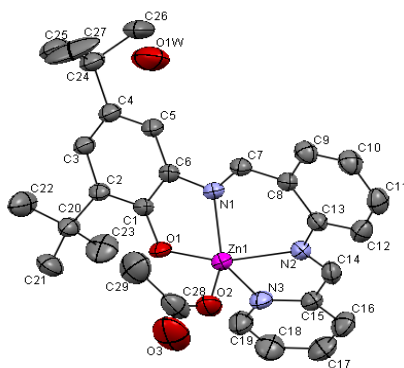

Fig.3 Molecular structure of $Zn^{II}L^{APIP}OAc$. Hydrogen atoms have been omitted for clarity.

Conclusion. In this work we investigated a water-mediated amide formation process involving oxidative radical formation on the ligand framework in copper. In contrast, zinc complex of same ligand includes the intact imine bond indicating that the redox active reactivity of this ligand varies significantly with the nature of metal center.

References

[1] T.D. Manuel, J.-U. Rohde, *J. Am. Chem. Soc.*, **2009**, 131, 15582.
[2] P.J. Chirik, K. Wieghardt, *Science*, **2010**, 327, 794.
[3] W. Kaim, B. Schwederski, *Coord. Chem. Rev.* **2010**, 254, 1580.
[4] M. Menon, A. Pramanik, A. Chakravorty, *Inorg. Chem.* **1995**, 34, 3310.

Aerobic Oxidative Coupling of Terminal Alkynes with a Copper Complex of new Redox-Active Aminophenol-Benzimidazole Ligand

Zahra Alaji [a], Elham Safaei [b*],

[a] *Institute for Advanced Studies in Basic Sciences (IASBS), 45137-66731, Zanjan, Iran*
[b] *Department of Chemistry, College of Sciences, Shiraz University, Shiraz, 71454, Iran*

E-mail*: e.safaei@shirazu.ac.ir

****

Introduction. C-H bond activation allows shortening the synthetic routes compared with traditional cross-coupling methods. It would be advantageous to employ less exotic metals such as copper or iron instead of precious metals for this reaction[1]. A notable example of such catalysis is the Glaser-Hay alkyne dimerization to form bi-alkyne C-C bonds[2,3]. Practically, coupled alkynes display good conduction properties, making them attractive for applications such as OLEDs (organic light-emitting diodes) and conducting polymers[4]. In this study, we reported a very efficient copper catalyst for homo-coupling of terminal alkynes. We also conducted kinetic studies to examine mechanism details of this interesting reaction.

Experimental methods. The ligand HL^{APIM} was prepared from the condensation of 3,5-Di-tert-butyl-quinone and amino methyl benzimidazole dihydrochloride in methanol under vigorous stirring to afford yellow precipitation. To the mixture of ligand in acetonitrile was added $CuBr_2$ and Et_3N to afford purple precipitation of CuL_2^{APIM}. In coupling reaction, the effect of base, solvent and temperature were examined to obtain the optimum condition.

Results and discussions. ESI-MASS analysis clearly indicated the formation of 1:2 complex of copper to ligand. The activity of this complex was investigated on phenyl acetylene homo-coupling reaction. We found that this complex is capable of catalyzing homo-coupling reaction in the presence of potassium hydroxide as a base in THF at room temperature. We conducted kinetic studies to obtain more details. The Raman/GC technique was employed to follow this reaction and indicate the concentration of product in the moment. The phenyl acetylene and its dimer product have active-peaks in Raman (Scheme 1).
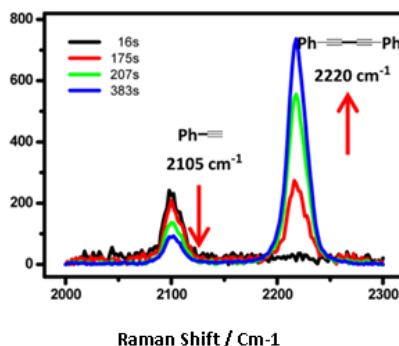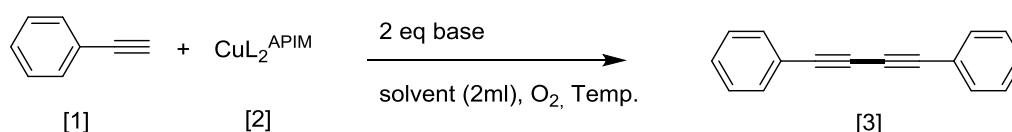
Scheme 1. Raman spectra change in the homo-coupling of phenyl-acetylene reaction

This study indicates the first order correlation between initial rate and the substrate and also copper complex concentrations (Figure 1).

In addition, the substrate and copper complex rate diagram (Figure 1, A and C) show that there is an induction period of 500 seconds to occur the product. This result implies that there is an active species in this process which requires time to form and precede the reaction. This remarkable achievement was also confirmed in other studies[5].
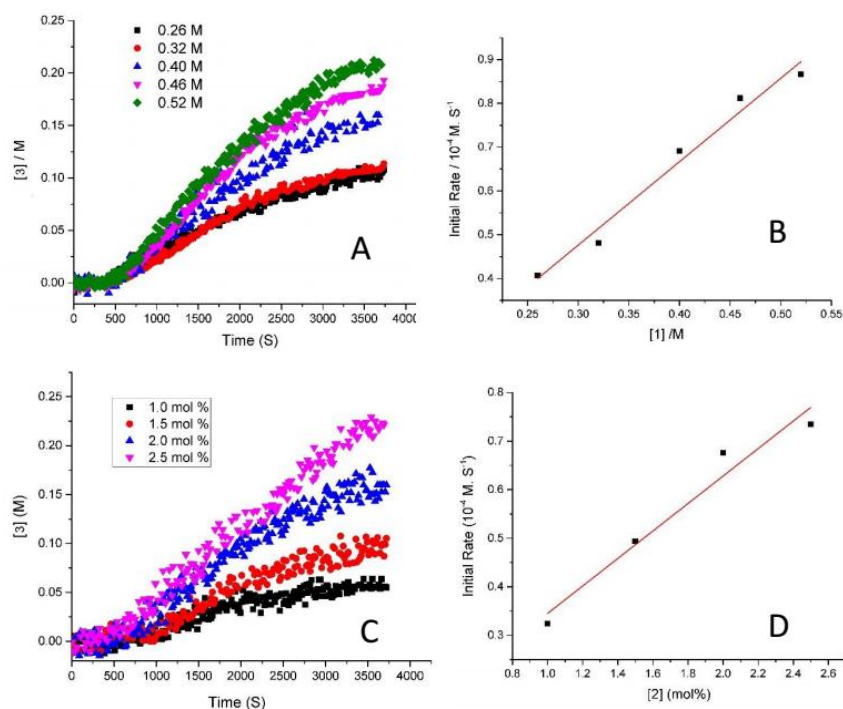

Figure 1. A) The effect of Phenyl acetylene concentration B) Kinetic profiles with different concentration of Phenyl acetylene C) The effect of copper complex concentration D) Kinetic profiles with different concentration of copper complex

Conclusion. The copper complex of new redox-active aminophenol-benzimidazole ligand was synthesized and employed in aerobic oxidative coupling of terminal alkynes.

This copper complex could efficiently catalyze the homo-coupling of different kinds of terminal alkynes in the presence of potassium hydroxide as a base in THF solvent in room temperature. The phenyl acetylene coupling reaction as a typical reagent follows the first order correlation relative to both substrate and copper complex concentrations.

References

[1] H.-Q. Do, O. Daugulis, J. Am. Chem. Soc. **2009**,131, 17052.

[2] L. Su, J. Dong, L. Liu, M. Sun, R. Qiu, Y. Zhou, S.-F. Yin, J. Am. Chem. Soc. **2006,**

[3] Y. Gao, G. Wang, L. Chen, P. Xu, Y. Zhao, Y. Zhou, L-.B. Han, J. Am. Chem. Soc. **2009,** 131 , 7956.

[4] L. van Gelderen, G. Rothenberg, V.R. Calderone, K. Wilson, N.R. Shiju, Appl Organomet. Chem. **2013**, 27, 23.

[5] R. Bai, G. Zhang, H. Yi, Z. Huang, X. Qi, C. Liu, J.T. Miller, A.J. Kropf ,E.E. Bunel, Y. Lan, J. Am. Chem. Soc. **2014**, 136, 16760.

Corrosion inhibition modeling of imidazole and its derivatives on iron metal using QSAR method

Mehdi Mousavi[a*], Sahar Ostovar [a]

[a] Department of Chemistry, Faculty of Sciences, Shahid Bahonar University of Kerman, P.O. Box 76175-133, Kerman, Iran
[*] mmousavi@uk.ac.ir

****

Introduction: Various attempts have been made to prevent the destructive effect of corrosion on metals and alloys. Corrosion control can be achieved by several methods, from which the use of corrosion inhibitors is one of the most effective methods [1].

Although experimental studies are straightforward, they are often expensive and time-consuming. Alternatively, theoretical and computational chemistry are useful and powerful means in choosing the appropriate and effective inhibitor by understanding the inhibition mechanism prior to any experiment. Quantitative structure inhibition (activity) relationship (QSIR or QSAR) is a theoretical method which is useful in relating structural based parameters to corrosion inhibition efficiencies [2,3].

Methods / experimental: In the development of a QSAR model for corrosion inhibitors, attempts are made to predict corrosion inhibition efficiency with a number of individual structural parameters (descriptors) obtained via various quantum chemical calculations. To fulfill this aim, a combination of cluster model and QSIR methods are considered[4]. In the present work, a series of imidazole and its derivatives was used as data set. The experimental inhibition efficiencies of the molecules were taken from zhe zhang et al work [5]. To optimize the iron cluster and inhibitor molecules, Gaussian 09 and Hyperchem 8.0 software's were used. In addition, SPSS/PC software was used to analyze and evaluate calculated descriptors and to generate linear models.

Results and Discussion: in order to calculate interaction energy of inhibitor molecules with the metal, iron cluster were extracted from literature. Then the structures of iron cluster, inhibitor molecules and the inhibitor-cluster were optimized at B3LYP/LANL1MB DFT level of theory implemented in Gaussian 09 software. Fig 1 shows optimized geometry of (E)-methyl 3-(4-((1H-imidazol-1-yl)methyl)phenyl)acrylate on the iron cluster.
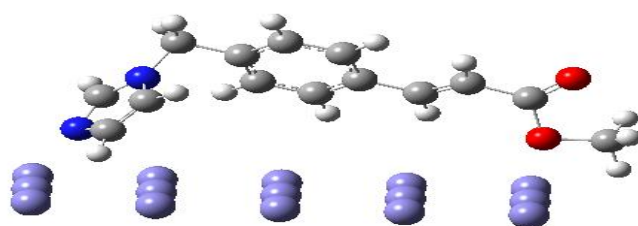

Fig1: optimized geometry of (E)-methyl 3-(4-((1H-imidazol-1-yl)methyl)phenyl)acrylate on the iron cluster.

In addition, some well-known quantum chemical and electronic descriptors such as HOMO, LUMO and GAP energies, polarizability and so on were calculated. Stepwise multiple linear regression (MLR) method was used to generate the model. The most suitable model and its statistics are shown in Eq. 1. Accordingly molar refractivity and E_{HOMO} are chosen as the most informative descriptor for the modeling.

Table1: optimized data set molecules

Inhibitors name	Experimental	Refractivity	E_{Homo}	Calculated

	inhibition efficiency			inhibition efficiency
imidazole	81.00	38.78	-.166	80.977
1-benzyl-1H-imidazole	84.40	53.66	-.168	84.382
1-buty1-1H-imidazole	77.70	20.01	-.170	77.718
1-tosyl-1H-imidazole	85.60	69.90	-.153	85.556
(E)-3-(4-((1H-imidazol-1-yl)methyl)phenyl)acrylic acid	86.80	74.67	-.156	86.805
(E)-methyl 3-(4-((1H-imidazol-1-yl)methyl)phenyl)acrylate	84.60	62.12	-.160	84.809

Inhibition efficiency $=47.537+0.209$ refractivity$-152.091E_{HOMO}$ (1)

$R=1.000$, $R^2_{adj}=0.999$, $F=2003$, $SE=0.120$, $R^2_{LOO}=0.997$

Plot of calculated versus experimental inhibition efficiencies indicate that the derived model can successfully explain experimental inhibition variation in sulfuric acid Media (Fig 2).
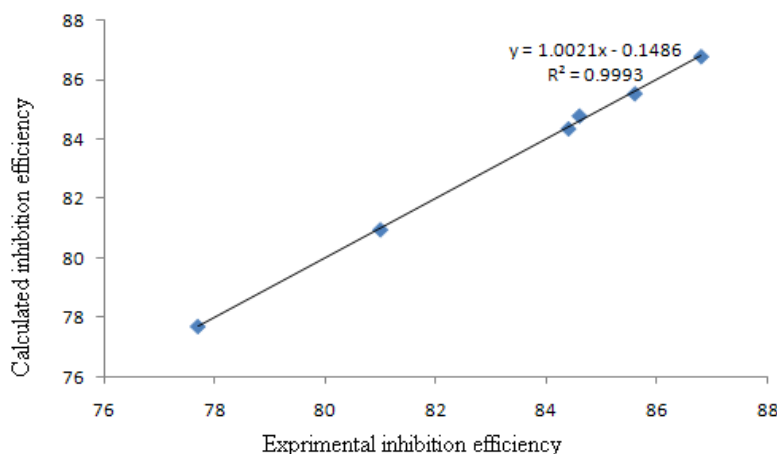

Fig2:plot of the calculated inhibition efficiency against the experimental inhibition efficiency

Conclusion: Experimental inhibition efficiencies of some imidazoles on iron corrosion were successfully modeled. The derived model may be used to test new candidate and propose new corrosion inhibitor in the same media.

Refrences
[1] R.M. Issa, M.K. Awad, F.M. Atlam, Appl. Surf. Sci. 255 (2008) 2433–2441.
[2]M.Mousavi,T.Baghgoli, Corros. Sci.105(2015)170-176
[3] S.G. Zhang, W. Lei, M.Z. Xia, F.Y. Wang, J. Mol.Struct. THEOCHEM 732 (2005) 173182.
[4] M.Mousavi , H.Safarizadeh ,A.Khosravan,Corros . Sci.65(2012)249.
[5]Z.Zhang, S.Chen,Y. Li,S. Li, L.Wang, Corros. Sci. 51(2009) 291-300.

Corrosion inhibition modeling of some Ortho-aniline derivatives on copper metal using quantum mechanical descriptors

Tayebeh Baghgoli, <u>Mehdi Mousavi</u>*

Department of Chemistry,Faculty of Sciences, Shahid Bahonar University of Kerman,P.O. Box ٧٦١٧٥-١٣,Kerman,Iran

*mmousavi@uk.ac.ir

Introduction

there has been a growing interest in the use of organic compounds as inhibitors for the aqueous corrosion of metals [١] The protective action of inhibitors is often associated with their chemical or physical adsorption on the metal surface and their role in elimination or parry of corrosive ions. To find a corrosion inhibitor molecule many chemical compounds are synthesized and evaluated experimentally. However, theoretical works reduce time and cost of inhibitor analysis for corrosion inhibition process [٢]. Quantum chemical and quantitative structure-inhibition relationship (QSIR) are theoretical methods which are used in inspection of corrosion processes [٣]. In the development of a QSIR model for a series of corrosion inhibitors, attempts are made to model corrosion inhibition efficiency with a number of efficient and interpretable descriptors. In the present work, in order to obtain chemically interpretable descriptors for QSIR modeling, the conditions of corrosion inhibition process were simulated by considering all major interactions in corroding media. Thus, some new quantum chemical descriptor were calculated based on the interactions. Efficiency of the proposed descriptors were compared with the well known descriptors which are usually applied in QSIR modeling process.

Computational method

At the present work, six ortho-substituted anilines with known experimental corrosion inhibition efficiencies were used as a data set [٤]. Quantum chemical calculations at DFT B٣LYP/LANL١MB level of theory were used for calculation of all quantum chemical descriptors. The interaction energies of inhibitor-metal cluster, inhibitor-hydronium ion (H_3O^+) and inhibitor-choloride ion (Cl^-) were considered as major chemical phenomena in the media. The interaction energy (E_{int}) was calculated according to Eq. ١:

$$E_{int}(A\text{-}B) = E_{A\text{-}B} - (E_A + E_B) \tag{١}$$

where, E_A, E_B and $E_{A\text{-}B}$ are electronic energies of the A and B species and the A-B complex system, respectively. All energies in Eq. ١ are calculated using DFT method at B٣LYP/LANL١MB level of theory for gas and water phases, they were corrected for zero point energy (ZPE), and basis set superposition error (BSSE). Then, a combination of the three interaction energies which are based on the inhibitors interaction with metal surface and corrosive ions were applied in the modeling process.

Results and discussion

In the conducted experimental work, corrosion inhibition efficiencies have been investigated in the aqueous solution including HCl electrolyte [٤]. We assumed that there are a number of competitive process in a corrosion process. Therefore, in addition to the interaction of inhibitor- metal cluster, the interaction energies of all components of solution which were in inhibitors contact, were calculated, separately. The electronic energies of the isolated copper cluster, H_3O^+ and Cl^- were -٦٨٠.٢٣٠٨٦٩٧, -٧٥.٧٦٨٠٧٦ and -١٥.٠٨١٢٠٤ hartrees (١hartree = ٢٢٠٧.١٠٢ kJ/mol) in water phase respectively. it is necessary to emphasis that, in calculation of inhibitor –metal cluster interaction, no restricted orientation was applied. The electronic energies of the inhibitor's interactions ($E_{inhibitor\text{-}Cu}$, $E_{inhibitor\text{-}Cl^-}$, $E_{inhibitor\text{-}H_3O^+}$) which were corrected for ZPE and BSSE are reported in Table ١.

Subsequently, interaction energies of the inhibitors with other components of solution were calculated according to Eq. ١ and are listed in Table ١.

Multiple linear regression (MLR) was used to build linear models that relate experimental inhibition efficiencies to a combination of the calculated interaction energies and other descriptors. The pool of descriptor were included interaction energies, E_{LUMO}, E_{HOMO}, *gap*, dipole moment, polarizability and some other electronic descriptors. Modeling process and descriptor selection were carried out for calculated corrosion inhibition efficiencies at ٠.٠٠١ M inhibitor concentration. Surprisingly, as shown in Eq. ٢ the most informative descriptors for the modeling are the proposed interaction energies. For the sack of comparison, a linear model is generated by using some well-known descriptors such as E_{LUMO}, E_{HOMO}, *gap*, dipole moment and polarizability (Eq. ٣). the obtained results indicate that the experimental corrosion inhibition imposed by the inhibitor molecules are explained more reasonably by using the interaction energies. In addition, calculated descriptors are reliable and interpretable descriptors and give a good insight about mechanism of action under study.

$$I = ١٢٠.٠٥٧\, E_{int}(inhibitor\text{-}Cu) - ٣٦٨.٩٥٩\, E_{int}(inhibitor\text{-}Cl^-) - ١٧٥.٠٤٤\, E_{int}(inhibitor\text{-}H_٢O^+) + ٩٥.٦٢ \qquad (٢)$$
$$R = ٠.٩٧٢ \qquad R^٢ = ٠.٩٤٤ \qquad F = ١١.٢٨ \qquad SE = ٢.١٣٦٩٩$$

$$I = ١٢٧٣.٦٢٩\, E_{homo} - ١٠٦٦.٠٥٤\, hardnesss + ١٨.٠١\, dipolmomemnt + ٢٧٣.٥٧ \qquad (٣)$$
$$R = ٠.٧٦٧ \qquad R^٢ = ٠.٥٨٩ \qquad F = ٠.٩٥٤ \qquad SE = ٥.٨٠١٢١$$

Table ١. Calculated energies for inhibitors interaction and E_{int} in aqueous phase using B٣LYP/LANL١MB method

NO.	Inhibitor	$E_{inhibitor\text{-}Cu}{}^{a}$	$E_{inhibitor\text{-}Cl}{}^{a}$	$E_{inhibitor\text{-}H_٢O+}{}^{a}$	E_{int}(inhibitor-Cu)	E_{int}(inhibitor-Cl⁻)	E_{int}(inhibitor-H₂O⁺)
١	٢-Chloro-aniline	-٩٧٨.٤٧٣١٤	-٣١٣.٢٥٠٨٦	-٣٧٤.٠٢١	٠.٠٢٨٥٢٠٠٧٠٦٤	٠.١٠١١٣٦١٥٥٣٨	٠.٠١٨٠٤٢٠٢٣٨٨
٢	٢-Ethyl-aniline	-١٠٤١.٧٤٨٠	-٣٧٦.٥٢٦٣٣	-٤٣٧.٣٠٦	٠.٠٢٣٠٧٥٠٩٧٦١	٠.٠٩٥١٠٠٠٨٠٦٣	٠.٠٠٢٧٨٨٥٠١٣٨٩
٣	٢-Fluoro-aniline	-١٠٦١.٨٨٣٢	-٣٩٦.٦٨٥٢٥	-٤٥٧.٤٠٩	٠.٠٤٣٩٥٠٨٨٥٥٣٩	٠.٠٩٢٢٨٥٤٢٩٨٣	٠.٠٥٤٩٥٢٤٩٤٩٦
٤	٢-Methyl-aniline	-١٠٠٢.٩٣٥٢	-٣٣٧.٧١٢٤٥	-٣٩٨.٤٤٨	٠.٠٢١٧٣٣٩٨٣٣٢	٠.٠٩٤٨٨٦٩٣٦٢	٠.٠٤٦٤٨٧٨٩٢٩٢
٥	٢-Ethoxy-aniline	-١١١٥.٩١٨١	-٤٥٠.٦٨٧٧١	-٥١١.٤٢٢	٠.٠٢٥٣٧٥١٣٩٦٨	٠.١٠٦١٣٦٦٩٩٤٩	٠.٠٥٩٠٢٤٢٣٧٧٤
٦	٢-Methoxy-aniline	-١٠٧٧.٠٩٩٢	-٤١١.٨٦٦٩١	-٤٧٢.٥٩٩	٠.٠٢٣٥١٤٩٢١٨٠	٠.١٠٦٢.٠٥٦٤٦١	٠.٠٦١٤٠٣٤٢٤٦٦

All energies are in hartree, a: energies are corrected for ZPE and BSSE.

Conclusion

Modeling and quantum chemical studies are useful and powerful means for selecting suitable inhibitor by realizing the inhibition mechanism of inhibitors.

A combination of $E_{inhibitor\text{-}Cu}$, $E_{inhibitor\text{-}Cl^-}$ and $E_{inhibitor\text{-}H_٢O+}$ in a linear model can satisfactorily describe experimental inhibition imposed by Ortho-aniline derivatives on copper metal in HCl solution.

It is realized that corrosion inhibition is a complicated chemical phenomena and there is not any reasonable relation between the experimental inhibition efficiency with parameters such as E_{homo}, E_{lumo}, gap ($E_{lumo} - E_{homo}$), dipole moment and polarizability.

References

[١] R.M. Issa, M.K. Awad, F.M. Atlam, Appl. Surf. Sci, ٢٠٠٨, ٢٥٥, ٢٤٣٣–٢٤٤١.

[٢] E.S.H. El Ashry, S.A. Senior, Corros. Sci, ٢٠١١, ٥٣, ١٠٢٥–١٠٣٤.

[٣] M. Mousavi , M. Mohammadalizadeh , A. Khosravan, Corros. Sci, ٢٠١١, ٥٣, ٣٠٨٦–٣٠٩١.

[٤] K.F. Khaled, N. Hacherman, Electrochimica Acta, ٢٠٠٤, ٤٩, ٤٨٥–٤٩٥.

Tributyl(3-sulfopropyl)phosphonium hydrogen sulfate as a robust ionic liquid catalyst for the synthesis of quinoline-4-carboxylic acid derivatives *via* an anomeric based oxidation mechanism

Meysam Yarie, Mahdi Saeidi-Rad, Mohammad Ali Zolfigol

Department of Organic Chemistry, Faculty of Chemistry, Bu-Ali Sina University, Hamedan, Iran. E-mail: mzolfigol@yahoo.com; Fax: +98 8138257407; Tel: +98 8138282807

Introduction

Due to the biological activities and pharmaceutical versatilities, the chemistry and synthesis of quinoline derivatives have been widely investigated. They have been applied as antagonists, analgesic agents, $5HT_3$, NK-3 receptors, and also some natural products bearing these active compounds [1, 2]. On the other hand, ionic liquids (ILs) have found their influential roles as ubiquitous compounds for different applications such as catalyst, reagent and solvent systems and due to their capabilities in the domain of eco-compatible systems, the chemistry of them have been well documented [3]. Herein, we wish to report tributyl(3-sulfopropyl)phosphonium hydrogen sulfate as a task-specific catalyst for the synthesis of quinoline-4-carboxylic acids *via* anomeric based oxidation mechanisem.

Experimentals

To a mixture of aryl aldehydes (1 mmol), aniline derivatives (1 mmol) and pyruvic acid (1 mmol, 0.09 g), tributyl(3-sulfopropyl)phosphonium hydrogen sulfate was added as ionic liquid catalyst and the mixture subjected to the reaction in an oil path at 70 $^{\circ}$C . After completion of the reactions as monitored by TLC, the reaction mixture was quenched to room temperature. In order to separate of the catalyst, distillated water added to the mixture and stirred foe a few minutes and decanted. Finally, the crud products were purified by recrystallization from ethanol.

Results and Discussion

After structural verification of the catalyst using suitable skills such as FT-IR, ^{1}H NMR, ^{13}C NMR, the catalytic applicability of the prepared tributyl(3-sulfopropyl)phosphonium hydrogen sulfate as ionic liquid was successfully explored in the synthesis of quinoline-4-carboxylic acid derivatives through the reaction of aryl aldehydes , anilines and pyruvic acid under mild and

solvent free conditions as portrayed in Scheme 1. The authors believe that the final step of the mechanistic pathway proceed *via* an anomeric based oxidation mechanism [4].
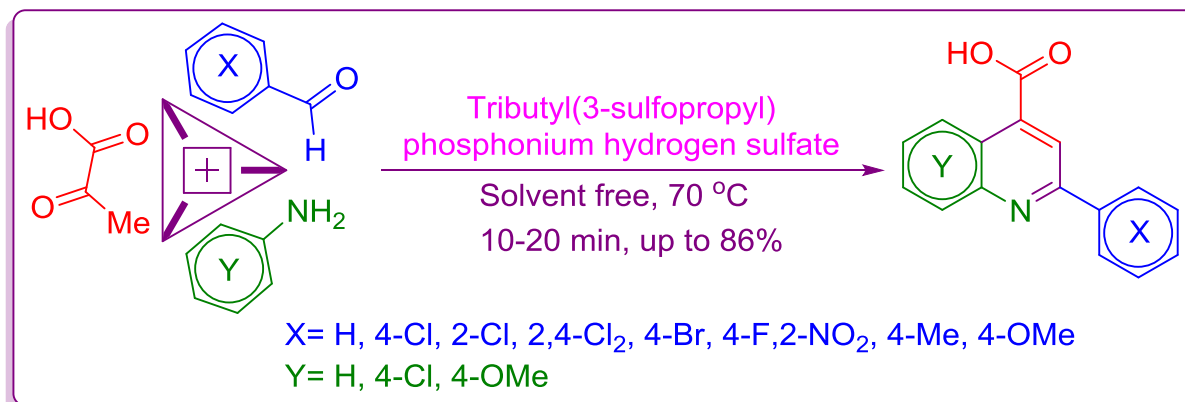
Scheme 1: Preparation of quinoline-4-carboxylic acid derivatives

Conclusion

In summary, in this investigation the design and synthesis of a novel ionic liquid namely tributyl(3-sulfopropyl)phosphonium hydrogen sulfate was explored. The structural verification of the catalyst was made by using techniques such as FT-IR, ^{1}H NMR, ^{13}C NMR. Afterwards, the catalytic applicability of the prepared ionic liquid was studied in the synthesis of quinoline-4-carboxylic acid derivatives under mild and solvent free conditions.

References

[1] L. M. Wang, L. Hu, H. J. Chen, Y. Y. Sui, W. Shen, *J. Fluorine Chem.* **2009**, *130*, 406.

[2] I. Bennacef, C. Perrio, M.C. Lasne, L. Barre, *J. Org. Chem.* **2007**, *72*, 2161.

[3] M. Yarie, M. A. Zolfigol, Y. Bayat, A. Asgari, D. A. Alonso and A. Khoshnood, *RSC Adv.*, **2016**, *6*, 82842

[4] M. Kiafar, M. A. Zolfigol, M. Yarie, A. A. Taherpour, *RSC Adv.* **2016**, *6*, 102280 and cited references within.

Photocatalytic activities of Cu_2O/TiO_2 Nanoparticles in degradation of methylene blue under visible light

Mona Hosseini-Sarvari[a]*, Fattaneh Jafari[a]

[a] Department of Chemistry, Faculty of Sciences, Shiraz University

Email address : hossaini@shirazu.ac.ir , fj70jafari@yahoo.com

Introduction : Environment problems related to the remediation of hazardous wastes and contaminated waters is a serious problem faced by most of the developing and industrialized countries in the world [1-3]. Dyes play a vital role in various branches of the dyeing and textile industries. Over 100 000 commercially available synthetic dyes are the most frequently used dyes in such industries.[4] In the past decades many methods have been developed for the removal of chemical pollutants, such as membrane filtration, ultrasonic degradation, biodegradation, chemical oxidation, adsorption, photocatalysis, etc. The adsorption and photocatalysis are promising metods for the removal of chemical pollutants which are difficult to biodegrade [5].

Experimentals: In this study we synthesized TiO_2/Cu_2O photocatalyst nanoparticles. TiO_2/Cu_2O composite oxides were prepared by the following method. Cupric acetate was dissolved in distilled water, followed by the addition of PEG 400 under vigorous stirring. Afterward tetrabutyl titanate was added to the solution of cupric acetate. A white precipitate was produced during the mixing. Then, NaOH and hydrazine were added dripwise into the above slurry under vigorous stirring. The precipitate was filtered, washed with distilled water and dry.

Results and Discussion: In this work, the visible light induced photocatalytic activities of the synthesized TiO_2/Cu_2O were evaluated by photocatalytic degradation of MB as a model contaminant. The change concentration of MB monitored by the UV–visible adsorption of 3.0 mL sample taken from the solution every 30 min. The TiO_2/Cu_2O can efficiently photo degrades MB under fluorescence lamp illumination after 120 min. For comparison, photo degrades performance of P25 and Cu_2O nanoparticles also included. It can be seen that pure P25 and Cu_2O nanoparticles displays the lowest photocatalytic degradation rate of MB under visible light irradiation due to its wide bandgap and prepared TiO_2–Cu_2O p–n heterojunction particles were quite effective.

Fig 1. Schematic of degradation of MB

Table 1. some representative data of the condition for degradation of MB

t	Abs.	C.
0	0/116	4/64
1	0/005	0/2
30	0/001	0/04
60	0/001	0/04
90	0/001	0/04
120	0	0

t = time (min) ,Abs. = Absorption , C = concentration

Conclusion: TiO_2–Cu_2O were prepared by the hydrolysis of titanium butoxide and reduction of copper acetate with hydrazine. The formation of composite oxides TiO_2–Cu_2O significantly enhanced the photocatalytic activity for the degradation of MB under visible lights.

 References:
 [1] Y.G. Adewuyi. *Environmental Science & Technology*, **2005**, *39*, 8557–8570.

[2] S. Annamalai; M. Santhanam; M. Sundaram; M.P. Curras. *Chemosphere*, **2014**, *117*, 673–678.

[3] J. Theron; J.A. Walker; T.E. Cloete. *Critical Reviews in Microbiology*, **2008**, *34*, 43-69.

[4] A. Ajmal; I. Majeed; R.N. Malik; H. Idriss; M.A. Nadeem. *The Royal Society of Chemistry Advances*, **2014**, *4*, 37003-37026.

[5] X. Fei; F. Li; L. Cao; G. Jia; M. Zhang. *Materials Science in Semiconductor Processing*, **2015**, *33*, 9–15.

Electronic Structure of Planar Tetra Coordinate Carbon

Afshan Mohajeri, Azade Yeganeh Jabri

Department of Chemistry, College of Sciences, Shiraz University, Shiraz, Iran

Email: amohajeri@shirazu.ac.ir

Introduction

Explorations of planar tetra coordinate carbon (ptC) began in 1968[1]. C_2Al_4 species, which is the most important ptC compound leads to a new type of ptC molecules, $C_2Al_4E_8$ (E = H, CH_3, NH_2, OH, F, Cl.) [2]. The inherent potential applications of these compound as hydrogen storage motivates us to study the electronic properties of $C_2Al_4E_8$ with E = CH_3, NH_2, OH. We are aiming to assess various electronic and magnetic properties for these systems and to investigate the effect of E group on the electronic structure of C_2Al_4.

Computational Method

The optimized geometric structures with all real frequencies of $C_2Al_4E_8$ (E =OH, CH_3, NH_2), obtained at the B3LYP/6-311G (d) level, were used. The considered method and basis set have been also used to calculate NMR parameters based on the gauge independent atomic orbital (GIAO) approach [3]. Moreover, we have performed the TD-DFT (B3LYP/6-31G(d)) calculation to obtain the excited state of considered species.

Results and Discussion

Table 1 is presents the energetic properties including ionization potential (IP), electron affinity (EA), chemical hardness (η) and mean polarizability (α) for the considered compounds which is shown in Figure 1. We have seen the C_2Al_4-CH_3 has the highest chemical hardness suggesting more reactivity as compared C_2Al_4-NH_2 and C_2Al_4-OH. Besides the highest mean polarizability has belonged C_2Al_4-CH_3.   On the other hand, we have investigated the magnetic the properties of $C_2Al_4E_8$ by calculating chemical shielding (CS) parameters at middle of C-C bond. The NICS of $C_2Al_4E_8$ are all negative indicating the electron delocalization in $C_2Al_4E_8$ compounds. In order to study compound in UV/VIS region, TD-DFT has been carried out and the excitation energy obtained for each compound which they are reported in table 1. C_2Al_4-OH shows obviously the greatest energy for exciting in this region
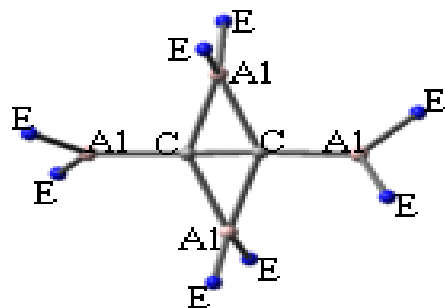
Figure 1: optimized structure C_2Al_4-E_8 (E = NH_2, OH, CH_3).

Table1: Electronic and Magnetic properties of different compound $C_2Al_4E_8$

	I_p(ev)	E_A(ev)	η(ev)	$<\alpha>A^3$	NICS(ppm)	Excited energy(eV)
C_2Al_4	-159.043	-81.4579	77.58534	11.496962	-7.8138	3.7916
C_2Al_4_Ch_3	-153.882	-30.3588	123.5234	18.304286	-37.6138	4.1131
C_2Al_4_NH_2	-124.59	-29.0482	95.54149	16.062609	-18.0871	3.8237
C_2Al_4_OH	-152.631	-44.235	108.3959	14.157787	-21.6171	4.3278

Conclusion

We theoretically described the incorporation of the central planar tetracoordinate molecules C_2Al_4. C_2Al_4- NH_2 exhibits the highest mean polarizability. Consequently, the present study is expected to enrich the knowledge of the planar tetracoordinate carbon chemistry and convinced us for possible use of these molecules as building blocks of linear and planar large molecules.

References

1. Xue-Feng Zhao, Yan-Bo Wu, Journal of Computational Chemistry, 37 (2016) 261–269
2. Jin-Liang Jiang, Yan-Bo Wu, Phys. Chem. Chem. Phys. , 12, 2010, 58–61
3. K. wolinski, J. F. Hilton, P. Pulary, j. Am. Chem. Soc. 112(1990) 8251

Fe$_3$O$_4$@SiO$_2$@DBA-SO$_3$H as an efficient and reusable catalyst for the synthesis of spiropyrans

Mostafa rajabi-salek, Mohammad Ali Zolfigol *, Ehsan Noroozizadeh, Mahmoud Zarei

Faculty of Chemistry, Bu-Ali Sina University, Hamedan, 6517838683, I. R.Iran, mzolfigol@yahoo.com & zolfi@basu.ac.ir

****

Abstract:

Spiropyrans including oxindoles are an important class of attractive heterocyclic compounds with useful biological properties such as spasmolitic, diuretic, anticoagulant, anticancer, and antianaphylactic activities [1–4]. Various catalysts have been applied for this transformation, including sodium stearate [4], sulfated choline based heteropolyanion[5], protic guanidinium ionic liquid [6], 4-dimethylaminopyridine [7], [BMIm]BF4, SBA-Pr-SO$_3$H, (SB-DBU)Cl [8], carbon-sulfonic acid [9], polyethylene glycol (PEG)-stabilized Ni nanoparticles [10]. Thus, considerable attention has been focused on the development of new methods for the synthesis of these compounds. Herein, we have utilized Fe$_3$O$_4$@SiO$_2$@DBA-SO$_3$H as an efficient and nano magnetic catalyst for the preparation of spiropyran derivatives (**Scheme 1**).
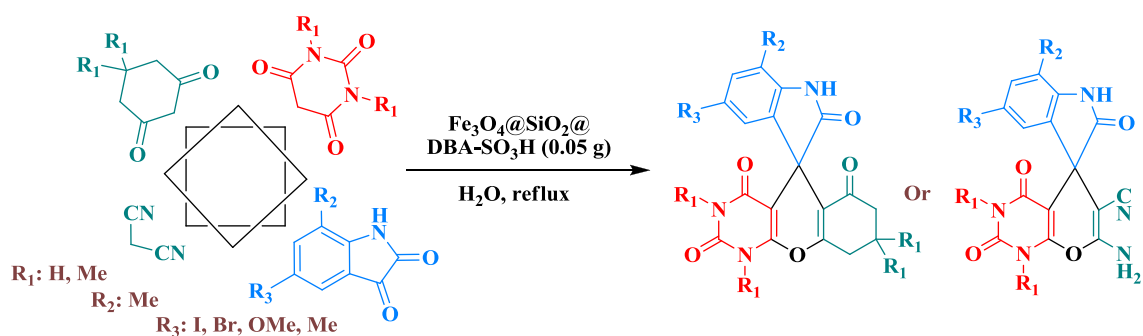
Scheme 1: The preparation of spiropyrans by the reaction of isatin and barbituric acid derivatives with malononitrile or 1, 3-dicarbonyl compounds using Fe$_3$O$_4$@SiO$_2$@DBA-SO$_3$H.
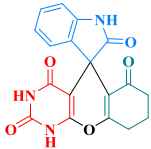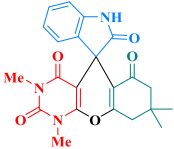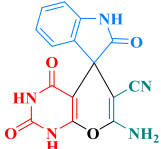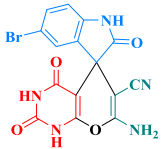
Experimentals

A mixture of isatin (1 mmol, 0.147 g) and barbituric acids (1 mmol, 0.128 g) derivatives, 1, 3-dicarbonylcompounds (1 mmol) or malononitrile (1 mmol, 0.067 g), Fe$_3$O$_4$@SiO$_2$@DBA-SO$_3$H (0.05 g) and H$_2$O (5 mL) was added to in 25 mL round-bottomed flask connected to a reflux condenser, and stirred under reflux conditions. After completion of the reaction, as monitored by TLC, the reaction mixture was cooled to room temperature. Methanol (20 mL) was added, stirred and refluxed for 30 min. Then, the resulting mixture was magnet for the separation of the catalyst from the product and remaining starting materials. After the separation of catalyst from the reaction mixture, methanol was removed and the solid residue (crude product) was triturated by a mixture of ethanol and water (9/1) to give the pure product.

Results and Discussion

To assess the efficiency and the scope of the catalyst in the preparation of spiropyrans, the condensation of 1,3-dicarbonyl compounds or malononitrile with isatin and barbituric acid

was examined in the presence of described catalyst at reflux condition. The corresponding results are displayed in below.

Entry	Products	Time (min)	Yielda (%)	M.p. °C (Lit.)
1		30	94	>300(>300)[11]
2		35	93	>300(>300)[11]
3		**35**	**96**	(276-278)[11]
4		**30**	**98**	(258-260)[11]

Conclusion

In summary, we have prepared $Fe_3O_4@SiO_2@DBA-SO_3H$ as a green, magnetic and nanostructured heterogeneous catalyst, and fully characterized by using FT-IR, XRD, TGA, DTG, SEM, EDX techniques. $Fe_3O_4@SiO_2@DBA-SO_3H$ was successfully tested for the multi-component condensation reaction between isatins barbituric acids, 1,3-dicarbonyl compounds, and malononitrile under reflux conditions to give spiropyrans. Short reaction time, high yield and reusability of the catalyst are some advantages of described research.

References

[1] (a) J. Skommer, D. Wlod kowic, M. Matto, M. Eray, J. Pelkonen, Leuk. Res, **2006**, 30,322–331(b) Y. Zou, Y. Hu, H. Liu, D. Shi, *ACS Comb. Sci*, **2012**, 14, 38.

[2] N. Yu, J.M. Aramini, M.W. Germann, Z. Huang, *Tetrahedron Lett*, **2000**,41, 6993–6996.

[3] L. Bonsignore, G. Loy, D. Secci, A. Calignano, *Eur. J. Med. Chem*, **1993**, 28, 517–520.

[4] L. M. Wang, N. Jiao, J. Qiu, J.-J. Yu, J.-Q. Liu, F.-L. Guo, Y. Liu, *Tetrahedron*, **2010**, 66, 339–343.

[5] S.P. Satasia, P.N. Kalaria, J.R. Avalani, D.K. Raval, *Tetrahedron*, **2014**, 70, 5763–5767.

[6] S.M. Baghbanian, M. Tajbakhsh, M. Farhang, *C.R. Chim*, **2014**, 17, 1160–1164.

[7]M. Zakeri, M.M. Nasef, E. Abouzari-Lotf, A. Moharami, M.M. Heravi, *J. Ind. Eng. Chem*, **2015**, 29, 273281.

[8] A. Hasaninejad, N. Golzar, M. Beyrati, A. Zare, M.M. Doroodmand, *J. Mol. Catal. A: Chem*, **2013**, 372, 137-150

[9] B.M. Rao, G.N. Reddy, T.V. Reddy, B.L.A.P. Devi, R.B.N. Prasad, J.S. Yadav, B.V.S. Reddy, *Tetrahedron Lett*, **2013**, 54, 2466–2471.

[10] J.M. Khurana, S. Yadav, *Aust. J. Chem*, **2012**, 65, 314–319.

[11] (a) A. R. Moosavi-Zare , M. A. Zolfigol, E. Noroozizadeh, R. salehi Moratab, M. Zarei, *J. Mol. Catal. A: Chem,* **2016**, 420, 246–253; (B) N. Khodabakhsh, P. Abolpour, *Monatsh Chem*, **2015**,146.4, 683-690.

Synthesis of some novel benzotriazolo-β-lactams and their antimalarial activities

Malihe Aye[a], Aliasghar Jarrahpour[a*], Véronique Sinou[b], Christine Latour[b], Jean Michel Brunel[c]

[a] Department of Chemistry, College of Sciences, Shiraz University, Shiraz 71946-84795, Iran.
[b] Aix-Marseille Université, UMR-MD3 Relation hôte-parasites, Physiopathologie & Pharmacologie, Faculté de pharmacie, Bd Jean Moulin, F-13385 Marseille, France.
[c] Centre de Recherche en Cancerologie de Marseille (CRCM), CNRS, UMR7258, Institut Paoli Calmettes, Aix-Marseille Université , UM 105, Inserm, U1068, Faculté de Pharmacie, 27 Bd Jean Moulin, 13385 Marseille Cedex 05, France.
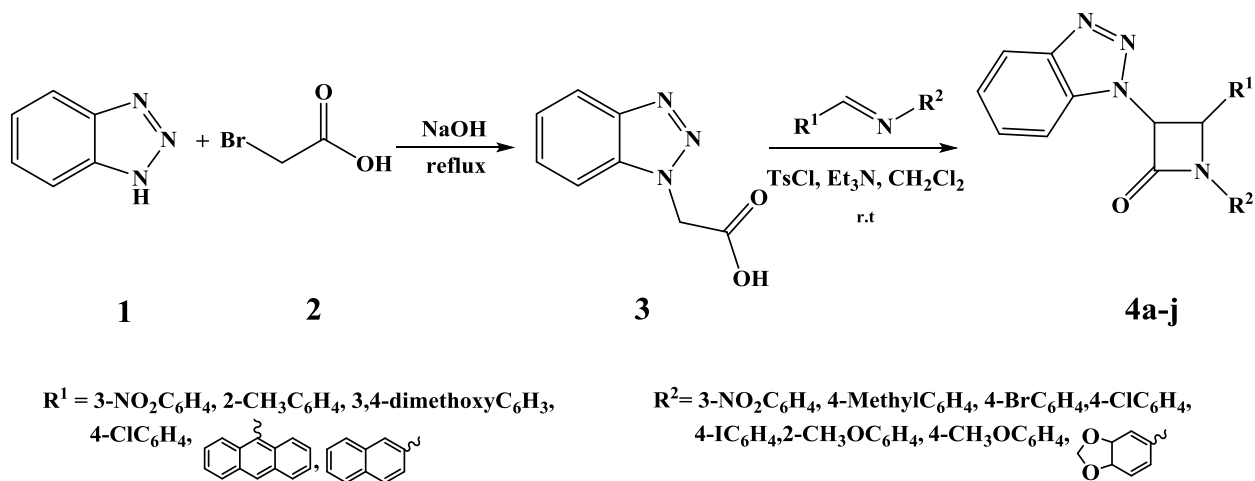Email: jarrah@susc.ac.ir; aliasghar6683@yahoo.com.

Introduction: 2-Azetidinones, commonly known as β-lactams with four member heterocyclic compound are very important class of compounds possessing wide range of biological activities that aimed to evaluate new products that possess interesting biological activities [1]. New research has been focused on the synthesis and modification of β-lactam ring to obtain compounds with diverse pharmacological activities [2,3]. In continuation of our research program aimed at developing new biologically active compounds, here we report the synthesis, characterization and biological investigation of new series of benzotriazolo-β-lactams.

Experimental: General procedure for the synthesis of benzotriazolo-*β*-lactams 4a-j. A mixture of 2-(1H-benzo[d][1,2,3]triazol-1-yl)acetic acid **3** (1.5 mmol) [4], in the presence of Et_3N (5.0 mmol), TsCl (1.5 mmol) and imine (1.0 mmol) was stirred in dry CH_2Cl_2 at room temperature. After 24 h, the mixture was washed with HCl 1 N, saturated $NaHCO_3$ and brine, dried over sodium sulfate and the solvent was evaporated to give the crude products. Then benzotriazolo-*β*-lactams **4a-j** were purified by recrystallization from EtOAc:n-Hexane (1:1).

Results and Discussion:

Chemistry: 1H-benzo[d][1,2,3]triazole **1** was chosen as the starting material for these studies. It was converted into 2-(1H-benzo[d][1,2,3]triazol-1-yl)acetic acid **3** by refluxing a mixture of 2-bromoacetic acid in the presence of NaOH in water. Subsequent reaction of 2-(1H-benzo[d][1,2,3]triazol-1-yl)acetic acid **3** in the presence of triethylamine, tosyl chloride and imine afforded β-lactams **4a-j** (Scheme 1).

R^1 = 3-$NO_2C_6H_4$, 2-$CH_3C_6H_4$, 3,4-dimethoxyC_6H_3, 4-ClC_6H_4,

R^2 = 3-$NO_2C_6H_4$, 4-MethylC_6H_4, 4-BrC_6H_4, 4-ClC_6H_4, 4-IC_6H_4, 2-$CH_3OC_6H_4$, 4-$CH_3OC_6H_4$,

Scheme 1. Synthesis of new benzotriazolo-β-lactams **4a-j**.

In all cases, TLC monitoring confirmed the presence of the expected new products. The structures of the cycloadducts have been fully characterized by spectral analyses. The IR spectra of these compounds showed absorption bands due to the carbonyl group at 1735–1751 cm^{-1}. For example, ^{1}H-NMR spectrum of **4a** exhibited the β-lactam ring protons H-3 and H-4 as two doublets at 5.67 and 5.87 ppm.

Biological activities: All of these newly synthesized β-lactam derivatives were evaluated for their biological activitie. Moderate to good antimalarial activities have been obtained against chloroquine resistant *P. falciparum K1* strain as outlined in **Table 1** with IC$_{50}$ varying from 5.56 to up to 25.65 µM. β-lactam benzotriazole hybrid **4a** showed best result for antimalarial activities in comparison of standard antimalarial chloroquine.

Table 1. Antimalarial activities of β-lactam benzotriazole hybrids **4a-j**.

Compound	IC$_{50}$ (µM) *P. falciparum* K1	Compound	IC$_{50}$ (µM) *P. falciparum* K1
Chloroquine	1.02	**4f**	10.68
4a	5.56	**4g**	11.44
4b	9.25	**4h**	14.40
4c	9.73	**4i**	14.64
4d	10.71	**4j**	25.65
4e	10.79		

Conclusion: In conclusion, the present work describes the synthesis of 10 new benzotriazolo-β-lactams in moderate to good yields. All newly synthesized β-lactams were characterized by FT-IR, ^{1}H NMR, ^{13}C NMR, mass spectra, and elemental analyses. All the compounds were evaluated for their *in vitro* antimalarial activities against chloroquine resistant *P. falciparum* K1 strain. the moderate to good antimalarial activities encountered.

Refrences:

[1]. Vatmurge,N. S.; Hazra, B. G.; Pore, V. S.; Shirazi, F.; Chavan, P. S.; Deshpande, M V. *Bioorg. Med. Chem. Lett.* **2008**, *18*, 2043–2047.

[2]. Mehta, P. D.; Sengar, N.P.S.; Pathak, A.K. *Eur. J. Med. Chem.* **2010**, *45*, 5541-5560.

[3]. Dive, G.; Bouillon, C.; Aline, S.; Valet, B; Verlaine, O.; Sauvage, E.; Brynaert,J. M. *Eur. J. Med. Chem.* **2013**, *64*, 365-376.

[4]. Chen, X.; Liu, C.; Wang, J.; Lia, Y. *J. Heterocyclic Chem.* **2010**, *47*, 1225-1229.

Three component reaction of 2-mercaptobenzimidazole, Acetylenic ester and triphenylphosphine: Different amount of Pph₃ obtained different structures of products

ElhamAfsari[a] **andHamid Reza Safaei**[a,*]

[b]*Department of Chemistry, Shiraz Branch, Islamic Azad University, Shiraz, Iran*

E-mail address:hrsafaei@yahoo.com

****

Abstract: The trend of reaction between 2-mercaptobenimidazole and acetylnic esters in the presence of different amount of triphenylphosphine was investigated. The newly synthesized compounds were systematically characterized by IR, ^{1}H NMR, ^{13}C NMR and elemental analysis.

Introduction: Phosphorous ylides are reactive systems which take part in many reactions of value in organic synthesis. especially the synthesisof naturally occurring products with biological and pharmacological activity over the last few years, several methods have been developed for preparation ofphosphorous ylides. recently, these ylides are prepared by treatment of phosphonium salts which is produced by Micheal addition of phosphorus nucleophiles to active olefins followed by nucleophiles attack. Recently, Maghsoodlou has reported tree-component reaction of 2-mercaptobenzimidazol and acetylenic estersin the presence of 100 mole% P(ph)₃[1]to obtain phosphorus ylide**1**. Moreover, Trost from university of Stanford synthesized a series of novel compounds through Nucleophilic α-addition to alkynoates. In these unprecedented reactions a 1:1 mixture of ethyl propiolate and phthalimidewere interacted at 105 °C in the presence of10 mol % triphenylphosphine. The reaction was produced 1:1 adduct **2** in 95% yield [2].
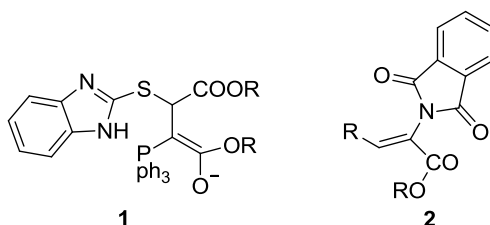

Beside,2-mercaptobenzimidazole derivatives, are one of the most important derivatives of benzimidazoleexhibited a wide variety of interesting biological activities such as antimicrobial, antihistamine, neutropic and analgesic activities. In recent years, the field of anticonvulsant drug development has become quite dynamic, affording many promising research oportunities.Considering the above reports and as a part of our interest [3]we encouraged to investigate the route of the reaction of 2-mercaptobenzimidazol and acetylenicesters in the presence of different amount of triphenylphosphyne.

Experimental: To a magnetically stirred solution of 2-mercaptobenzimidazol (1 mmol), DMAD or methylpropiolate (1 mmol) different amounts of triphenylphosphine 1 mmol, 0.1 mmole and absence of Pph₃,were addedin solvent or neat and catalyst free conditions,separately. The reaction mixture was stirred for proper times and after completion of the reaction the crud

products were dried and the residues were purified via crystallization orcolumn chromatography. The chemical structures of solid products were determined by instrumental analysis.
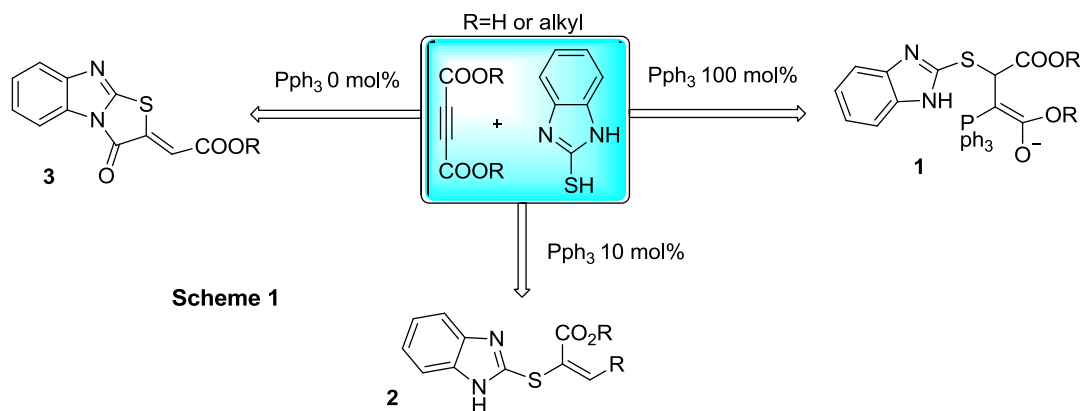
Scheme 1

Results and Discussions: On the basis of NMR data and comparison ofwe found that the amount of triphenylphosphine has played critical role on structures of obtained products (Scheme 1). When 2-mercaptobenzimidazole was reacted with acetylenic methyl ester in the absence of triphenylphosphine the product **3** was obtained in 95% yield under neat condition. The ^{1}H NMR spectrum of product **3**was shown one sharp singled at δ(H) 4.1 related to methyl group and multipletsat δ(H) 7.0 – 8.6 corresponding to four aromatic H-atoms and one olefinic hydrogen.
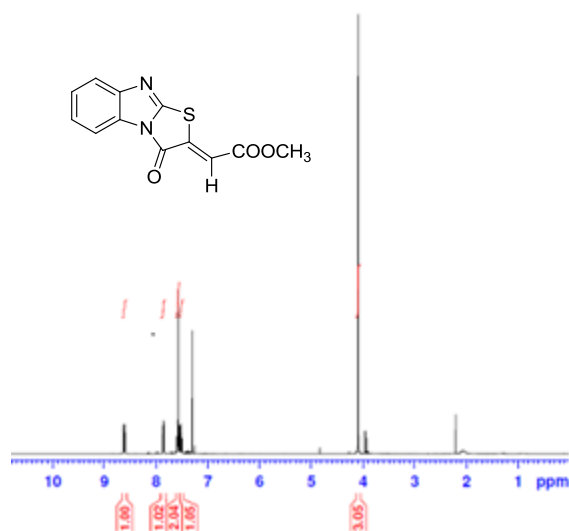
conclusion: We successful changed the reaction pathway in order to achieve different products by different amount of Ph$_3$P in three-component reaction.

References:

3) A.Shaabani,H.R.Safaei, K.Hamyari, A. Moghim, *J. Chem. Research.,***2001**, 192–194.;H.R. Safaei,L Rohani*J of bioprocessing and chemeng*, **2015**, 2(2), 1-7.

1) M.T.Maghsoodlou, R.Heyari, S.M.HabibiKhorassani, M.K. Rofouei, M. Nassiri,E.Mosaddegh, A.Hassankhani*Journal of Sulfur Chemistry*Vol. 27, No. 4, August **2006**, 341–346

2) B.M. Trost, G.R. Dake*J. Am. Chem. Soc.* **1997**, 119, 7595-7596

Synthesis of Some New Diastereoselective Quinoline β-lactam Hybrids

Aliasghar Jarrahpour[a,*,] Zahra Liravi[a] , Javad Ameri Rad[a]

[a]Department of Chemistry, College of Sciences, Shiraz University, Shiraz 71946-84-795, Iran

Email address: jarrah@susc.ac.ir, aliasghar6683@yahoo.com

Introduction: β-Lactam antibiotics are a broad class of antibiotics contains a β-lactam ring in their molecular structures. They work by inhibing cell wall biosynthesis in bacterial organisms and are the most widely used group of antibiotics [1-3]. Many other interesting biological properties, such as cholesterol absorption inhibitors, human cytomegalovirus protease inhibitors, thrombin inhibitors, anti-hyperglycemic, anti-tumor, anti-HIV, anti-inflammatory, analgesic activities, antifungal, antimalarial activities and serine-dependent enzyme inhibitors, have been highlighted [4]. It is known that quinolines and its derivatives exhibit extensively biological and pharmacological activities, thus considerable efforts have been devoted to design and synthesize functional quinoline derivatives over the past decades [5].

Experimental: General procedure for the synthesis of quinolin β-lactam conjugates 4a-j

A mixture of 2-oxo-1,2-dihydroquinoline-3-carbaldehyde **1** (1mmol) with 3-bromoprop-1-ene **2** (1.5mmol) was stirred magnetically in DMF for 24h. Then compound **3** reacted with various aromatic amines to afford Schiff bases. Finally a mixture of Schiff bases (1.00 mmol), triethylamine (5.00 mmol), substituted acetic acid (1.50 mmol) and tosyl chloride (1.50 mmol) in dry CH_2Cl_2 (15 mL) was stirred at room temperature for several hours. Then it was washed with HCl 1N (20 mL), saturated $NaHCO_3$ (20 mL) and brine (20 mL). The organic layer was dried (Na_2SO_4), filtered and the solvent was evaporated to give the crude products **4a-j**. Crude conjugates **4a-j** were purified by recrystallization from acetone (Scheme 1).

Results and Discussion: The synthesis of β-lactam hybrids **4a-j** was achieved according to the outlined procedure in Scheme 1. A mixture of Schiff base, triethylamine, substituted acetic acid and tosyl chloride in dry CH_2Cl_2 was stirred at room temperature overnight to give β-lactams **4a-j** by the ketene–imine [2+2] cycloaddition reaction (Staudinger reaction). Then we observed our products are *cis* stereoisomer. The stereochemistry of β-lactams was either *cis* or *trans* due to the coupling constants of H-3 and H-4 of the β-lactam ring. The *cis* geometry was assigned for the $^3J_{3,4}> 3$ Hz and the *trans* geometry for those $^3J_{3,4}< 3$ Hz [6]. The structure of the products was characterized by IR and ^{1}H and ^{13}C NMR spectra. The ^{1}H NMR spectrum of **4a** exhibited two doublets at $\delta = 5.61$ and 6.00 ppm ($^3J_{HH}= 4.75$ Hz) for vicinal methine protons along with a multiplet at $\delta = 6.83-7.73$ ppm for phenyl ring protons. The ^{1}H-decoupled ^{13}C NMR spectrum of **4a** showed 21 distinct resonances in agreement with the suggested structure. Characteristic ^{13}C NMR signals were shown due to carbonyl group at $\delta = 160.7$ ppm and signals at $\delta = 68.1$ and 70.2 ppm for CH groups. Also the IR spectrum of compound **4a** indicated a characteristic absorption band of a β-lactam carbonyl moiety at 1751 cm^{-1}.
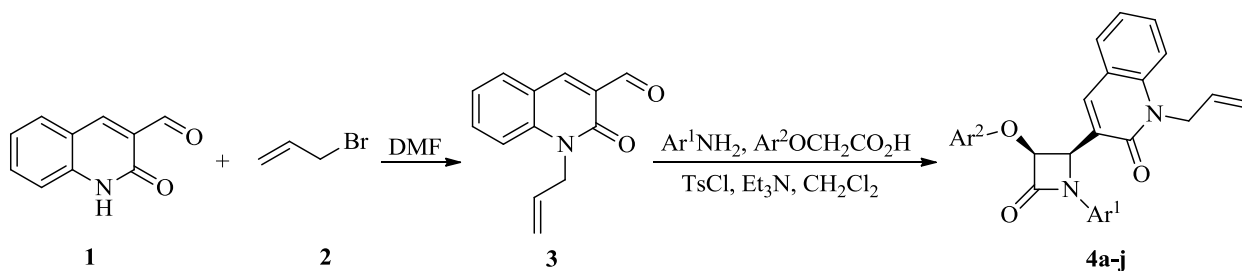
Scheme 1: synthesis of new quinolin β-lactam hybrids **4a-j**

Conclusion: A series of novel quinolone β-lactam conjugates were synthesized via the [2 + 2] ketene imine cycloaddition reaction. All of the synthesized β-lactam hybrids were *cis* stereoisomers. These β-lactams are now under process to investigate their biological activity such as anticancer, antifungal, antimalarial, and antibacterial, that it will be reported in due course. This research will offer many additional opportunities to use β-lactams in the synthesis of new compounds.

References:

[1]. Saitoh, T.; Shibayama, T. *J. Hazard. Mater*. **2016**, *317*, 677–685.
[2]. Jarrahpour, A.; Shirvani. P.; Sinou, V.; Latour, C.; Brunel, J. M. *Med. Chem. Res*. **2016**, *25*, 149-162.
[3]. Jarrahpour. A.; Nazari, M. *Iran. J. Sci. Technol. Trans A. Sci*. **2015**, *39*, 259-265.
[4]. Ebrahimi, E.; Jarrahpour, A.; Heidari, N.; Sinou, V.; Latour, C.; Brunel, J. M.; Zolghadr, A. R.; Turos, E. *Med. Chem. Res*. **2016**, *25*, 247-262.
[5]. Zhang, Y.; Fang, Y.; Liang, H.; Wang, H.; Hu, K.; Liu, X.; Yi Yan Peng, X. *Bioorg. Med. Chem. Lett*. **2013**, *23*, 107–111.
[6]. Jarrahpour, A.; Aye, M.; Sinou, V.; Latour, C.; Brunel, J. M. *J. Iran. Chem. Soc*. **2015**, *12*, 2083-2092.

Introduction and investigation of electronicstructure of N-ethyl-N-methylethanamine [1,9](C_{60}-I_h)[5,6]fullerene as HIV protease inhibitor

Sara Fakhraee . Najme Solimani

Email: Fakhraee@pnu.ac.ir

Abstract: In this study a new HIV protease inhibitor has been introduced based on the substituted fullerene structure. The chemical and electronic properties of this drug have been investigated using atoms in molecules theory. The topological properties of electron density for the bond critical points involved in the areas with the greatest impact of substitution have been analyzed to compare with fullerene. The results approved the deformation of electron density on substituted fullerene based drug causes the binding affinity of HIV inhibitors.

Introduction:
HIV protease inhibition is one of the most effective methods of preventing HIV disease. The molecules of substituted fullerenes occupy the HIV protease active sites and therefore they have been used as effective HIV protease inhibitor. These compounds due to their polar interactions with harmful or helpful enzymes in the body, work better than pure fullerene. The substituted fullerenes are non-toxic to inhibit viruses affecting DNA and RNA[1]. In this study the N-ethyl-N-methylethanamine [1,9](C_{60}-I_h)[5,6]fullerene has been introduced as an HIV-inhibitor and compared with C_{60} using atoms in molecules theory(AIM) [2].

Methods/experimental: In this study the N-ethyl-N-methylethanamine substitution has been replaced on C_{60}. All calculations including geometry optimization and frequency calculations have been performed at the B97D/6-311++g** [3] extensive density functional level of theory using Gaussian09[4] package. Then, atoms in molecules (AIM) analyses have been applied at the same level of theory to analyze the wave function of the molecule and determine the nature of bonds using AIM2000[5] program. The optimized structure and AIM molecular graph of the drug have been presented in Fig. 1
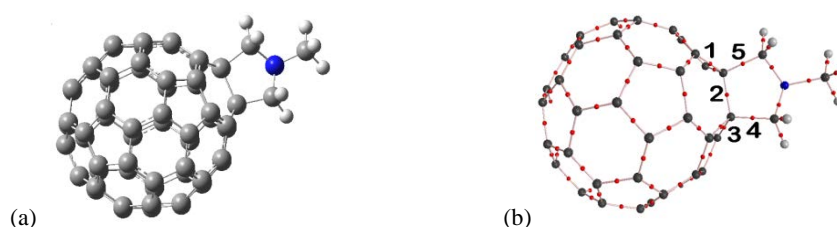

Fig. 1: (a) Optimized structure of the substituted fullerene based drug. (b) The AIM graph of the drug, including the bond critical points and bond paths.

Result and Discussion:

Table 1 represents the AIM descriptors of bond critical points (BCPs) numbered as 1-5 in Fig. 1, including: the electron density, $\rho(r)$, laplacian of electron density, $\nabla^2\rho(r)$, electronic potential energy, V(r), electronic kinetic energy G(r), the total Hamiltonian energy, H(r).

Table 1: The AIM descriptors for the BCPs 1-5 in fullerene based drug of Fig. 1.

BCP	ρ	$\nabla^2\rho$	$G(r)$	$V(r)$	$H(r)$
1	0.243	-0.532	0.060	-0.253	-0.193
2	0.204	-0.356	0.048	-0.185	-0.137
3	0.242	-0.528	0.060	-0.252	-0192
4	0.229	-0.476	0.054	-0.228	-0.174
5	0.229	-0.476	0.054	-0.228	-0.174

According to the results at Table 1 the nature of the BCPs 1-5 are totally covalent.

Table 2. The AIM descriptors for the BCPs 1-3 in pure C_{60} fullerene correspond to the BCPs 1-3 in drug.

BCP	ρ	$\nabla^2\rho$	$G(r)$	$V(r)$	$H(r)$
1	0.275	-0.672	0.082	-0.333	-0.251
2	0.300	-0.796	0.102	-0.403	-0.301
3	0.275	-0.672	0.082	-0.333	-0.251

Comparing the results of Table 1 and 2 shows that in substituted fullerene drug, the electron density at BCP 1-3 and the absolute values of $\nabla^2\rho(r)$ and H(r) decrease. This implies that the covalent nature of 1-3 bonds decreases and these bonds becomes weaker than that of pure C_{60}. In fact, connection of the substitution to C_{60} and formation of the covalent BCPs 4 and 5 in the drug affects on the electronic structure of the drug. It transfers the electron density from BCPs 1-3 to the BCP 4 and 5 and substitution. This deforms the symmetrical distribution of electron density on fullerene. This effect also has been approved by calculation of the AIM atomic charges of the drug which to save space we have not presented it here.The more deformation of electron density causes the more capability of binding to the HIV enzymes.

Conclusion: Replacement of substitution of fullerene forms an effective HIV enzyme inhibitor. The N-ethyl-N-methylethanamine substitution alters the distribution of electron density on C_{60} and increases the ability of this drug to connect to the active sites of enzymes.

References:

[1]Marchesan, S., et. al. *Bioorg. Med. Chem. Lett.* (2005), 15, 3615-3618.

[2] Bader, R. F. W., *Atoms in Molecules: A Quantum Theory*; Oxford University Press: Oxford, UK, (1990).

[3]Grimme s (2011) Density functional theory with london dispersion corrections. WIRE$_S$ I Comput MOL Sci 1:21-228

[4] FrischMJ, Trucks GW, Schlegel HB, Scuseria GE, Robb MA, Cheesema JR, Scalemani G, Barone V, Mennucci B, et. al., (2009), Gaussian 09, revision A.02, Gaussian, Inc.: Pittsburgh, PA.

[5] Bader R. F. W., *AIM 2000 program*, Version 2.0, McMaster University, Hamilton, Ontario, (2002).

Oxidative desulfurization of DBT with TBHP catalysed by zeolite Imidazolate framework-٨ (ZIF-٨)

Fatemeh Pakdel [a], Mahboube Ghahramaninezhad [a], Mahdi Niknam Shahrak [a] *

[a] Department of Chemical Engineering, Quchan University of Advanced Technology, Quchan, Iran
Email Address: M.niknam.sh@qiet.ac.ir

١. Introduction: Oxidative desulfurization (ODS) method is one of the most important methods to remove sulfur compounds [١-٣]. In this way, Sulfur compounds in the presence of suitable oxidants and catalysts oxide to their corresponding sulfonates (Figure ١: A simple schematic of oxidative desulfurization process). Zeolite Imidazolate Framework-٨ is a kind of Metal-organic frameworks that has great surface area, high porosity and tunable pore size [٤]. In this article, ZIF-٨ is used to catalyze the oxidation dibenzothiophene in a model fuel. The ZIF-٨ catalyst showed desired activity in the oxidation of dibenzothiophene using tert-butylhydroperoxide (TBHP) as an industrially and environmentally important oxidant.
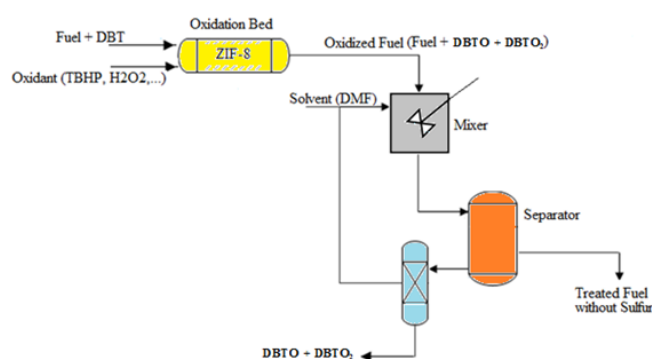

Figure ١: A schematic of an industrial oxidative desulfurization process

٢. Methods / Experimental:

The catalytic oxidative desulfurization was performed with dibenzothiophene (DBT). To a mixture of DBT (٥٠٠ ppml) and ZIF-٨ (١٠٠ mg) in toluene (٥ mL) TBHP was added, and the reaction mixture was stirred at ٨٠ °C for the required time. The reaction progress was monitored by GC (gas chromatography), and the yields of the products were determined by GC.

٢. ١. Materials

All materials used in these experiments, dibenzothiophene, tert-butyl hydroperoxide (TBHP), toluene, ZIF-٨, hexane, dichloromethane and octane, except ZIF-٨ that is purchased from Sigma-Aldrich, were prepared from Merck.

٣. Results and discussion

in this section, the effect of various parameters on DBT conversion were investigated.

٣. ١. Effect of temperature on DBT conversion:

We first examined the reaction at room temperature but no conversion was observed. Then temperatures of ٦٠, ٨٠ and ١٠٠ °C were employed to investigate their effect on the process conversion. The results can be considerate in figure ٢. As it's been shown, with increasing temperature, the reaction has improved significantly and is able to remove a high percentage of DBT.
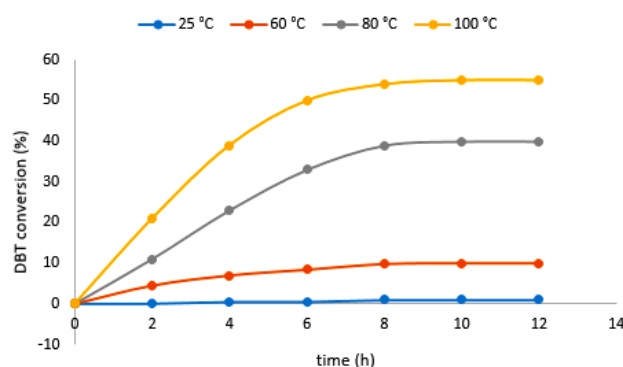
Figure ٢: The effect of temperature on oxidation of DBT (٥٠٠ ppm) using TBHP in toluene catalyzed by ZIF-٨ (١٠٠ mg).

٣.٢. Effect of the initial concentration on DBT conversion:

In order to examine the influence of the DBT concentration on its conversion, additional experiments were conducted by changing the DBT initial concentrations. The results are demonstrated in figure ٣. In case of the DBT solution with an initial concentration of ٤٠٠٠ ppm, ZIF-٨ showed the best catalytic reactivity. This issue is very important from industrial application point of view.

٣.٣. Effect of the solvent on DBT conversion:

Various solvents such as toluene, hexane, dichloromethane, octane and toluene-hexane mixture(٥٠:٥٠) have been tested to produce fuel models. Among all of them, as it is shown in Figure ٤, only toluene and toluene-hexane (٥٠:٥٠) reveal DBT conversion under specific conditions.Obviously, toluene solvent appear better performances in all times of reaction.
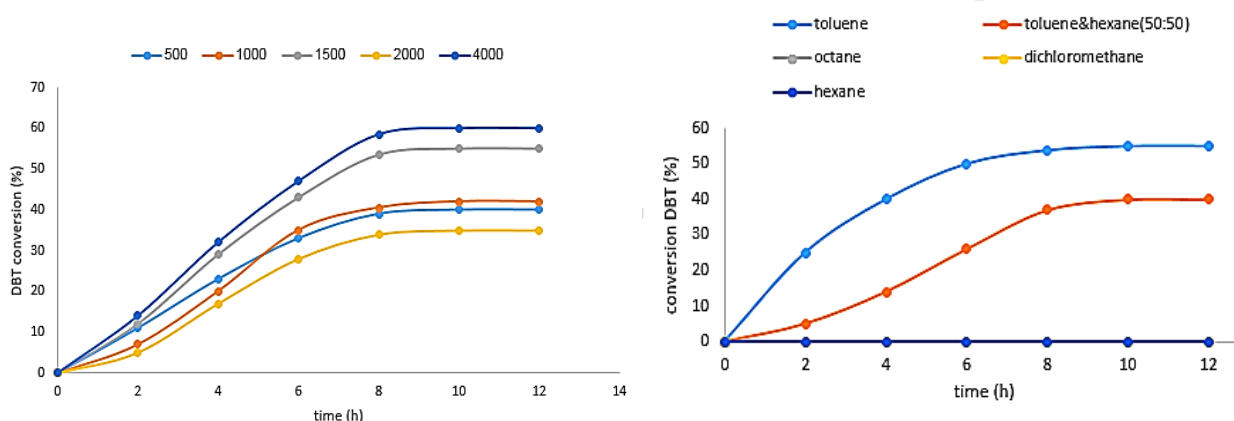

Figure ٣: a)The effect of initial concentration of DBT on oxidation reaction using TBHP in toluene catalyzed by ZIF-٨ (١٠٠ mg)at ٨٠ °C, b) The effect of solvent (٥ mL) nature on oxidation of DBT (٥٠٠ ppm) using TBHP catalyzed by ZIF-٨ (٥٠ mg) at ٨٠ °C

٤.Conclusion

Investigating the effect of various operational parameters on the ODS process catalysed by ZIF-٨ revealed that almost moderate temperature of ٨٠°C, ٥٠٠ppm initial concentration of DBT and toluene solvent as model fuel are the best conditions for efficient oxidative desulfurization. Furthermore, application of ZIF-٨ in real industrial sulphur concentration of ٤٠٠٠ppm is also recommended. Facile and efficient reusability of the solid catalyst at the end of reaction is observed.

٥. References

[١] Jorge Palomeque, Jean-Marc Clacens, and Fran¸coisFigueras, Journal of Catalysis, ٢١١ (٢٠٠٢),١٠٣–١٠٨.

[٢] Karina Castillo, J.G. Parsons, David Chavez, Russell R. Chianelli, Journal of Catalysis ٢٦٨ (٢٠٠٩) ٣٢٩–٣٣٤.

[٣] Dong Xie, Qihui He, Yangyang Su, Tongwei Wang, RenfuXu, Baixing Hu, Chinese Journal of Catalysis ٣٦ (٢٠١٥) ١٢٠٥–١٢١٣.

[٤] Surendar R. Venna, Jacek B. Jasinski,andMoises A. Carreon, J. AM. CHEM. SOC., VOL. ١٣٢, NO. ٥١, ٢٠١٠.

Synthesis and Characterization of Cu(II) Complexes as Biomimetic Models for Enzyme Substrate Adducts of Galactose Oxidase

**Mina Nasibipour[a], Elham Safaei[a*]**

[a] *Department of Chemistry, College of Science, Shiraz University, Shiraz, 71454, Iran*

E-mail*: e.safaei@shirazu.ac.ir

****

Background: Galactose oxidase (GOase) is a copper enzyme in which the active site contains a tyrosyl radical coordinated to a Cu ion and catalyzes the oxidation of D-galactose with concomitant reduction of dioxygen to hydrogen peroxide [1]. In this work, synthesis of copper complexes (CuL^{ABN}) of 2-amino benzonitrile ligand (H_2L^{ABN}) have been reported.

Method: To the stirred mixture of H_2L^{ABN} and Cu powder in acetonitrile, triethylamine was added. The resulting mixture was stirred for one day. Crystals suitable for X-Ray diffraction were obtained by slow evaporation of dichloromethane/methanol mixture.

Results: Copper complexes were characterized by IR, UV-vis, single crystal X-Ray diffraction, magnetic susceptibility studies and cyclic voltammetry techniques. X-Ray analysis revealed that Cu core in the model compound is a distorted square planar coordination sphere and surrounded by two phenolate O and two amine N atoms (scheme 1). The magnetic property, catalytic and redox activity of the mentioned complex was investigated.
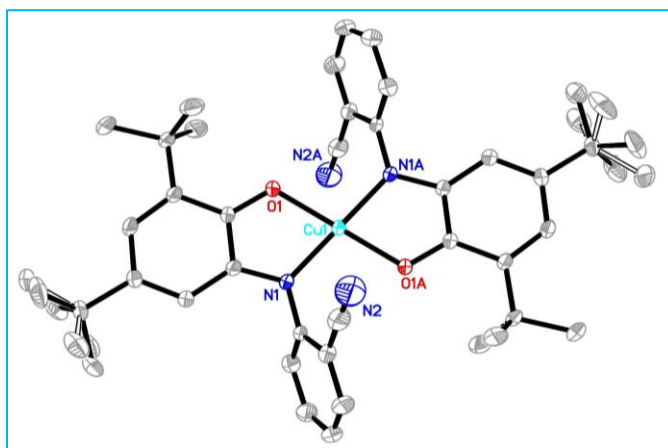
Scheme 1. Molecular structure of CuL^{ABN}

Conclusion: New CuL^{ABN} complexe were synthesized as biomimetic model for galactose oxidase enzyme. Mild and efficient oxidation of alcohol substrate to the corresponding aldehydes was achieved with molecular oxygen as the oxidant using CuL^{ABN} as catalyst.

References:

1. Balaghi, S.; Safaei, E.; Chiang, L.; Wong, E.; Savard, D.; Clarke, R.; Storr, T. *Dalton Trans*, **2013**, *42*, 6829-6839.

Titanium Dioxide Nanoparticles Size Effects On Dye Sensitive Solar Cells Efficiency With Different Dyes

Pooya Tahay, Zahra Parsa, Meysam Babapour, Maryam Adineh, Ali Alavi, Nasser Safari[*]

Department of Chemistry, Shahid Beheshti University, Evin, 1983963113 Tehran, Iran

E-mail: n-safari@sbu.ac.ir

****

Introduction: Dye-sensitized solar cells (DSSC) have become a topic of significant research in the last two decades because of their fundamental and scientific importance in the area of energy conversion [1]. Ruthenium and porphyrin dyes are two different generation of dye which shows high photocurrent efficiency over 10% [2]. The photocurrent efficiency of DSSC highly depends on titanium dioxide size and interaction between dye and titanium oxide [3]. Consequently, we have investigated dye type relation with TiO_2 size and their effect on photocurrent efficiency of dye-sensitized solar cells.

Methods / Experimentals: Three sizes of TiO_2 nanoparticles had been synthesized by varying hydrothermal temperature and their physical properties investigated with XRD powder diffraction, tapping mode AFM, FESEM and cyclic voltammetry. The porphyrin dye (T1) and the ruthenium dye synthesized and characterized with ^{1}HNMR, FTIR and UV-vis spectroscopy. The cells efficiency and properties analyzed with photocurrent efficiency measurement and impedance spectroscopy.

Results and Discussion: The synthesized TiO_2 nanoparticles were sintered on the surface of fluorine-doped tin oxide (FTO) Glasses and used for fabrication dye-sensitized solar cells with two types of dye: a porphyrin dye (T1) and a ruthenium dye (N3). The results for N3 dye shows that increasing TiO_2 nanoparticles size reduced photocurrent efficiency and surface area of the TiO_2 nanoparticles is a key factor for N3 cells. In contrast to N3 cells, porphyrin cells efficiency increase with TiO_2 nanoparticle size and electron transfer dominated factor in solar cell efficiency.

Conclusion: The photocurrent efficiency measurements and other experimental results demonstrate that the favorite TiO_2 nanoparticles size depends on dye intrinsic properties and the best size changes with dye types.

References

[1] S. Shalini, R. B. Prabhu, S. Prasanna, T. K. Mallick and S. Senthilarasu, *Renewable & Sustainable Energy Reviews* **2015**, *51*, 1306-1325.

[2] A. Hagfeldt, G. Boschloo, L. C. Sun, L. Kloo and H. Pettersson, *Chemical Reviews* **2010**, *110*, 6595-6663.

[3] a) Y. Bai, I. Mora-Sero, F. De Angelis, J. Bisquert and P. Wang, *Chemical Reviews* **2014**, *114*, 10095-10130; b) H. van der Salm, S. J. Lind, M. J. Griffith, P. Wagner, G. G. Wallace, D. L. Officer and K. C. Gordon, *Journal of Physical Chemistry C* **2015**, *119*, 22379-22391.

A NOVEL USE OF CALMAGITE AS THE COLORIMETRIC ANION CHEMOSENSOR FOR CARBONATE ION

Hossein Tavallali [*], Gohar Deilamy-Rad, Pegah Peykarimah

Department of Chemistry, Payame Noor University 19395-4697 Tehran, Islamic Republic of Iran

*Corresponding author E-mail address: Tavallali@pnu.ac.ir, Tavallali@yahoo.com

Introduction:

Carbonate is a physiologically important ion in human body [1] which has been detected through different analysis methods [2-5]. However, the used methods were cumbersome, time-consuming and naked-eye-invisible [6]. Over the past 10 years, several excellent chemosensors have been reported for recognition and sensing of anions [7, 8]. However, only very few sensors have been reported for carbonate [9, 10]. Herein, we report the use of 1-(1-hydroxy-4-methyl-2-phenylazo)-2-naphthol-4- sulfonic acid (Calmagite) as a colorimetric sensor for detection of carbonate with high selectivity. According to our knowledge, the application of this azo dye as an anion sensor has not been documented.

Experimental:

The 1.0×10^{-2} mol L^{-1} solutions of PO_4^{3-}, NO_3^-, SO_4^{2-}, SO_3^{2-}, AcO^-, CO_3^{2-}, I^-, Br^-, Cl^-, F^-, SCN^-, Ascorbate and Citrate ions were prepared. To cells containing 5×10^{-5} mol L^{-1} Calmagite in 10% $DMSO/H_2O$, proper amount of mentioned anion solutions was added. Only CO_3^{2-} induced a blue color while other anions had no significant effects on the color of solution. The UV-vis titration was subsequently conducted. The practical applicability of calmagite as a selective colorimetric chemosensor for CO_3^{2-} was examined by performing the competitive anion interference experiments.

Results and Discussion:

Upon the addition of CO_3^{2-} to the Calmagite solution, a new peak at 592.5 nm appeared while the absorbance at 534 nm decreased concomitantly. The binding mode between Calmagite and the carbonate ion was studied using their Job's plots analysis. The plot indicated the maximum absorbance at the concentration ratios of 0.5 which confirmed a simple 1:1 binding mode. The optical property of the chemosensor was studied in the presence of different anions. Among all anions studied, only CO_3^{2-} could generate a new complex through its addition into calmagite. These results demonstrated that the CO_3^{2-} recognition by calmagite was barely interfered by other coexisting anions. LOD for CO_3^{2-} was 0.2 μmol L^{-1} (R.S.D. 2.4% calculated from a triplicate). To evaluate the repeatability and the intermediate precision, aqueous carbonate samples (n=3) at three concentration levels (9.0×10^{-6}, 0.5×10^{-5} and 1.3×10^{-5} μmol L^{-1}) were measured in one single day per week during 1 month, for CO_3^{2-} ions. The repeatability,

expressed as RSD, was in the range of 2.7–3.7%. Intermediate precision, expressed as RSD, was in the range of 3.1–4.2%.

The accuracy of the proposed method for carbonate ions was checked by preparing different synthetic samples with different amounts of $CaCO_3$ and analyzing them, using the proposed method. Recoveries between 98.8 and 102.0% were obtained in all cases.

Conclusion:

In summary, we have developed a colorimetric method to recognize CO_3^{2-} with high selectivity and sensitivity using a readily available azo dye, Calmagite. In this study, the formation of the complex and the anion recognition were monitored by anion complexation induced changes in UV-vis spectroscopic studies. The proposed straightforward and inexpensive manner which was also used to detect carbonate in practical analysis, showed that Calmagite has a potential application in naked-eyes carbonate detection.

References:

[1] M. Maj-Zurawska; D. Ziemianek; A. Mikolajczuk; J. Mieczkowski; A. Lewenstam; A. Hulanicki; T. Sokalski. *Anal. Bioanal. Chem.*, **2003**, *376*, 524–526.

[2] M. Zougagh; A. Rios; M. Valcarcel. *Talanta*, **2005**, *65*, 29–35.

[3] H.K. Lee; H. Oh; K.C. Nam; S. Jeon. *Sens. Actuator B*, **2005**, *106*, 207–211.

[4] O. Doka; D. Bicanic; M. Szucs; M. Lubbers. *Appl. Spectrosc.*, **1998**, *52*, 1526–1529.

[5] E.E. Burt; A.H. Rau. *Drug Dev. Industrial Pharm.*, **1994**, *20*, 2955–2964.

[6] L. He; Ch. Liu; J. H. Xin. *Sens. Actuator B*, **2015**, *213*, 181–187.

[7] M. Yıldız; Ö. Karpuz; C. T. Zeyrek; B. Boyacıoğlu; H. Dal; N. Demir; N. Yıldırım; H. Ünve. *J. Mol. Struct.*, **2015**, *1094*, 148–160.

[8] S. Dalapati; S. Jana; N. Guchhait. *Spectrochim. Acta Part A*: Mol. Biomol. Spect., **2014**, *129*, 499–508.

[9] G. Hennrich; H. Sonnenschein; U. Resch-Genger. *Tetrahedron Lett.*, **2001**, *42*, 2805‑2808.

[10] H. Tavallali; G. Deilamy-Rad; A. Parhami; S. Lohrasbi. *Talanta*, **2016**, *149*, 168–177.

Synthesis of some novel quinoxaline β-lactam conjugates

Aliasghar Jarrahpour[a,*], Motahareh Mozaffari khalfebadam[a], Javad Ameri Rad[a]

[a]Department of Chemistry, College of Sciences, Shiraz University, Shiraz 71946-84-795, Iran

Email address: jarrah@susc.ac.ir, aliasghar6683@yahoo.com

Introduction: The azetidine-2-one (β-lactam) ring system is a common structural feature of a number of broad spectrum β-lactam antibiotics, like penicillins, cephalosporins, carbapenems, nocardicins and monobactams, which have been widely used as chemotherapeutic agents for treating microbial diseases [1]. However, microorganisms have built up resistance against the most traditional β-lactam antibiotics due to the wide-spread overuse of antibiotics. Therefore, the phenomenon of bacterial resistance forces the continuous modification of structure of known active compounds and the development of new ones [2]. Nitrogen containing heterocycles are present in a wide pectrum of organic molecules, and they are foremost in synthetic chemistry. Quinoxalines, which are an important class of nitrogen containing heterocyclic compounds, have diverse biological properties such as anti-HIV [3]. Our interest in the biological applications of β-lactams and quinoxaline led us to assess molecular constructs that contain both bioactive moieties.

Experimental: General procedure for the synthesis of quinoxalino-β-lactams 3a-j. A mixture of 2,3-Diphenyl-quinoxalin-6-yl amine **1** in the presence of various aromatic aldehydes was refluxed in ethanol to afford imines **2**. Then a mixture of imine **2** (1.45 mmol), triethylamine (7.27 mmol), substituted acetic acid (2.18 mmol) and TsCl (2.18 mmol) in dry CH_2Cl_2 (15 mL) was stirred at r.t over night. Then it was washed with HCl 1N, saturated $NaHCO_3$ and brine. The organic layer was dried (Na_2SO_4), to give the crude products **3a-j**, then were purified by recrystallization from acetone.

Results and Discussion: The synthesis of β-lactam hybrids **3a-j** was achieved according to the outlined procedure in Scheme 1. A mixture of imine, Et_3N, substituted acetic acid and TsCl in dry CH_2Cl_2 was stirred at room temperature for 24 h. to give 2-azetidinones **3a-j** by the ketene–imine [2+2] cycloaddition reaction (Staudinger reaction). Then we observed our products are *cis* stereoisomer. The stereochemistries of these 2-azetidinones were either *cis* or *trans* due to the coupling constants of H-3 and H-4 of the β-lactam ring[4]. The structure of the products was fully characterized by IR and ^{1}H and ^{13}C NMR spectra. The ^{1}H NMR spectrum of **3a** exhibited two doublets at $\delta = 6.01$ and 6.14 ppm ($^3J_{HH}= 5$ Hz) for vicinal methine protons along with a multiplet at $\delta = 7.25$-8.21 ppm for phenyl ring protons. The ^{13}C NMR spectrum of **3a** showed 19 distinct resonances in agreement with the suggested structure. Characteristic ^{13}C NMR signals were shown due to one carbonyl groups at $\delta = 163$ ppm and signals at $\delta = 89.6$ and 61.5 ppm for CH groups. Also the IR spectrum of compound **3a** indicated a characteristic absorption band of a β-lactam carbonyl moiety at 1754 cm^{-1}.
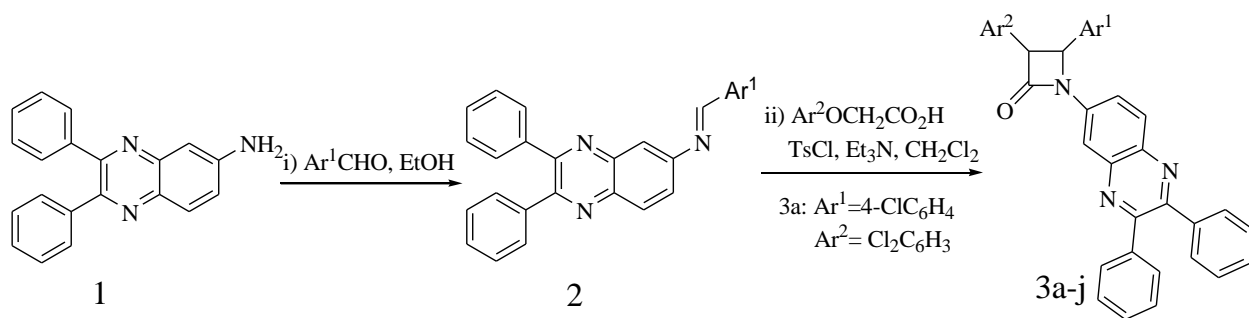
Scheme1: Synthesis of 2-azetidinone ring **3a-j**.

Conclusion: 10 new β-lactams were synthesized. All of the synthesized β-lactam hybrids were *cis* stereoisomers. These newly synthesized β-lactams will be evaluated for their potential biological activities

[1] Halve, A. K.; Bhadauria, D.; Dubey, R. *Bioorg. Med. Chem. Lett*. **2007**, *17*, 341-345.

[2] Vatmurge, N. S.; Hazra, B. G.; Pore, V. S.;l Shirazi, F.; Chavan, P. S.; Deshpande, M. V. *Bioorg. Med. Chem. Lett*. **2008**, *18*, 2043-2047.

[3] Keivanlo, A.; Kazemi, Sh.S.; Nasr-Isfahani, H.; Bamoniri, A. *Tetrahedron*, **2016**, *27*, 6536-6542

[4] Jarrahpour, A.; Heiran, R. *J. Iran. Chem. Soc.* **2014**, *11*, 75–83

Electronic and Structure Properties of Ir$_4$ Cluster

Afshan Mohajeri*, Nasim Hassani

Department of Chemistry, College of Science, Shiraz University, Shiraz, Iran
Email: amohajeri@shirazu.ac.ir

Introduction: Nano sized clusters perusal has been one of the attractive topics of research in some science for example physics, biology and chemistry [1]. Clusters can be applied to catalysis, data storage, medical diagnosis, bio sensing and etc. [2]. However, properties of metal clusters are different from those of bulk metals, due to their size. During the last decade, iridium-based catalysts have attracted much attention, because of their ready availability and high reactivity. Accordingly, the present work reports density functional study on the electronic and structural properties of Ir$_4$ cluster.

Methods: All calculations were carried out by Gaussian 09 suite of program [3]. We used standard LANL2DZ basis set [4] and Ir was described by pseudo effective core potential (ECP) of Wadt and Hay [5]. Geometry optimization and calculations of electronic properties were performed by seven DFT methods; B3LYP, BLYP, BPW91, BP86, BB95, B3P86 and TPSSH.

Results and Discussion: To ensure physically meaningful results for the electronic properties, the correct atomic arrangements for the clusters must be considered. The stability of the clusters was assessed based on the binding energy (E$_B$):

$$E_B = [E(Ir_n) - n\,E(Ir)]$$

where $E(Ir_n)$ and $E(Ir)$ are the total electronic energy of a cluster and iridium atom, respectively [6]. We considered two possible configurations for Ir$_4$ cluster that were previously reported in literature. Seven different DFT methods were used to optimize these initial configurations with all possible spin multiplicities. The results are shown in Table 1. The lowest energy of Ir$_4$ is predicted to be a nonet state with planar square structure, at all tested computational levels. The BB95 functional show the most stable planar square Ir$_4$ with E_B = -13.74 eV. Its structure is shown in Figure 1. The lowest energy tetrahedral Ir$_4$ that commonly exists in Ir$_4$ complexes, e.g. Ir$_4$(CO)$_{12}$, is a singlet molecule [7] and its binding energy is higher than that of the nonet ground state (E_B = -13.167 eV) at BB95 level.

Conclusion: This study reports the structural and electronic properties of Ir$_4$ clusters by using density-functional theory at B3LYP, BLYP, BPW91, BP86, BB95, B3P86 and TPSSH levels of

theory. After considering lowest energy configurations with different possible spin multiplicities, it was found that planar square Ir_4 cluster is more stable in nonet spin state.

Table 1. Binding energy (eV) of Ir_4 cluster at several levels of theory.

Configuration	Spin state	BLYP	B3LYP	BPW91	BP86	BB95	B3P86	TPSSH
planar square	Singlet	-10.75	-7.71	-11.75	-12.22	-13.09	-8.57	-10.18
	Triplet	-11.06[*]	-8.55	-11.99[*]	-12.61	-13.57	-9.34[*]	-10.17
	Quintet	-11.32	-8.96	-12.42[*]	-12.88[*]	-13.71[*]	-9.59	-10.56
	Septet	-11.50[*]	-9.26[*]	-12.49	-12.92	-13.68	-10.05[*]	-10.90
	Nonet	-11.62	-9.45	-12.69	-13.09	-13.74	-10.40	-11.21
	11-et	-10.91	-9.28	-12.00	-12.35	-12.90	-10.20	-10.85
tetrahedral	Singlet	-10.49	-8.96	-11.63	-11.99	-13.16	-9.98	-10.72

[*] The asterisk sign indicates structures with imaginary frequency.
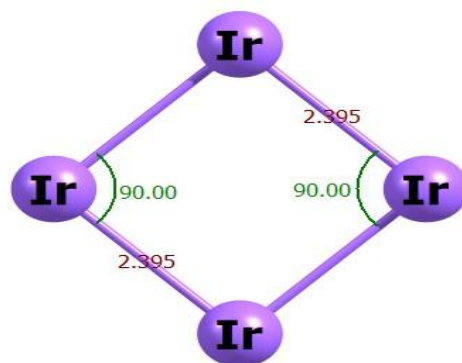
Figure 1. Optimized structure of planar square Ir_4, at BB95/LANL2DZ level of theory.

References

[1] A. M. Argo; J. F. Odzak; B. C. Gates. *Am Chem Soc*, **2003**, *125* (23), 7107 -7115.
[2] R. Ferrando; J. Jellinek. *Chem. Rev*, **2008**, *108* (3), 845–910.
[3] M. J. Frisch; G. W. Trucks; H. B. Schlegel; et al. Gaussian 09w, version 7.0, Gaussian. Inc, Wallingford, **2009**.
[4] P. J. Hay; W. R.Wadt. *J. Chem. Phys*, **1985**, *82*, 270-283.
[5] P. J. Hay; W. R.Wadt. *J. Chem. Phys*, **1985**, *82*, 299-310.
[6] M. Chen; D. A. Dixon. *J. Phys. Chem. A,* **2013**, *117,* 3676−3688.
[7] S. Kawi; J. R. hag; B. C. Gates. *J. Phys. Chem.* **1993**, *97*, 5375-5383.

Interpolated potential energy surface for abstraction and exchange reactions of HCN⁻ + H and deuterated analogues

Raziyeh Sharafdini, Shapour Ramazani*

Department of chemistry, Yasouj University, ٧٥٩١٤ Yasouj, Iran

ramazani@yu.ac.ir

Introduction:

HCN has been finded in such diverse molecular astrophysical environments as diffuse interstellar clouds. It is especially dense interstellar clouds [١]. HCN molecule has been used to analyze a variety of species and processes in the interstellar medium [٢]. The study of reactive or nonreactive chemical processes on a molecular level requires knowledge of the potential energy surface (PES) for the system considered. Collins performs ab initio molecular orbital theory calculations at a number of discrete atomic configurations, referred to as data points, as per the well-known Grow prescription. Actually, he introduces a method named Growing Potential Energy Surfaces to construct molecular PES with classical trajectory simulations to provide an iterative scheme for successively improving the surface. The Grow methodology does not assume a functional form for the PES [٣].

Methods:

A modified Shepard interpolation gives the total potential energy at any configuration Z as a weighted average of the Taylor series about all N_d initial data points and their symmetry equivalents: $E(Z) = \sum_{g \in G} \sum_{i=1}^{N_{data}} w_{goi}(Z) T_{goi}(Z)$ where each Taylor expansion, T_i, has associated weight, w_i. In this expression G denotes the symmetry group of the molecule. The weight function, w_i, which weights the contribution of the Taylor expansion about each of the $Z(i)$ data points to the total potential energy at the configuration Z. Ab initio calculations were carried out using the Gussian ٠٣ program [٤]. The geometries of all stationary points were optimized at The MP₂ level with the ٦-٣١١++G (d,p) basis set.

Results and discussion:

An important aspect of the grow methodology is monitoring derived dynamical quantities as points are added to the ab initio data set defining the interpolation. we investigate R١ reaction and isotopically substituted analogues that as shown: HCN⁻ +H → CN⁻ + H₂ (R١), HCN⁻ +D → CN⁻ + HD (R٢), DCN⁻ +H → CN⁻ + HD (R٣), DCN⁻ +D → CN⁻ + HD (R٤). An example of the convergence of the probability of the R١ reaction with increasing data set size is shown in figure ١. Figure ٢ shows the effect of increasing the impact parameter on the probability of the R١ reaction as a function of relative translational energy. The total reaction cross section as a function of relative translational energy has been shown in figure ٣. Figure ٤ shows rate constants for the all reactions that have been calculated from evaluated reactive cross sections and reaction probabilities, at temperature T.

Conclusion:

An accurate ab initio interpolated PES has been constructed to describe the dynamics of the reactions $HCN^- + H \rightarrow CN^- + H_\Upsilon$ and deuterated substituted analogues. This PES is based on a combination of QCISD/٦-٣١١++G (d,p) energies with QCISD/ ٦-٣١١++G (d,p) first and second energy derivatives for ٢٨٣٦ molecular configurations. The rate constants for all reactions are calculated over the temperature range ٣١٦-١٢٠٠ K and Arrhenius plot for these are shown in figure ٤.
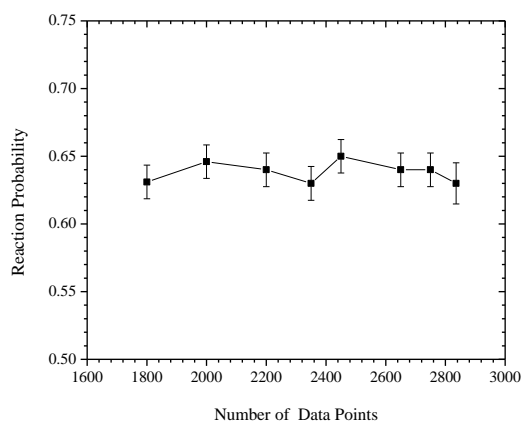
FIG. ١. The calculated reaction probability as a function of the PES data set size.
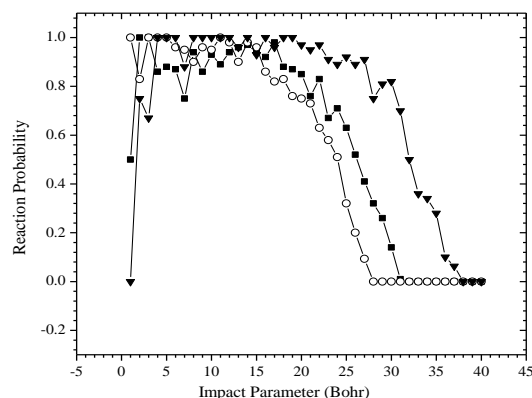
FIG. ٢. Reaction probability as a function of impact parameter for R١ reaction at relative translation energies of ٤.٤٦ (kJ mol^{-1}) (▼), ٧.٠٩ (kJ mol^{-1}) (■), ٧.٨٨ (kJ mol^{-1}) (○)
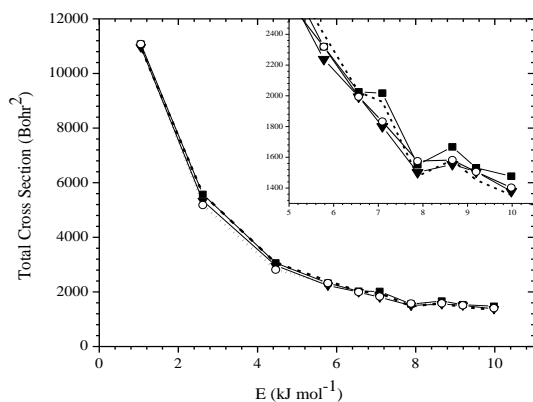
FIG. ٣. The reaction cross section as a function of the relative translation energy for all reactions, (—■—) R١, (—▼—) R٢, (-----) R٣, (—○—) R٤ in ٧.٨٨ kJ mol^{-1}
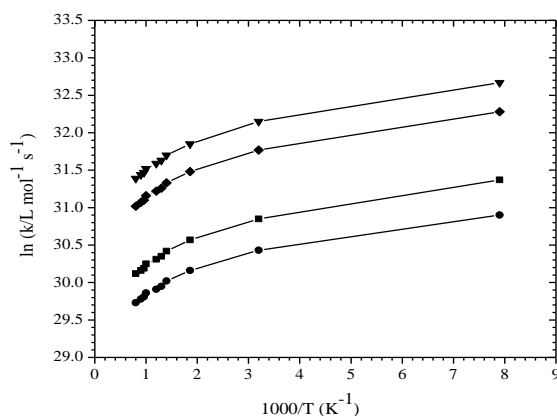
FIG. ٤. Arrhenius plot for all the reactions of (■) R١, (♦) R٢, (▼) R٣, (●) R٤

References:

[١] S. Petrie, J. *Phys. Chem. A*, ٢٠٠٢, ١٠٦, ١١١٨١-١١١٨٩.

[٢] Y. Gao ; P. M. Solomon, *The Astrophysical Journal*, ٢٠٠٤, ٦٠٦, ٢٧١-٢٩٠.

[٣] M. A. Collins, Theor. *Chem. Acc*, ٢٠٠٢, ١٠٨, ٣١٣-٣٢٤.

[٤] M. J. Frisch, G. W. Trucks, H. B. Schlegel *et al.*, GAUSSIAN ٠٣, Revision B.٠١, Gaussian, Inc., Pittsburgh, PA, ٢٠٠٣.

Synthesis and optical properties of the binuclear cyclometalated platinum complexes containing bridging azobispyridine ligands

Sirous jamali[a,*], <u>Sara Nayeri[b]</u>
[a,b]Chemisty Department, Sharif University of Technology, P.O. Box 11155-3516, Tehran, Iran.
Email addrss: sjamali@sharif.ir

Introduction: Azo aromatic compounds have attracted attention in chemistry because of their unique combination of geometrical and electronic structures, which lead to interesting optical properties. In this regard, these compounds can undergo a photoinduced isomerization which has been used to prepare photoresponsive materials [1]. In this class of compounds, the most stable *trans* isomers convert to the *cis* isomers upon UV irradiation (around 365 nm) (Figure 1)[2]. For example, azobispyridine ligands 2,2'-azobispyridine (2-abpy) and 4,4'-azobispyridine (4-abpy) able to coordinate metal fragments and act as switches under UV irradiation [3].
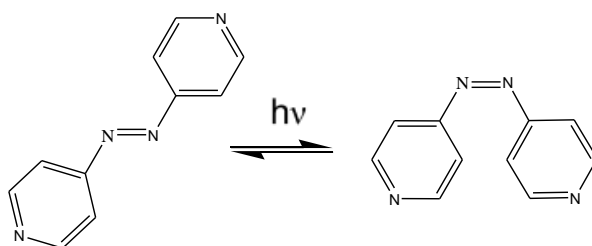

Figure 1

Experimentals: All manipulations were performed under an atmosphere of argon, using glove box techniques. The cyclometalated complex [PtMe(SMe$_2$)(CN)], in which CN = 2-phenylpyridine, **1**; CN = benzo{h}quinolone, **2**, were prepared from the reaction of [Pt(μ-SMe$_2$)Me$_2$]$_2$ with 1 equiv of corresponding cyclometalating ligand in acetone. The reactions of **1** and **2** with ½ equiv of 4,4'-azobispyridine (4-abpy)gave the binuclear cyclometalated platinum complexes [Pt$_2$Me$_2$(CN)$_2$(μ-4-abpy)] in which CN= 2-phenylpyridine, **3**; CN = benzo{h}quinolone, **4**.

Discussion and Conclusion: The binuclear complexes **3** and **4** have been prepared and characterized using multinuclear 1D and 2D NMR spectroscopies. Complexes **3** and **4** are stable in acetone solvent and show isomerization under UV lamp. The optical properties and *cis* to *trans* isomerization of **3** and **4** have been investigated under UV-vis irradiation.
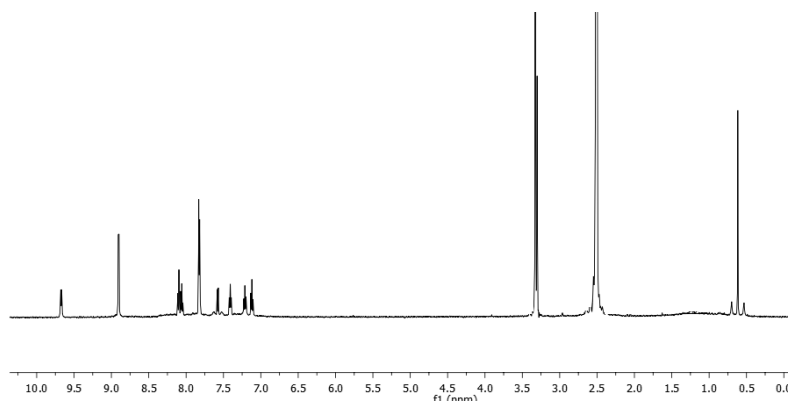

Figure 2 NMR spectrum

References

[1] M. Bardaj; M. Barrio; P. Espinet. *Dalton Trans.*, **2011**, *40*, 2570–2577.

[2] S. Das; S. Varghese; N. S. S. Kumar. *Langmuir*, **2010**, *26*, 1598-1609.

[3] Y. Yu; T. Maeda; J. Mamiya. *Angew. Chem., Int. Ed.*, **2007**, *46*, 881-883.

Synthesis of Some Novel Morpholinoquinoline β-Lactam hybrids

Maryam Sasanipour[a], Aliasghar Jarrahpour[a,*], Hashem Sharghi[a], Mahdi Aberi[a]

[a] Department of Chemistry, College of Sciences, Shiraz University, Shiraz 71454, Iran

Email address: jarrah@susc.ac.ir; aliasghar6683@yahoo.com

Introduction: β-lactams are a biologically important class of heterocyclic compounds [1] and have been recognized as the central motif of antibiotics such as penicillins, cephalosporins, and carbapenems [2]. β-lactams have a broad range of pharmacological activities, such as chemotherapeutic agents for treating microbial diseases, antimalarial activities, cholesterol absorption inhibitors, anti-HIV, antifungal [3] and anticancer agents [4]. Quinoline scaffold plays an important role in anticancer drug development as their derivatives have shown excellent results through different mechanism of action such as growth inhibitors by cell cycle arrest, apoptosis, inhibition of angiogenesis, disruption of cell migration, and modulation of nuclear receptor responsiveness. The anticancer and biological potential of these derivatives have been demonstrated on various cancer cell lines [5, 6].

Experimental: This study involves the treatment of an imine with a ketene. Initially, a mixture of 2-morpholinoquinoline-3-carbaldehyde (**1**) (10.0 mmol) and an aromatic amine derivative (10.0 mmol) was refluxed in ethanol for an appropriate time. After the solution cooling, the precipitate was filtered and washed with ethanol to give the crude Schiff base (**2a-i**), a mixture of this Schiff base (1.0 mmol), Triethylamine (5.0 mmol), substituted Acetic acid (1.5 mmol), and Tosylchloridein (1.5 mmol), in dry CH_2Cl_2 (15.0 mL) was stirred at room temperature for several hours. Then the mixture was washed with HCl 1N (20.0 mL), saturated $NaHCO_3$ (20.0 mL), and brine (20.0 ml).The organic layer was dried (with Na_2SO_4), filtered and the solvent evaporated to give the crude product. Finally the crude product was purified by recrystallization from Ethyl acetate to give β-lactams (**3a-n**) (Scheme 1).

Results and Discussion: In this work, the synthesis and characterization of novel β-lactam-quinoline conjugates are described. 2-Morpholinoquinoline (**1**) was synthesized by Professor Sharghi's research group. Treatment of (**1**) with different anilines afforded Imines **2a-i**. Then imines were treated with substituted Acetic acids in the presence of Tosylchloride and Triethylamine to afford Morpholinoquinoline β-Lactams (**3a–n**). The structure of the products was fully characterized by IR, ^{1}H and ^{13}C NMR spectra. The ^{1}H NMR spectrum of **3a** exhibited two doublets at δ = 7.14 and 7.20 ppm ($^3J_{HH}$= 4.8 Hz) for vicinal methane of β-lactam protons along with a multiplet at δ = 7.49−9.26 ppm for phenyl ring protons. The ^{1}H-decoupled ^{13}C NMR spectrum of **3a** showed 20 distinct resonances in agreement with the suggested structure. Characteristic ^{13}C NMR signals were shown due to carbonyl groups at δ = 163.2 ppm, signals at δ = 82.2 and 68.2 ppm for C-3, and C-4 (β-lactam ring), and at δ = 55.3 ppm for methoxy group. Also the IR spectrum of compound **3a** indicated a characteristic absorption band of a β-lactam carbonyl moiety at 1747 cm^{-1}.
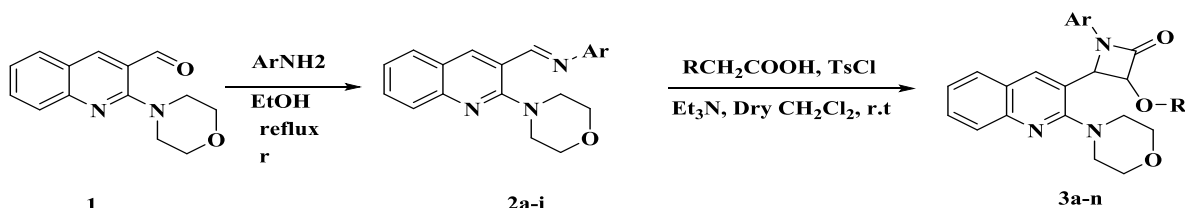
Ar = 2,4-dimethoxyaniline, 4-methylaniline, 4-OMe aniline, 4-Br aniline, 4-I aniline, 4-Cl aniline, 2,4-dimethoxyaniline, 3-5-dimethoxyaniline, 4- ethoxyaniline, 3-Br aniline

R=2,4-Cl$_2$C$_6$H$_3$O, PhO, 4-ClC$_6$H$_4$O, 2-NaphthO

Scheme 1: Synthesis of morpholinoquinoline β-lactam hybrids **3a–n**

Conclusion: In summary, 14 new morpholinoquinoline β-lactam hybrids were prepared and characterized from a novel bioactive aldehyde. Compounds **3a-j** were characterized as *cis* stereoisomers whilst **3k-n** were obtained as *trans* isomers. These newly synthesized β-lactams will be evaluated for their potential biological activities, such as anticancer, antifungal, antimalarial, and antibacterial.

References:

[1] Ebrahimi, E.; Jarrahpour, A.; Heidari, N.; Sinou, V.; Brune, J. M.; Zolghadr, A. R.; Turos, A. *Med. Chem. Res.*, **2015**, 25, 247-262

[2] Wilke, M. S.; Lovering, A. L.; Natalie, C. J. *Curr. Opin. Microbiol.*, **2005**, 8, 525–533.

[3] Ceric, H.; Sindler-Kulyk, M.; Kovacevic, M.; Peric, M.; Zivkovic, A. *Bioorg. Med. Chem.,* **2010**, 18, 3053–3058.

[4] Gowda,V. C.; Klaustermeyer, B. W. *Mil. Med.,* **2005**, 170, 701–704.

[5] Kumar, S.; Gupta, H. *Med. Chem.,* **2009**, 9, 1648–1654.

[6] Bawa, S.; Kumar, S.; Drabu, S.; Kumar, K. *J. Pharm. Bioallied.,* Sci., **2010**, 2, 64–71.

Centrifuge-less dispersive liquid–liquid microextraction by use of magnetic room temperature ionic liquid for the determination of parabens

Kobra Zavvar Mousavi[a] and Yadollah Yamini[a,*]

[a] Department of Chemistry, Tarbiat Modares University, P.O. Box 14115-175, Tehran, Iran

yyamini@modares.ac.ir

****

Introduction: Magnet-based separations constitute a quite interesting and evolving advancement in sample preparation [1]. Lately, considerable attention has been focused on magnetic ionic liquids (MILs). Metal-containing ionic liquids can combine the general properties of RTILs with those associated with the incorporation of a metal ion in their structure such as a strong response to an external magnetic field [2-4]. This work presents application of a magnetic room temperature ionic liquid (MRTIL) as a new extraction solvent for preconcentration and determination of parabens using centrifuge-less dispersive liquid–liquid microextraction (DLLME) followed by HPLC-UV.

Methods/ Experimental: Thirty microliter of MIL, as extraction solvent, diluted in 200 μL of acetone, as disperser solvent, was injected rapidly into 20 mL of sample solution containing **a** mixture of parabens. Then, a magnet was placed at one side of the extraction tube. The MIL was immediately attracted to the magnet and retained on the wall of the tube. Once parabens were enriched in the MIL droplet separated from the remaining aqueous sample.

Results and Discussion: The magnet-assisted approach with these MILs was performed in combination with high performance liquid chromatography and UV detection. Some important parameters, such as kind of extraction and disperser solvent and volume of them, extraction time, rate of vortex agitator and ionic strength content were investigated and optimized. Under optimum conditions the fast extraction step required 30 μL of MIL for 20 mL of aqueous sample, 200 μL of acetone as dispersive solvent, 5 min of vortex and high ionic strength content of NaCl (25% (w/v)). The preconcentration factor (PF) was defined as the ratio of the analyte concentration in the ionic liquid phase and the initial concentration of analyte in the sample solution was estimated 150. This work is currently conducting in our laboratory to evaluate linearity of calibration curve, limit of detection (LOD) and relative standard deviations (RSD).

Conclusion: Magnetic ionic liquids have been successfully studied in a magnet-based microextraction approach for the determination of a mixture of parabens. The overall method is quite simple because it does not require centrifugation or filtration to separate the magnetic material from the sample once extraction has been accomplished. The effective parameters on the extraction procedure were optimized and further detailed studies are currently ongoing in our laboratory.

References

[1] M. J. Trujillo-Rodríguez, O. Nacham, K. D. Clark, V. Pino , J. L. Anderson , J. H. Ayala, A. M. Afonso. *Analytica Chimica Acta,* **2016**, 934, 106-113

[2] E. Santos, J. Albo, A. Irabien. *RSC Advances*, **2014**, 4, 40008

[3] A. Beiraghi, M. Shokri, Sh. Seidi, B. M. Godajdar. *Journal of Chromatography A*, 1376, **2015**, 1–8

[4] N. Deng, M. Li, L. Zhao, Ch. Lu, S. L. de Rooy, I. M. Warnera. *Journal of Hazardous Materials*, 192, **2011**,1350– 1357

Physisorption of DNA/RNA Nucleobases on graphene and Single-Layer MoS$_2$ Using Dispersion-Corrected DFT Calculations

Meisam sadeghi[a,*] Mohsen Jahanshahi[b], Morteza Ghorbanzadeh Ahangari[c]

[a,b] Department of Nanotechnology Research, Babol Noshirvani University of Technology, Babol
c Department of Mechanical Engineering, University of Mazandaran, Babolsar
 Email address : meysam.sadeqi1366@gmail.com

****

Introduction: The kind of sensing platforms in biosensors play an important role in nucleic acid sequence detection. In this paper, a comparative study of methods with graphene and single-layer molybdenum disulfide (MoS$_2$) nanosheet as sensing platforms was proposed. In this strategy, DNA/RNA nucleobase [guanine (G), adenine (A), thymine (T), cytosine (C) and uracil (U)] adsorbed on graphene and MoS$_2$ via the van der Waals force between nucleobases and the basal plane of nanosheet and calculated using Dispersion-corrected density functional theory (DFT-D).

Methods / Experimentals: In this section individual starting configurations of DNA/RNA nucleobases were considered for interacting systems and physisorbed onto graphene and MoS$_2$ through π–π interaction and expresserd different quantity of interaction strengths, charge transfer and binding energies for the various nucleobase molecules.

Results and Discussion: Results revealed that the binding energies of the five nucleobases in graphene decreases in the range of 16 to 24 (kcal/mol) and ordered with G > A ≥ T ≥ C > U scheme which is consistent with the experimental values and is in agreement with theoretical data obtained from literature by using the B3LYP method. It has been demonstrated that Graphene does not have a band gap, which is not desirable for electronic base detection. Beside, a monolayer of MoS2 exhibits a better ON/OFF current ratio than graphene and hence, can potentially be used for sensing. On the other hand, the high affinity between DNA/RNA and MoS$_2$ nanosheet and the renewable property of the biosensing platform demonstrated that MoS$_2$ nanosheet is biocompatible and suitable for nucleic acid analysis. The calculated binding energies of the five nucleobases in MoS$_2$ follow the hierarchy G > C ≥ T ≥ A ≥ U using the DFT-D scheme and are in the range of 5 to 8 (kcal/mol), respectively which rather are lower than in graphene.

Conclusion: Our Dispersion-corrected DFT findings present evidence for a rational benchmark to the applicability of the single-layer MoS$_2$ for DNA/RNA nucleobases physisorption. In addition, we find that the van der Waals (vdW) interaction between the DNA/RNA base and the single-layer MoS$_2$ play a dominant role in the physisorption process, when nucleobases are placed on top of the single-layer MoS$_2$.

References: [1] Hossein Tavassoli Larijani; M. D. Ganji; Mohsen Jahanshahi. RSC Advances, 2015, 5,92843–92857

Human serum albumin and DNA Binding properties of a new diplatinum complex

Shiva Aryamanesh, Marzieh Dadkhah Aseman*, S. Masoud Nabavizadeh*

Department of Chemistry, College of Sciences, Shiraz University, Shiraz, Iran

nabavi@chem.susc.ac.ir

Introduction: Cisplatin is a widely used anticancer drug that is highly effective against testicular and ovarian cancers but has a number of side effects such as nephrotoxicity, ototoxicity, and allergy and a limited spectrum of activity due to inherent and/or acquired resistance. Therefore, much attention has been focused on designing new platinum compounds with improved pharmacological properties, broader range of antitumor activity, and wider spectrum of activity [1]. Recently, many efforts have been made to introduce non-conventional structures of platinum compounds that violate their empirical structure–activity relationships. These labours have been made with the aim to overcome the above mentioned restrictions which are associated with application of the classical platinum complexes. The multinuclear Pt complexes are good example of such compounds bearing non-classical structures. These platinum complexes contain two or more linked platinum centres that can each covalently bind to DNA, and hence are talented to forming an entirely diverse range of DNA adducts compared to cisplatin which forms principally intra strand crosslink between two adjacent guanine bases. Therefore, the multi-nuclear complexes signify an absolutely new model of platinum based drugs, and seem to be a great potential as new anticancer agents [2]. It has also been suggested that more than 90% of platinum in the blood, following intravenous administration of cisplatin, is covalently bound to the plasma proteins. Therefore, the study of cisplatin−protein is of a major biological interest that can provide useful information regarding the cisplatin−DNA protein recognition. Among the possible non-DNA targets, albumin is the most used. The affinities of drugs to protein would directly influence the concentration of drugs in the blood and in the binding sites and the duration of the effectual drugs and consequently contribute to their magnitude of biological actions in vivo [3].

Methods / Experimentals: As shown in Scheme 1, reactions of the Pt(II) starting complexes [PtMe(ppy)(SMe$_2$)], 1, in which ppy = deprotonated 2-phenylpyridine, with mercaptopurine (C$_5$H$_4$SN$_4$) in a 1:1 molar ratio, followed by the replacement of the labile ligand SMe$_2$ to give a dimeric complex [Pt(ppy)(N^S)]$_2$, 2, with two bridging deprotonated mercaptopurine(N^S) ligands, and CH$_4$.
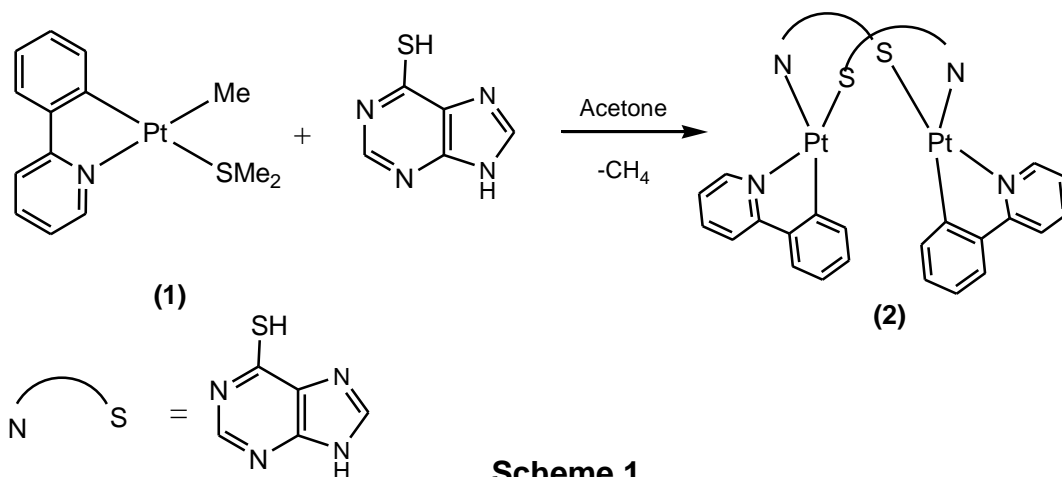
Scheme 1

Results and Discussion: As is depicted in Scheme ١, the reaction of organoplatinum(II) precursor [PtMe(ppy)(SMe٢)], ١, with ١ eq mercaptopurine ligand, in acetone, gave in good yield, the dimeric complex [Pt(ppy)(N^S)]٢, ٢. This complex are an air-stable brown solid that was fully characterized by (¹H, ¹³C) NMR spectroscopy and also mass spectroscopy. The interactions of complex ٢ as antitumor agents, with human serum albumin (HSA) have been studied by fluorescence and UV-vis absorption spectroscopic techniques at pH ٧.٤٠. The quenching constants and binding parameters (binding constants and number of binding sites) were determined by fluorescence quenching method. The obtained results revealed that there is a strong binding interaction between the complex ٢ and protein (Table ١). This complex also evaluated for anticancer activities and DNA binding properties.

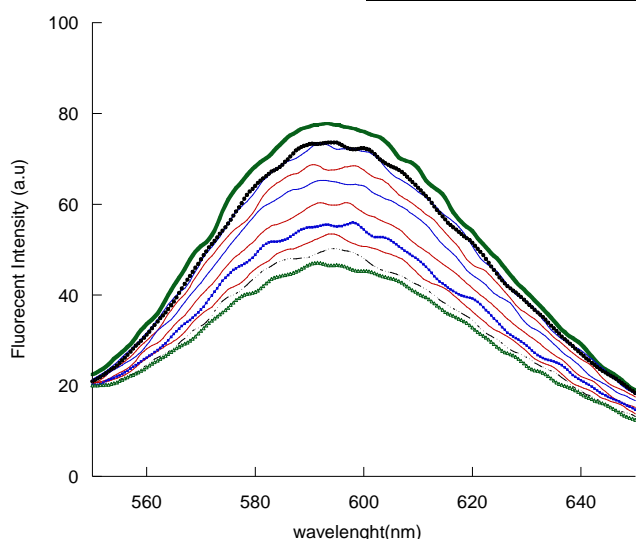| **Table ١** Binding Parameters of the System of the Interaction of Pt Complex (٢) with HSA at Different Temperatures			
T (K)	10^{-5} K_b	n	R
٢٩٨	٧.٨٤	١.٠٣٣	٠.٩٩٤٨
٣٠٣	٧.٢٣	١.٠٤٥	٠.٩٩٩٠
٣١٠	٦.٦٥	١.٠٤٤	٠.٩٩٦٤
[a] R is the linear correlated coefficient.			

Fig. ١. The fluorescence analysis of interaction between binuclear Pt (II) complexes and DNA. A) The fluorescence titration curve of EB-DNA ([EB]= ٤.٣μM, [DNA]=٠.٠٤ μM) in the presence of each complex ([Pt complex]=٠–٣٢ μM) performed in TN buffer, as the excitation wavelength was ٥٤٦ nm and the emission spectra were collected between ٥٥٠ and ٧٠٠

Conclusion: Overall, The binding mechanisms of newly designed binuclear Pt (II) complex contain mercaptopurine ligand with HSA, as important carrier proteins, were investigated by spectroscopic methods. Experimental results suggested that this Pt(II)complexes could bind to the serum albumins by high affinity. Also different spectroscopic methods were employed to investigate its interaction with DNA.

References:

[١] T. C. Johnstone, K. Suntharalingam, S, J. Lippard, *Chem. Rev.,* ٢٠١٦, ١١٦, ٣٤٣٦–٣٤٨٦.

[٢] M. B. Shahsavani, R .Yousefi, *Journal of Photochemistry and Photobiology B: Biology*, ٢٠١٦, ١٦١, ٣٤٥–٣٥٤.

[٣] F. Samari, B. Hemmateenejad, M. Shamsipur, M. Rashidi, H. Samouei, *Inorg. Chem.* ٢٠١٢, ٥١, ٣٤٥٤-٣٤٦٤.

Development of a new carbon paste sensor for low level measurement of rifampicin in pharmaceutical and biological samples

Ahmad Soleymanpour[a,*], **Azar Dehnavi**[b]

ᵃ School of Chemistry, Damghan University, Damghan 3671641167, Iran

E-mail address: soleymanpour@du.ac.ir (A. Soleymanpour)

****

Introduction: Rifampicin (RIF), 3-[(4-methyl-1-piperazinyl)imino]-methyl (Fig. 1), is an important antibiotic which is widely used for the chemotherapy of tuberculosis. Since RIF is one of the most effective antituberculosis regimens used in many countries, considerable effort has been spent on improving the efficacy of this therapy [1]. The analytical methods reported for the assay of rifampicin individually in the bulk form and pharmaceutical formulations are included thin-layer chromatography (TLC) with electrochemical detection [2], flow-injection chemiluminescence, spectrometry, differential pulse polarography and adsorptive stripping voltammetry [3,4]. However, no potentiometric sensor for this drug has been reported so far. Thus, the introduction of a sensor for fast, simple and selective determination of RIF is an urgent need. In this study, it was tried to construct a sensitive carbon paste sensor for determination of RIF in different pharmaceutical and biological samples.
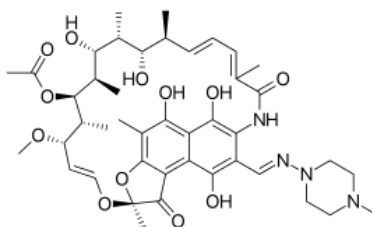

Fig. 1. The chemical structure of rifampicin

Experimental

Reagents: All of the chemical used were of highest purity available and doubly distilled water was used for the preparing all aqueous solution. Reagent paraffin oil (PO), graphite powder, tridodecyl methyl ammonium chloride (TDMACl) and 2-hydroxypropyl ß-cyclodextrin (HP-ß-CD) were used as received (all from Merck). Rifampicin was obtained from Damavand Darou Mfg. Company, Damghan, Iran.

Preparation of the electrode: The modified carbon paste electrodes were generally prepared by hand-mixing various amounts of graphite powder, additive and ionophore in a mortar for at least 10 min, Then, pasting liquid was added to this mixture and the mixture was mixed again until a uniform paste was obtained. The paste was packed in the end of a disposable polyethylene syringe (3 mm i.d.), the tip of which had been cut off with a razor blade. Electrical contact to the carbon paste was made with a copper wire. Fresh surface was obtained by applying manual pressure to the piston. The resulting fresh surface was polished on a white paper until the surface had a shiny surface.

Results and discussion: In order to achieve the best performance of the carbon paste sensor such as slope, linear range and detection limits, different factors such as the amount of ionophore (ß-CD), type of pasting liquid [5], additive and effect of pH, on the potentiometric response of

the sensor was investigated. The response characteristics of the modified carbon paste sensor at optimized conditions were summarized in Table1. The calibration curve of the modified sensor was also shown in Fig 2. The performance of the sensor was obtained in phosphate buffer solution (pH=8.0).
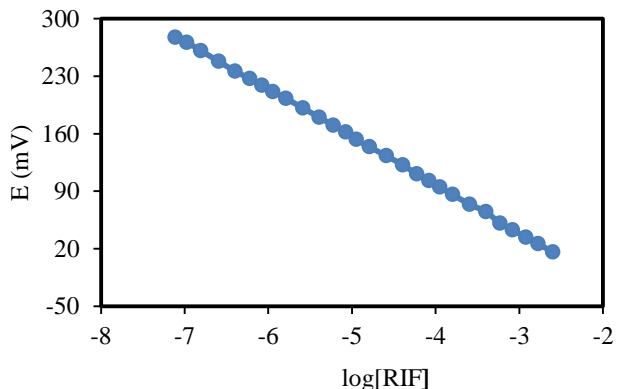

Fig. 2. Calibration graph for the rifampicin sensor under optimum conditions.

Table 1 Optimization of the carbon paste ingredients.

Optimized CPE ingredient	Linear range (M)	Detection limit (M)	Slope	pH	Response time (s)	Life time
Grafite (%64.5) Nojul (%32.3) Ionophore (%3.0) Additive (%0.2)	7.7×10^{-8} – 2.5×10^{-3}	5.0×10^{-8}	58.2	7.5-8.5	4	2 months

Analytical applications of the sensor: The sensor was successfully applied as an indicator electrode in potentiometric titration of RIF solution and also determination of RIF in rifampicin tablet (300 mg) and blood serum samples. The result of the titration curve has a distinct and accurate equivalent point which shows that the amount of RIF concentration can be accurately determined by the proposed sensor. Moreover, all of the determinations in real samples have the recoveries between 97 to 102 percent, indicating that the determination of RIF concentration can be performed by the sensor with satisfactory accuracy in biological and pharmaceutical matrices.

Conclusion: This work revealed that the modified carbon paste sensor based on 2-hydroxypropyl ß-cyclodextrin as ionophore, can be used as useful analytical tools and interesting alternative for the determination of RIF in pharmaceutical and biological samples. A rifampicin concentration as low as 7.7×10^{-8} M can be determined by the proposed sensor. The sensor shows good sensitivity, low detection limit, long-term stability, high selectivity and suitable applicability.

References

[1] C.A. Peloquin; S.E. Berning. Ann. Pharmacother, 1994, 28, 72-84.
[2] J.Nowakowska; J. Halkiewicz; J.W. Lukasiak. Chromatographia, 2002, 56, 367-373.
[3] M.A.A. Lomillo; O.D. Renedo; M.J.A. Martinez. Electroanalysis, 2002, 14, 634-637.
[4] M.A.A. Lomillo; O.D. Renedo; M.J.A. Martinez. Helv. Chim. Acta, 2002, 85, 2430-2439.
[5] E. Bakker; P. B uhlmann; E. Pretch. Chem. Rev, 1997, 97, 3083-3132.

A carbon nanotube –Ag nano particle modified electrochemical sensor for determination of bisphenol A in real samples

Shahab Maghsoudi*,a , Mehdi Mousavi[a], Maryam Mohammadkhah[a]

a *Department of Chemistry, Faculty of Sciences, Shahid Bahonar University of Kerman, P.O. Box*

76175-133 , Kerman, Iran

* *Email:* shahabmaghsoudi@yahoo.com

Introduction: Bisphenol A (BPA), 2,2-bis(4-hydroxyphenyl)propane is a commonly used raw material for polycarbonate (PC) and epoxy resin (EP) production which are widely used as plastic food containers, food can linings and water bottles[1]. Accordingly, it is widely used in many industries as an industrial chemical. In many reports, it is indicated that exposure to BPA in the environment would be a threat to human health and can cause reproductive disorders including the decrease of sperm quality in humans, birth defects due to fetal exposure and various kinds of cancers. Recently, several analytical methods including liquid chromatography (LC), gas chromatography (GC) and electrochemical methods have been used to measure BPA quantity. LC and GC provide sensitive, convenient, and effective methods for BPA, but the methods are costly and time-consuming. Electrochemical methods have the advantage of simplicity and high sensitivity with low-cost instrumentation. Electroanalysis can also be used to give appropriate results within a short time under field conditions and for on-line monitoring [2]. Electrochemical sensors can be used in this work owing to the good electrochemical activity of BPA, which can be detected successfully using electrochemical oxidation. Multi-walled carbon nanotube (MWCNTs) has attracted much attention due to their unique structure, good biocompatibility, excellent electrical conductivity, high surface area and chemical stability. Moreover, its large surface-to-volume ratio, leading to a good catalytic property for BPA[3]. The combination of a multi-walled carbon nanotube electrode and Ag nanoparticles may produce sensors with good sensitivity and selectivity. Cyclic voltammetry (CV) and differential pulse voltammetry (DPVs) were used to investigate the electrochemical behavior of BPA at the modified electrodes.

Methods / Experimental: A modified Au electrode (or multi-walled carbon nanotube-Ag nanoparticles modified Au electrode) serves as the working electrode, a platinum wire as the auxiliary electrode, and an Ag/AgCl as the reference electrode.
Sensor Preparation: A bare Au electrode was polished with alumina powder, rinsed ultrasonically with deionized water and dried at room temperature before use. Approximately 70 µL of MWCNT, 50 µL of Ag nanoparticle (3.8×10^{-4}) in 80 µL of ultra pure water were dispersed for 15min. About 30 µL of the mixture was cast on the surface of Au electrode and dried in air. Prior to use, the modified electrode was carefully rinsed with water to remove the loosely attached MWCNT on the electrode surface.

Results and Discussion: Cyclic voltammograms for oxidation of 1.0×10^{-4} M BPA in 0.04 M phosphate buffer solution (pH 3.0) at bare and modified Au electrode are shown in Figure 1.

Cyclic voltammetry (CV) is a convenient and effective method to monitor electrochemical behaviors. Fig. 2 shows the CV responses of the bare Au electrode, Ag/Au electrode, MWCNTs/Au electrode and Ag–MWCNTs/Au electrode in the mixture solution of 1.0×10^{-4} M BPA and PBS.
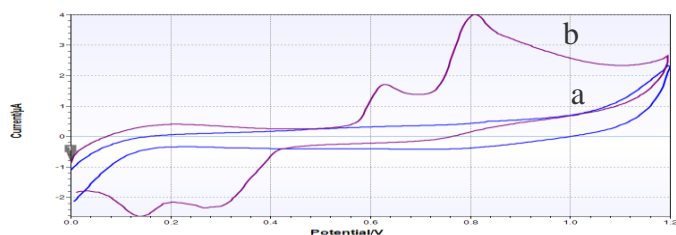

Fig.1 Cyclic voltammograms of a) blank and b) 1.0×10^{-4} M BPA solutions on the modified electrode.
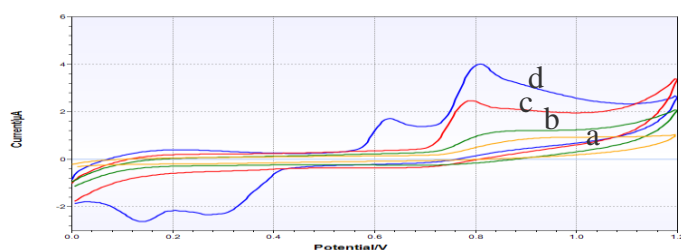

Fig. 2 Cyclic voltammograms of a 1.0×10^{-4} M BPA in phosphate buffer solution on (a) Ag/Au electrode , (b) bare Au electrode, (c) modified MWCNT electrode and, (d) MWCNT–Ag/Au electrode .

The effects of pH, time and potential of deposition, pH of Ag nanoparticle solution and the amounts of MWCNT and Ag nanoparticle were optimized. DPV was used to obtain the figures of merit of the method (linear range, detection limit and precision). The results showed a linear relationship versus BPA concentrations in the range of 1×10^{-7} to 1×10^{-6} and a detection limit 1.2×10^{-7}.

Conclusion: A electrochemical sensor based on modified carbon nanotube- Ag nanoparticle was fabricated for the determination of bisphenol A in real samples . The present BPA sensor shows good selectivity and thus the practical application of BPA in food package samples was satisfactory with good recovery. The results showed that the combination of Ag nanoparticle and MWCNT could remarkably enhance the analytical signal due to their higher effective surface area and excellent conductive effect.

References
[1] Ntsendwana, B., Mamba, B. B., Sampath, S., & Arotiba, O. A. (2012). Int J. Electrochem Sci, 7(4), 3501-3512.
[2] Han, J., Li, F., Jiang, L., Li, K., Dong, Y., & Li, Y. (2015). Analytical Methods, 7(19), 8220-8226.
[3] Chen, Z., Tang, C., Zeng, Y., Liu, H., Yin, Z., & Li, L. (2014). Analytical Letters, 47(6), 996-1014.

Synthesis and Characterization of Two Copper(II) Complexes of Redox-active *O*-iminobenzosemiquinone Benzoxazole Ligands

Salimeh Nazari Mazidi, Elham Safaei[*]

Department of Chemistry, College of Sciences, Shiraz University, Shiraz, 71454, Iran

E-mail*:* e.safaei@shirazu.ac.ir

****

Introduction: The chemistry of metal complexes with redox-active ligands has received considerable attention largely in both bioinorganic and catalytic chemistry [1]. *O*-aminophenols are one of the most common classes of redox-active ligands as a biomimetic model of enzymes acting via metallotyrosyl radicals such as: galactose oxidase (GOase), they can be bound to transition metal ion in three oxidation levels either as an *O*-aminophenolate dianion, *O*- iminobenzosemiquinonate π radical monoanion and neutral iminoquinonate ligand [2]. In this work, synthesis of two copper complexes of tridenate *O*-aminophenol benzoxazole [2] and cyano or thiocyano ligands has been reported. In addition, the axial ligand effect on the tuning of complexes redox potential has been investigated.

Experimental: H_2L^{BAP} and triethylamine were dissolved in a 2:1 acetonitrile/dichloromethane mixture, and then copper acetate and NaCN or KSCN salts were added. The reaction mixture was stirred for 6 hours at room temperature. X-ray quality brown single crystals of $CuL^{BIS}SCN$ and $CuL^{BIS}CN$ were grown from a solvent mixture of dichloromethane/ethanol and dichloromethane/acetonitrile solution respectively. The redox potential of transition metal complexes of these ligands has been shown to correlate with the Lewis acidity of a redox-inactive species coordinated to the redox-active transition metals.

Results and Discussion: Copper complexes were characterized by IR, UV-vis, 1H NMR, element analysis, single crystal X-Ray diffraction, magnetic susceptibility studies and cyclic voltammetry techniques. X-ray crystallography analysis of both complexes revealed that the coordination sphere of the Cu(II) center is a deformed tetrahedron. The structure of both complexes involves one ligand molecule coordinated to the copper ion through the nitrogen atom of benzoxazole, nitrogen and oxygen atoms from *O*- iminosemiquinone moiety, and the NCS or

CN anions coordinated via their N atoms (figure 1). Magnetic measurements, X-ray crystallography studies and ^{1}H NMR sharp peaks prove the diamagnetic character of CuL[BIS]X complexes.

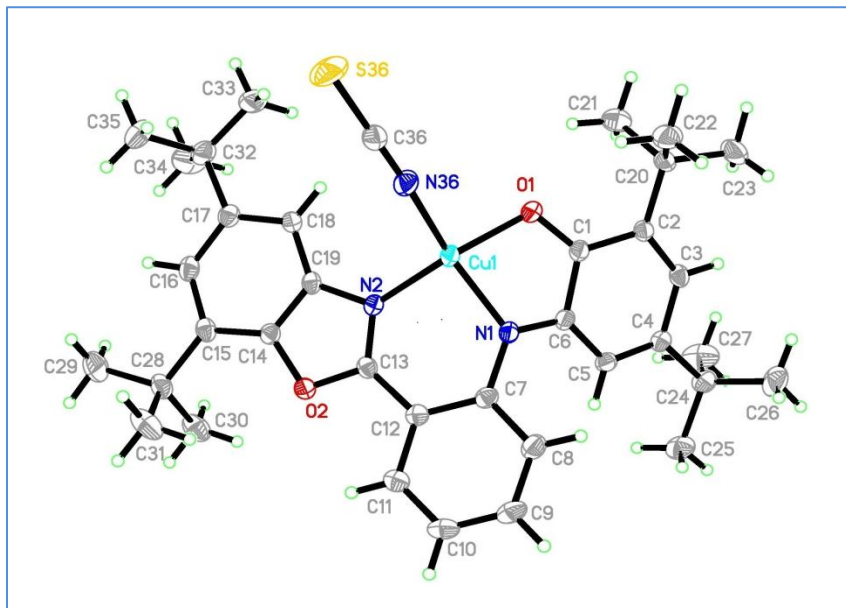figure 1. Molecular structure of CuL[BIS]SCN

Conclusion: New CuLX complexes of non-innocent ligands were synthesized and characterized. Our studies show that the electrochemical redox potential of complexes have been tuned by X anion coordinated to Cu(II) center.

References:

1. Luca, O. R; Crabtree, R. H. *Chem. Soc. Rev*, **2013**, *42,* 1440–1459.

2. Balaghi, S. E; Safaei, E; Chiang, L; Wong, E. W; Savard, D; Clarke, R. M; Storr, T. *Dalton Trans*, **2013**, *42*, 6829–6839.

Separation and determination of the enantiomers of fluoxetine by high performance liquid chromatography on achiral column C18 and chiral mobile phase

Mahsa taheri jahromi[a], Ali Asghar Amiri[a*]
[a] Department of Applied Chemistry, Shiraz Branch, Islamic Azad University, Shiraz, Iran
*amiri1355@gmail.com

Introduction: The separation of chiral compounds has been of great importance in many research and factory, particularly the pharmaceutical industry. This interest is due to the different pharmacokinetic characteristics and pharmacological activities of each enantiomer in a racemic drug. Thus, there has been a great demand for the development of analytical techniques for the enantioseparation [1]. Separation of enantiomers can be achieved using different chromatographic techniques such as gas chromatography, liquid chromatography [2], supercritical fluid chromatography [3] and capillary electrochromatography. Among these methods, high-performance liquid chromatography (HPLC) is well recognized as a powerful, fast, selective and highly efficient technique, successfully employed for separation and determination of enantiomers of drugs. The chiral mobile phases (CMPs) HPLC have become a powerful and widely applicable analytical tool for enantioseparation purpose, which is a convenient to separate the underivatized enantiomer compounds and the reagent used is cheaper than chiral solid-phase HPLC [1]. Fluoxetine hydrochloride, (±)-*N*-methyl-3-Phenyl-3-[(*α, α,α*-trifluoro-*p*-tolyl)] propylamine hydrochloride is an antidepressant drug used for the handling of unipolar mental depression. Fluoxetine (FLX) is the most widely prescribed selective serotonin reuptake inhibitor antidepressant drug [4]. FXT has been shown to have comparable efficacy to tricyclic antidepressants but with fewer cardiovascular and anticholinergic side effects [5]. Since FXT is a compound of great pharmacological and analytical importance there has been an interest to develop accurate analytical method for the quantification of FXT in biological and pharmaceutical samples.

Methods / Experimentals: The chromatographic equipment consisted of two PU-2080 plus delivery pumps (Jasco, Japan), an injector valve Rheodyne 7725i (USA) with 20-µL sample loop and a variable-wavelength absorbance detector UV-2070 plus (Jasco, Japan) operating at 254 nm. The chromatographic system was controlled by HSS-2000 provided by Jasco using the LC-Net II/ADC interface. Analysis was carried out at room temperature on a (Waters, Ireland) µBondapak C18, 5 µm particle size, 300 × 3.9 mm I.D. column. Acetonitrile-triethylamine acetate (TEAA) buffer (pH 9, 15 mM) (35:65, v/v) containing 11 mM DAM-α-CD as the mobile phase was used. The mobile phase was filtered through suitable 0.45 µm pore size membrane filters prior to introduce to pumps. Mobile phase degassing was performed automatically, on line, under stream of He. Fluoxetine was eluted isocratically with this mobile phase at the flow rate of 1.0 mLmin^{-1}.

Results and Discussion: For HPLC analysis, 20 µl of the racemate of fluoxetine solution (10 µg mL^{-1}) was injected into HPLC system and the enantioselectivity (α) is calculated from the equation α= k_R / k_S, where k_R and k_S are capacity factors of *(R)-* and *(S)-* fluoxetine, respectively. In order to bring about chiral separations, a difference in

retention behavior between the complexed and free enantiomers is necessary. The main operating parameters optimized in the proposed HPLC method were the type and concentration of the chiral selectors, the concentration of acetonitrile in mobile phase, pH of buffer and the temperature. In the present study, four CDs, namely α-, β-, γ-CD and DAM-α-CD, were used for enantioseparation of fluoxetine. Experiments were performed with solutions containing 10 μg mL^{-1} fluoxetine and mobile phase having different concentrations of CDs. Among these four CDs, The separation factor achieved with DAM-α-CD as chiral selector for fluoxetine enantiomers was good and with other CDs poor enantioselectives for the enantiomers examined was achieved. Obviously, DAM-α-CD possesses a stronger ability for chiral separation than the other CDs. This probably reflects the ability of flexible permethylated CD to better adapt its shape to that of the included guest molecules, resulting in diasteromeric complexes having distinctive structures. Weak bonds between functional groups on the analyte and those of the cyclodextrin ring may also contribute to the effective chiral recognition. Overall, enantioselection with CDs is difficult to predict since it depends not only on the nature of the functional groups present in both host and guest, but also on structural factors that may control the host–guest complementarity. In order to optimize the concentration of chiral selector of DAM-α-CD, different amounts of chiral selector were added to mobile phase. The enantioselectivity is shown to increase with an increase in DAM-α-CD concentration in mobile phase from 3.0 to 15.0 mM, followed by a slight decrease at DAM-α-CD concentration between 11.0 and 15.0 mM.

Conclusion: The quantification of mixtures of *(R)*- and *(S)*-fluoxetine in the pure form and in the pharmaceutical preparations is described. The methodology is based on chiral recognition of fluoxetine by formation of an inclusion complex with DAM-α-CD, as a chiral auxiliary. Effects of the type and concentration of chiral selector, content of acetonitrile and TEAA buffer pH on the enantioseparation were investigated. The method was validated for linearity, repeatability, limits of detection (LOD) and limits of quantification (LOQ). Among the α-, β- and γ-cyclodextrins, linear polysaccharides (maltodextrin with dextrose equivalents of 4.0–7.0, 13.0–17.0 and 16.5–19.5) and diamino derivative of methylated α-cyclodextrin (DAM-α-CD), as chiral selectors DAM-α-CD showed high abilities of enantioseparation.

Refrences
[1] L.-M. Yuan, *Sep. Sci. Technol.* 29 (2008) 375.

[2] G. Torok, L. Goetelen, R. Luyckx, P. V. Broeck, *J. Pharm. Biomed. Anal.* 39 (2005) 425.

[3] M. Maftouh, C. Granier-Loyaux, E. Chavana, J. Marini, A. Pradines, Y. V. Heyden, *J. Chromatogr. A* 1088 (2005) 67.

[4] K. Parfitt, "Martindale: The Complete Drug Reference," 33rd Edition, Pharmaceutical Press, London, 2002.

[5] J. Shah, M.R. Jan, M.N. Khan, S. Durrani, *American Journal of Analytical Chemistry*, 3 (2012) 828.

Synthesis of nanotube Ag doped TiO$_2$ for surface adsorption and photo decomposition of methylene blue under visible light

Mona Hosseini.Sarvari*[a], Zeinab Hosseinpoaur[a]

[a] Department of Chemistry, Faculty of Sciences, Shiraz University

 Email: hosseini@shirazu.ac.ir, zeinab.hosseinpour@yahoo.com

Introduction: TiO$_2$ particles have been used as photocatalyst for degradation of various organic compounds. The photocatalytic efficiency of TiO$_2$ is greatly influenced by crystal structure, particle size, surface area, and porosity, as determined by different preparation methods[1].

Silver (Ag) particles are often applied to act as electron reservoirs to suppress the electron–hole pairs recombination, thus more holes are available for the oxidation reactions, which cause a lot of attention in the modification of TiO$_2$ NTs [2].

Wastewater containing pigments and/or dyes can cause serious water pollution problems .Semiconducting titania materials are currently attracting attention due to their marked photocatalytic effect in removing pollutants [3].

Experimental:

Preparation of TiO$_2$-NTs : A hydrothermal method for TiO2-NTs preparation was applied. TiO$_2$ (p25) was added into 25 mL NaOH solution, and the mixture refluxed for 24 h. After filtration , the white product was treated with 1mol/L HCl and distilledwater. Subsequently the nanotubewas dried at room temperature and calcined at 300 ∘C for 1 h to remove any impurity on the TiO$_2$-NTs surface.[4]

Preparation of Ag/TiO$_2$-NTs: Hydrothermal method for TiO$_2$-NTs preparation was applied. TiO$_2$ NTs were immersed into AgNO$_3$ ethanol solution with a concentration of 0.25 mM and the mixture refluxed for 24 h at 83 ∘C, then cooled down naturally, the sample was taken out and ultrasonically cleaned with ethanol and deionized water [5].

Results and Discussion: Prepared nanotube Ag/TiO$_2$ was characterized by IR, XRD, and SEM. The morphologies of Ag/TiO$_2$ nanotubes were studied using SEM and TEM. Figure 1 shows the SEM images of Ag/TiO$_2$ particles.
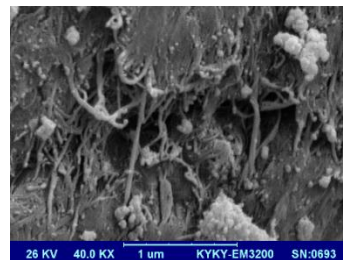

Figure 1:

Decolorization experiments were conducted in white irradiation source. All systems were stirred continuously and first mechanical stirring for 30 min in the dark environment. The change in MB concentration was monitored by determining the UV–visible adsorption of 3.0 mL sample taken from the solution every 15 min at 660 nm. In this test investigate decolorization in different conditions and the concentration of methylene blue Become zero. The dye concentration was measured using a spectrophotometer (name) at 660 nm; decolorization efficiency was determined from the difference between dye concentrations before and after each test. The dye concentration was zero after 30 min . The amount of catalyst for decolorization was Lowest and we use Concentrate solution . The result was perfect for this situation.

Conclusions: In summary, we have successfully decorated TiO_2 NTs with Ag nanoparticles by a hydrothermal method. The Ag nanoparticle modified TiO_2 NTs largely enhanced the photocatalytic degradation of methylene blue under visible light irradiation. [6]

References
[1]1;Yiming Xu 2; Cooper H. Langford. *J. Phys. Chem. B*, *101,* **1997***,* 3115-3121.

 [2]1;Qingyao Wang2;Xiuchun Yang3;Dan Liu4; Jianfu Zhao. *Journal of Alloys and Compounds*,**2012**,*527* ,106– 111.

[3]1;P.V. Messina2; P.C. Schulz .*Journal of Colloid and Interface Science*,**2006***,299*, 305–320.

[4]1;Guangmei Guoa2; Binbin Yub3; Ping Yuc4;Xi Chenb. *Talanta***, 2009***,79*, 570–575.

[5]1; J.S. Zhong 2; Q.Y. Wang3; Y.F. Yuc. *Journal of Alloys and Compounds,* **2015,** *620* ,168– 171.

[6]1;Qingyao Wang2;Xiuchun Yang3;Dan Liu4; Jianfu Zhao. *Journal of Alloys and Compounds*,**2012**,*527* ,106– 111.

Aggregation-Based Colorimetric Sensor for Determination of Prothioconazole Fungicide Using Colloidal Silver Nanoparticles (AgNPs)

Zahra Jafar-Nezhad Ivrigh[a], Nafiseh Fahimi-Kashani[a], M.R. Hormozi-Nezhad[a,b,*]

[a] Department of Chemistry, Sharif University of Technology, Tehran 11155-9516, Iran
[b] Institute of Nanoscience and Nanotechnology, Sharif University of Technology, Tehran, Iran
E-mail :* hormozi@sharif.edu

Introduction: Triazole fungicides have received increasing attention in recent years. Triazoles are classified as acutely toxic substances for potentially inducing adverse chronic effects by changing liver functionality, decreasing kidney weight, altering urinary bladder structure, and arousing acute effects in the central nervous system of animals. Prothioconazole is one of the most abundant triazole fungicides which is used to control infection of wheat[2]. It features high chemical and photochemical stability, low biodegradability and easy transport in the environment; thus monitoring traces of these compound has been spotlighted owing to the possible contamination of water resources. Several analytical methods have been developed for determination of triazoles which are costly and time-consuming [2]. Consequently, the development of cheap and sensitive and analytical methods measuring prothioconazole residues is of great interest. Recently, plasmonic nanomaterials, have been exploited as powerful sensing materials in pesticide colorimetric assays. These assays are based on plasmon resonance wavelength changes of NPs triggered by the analyte and can be colorimetrically detected. Herein, we have developed a colorimetric sensor, based on aggregation of citrate-capped AgNPs, capable of identifying prothioconazole fungicide.

Methods/ Experimental: Silver nanoparticles were synthesized by reduction of 0.25 mL AgNO$_3$ 0.1 M by 1 mL NaBH$_4$ 0.005 M in the presence of sodium citrate 0.1 M. In a typical procedure, 375 µL AgNPs was mixed with 1350 µL of Deionized water, 750 µL NaCl 0.1 M. Then different concentration of prothioconazole was added, and equilibrated for 25 min at room temperature before the spectral measurements.

Result and Discussion: Scheme 1 depicts the method to analyze Prothioconazole (PC) through the aggregation of AgNPs. Initially, AgNPs are well dispersed and yellow-colored in the absence of PC. The presence of PC induces the aggregation of AgNPs whithin 25 minutes, resulting in a color change from bright yellow to orange.
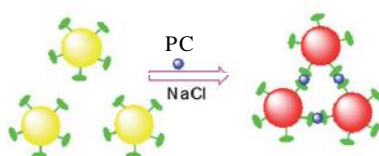
Scheme 1 Aggregation of AgNPs in presence of NaCl and prothioconazole

Fig. 1 shows the change in UV-Vis spectra of AgNPs solution before and after the addition of 0.4 ppm PC. As shown if Fig. 1 the AgNPs plasmon intensity is decreased at 395 nm and a new peak is appeared at 500 nm after 25 min incubation.

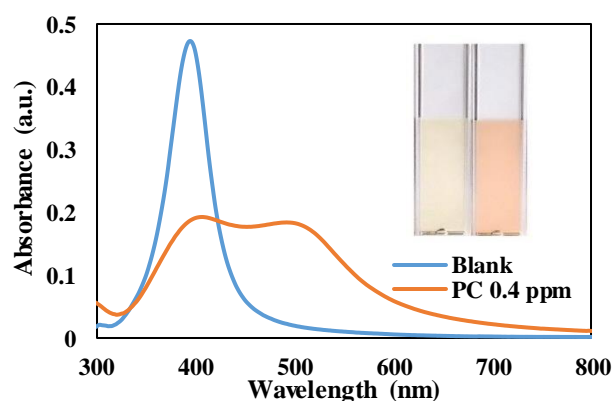

Figure 1 UV-Vis spectra and photographic images of 2.5 mL AgNPs (A) before (B) after addition of 0.4 ppm PC

Quantitative analysis was performed by the addition of various concentrations of PC into AgNPs solution (containing 30 mM of NaCl at pH=6.2) and monitoring the UV-Vis absorption spectra and color changes after 25 min. The results obtained in Fig. 2 show that significant changes in absorbance occur at PC concentrations range of 0.01 To 0.4 ppm. The quantitative characteristics of the proposed method was based on a linear relationship between A_{500}/A_{395} and concentrations of PC.
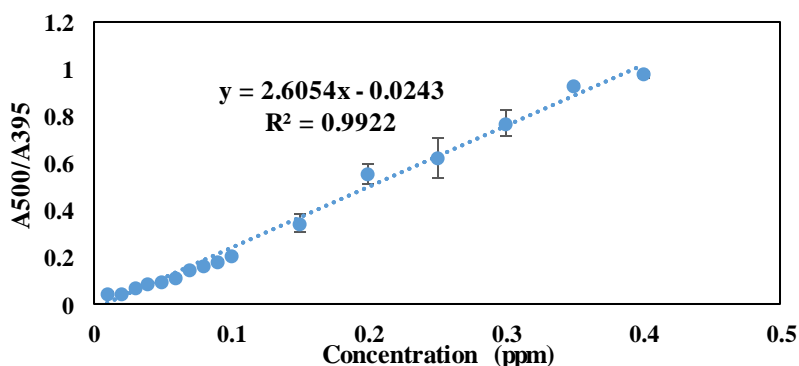

$$y = 2.6054x - 0.0243$$
$$R^2 = 0.9922$$

Fig. 2 Calibration curve for determination of PC (A_{500}/A_{395} versus concentration of PC)

Conclusion: In conclusion, we have developed a new sensitive method for detection of prothioconazole, based on aggregation of AgNPs in the presence of NaCl. Upon adding PC, the AgNPs solution changes from yellow to orange which is easy to detect by the naked eye.

References:

(1) Liu, N.; Dong, F.; Xu, J.; Liu, X.; Chen, Z.; Tao, Y.; Pan, X.; Chen, X.; Zheng, Y. *J. Agric. Food Chem.* 2015, *63*, 6297-6303.
(2) Li, Y.; Yang, X.; Zhang, J.; Li, M.; Zhao, X.; Yuan, K.; Li, X.; Lu, R.; Zhou, W.; Gao, H. *Anal. Methods* 2014, 6, 8328-8336.
(3) Rohit, J. V.; Kailasa, S. K. *Anal. Methods* 2014, 6, 5934-5941.

Synthesis and Chromotropism Investigation of a Copper Complex containing tridentate Amide and Azide Ligands

Leila Rostami*, Hamid Golchoubian
Department of Chemistry, University of Mazandaran, Babol-sar
E-mail: Leila_rostami64@yahoo.com

1. Introduction

The term Chromotropism is defined as a reversible change in absorption spectra of compounds in different physical or chemical conditions. There are much interest in investigation of chromotropism phenomenon because of its applications in various fields such as thermosensitive, imaging, photo-switching and sensor-materials [1]. Halochromism is an interesting aspect of chromotropism behavior which is related to the color change of a compund when pH changes occur. Amide ligands are an attractive class of ligands that with pH variation their coordination as protonated/deprotonated change through amide oxygen or imine nitrogen [2]. In view of the attractive amide ligand motivated us to prepare, characterize and investigate chromotropism in a complex with a tridentate amide (L) and N_3 ligands.

2. Methods / Experimental:

The ligand was prepared according to published procedure [2]. The complex was prepare by mixing of the ligand (L), $Cu(ClO_4)_2.6H_2O$ and NaN_3 with the molar ratio 1.1.1 in methanol. The resultant complex was characterized on the basis of elemental analysis, molar conductance, UV-Vis and IR spectroscopies. The structure of the complex was elucidated by x-ray diffraction.

3. Results and Discussion

The complex is halochromic so that its original blue color turns to purple upon addition of a base (NaOH) and colorless in presence of an acid ($HClO_4$) as shown in Fig 1. This phenomenon is totally reversible.

There are two isosbestic points in absorption spectra of the compound with variation of pH. The first isosbestic point is attributed to deprotonation of amide group and the second one is

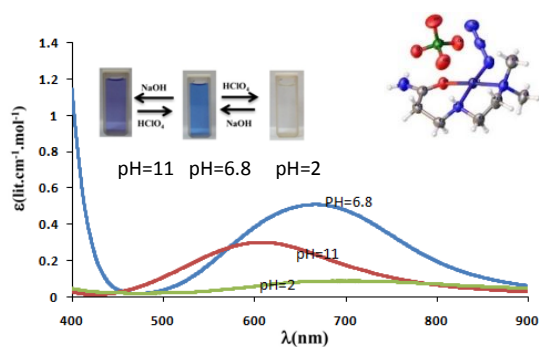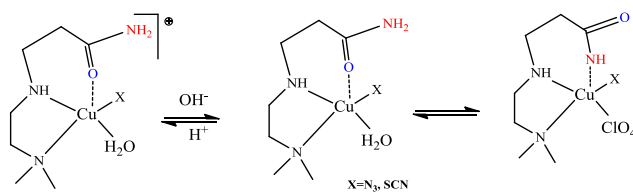due to interchange of Cu-O to Cu-N coordination as shown in scheme 1.

Fig. 1. The pH dependent visible spectrum in aqueous solution at 25 °C.

Scheme 1. Interconversion of The complex triggered by acid and base (pH = 6.5-11.5)

The electronic absorption spectra of the complex in several common organic solvents with different donor power are illustrated in Fig 2. The complex demonstrates solvatochromism properties that is possibly due to the dissociation of the weakly coordinated perchlorate anion from the coordination sphere that facilitates the approach of the solvent molecules to the copper(II) center.
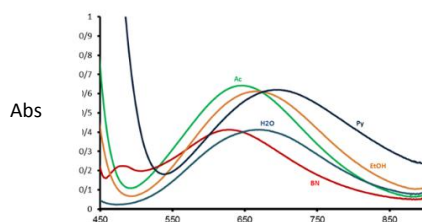

Fig. 2. Solvatochromic behavior of the compound in different solvents

4. Conclusion:

The prepared new complex containing hemilabile amide group demonstrated chromotropism behavior. The complex with structurally switchable response to change pH, absorption changes were arise from ionization of the amide protons and followed by the Cu-O to Cu-N interchange. The compound is also solvatochromic. SMLR investigation results indicated that the donor number parameter of the solvent is the most effective factor in shift of d-d absorption of the complex.

References:

[1] H. Golchoubian; E. Rezaee ; G. Bruno; H. Amiri Rudbari, Inorganic Chimica Acta, 366(2011)290-297.

[2] H. Golchoubian ; A. Heidarain; E. Rezaee; F. Nicolò, , Dyes and Pigments 104 (2014) 175-184.

Electronic and magneto structural Investigation of some new Copper complexes of Amine Bis (Phenolate) Ligands

Mahboobeh Shahsavari[a], Elham Safaei[a]

[a]Department of Chemistry, College of Sciences, Shiraz University, Shiraz 71454, Iran

E-mail: e.safaei@shirazu.ac.ir

Introduction: Galactose oxidase (GOase) is a kind of radical-coupled copper oxidases that catalyze the oxidation of primary alcohols into aldehydes [1]. The crystal structure of galactose oxidase has shown that the active site of this enzyme is including two tyrosine and two cysteine residues of amino acides. This cofactor serves as a redox center by shuttling between the phenol and phenoxyl radical forms during the course of the redox cycle. Thus, the active species (fully oxidized state) of the enzyme is the Cu(II)–phenoxyl radical of tyrosine that can oxidize alcohols to the corresponding aldehydes [2]. In the present work, synthesis of some copper complexes of bis(phenol) amine ligands has been reported. In addition, the effect of substituent on phenol groups on magnetic moments of complexes has been investigated.

Method: At first step bis (phenol) amine ligands were synthesize from the reaction of phenol, formaldehyde and corresponding amine. Triethylamine was added to a solution of bis(phenol) amine in ethanol. $Cu(OAc)_2.H_2O$ was added to this solution and the resulting mixture was stirrer for 2 h. Crystals suitable for X-ray diffraction were obtained by the slow evaporation of dichloromethane/methanol mixture. Copper complexes were characterized by IR, UV-vis, X-Ray diffraction and magnetic susceptibility studies. Electrochemical oxidation of these complexes yields the corresponding Cu(II)–phenoyl radical species.

Results: The X-Ray crystal analysis show that the complexes are dimer in nature in which copper atom has been surrounded by oxygen and nitrogen atoms of ligand and two bridge phenolate groups. The magnetic results confirm binuclear character of complexes with Cu(II) (S=1/2) centers.
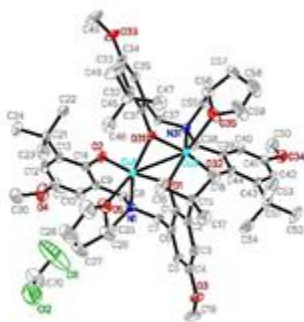
Conclusion: Some new copper(II) complexes were synthesized and characterized. Our studies show that the magnetic moments of complexes have been tuned by the variation of the substituents on phenol groups coordinated to Cu(II) center.

Refrences:

1. L. Que Jr., W.B. Tolman, Nature 455 (2008) 333

2. S. Itoh, M. Taki, and S. Fukuzumi, "Active site models for galactose oxidase and related enzymes," *Coordination Chemistry Reviews,* vol. 198, pp. 3-20, 2000

Linear Relationship of the Solubility of Trans-Stilbene with doner strength, acidity, polarity and polarizability of solvents

Marziyeh Mosahebfard [a], Saeed Yousefinejad *,[b]

[a] Department of Chemistry, Shiraz Branch, Islamic Azad University, Shiraz, Iran
[b] Department of Occupational Health Engineering, School of Health, Shiraz University of Medical Sciences, Shiraz, Iran
* Corresponding author (Email: yousefinejad.s@gmail.com; yousefisa@sums.ac.ir)

Introduction: Lots of reports on stilbenes and its derivatives have been published because of their applications in different branches of sciences [1]. Because of the unique properties of stilbenes (fluorescence, phosphorescence, photophysical, photochrome and photochemical properties) various researchers have focused on this subject. Despite of these potentials, one of the problems in stilbenes is their poor solubility which limits some of their applications. Linear solvation energy relationship (LSER) is a well-known approach in quantitative structure property relationship which involves the effects of solvent–solute interactions on physicochemical properties and reactivity parameters [1, 2]. Here, a LSER model was proposed based on solvent empirical parameters to investigate the solubility of trans-stilbene (Fig. 1) in some different solvents.
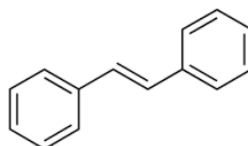

Fig. 1 Molecular structure of trans-stilbene

Methods: Herein, a set of empirical scales (i.e. spectroscopic based, equilibrium-kinetic based, and multiparameters of other measurements) were used as independent variables of the model. Appropriate solvent scales were distinguished by variable selection to use in LSER model. 42 solvents in data set were divided into training (80% of total solvents) and external test set (20% of total solvents) in in order to test the final model performances. Various statistical evaluations were used to check the model's performance [3].

Results and Discussion

Cross validation was used to select the following four-parametric LSER model among those which were selected by variable selection strategy:

$$\log L_{stilbene} = -0.594(\pm 0.110)\, logK + 0.523(\pm 0.107)\, p^* - 0.350(\pm 0.114)\, d - 0.261(\pm 0.112)\, Cu\text{-}\lambda_{max} - 0.204(\pm 0.101)\, Kq^{MMA} \tag{1}$$

$N_{total} = 42$, $N_{train} = 34$, $N_{test} = 8$, $R^2_{train} = 0.84$, $Q^2_{LOO} = 0.80$, $F = 29.186$, $F_{crit\ (95\%).} = 2.56$

In the above suggested quantitative relationship $logK$ denotes the solvatochromic parameter α obtained from some other solvent scales, p^* is a solvatochromic parameter, which implies the solvent ability to stabilize a dipole or a charge by virtue of its dielectric effect and d is the dielectric constants of the solvents. Cu-λ_{max} denotes the maximum absorption band of a copper (II) complex in different solvents and finally Kq^{MMA} is the quenching rate constants to deactivate the triplet thioxanthone by methyl methacrylate. These utilized empirical scales are indicators of donor strength of solvents, solvent acidity polarity of solvents, dipolarity and polarizability of investigated solvents. Defining such relationship is important from the view of solution thermodynamic ($\Delta G_s = -2.3RT\ log\ L$). To indicate chance correlation, y-scrambling was done 50 times and Q^2_{MP} was calculated equal to 0.19 which showed no chance correlation in the proposed LSER model when was compared with Q^2 of original model (=0.80).

Conclusion: Suggested LSER model was based on empirical solvent scales which is a rich source of information about the solvent-solute interactions. Results showed that various solvent characteristics and solvent-solute interactions are effective in the solubility of trans-stilbene in organic phase. Donor strength, solvent acidity, polarity, and polarizability of solvents were some of these effective properties. It can be concluded that polar interactions has a basic role in the solubility of trans-stilbene.

References

[1] Silva F., Figueiras A., Gallardo E., Nerín C., Domingues F. C., *Food Chemistry*, **2014**, 145, 115-125.

[2] Likhtenshtein G. I., Stilbenes Synthesis and Applications. Kirk-Othmer Encyclopedia of Chemical Technology.

[3] Yousefinejad S., Honarasa F., Montaseri H., *RSC Advances*, **2015**, 5, 42266-42275.

A Quantitative Structural Study on the Gas-Organic Solvent Partition Coefficient of Anthracene

Fahime Zangene [a], Saeed Yousefinejad [b,*]

[a] *Department of Chemistry, Shiraz Branch, Islamic Azad University, Shiraz, Iran*

[b] *Department of Occupational Health Engineering, School of Health, Shiraz University of Medical Sciences, Shiraz, Iran*

[*] Corresponding author (Email: yousefinejad.s@gmail.com; yousefisa@sums.ac.ir)

Introduction

Solubility of Polycyclic aromatic hydrocarbons (PAHs) such as anthracene in non-organic electrolytes is of great importance in the oil and gas industry. Bad estimation of PAHs' solubility can cause undesirable deposition and crystallization in the oil and petrochemical equipment. For this purpose, knowledge of the factors affecting solubility of these compounds is important from the industry perspective. In this study, a quantitative solvent's structure-property relationship [1] was developed to investigate the gas-organic solvent partition coefficient of anthracene in 56 pure organic solvents from different categories of non-polar, polar protic and dipolar aprotic.

Materials and Methods

The optimized structure files of solvents (using AM1 as a semi-empirical method) were prepared in Hyperchem software (Version 7, Hypercube Inc., http://www.hyper.com, USA) and were followed by Dragon to calculate different kind of structural descriptors. All of regression and statistical evaluation steps [2] were done in MATLAB (Varsion 7.6.0) environment.

Results and Discussion

Thermodynamic relationship of $\log_{10}L$ (gas-organic solvent partition coefficient or Ostwald Coefficient) and solute's free energy of solvation can be expressed by the following well-known equation [3]:

$$\Delta G_s = -2.3RT \, \log_{10}L \tag{1}$$

To obtain a predictive model for $\log_{10}L$, variable selection by stepwise MLR was done and seven models which some of them may be overfitted. Cross validation confirmed the five-parametric model as the optimized which is presented in the following equation:

log L =4.417 (±0.259) +0.610(±0.053)BLTF96 + 0.143(±0.022)RDF050m −

0.229(±0.090)MATS3p −1.258(±0.507)E1V   (2)

N_{total} = 56, N_{train} = 44, N_{test} = 12, R^2_{train} = 0.84, Q^2_{LOO} = 0.77, F = 39.69, $F_{crit\ (95\%)}$ = 2.46

Five selected parameters included in the proposed model are defined in Table 1. F-test and t-test confirmed the significance of model and the obtain coefficients as well. The pair correlation and muli-correlation between the five utilized descriptors were checked and no significant correlation was observed. Thus the sign and magnitude of MLR coefficient (after standardization) was used to descript the developed model. The above model was constructed using 80% of data set and results were used to predict remaining 20% which was reserved as the test set.

Table 1 Brief definitions and description of variables of the QSPR model

Solvent scale	Definition	Property of scale
GATS1m	Geary 2D-autocorrelation index of lag 1 weighted by mass	Geometry and mass
Hy	hydrophilic factor	Hydrophilic property
E2e	2nd component accessibility directional WHIM index weighted by Sanderson electronegativity	Geometry and Sanderson electronegativity
qneg	total negative charge	Charge interactions
GATS3e	Geary 2D-autocorrelation index of lag 3 weighted by Sanderson electronegativity	Geometry and Sanderson electronegativity

Conclusion

New quantitative models using QSPR was proposed to predict the gas-organic solvent partition coefficient of anthracene in the organic phase as a free energy dependent parameter. The advantage of proposed model is its simplicity for application in the solvent that has not even synthesized experimentally. Extension of this work to the mixed solvents rather than a single solvent is in progress for future studies.

References

1. Yousefinejad, S., Hemmateenejad, B., *Chemom. Int. Lab. Syst.,* **2015**, *149*, 177-204.
2. Yousefinejad, S., Honarasa, F., Abbasitabar, F., Arianezhad, Z., *J. Solution Chem*., **2013**, *42*, 1620-1632.
3. Tulp, I., Dobchev, D. A., Katritzky, A. R., Acree Jr, W., & Maran, U.*, J. Chem. Inf. Model.*, **2010**, 50, 1275-1283.

Synthesis of a Novel Magnetic Reusable Organocatalyst Based on 4-Dialkylaminopyridines for One-pot green Synthesis of Pyrimido[4,5-d]pyrimidine Derivatives in Water

S. Khajeh Dangolani[a,] , F. Panahi[b]*, A. Khalafi Nezhad[a]*

[a]*Department of Chemistry, College of Science, Shiraz University, Shiraz, Iran*
[b]*Department of Polymer Engineering and Color Technology, Amirkabir University of Technology, Tehran, Iran.*
**Email address:** fpanahi@aut.ac.ir
                khalafi@susc.ac.ir

Introduction: 4-(Dimethylamino)pyridine (DMAP) is an important organocatalyst for a large variety of organic reactions [1, 2]. Recovery and reuse of organocatalysts after catalytic reactions are important factors in view of sustainable and green chemistry [3, 4]. In this study, we have introduced a new synthetic pathway to graft DMAP moiety on magnetic nanoparticles (MNPs) through the ring opening of oxiran groups on the MNPs surface with N-methylpyridin-4-amine. Then the MNP–DMAP was investigated as catalytic applicability because of simple, rapid and one-pot water-mediated procedure for the synthesis of pyrimido[4,5-d]pyrimidines derivatives in high yield and purity.

Experimentals A mixture of aldehyde (1 mmol), barbituric acid (1 mmol), urea/thiourea (1 mmol) and MNP–DMAP (30 mg, 5 mol%) in H_2O (4 mL) was stirred at room temperature for appropriate time. The progress of the reaction was monitored by TLC. After completion of the reaction, as showed by TLC, the catalyst was recovered magnetically by attaching a general magnet to the external of the reactor vessel and the reaction mixture was filtered and the residual washed with ethanol.

Results and Discussion: The synthetic pathway for the synthesis of the heterogeneous MNP–DMAP catalyst is shown in Scheme 1. The MNP-DMAP catalyst was fully characterized using various techniques such as TEM, SEM, EDX, TGA, XRD, VSM and elemental analysis (Fig 1, 2). Catalyst particles with near spherical morphology are observable in the TEM images of the MNP–DMAP (Fig 1a). The SEM image shows a relatively homogeneous and uniform particles distribution which suitable for catalysis purposes (Fig 1b). After preparation and characterization of the MNP-DMAP catalyst, its catalytic activity was evaluated in a multi component reaction between aldehyd, barbituric acid, urea/thiourea for the preparation of Pyrimido[4,5-d]pyrimidine under green conditions. Thus, a simple system including MNP-DMAP (5 mol%) and H2O at 80 °C was chosen as the optimized reaction conditions (Scheme 2). In order to show that the catalyst activity of the MNP–DMAP catalyst did not change significantly during the reaction process, the nitrogen content of catalyst after 10 cycles of reusability was investigated using the elemental analysis method and the results show that only about 0.2% of nitrogen was lost. These results are in good agreement with the reactivity of MNP–DMAP catalyst after recovery.
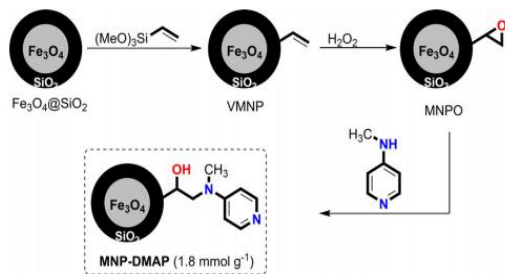
Scheme 1. Synthesis of a new MNP supported DMAP-based catalyst using the ring opening of oxiran-functionalized magnetic nanoparticles with N-methylpyridin-4-amine.
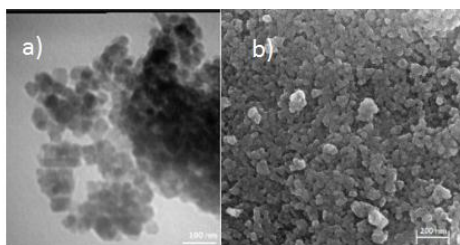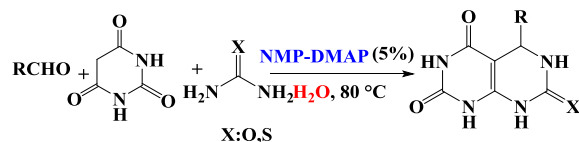

Scheme 2. General strategy for the synthesis of pyrimido[4,5-d]pyrimidines in the presence of MNP–DMAPcatalyst.

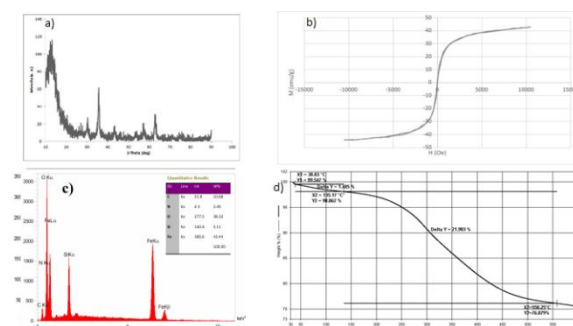Fig. 1. A TEM images MNP-DMAP catalyst particles (a). A SEM image of the MNP-DMAP catalyst (b)

Fig. 2. The XRD pattern of MNP-DMAP catalyst (a). The vibrating sample magnetometer (VSM) of the MNP-DMAP catalyst(b). The EDX analysis of the MNP-DMAP catalyst (c). A thermal gravimetric analysis of the MNP-DMAP catalysts.

Conclusion: we have introduced an efficient and simple method for chemical stabilization of DMAP on magnetic nanoparticles. This is an efficient strategy for chemical modification of magnetic nanoparticles with DMAP. The MNP–DMAP was used as an efficient heterogeneous organocatalyst in a three-component coupling reaction for one pot synthesis of Pyrimido[4,5-d]pyrimidine derivatives under mild and green conditions. This organocatalyst system was reused 10 times in the designed protocol without any change in its catalytic activity.

References

[1] (a) Xu, S. ; Held, I.; Kempf, B.; Mayr, H.; Steglich, W.; Zipse, H. Chem. Eur. J., 2005, 11, 4751-4757.

[2] Heinrich, M. R.; Klisa, H. S.; Mayr, H.; Steglich, W.; Zipse, H. Angew. Chem., Int. Ed., 2003, 42, 4826-4828.

[3] Wende, R. C.; Schreiner, P. R. Green Chem., 2012, 14, 1821-1849.

[4] Ferre, M.; Pleixats, R. M.; Man, W. C.; Cattoen, X. Green Chem., 2016, 18, 881-922.

A New Acrylamide-Based Monomer with Metal Coordination Ability: Surface Grafting of Polymer onto Magnetite Nanoparticles via ATRP

**Masoumeh Mirzaeinejad[-a], Yagoub Mansoori [a*]**

[a] *Department of Applied Chemistry, University of Mohaghegh Ardabili, 56199-11367, Ardabil, Iran.*
Email: ya_mansoori@yahoo.com, ya_mansoori@uma.ac.ir

****

Introduction:

Among different nanoparticles, magnetite nanoparticles (MNPs) are widely studied and have found their way into various domains including drug delivery [1], catalysis [2] and waste water treatment [3]. Removing harmful heavy metal ions from industrial effluent is one of the most important challenges focused by many researchers [4]. Functionalized magnetic nanoparticles are excellent candidates for the selective extraction of metal traces from waste water streams or industrial effluents. These sophisticated adsorbents can act toward metal ions as a kind of "nanosponges" and they can easily be retrieved with a magnet [5].

Methods / Experimentals: At first, commercially available pyiridine-2-carbonitrile (I), was converted into pyridine-2-(1H)-tetrazole (II) upon reaction with sodium azide in refluxing DMF in the presence of ammonium chloride. The subsequent reaction of pyridine-2-(1H)-tetrazole (II) with 4-nitrobenzoyl chloride, Huisgen rearrangement, followed by reduction of (III) with Pd/C in the presence of hydrazine, gave the aromatic amine (IV). The monomer (V) was prepared successfully from reaction of acryloyl chloride with aromatic amine (IV), Scheme 1.
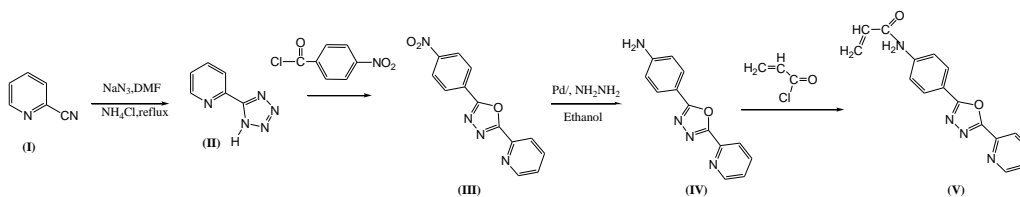
Scheme 1: Synthesis of monomer **V**.

Results and Discussion: In this work, a novel monomer, 2-(4-aminophenyl)-1,3,4-oxadiazole-2-yl) pyridine, containing a pyridine ring and a 1,3,4-oxadiazole moiety, was designed and synthesized in 4 steps, Scheme 1. The monomer **V** was characterized with the conventional methods. ^{1}HNMR and ^{13}CNMR spectra are shown in the Figure 1. Surface-initiated atom transfer radical polymerization (ATRP) technique was used to grafting the homopolymer of the monomer **(V)** onto MNPs, Scheme 2. The surface grafted MNPs was used for Co(II) removal from aqueous solutions via magnetic separation. Kinetic of adsorption was also investigated.
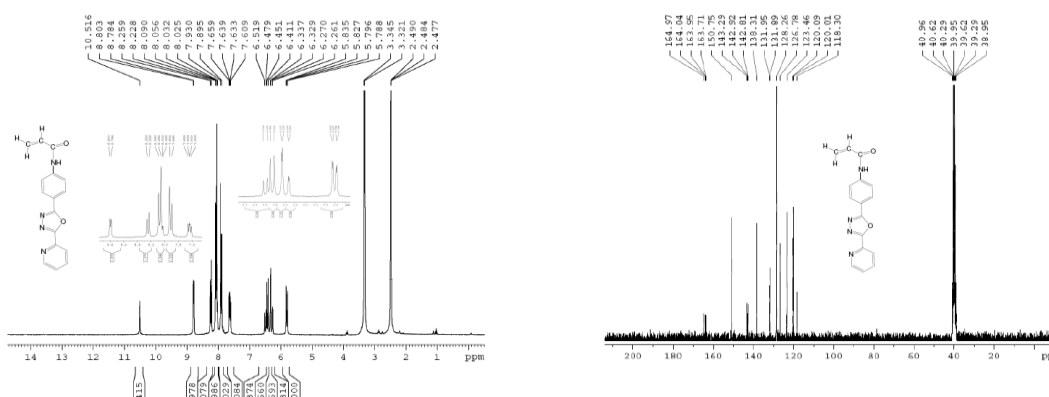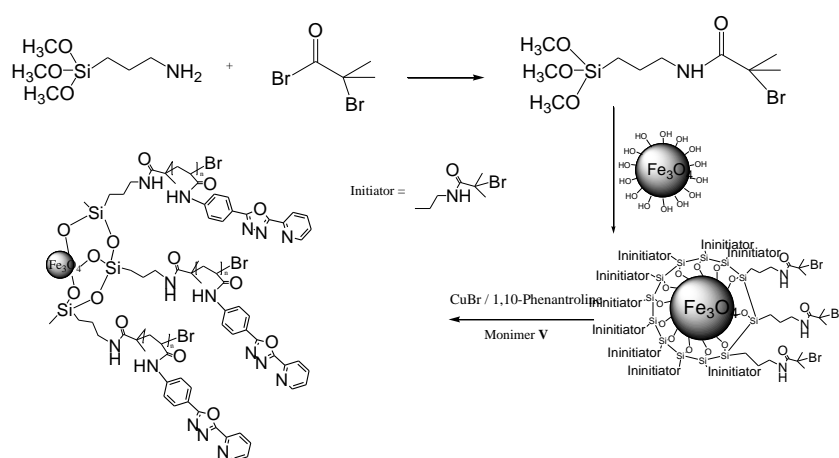
Figure 1: ^{1}HNMR (250 MHz) and ^{13}CNMR (62.5 MHz) spectra of the monomer **V** (DMSO-d$_6$).

Scheme 2: ATRP polymerization of monomer **V** on magnetite.

Conclusion: New acryamide based monomer containing metal ion coordination site was designed synthesized. Surface-initiated ATRP of the monomer on Fe$_3$O$_4$ nanoparticles led to grafting of the homopolymer onto magnetite surface. The prepared nanoparticles were subjected to Co(II) removal from aqueous solution. Kinetic of the adsorption was also studied.

References

[1] Mohapatra, S.; Mallick, S. K.; Maiti, T. K.; Ghosh, S. K., Pramanik, P., *Nanotechnology*. **2007**, *18*, 385102.

[2] Ramasahayam, S.; Gunawan, G.; Finlay, C., Viswanathan, T., *Water, Air, & Soil Pollution*. **2012**, *223*, 4853-4863.

[3] Hashemian, S.; Saffari, H., Ragabion, S., *Water, Air, & Soil Pollution*. **2014**, *226*, 2212.

[4] Ramakrishna, K. R. Viraraghavan, T., *Water Science and Technology*. **1997**, *36*, 189-196.

[5] Mansoori, Y.; Koohi-Zargar, B.; Shekaari, H.; Zamanloo, M. R., Imanzadeh, G. H., *Chinese Journal of Polymer Science (English Edition)*. **2012**, *30*, 112-121.

Determination of the Surface Tension of Some Binary Systems of Imidazolium Based Ionic Liquids by Using Potential Function

S. Behroozi, M. Bahadori*

Department of Chemistry, Marvdasht Branch, Islamic Azad University, Marvdast, Iran

Email mbahadorida@yahoo.com

Introduction: Surface tension is one of the most important subjects of the thermodynamics of ionic liquids. The effect of solvents on the physical properties of ionic liquids is very important. Only a relatively small quantity of data focuses on surface properties of their binary systems. The surface tension of mixtures is not easily correlated with the surface tension of the pure components. Different approaches have been used to predict the surface tension of mixtures but they usually require parameters that are difficult to obtain. Since 2001 many papers have been published on surface tension data on ionic liquid solutions. [1-4]

Methods: A new correlation for surface tension was derived by using the Stock Mayer potential model (Eq. (1)) and some thermodynamic arguments

$$u(r_{ij}) = 4\varepsilon\left[\left(\frac{\sigma_{ij}}{r_{ij}}\right)^{12} - \left(\frac{\sigma_{ij}}{r_{ij}}\right)^{6}\right] + \frac{\mu_i\mu_j}{r_{ij}^3} - \frac{\alpha_i\mu_j^2 + \alpha_j\mu_i^2}{r_{ij}^6} \qquad (1)$$

ε and σ are LJ parameters , μ and α are dipole moment and polarizability. The required parameters components of system were calculated by fitting the experimental data in the equation of state. By using mixing rules the potential parameters, the internal pressure and the pair correction function were determined for mixtures. Finally, the surface tension was calculated from integration.

Results and Discussion: The investigated systems are mixtures of some imidazolium based ionic liquids with ethanol and water. The Stock Mayer potential model was applied as a suitable potential. For a dense fluid, the thermodynamic equation of pressure is:

$$P = T\left(\frac{\partial P}{\partial T}\right)_V - P_{int} \qquad (2)$$

P_{int} is the internal pressure, and is derivation of the potential energy with respect to the volume. To determine P_{int} we suggest $r = K_{cell}V^{1/3}$, where K_{cell} is a constant.

$$P_{int} = -A'\rho^5 + B'\rho^3 + C'\rho \qquad (3)$$

A', B' and C' are constants and ρ is the molar density. By applying Eq. (3) in the pressure equation of state, Eq. (2), the isothermal regularity was attained.

$$(Z - 1)V = A\rho^3 + B\rho + C \qquad (4)$$

Eq.(4) was fitted in the experimental data to find the isotherm parameters A, B and C. They are linear functions of $1/T$ with the slopes A', B' and C'. The magnitude of the slopes, were tabulated in table 1.They were applied to calculate P_{int} of the mixture by using the fallowing mixing rule for each of them.

$$Y'_{mix} = \sum_i \sum_j x_i x_j Y'_{ij} \qquad Y'_{ij} = \left(Y'_i Y'_j\right)^{\frac{1}{2}} \qquad (5)$$

Table 1. The magnitude of A', B' and C' for ionic liquids and solvents.

	$A' \times 10^{10} \left(\dfrac{j\,m^{12}}{K\,mol^5}\right)$	$B' \times 10^2 \left(\dfrac{j\,m^6}{K\,mol^3}\right)$	$D' \left(\dfrac{j\,m^3}{K\,mol^2}\right)$
H_2O	-0.00167	1.663	-73.97
Ethanol	-0.0037	1.714	-44.44
[Bmim]BF$_4$	-1.01	2.155	-116.32
[Hmim]BF$_4$	-1.11	4.66	-217.47
[Bmim]Ntf$_2$	-2.99	14.39	-514.69
[Bmim]PF$_6$	-0.960	2.802	-141.78

Surface tension of a fluid has been expressed directly by Kirkwood and Buff.

$$\gamma = \frac{\pi \rho^2}{8} \int_0^\infty r^4 \frac{du(r)}{dr} g(r)\,dr \tag{6}$$

By using some thermodynamic arguments, this equation was rearranged as:

$$\gamma = -\frac{\pi \rho^2}{8} \int_0^\infty r_m^4 p_{int} \frac{1}{4\eta} \left[\frac{p_{int}}{\rho k_B T} - 1\right] dv \tag{7}$$

η is the packing fraction. The entirely required quantities in Eq. (7) were obtained from the parameters of Eq. (4). Lastly the surface tension in each temperature was estimated by solving the integral. The integral constant was found from the surface tension at 293.15K.

Table 2. The calculated surface tension in a wide temperature and mole fraction range

Mixture	X	T(k)	γ (mN/m)
[Bmim]BF$_4$- EtOH	0.2-0.9	313.15-433.15	16.8-41.6
[Bmim]Ntf$_2$- EtOH	0.194-.818	278.15-338.15	16.6-32.5
[Hmim]PF$_6$- EtOH	0.1-0.85	293.15-318.15	20.7-34.5
[Bmim]PF$_6$- H$_2$O	0.0003-0.0013	298.15-318.15	45.8-39.6
[Bmim]BF$_4$- H$_2$O	0.2-0.9	293.15-353.15	20.4-46.0

Conclusion: In this work, the surface tension of some mixtures of ionic liquid was calculated by using the Stock Mayer potential function. In this method only the experimental PVT data and the surface tension of an individual temperature are required for calculating the surface tension in a wide temperature and mole fraction range. The value and the trend of the calculated surface tensions are in agreement with the experimental data.

References

[1] F. Geng, L. Zheng, L. Yua, G. Li and C. Tung, Process Biochem., **2010**, *45*, 306–311.
[2] V. Pino, C. Yao and J. L. Anderson, J. Colloid Interface Sci., **2009**, *333*, 548–556.
[3] W. Liu, L. Cheng, Y. Zhang, H. Wang and M. Yu, J. Mol. Liq.,**2008**, *140*, 68–72.
[4] M. Ao, P. Huang, G. Xu, X. Yang and Y. Wang, Colloid Polym. Sci., **2009**, 287, 395–402.

Increased Sensitivity and Selectivity of Zinc oxide Nano-Rod by using Al-Dopant as Oxygen Sensor

Mona Nourzadeh[1], Mahdi behzad[1*], Hamideh Samari Jahromi[2], Maryam Barzegar[2]

[1]Department of Chemistry, Semnan University, Semnan, Iran

[2]Institute for environmental research and Biotechnology, RIPI, Tehran, Iran

Corresponding author Email address: mbehzad@semnan.ac.ir

Abstract

In this work, with the purpose of preparing an active sensor for the detection the amount of oxygen for oil tanks application, ZnO nanoparticles were synthesized via a facile hydrothermal method. In order to improve gas sensing performance of the synthesized nanoparticles, aluminum nanoparticles were added as dopant. Synthesized nanomaterials (ZnO and Al-ZnO) were characterized by X-ray diffraction (XRD), Brunauer–Emmet–Teller (BET), Scanning Electron Microscope (SEM) and Energy Dispersive Spectroscopy (EDS). XRD results confirmed that wurtzite hexagonal crystal structure of ZnO was produced. SEM images showed that high quality nanorod and nanoflower structures of ZnO and Al-doped ZnO were successfully produced. Measured active surface area of 33 m^2/g and 15 m^2/g corresponded to ZnO and Al-doped ZnO, respectively. Gas sensing results in the presence of different concentrations of oxygen showed that sensitivity and gas selectivity were increased up to 92 percent by adding aluminum to zinc oxide.

Keywords

Metal Oxide ; Sensor ; Oxygen

Introduction : Oxygen gas monitoring is an important issue in various fields such as the environment, transportation, medicine and agriculture [1,2]. Metal-oxide-semiconductor gas sensors offer an inexpensive and simple method for monitoring gases due to low-cost, small size and real-time detection [3,5]. Oxygen gas sensors have been widely used in industrial heating furnaces, to monitor environments as underground mines, oil fields, and to prevent gas poisoning. However, most of the sensors made up of semiconducting oxide materials have high operating temperature, which is becoming an obstacle in its application in different areas.

Doping of metal elements is an important and effective method for improving the sensing performance of ZnO-based sensors, due to that doping can effectively modulate morphologies and electronic structures of ZnO. For example, We studied the effect of Al dopant on the response of thin film ZnO gas sensors to oxygen[13].

Zinc oxide (ZnO) is a unique II-IV semiconductor material having wide band gap of 3.37 eV and large excitation binding energy of 60 meV, which allows excitonic emission process happens at or even above room temperature [1]. ZnO poses the wurzite family of structures. ZnO also has several interesting types of morphology such as nanocombs, nanowires, nanorings, nanorods, nanoflakes and nanotubes. Generally, the variety growths of morphology could be mainly caused by the variation of the parameters during deposition. ZnO thin films also reported can be deposited on various substrates by numerous methods like magnetron sputtering [2], spray pyrolisis [3], CVD [4] and sol-gel [5]. ZnO can be used in much application such as gas sensors, varistors, optical waveguides, and surface acoustic wave devices. Through this recent year, researcher has found nanotechnology as a solution of a lot of problem. The nanomaterial is a material that scales up to 100 nm. By introducing

nanotechnology in the device fabrication and material preparation process, it can enhance the material or device performances using the nanoscale structure. Above all, many researcher found that the sensitivity of nanostructured ZnO based gas sensors is due to the grain size effect. However, a control growth of nanostructures has always been a challenge in this area. Thus investigation and research on the effect of surface characteristic by varying the deposition parameters is essential. Many researchers reported deposition of ZnO thin film using magnetron sputtering and CVD but both are expensive. Therefore, sol-gel spin-coating method which is comparatively low cost and simple technique has been chosen to prepare nanostructured ZnO thin films. In this work, we study the effect of oxygen flow rate of nanostructured Al-doped ZnO thin films.

Experimental:

CTAB was dissolved in deionized water to produce a clear result. Then zinc powder was added under stirring to the supernatant. The suspension into a stainless steel autoclave was transferred 40 ml with Teflon layer to be tightly sealed. Hydrothermal processes in 140 ℃ for 15 hours. Then the autoclave was cooled naturally. The sediment was collected and was washed several times with deionized water and air dried 80 ℃. Finally 5wt% to about 1 gram of aluminum-doped zinc oxide synthesis has And at 70 ° C for 2 hours, stirring placed And finally in the oven overnight at 150 ° placed and is calcined at 400 degrees for 3 hours. After the powders were prepared for coating to a substrate of alumina was used. Before the final coating, the substrate using ultrasonic bath with ethanol and acetone were washed under, finally using spin coating techniques (spin coating) at 3000 rpm on the cover was given.

Resalts and Disscussion

The morphology, microstructure, crystal structure and chemical composition of aluminum oxide semiconductor adding the impact on the structure of zinc oxide using the technique XRD, SEM , EDS, were studied.

ZnO nanorod and Al-ZnO nanoflower with 5wt% Al loading were prepared using a modifide hydrotermal route , as reported in detail in a previous paper. The SEM images in Fig 1 and 2

The X-ray diffraction (XRD) patterns for various concentrations of Al (5wt%) in ZnO. All of the peaks are indexed to wurtzite hexagonal-shaped ZnO with space group P63mc (Joint Committee on Powder Diffraction Standards (JCPDS) card file 36-1451 . Another technique that helps identify nanoparticles, electron microscopy. The samples were coated with a coating of 10 nm of gold. Resolution transmission electron microscope images taken by the scanning electron accuracy is better, But due to it being expensive and harder as sample preparation steps for getting the most out of SEM is used under an electron microscope.

Conclution

ZnO sensor made based on performance compared to 18% and 23% concentration of oxygen in the system was tested intelligent sensor evaluation. Response of the sensor in the presence of gas at a temperature of 350 ° C and a relative humidity of 20% was investigated. The results show that the response of the sensor sensing made less than 20 seconds. According to the curves in the presence of oxygen gas sensor resistance increases due to regenerative properties And then cut saturated with oxygen gas sensor Initial resistance is to recover.
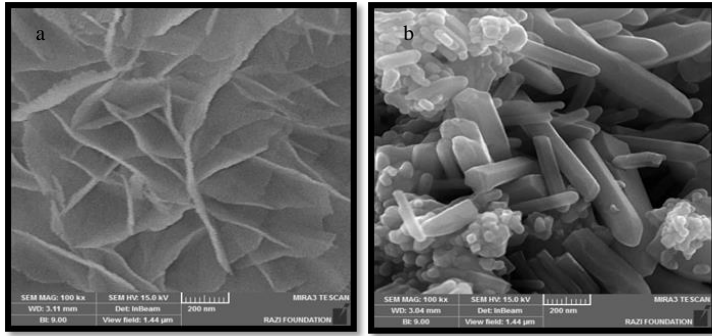
Fig. 1.SEM image of undoped ZnO and (b) SEM image of 5 wt% Al-doped ZnO.

Table 1

Al-doping in ZnO as detected by EDS

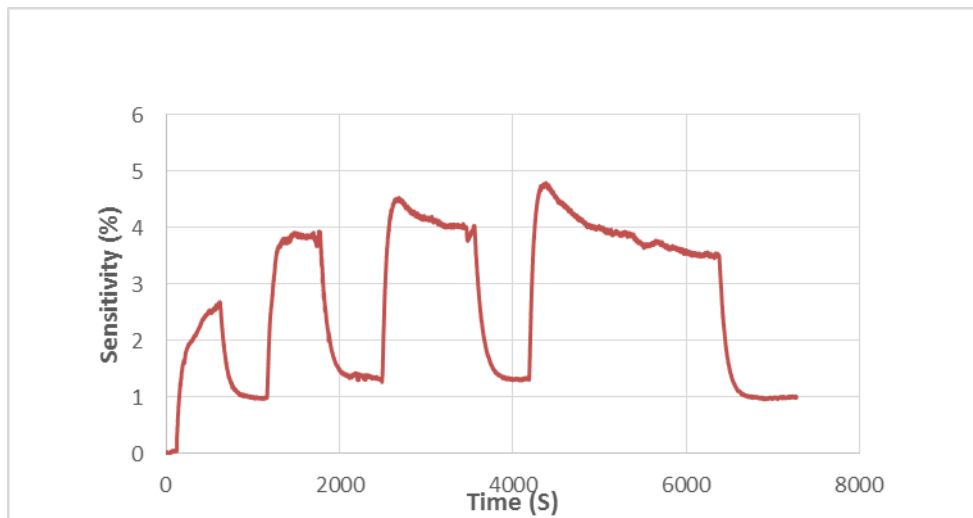| wt% Al added	wt% Al	at.% Al
5wt%	0.19	0.29

Fig. 2 . graph element Al-ZnO sensitivity to concentrations 23% O_2 at 350 ° C
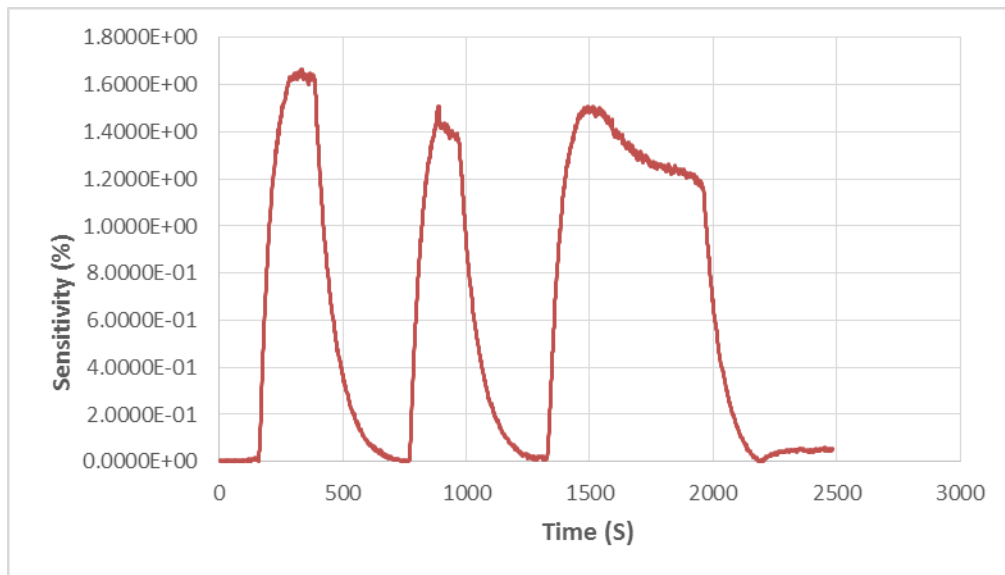
Fig. 3.graph element Al-ZnO sensivity to concentrations 18% O_2 at 350 ° C

References

[1] C. Klingshirn, "The Luminescence of ZnO under High One- and Two- Quantum Excitation," *physica status solidi (b),* vol. 71, pp. 547-556, 1975.

[2] R. Ondo-Ndong, F. Pascal-Delannoy, A. Boyer, A. Giani, and A. Foucaran, "Structural properties of zinc oxide thin films prepared by r.f. magnetron sputtering," *Materials Science and Engineering: B,* vol. 97, pp. 68-73, 1/15/ 2003.

[3] S. M. Rozati, F. Zarenejad, and N. Memarian, "Study on physical properties of indium-doped zinc oxide deposited by spray pyrolysis technique," *Thin Solid Films,* vol. 520, pp. 1259-1262, 12/1/ 2011.

[4] C. L. Wu, L. Chang, H. G. Chen, C. W. Lin, T. F. Chang, Y. C. Chao*, et al.*, "Growth and characterization of chemical-vapor-deposited zinc oxide nanorods," *Thin Solid Films,* vol. 498, pp. 137-141, 3/1/ 2006.

[5] M. H. Mamat, Z. Khusaimi, M. Z. Musa, M. F. Malek, and M. Rusop, "Fabrication of ultraviolet photoconductive sensor using a novelaluminium-doped zinc oxide nanorod–nanoflake network thin film prepared via ultrasonic-assisted sol–gel and immersion methods," *Sensors and Actuators A: Physical,* vol. 171, pp. 241-247, 2011.

Increased Sensitivity and Selectivity of Zinc oxide Nano-Rod by using Al-Dopant as Oxygen Sensor

Mona Nourzadeh[1,2], Mahdi behzad[1*], Hamideh Samari Jahromi[2], Maryam Barzegar[2]

[1]Department of Chemistry, Semnan University, Semnan, Iran

[2]Institute for environmental research and Biotechnology, RIPI, Tehran, Iran

Corresponding author Email address: mbehzad@semnan.ac.ir

Introduction : ZnO poses the wurzite family of structures. ZnO also has several interesting types of morphology such as nanocombs, nanowires, nanorings, nanorods, nanoflakes and nanotubes. Generally, the variety growths of morphology could be mainly caused by the variation of the parameters during deposition. ZnO thin films also reported can be deposited on various substrates by numerous methods like magnetron sputtering , spray pyrolisis , CVD ,hydrothermal , and sol-gel [١] . Through this recent year, researcher has found nanotechnology as a solution of a lot of problem. The nanomaterial is a material that scales up to ١٠٠ nm. By introducing nanotechnology in the device fabrication and material preparation process, it can enhance the material or device performances using the nanoscale structure. Above all, many researcher found that the sensitivity of nanostructured ZnO based gas sensors is due to the grain size effect. However, a control growth of nanostructures has always been a challenge in this area. Thus investigation and research on the effect of surface characteristic by varying the deposition parameters is essential . therefore Oxygen gas monitoring is an important issue in various fields such as the environment, transportation, medicine and agriculture [٢]. Oxygen gas sensors have been widely used in industrial heating furnaces, to monitor environments as underground mines, oil fields, and to prevent gas poisoning. Doping of metal elements is an important and effective method for improving the sensing performance of ZnO-based sensors . In this work , we study the effect of oxygen flow rate of nanostructured Al-doped ZnO thin films .

Experimental

CTAB was dissolved in deionized water to produce a clear result. Then zinc powder was added under stirring to the supernatant. The suspension into a stainless steel autoclave was transferred ٤٠ ml with Teflon layer to be tightly sealed. Hydrothermal processes in ١٤٠ ºC for ١٥ hours. Then the autoclave was cooled naturally. The sediment was collected and was washed several times with deionized water and air dried ٨٠ ºC [٣] . Finally ٥wt%

to about ١ gram of aluminum-doped zinc oxide synthesis has And at ٧٠ ° C for ٢ hours, stirring placed And finally in the oven overnight at ١٥٠ ° placed and is calcined at ٤٠٠ degrees for ٣ hours.

Resalts and Disscussion

The morphology, microstructure, crystal structure and chemical composition of aluminum oxide semiconductor adding the impact on the structure of zinc oxide using the technique XRD, SEM , EDS, were studied. ZnO nanorod and Al-ZnO nanoflower with ٥wt% Al loading were prepared using a modifide hydrotermal route , as reported in detail in a previous paper. The X-ray diffraction (XRD) patterns for various concentrations of Al (٥wt%) in ZnO. All of the peaks are indexed to wurtzite hexagonal-shaped ZnO ,Joint Committee on Powder Diffraction Standards (JCPDS) card file ٣٦-١٤٥١ . Another technique that helps identify nanoparticles, electron microscopy. The samples were coated with a coating of ١٠ nm of gold. Resolution transmission electron microscope images taken by the scanning electron accuracy is better, But due to it being expensive and harder as sample preparation steps for getting the most out of SEM is used under an electron microscope.

Conclution

ZnO sensor made based on performance compared to ١٨٪ and ٢٣٪ concentration of oxygen in the system was tested intelligent sensor evaluation. Response of the sensor in the presence of gas at a temperature of ٣٥٠ ° C and a relative humidity of ٢٠٪ was investigated. The results show that the response of the sensor sensing made less than ٢٠ seconds. According to the curves in the presence of oxygen gas sensor resistance increases due to regenerative properties And then cut saturated with oxygen gas sensor Initial resistance is to recover.

References

[١] C. Klingshirn, "The Luminescence of ZnO under High One- and Two- Quantum Excitation," *physica status solidi (b),* vol. ٧١, pp. ٥٤٧-٥٥٦, ١٩٧٥.

[٢] R. Ondo-Ndong, F. Pascal-Delannoy, A. Boyer, A. Giani, and A. Foucaran, "Structural properties of zinc oxide thin films prepared by r.f. magnetron sputtering," *Materials Science and Engineering: B,* vol. ٩٧, pp. ٦٨-٧٣, ١/١٥/ ٢٠٠٣.

[٣] X.M. Sun, X. Chen, Z.X. Deng, Y.D. Li "A CTAB-assisted hydrothermal orientation growth of ZnO nanorods," *Materials Chemistry and Physics,* vol. ٧٨, pp. ٩٩-١٠٤, ٢٩/١/ ٢٠٠١.

Theoretical predictions on the structures and stability of the di noble gas compounds HNgNg'F (Ng=Ar, Kr, Xe)

Authors <u>Zeinab Abdeveiszadeh</u> and Siamak Noorizadeh[*]

Chemistry Department, Faculty of Sciences, Shahid Chamran University of Ahvaz, Ahvaz, Iran

Email noorizadeh_s@scu.ac.ir

Introduction Reporting the first noble-gas compound (xenon hexafluoroplatinate) by Neil Bartlett [1] has been followed by successful synthesis of many other noble-gas compounds. Although it seems that two noble gases do not engage in chemical bonding with each other, many attempts have been made for synthesis of compounds which contain two noble gas atoms connected by a chemical bond [2,3]. In this study, both kinetic and thermodynamic stabilities of noble gas compounds HNgNg'F that Ng and Ng' are two different noble gases (Ar, Kr, Xe), which have not been experimentally observed so far, have been investigated.

Computational methods The geometries of the ground state HNgNg'F molecules (Ng=Ar, Kr, Xe) were optimized using wB97XD functional with def2-TZVPP basis set and M05-2X method with both def2-TZVPP and aug-cc-pVTZ basis sets implemented in the Gaussian09 program. The NBO charge analysis and transition state calculation were performed at M05-2X/def2-TZVPP level of theory for each compound. Transition structures show only one negative frequency and it's associated vibration was confirmed to correspond to the motion along the reaction coordinate using IRC method.

Results and Discussion All species present linear (or quasi linear) structures. NBO charge showed that F atom has negative charge whereas noble gas and H atoms possess positive charges. Bond lengths and NBO charges of the optimized HKrXeF molecule are shown in Fig. 1. The stability of the compounds was studied by computing the transition states for decomposition of HNgNg'F to HF, Ng and Ng'. Two different fragmentation pathways were considered:

$$HNgNg'F \xrightarrow{TS_1} HNgF+Ng' \xrightarrow{TS_2} HF+Ng$$

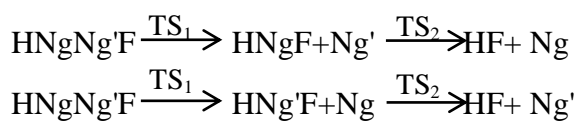$$HNgNg'F \xrightarrow{TS_1} HNg'F+Ng \xrightarrow{TS_2} HF+Ng'$$

Fig.2 shows the transition state structures (TS1). We have focused on the first step of the process which indicates how far a Ng-Ng' compound is prone to decomposition. A low activation barrier indicates low stability for a given compound (table 1).
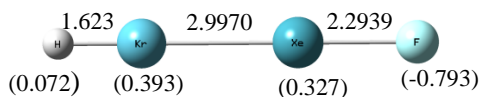

Fig.1. Bond lengths and NBO charges (values in parenthesis) of HKrXeF by M052x/def2-TZVPP.

(a)   (b)

Fig.2. Transition state structures of the pathways (a) HNgNg'F→HNgF+Ng' and (b) HNgNg'F→HNg'F+Ng.

Table 1. Activation barriers ($\Delta E^{\neq}$) computed at M05-2X/def2-TZVPP level.

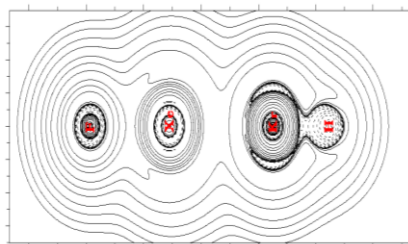| Decomposition pathway	$\Delta E^{\neq}$(Kcal/mol)
HArKrF→HArF+Kr	3.1068
HArKrF⃗→HKrF+Ar	9.3436
HkrArF→HKrF+Ar	0.6300
HKrArH→HArF+Kr	8.5303
HArXeF→HArF+Xe	7.3738
HArXeF→HXeF+Ar	12.8790
HXeArF→HXeF+Ar	1.6666
HXeArF→HArF+Xe	10.9180
HXeKrF→HXeF+Kr	3.9909
HXeKrF→HKrF+Xe	16.5311
HKrXeF→HKrF+Xe	8.9300
HKrXeF→HXeF+Kr	19.6121

Fig.3. Contour line diagram of HKrXeF.

Conclusions. Spherically symmetrical Laplacian distribution ($\nabla^2\rho(r)$) of the fluorine atom in all the compounds shows it's anionic character. positive values of $\nabla^2\rho(r)$ at critical point of Ng'-F bond indicate electrostatic nature of this bond. The critical point of H-Ng bond has negative values of $\nabla^2\rho(r)$ which shows that H-Ng is a covalent bond.
The more stable molecule, HKrXeF, presents higher activation barrier with respect to the other compounds.

References

1. N. Bartlett, *Proc. Chem. Soc*.,**1962**, 218.

2. C. Jimenez-Halla; I. Fernandez; G.Frenking. *Angew. Chem.. Int. Ed*. **2009**, 48, 366-369.

3. I. Fernandez; G.Frenking. *phys. Chem. Chem. Phys*, **2012**, 14, 14869-14877.

Study of Thermophysical Bulk Properties of Morpholinium-based Ionic Liquids by Molecular Dynamics Simulation

Mohammad Hadi GHatee[a,*], Maliheh Pezeshki[a]

[a] Department of Chemistry, Shiraz University, Shiraz 71454, Iran

* ghatee@susc.ac.ir

Introduction: Ionic liquids (ILs) have been interestingly used for diverse applications such as organic synthesize, catalysts, electrochemical devices [1] and so on. ILs show good conductivity as well as suitable electrolytic properties in electrochemical devices [2, 3] and battery industry[4]. Transport properties including diffusion and viscosity of electrolytes play an important role in the electrochemical processes and battery technology. There is a great number of simulation study on the diverse ionic liquids in recent years, but relatively little attention on the simulation of dynamic properties of morpholinium based ionic liquids.

Method: We performed the simulations under conditions of constant pressure and temperature (*NPT* ensemble for density) and constant volume and temperature (*NVT* ensemble) for transport. To calculate density, we performed 5 ns *NPT* simulation on ensemble of methylmorpholinium-based ILs including formate anion, [MeMorph][For]. We study radial distribution function (g(r)) by using output of 10 ns *NVT* simulation with DL_POLY program version 2.17.

Results and Discussion:

1. Temperature dependence of density

We investigated density for [MeMorph][For] from simulation with 25% reduced charge as well as original atomic charges. Result show that there is good agreement with experimental data using main charges.

		[MeMorph][For]	
		a	*b*
T/K	$\rho_{exp.}$/g cm−3	ρ_{sim}/g cm−3 (% Dev.)	ρ_{sim}/g cm−3 (% Dev.)
298.15	1.1297	1.097478(-2.85)	----
308.15	1.1222	1.058473(-5.68)	----
318.15	1.1140	1.046337(-6.07)	1.10344677(-0.95)
328.15	1.1064	1.043319(-5.70)	1.09139558(-1.36)
338.15	1.0991	1.029462(-6.34)	1.07940233(-1.79)
348.15	1.0905	1.026753(-5.85)	----

Table I. Comparison of densities obtained from molecular dynamics simulation and experiment .column (*a*) show density for charges reduced by 25% and (*b* for original charges.

2. Structural properties: Radial distribution function

The bulk structure of [MeMorph][For] IL are studied using site-site radial distribution function. $g(r)$ between H atom (connected to nitrogen of morpholinium cation) and different anion site are shown is Figure II. The first peak with high probability and small dynamic indicate effective interaction between H atom and two oxygens of anion. The broad and shorter peak at about 7 A ° between H and N atoms indicates a weak correlation. According to the simulated $g(r)$, the H atom tends positioning towards anion than the anion.
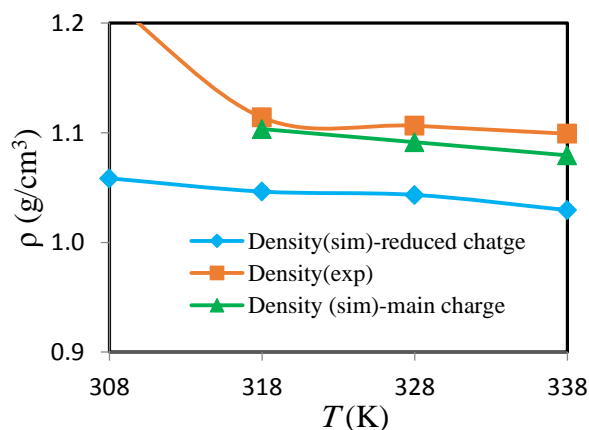

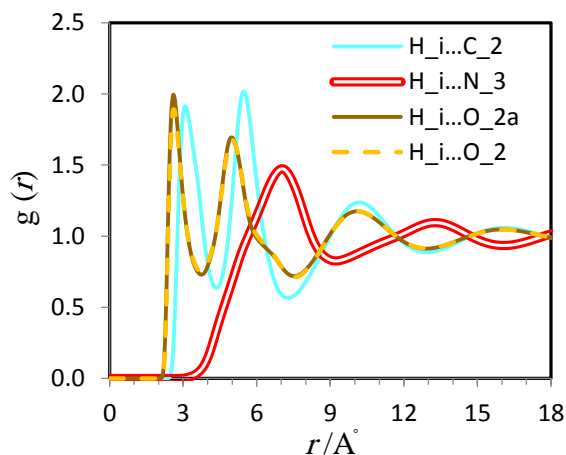Figure I. Comparison of simulated densities with experiments.

Figure II. Radial distribution functions of H atom with different atomic sites of anion for [MeMorph][For] at 328 K.

Conclusion: From calculated density we notice that simulated density with the main charges have more conformity with experimental data. Density is decreased with reduce charge, because charge reduction decreases the cation-anion attraction. From simulated $g(r)$ for [MeMorph][For], we understand that the cation and the anion are not position on average symmetrically with respect to the H atom. The values of simulated viscosities are within 25% reduced charge is calculated. There is good agreement with respect to the experimental values at 308 to 348 K.

References

[1]   N. D. Khupse and A. Kumar, *Indian journal of chemistry. Section A, Inorganic, bio-inorganic, physical, theoretical & analytical chemistry,* 2010, vol. 49, p. 635, 2010.
[2]   A. Lewandowski, M. Zajder, E. Frąckowiak, and F. Béguin, *Electrochimica Acta*, 5/31/ 2001, vol. 46, pp. 2777-2780.
[3]   M. C. Buzzeo, R. G. Evans, and R. G. Compton, *ChemPhysChem*, 2004, vol. 5, pp. 1106-1120.
[4]   X. Wang, Y. Chi, and T. Mu, *Journal of Molecular Liquids*, 2014, vol. 193, pp. 262-266.

Introducing the monotonicity as an effective chemistry based constraint in self modeling curve resolution

Somaye Valizade[a], Mathias Sawall[b], Hamid Abdollahi[a,*], Klaus Neymeyr[b], Mohammad Reza Khoshayand[c]

[a]Faculty of Chemistry, Institute for Advanced Studies in Basic Sciences, Zanjan, Iran
[b]Universit¨at Rostock, Institut f¨ur Mathematik, Ulmenstrasse 69, 18057 Rostock, Germany
[c]Department of Food and Drug Control, School of Pharmacy, Medical Sciences/University of Tehran, Tehran, Iran
abd@iasbs.ac.ir

Introduction: The objective of self modeling curve resolution (SMCR) methods is to decompose a second-order bilinear data matrix into a range of chemically meaningful matrices without any knowledge about the chemical or physical model.

The reduction of the rotational ambiguity in multivariate curve resolution problems is a major challenge in SMCR methods. Constraints such as unimodality and monotonicity for certain concentration profiles is used to reduce the Area of Feasible Solutions (AFS).

The unimodality constraint allows the presence of only one maximum per profile. In the monotonicity constraint, concentration profiles of the reactants and products of a chemical reaction can usually be assumed as monotone decreasing or increasing functions.

Methods / Experimentals: for computing the AFS of two and three component systems, we used the grid search method with used nonnegativity constraint. In order to investigate monotonicity and unimodality constraints, were implemented in grid search algorithm.

Results and Discussion: we used the simulated data for investigation of monotonicity constraint. Two kinetics of first order was considered for simulating data set. The associated bands of solutions simulated data and their area of feasible solution are shown in figure (1):
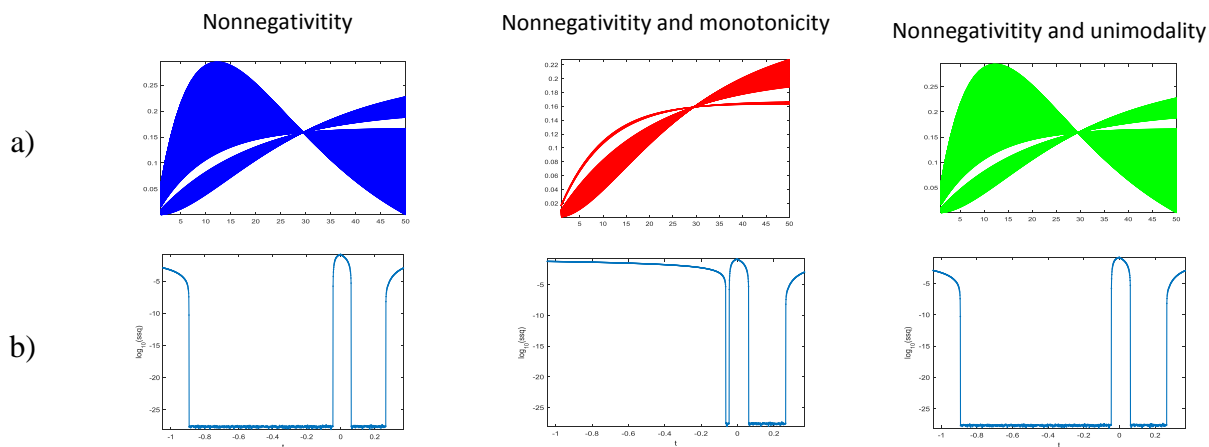
Figure 1: a) The associated bands of concentration profiles for simulated data with nonnegativity, monotonicity and unimodality constraint, respectively and b) their area of feasible solution.

Conclusion: the aim of this work is to introduce and demonstrate the impact of monotonicity and unimodality constraints on the full set of all feasible, nonnegative solutions, and comparing these two constraints in different systems. As illustrated in the result section, monotonicity is a meaningful chemistry based constraint which in some cases is more effective than unimodality.

[1] M. Sawall, N. Rahimdoust, C. Kubis, *Chemometrics and Intelligent Laboratory Systems*, **2015**, 149, 140-150.

Graphene oxide (GO) catalyzed Aza Michael Addition of Amines to Chalcones Through in situ Generation of Michael Acceptors

Salime Lavian, Dariush Khalili*

Department of Chemistry, College of Sciences, Shiraz University, Shiraz 71454, Iran

*Corresponding Author E-mail: khalili@shirazu.ac.ir

Introduction

Harnessing the efficiency of graphene oxide (GO) as a carbocatalyst for various synthetic reactions is a recently sought after challenge [1-3]. GO possesses a rich chemical functionality, is slightly acidic and has long been recognized as having strong oxidizing properties [4]. Owing to the unique properties of this carbon material, the use of GO as a metal-free catalyst is a growing area of interest [5,6]. The formation of new carbon-heteroatom bonds via aza-Michael addition is an important transformation in organic chemistry, as these compounds are extensively used in the synthesis of a variety of biologically active and natural products [7]. In recent years, various methodologies have been reported for this reaction [8]. Now we wish to report the use of GO as heterogeneous carbocatalyst for the synthesis of various β-amino compounds through in situ generation of chalcones and then Aza-Michael addition of amines to the prepared chalcones.

Methods / Experimentals

General Procedure for the Aza-Michael addition reaction: A 10 mL flask was charged with 50 mg of GO, methyl ketone (0.5 mmol), aldehyde (0.5 mmol) and a magnetic stir bar. The flask was heated at 80 ° C for 12 h. Afterward, amine (0.5 mmol) was added to the reaction mixture and heated at 80 ° C for an additional 12 h. After completion the reaction, the reaction mixture was diluted with CH_2Cl_2 and GO was separated by simple filtration. After evaporation of the solvent, the obtained crude product was purified by column chromatography.

Results and Discussion

GO obtained by oxidation of graphite using the modified Hummer's method [9]. The synthetic GO was characterized using FT-IR and XRD. Then we used GO as catalyst for solvent free aldol condensation reaction and sequentially Aza-Michael addition in one step (Scheme 1).
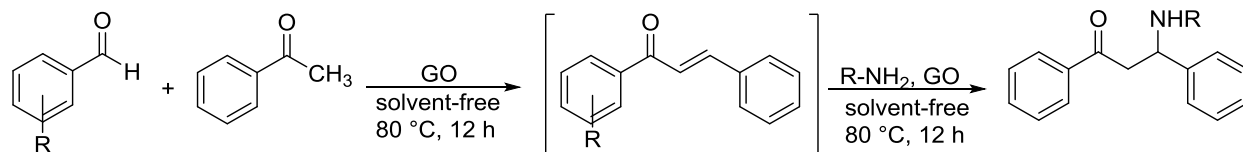
Scheme 1. Aldol condensation reaction and sequentially Michael addition by using GO as catalyst

Next, we extended the scope of the reaction by using a variety of primary and secondary amines with various in situ generated α,β-unsaturated compounds under the described reaction conditions to afford the corresponding β-amino compounds. These results are presented in Table 1.

Table 1: GO promoted Aza-Michael addition of amines to chalcones

Entry	Aldehyde	Ketone	Amine	Yield (%)
1	Benzaldehyde	Acetophenone	Aniline	74
2	4-Methylbenzaldehyde	Acetophenone	Aniline	58
3	4-Chlorobenzaldehyde	Acetophenone	Aniline	79
4	4-Nitrobenzaldehyde	Acetophenone	2,4-Dimethoxy aniline	82
5	Benzaldehyde	Acetophenone	2,4-Dimethoxy aniline	86

Conclusion

In conclusion, graphene oxide was found to be an efficient catalyst for the synthesis of various amino-substituted compounds *via* aza-Michael addition of amines and chalcones. In addition, GO also catalyzed in situ generation of chalcones through Aldol condensation reaction of aldehydes and ketones.

References

[1] Su, C.; Tandiana, R.; Balapanuru, J.; Tang, W.; Pareek, K.; Nai, C. T.; Hayashi, T.; Loh, K. P. *J. Am. Chem. Soc.*, **2015**, *137*, 685.
[2] Sengupta, A.; Su, C.; Bao, C.; Nai, C. T.; Loh, K. P. *ChemCatChem*, **2014**, *6*, 2507.
[3] Garg, B.; Bisht, T.; Ling, Y. C. *RSC Adv.*, **2014**, *4*, 57297.
[4] Zhou, K. G.; Mao, N. N.; Wang, H. X.; Peng, Y.; Zhang, H. L.; *Angew.Chem., Int. Ed.*, **2011**, *50*, 10839.
[5] Trandafir, M. M.; Florea, M.; Neaţu, F.; Primo, A.; Parvulescu, V. I.; García, H. *ChemSusChem*, **2016**, *9*, 1565.
[6] Primo, A.; Puche, M.; Pavel, O. D.; Cojocaru, B.; Tirsoaga, A.; Parvulescu, V.; García, H. *Chem. Commun.*, **2016**, *52*, 1839.
[7] Xu, L. W.; Xia C. G.; Hu, X. X.; *Chem. Commun.*, **2003**, 2570.
[8] a) Verma, S.; Jain, S. L.; Sain, B.; *Org. Biomol. Chem.,* **2011**, *9*, 2314; b) Polshettiwar, V.; Varma, R. S. *Tetrahedron*, **2010**, *66*, 1091.
[7] Hummers, W. S.; Offeman.; R. E. *J. Am. Chem. Soc.,* **1958**, *80*, 1339.

QSAR for Antibacterial Activity in a New Set of Formyl Hydroxyamino Derivatives

Sahar Rasekh [a], **Saeed Yousefinejad** *,[b]

[a] *Department of Chemistry, Shiraz Branch, Islamic Azad University, Shiraz, Iran*

[b] Research Center for Health Sciences , *School of Health, Shiraz University of Medical Sciences, Shiraz, Iran*

* Corresponding author (Email: yousefinejad.s@gmail.com; yousefisa@sums.ac.ir)

Introduction: Increasing the prevalence of multi drug-resistant (MDR) bacteria from clinical isolates is a problem which has raised the importance of the search for new antibacterial agents with novel modes of action. Peptide deformylase (PDF) has been identified as a promising target for novel antibacterial agents [1]. In this study, a quantitative structure relationship was developed for a set of new formyl hydroxyamino derivatives as PDF inhibitors to evaluate their antibacterial activities. It is worthy to note that one of the new targets currently receiving widespread attention from both academic and industrial research groups is peptide deformylase(PDF) [2]. PDF is an iron-containing metalloenzyme involved in the post-translational modification of nascent polypeptides in bacterial cells [2].

Materials and methods: QSAR is a tool in drug design and its roles in the estimation of non-synthesized active compounds should not be overlooked [3]. In the present study, 44- new Formyl Hydroxyamino derivatives (Fig. 1) with defined activities against three bacteria were modeled by QSAR. Feed-forward artificial neural network (ANN) with Levenberg-Marqart algorithm was used as the non-linear regression method and different statistical methods were used to evaluate the results.
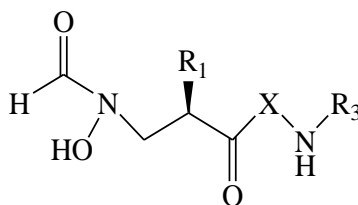
Fig. 1 The structural skeleton of 44 antibacterial compounds used in the current work

Results and Discussion: After extraction of different kind of descriptors from the structure of 44 Formyl Hydroxyamino derivatives and performing variable selection, linear modeling approaches such as MLR and PLS were not successful in finding relationship between structural information and activities of these compound against, MRSA, and MSSA. Thus, ANN was used as a non-linear approach and good relationships were found to predict their activities against

three bacterial infections. As an example the agreement of experimental and predicted values for the model constructed for activity against MSSA (based on our suggested non-linear QSAR model) is represented in Fig. 2.

The squared correlation coefficients for training, validation and test sets in the model suggested for anti-MSSA activity were 0.937, 0.916 and 0.903 respectively. The quality of five-parametric models suggested for activities against S.aures and MRSA were also good.
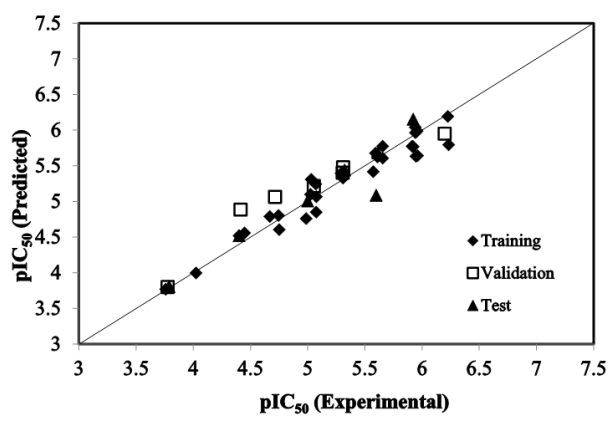

Fig. 2 The predicted pIC$_{50}$ (against MSSA) versus experimental values in training, validation and test sets which were randomly selected form 44 under-evaluation compounds.

Conclusion: According to the importance of anti-bacterial drug design because of multi drug-resistant (MDR) problems, attempts in making predictive models for screening and estimation of the activities of new compound is very important in drug synthesis laboratories. In the current work two layer feed-forward ANN was used successfully for such goal in 44 new anti-bacterial Formyl Hydroxyamino compounds.

References:

[1] Yang S., Shi W., Xing D., Zhao Z., Lv F., Yang L., Yang Y., Hu W.,. *Europ. J. Med. Chem.*, **2014**, *86*, 133-152.

[2] Leeds J.A., Dean C.R., *Curr. opin. pharmacol.***2006**, *6*, 445-452

[3] Yousefinejad S., Hemmateenejad B., *Chemom. Int. Lab. Syst.,* **2015**, *149*, 177-204.

A quantum mechanical investigation on electronic structure of star-shaped poly-titanium oxide nanostructure

Sara Fakhraee*,a, Mona Razi[a]

a Department of Chemistry, Payame Noor University, Shiraz, Iran

Email address: fakhraee@pnu.ac.ir

Key words: poly-titanium oxide, atoms in molecules ,electrical conductivity, electronic structure

Introduction: TiO_2 has been attracted a lot of attention because it eliminates the need of post-treatment separation processes as a suitable catalyst for environmental remediation[1]. It has been shown that when the size of TiO_2 particles transmits from micro to nano, the interfacial interactions between inorganic and organic phases of the composites increase and the size-dependent properties of the nanocomposites can be improved compared to micro-composites[2-5]. The nanocomposites based on poly-titanium oxide (PTO) play a crucial role as photocatalysts in environmental remediation. We have investigated the electronic structure and bond nature of this compound using the atoms in molecules (AIM).

Methods: The geometry optimization, frequencies and wave function calculations were performed using Gaussian 09 at HF/6-31G* level of theory. The wave function of the PTO was analyzed using AIM2000 software. The electronic structures and nature of Ti-O bonds were determined using the descriptor of BCPs based on the AIM theory including: electron density $\rho(r)$, laplacian of electron density $\nabla^2\rho(r)$, electronic potential energy V(r), electronic kinetic energy G(r) and total electronic energy H(r). The optimized structure and molecular graph of PTO have been presented in Fig. 1.
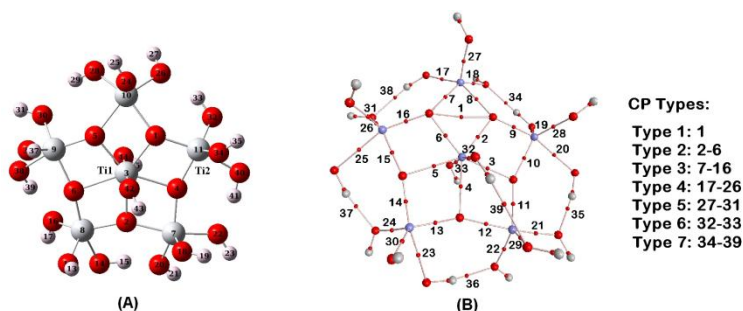
Fig 1: (a) Optimized structure of PTO, (b) Molecular graph of PTO
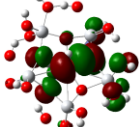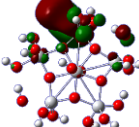
Results and discussion: The PTO includes six Ti atoms, 22 oxygen atoms and 17 hydrogen atoms. Ti atoms in the molecule are of two types: 5-coordination Ti (Ti2) and 7-coordination Ti(Ti1) that have been shown in Fig. 1(a). The structure has 7 types of bonds based on the categorization of Ti-O bonds in Fig. 1(b). The 39 BCPs have been identified between Ti and O atoms. The descriptors of AIM and the nature of Ti-O BCPs have been represented in Table 1. The results show that most BCPs have partially electrostatic-partially covalent nature including the BCP 1 for O-O bond. The other remaining are totally electrostatic in nature.

Table1. The values of descriptors related to the BCPs numbered in Fig 1.

BCP	ρ	$\nabla^2\rho$	G	V	H	nature of BCP
1	O-O	0.0371	0.1336	0.0351	-0.0369	-0.0018	Partially electrostatic partially covalent
2	O-Ti1	0.0944	0.4272	0.1162	-0.1256	-0.0094	Partially electrostatic partially covalent
3	O-Ti1	0.0586	0.2848	0.0685	-0.0658	0.0027	Totally electrostatic
4	O-Ti1	0.0554	0.2724	0.0649	-0.0617	0.0032	Totally electrostatic
5	O-Ti1	0.0460	0.2304	0.0536	-0.0496	0.004	Totally electrostatic
6	O-Ti1	0.0865	0.4072	0.1072	-0.1126	-0.0054	Partially electrostatic partially covalent
7	O-Ti2	0.0723	0.3872	0.0945	-0.0923	0.0022	Totally electrostatic
8	O-Ti2	0.0860	0.4528	0.1157	-0.1183	-0.0026	Partially electrostatic partially covalent
9	O-Ti2	0.1397	0.6212	0.1955	-0.2356	-0.0401	Partially electrostatic partially covalent
10	O-Ti2	0.1122	0.5644	0.1584	-0.1756	-0.0172	Partially electrostatic partially covalent
11	O-Ti2	0.1304	0.6056	0.1831	-0.2149	-0.0318	Partially electrostatic partially covalent
12	O-Ti2	0.0998	0.5148	0.1379	-0.1470	-0.0091	Partially electrostatic partially covalent
13	O-Ti2	0.1508	0.6716	0.2184	-0.2688	-0.0504	Partially electrostatic partially covalent
14	O-Ti2	0.1465	0.6648	0.2118	-0.2575	-0.0457	Partially electrostatic partially covalent
15	O-Ti2	0.1220	0.6008	0.1743	-0.1984	-0.0241	Partially electrostatic partially covalent
16	O-Ti2	0.1586	0.6608	0.2244	-0.2835	-0.0591	Partially electrostatic partially covalent
17	O-Ti2	0.1610	0.6856	0.2328	-0.2943	-0.0615	Partially electrostatic partially covalent
18	O-Ti2	0.1368	0.5742	0.1821	-0.2207	-0.0386	Partially electrostatic partially covalent
19	O-Ti2	0.1786	0.6622	0.2488	-0.3321	-0.0833	Partially electrostatic partially covalent
20	O-Ti2	0.0384	0.2061	0.0457	-0.0399	0.0058	Totally electrostatic
21	O-Ti2	0.1182	0.5604	0.1620	-0.1838	-0.0218	Partially electrostatic partially covalent
22	O-Ti2	0.1204	0.5472	0.1612	-0.1856	-0.0244	Partially electrostatic partially covalent
23	O-Ti2	0.0370	0.1984	0.0440	-0.0358	0.0082	Totally electrostatic
24	O-Ti2	0.1280	0.5888	0.1772	-0.2073	-0.0298	Partially electrostatic partially covalent
25	O-Ti2	0.0331	0.1768	0.0389	-0.0337	0.0052	Totally electrostatic
26	O-Ti2	0.1442	0.6428	0.2049	-0.2491	-0.0442	Partially electrostatic partially covalent
27	O-Ti2	0.1632	0.6632	0.2299	-0.2941	-0.0642	Partially electrostatic partially covalent
28	O-Ti2	0.1564	0.6996	0.2305	-0.2861	-0.0556	Partially electrostatic partially covalent
29	O-Ti2	0.1564	0.6352	0.2161	-0.2734	-0.0573	Partially electrostatic partially covalent
30	O-Ti2	0.1615	0.7104	0.2387	-0.2997	-0.0610	Partially electrostatic partially covalent
31	O-Ti2	0.1640	0.6972	0.2385	-0.3027	-0.0642	Partially electrostatic partially covalent
32	Ti1-O	0.1470	0.6624	0.2125	-0.2594	-0.0469	Partially electrostatic partially covalent
33	Ti1-O	0.1308	0.5904	0.1800	-0.2124	-0.0324	Partially electrostatic partially covalent

The HOMO and LUMO orbitals and energy gap of PTO have been calculated in Table 2. The energy gap of PTO has been calculated about 2.43 e.v which shows a decrease relative to the semiconductor TiO$_2$ nanoparticles with energy gap about 3.21 e.v[6].

Table2. The HOMO and LUMO orbitals energy gap in terms of electron volt.

HOMO	LUMO	Energy gap (e.v)
		2.43

Conclusion: The topological electron density analysis for star-shaped PTO shows that all BCPs between Ti and O are partially electrostatic-partially covalent except for seven bonds which are totally electrostatic. Also, the energy gap for PTO is calculated to be 0.78 e.v less than TiO2 nanoparticles[6].

References:

[1] Singh. S.; Mahalingam.; Singh. P. K.; *Journal of Applied Catalysis A: General.,*(2013), *462,* 178-195.

[2] Saujanya.C.; Radhakrishnan. S.; *Journal of Polymer.,*(2001), *42,* 6723-6731.

[3] Zheng.Y.; Zhengb.Y.; Ning. R.; *Journal of Materials Letters.,*(2003), *57,* 2940-2944.

[4] Estahappan. S. K.; Kuttappan. S. K.; Joseph. R.; *Journal of Polymer Degradation and Stability.,*(2012), *97,* 615-620.

[5] Akkapeddi. M.K.; *Journal of Composites.,*(2002), *21,* 576-585.

[6] Sagadevan. S.; *American Journal of Nanoscience and Nanotechnology.*, (2013), *1(1),* 27-30.

Evaluation of graphene oxide for fuel denitrogenation

M. Shams[a], E. Shams *[a]

[a] Department of Chemistry, university of Isfahan, Isfahan, Iran

e_shams@chem.ui.ac.ir

Introduction:

Desulfurization and denitrogenation of liquid fuels has been receiving dramatic attention. Fuels containing sulfur and nitrogen compounds leads to SO_x and NO_x emissions and especially acid rain. Hence it is necessary to remove S and N compounds from liquid fuels [1]. Among the various methods for denitrogenation and desulfurization of fossil fuels, adsorption-based methods have attracted much attention in the last decade due to the fact that they are performable at ambient pressure and temperature and do not require much energy. In this regard, various adsorbents have been used in order to achieve deep desulfurization and denitrogenation levels. Activated carbon [2], zeolites [3], mesoporous silica [4] has been widely applied to adsorptions of N-compounds. In this studied, adsorptive denitrogenation method from fossil fuels by graphene oxide (GO) has been discussed.

Methods / Experimental:

Batch adsorption studies of pyridine on grapheme oxide were done using a pyridine solution (1000 ppm in n-hexane) 20.00 mg of adsorbent was added into 5.0 mL pyridine solution and it was shaken for 60 min at 25 °C. After the pyridine removal by GO, the remained amount of pyridine in solution was measured with a UV–Vis spectrometer at its maximum absorbance wavelength (240 nm). The amount of equilibrium concentration of pyridine was obtained with the aid of equation $q_e = (C_. - C_e)w/m$, where $C_.$ and C_e are respec- tively the initial and equilibrium concentrations(mg.kg^{-1}) of pyridine in the bulk phase, w is the amount of the liquid phase(kg) and m is the amount of adsorbent(g).

Results and Discussion:

GO was studied as adsorbents for the denitrogenation of liquid hydrocarbon fuels. The adsorbent was synthesized through the oxidation of graphite layers by sulfuric acid and potassium permanganate according to Hummer method. The synthesized GO was characterized by X-ray diffraction and FT-IR technique.

The effects of temperature and shaking time was investigated on the adsorption of pyridine on GO. The results showed that the equilibrium adsorption amount (q_e) of pyridine onto GO is independent of shaking time and decreases by increasing the temperature(Fig. 1), a predictable result due to the exothermic property of adsorption process.

The effect of initial pyrodine concentration in on the extent of its adsorption onto GO at 25 °C using contact time of 60 min is shown in Fig. 2. As can be seen from this figure, the amount of equilibrium adsorption is dependent on the initial pyridine concentration, and also the equilibrium uptake increases with the rise in the adsorbent concentration. In order to better describe the mechanism of DBT adsorption onto GO, three adsorption isotherms including Langmuir, Freundlich and Temkin models were used to fit the equilibrium experimental adsorption data. The results showed that the Langmuir isotherm is better than other isotherms in describing adsorption of pyridine on GO. The maximum adsorption capacity (q_{max}) of GO is 178.6 mg.g^{-1}. Finally, the regeration of the used adsorbent was carried out using different solutions. Tthe carbon adsorbent easily regenerated by washing with HCl/water (2 M) solution.
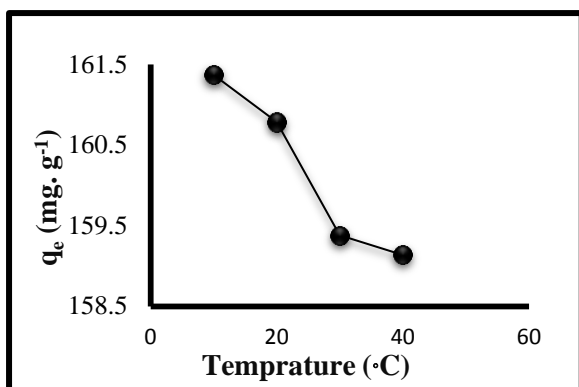
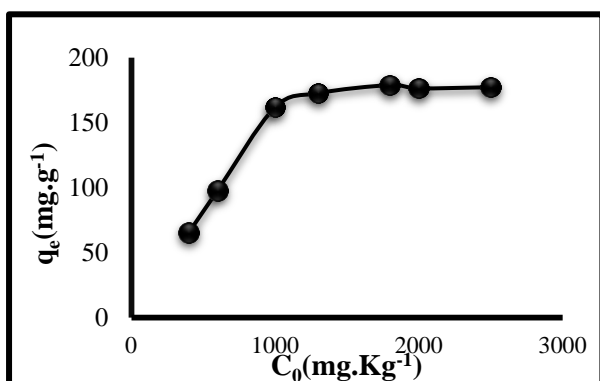Fig ١. Influence of temperature in the range of on the adsorption of pyridine onto GO

Fig ٢. Effect of initial concentration of pyridine on adsorption.

Conclusion:

This work has focused on the removal of liquid phase aromatic nitrogen compound (i.e. pyridine) by GO nanostructure carbonaceous materials. The results of adsorption isotherm study indicated that Langmuir model best represents the equilibrium adsorption data. Typically, ١٧٨.٦ mg g^{-1} pyridine removal by GO was obtained at ٢٥ ^{o}C and after ٦٠ min equilibrium time. The spent N-containing adsorbent can be regenerated with HCl/water (٢ M) by simple extraction process.

References:

[١] Touhoat, H; Kessas, R. Hydrodenitrogenation of Distillates Issuing from the Conversion of Heavy Hydrocarbons, *Revue De L Institut Francais Du Petrole,* ١٩٨٦, ٤١, ٥١١-٥٢٧.

[٢] Han, X; Lin, H; Zheng, Y. Understanding capacity loss of activated carbons in the adsorption and regeneration process for denitrogenation and desulfurization of diesel fuels, *Sep. Purif. Technol.,* ٢٠١٤, ١٣٣, ١٩٤-٢٠٣.

[٣] Hernández-Maldonado, A. J; Yang, R. T. Denitrogenation of Transportation Fuels by Zeolites at Ambient Temperature and Pressure, *Angew. Chem.,* ٢٠٠٤, ١١٦, ١٠٢٢-١٠٢٤.

[٤] Ahmed, I; Jhung, S.H. Adsorptive denitrogenation of model fuel with cucl-loaded metal–organic frameworks (MOFs), *Chem. Eng. J.,* ٢٠١٤, ٢٥١, ٣٥-٤٢.

Head space solid-phase microextraction of phthalate esters from aqueous media by activated carbon/polyaniline nanofiber composite on a stainless steel fiber

Mostafa Ghaemmaghami, Yadollah Yamini[*], Hatam amanzadeh

Department of Chemistry, Tarbiat Modares University, P.O. Box 14115-175, Tehran, Iran

yyamini@modares.ac.ir*

Introduction: The coating type of solid phase microextraction plays a crucial role in the efficiency of the extraction, as it is the main factor affecting the distribution constant between the sample matrix and the immobilized phase. In recent years, nanomaterials have been attractive for extraction techniques because of their high porosity, which improves the extraction rate and the extraction efficiency. The remarkable thermal, mechanical and chemical stability of nanomaterials has resulted in their usage as SPME coatings [1-2]. In this study, a novel coating, namely activated carbon/polyaniline (AC/PANI) nanocomposite was prepared on a stainless steel (SS) wire and evaluated as a SPME fiber coating for the headspace solid-phase microextraction of phthalate esters (PEs) from aqueous media.

Experimental: The activated carbon/polyaniline nanofiber (AC/PANI-NF) composite was synthesized by an in-situ chemical polymerization method. Chemical oxidation of aniline was carried out at high acidity (0.5 M HCl). 0.05 M of aniline monomers was prepared in 0.5 M HCl solution containing 100 mg activated carbon . Then, 0.2 M ammonium persulfate (APS) in deionized water as an oxidizing agent was used for oxidative polymerization. Both solutions were rapidly mixed together in the same proportion at room temperature.

To perform the extraction of phthalate esters, 10 mL sample solution containing (0-3) g NaCl was added into a 15 mL glass vial with PTFE–silicon septum. After adding a magnetic stirring bar the vial was tightly sealed with an aluminum cap. The vial was then placed on a magnetic stirrer with a water bath and the stirring rate was fixed at (0-1200) rpm. When the temperature reached to the fixed value (40-90) $^\circ$C the syringe needle was pushed through the septum of vial and the SPME fiber was exposed to the head space over the stirred solution for (5-40) min. Then the fiber was withdrawn into the needle, removed from the vial and immediately introduced into

the GC injection port for thermal desorption desorption at (260-290) $^\circ$C in the splitless mode for 8 min.

Results and Discussion: The optimization strategy of the extraction process was carried out using the one-variable-at-a-time (OVAT) process. the developed method gave a low limit of detection (0.03–0.08 µg L^{-1}) and good linearity (0.1–100 µg L^{-1}) for the determination of the PEs under the optimized conditions (extraction temperature, 90 ± 1°C; extraction time, 30 min; salt concentration, 25% w/v; stirring rate, 1000 rpm; desorption temperature, 280 $^\circ$C;and desorption time, 8 min) whereas the repeatability and fiber-to-fiber reproducibility were in the range 6.5–8.7% and 9.7–11.3%, respectively. Finally, the proposed method was successfully applied to the analysis of PEs in waters sample with good recoveries (88–114%) and satisfactory precisions (RSDs < 8.7%).

Conclusions: A new laboratory-made SPME fiber was prepared and successfully applied for the detection of the trace levels of PEs in the water samples. The proposed fiber has the following merits: (i) high temperature and mechanical resistance, (ii) long life span, and (iii) high extraction efficiency. The method showed satisfactory accuracy, linearity, precision, and LODs.

References

[1] Xu, J.; Zheng, J.; Tian, J.; Zhu, F.; Zeng, F.; Su, C.; Ouyang, G. TrAC Trends in Analytical Chemistry 2013, 47, 68.

[2] Spietelun, A.; Kloskowski, A.; Chrzanowski, W.; Namieśnik, J. Chemical Reviews 2013, 113, 1667.

Simultaneous determination and quantification of picoline derivatives using UV-vis spectroscopy and multivariate calibration methods

AlirezaHoseini Madani [a], **Ahmad Mani-Varnosfaderani** [*a], **Nadeer Alizadeh Motlagh**[a]

a Department of Chemistry, Tarbiat Modares University, Tehran, Iran

* Corresponding author, email: a.mani@modares.ac.ir

Introduction

Picolines are methyl-substituted pyridine derivatives which are also structural isomers. Pyridine and its derivatives are widely used in various processes and industries. As the usage of these compounds as solvent or precursors for chemical reactions increases, therefore they are widely distributed in environment. Separation and determination of isomeric compounds (compounds with an identical molecular weight but different structures) has been a challenging issue for many years (1-3). In the present contribution, we have used the UV-vis spectra to determine and quantify α, ß, and γ picoline isomers, simultaneously.

Methods / Experimental

First step was to find the best solvent which provides the most dissimilar UV-vis spectra for the picoline isomers. Effect of four solvents of methanol, 2-propanol, 2-buthanol and deionized water has been explored. The UV spectra were gained by SCINCO 2100 UV-VIS Spectroscopy. In the next step, we considered the pH effect on the resolution of the UV-vis spectra of picolines. The pH effect was examined in five levels (i.e. pH=1, pH=4, pH=6.5, pH=9, pH=12).

The central composite design (CCD) approach has been used to make the calibration set. DESIGN EXPERT software (version 7.5.) was used for generation of the design matrix.

Results and Discussion

First of all, we found an appropriate solvent for isomers of picoline to have a good solubility and differentiation (dissimilarity of UV spectra). Water has shown the best difference between the UV spectra of the isomers. The optimization procedure has been continued by exploring the pH effect on the resolution of the UV spectra. After the optimization procedure, the deionized water with pH equals to 4 was chosen as the solvent to make the calibration set. An orthogonal CCD design with three factors (3 picolines isomers) suggested performing 20 runs for making the calibration set. Each run repeated 3 times to yield 60 experiments. The obtained UV spectra have been used for development of the multivariate calibration models. Different strategies such as multiple linear regression (MLR), principle component regression (PCR) and partial least square

(PLS) have been used for making the mathematical relationships between the UV spectra and the concentration profiles. The results are given in Table 1[]. The results in Table 1 illustrate that the multivariate calibration methods accurately determines the concentration of the isomeres of picolines in aqueous samples. Generally, the present work suggest that it is possible to design situation which a simple and easy technique provides as systematic way for determination of isomeric compounds using multivariate calibration methods.

	MLR		PCR		PLS	
	R^2	RMSE	R^2	RMSE	R^2	RMSE
α- Picoline	0.96	0.98	0.95	1.06	0.95	1.14
ß-Picoline	0.97	0.9	0.96	0.97	0.94	1.18
γ-Picoline	0.99	0.58	0.98	0.59	0.98	0.69

Conclusion

Separation of isomeric compounds (compounds with an identical molecular weight but different structures) has been a challenging issue for many years. The researchers in the field of analytical chemistry have used some complicated instruments such as mass spectrometry, ion mobility spectroscopy and chiral columns in chromatography for separation and quantification of isomeric compounds. In the present contribution, a simple and rapid strategy based on the combination of UV-Vis spectroscopy and multivariate calibration methods has been successfully suggested for simultaneous determination of picoline isomers. The results in this work revealed that the coefficient of determination between the predicted concentration and real concentrations were more than 0.95 and it reveals the robustness and reliability of the developed models in this work.

References

1.   Ghaemi E, Alizadeh N. Nanoclusters formation in ion mobility spectrometry and change separation selectivity of picoline isomers. International Journal for Ion Mobility Spectrometry. 2014;17(3-4):117-24.
2.   Lebrilla CB. The gas-phase chemistry of cyclodextrin inclusion complexes. Accounts of chemical research. 2001;34(8):653-61.
3.   Liang Y, Bradshaw JS, Dearden DV. The thermodynamic basis for enantiodiscrimination: Gas-phase measurement of the enthalpy and entropy of chiral amine recognition by dimethyldiketopyridino-18-crown-6. The Journal of Physical Chemistry A. 2002;106(42):9665-71.

Rigid Co-Poly(Benzimidazole-Imide)s Prepared from a Synthetic Dianhydride and a Pyridine-containing Diamine

Mohammad Reza Zamanloo[a]*, Yaghoub Mansoori[a], Fatemeh Babazadeh

[a] *Department of Applied Chemistry,Faculty of Basic Science, University of Mohaghegh Ardabili, Ardabil 56199-11367, Iran*
*E-mail: zamanlou@yahoo.com, mrzamanloo@uma.ac.ir*

Introduction: **A**romatic polyimides possess growing importance due to rigid glassy structure with a polar nature along with a high glass transition temperature. Incorporating heterocyclic units into the polyimide backbone could integrate the advantages of both PI and modifying structural unit which improves the PI properties for specific applications. Recently poly(benzimidazole-imide)s have attracted great attention owing to excellent proton conductivity, good thermo-oxidative stability as well as adhesive properties [1-2]. Due to the H-bonding possibility in PBI and PI combinations between imide and benzimidazole units, high-performance fibers with superior mechanical properties could be obtained in poly(benzimidazole-imide)s [3-5].

Experimentals: To 0.93 mmol of BTDA (1ml DMF), 0.465 mmol of ODA (4ml HOAc) was added dropwise and mixed overnight at R.T under Ar. The mixture was heated at 160^oC for 5hrs by 10ml toluene. The solvent was removed and dianhydride product (S-DA) was dried. To 2.92 mmol of P-DA, 2.92mmol of ODA and 11.472mmol of TMSCl (5ml NMP) was added 5.84 mmol of S-DA and mixed at 30 ^{o}C for 24hrs under Ar. The mixture was heated at 150^oC for 5hrs and then precipitated in MeOH as cold.

 Results and Discussion: S-DA was prepared from BTDA and ODA in order to inserting flexible bonds in polymer backbone. TLC following along with IR and MS was used to confirm the reaction. The polycondensations to poly(benzimidazole-imide)s was conducted in the presence of activating agent, TMSCl, according to the following pathway, Scheme 1. Based on the characteristic IR absorption peaks of imide and imidazole FGs as well as solubility in NaHCO3 (5%), the PBI-IMs were characterized. Some of the physical properties of PBI-IM have been shown in table 1. The synthesized polymers did not show any solubility in all organic solvents at R.T., but limited solubility was observed by heating in DMSO and NMP. All of them were completely in conc. H_2SO_4. The thermal properties of PBI-IMs were investigated using TGA-DTA measurements, Fig. 1. Duo to moisture characteristic of benzimidazole units, all the thermoghrams of first scan was shown initial weight loss. So, second heating TGA-DTA traces were used to evaluate the thermal stability of the polymers, Table 1. The morphology of PBI-IMs was assessed by means of WAXD measurements on powder samples, Fig. 2. A Gaussian distribution with three peaks showing the ordered structure around 2θ = 16, 23 and 27 with FWHM = (0.83, 1.18 and 2.83 2θ) was deduced.

Conclusion: Co-polyimides containing benzimidazole units were prepared and evaluated for solution, thermal and aggregation properties. They were soluble only in conc. H_2SO_4 and showed solubility in NMP and DMSO by heating. High thermal stability and T_g were illustrated in TGA-DTA thermograms resulting from rigid structure and strong interchain interactions. Also, an ordered morphology in an amorphous matrix was detected in WAXDs.
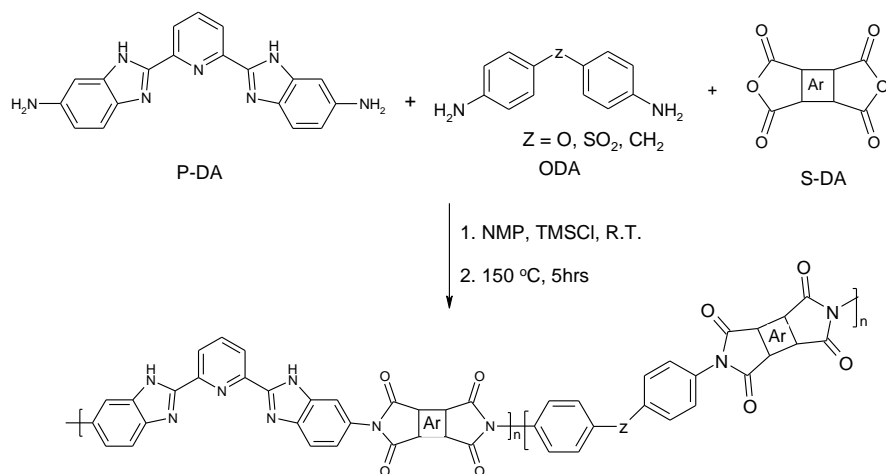
Scheme 1. The polycondensation pathway

Table 1. Reaction results and some physical properties of PBI-IM

Polymer Code	η_{inh} (dL/g)	Film	T_5 (°C)	T_{10} (°C)	T_g (°C)	C.Y (%)	LOI
Co-PBI-IM-a	0.65	Transparent, shattered	420	490	350	65	43.5
Co-PBI-IM-b	0.60	Transparent, shattered	430	490	325	67	44.3
Co-PBI-IM-c	0.51	Transparent, shattered	460	500	338	70	45.5

References

[1] S. Yuan; X. Guo; D. Aili; C. Pan; Q. Li; J. Fang. *J. Membr. Sci.*, **2014**, *454*, 351-358.

[2] Q. Xia; J. Liu; J. Dong; C. Yin; Y. Du; Q. Xu; Q. Zhang. *J. Appl. Polym. Sci.,* **2013**, *129*, 145-151.

[3] J. Liu; Q. Zhang; Q. Xia; J. Dong; Q. Xu. *Polym. Degrad. Stab.,* **2012**, *97*, 987-994.

[4] Y. Feng; L.B. Luo; J. Huang; K. Li; B. Li; H. Wang; X. Liu. *J. Appl. Polym. Sci.*, **2016**, *133*, 43677-43686.

[5] X. Ma; C. Kang; W. Chen; R. Jin; H. Guo; X. Qiu; L. Gao. *J. Polym. Sci., Part A: Polym. Chem.*, **2016**, *54*, 570-581.